LEABHARLANN CHOLÁISTE NA TRÍONÓIDE, BAILE ÁTHA CLIATH | TRINITY COLLEGE LIBRARY DUBLIN
Ollscoil Átha Cliath | The University of Dublin

Terms and Conditions of Use of Digitised Theses from Trinity College Library Dublin

Copyright statement

All material supplied by Trinity College Library is protected by copyright (under the Copyright and Related Rights Act, 2000 as amended) and other relevant Intellectual Property Rights. By accessing and using a Digitised Thesis from Trinity College Library you acknowledge that all Intellectual Property Rights in any Works supplied are the sole and exclusive property of the copyright and/or other IPR holder. Specific copyright holders may not be explicitly identified. Use of materials from other sources within a thesis should not be construed as a claim over them.

A non-exclusive, non-transferable licence is hereby granted to those using or reproducing, in whole or in part, the material for valid purposes, providing the copyright owners are acknowledged using the normal conventions. Where specific permission to use material is required, this is identified and such permission must be sought from the copyright holder or agency cited.

Liability statement

By using a Digitised Thesis, I accept that Trinity College Dublin bears no legal responsibility for the accuracy, legality or comprehensiveness of materials contained within the thesis, and that Trinity College Dublin accepts no liability for indirect, consequential, or incidental, damages or losses arising from use of the thesis for whatever reason. Information located in a thesis may be subject to specific use constraints, details of which may not be explicitly described. It is the responsibility of potential and actual users to be aware of such constraints and to abide by them. By making use of material from a digitised thesis, you accept these copyright and disclaimer provisions. Where it is brought to the attention of Trinity College Library that there may be a breach of copyright or other restraint, it is the policy to withdraw or take down access to a thesis while the issue is being resolved.

Access Agreement

By using a Digitised Thesis from Trinity College Library you are bound by the following Terms & Conditions. Please read them carefully.

I have read and I understand the following statement: All material supplied via a Digitised Thesis from Trinity College Library is protected by copyright and other intellectual property rights, and duplication or sale of all or part of any of a thesis is not permitted, except that material may be duplicated by you for your research use or for educational purposes in electronic or print form providing the copyright owners are acknowledged using the normal conventions. You must obtain permission for any other use. Electronic or print copies may not be offered, whether for sale or otherwise to anyone. This copy has been supplied on the understanding that it is copyright material and that no quotation from the thesis may be published without proper acknowledgement.

Preclinical Evaluation of Novel Tumour Vasculature Disrupting Agents

TRINITY COLLEGE
2 6 MAY 2010
LIBRARY DUBLIN

Ekatherine M Prokopiou

TRINITY COLLEGE
2 4 MAY 2013
LIBRARY DUBLIN

Thesis 9864.

Declaration

I hereby declare that the work presented in this thesis has not been submitted as an exercise of a degree at this or any other University. I also declare that the work presented in this thesis is entirely my own work, except where duly acknowledged. I agree that the library may lend or copy this thesis upon request.

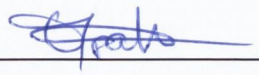

Ekatherine Prokopiou

Summary

Targeting of tumour vasculature and angiogenesis represents an ideal approach in the design of cancer therapeutics since all types of solid tumours are dependent upon a blood supply for growth and survival. The best known vascular disrupting agents are the tubulin binding agents, which as a result of their effect on microtubule dynamics; cause cell cycle arrest, morphological changes to endothelial cells and subsequent tumour vascular shutdown.

Aminopeptidase N (APN) is an exopeptidase which plays a key role in tumour cell invasion, extracellular matrix degradation and tumour metastasis. It is expressed in proliferating endothelial cells undergoing angiogenesis but not in quiescence endothelial cells, as well as in a variety of tumour cells (*e.g.* PC-3 cells). Thus, APN is an ideal therapeutic target for angiogenesis, invasion and APN-expressing tumours.

In our laboratory, single tubulin polymerisation inhibitors, dual-acting hybrids and designed multiple ligands, targeting tubulin polymerisation and APN (using bestatin) were designed, synthesised and evaluated in preliminary protein-based assays. The purpose of the studies described in this doctoral thesis was to extend this work and evaluate test compounds' anti-vascular, anti-angiogenic and anti-tumour activity in enzyme, cellular, *ex vivo* and *in vivo* settings.

The effect of the novel tubulin polymerisation inhibitors and dual-acting compounds on cell proliferation was evaluated using the (3-(4,5-Dimethylthiazol-2-yl)-2,5-diphenyltetrazolium) bromide (MTT) assay on human umbilical vein endothelial cells (HUVECs) and PC-3 human adenocarcinoma prostate cancer cells. The effect of test compounds on the cell cycle was established using flow cytometric analysis, while immunofluorescence staining determined their effect on the tubulin cytoskeleton. Morphological changes to endothelial cells were examined microscopically following addition of test compounds. An *in vitro* human angiogenesis assay was used to investigate the anti-angiogenic effect of a particular compound, namely RS180. The effect of dual-acting compounds on APN was investigated both in an enzyme-based assay, using a colorimetric technique, and a cellular-based assay, using HUVECs and PC-3 cells. The *ex vivo* rat aortic ring assay was performed in order to examine both the anti-vascular and the anti-angiogenic effects of test compounds, while the PC-3 tumour xenograft model was developed in order to determine the anti-tumour activity of the

most promising compounds *in vivo*. In addition, the degree of tumour necrosis and the *in vivo* anti-vascular/anti-angiogenic effects of test compounds were assessed by histological examination of tumour samples.

The *in vitro* data obtained from the evaluation of tubulin polymerisation inhibitors and dual-acting compounds showed that the majority displayed potent anti-proliferative activity, with varied potency depending upon their design. In addition, test compounds induced cell cycle arrest at the G_2/M phase, disrupted the tubulin cytoskeleton, caused reversible morphological changes to endothelial cells, inhibited *in vitro* and *ex vivo* angiogenesis and caused rapid microvessel breakdown in the aortic ring assay.

Furthermore, the dual-acting compounds demonstrated potent inhibition of APN both in the enzymatic and the cellular level and showed superiority over bestatin. Cell cycle analysis of DNA fragmentation (sub-G_0/G_1 arrest) showed that the design of these compounds was advantageous over single agents alone or in combination, and may suggest a different mechanism of action (other than the mitotic arrest) in which the compounds induced their apoptotic effect.

Selected tubulin polymerisation inhibitors and dual-acting compounds were chosen for further *in vivo* evaluation, whereby their anti-tumour efficacy and their effect on tumour vasculature were dependent upon their design, and which correlated with their *in vitro* and *ex vivo* data.

In conclusion, novel tubulin polymerisation inhibitors and dual-acting compounds targeting tubulin polymerisation and APN showed promising activity in several *in vitro*, *ex vivo* and *in vivo* models. The emergence of several potent vascular disrupting agents from these studies is encouraging; therefore demonstrating the need for further investigation to determine their true potential as anti-vascular, anti-angiogenic and anti-tumour agents.

Acknowledgments

First of all, I would like to thank my supervisors John Walsh and Sheila Ryder for all the support and help they offered me over the duration of my Ph.D. studies. Thank you for giving me the opportunity to work along site with you, providing me with your knowledge and the benefit of your experience.

I would like to thank Enterprise Ireland for their funding support and for giving me the chance to accomplish the research studies involved in this project.

A very big thank you to my colleagues Gary, Brian, Adrian and Elaine for sharing this project with me, for the long hours spent to synthesise the compounds and provided me with the material to work with. Thank you for your understanding and patience and for not getting annoyed when I asked you for a few more milligrams of compound! I have enjoyed working with you and I wish you the very best for the future!

A massive thank you to Orla for her support and advices, especially at the beginning of the project, and for the times she made me feel better when I was feeling lost. Also, many thanks to Deirdre, Tao and Paul for their encouragement and positivity. A big thank you to Cathal and Niamh for sharing the office with me and for always supporting me. Thank you guys, I wish you the best, to all of you!

In addition, I would like to thank Orla, Cathal, Gary, Brian and Adrian for proof reading parts of my thesis.

Many thanks to Jose and Anita, for sharing their knowledge with me and giving me advices when I was planning to start cell culture techniques.

I would also like to thank Anne, Sylvie, Tom, Mark, Peter, Monica and William in BioResources, TCD, for being so supportive and always trying to help me out. In particular, I would like to thank Ciaran Gavagan for giving me advices from his own experience and offered to train me with technical skills related to the animal models. In addition, a big thank you to Neil Marshall for his constant support throughout my *in vivo* studies and for teaching me techniques required for the purpose of the project.

Many thanks to Barry Moran from the School of Biochemistry and Immunology, for his assistance while using the flow cytometer, and for always willing to help me out. A big thank you to Gavin McManus from the School of Biochemistry and Immunology,

for being so supportive while using the confocal microscope and trying to help me resolve issues related to staining protocols.

Sincere thanks to Peter Stafford from the Department of Zoology, for kindly providing equipment and materials for paraffin-embedding processing of tumour samples. Thank you for sharing your valuable experience with me and offering me your precious knowledge.

To Dr Andrew Harkin, many thanks for kindly supplying the cryotome in the Institute of Neuroscience. I would also like to thank Valentina for showing me how to use the cryotome and giving me advice from her own experience.

Thank you to Brian Talbot, for his assistance with the LCMS and to Maureen, Pauline, Ray and Anne, but especially Joe for always being there to help me out with whatever I needed.

To Dr Fabio Boylan and Dr Helen Sheridan, thank you for giving me the opportunity to demonstrate undergraduate practicals.

Many thanks to John O'Brien and Emmanuel from the School of Chemistry, for their kind supply of liquid nitrogen.

I would like to thank my good friends Yianna, Laoura, Katerina and Elena who were always there to hear me out and who made my days brighter when I needed them!

To Iacovos, a massive thank you for being by my site throughout these years, always understanding, supporting and encouraging me and never complained when I was whining! I couldn't have done it without you, and for that I sincerely thank you.

Last but not least, I would like to thank my parents Angie and Andreas, and my lovely sister Danae for their unconditional love and support they always give me, even from far away, for spending hours chatting on Skype trying to encourage me, but most importantly for believing in me!

This thesis is dedicated to my youngest sister

Abbreviations

5-FdUrd	5-fluoro-2-deoxyuridine
5-FU	5-fluorouracil
AAVP	Adeno-Associated Virus Phage
ALCL	Anaplastic Large Cell Lymphoma
AML	Acute Myeloid Leukaemia
ANLL	Acute Non-Lymphocytic Leukaemia
APN/CD13	Aminopeptidase N
AR	Amphiregulin
BAEC	Bovine Aortic Endothelial Cell
BCEC	Brain Capillary Endothelial Cell
BRU	BioResources Unit
BSA	Bovine Serum Albumin
BTC	Betacellulin
BW	Body Weight
CA-4	Combretastatin A-4
CA-4P	Combretastatin A-4 Phosphate
CAM	Chorioallantoic Membrane
CAMs	Cell-cell Adhesion Molecules
CML	Chronic Myelomonocytic Leukaemia
CPT	Camptothecin
d.w	Distilled Water
DAPI	4', 6-diamidino-2-phenylindole
DCE-MRI	Dynamic Contrast Enhanced-Magnetic Resonance Imaging
DHI	Dihydroindazolocarbazole
DHN	DOX-loaded Heparin Nanoparticle
DLT	Dose Limiting Toxicity

DM1	Maytansinoid
DML	Designed Multiple Ligand
DMSO	Dimethyl Sulfoxide
DMXAA	5, 6-dimethylxanthenone-4-acetic acid
DOX	Doxorubicin
EBM	Endothelial cell Basal Medium
ECM	Extracellular Matrix
EGFR	Epidermal Growth Factor Receptor
EGM	Endothelial Growth Medium
ELISA	Enzyme-Linked Immunosorbent Assay
EPG	Epigen
Eph	Ephrin
EPR	Enhanced Permeability and Retention
EPR	Epiregulin
FAA	Flavone Acetic Acid
FBS	Foetal Bovine Serum
FGF	Fibroblast Growth Factor
FHL	Folate Heparin-Lithocholic Acid
Flt-1	Fms-Like Tyrosine Kinase-1
g	Gram
GDP	Guanosine Diphosphate
GIST	Gastrointestinal Stromal Tumour
GTP	Guanosine Triphosphate
H&E	Haematoxylin and Eosin
HAEC	Human Aortic Endothelial Cell
HAH	Heparin Adipic Hydrazide
HB-EGF	Heparin-Binding EGF-like Growth Factor

HCC	Hepatocellular Carcinoma
HCPS	Heparin-Carrying Polystyrene
HD	Heparin-Deoxycholic Acid
HGF	Hepatocyte Growth Factor
HIF-1	Hypoxia Inducible Factor-1
HL	Heparin-Lithocholic Acid
HMVEC	Human Dermal Microvascular Endothelial Cell
HSA	Human Serum Albumin
HSPG	Heparin Sulphate Proteoglycan
HUVEC	Human Umbilical Vein Endothelial Cell
i.p.	Intraperitoneal
i.v.	Intravenous
IC_{50}	Concentration at which 50% inhibition occurs
IGF	Insulin-like Growth Factor
IL	Interleukin
IVC	Individual Ventilated Cage
Kg	Kilogram
LDH	Lactate Dehydrogenase
LMWH	Low Molecular Weight Heparin
LYP	Bestatin Dimethylaminoethyl Ester
M	Molar
MAP	Microtubule Associated Protein
MAPK	Mitogen-Activated Protein Kinase
mg	Milligram

MHC	Major Histocompatibility Complex
mL	Millilitre
mM	Millimolar
MMAE	Monomethyl Auristatin E
MMAF	Monomethyl Auristatin F
MMP	Matrix Metalloproteinase
mol	Mole
MTC	Medullary Thyroid Carcinoma
MTD	Maximum Tolerated Dose
MTOC	Microtubule Organising Centre
mTOR	Mammalian Target of Rapamycin
MTT	3-(4,5-Dimethylthiazol-2-yl)-2,5-diphenyltetrazolium bromide
μg	Microgram
μL	Microlitre
μm	Micrometre
μM	Micromolar
n	Number of Experiments
ng	Nanogram
nM	Nanomolar
NP-1	Neuropilin-1 Receptor
NRG	Neuregulins
NS	Not Significant
NSCLC	Non-Small Cell Lung Cancer
p	P value
PBS	Phosphate Buffered Saline
PDGF	Platelet-Derived Growth Factor

PEG	Polyethylene Glycol
PEI	Polyethylenimine
pH	The measure of Acidity or Alkalinity
PI	Propidium Iodide
PI3K	Phosphatidylinositol 3-Kinase
pO_2	Partial oxygen pressure
pRb	Retinoblastoma Protein
PSA	Prostate-Specific Antigen
PSMA	Prostate-Specific Membrane Antigen
PTX	Paclitaxel
RCC	Renal Cell Carcinoma
RNase A	Ribonuclease A
rpm	Rotations per Minute
RT	Room Temperature
RTV	Relative Tumour Volume
s.c.	Subcutaneous
SAC	Spindle Assembly Checkpoint
SAPK	Stress-Activated Protein Kinase
SAR	Structure-Activity Relationship
SCC	Squamous Cell Carcinoma
SEM	Standard Error of Mean
SMC	Smooth Muscle Cell
STAT	Signal Transducers and Activators of Transcription
TAM	Tumour-Associated Macrophage
TAP	Tumour-Associated Protease
TCD	Trinity College Dublin

TGEV	Transmissible Gastroenteritis Virus
TGF-α	Transforming Growth Factor-α
Tie-2	Angiopoietin-1 Receptor
TIMP	Tissue Inhibitor of Metalloproteinase
TKI	Tyrosine Kinase Inhibitor
TNF-α	Tumour Necrosis Factor-α
TSP-1	Thrombospodin-1
UFH	Unfractionated Heparin
VCAM-1	Vascular Cell Adhesion Molecule-1
VDA	Vascular Disrupting Agent
vs	Versus
VE-cadherin	Vascular Endothelial-Cadherin
VEGF	Vascular Endothelial Growth Factor
wfi	Water for Injection

Table of Contents

-- Chapter 1 -- 1

1. Introduction 2

1.1 Cancer 2

1.1.1 Sustaining Proliferative Signalling 3

1.1.2 Evading Growth Suppressors 3

1.1.3 Resisting Cell Death 4

1.1.4 Enabling Replicative Immortality 4

1.1.5 Inducing Angiogenesis 5

1.1.6 Activating Invasion and Metastasis 5

1.2 Angiogenesis 7

1.2.1 Angiogenic Regulators 9

1.3 Tumour Vasculature 18

1.3.1 Tumour Vasculature as a Target 19

1.4 Anti-angiogenic Approach 20

1.4.1 Monoclonal Antibodies 20

1.4.2 Tyrosine Kinase Inhibitors 21

1.5 Aminopeptidase N 27

1.5.1 Bestatin 29

1.5.2 APN Inhibitors 31

1.6 Vasculature Normalisation 33

1.6.1 Vascular Disrupting Approach 34

1.6.2 Tubulin Targeting Agents 36

1.6.3 Cytokine Inducers 38

1.6.4 Ligand-directed Approach 39

1.7 Combination Therapy 39

1.8 Hybrid Drugs 40

1.8.1 Hybrid Approaches 41
1.8.2 RGD/NGR - Related Conjugates 46
1.8.3 Heparin - Related Conjugates 53
1.8.4 Multi - Targeted Compounds 60
1.9 Project aims 67
1.9.1 Overall Aims 69
-- Chapter 2 -- 70
2. Introduction 71
2.1 Compound Series 71
2.1.1 Group I Compound 71
2.1.2 Group II Compounds 72
2.1.3 Group III Compounds 73
2.1.4 Group IV Compounds 74
2.1.5 Tubulin Polymerisation Inhibitors as VDAs 76
2.1.6 Aims 77
2.1.7 Background to the Protocols Used 77
2.2 Materials and Methods 80
2.2.1 Materials 80
2.2.2 Test Compounds 80
2.2.3 Cell Lines 80
2.2.4 Cell Maintenance and Sub-culture 81
2.2.5 Cell Count 81
2.2.6 Cell Proliferation Assay 82
2.2.7 Cell Cycle Analysis – G_2/M Phase 83
2.2.8 Immunofluorescence Staining of the Microtubules 83
2.2.9 Analysis of Endothelial Cells' Morphology 84
2.2.10 *In Vitro* Angiogenesis Assay 84

2.2.14 Statistical Analysis 85
2.3 Results 86
2.3.1 Cell Proliferation Assay 86
2.3.2 Cell Cycle Analysis – G_2/M Phase 89
2.3.3 Immunofluorescence Staining of the Microtubules 94
2.3.4 Analysis of Endothelial Cells' Morphology 97
2.3.5 *In Vitro* Angiogenesis Assay 101
2.4 Discussion 104
2.4.1 Cell Proliferation Assay 104
2.4.2 Cell Cycle Analysis 106
2.4.3 Immunofluorescence Staining of the Microtubules 108
2.4.4 Analysis of Endothelial Cells' Morphology 109
2.4.5 *In Vitro* Angiogenesis Assay 111
2.5 Conclusions 112
-- Chapter 3 -- 113
3. Introduction 114
3.1. Aims 115
3.2 Background to the Protocols Used 115
3.2.1 Aortic Ring Assay 115
3.2.2 Tumour Xenograft Models 116
3.2.3 Assessment of Tumour Necrosis 118
3.2.4 Assessment of the Tumour Vasculature 118
3.3 Materials and Methods 120
3.3.1 Materials 120
3.3.2 Cell Line 120
3.3.3 Test Compounds 120
3.3.4 Animals 121

3.3.5 Aortic Ring Assay (anti-vascular model) 121
3.3.6 Aortic Ring Assay (anti-angiogenic model) 122
3.3.7 Maximum Tolerated Dose 122
3.3.8 Tumour System 123
3.3.9 Chemotherapy Studies 123
3.3.10 Assessment of Tumour Necrosis 124
3.3.11 Assessment of the Tumour Vasculature 125
3.3.12 Statistical Analysis 126
3.4 Results 127
3.4.1 Aortic Ring Assay (anti-vascular model) 127
3.4.2 Aortic Ring Assay (anti-angiogenic model) 132
3.4.3 *In Vivo* Evaluation of ECB206 139
3.4.4 *In Vivo* Evaluation of GS291 143
3.5 Discussion 150
3.5.1 Aortic Ring Assay (anti-vascular model) 150
3.5.2 Aortic Ring Assay (anti-angiogenesis) 151
3.5.4 *In Vivo* Anti-tumour Effect of GS291 153
3.5.5 Assessment of Tumour Necrosis 155
3.5.6 Assessment of the Tumour Vasculature 157
3.6 Conclusions 159
3.7 Overall Conclusions 161
-- Chapter 4 -- 162
4. Introduction 163
4.1 Background to the Dual-Acting Compounds Designed in our Group 163
4.1.1 Compound Series 164
4.1.2 Aims 167
4.1.3 Background to the Protocols Used 168

4.2 Materials and Methods 171
4.2.1 Materials 171
4.2.2 Test Compounds 171
4.2.3 APN Assay Buffer 171
4.2.4 Cell Lines 171
4.2.5 APN Expression of HUVECs and PC-3 cells 172
4.2.6 APN Enzyme-based Assay 172
4.2.7 Cytotoxicity Assay 173
4.2.8 APN Cell-based Assay 173
4.2.9 Inhibition of APN Expression 173
4.2.10 Cell Proliferation Assay 174
4.2.11 Immunofluorescence Staining of the Microtubules 174
4.2.12 Cell Cycle Analysis – G_2/M Phase 174
4.2.13 Cell Cycle Analysis – Sub-G_0/G_1 Phase 175
4.2.14 Analysis of Endothelial Cells' Morphology 175
4.2.15 Statistical Analysis 175
4.3 Results 176
4.3.1 APN Enzyme-based Assay 176
4.3.2 APN Expression of HUVECs and PC-3 Cells 178
4.3.3 Cytotoxicity Assay 179
4.3.4 APN Cell-based Assay 182
4.3.5 Inhibition of APN Expression 191
4.3.6 Cell Proliferation Assay 195
4.3.7 Immunofluorescence Staining of the Microtubules 199
4.3.8 Cell Cycle Analysis – G_2/M Phase 202
4.3.9 Cell Cycle Analysis – Sub-G_0/G_1 Phase 210
4.3.10 Analysis of Endothelial Cells' Morphology 231

4.4 Discussion 235
4.4.1 APN Enzyme-based Assay 235
4.4.2 APN Cell-based Assay 236
4.4.4 Cell Proliferation Assay 238
4.4.5 Immunofluorescence Staining of the Microtubules 242
4.4.6 Cell Cycle Analysis – G_2/M Phase 243
4.4.7 Cell Cycle Analysis – Sub-G_0/G_1 Phase 244
4.4.8 Analysis of Endothelial Cells' Morphology 249
4.5 Conclusions 250
-- Chapter 5 -- 253
5. Introduction 254
5.1 Aims 255
5.2 Materials and Methods 256
5.2.1 Materials 256
5.2.2 Cell Line 256
5.2.3 Test Compounds 256
5.2.4 Animals 257
5.2.5 Aortic Ring Assay (anti-vascular and anti-angiogenic model) 257
5.2.6 Dose Establishment 258
5.2.7 Tumour System 258
5.2.8 Chemotherapy Studies 258
5.2.9 Assessment of Tumour Necrosis 259
5.2.10 Assessment of the Tumour Vasculature 259
5.2.11 Statistical Analysis 259
5.3 Results 260
5.3.1 Aortic Ring Assay (anti-vascular model) 260
5.3.2 Aortic Ring Assay (anti-angiogenic model) 263

5.3.3 *In Vivo* Anti-tumour Evaluation 267
5.3.4 Assessment of Tumour Necrosis 276
5.3.5 Assessment of the Tumour Vasculature 277
5.4 Discussion 285
5.4.1 Aortic Ring Assay (anti-vascular model) 285
5.4.2 Aortic Ring Assay (anti-angiogenic model) 285
5.4.3 *In Vivo* Anti-tumour Efficacy 286
5.4.4 Assessment of Tumour Necrosis 289
5.4.5 Assessment of the Tumour Vasculature 290
5.5 Conclusions 292
5.6 Overall Conclusions 294
6. Future Work 297
6.1 Inhibition of Cell Proliferation 297
6.2 Inhibition of Tubulin Polymerisation 297
6.3 Inhibition of Cell Migration, Invasion, Adhesion and Angiogenesis 298
6.4 Inhibition of APN 298
6.5 Induction of Apoptosis 299
6.6 *In Vivo* Anti-tumour Efficacy 299
6.7 Examination of Tumour Samples 301
6.8 Hybrids' Design 301
Bibliography 302

Table of Figures

Figure 1.1: The hallmarks of cancer [4]. 2

Figure 1.2: Therapeutic targeting of the hallmarks of cancer [4]. 7

Figure 1.3: The steps involved in the process of angiogenesis. 9

Figure 1.4: Angiogenesis is orchestrated by a variety of activators and inhibitors. Changes in the angiogenic balance mediate the "angiogenic switch" [54]. 11

Figure 1.5: The VEGF family and its receptors [66] 12

Figure 1.6: Intracellular signalling pathways activated through FGFRs [77]. 13

Figure 1.7: PDGF ligands and their corresponding receptors [90]. 15

Figure 1.8: EGFR signalling pathway [101]. 16

Figure 1.9: MMP composition and expression in endothelial and fibroblast cells. 18

Figure 1.10: The differences between the normal and the tumour vasculature [66]. 19

Figure 1.11: FDA-approved multi-targeted inhibitors of angiogenesis sunitinib 1 [137-141], sorafenib 2 [142-147], pazopanib 3 [148-150], axatinib 4 [152, 156], gefitinib 5 [158-167] and erlotinib 6 [168-173]. 24

Figure 1.12: Multi-tyrosine kinase inhibitors lapatinib 7 [174] and vandetanib 8. 26

Figure 1.13: The structure of APN [221]. 28

Figure 1.14: Aminopeptidase inhibitors, bestatin 9 [239, 241], amastatin 10 [272], phebestin 11 [273] and probestin 12 [274]. 32

Figure 1.15: Normalisation of tumour vasculature following anti-angiogenic therapy. 34

Figure 1.16: Microtubules dynamics [301]. 36

Figure 1.17: Tubulin targeting agents: colchicine 13 [303], vincristine 14 [304], PTX 15 [306-307] and CA-4 16 [308]. 38

Figure 1.18: Cytokine inducer DMXAA 17 [322]. 39

Figure 1.19: Schematic illustrating a hybrid/conjugate design. Two distinct moieties are conjugated using a linker unit. 41

Figure 1.20: PTX-RGD conjugate 18 [395]. 48

Figure 1.21: RGD and NGR platinum-based conjugates 19 a, b and 20 a, b [338]. 52

Figure 1.22: HAH-cortisol conjugate 21 [436] and heparin-DOCA or HD conjugate 22 [439, 441]. Heparin is a sulphated polysaccharide with repeating uronic acid and glucosamine residues that vary in number. 56

Figure 1.23: Folate-heparin-lithocholate conjugate (FHL) 23 [352] and cRGD-heparin-lithocholic acid congugate, (cRGD-HL) 24 [452]..... 59

Figure 1.24: Multi-TKIs of angiogenesis cediranib 25 [453] and motesanib 26 [459].. 61

Figure 1.25: Multi-targeted TKIs canertinib 27 [462], vatalanib 28 [467] and leflunomide 29 [476]. 63

Figure 1.26: Multi-target inhibitors of VEGFR2 and Tie-2 tyrosine kinases 30 [483] and 31 [484], VEGFR2/c-Met 32 [489] and $\alpha_n\beta_3/\alpha_5\beta_1$ 33 [491]. 66

Figure 1.27: The group of compounds evaluated include tubulin polymerisation inhibitors, dual-targeting hybrids and DML..... 68

Figure 2.1: Phenstatin and group I compound RS133..... 72

Figure 2.2: Group II compounds: RS180, GS117 and GS170. 73

Figure 2.3: Group III compounds, ADR269, ADR354, ADR382, ADR384 and ADR393..... 74

Figure 2.4: Group IV compounds, GJH140, ADR084, ADR116, ADR118, ADR119 and ADR149. 75

Figure 2.5: The DML ADR241. 75

Figure 2.6: Cell cycle histograms of the gated $G_1/S/G_2/M$ cells treated with CA-4 and RS133.. 89

Figure 2.7: Percentage of cells in the G_2/M phase treated with RS133 and CA-4. Data represents mean ± SEM (n=3). 90

Figure 2.8: Cell cycle histograms of the gated $G_1/S/G_2/M$ cells treated with RS180 and GS117. 91

Figure 2.9: Percentage of cells in the G_2/M phase treated with RS180, GS117 and CA4. Data represents mean ± SEM (n=3). 91

Figure 2.10: Cell cycle histograms of the gated G_2/M cells treated with ADR269.. 92

Figure 2.11: Percentage of cells in the G_2/M phase treated ADR269. Data represents mean ± SEM (n=3). 92

Figure 2.12: Cell cycle histograms of the gated $G_1/S/G_2/M$ cells treated with GJH140 and ADR149.. 93

Figure 2.13: Percentage of cells in the G_2/M phase treated with GJH140, ADR149 and CA-4. Data represents mean ± SEM (n=3). 94

Figure 2.14: Microtubule disruption of endothelial cells by CA-4. 95

Figure 2.15: Microtubule disruption of endothelial cells by RS133.. 95

Figure 2.16: Microtubule disruption of endothelial cells by RS180 and GS117.. 96

Figure 2.17: Microtubule disruption of endothelial cells by ADR269..... 96

Figure 2.18: Microtubule disruption of endothelial cells by GJH140 and ADR149..... 97

Figure 2.19: The effect of RS133 on endothelial cells' morphology.. 98

Figure 2.20: The effect of RS180 and CA-4 on endothelial cells' morphology. 99

Figure 2.21: The effect of GS117 on endothelial cells' morphology..... 99

Figure 2.22: The effect of ADR269 on endothelial cells' morphology 100

Figure 2.23: The effect of GJH140 on endothelial cells' morphology..... 101

Figure 2.24: The effect of ADR149 on endothelial cells' morphology. 101

Figure 2.25: The anti-angiogenic effect of RS180 as determined by the AngioKit assay. 102

Figure 2.26: The effect of RS180 on microvessels formation..... 103

Figure 3.1: ECB206 is the leucine prodrug of ADR149 and GS291 is the disodium phosphate prodrug of RS180. 114

Figure 3.2: The anti-vascular effect of CA-4.. 127

Figure 3.3: The anti-vascular effect of RS133.. 128

Figure 3.4: The anti-vascular effect of RS180. 129

Figure 3.5: The anti-vascular effect of GS117. 129

Figure 3.6: The anti-vascular effect of ADR269.. 130

Figure 3.7: The anti-vascular effect of GJH140.. 131

Figure 3.8: The anti-vascular effect of ADR149. 131

Figure 3.9: The anti-angiogenic effect of CA-4.. 132

Figure 3.10: The microvessel density of CA-4-treated cultures was obtained using Image J. Data represents mean pixel density area ± SEM (n=3)..... 133

Figure 3.11: The anti-angiogenic effect of RS133.. 133

Figure 3.12: The microvessel density of RS133-treated cultures was obtained using Image J. Data represents mean pixel density area ± SEM (n=3)..... 134

Figure 3.13: The anti-angiogenic effect of RS180.. 134

Figure 3.14: The microvessel density of RS180-treated cultures was obtained using Image J. Data represents mean pixel density area ± SEM (n=3)..... 135

Figure 3.15: The anti-angiogenic effect of GS117..... 135

Figure 3.16: The microvessel density of GS117-treated cultures was obtained using Image J. Data represents mean pixel density area ± SEM (n=3)..... 136

Figure 3.17: The anti-angiogenic effect of ADR269..... 136

Figure 3.18: The microvessel density of ADR269-treated cultures was obtained using Image J. Data represents mean pixel density area ± SEM (n=3)..... 137

Figure 3.19: The anti-angiogenic effect of GJH140..... 137

Figure 3.20: The microvessel density of GJH140-treated cultures was obtained using Image J. Data represents mean pixel density area ± SEM (n=3)..... 138

Figure 3.21: The anti-angiogenic effect of ADR149..... 138

Figure 3.22: The microvessel density of ADR149-treated cultures was obtained using Image J. Data represents mean pixel density area ± SEM (n=3)..... 139

Figure 3.23: Evaluation of the efficacy of 50 mg/kg ECB206 administered once a week for three weeks in a PC-3 tumour xenograft model.. 141

Figure 3.24: Body weight measurements were recorded to monitor any systemic toxicity following treatment with ECB206.. 142

Figure 3.25: H&E stained tumour samples obtained from A-B) the control treated group and C-D) the ECB206-treated group, following 24h of a single i.p. injection (V=Viable, N=Necrotic, n=3). 143

Figure 3.26: Evaluation of the efficacy of 200 mg/kg GS291 and 150 mg/kg CA-4... 145

Figure 3.27: Body weight measurements were recorded to monitor any systemic toxicity following treatment with GS291 and CA-4 145

Figure 3.28: H&E stained tumour samples obtained from A-C) the control treated group, D-F) the CA-4P-treated group and G-I) the GS291-treated group (V=Viable, N=Necrotic, n=3)..... 147

Figure 3.29: The effect of GS291 treatment on the tumour vasculature.. 148

Figure 3.30: Quantification of functional vasculature area of tumours following 6h after a single i.p. administration of 200 mg/kg GS291. 149

Figure 4.1: Group I hybrids ECB377 and ECB378 which incorporate ECB394 and bestatin. 165

Figure 4.2: Group II hybrids ECB399 and ECB404 which incorporate GS117 or RS176 and bestatin, respectively. 165

Figure 4.3: Group III hybrid ECB397 which incorporates RS180 and bestatin. 166

Figure 4.4: Group IV hybrid ADR469 which incorporates ADR269 and bestatin. 166

Figure 4.5: BWM120, a DML which incorporates RS180 and a hydroxamic acid. 166

Figure 4.6: The effect of ADR469 on APN inhibition using the enzyme-based assay. Data represents mean ± SEM (n=3). 178

Figure 4.7: APN expression of HUVECs and PC-3 cells.. 179

Figure 4.8: The cytotoxic effect of A) ECB377 and B) ECB378 on HUVECs after 2h incubation, as determined by the MTT assay 180

Figure 4.9: The cytotoxic effect of A) ECB399 and B) ECB404 on HUVECs after 2h incubation, as determined by the MTT assay. 181

Figure 4.10: The cytotoxic effect of ADR469 on HUVECs after 2h incubation, as determined by the MTT assay.. 182

Figure 4.11: The cytotoxic effect of BWM120 on HUVECs after 2h incubation, as determined by the MTT assay. 182

Figure 4.12: APN inhibition of HUVECs after 2h incubation with A) bestatin, B) ECB377 and C) ECB378. 184

Figure 4.13: APN inhibition of PC-3 cells after 2h incubation with A) bestatin, B) ECB377 and C) ECB378.. 186

Figure 4.14: APN inhibition of HUVECs by A) ECB399 and B) ECB404 after 2h incubation.. 187

Figure 4.15: APN inhibition of PC-3 cells by A) ECB399 and B) ECB404 after 2h incubation. 188

Figure 4.16: APN inhibition by ECB397 of A) HUVECs and B) PC-3 cells after 2h incubation.. 189

Figure 4.17: APN inhibition by ADR469 of A) HUVECs and B) PC-3 cells after 2h incubation.. 190

Figure 4.18: APN inhibition by BWM120 of A) HUVECs and B) PC-3 cells after 2h incubation.. 191

Figure 4.19: Detection of APN expression level (PE CD13) in HUVECs after 2h incubation with A) 0.1 mM bestatin, B) 0.5 mM bestatin, C) 0.1 mM BWM120 and D) 0.5 mM BWM120. 192

Figure 4.20: Percentage PE CD13 fluorescence median of HUVECs after 2h incubation with A) bestatin and B) BWM120..... 193

Figure 4.21: Detection of APN expression level (PE CD13) in PC-3 cells after 2h incubation with A) 0.1 mM bestatin, B) 0.5 mM bestatin, C) 0.1 mM BWM120 and D) 0.5 mM BWM120. 194

Figure 4.22: Percentage PE CD13 fluorescence median of PC-3 cells after 2h incubation with A) bestatin and B) BWM120..... 195

Figure 4.23: Microtubule disruption of endothelial cells by ECB378.. 200

Figure 4.24: Microtubule disruption of endothelial cells by ECB397.. 201

Figure 4.25: Microtubule disruption of endothelial cells by ADR469..... 201

Figure 4.26: Microtubule disruption of endothelial cells by BWM120.. 202

Figure 4.27: Cell cycle histograms of the gated G_2/M cells treated with ECB378..... 203

Figure 4.28: Percentage of cells in the G_2/M phase A) HUVECs and B) PC-3 cells incubated with ECB378. Data represents mean ± SEM (n=3). 204

Figure 4.29: Cell cycle histograms of the gated G_2/M cells treated with ECB397..... 205

Figure 4.30: Percentage of cells in the G_2/M phase A) HUVECs and B) PC-3 cells incubated with ECB397. Data represents mean ± SEM (n=3). 206

Figure 4.31: Cell cycle histograms of the gated G_2/M cells treated with ADR469.. ...207

Figure 4.32: Percentage of cells in the G_2/M phase A) HUVECs and B) PC-3 cells incubated with ADR469. Data represents mean ± SEM (n=3). 208

Figure 4.33: Cell cycle histograms of the gated G_2/M cells treated with BWM120....209

Figure 4.34: Percentage of cells in the G_2/M phase A) HUVECs and B) PC-3 cells incubated with BWM120. Data represents mean ± SEM (n=3)..... 210

Figure 4.35: Cell cycle histograms of the gated sub-G_0/G_1 cells treated with CA-4.. .211

Figure 4.36: Percentage of cells in the sub-G_0/G_1 phase A) HUVECs and B) PC-3 cells incubated with CA-4. Data represents mean ± SEM (n=3). 212

Figure 4.37: Cell cycle histograms of the gated sub-G_0/G_1 cells treated with ECB394.. 214

Figure 4.38: Percentage of cells in the sub-G_0/G_1 phase A) HUVECs and B) PC-3 cells incubated with ECB394. Data represents mean ± SEM (n=3). 215

Figure 4.39: Cell cycle histograms of the gated sub-G_0/G_1 cells treated with bestatin.. 216

Figure 4.40: Percentage of cells in the sub-G_0/G_1 phase A) HUVECs and B) PC-3 cells incubated with bestatin. Data represents mean ± SEM (n=3). 217

Figure 4.41: Cell cycle histograms of the gated sub-G_0/G_1 cells treated with ECB394 and bestatin. 217

Figure 4.42: Percentage of cells in the sub-G_0/G_1 phase A) HUVECs and B) PC-3 cells incubated with 1:1 ECB394/bestatin combinations. Data represents mean ± SEM (n=3). 218

Figure 4.43: Cell cycle histograms of the gated sub-G_0/G_1 cells treated with ECB378.. 219

Figure 4.44: Percentage of cells in the sub-G_0/G_1 phase A) HUVECs and B) PC-3 cells incubated with ECB378. Data represents mean ± SEM (n=3). 220

Figure 4.45: Cell cycle histograms of the gated sub-G_0/G_1 cells treated with RS180..222

Figure 4.46: Percentage of cells in the sub-G_0/G_1 phase A) HUVECs and B) PC-3 cells incubated with RS180. Data represents mean ± SEM (n=3). 223

Figure 4.47: Cell cycle histograms of the gated sub-G_0/G_1 cells treated with RS180 and bestatin. 224

Figure 4.48: Percentage of cells in the sub-G_0/G_1 phase A) HUVECs and B) PC-3 cells incubated with 1:1 RS180/bestatin combinations. Data represents mean ± SEM (n=3). 225

Figure 4.49: Cell cycle histograms of the gated sub-G_0/G_1 cells treated with ECB397.. 226

Figure 4.50: Percentage of cells in the sub-G_0/G_1 phase A) HUVECs and B) PC-3 cells incubated with ECB397. Data represents mean ± SEM (n=3). 227

Figure 4.51: Cell cycle histograms of the gated sub-G_0/G_1 cells treated with BWM120.. 229

Figure 4.52: Percentage of cells in the sub-G_0/G_1 phase A) HUVECs and B) PC-3 cells incubated with BWM120. Data represents mean ± SEM (n=3). 230

Figure 4.53: The effect of ECB378 on endothelial cells' morphology. 231

Figure 4.54: The effect of ECB378 on endothelial cells' morphology.. 232

Figure 4.55: The effect of ECB397 on endothelial cells' morphology. 233

Figure 4.56: The effect of ADR469 on endothelial cells' morphology.. 234

Figure 4.57: The effect of BWM120 on endothelial cells' morphology. 234

Figure 5.1: Hybrids ECB397, ECB378, ADR469 and DML BWM120. 254

Figure 5.2: The anti-vascular effect of ECB378. 260

Figure 5.3: The anti-vascular effect of ECB397. 261

Figure 5.4: The anti-vascular effect of ADR469.. 262

Figure 5.5: The anti-vascular effect of BWM120. 263

Figure 5.6: The anti-angiogenic effect of ECB378.. 264

Figure 5.7: The microvessel density of ECB378-treated cultures was obtained using Image J. Data represents mean pixel density area ± SEM (n=3)..... 264

Figure 5.8: The anti-angiogenic effect of ECB397.. 265

Figure 5.9: The microvessel density of ECB397-treated cultures was obtained using Image J. Data represents mean pixel density area ± SEM (n=3)..... 265

Figure 5.10: The anti-angiogenic effect of ADR469..... 266

Figure 5.11: The microvessel density of ADR469-treated cultures was obtained using Image J. Data represents mean pixel density area ± SEM (n=3)..... 266

Figure 5.12: The anti-angiogenic effect of BWM120. 267

Figure 5.13: The microvessel density of BWM120-treated cultures was obtained using Image J. The data represents mean pixel density area ± SEM (n=3). 267

Figure 5.14: Evaluation of the efficacy of 40 mg/kg ECB378 administered i.p. on alternate days for 12 days in a PC-3 tumour xenograft model. A) Control and treated tumours obtained after completion of the study, B) data represents the mean relative tumour volume ± SEM (n=7-8). 268

Figure 5.15: Body weight measurements were recorded to monitor any systemic toxicity following treatment with ECB378. 269

Figure 5.16: A) Control and treated tumours obtained after completion of the study. Evaluation of the efficacy of B) 40 mg/kg ECB397 and C) 1:1 RS180-leu/bestatin combination at equimolar concentration as per ECB397 administered i.p. on alternate days for 12 days in a PC-3 tumour xenograft model..... 271

Figure 5.17: Body weight measurements were recorded to monitor any systemic toxicity following treatment with ECB397 and RS180-leu/bestatin. 272

Figure 5.18: A) Control and treated tumours obtained after completion of the study. B) Evaluation of the efficacy of 50 mg/kg ADR469 administered i.p. on alternate days for 24 days in a PC-3 tumour xenograft model. 273

Figure 5.19: Body weight measurements were recorded to monitor any systemic toxicity following treatment with ADR469. 274

Figure 5.20: A) Control and treated tumours obtained after completion of the study. B) Evaluation of the efficacy of 40 mg/kg BWM120 administered i.p. on alternate days for 12 days in a PC-3 tumour xenograft model. 275

Figure 5.21: Body weight measurements were recorded to monitor any systemic toxicity following treatment with BWM120. 276

Figure 5.22: H&E stained tumour samples obtained from the A-B) control treated group and C-D) the ADR469-treated group. 277

Figure 5.23: The effect of ECB378 treatment on the tumour vasculature.. 278

Figure 5.24: Quantification of functional vasculature area of tumours following i.p. administration of 40 mg/kg ECB378 on alternate days for 12 days, using Image J. ... 279

Figure 5.25: The effect of I. 40 mg/kg ECB397 and II. equimolar dose of RS180-leu/bestatin (1:1) treatment on tumour vasculature. 280

Figure 5.26: Quantification of functional vasculature area of tumours following i.p. administration of 40 mg/kg ECB397 or equimolar dose of RS180-leu/bestatin combination on alternate days for 12 days, using Image J. A) Analysis of individual control and ECB397-treated tumours and B) overall analysis. 281

Figure 5.27: The effect of ADR469 treatment on tumour vasculature. 282

Figure 5.28: Quantification of functional vasculature area of tumours following i.p. administration of 50 mg/kg ADR469 on alternate days for 24 days, using Image J. A) Analysis of individual control and ADR469-treated tumours and B) overall analysis. 283

Figure 5.29: The effect of BWM120 treatment on tumour vasculature.. 284

Figure 5.30: Quantification of functional vasculature area of tumours following i.p. administration of 40 mg/kg BWM120 on alternate days for 12 days, using Image J. . 284

Table of Tables

Table 1.1: Summary of the FDA-approved tyrosine kinase inhibitors (TKI). 27

Table 1.2: Hybrid/Conjugate designs targeting tumour angiogenesis or vasculature. ... 42

Table 2.1: Best fit IC_{50} values ± SEM of group I compound, following the MTT assay (n=3). 86

Table 2.2: Best fit IC_{50} values ± SEM of group II compounds, following the MTT assay (n=3). 86

Table 2.3: Best fit IC_{50} values ± SEM of group III compounds, following the MTT assay (n=3). 87

Table 2.4: Best fit IC_{50} values ± SEM of group IV compounds, following the MTT assay (n=3). 88

Table 2.5: Best fit IC_{50} values ± SEM of ADR241, following the MTT assay (n=3).... 88

Table 3.1: Summary of ECB206 *in vivo* data. 142

Table 3.2: Summary of GS291 and CA-4P *in vivo* data 146

Table 4.1: APN enzyme-based assay data of group I hybrids, IC_{50} ± SEM (n=3)..... 176

Table 4.2: APN enzyme-based assay data of group II hybrids, IC_{50} ± SEM (n=3). 177

Table 4.3: APN enzyme-based assay data of group III hybrid, IC_{50} ± SEM (n=3)..... 177

Table 4.4: APN enzyme-based assay data of BWM120, IC_{50} ± SEM (n=3). 178

Table 4.5: Best fit IC_{50} values ± SEM of group I hybrids, following the MTT assay (n=3). 196

Table 4.6: Best fit IC_{50} values ± SEM of group II hybrids, following the MTT assay (n=3). 197

Table 4.7: Best fit IC_{50} values ± SEM of group III hybrid, following the MTT assay (n=3). 198

Table 4.8: Best fit IC_{50} values ± SEM of group IV hybrid, following the MTT assay (n=3). 198

Table 4.9: Best fit IC_{50} values ± SEM of BWM120, following the MTT assay (n=3). 199

Table 4.10: Percentage of cells in the sub-G_0/G_1 ± SEM (n=3), for group I hybrid. ... 213

Table 4.11: Percentage of cells in the sub-G_0/G_1 ± SEM (n=3), for group III hybrid. 222

Table 4.12: Percentage of cells in the sub-G_0/G_1 ± SEM (n=3), for BWM120. 228

Table 5.1: Summary of ECB378 *in vivo* data. 269

Table 5.2: Summary of ECB397 and RS180-leu/bestatin *in vivo* data. 272

Table 5.3: Summary of ADR469 *in vivo* data. 274

Table 5.4: Summary of BWM120 *in vivo* data.....276

-- Chapter 1 --

Introduction

1. Introduction

1.1 Cancer

The first known description of cancer dates back to ancient times, when Hippocrates described cancer in detail, using the Greek terms "*carcinos*" and "*carcinoma*" to refer to chronic ulcers or growths that appeared to be malignant tumours [1]. According to the National Cancer Registry in Ireland, cancer is currently the second most common cause of deaths in Ireland. An average of 30 000 new cases of cancer are diagnosed each year, with the five most common cancers being non-melanoma skin cancer, prostate, breast, bowel and lung cancer. Statistics suggest that cancer will affect one in three people in Ireland [2].

Cancer is a disease involving dynamic changes in the genome which drive the progressive transformation of normal human cells into highly malignant derivatives. Hanahan and Weinberg characterised cancer by six distinct hallmarks; sustaining proliferative signalling, evading growth suppressors, resting cell death, enabling replicative immortality, inducing angiogenesis and activating invasion and metastasis [3-4]. A summative illustration of the hallmarks of cancer is shown in Figure 1.1; each aspect will be discussed in detail in the following sections.

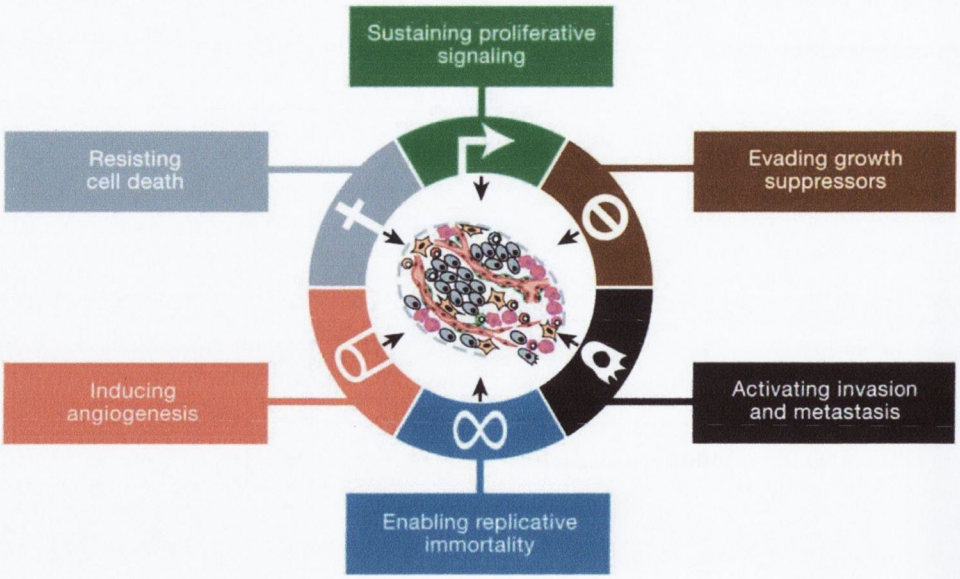

Figure 1.1: The hallmarks of cancer [4].

1.1.1 Sustaining Proliferative Signalling

In order for normal cells to move from a quiescent stage to a proliferative stage, mitogenic growth signals are required. An oncogene is any gene which, when mutated or expressed at high levels, has the potential to cause cancer. Due to their nature, many oncogenes can mimic normal growth signalling. For example, mutant *ras* oncogenes are responsible for approximately 50% of human colon carcinomas [5]. Tumour cells reduce their dependence on stimulation from their non-tumour tissue microenvironment, and sustain proliferative signalling, by generating their own growth signals, involving alterations of extracellular signalling of transcellular transducers or intracellular circuits, which translate signals into action.

An example of signalling pathways which are implicated in cancer are those of tyrosine kinase growth factor receptors. Over-expression of tyrosine kinase receptors enables cells to become hyper-responsive to ambient levels of growth factors that would normally not trigger proliferation. The epidermal growth factor receptor (EGFR) is up-regulated in stomach, brain and breast tumours and the type 2 receptor (EGFR2) is over-expressed in stomach and mammary carcinomas [6-7]. Also, alterations of growth signalling pathways, such as the SOS-Ras-Raf-MAPK (mitogen-activated protein kinase) cascade, play a central role in the development of human tumours. Ras proteins are found to be structurally different in 25% of human tumours, in this way enabling them to release mitogenic signals into the cells without stimulation by their normal regulators [8].

1.1.2 Evading Growth Suppressors

There are multiple anti-proliferative signals within the normal tissue that operate to maintain cellular quiescence. Normal cells can be removed from the active proliferation cycle to a resting, quiescent phase (G_0) or induced to enter into a post-mitotic state. Anti-proliferative signals are regulated through the retinoblastoma protein (pRb) and its two related proteins, p107 and p130. Hyper-phosphorylation or loss of pRb allows tumour cells to become insensitive to anti-growth signals [9].

1.1.3 Resisting Cell Death

Apoptosis is the programmed cell death, which along with cell proliferation, regulates the ability of cell populations to expand. Once apoptosis is triggered by a variety of physiologic signals, a series of steps unfold, including disruption of cellular membranes, breakdown of cytoplasmic and nuclear skeletons, extrusion of cytosol, degradation of chromosomes and fragmentation of the nucleus [10]. There are two classes of components that regulate apoptosis; the sensors and effectors. Extracellular and intracellular environment conditions (*e.g.* DNA damage, signalling imbalance, hypoxia) of normality or abnormality are monitored by the sensors. These signals control the effectors, including cell surface receptors which bind to survival or death factors. For example, survival signals are transmitted through insulin-like growth factors IGF-1/IGF-2 and interleukin-3 (IL-3) [11-12], whereas death signals are modulated by interaction of Fas ligand and tumour necrosis factor-α (TNF-α) with their receptors [13]. Cytochrome C, a potent catalyst of apoptosis which is released by the mitochondria [14] can activate, along with Fas, an array of intracellular proteases termed caspases, [15] such as caspase-8 and -9, which then trigger several effector caspases that execute the cell death program.

The discovery of the up-regulation of the *bcl-2* oncogene in follicular lymphoma and its anti-apoptotic ability [16] was the first correlation which warranted further investigation into apoptosis and cancer. In addition, co-expression of *bcl-2* with *myc* oncogene in transgenic mice promotes the growth of B cell lymphomas, by enhancing lymphocyte survival and not by further *myc*-induced proliferation. Resistance to apoptosis is achieved through a number of mechanisms, including inactivation of pro-apoptotic stimuli and the over-expression of anti-apoptotic genes [17].

1.1.4 Enabling Replicative Immortality

Normal cells have a finite replicative potential and once they have progressed through a certain number of doublings, they stop growing in a process referred to as senescence [18]. By disabling the pRb and p53 tumour suppressor proteins of senescence, cultured human fibroblasts continue multiplying until they enter a second stage, termed crisis. At this stage, cells undergo massive cell death, karyotypic disarray and end-to-end fusion of chromosomes. Occasionally there is an emergence of a variant cell, coined

"immortal cell", that has acquired the ability to multiply without limit [19]. Telomeres, the ends of chromosomes, are characterised as the counting device for cell generations and are composed of several thousand repeats of a short 6 base pair sequence element. During each cycle, there is a 50-100 base pair loss of telomeric DNA from the ends of every chromosome which results in the inability of DNA polymerases to completely replicate the 3′ends of chromosomal DNA. The progressive erosion of the telomeres leads the unprotected ends of chromosomal DNA to participate in end-to-end chromosomal fusions creating the karyotypic disarray associated with crisis and cell death [20]. Up-regulation of telomerase enzyme, which adds hexanucleotide repeats onto the ends of telomeric DNA [21], is evident in almost all types of malignant cells [22]. When telomeres' length is maintained at a critical threshold, it allows constant and unlimited multiplication of descendant cells and thus induces a malignant phenotype.

1.1.5 Inducing Angiogenesis

The provision of oxygen and nutrients supplied by the vasculature is crucial for cell function and survival. Solid tumours require the growth of new blood vessels, in a process termed angiogenesis, in order to remain viable and continue to grow. Initially, cells within the aberrant proliferation lesions lack angiogenic ability but subsequently develop the potential to promote angiogenesis through positive signals [23-24]. The balance between positive and negative signals regulates this process and involves the interaction between soluble factors, their receptors which are displayed on the surface of endothelial cells, and adhesion molecules which mediate cell-matrix or cell-cell associations. This section will be discussed in detail in section 1.2.

1.1.6 Activating Invasion and Metastasis

Once a solid tumour has developed, pioneer cells move out of the primary site and invade adjacent tissues where they establish new colonies. The distant settlement of tumour cells from the primary tumour is referred to as metastasis and is primarily responsible for 90% of human cancer deaths [25]. Cells with invasive and metastatic potential have alterations in proteins including cell-cell adhesion molecules (CAMs, *e.g.* members of the calcium-dependent cadherin families), and integrins which associate cells to extracellular matrix (ECM) substrates. The most important adhesion molecule is thought to be E-cadherin, a cell-cell interaction molecule, which is

expressed on epithelial cells. E-cadherin coupling to adjacent cells generates anti-growth signals, while loss of its function represents a key step in the prevention of invasion and metastasis [26]. Likewise, changes in the level of integrin expression [27], up-regulation of protease genes and down-regulation of protease inhibitors genes, influence the invasive and metastatic capability of cancer cells [28].

In addition to the six cancer hallmarks, Hanahan and Weinberg also suggested that cancer cells acquire functional capabilities for survival and proliferation by two enabling characteristics, including the development of genomic instability and the inflammatory state of malignant lesions, driven by the immune system cells [4]. Thus, an additional two emerging hallmarks have been proposed to be functionally important for cancer cells' progression: (i) deregulation of cellular energetics in order to support continuous cell growth [29-30] and (ii) evasion of immune destruction by cancer cells [31-32].

In summary, cancer is an extremely complex disease which is characterised by the hallmarks discussed above. An understanding of these mechanisms and their molecular targets allows for the development of therapeutics which is directed towards these specific molecular targets (Figure 1.2). In theory, inhibition of these processes should result in the development of new therapies which acquire fewer side effects and reduced toxicity profiles than those currently used for the treatment of cancer.

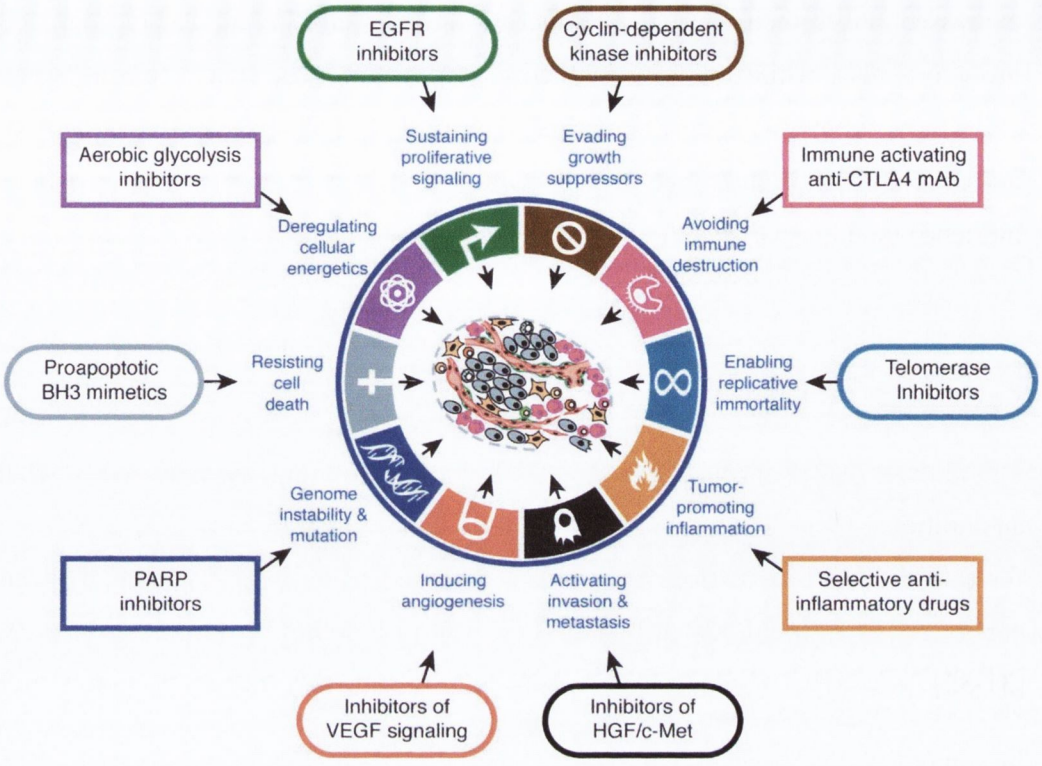

Figure 1.2: Therapeutic targeting of the hallmarks of cancer [4].

The work carried out in this doctoral thesis involves the evaluation of novel anti-cancer agents which were designed to target and inhibit one of the main cancer hallmarks described earlier; tumour vasculature and angiogenesis. Accordingly, the anti-vascular, anti-angiogenic and anti-tumour properties of the newly synthesised tubulin polymerisation inhibitors and dual-acting compounds, targeting tubulin polymerisation and aminopeptidase N (APN), were examined *in vitro*, *ex vivo* and *in vivo*.

1.2 Angiogenesis

Tumour growth and survival requires nutrients and oxygen, as well as the elimination of metabolic wastes and carbon dioxide. Central to these processes is the requirement of an adequate vasculature system. Angiogenesis is defined as the process in which new blood vessels form from the existing vasculature. During this process, endothelial cell proliferation is induced which results in alignment of these cells into tubes (vasculogenesis). Physiologically, this process takes place during embryogenesis, female reproductive cycle, as well as wound healing. During tumour angiogenesis, the "angiogenic switch" is turned on causing the normally quiescent vasculature to

constantly sprout new vessels and thus facilitate tumour growth [23-24]. Evidence in an *in vivo* study, whereby implanted tumour and non-tumour tissue in non-vascularised cornea in rabbits, has shown that tumour growth was angiogenesis-dependent. Tumour tissues were able to grow once newly formed vasculature was developed, whereas non-tumour tissue did not attract new blood vessel formation and therefore was not increased in size [33].

Angiogenesis is a complex process which involves a number of steps including the production and release of angiogenic factors (upon activation by hypoxia or genetic mutations) [34-36], and the binding of these factors to vascular endothelial cell receptors, thereby causing activation and cell proliferation (Figure 1.3). Extracellular metalloproteinases mediate many of the changes in the microenvironment by degrading the ECM in front of the proliferating endothelial cells [37]. Endothelial cells then migrate towards the tumour tissue where they align to form new blood vessels *via* adhesion molecules, and connect to create a loop that allows the blood to circulate. Specialised muscle cells (*e.g.* smooth muscle cells and pericytes) stabilise the vessel tubes providing structural support [38]. Figure 1.3 is a schematic illustration showing individual steps involved in the process of angiogenesis.

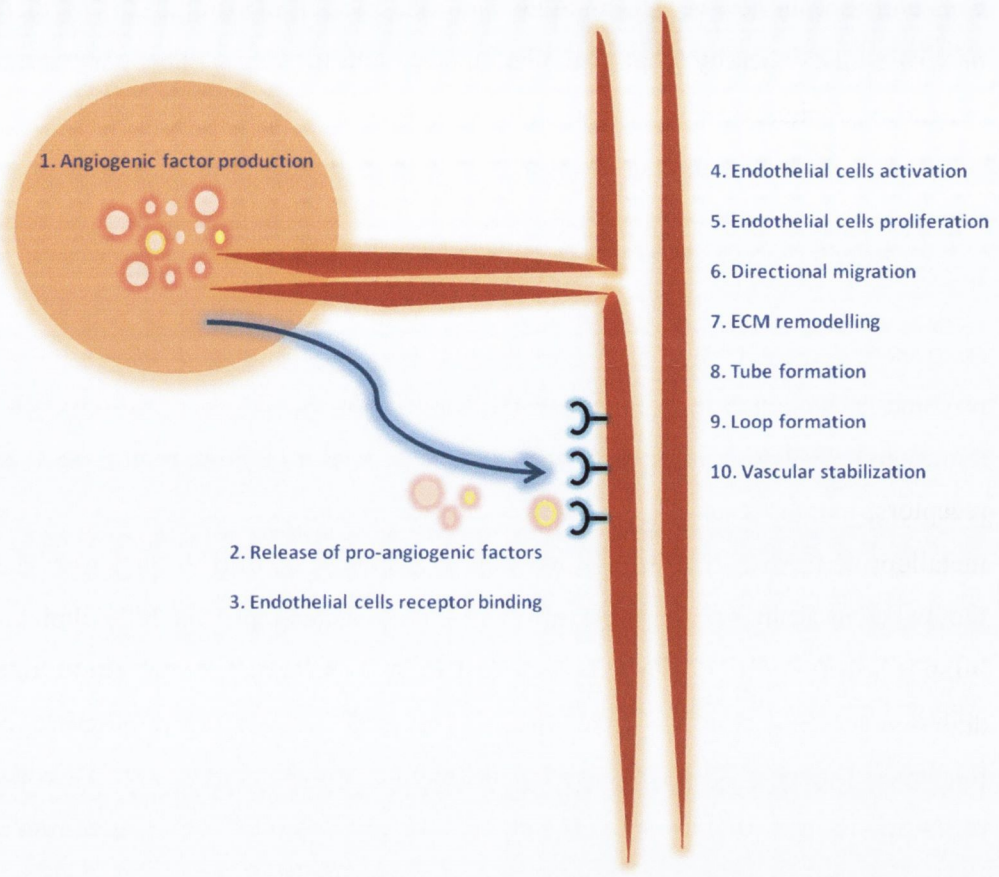

Figure 1.3: The steps involved in the process of angiogenesis.

1.2.1 Angiogenic Regulators

Many endogenous molecules are involved in the control of angiogenesis and several of these are studied for potential therapeutic applications. Pro-angiogenic regulators include vascular endothelial growth factors (VEGFs), the fibroblast growth factors (FGFs), the platelet-derived growth factors (PDGFs), the EGFs and their associated tyrosine kinase receptors, VEGFRs, FGFRs, PDGFRs and EGFRs. Two distinct therapeutic approaches currently employed which target angiogenic regulators in various human malignancies are monoclonal antibodies, which bind to the extracellular domains of the receptors and small-molecule tyrosine kinase inhibitors (TKIs) which target the intracellular tyrosine kinase domain of the receptors.

Further angiogenic regulators include the matrix metalloproteinases (MMPs) and their inhibitors, tissue inhibitors metalloproteinases (TIMPs). Thrombospodin-1 (TSP-1) is an angiogenesis inhibitor which counteracts pro-angiogenic stimuli by evoking

suppressive signals through activation of endothelial cell receptors [39]. Furthermore, a network of interconnected signalling pathways involving newly characterised ligands of signal-transducing receptors displayed by endothelial cells, include Notch, Neuropilin, Robo and ephrin receptors (Eph-A/B). These pathways were associated with the developmental and tumour-driven angiogenesis and which demonstrate the complexity of endothelial cells' regulation [40-43].

Endogenous angiogenesis inhibitors include angiostatin (a fragment of plasminogen that binds ATP synthase and annexin II), which is inversely correlated with VEGF and associated with longer patient survival [44]. Endostatin (a fragment of the C-terminal collagen XVIII) that showed anti-angiogenic activity *in vitro* and *in vivo* demonstrated inhibition of primary tumour growth and maintained metastasis in a dormant state, without exhibiting apparent side effects [45-48]. Tumstatin (the NC1 domain of $\alpha 3$ chain of type IV collagen) was identified as possessing anti-angiogenic activity mediated by $\alpha_v\beta_3$ integrin interaction in an RGD (arginine-glycine-aspartic acid)-independent manner [49]. Canstatin, (a fragment of the $\alpha 2$ chain of type IV collagen) is an additional human basement membrane-derived inhibitor of angiogenesis, which demonstrated inhibition of endothelial cells migration and tube formation and suppression of tumour growth *in vivo* [50].

The expression of angiogenic factors can be induced by environmental stress including glucose deprivation, formation of reactive oxygen species, cellular acidosis and iron deficiency, by the loss of the function of tumour-suppressor genes or by the activation of oncogenes [51-53]. Changes in the relative balance of inducers and inhibitors of angiogenesis can activate the "angiogenic switch" as illustrated in Figure 1.4.

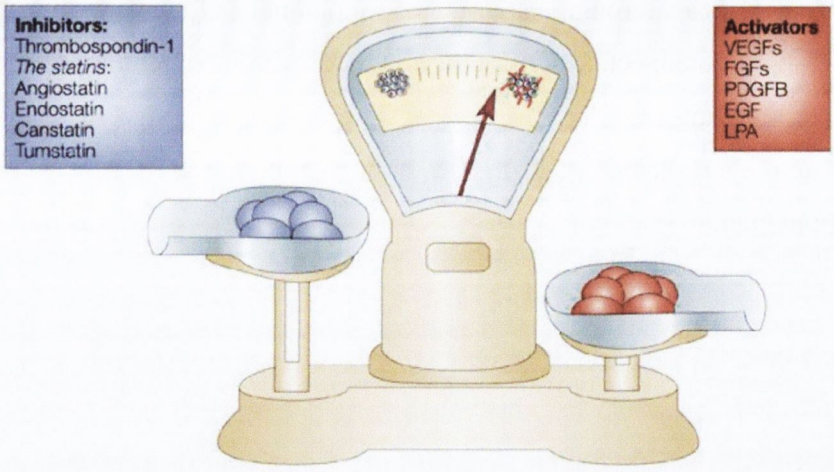

Figure 1.4: Angiogenesis is orchestrated by a variety of activators and inhibitors. Changes in the angiogenic balance mediate the "angiogenic switch" [54].

1.2.1.1 Vascular Endothelial Growth Factors

The VEGF family are the most potent and specific factors for endothelial cell growth, which can increase vascular permeability, activate proteases for ECM degradation and inhibit apoptosis of endothelial cells. The rise in vascular permeability enables the formation of a fibrin gel by extravasation of plasma proteins and other circulating macromolecules, in this way providing a new provisional matrix. This results in the attraction and support of endothelial cells' and fibroblasts' growth, leading to the initiation of angiogenesis and synthesis of matrix connective tissue [55].

There are at least four structurally related isoforms of human VEGF including $VEGF_{121}$, $VEGF_{165}$, $VEGF_{189}$ and $VEGF_{206}$, with the most potent and abundant subtype *in vivo* being $VEGF_{165}$ [56-58]. VEGF stimulates capillary formation *in vivo* and has direct mitogenic actions that are restricted to endothelial cells [59-60]. Its expression is regulated by a number of growth factors and cytokines, for example PDGF and interleukin-1β (IL-1β). In addition, VEGF is up-regulated by both hypoxia and oncogene signalling [35-36, 61].

The most well known angiogenesis inducer is the VEGF-A which signals *via* three receptor tyrosine kinases (VEGFR-1-3, as shown in Figure 1.5). These receptors are expressed largely in the endothelium but also in some non-vascular endothelium and cancer cells. VEGFR-3 is mostly restricted to the lymphatic endothelium [55].

VEGF withdrawal has been shown to result in regression of blood vessels in several physiological and pathological circumstances, indicating its importance in endothelial cell survival. Moreover, VEGF mRNA is up-regulated in a large number of tumours [62-63], whereas inhibition of VEGF activity results in suppression of tumour cell lines growth in murine models [64-65].

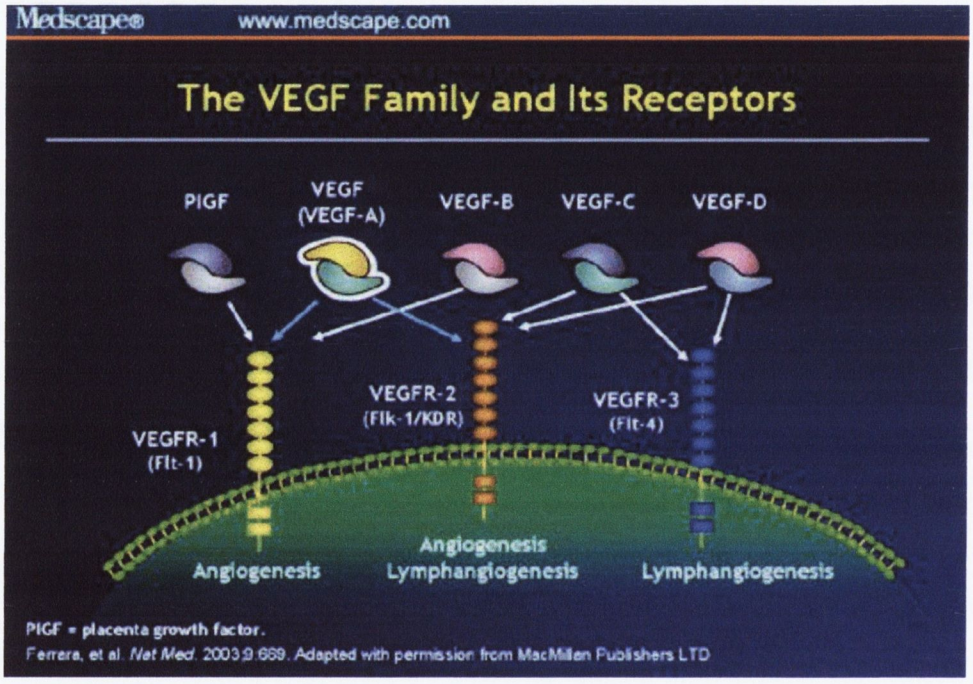

Figure 1.5: The VEGF family and its receptors [66].

1.2.1.2 Fibroblast Growth Factors

Additional pro-angiogenic regulators include members of the FGFs. The FGF family comprises of 23 members and four tyrosine kinase receptors (FGFR1-4) [67]. The FGF prototypes, FGF-1 (acidic) and FGF-2 (basic), are unique due to the absence of classical signal sequence to direct their secretion through the endoplasmic reticulum-Golgi apparatus [68].

The FGFR activation requires heparin sulphate proteoglycans (HSPGs), such as syndecan or glypicans as co-receptors [69]. Upon FGFR stimulation by FGFs, the classical MAP kinase pathway is activated which recruits a number of binding partners, such as FRS2 or GRB2. p38 MAP kinase appears to be an essential mediator of FGF activity in vascular endothelial cells (Figure 1.6) [70].

FGFR1 is the main FGFR expressed in endothelial cells *in vitro* and has also been detected in activated endothelial cells *in vivo* [71]; however FGFR2 has also found in endothelial cells in small amounts [72]. Activation of FGFR1 induces proliferation and migration of endothelial cells, protease production and tubular morphogenesis, whereas FGFR2 activation increases cell motility. Up-regulation of FGF expression demonstrated to be involved in maintaining tumour angiogenesis [73]. FGF2 secretion in fibrosarcoma cells was correlated with tumour progression [74] and FGF2 levels in urine or serum were correlated with the degree of malignancy and tumour progression [75-76].

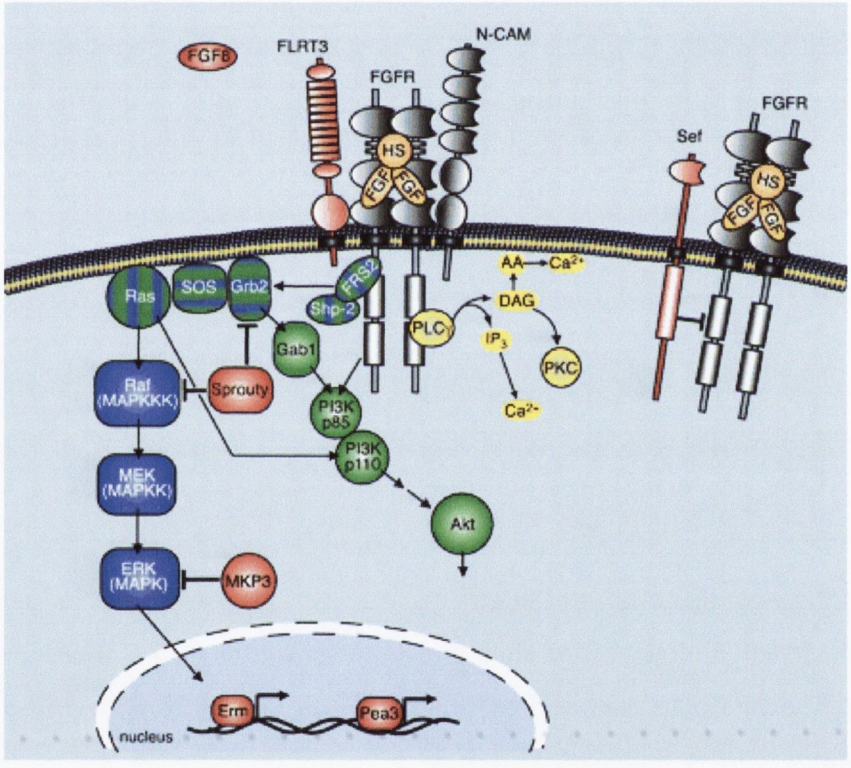

Figure 1.6: Intracellular signalling pathways activated through FGFRs [77].

1.2.1.3 Platelet-derived Growth Factors

There are two genes (*PDGF-A* and *PDFG-B*) encoded in the PDGF family which result in five dimeric isoforms of proteins: PDGF-AA, PDGF-BB, PDGF-AB, PDGF-CC and PDGF-DD. The biological action of these growth factors is mediated by three receptor dimeric structures, including PDGFR-αα, PDGFR-ββ and PDGFR-αβ, which upon ligand activation induce tyrosine phosphorylation and activate signal transduction

through the phosphatidylinositol 3-kinase (PI3K) pathway, as shown in Figure 1.7 [78-83]. PDGF-CC was reported to be an oncogenic protein which transformed a murine fibroblast cell line, induced tumour formation [83] and stimulated vascular smooth muscle cell growth *in vitro* [84].

In addition, PDGF functions as a potent mitogen in mesenchymal and glial cells, regulates cell morphology and movement and is involved in embryogenesis, carcinogenesis, atherosclerosis and wound healing [85-87].

PDGF signalling exerts paracrine stimulation on stromal cells during tumour angiogenesis, which has been observed in melanoma, breast, colorectal, and small cell lung cancers [86]. The density of blood vessel tumours is correlated with the level of PDGFs. It is reported that melanoma xenografts, with PDGF-BB expression, form highly vascularised and stromal-rich tumours, whereas melanomas without PDGF form poorly vascularised or necrotic tumours, with undetectable stroma [85]. PDGFR-ββ can induce the transcription and secretion of VEGF where can indirectly regulate angiogenesis.

In addition to the paracrine stimulation, PDFG signalling exerts autocrine regulation of tumour growth. PDGFRs and their ligands are frequently over-expressed during carcinogenesis; PDGF-AA and PDGFR-αα are over-expressed in human glioma tumours, with an increase observed in the high grades [85]. The gain-of-function mutations in the *c-kit* or *PDGFR-αα* genes are considered to be causative for mesenchymal tumours of the human gastrointestinal tract [88]. Translocation in chronic myelomonocytic leukaemia (CML) generates fusion of *BCR-PDGFR-αα*, resulting in constitutive activation of PDGFR-αα [89].

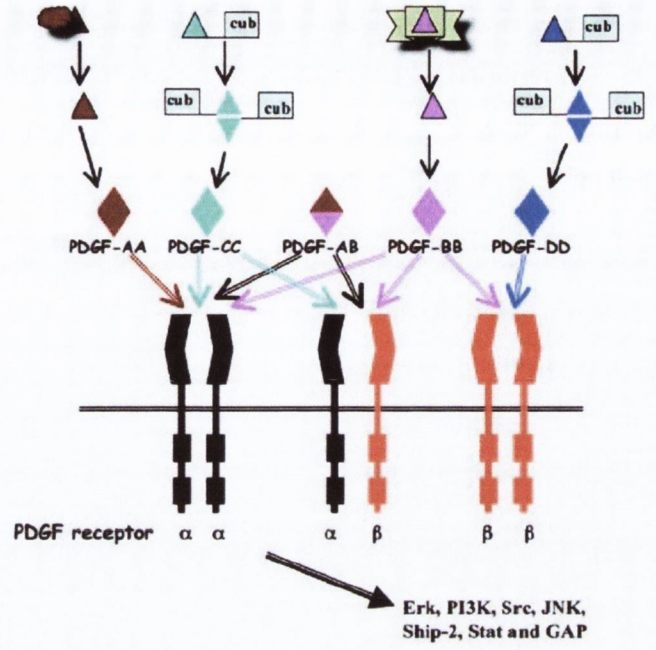

Figure 1.7: PDGF ligands and their corresponding receptors [90].

1.2.1.4 Epidermal Growth Factors

The EGF/ErbB/HER family of receptors consists of four known members namely EGFR/ErbB1/HER-1, EGFR-2/ErbB2/HER-2/Neu, EGFR-3/ErbB3/HER-3 and EGFR4/ErbB4/HER4 which are transmembrane glycoproteins [91] comprised of: (i) a cysteine-rich, extracellular N-terminal ligand-binding domain and a dimerisation arm, (ii) a hydrophobic transmembrane domain and (iii) an intracellular, highly conserved cytoplasmic C-terminal tyrosine kinase domain with several phosphorylation sites. The variable extracellular ligand-binding domain enables binding to different ligands due to the highly conserved tyrosine kinase domain. In addition, the extracellular region of EGFR is subdivided into four domains (I, II, III and IV) [92-93].

The EGFRs can be activated by 13 known ligands, which include EGF, transforming growth factor-α (TGF-α), amphiregulin (AR), betacellulin (BTC), heparin-binding EGF-like growth factor (HB-EGF), epiregulin, (EPR), epigen (EPG) and neuregulins 1-6 (NRG) [94-95]. Upon ligand activation, EGFR can either homodimerise or heterodimerise with the rest of the EGF receptors to initiate cellular signalling cascades. In this way EGF can induce heterodimerisation of EGFR with HER-2, HER-3 or HER-4. Likewise, NRG4 induces heterodimerisation of HER-4 with EGFR, HER-2 and HER-3 [94]. Following receptor dimerisation signalling cascades are stimulated

including the KRas-BRaf-MEK-ERK, PI3K, phospholipase C gamma protein, anti-apoptotic AKT kinase pathways and the signal transducers and activators of transcription (STAT) signalling pathway, which lead to cell proliferation, angiogenesis, migration, survival and adhesion (Figure 1.8) [94, 96].

EGFR signalling activation has an indirect effect in the regulation of angiogenesis, *i.e.* EGFR activation can stimulate the synthesis and secretion of a number of angiogenic factors, including VEGF, interlukin-8 (IL-8) and bFGF [97], whereas EGF and TGF-α can regulate tumour stimulated angiogenesis [98]. Over-expression of VEGF was observed in glioma cells stimulated by EGF, which was found to be associated with PTEN, a negative regulator of PI3K/AKT signalling [99-100].

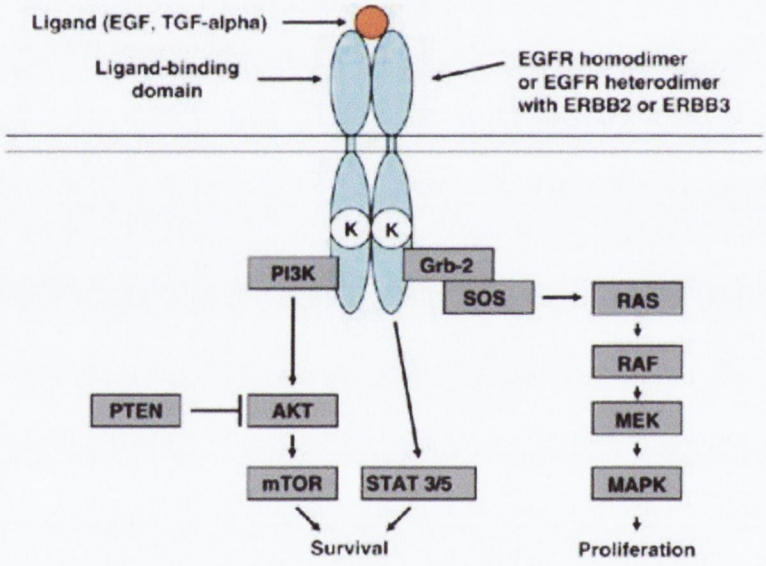

Figure 1.8: EGFR signalling pathway [101].

1.2.1.5 Matrix Metalloproteinases

Extracellular proteinases, such as MMPs, are a family of zinc-dependent endopeptidases which regulate various physiological processes, including tissue remodelling and organ development [102], and also regulate inflammatory processes [103] and cancer development [104]. MMPs' structure consists of three domains: the pro-peptide, the catalytic domain and the hemopexin-like C-terminal domain, which is linked to the catalytic domain *via* a flexible hinge region (Figure 1.9). MMPs are enzymatically inactive due to the interaction of a cysteine residue of the pro-domain with the zinc ion of the catalytic site. Once this interaction is disrupted by a mechanism

called "cysteine switch", the enzyme becomes proteolytically active [105]. The activity of MMPs can be regulated at different levels: gene expression, compartmentalisation, conversion from zymogen to active enzyme, and, finally, in the presence of specific inhibitors, such as the TIMPs. The inhibition of MMPs proteolytic activity is achieved by stochiometric complexes of TIMP-1, -2, -3 and -4 with active MMPs [106].

A number of MMPs are involved in tumour angiogenesis including MMP-2, -9, -14 and to a lesser extent MMP-1 and -7, whereby each can contribute to distinct vascular events in the same tumour [37]. MMP-9 regulates the bioavailability of VEGF and enables an "angiogenic switch" by making sequestered VEGF bioavailable for its receptors VEGFR2, in pancreatic islet tumours [107]. It has been reported that tumours transplanted into tissue irradiated to prevent angiogenesis, were unable to grow in MMP-9 deficient mice, suggesting that MMP-9 is required for tumour vasculogenesis [108]. In addition, MMPs regulate vascular stability and permeability; in particular MMP-14 appeared to mediate the vascular response to tissue injury and tumour progression, through activation of TGF-β [109].

Egeblad and Werb reviewed that over-expression of several MMPs, including MMP-3, -7 and -14, is associated with carcinoma formation [104]. MMP-mediated signal transduction is linked with increased metastasis in the presence of MMP-1. A separate study reported a critical role for MMP-1 in cell migration and invasion of tumours in a breast carcinoma xenograft model [110].

A different type of zinc-dependent proteases are the ADAMs family (a disintegrin and metalloprotease), which are characterised by the presence of metalloprotease and integrin receptor-binding activities. The ADAMs family has been associated with the control of membrane fusion, cytokine and growth factor shedding and cell migration. In addition, their over-expression has been implicated in pathological conditions, such as cancer and inflammation [111]. For instance, a number of carcinoma tissues and cell lines, including breast and colon, demonstrated over-expression of ADAM12 [112-113], whereas high expression levels of ADAM10 has been detected in pheochromocytomas and neuroblastomas [114].

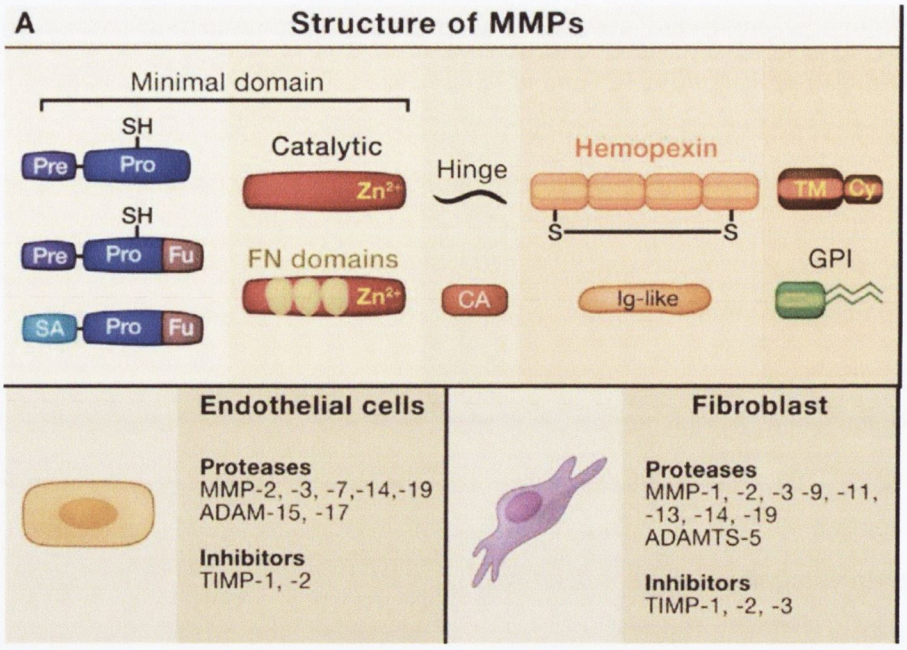

Figure 1.9: MMP composition and expression in endothelial and fibroblast cells [115].

1.3 Tumour Vasculature

The fact that tumour vasculature differs from the normal vasculature presents an additional advantage for the development of new vascular targeted therapies. The abnormal increased rate of angiogenesis results in undeveloped tumour blood vessels which are often distinguished by abnormal characteristics including: fragility, chaotic arrangements, imperfect vessel wall due to discontinuous endothelial cell lining and weak investiture with vascular smooth muscle cells. Additionally, there are poor connections between pericytes and endothelial cells which themselves are usually irregularly shaped, forming an uneven luminal layer with loose interconnections and focal intercellular openings [116-119]. Tumour blood vessels have an irregular, structurally abnormal basement membrane [120-121], uneven diameter and very long distance between branching points, resulting in a chaotic vascular network with complex branching patterns and lack of hierarchy (Figure 1.10) [122-124].

These characteristics of the newly developed tumour vasculature means it is leaky to macromolecules, aids the metastatic process by facilitating the tumour cells into the bloodstream and accumulates fibrin in the ECM, therefore favouring angiogenesis. The

histological grade and malignant potential of the tumour correlates to the degree of blood vessel leakiness [125].

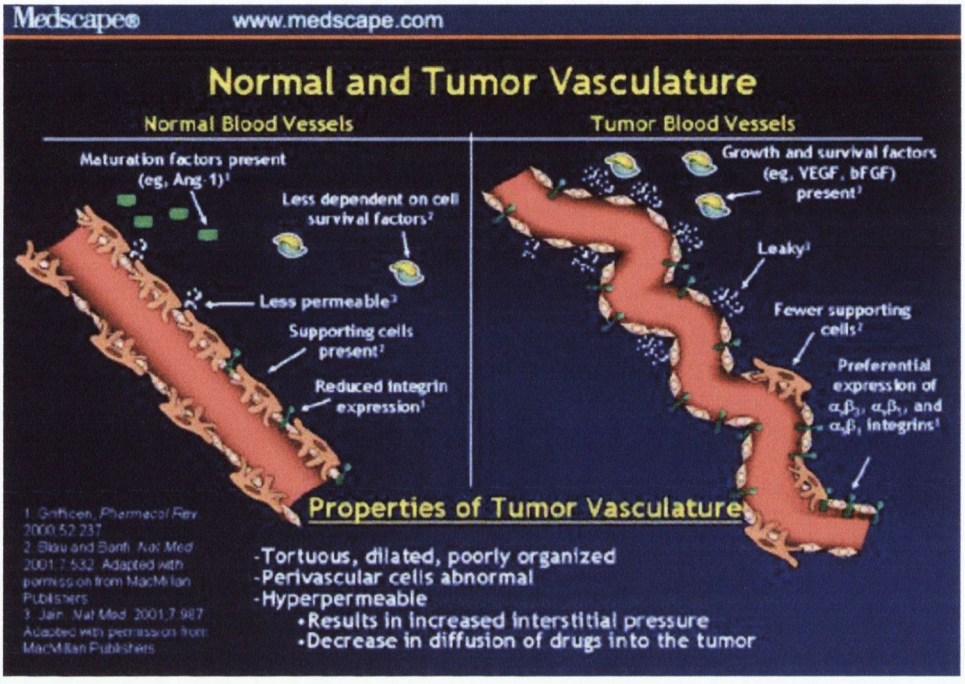

Figure 1.10: The differences between the normal and the tumour vasculature [66].

1.3.1 Tumour Vasculature as a Target

The ability to selectively target established tumour vasculature is a very appealing strategy for the treatment of cancer, which allows rapid vascular shutdown, leading to secondary tumour cell death. The differences between tumour and normal blood vessels described earlier might be the reason why tumour vasculature is more susceptible to vascular disrupting agents (VDAs) than normal vasculature. These types of agents have several advantages over conventional chemotherapeutic agents: (i) the therapy is effective in the majority of solid tumours, regardless of histological sub-type, (ii) the killing of relatively few vascular endothelial cells may result in the death of a large area of tumour *via* widespread central necrosis, whereas other strategies target individual cancer cells and all the cells are required to be killed in order for the therapy to be effective, (iii) VDAs have the ability to minimise the acquired drug resistance, due to the fact that they target normal vascular endothelial cells (which are more genetically stable than tumour cells) and (iv) drug delivery to cellular targets lining blood vessels is

easier to achieve compared with targets in the tumour area distant from capillaries [126].

There are two different approaches used to cause disruption of the blood supply to the tumours: a) deplete tumour angiogenesis (anti-angiogenic approach) and b) target the established tumour vasculature (vascular disrupting approach). Inhibition of either of those processes by agents that suppress the growth of vascular endothelial cells, is likely to result in restricted tumour growth and tumour cell death [127].

1.4 Anti-angiogenic Approach

There are several anti-angiogenic approaches that aim to target specific over-expressed receptors or ligands involved in the process of angiogenesis. The two most successful approaches to date are: a) the design of monoclonal antibodies specific to certain angiogenic regulators and b) the design of single or multi-TKIs.

1.4.1 Monoclonal Antibodies

1.4.1.1 Bevacizumab

VEGF has been identified as a key molecule for angiogenesis and this led to the development of VEGF inhibitors. One example is the humanised anti-VEGF monoclonal antibody named bevacizumab (Avastin®) which is used for the treatment of metastatic colorectal cancer and advanced non-small cell lung cancer (NSCLC) in combination with cytotoxic chemotherapy [128]. One of the main concerns with bevacizumab treatment is its interference with conditions such as coronary artery or peripheral artery disease [129].

1.4.1.2 Trastuzumab

Trastuzumab (Herceptin®) is an additional recombinant humanised monoclonal antibody which targets the extracellular domain of HER-2 and it's currently used for the treatment of both metastatic and early-stage HER-2-positive breast cancer [130-131]. Trastuzumab's clinical benefit is attributed to internalisation and down-regulation of cell surface HER-2 [132], preventing AKT activation by interfering with PI3K-PTEN pathway [133], cell cycle arrest in G_1 [134] and inhibition of angiogenesis [135]. Trastuzumab treatment is associated with cardiac dysfunction in 2-7% of cases [136].

1.4.2 Tyrosine Kinase Inhibitors

1.4.2.1 Sunitinib

Sunitinib **1** (Sutent®) is a small molecule which targets multiple receptor tyrosine kinases and it is licensed for the treatment of renal cell carcinoma (RCC) and imatinib-resistant gastrointestinal stromal tumours (GIST). Sunitinib inhibits the kinase activity of PDGFR, VEGFR-2 and FLT-3, all of which play central roles in angiogenesis and tumour cell proliferation, as well as CD117, a RTK which drives the majority of GIST [137-139]. Phase II studies have shown that sunitinib has a potentially beneficial effect in previously treated advanced NSCLC and unresectable neuroendocrine tumours [140-141]. Treatment with sunitinib is associated with haematological adverse effects such as fatigue, diarrhoea, nausea, sore mouth and skin discolouration.

1.4.2.2 Sorafenib

Sorafenib **2** (Nexavar®) is an oral TKI approved for the treatment of advanced RCC and hepatocellular carcinoma (HCC). Sorafenib inhibits VEGFR, PDGFR, Raf-1 and intracellular serine/threonine kinases, and targets the MAPK pathway (Raf/MERK/ERK) [142-143]. Treatment with sorafenib exhibited anti-tumour effects in colon, pancreas and breast cancer cell lines as well as in colon, breast and NSCLC xenograft models [144]. Dose limiting toxicities (DLTs) following treatment with sorafenib included haematological toxicity, diarrhoea, fatigue, hypertension and skin rash. It has been suggested that because the presence of rash is commonly associated with EGF-pathway inhibition, its onset may be a predictor of the treatment outcome and therefore may be used for optimal dose titration [145]. Interestingly, reports from four Phase I clinical trials have indicated that patients experiencing skin toxicity and/or diarrhoea after treatment with sorafenib, had a significantly increased time to progression, compared with patients without such toxicity [146]. Blood pressure is another possible biomarker indicating the treatment outcome in patients treated with sorafenib or other VEGF inhibitors [147].

1.4.2.3 Pazopanib

Pazopanib **3** (Votrient®) is a small molecule TKI of VEGFR-1, -2, and -3, PDGFR-α and -β, FGFR, cytokine receptor (Kit), IL-2 receptor inducible T-cell kinase (Itk),

leukocyte-specific protein tyrosine kinase (Lck), and transmembrane glycoprotein receptor tyrosine kinase (c-Fms) [148]. Pazopanib was approved for the treatment of advanced or metastatic RCC, following a Phase III trial which showed improvement of progression-free survival and tolerability in the selected population [149]. The most common adverse effects associated with pazopanib treatment included diarrhoea, hypertension, lymphocytopenia and asthenia. Hepatotoxicity was also observed in the pazopanib group which was associated with two treatment-related deaths, but was thought to be similar to that seen with sunitinib during its Phase III trial [149]. Compared to other TKIs, pazopanib has a lower incidence of skin toxicities [150].

1.4.2.4 Axitinib

Axitinib **4** (Inlyta®) is a potent small molecule inhibitor of VEGFR-1, -2 and -3 and which also demonstrated lower potency against PDGFR and c-Kit [151]. Axitinib has been approved for the treatment of clear cell metastatic RCC. A comparison trial between axitinib and sorafenib in patients with metastatic RCC demonstrated a significant improvement in progression free survival in patients receiving axitinib [152]. The adverse effect noted following treatment with axitinib were similar to those observed with sorafenib and other TKIs. Axitinib demonstrated efficacy in patients with other cancer types including thyroid [153], melanoma [154] and NSCLC [155], when given as a monotherapy and in metastatic breast [156] and colorectal cancer patients [157], when given in combination with chemotherapy.

1.4.2.5 Gefitinib

Gefitinib **5** (Iressa®) was the first commercially available EGFR tyrosine kinase blocker, which has been approved as second or third line therapy for advanced NSCLC [158-159]. Additional studies using a combination of chemotherapies with gefitinib did not demonstrate improved efficacy over chemotherapy alone [160-161]. It is important to note that tumour EGFR status was not included in the selecting criteria of patients. Responsiveness to EGFR-inhibition treatment is associated with histologic features of adenocarcinoma, female sex, no history of smoking and Asian ancestry. However, the EGFR level of expression in immunohistochemical staining does not predict response to therapy and does not correlate with poor survival [162-164]. Recently, it has been reported that an activating mutation in the tyrosine kinase side of the EGFR gene in

NSCLC seems to predict the response to gefitinib treatment [165-167]. Evidence to date suggests that it is important to select those patients who are more likely to benefit from the EGFR-TKI, because non-selection is probably the main reason of disappointing results following gefitinib treatment.

1.4.2.6 Erlotinib

Erlotinib **6** (Tarceva®) is another EGFR TKI which is used for the treatment of non-metastatic pre-treated NSCLC, and in combination with gemcitabine for the treatment of advanced pancreatic cancer in patients who have not previously received chemotherapy. Erlotinib was reported to be effective in combination with other agents in patients with metastatic colorectal carcinoma; however EGFR expression was not an entry criterion. Currently, the tumour samples taken in this study are being examined for their EGFR expression patterns [168-169]. Therapeutic benefit was also observed in patients with advanced biliary cancer [170], advanced HCC [171] and metastatic RCC [172]. In addition, a recent study suggested that erlotinib may be an alternative option for patients resistant to cytotoxic chemotherapy, even in those with EGFR wild-type NSCLC [173].

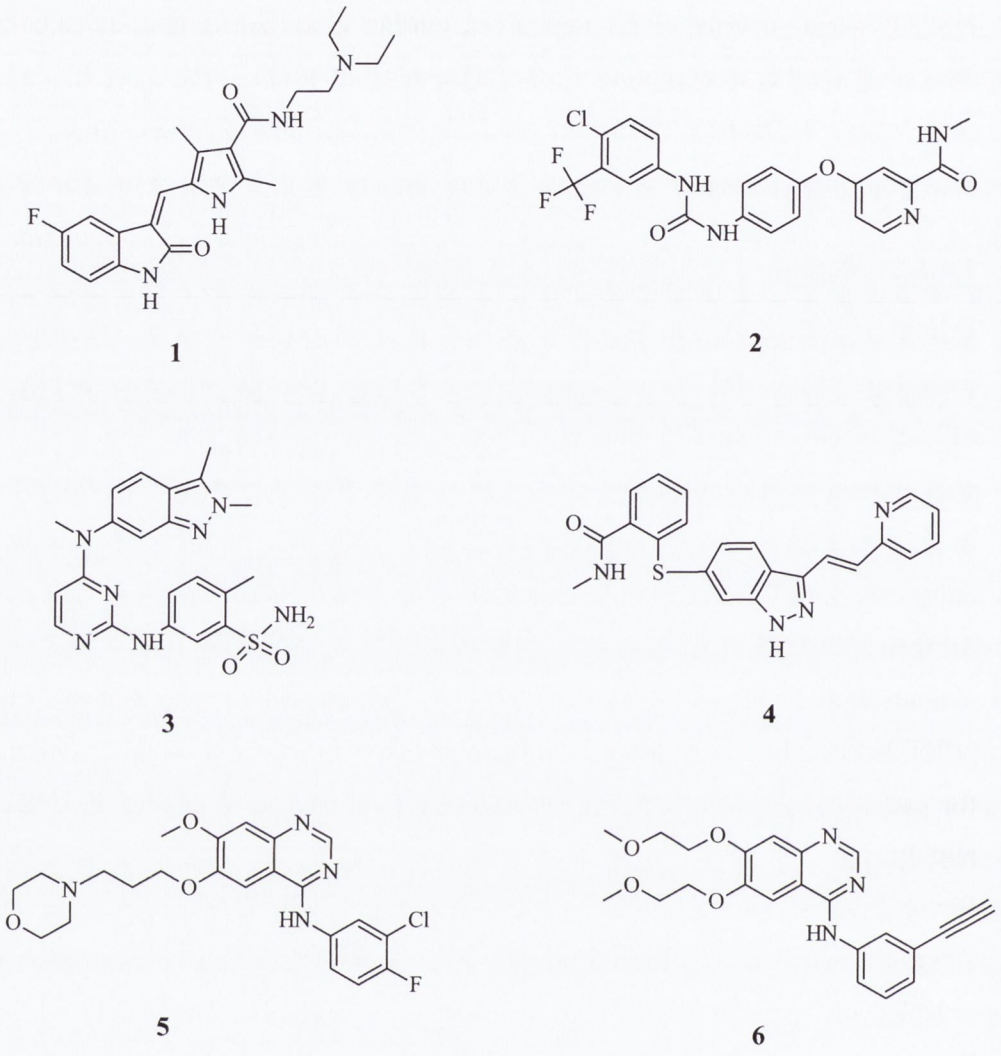

Figure 1.11: FDA-approved multi-targeted inhibitors of angiogenesis sunitinib **1** [137-141], sorafenib **2** [142-147], pazopanib **3** [148-150], axatinib **4** [152, 156], gefitinib **5** [158-167] and erlotinib **6** [168-173].

1.4.2.7 Lapatinib

Further TKI have been synthesised, including lapatinib **7** (Tyverb®), which targets EGFR and HER-2 tyrosine kinases [174]. Clear tumour responses were observed in Phase I studies using lapatinib in trastuzumab-refractory breast cancer and NSCLC patients [175]. In a Phase II study involving patients with metastatic colorectal cancer, lapatinib showed minor effects [176]. Interestingly, a Phase III trial with HER-2 over-expressing refractory advanced or metastatic breast cancer patients, lapatinib demonstrated an increased time to progression in combination with capecitabine

compared with capecitabine alone [177]. Further Phase III trials established that there was no difference between the median time to progression of RCC patients treated with lapatinib or hormone therapy; however the median time to progression in the EGFR over-expressing patients was higher in the lapatinib group than in the hormone treated patients; 15.1 months *versus* (*vs*) 10.9 weeks, respectively [178]. The outcome of these studies highlighted the importance of the criteria selection of the participating patients. For that reason, recent studies have shown more success using lapatinb in combination with other agents for the treatment of HER-2-positive breast cancer [179-180]. In 2010, lapatinib in combination with letrozole was approved for the treatment of hormone receptor positive metastatic breast cancer tumours that over-express HER-2 and with whom hormonal therapy is indicated [181].

1.4.2.8 Vandetanib

Vandetanib **8** (Caprelsa®), another orally available small molecule, is a dual inhibitor of VEGFR2 and EGFR tyrosine kinases. Vandetanib showed a broad spectrum of anti-tumour activity in several *in vivo* models, through targeting VEGF signalling and angiogenesis [182-183]. DLTs associated with vandetanib treatment were observed in Phase I trials, including diarrhoea, hypertension and thrombocytopenia [184-185]. Assessment of vandetanib in Phase II trials alone or in certain combination regimens revealed diverse results in a variety of tumours including NSCLC [186], metastatic breast cancer [187], multiple myeloma [188] and hereditary medullary thyroid carcinoma (MTC) [189]. The promising results of vandetanib anti-tumour efficacy in patients with advanced MTC resulted in the initiation of a Phase III trial which demonstrated therapeutic efficacy against MTC [190]. Therefore, vandetanib became the first drug to be approved for the treatment of metastatic MTC in patients who are ineligible for surgery. However, vandetanib alone was ineffective for the treatment of patients with NSCLC patients [191-192], but showed clinical benefit when combined with docetaxel [193].

1.4.2.9 Imatinib

Imatinib (Gleevec®) was the first commercially available small molecule tyrosine kinase inhibitor which reversibly competes with ATP for binding to the kinase domain of the c-Kit, c-Abl and PDGFR-BB tyrosine kinases [194-195]. Imatinib has been

approved for the treatment of CML, by inhibiting the phosphorylation of Bcr-Abl tyrosine kinase and thereby suppressing the proliferation of Bcr-Abl-expressing leukemic cells. Although imatinib is not considered a true anti-angiogenic inhibitor, it is being used in treatment of patients with GIST who have *c-Kit* gene expression [196-198].

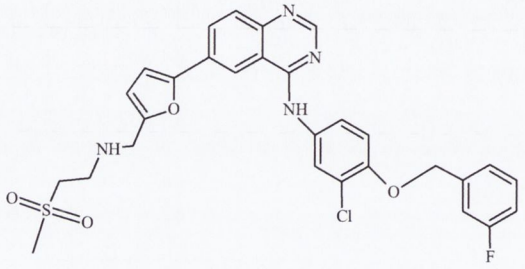

7

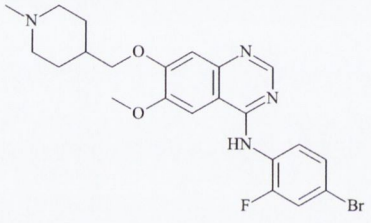

8

Figure 1.12: Multi-tyrosine kinase inhibitors lapatinib **7** [174] and vandetanib **8** [182].

Given that multi-targeted compounds have shown clinical success, it is worthwhile to closely examine other molecules that may be expected to have similar profiles of activity and to investigate their effects in several cell-regulated pathways.

Lack of tumour vessel selectivity exhibited by current therapies and those under investigation, remains a major obstacle in the development of effective cancer therapeutics. Angiogenic blood vessels express markers that are either entirely absent from the normal blood vessels or present at very low levels. Such markers include APN [199], the $\alpha_v\beta_3$ and $\alpha_v\beta_5$ integrins [200-201], certain receptors for vascular growth factors [202-203], MMPs [204-205], and high-molecular-weight proteoglycan [206-207]. There is an urgent and necessary need to develop compounds which are specific to these tumour angiogenic markers; compounds which should, because of this specificity, demonstrate superior anti-cancer activity and minimised toxicities than conventional chemotherapies.

Table 1.1: Summary of the FDA-approved tyrosine kinase inhibitors (TKI).

TKI	Targets	Treatment
Sunitinib	PDGFR, VEGFR-2, FLT-3 and CD117	RCC and imatinib-resistant GIST
Sorafenib	VEGFR, PDGFR, Raf-1 and MAPK pathway	Advanced RCC and HCC
Pazopanib	VEGFR-1,-2, -3, PDGFR-α, -β, FGFR, c-Kit, Itk, Lck and c-Fms	Advanced or metastatic RCC
Axitinib	VEGFR-1, -2, -3, PDGFR and c-Kit	Clear cell metastatic RCC
Gefitinib	EGFR	Advanced NSCLC
Erlotinib	EGFR	Non-metastatic pre-treated NSCLC and advanced pancreatic cancer
Lapatinib	EGFR and HER-2	HER-2 over-expressing metastatic breast cancer
Vandetanib	VEGFR-2 and EGFR	Metastatic MTC
Imatinib	c-Kit, c-Abl and PDGFR-BB	CML and c-Kit-expressing GIST

1.5 Aminopeptidase N

Aminopeptidases are ubiquitous exopeptidases involved in many biological processes, such as antigen processing and presentation, scavenging of amino acids, catabolism of regulatory peptides, degradation of vasoactive and neuroactive peptides and tumour invasion and metastasis [208-209]. Although some aminopeptidases are secreted, the vast majority are either cytosolic or membrane-bound enzymes [210-211]. APN is a zinc-dependent exopeptidase, which is anchored to the plasma membrane by its N-terminal segment and acts as an ectoenzyme by cleaving neutral amino acids from the N-terminal residues of peptides (Figure 1.13). APN is identical to the cell surface antigen CD13 [212] and is also known as aminopeptidase M and human alanyl

aminopeptidase [213]. Soluble APN is detectable in plasma/serum and urine but the mechanism of release of membrane APN still remains unknown [214-215].

Membrane bound APN is present on the brush border membranes of the small intestine, where it is involved in the final hydrolysis of ingested nutrients, as well as on the renal proximal tubules, breast, colon and synaptic membranes of the central nervous system. Degradation of neuropeptides, enkephallins and endorphins is facilitated by APN [216]. The enzymatic activity of APN is regulated either by its synthesis or degradation, by natural peptides such as bradykinin or substance P [217], as well as its varying expression pattern (*e.g.* maturation and differentiation of monocytes is accompanied by increased APN expression [218]). In addition, APN serves as the major receptor for the transmissible gastroenteritis virus (TGEV) [219] and for the human coronavirus 229E, which causes upper respiratory infections [220].

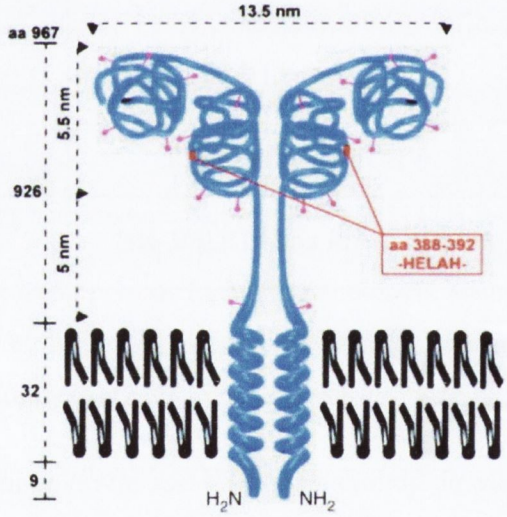

Figure 1.13: The structure of APN [221].

APN has previously been shown to play a key role in tumour cell invasion, extracellular matrix degradation by tumour cells and tumour metastasis *in vitro* and *in vivo* [222-225]. According to the characteristics of the tumour microenvironment, such as hypoxia or elevated concentration of angiogenic growth factors, APN is transcriptionally up-regulated [226]. Newly formed tumour vessels, as well as other types of new blood vessels, express APN in high levels [199], thereby making it a novel marker for angiogenesis on endothelial cell surfaces. *In vitro* studies have shown that APN is

highly expressed in human umbilical vein endothelial cells (HUVECs), human aortic endothelial cells (HAECs) and in a majority of tumour cell lines. In the absence of functional APN, capillary tube formation, cell migration and adhesion were all suppressed [227]. Its functions are regulated by influencing the organisation of specific plasma membranes [228] and by modulating endothelial morphogenesis during angiogenesis [226]. Further studies have shown that APN-null mice developed normally without physiological alterations and can undergo physiological angiogenesis but demonstrated a severely impaired angiogenic response under pathological conditions [229].

High expression levels of APN have been detected in various solid tumours [230-232]. APN may be a useful indicator of poor prognosis for node-positive patients with colon cancer, as patients with APN-positive tumours showed significantly lower disease-free and overall survival rate than patients with APN-negative tumours [233]. Furthermore, NSCLC patients with high serum APN levels have been associated with more advanced stage, poor performance status and lower survival rate [234-235]. APN has therefore been considered as a potential target for proliferating tumour vasculature and APN-positive tumours. Another study examining the expression level of APN in prostate tumour samples found that APN was located in the cytoplasmic membranes of prostate gland epithelial cells. Increased APN expression was associated with prostate cancer, while the expression of prostate-specific antigen (PSA, a marker for prostate cancer) was shown in normal and cancer tissue. Interestingly, this evidence suggests that APN may potentially be a good histological marker of prostate cancer [236].

1.5.1 Bestatin

A number of APN inhibitors have been synthesised and which showed promising results, including anti-invasive and anti-metastastic activity. A well known inhibitor of APN, aminopeptidase B and leucine aminopeptidase is (2S,3R)-3-amino-2-hydroxy-4-phenylbutanoyl-L-leucine), namely bestatin **9** (Ubenimex®), which was originally isolated from the culture filtrates of *Streptomyces olivoreticuli* [237]. Bestatin has also demonstrated inhibitory activity against a metallo-enzyme leukotriene A4 hydrolase that plays an important role in the arachidonic acid cascade [238]. APN inhibition by bestatin significantly reduced the *in vitro* migration of eosinophils across HUVEC

monolayers [239]. In addition, bestatin (50-150 μM) blocked the invasion of various human metastatic tumour cells into reconstituted basement membrane [223-224] or into matrigel [236, 240], inhibited the *in vitro* chemotactic migration of T lymphocytes at 580 μM [223, 240] and inhibited the capillary tube formation [241]. Bestatin showed a direct anti-tumour effect against NSCLC cell lines and particularly against various carcinomas (squamous, fibrosarcoma, cervical, and lung carcinoma) [242-243] and myeloid cells (P39/TSU, HL-60, U937, NB4) [244-246] through the induction of apoptosis.

In the chorioallantoic membrane (CAM) assay, bestatin inhibited FGF-2 induced angiogenesis, and blocked the hypoxia-induced retinal neovascularisation in the mouse retinal neovascularisation model [199]. Following intraperitoneal (i.p.) administration of bestatin (50-100 mg/kg/day), the number of vessels on the primary tumour mass of B16-BL6 melanoma were significantly reduced [241].

The anti-tumour effect of bestatin was observed against syngeneic colon tumours through indirect immunomodulation *via* spleen cells and possibly *via* T cells [247]. *In vivo* anti-tumour activities have been reported in several syngeneic tumours such as leukaemia, melanoma, ovarian, HCC and gastric carcinoma [199, 247-251].

Following successful preclinical evaluation, bestatin entered into different clinical trials. An increase in the number of T cells and enhanced natural killer cells' activity was observed, following treatment with bestatin. In addition, anti-tumour effects were noted in one case of residual penile tumour after bleomycin treatment, and marked regression was detected in two cases of skin metastasis of mammary carcinoma. Combination of bestatin treatment and radiation resulted in complete regression in three cases of Virchow's nodes; pepleomycin and bestatin showed complete regression in one case of metastatic skin carcinoma and the combination of the three had a favourable effect against oesophageal carcinoma [252]. Moreover, positive preliminary results were obtained on the disease-free survival in bladder cancer patients receiving adjuvant treatment with bestatin, following radiation therapy [253]. The data obtained from a different clinical trial evaluating the effect of bestatin in NSCLC patients showed a non-significant trend in favour of bestatin in terms of disease-free survival [254]. Further clinical trials suggested that bestatin may be a useful agent for treating

stage Ib and II malignant melanomas, squamous cell carcinoma (SCC), gastric cancer, urogenital cancer and squamous cell lung cancer [255-259].

The effect of bestatin was not only observed in solid tumours but also in haematological cancers. APN was found on cells of myelomonocytic lineage [260], while mature B cells and resting T cells lack detectable APN expression. An abnormal surface expression of APN has been identified in acute and chronic B cell leukaemia and is associated with poor prognosis in the case of adult acute B cell leukaemia (B-ALL) [261-262]. The highly selective haemopoietic distribution of APN makes it an effective marker of myeloid leukaemia, with considerable value in immuno-phenotyping studies [263].

Clinical trials were designed to evaluate bestatin for the treatment of acute non-lymphocytic leukaemia (ANLL). Promising outcomes, such as significantly longer remission duration and survival time were observed in bestatin treated patients, compared with the control group [264-267]. A separate study investigating treatment for acute myeloid leukaemia (AML) patients, showed that immunotherapy with bestatin after the end of chemotherapy did not improve the disease free survival [268]. Treatment with bestatin at high doses (90 and 180 mg daily) activates macrophage/monocyte production, providing augmentation of neopterin and colony-stimulating activity in the serum of lymphoma patients following autologous bone marrow transplant [269]. Bestatin is licensed in Japan for the treatment of AML.

1.5.2 APN Inhibitors

The inherent low toxicity of bestatin and its effectiveness as a cancer therapy have encouraged further studies using different analogues or compounds with similar activity profile as bestatin. Amastatin **10**, (2S,3R)-3-amino-2-hydroxy-5-methylhexanoyl-L-valine-L-valine-L-aspartic acid), which was isolated from the culture filtrate of *Streptomyces* sp. ME98-M3 [270], has been reported to be a slow-binding competitive inhibitor of APN [271]. It has been reported that amastatin enhanced the chemotactic response of human neutrophils toward f-MLP, however it weakly inhibited APN enzymatic activity over the range of concentrations (which were effective on neutrophil migration) [272]. Amastatin demonstrated inhibition of capillary tube formation without altering the proliferation rate of HUVECs between 10-250 μM [226]. Phebestin

11, (2S,3R)-3-amino-2-hydroxy-4-phenylbutanoyl-L-valyl-L-phenylalanine) is a tripeptide produced by *Streptomyces* sp. MJ716-m3 [273] and probestin **12**, (2S,3R)-3-amino-2-hydroxy-4-phenylbutanoyl-L-valyl-L-prolyl-L-proline), is a tetrapeptide isolated from *Steptomyces azureus* sp. MH663-2F6 [274].

Different series of compounds were also designed as APN inhibitors including α-aminoaldehydes [275], aminophosphonates [276], quinoline-based compounds [277], bisphosphonates [278] and tetralones [279].

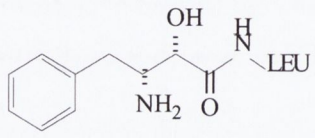

9

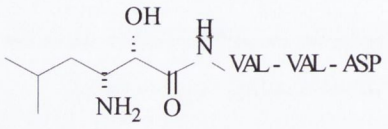

10

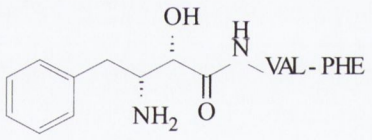

11

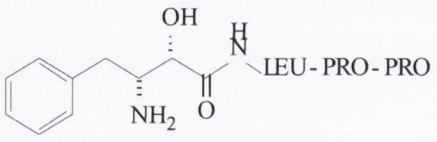

12

Figure 1.14: Aminopeptidase inhibitors, bestatin **9** [239, 241], amastatin **10** [272], phebestin **11** [273] and probestin **12** [274].

Recent studies reported the design and synthesis of a bestatin dimethylaminoethyl ester, LYP, which displayed a greater APN inhibitory effect than bestatin and inhibition of cell growth in ES-2 human ovarian carcinoma cells *in vitro* [280], in the *in vivo* ES-2 xenograft model [281], and in assays of *in vitro* and *in vivo* angiogenesis [282].

A summary of APN inhibitors is well presented in a review by Bauvois and Dauzonne [283], and in a more recent review by Zhang *et. al* [284].

It has been identified that endothelial cells express APN as a surface receptor for the tumour-homing motif NGR (asparagine-glycine-arginine), thus APN is capable of

homing selectively to the tumour vasculature. NGR conjugates which target the tumour vasculature will be discussed later in section 1.8.2.

1.6 Vasculature Normalisation

Additional rationale for anti-angiogenic therapy implies that treatment with anti-angiogenic agents can result in a more "normal" vasculature that is more conducive to the delivery of nutrients and therapeutics (Figure 1.15). Tumour hypoxia results in tumour cell resistance to radiotherapy or cytotoxic agents and induces genetic instability [285]. Previous studies have shown that anti-angiogenic treatment resulted in vascular normalisation by blocking of VEGF or its receptor VEGFR-2, leading to endothelial cell apoptosis and a reduction in vessel diameter, density and permeability [58, 286-287]. Subsequently, interstitial fluid pressure decreased and, in some tumours, oxygen tension increased [288-289]. Interestingly, treatment with endostatin revealed a decrease in tumour blood flow at certain intermediate doses and an increase in other lower doses. Taking into consideration that only few examples of anti-angiogenic drugs exist which support their efficacy as single agents [290], it is still unclear whether the effect of these agents occur as a result of vascular normalisation [291]. A better understanding of the molecular mechanism of vascular normalisation may lead to more efficient anti-cancer therapies as well as for other vascular-related diseases. A more comprehensive review on vascular normalisation is discussed by Jain [292].

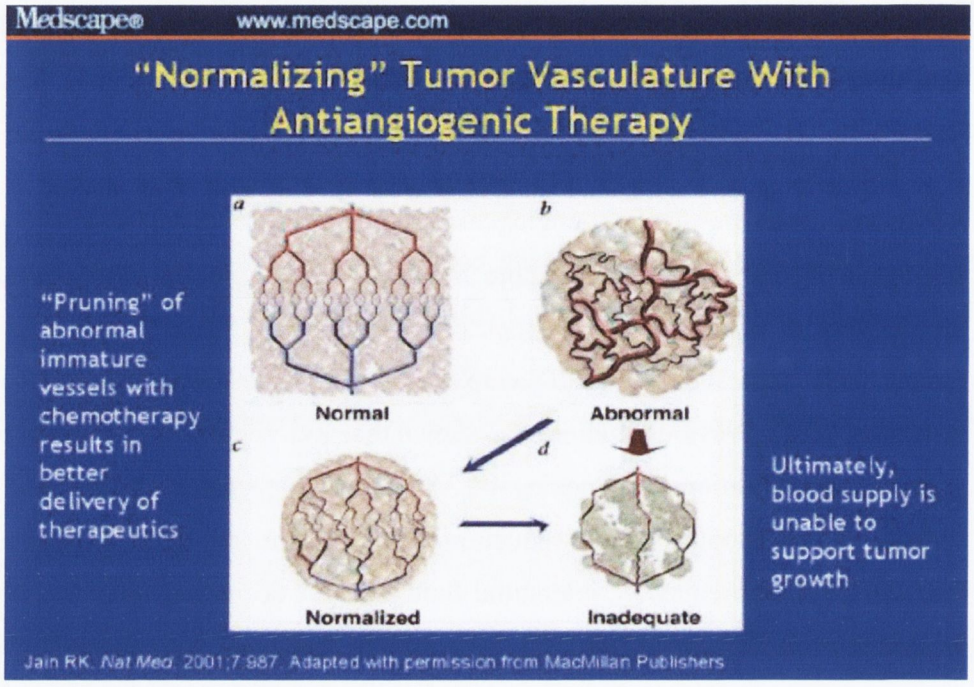

Figure 1.15: Normalisation of tumour vasculature following anti-angiogenic therapy [66].

1.6.1 Vascular Disrupting Approach

The ability to selectively target established tumour vasculature is a very appealing strategy which allows for rapid vascular shutdown, leading to secondary tumour cell death. There are two classes of VDAs: small molecule VDAs and ligand-directed VDAs. Small molecule VDAs are not specific to tumour vessels, however they exploit pathophysiological differences between normal and tumour tissue endothelium to achieve tumour vessel selectivity. This type of class includes tubulin targeting agents and cytokine inducers.

1.6.1.1 Tubulin

Tubulin is a globular protein that polymerises to form microtubules, one of the components of the cytoskeleton which is involved in many cellular processes including mitosis, cytokinesis, and vesicular transport [293]. Tubulin is composed of a heterodimer of two closely related proteins, α- and β-tubulin which bind together to form a $\alpha\beta$-tubulin heterodimer. Two energy rich guanosine triphosphate (GTP) molecules are bound to these heterodimers, one of which cannot be removed without denaturing the heterodimer and the other is freely exchangeable with unbound GTP. In

the presence of excess GTP at 37 °C, repeating $\alpha\beta$-tubulin heterodimers polymerise head to tail to form protofilaments [294], which then associate in parallel (number can vary from nice to sixteen) to create a C-shaped protein sheet, that curls around to give a pipe-like structure known as microtubule (Figure 1.16) [293-295].

Microtubules consists of long tube-like structures, that are approximately 240 angstrom in diameter, with a hollow core [296]. The microtubule polymers are constantly in a state of flux, allowing them to mediate their various cellular functions, such as serving as tracks on which motor proteins (kinesins) transport vesicles during interphase. Microtubules form the key structural component of the mitotic spindle during cell division and the equilibrium between the monomers (tubulin) and the polymers (microtubule) changes according to the cell cycle stage [297]. During mitosis, the elongating ends of the microtubules bind to the chromosomes at each kinetochore and align the chromosome on the metaphase plate. Any disruption of this alignment causes cells to undergo mitotic arrest [298].

The ability of microtubules to switch between growing and shrinking phases is crucial to their function. Each tubulin monomer binds one molecule of GTP; the nucleotide bound to the α-tubulin at the N-site is non-exchangeable and the one bound to the β-tubulin at the E-site is exchangeable. In order for tubulin to polymerise, GTP is required at the E-site, however once this nucleotide is hydrolysed it becomes non-exchangeable. A cap of GTP-tubulin subunits at the ends is believed to result in the metastable microtubule structure, whereas upon its loss it causes rapid depolymerisation [293]. Since tubulin can polymerise from both ends but at a different rate from each side, the rapidly polymerising end is called the plus end of the microtubule and the slowly polymerising end the minus end. The microtubule organising centre (MTOC) functions to modify the concentration of $\alpha\beta$-tubulin inside the cells according to the required level for spontaneous nucleation. In this centre, a third, less abundant protein called γ-tubulin is found. The dynamics of microtubule assembly are further regulated by a host of microtubule-binding proteins and complexes [299], known as microtubule associated proteins (MAPs) which stabilise microtubules. MAPs are able to increase mitotic spindle dynamics by hyper-phosphorylation and are released from microtubules during cell division [300]. Also they serve to protect

microtubules from depolymerisation which could be induced by low temperature and calcium ions [294].

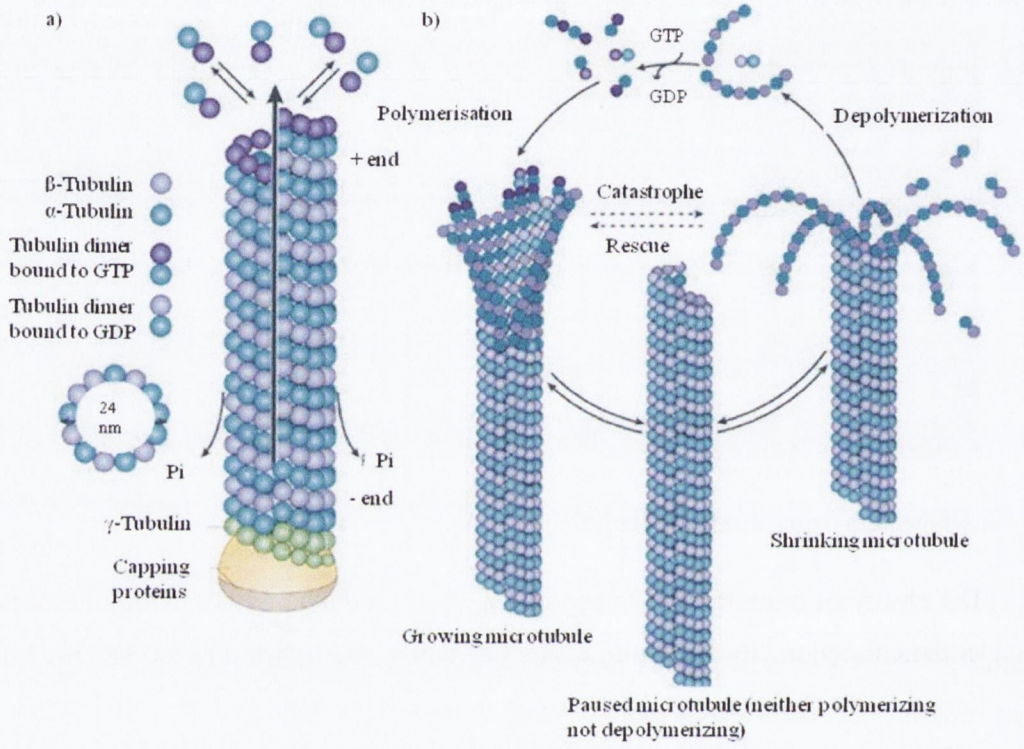

Figure 1.16: Microtubules dynamics [301].

1.6.2 Tubulin Targeting Agents

Perhaps the best known class of VDAs are the tubulin targeting agents which have both anti-mitotic and anti-vascular effects, leading to inhibition of spindle formation (mitotic arrest) and reduced tumour blood flow, respectively [302]. The earliest tubulin binding agents which demonstrated anti-mitotic and anti-vascular activity were compounds such as colchicine **13** [303], the vinca alkaloids *e.g.* vinblastine and vincristine **14** (Oncovin®) [304] and the taxanes *e.g.* paclitaxel **15** (PTX, Taxol®) [305]; however these compounds have a very narrow therapeutic window associated with consequent DLTs [306-307].

The first small molecule VDA that was shown to have anti-vascular effects at doses below the maximum tolerated dose (MTD) was Combretastatin A-4 **16** (CA-4) [308], a tubulin binding agent with structural similarities to colchicine that was isolated from

the Cape Bushwillow tree, *Combretum caffrum* [309-310]. CA-4 treatment has shown to cause extensive tumour vascular damage and necrosis *in vivo* at relatively non-toxic doses [308]. The more soluble disodium phosphate prodrug form of this compound (CA4-P) has been developed. CA-4P is rapidly cleaved by endogenous non-specific phosphatases to release the active CA-4 [311]. Preclinical studies in mouse and rat tumour models demonstrated that CA-4-P was able to cause rapid tumour vascular shutdown and reduce blood flow at doses well below the MTDs, offering a wide therapeutic window [308]; while normal tissue was much less affected [312-313]. The vascular shutdown induced by CA-4-P in tumours is due to the change in shape of newly formed endothelial cells [314], causing microtubule breakdown and reorganisation in the actin cytoskeleton, resulting in membrane blebbing [315].

In 1998, CA-4-P entered clinical trials with reported distinct DLTs from those of conventional chemotherapies such as cardiopulmonary toxicities (dyspnoea or hypoxia) [316-318]. CA-4-P completed Phase I and II clinical trial evaluation in patients with advanced solid tumours such as anaplastic thyroid cancer and lung cancer and is undergoing Phase III trials in combination with conventional chemotherapy/radiotherapy, against a variety of tumour types [310, 316-319].

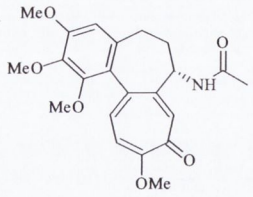

13

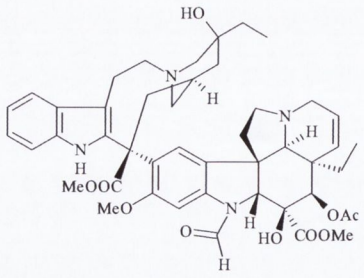

14

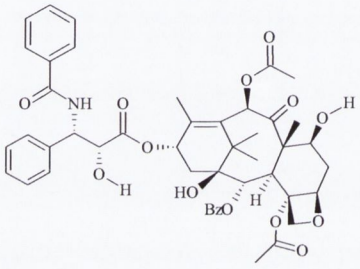

15

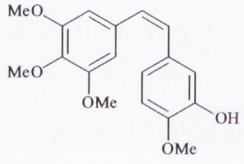

16

Figure 1.17: Tubulin targeting agents: colchicine **13** [303], vincristine **14** [304], PTX **15** [306-307] and CA-4 **16** [308].

1.6.3 Cytokine Inducers

Flavone acetic acid (FAA) is a small molecule cytokine inducer which was originally synthesised as a non-steroidal anti-inflammatory agent. The anti-vascular effects of FAA in experimental tumours are mediated *via* the release of TNF-α from activated mouse macrophages [320-321]. FAA's lack of clinical activity led to the synthesis of 5, 6-dimethylxanthenone-4-acetic acid (DMXAA, AS1404, **17**), an analogue of FAA. DMXAA's mechanism of action is more complex and the exact target is not fully understood; however data supports a direct effect on endothelial cells (possibly through nuclear factor-κ B) leading to apoptosis. In addition, indirect effects include release of vasoactive agents within the tumour tissue, such as serotonin, TNF-α, nitric oxide and possibly other cytokines [322]. DMXAA has been further developed and is currently undergoing Phase III trials in combination with conventional chemotherapy [323].

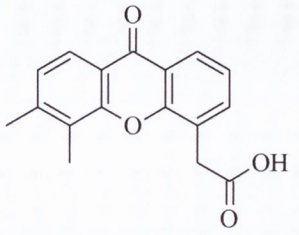

17

Figure 1.18: Cytokine inducer DMXAA **17** [322].

1.6.4 Ligand-directed Approach

The ligand-directed approach is designed to selectively target components of tumour vessels. Therefore, ligand-directed VDAs are composed of targeting moieties that are linked together, usually *via* chemical cross-linkers or peptide bonds. Antibodies or peptides are usually used as a targeting moiety that could be directed against a marker which is over expressed in the tumour cells but not in normal cells. Tumour vessel markers include major histocompatibility complex (MHC) class II [324], the vascular cell adhesion molecule-1 (VCAM-1) [325], the ED-B domain of fibronectin [326] and prostate-specific membrane antigen (PSMA) [327]. Ligand-directed VDAs have successfully and selectively targeted tumour vessels *in vivo*, causing the central region of the tumour to degenerate.

1.7 Combination Therapy

Single agent administration of VDAs can cause massive central tumour necrosis due to vascular collapse; however a narrow viable rim on the periphery of tumour tissue often remains, allowing tumour cells to repopulate and avoiding complete tumour cell death. A possible explanation for this is that the peripheral tumour cells can obtain oxygen and nutrients from the surrounding non-tumour blood vessels, which are less responsive to VDAs [328-329]. The tumour periphery is the only tumour region that is easily accessible to therapeutic agents, leading to the suggestion that the optimal clinical use of VDAs would be in combination with other treatments such as cytotoxic chemotherapy/radiotherapy, most notably the platinum drugs. In this way, the remaining viable rim of the tumour may be eliminated, eventually causing total tumour cell death [329-332].

Use of current anti-angiogenic treatments alone has provided only a modest survival benefit, thus interest in combining anti-angiogenic drugs with conventional cytotoxic chemotherapies has been shown and has proved to maximise the therapy's effect. For instance, bevacizumab has been approved in combination with 5-fluorouracil-based (5-FU) regimen, for first and second-line treatment of patients with metastatic colorectal carcinoma [333]. In addition, a recent Phase I clinical trial showed that treatment with CA-4P in combination with bevacizumab resulted in profound tumour vascular changes, which were maintained in the presence of bevacizumab [334].

1.8 Hybrid Drugs

A relatively new approach which has emerged in the last decade is the design of hybrid based therapies using different modalities. Two or more targeting ligands, which are joined together with a linker, form one individual compound, called a hybrid (Figure 1.19). Walsh and Bell have discussed the concept of hybrid based approaches for malaria [335], while Chow *et al.* have outlined the concept of hybrid based anti-tumour drug candidates [336]. This concept is based on the premise that drugs in hybrid form may overcome the disadvantages associated with monotherapy or indeed combination chemotherapy in terms of drug resistance, pharmacokinetics and solubility concerns associated with the individual constituents. In addition, the effect of the hybrid drug could be synergistically greater than the free agents. Most importantly, selectivity could be vastly improved because VDAs which have been examined so far have demonstrated a lack of selectivity. In this respect, one component of the hybrid drug could act as a tumour-homing device in order to target specifically tumour vessels while the other component may be the active agent [337-338]. Nevertheless, hybrid drugs' administration may have a reduced effect compared to the combination of single constituents, perhaps because of the increased bulk of the molecule which may decrease penetration to the target site. Combination treatment with individual drugs should be examined at an early stage and then compared to the hybrid in order to observe any potential benefits of the hybrid over the individual components.

Figure 1.19: Schematic illustrating a hybrid/conjugate design. Two distinct moieties are conjugated using a linker unit.

1.8.1 Hybrid Approaches

There are several design strategies for the development of hybrids: (i) one component may be used to present the other component in prodrug form, (ii) both moieties can be presented in an active form and (iii) both moieties can be presented in a prodrug form, giving an overall pro-prodrug form. Frequently, hybrids depend upon specific enzymes or chemical transformation to release their two components as active agents; in this way systemic toxicity may be reduced and drug delivery may be optimised to the target site [339].

A variety of hybrid designs have been proposed and evaluated for use as anti-cancer agents, revealing their benefits in drug delivery, as well as their inherent associated complexity. Such designs include hybrids/conjugates with either one or both components aiming to: i) inhibit tumour angiogenesis, ii) disrupt the existing tumour vasculature or iii) directly target and eradicate tumour cells.

Rejniak *et al.* have published a review on hybrid models of tumour growth emphasising the mathematical modelling approaches that can handle multiple intracellular and extracellular factors, and assist in the design of hybrid molecules [340].

The preclinical evaluation of hybrids/conjugates which have been designed to target tumour vasculature will be discussed including: i) tubulin targeting - cytotoxic hybrids, ii) antibody - drug hybrids, iii) toxin - drug hybrids, iv) RGD/NGR - related conjugates and v) heparin - associated conjugates. In addition, the preliminary evaluation of multi-targeted inhibitors of angiogenesis will be discussed. Table 1.2 summarises theses hybrid designs and includes one example from each group.

Table 1.2: Hybrid/Conjugate designs targeting tumour angiogenesis or vasculature.

Hybrid/Conjugate Design	Example	Ref.
Tubulin targeting - Cytotoxic hybrids	PTX – Camptothecin	[341]
Antibody - Drug hybrids	Trastuzumab – Maytansinoid	[342-344]
Toxin - Drug hybrids	Irofulven – Anginex	[345]
RGD/NGR - Related conjugates	RGD/NGR - TNF-α	[346-351]
Heparin - Associated conjugates	Heparin-lithocholic acid – Folate	[352]

1.8.1.1 Tubulin Targeting - Cytotoxic Hybrids

Tubulin targeting-cytotoxic hybrids have been designed to have one tubulin binding component (for either anti-vascular or anti-tumour purposes) joined to a cytotoxic agent. For example, a PTX-octreotide hybrid showed specificity to somatostatin receptor-expressing cells [353]. Nakagawa-Goto *et al.* have designed different taxoid conjugates by linking various anti-cancer agents, including glycyrrhetinic acid, colchicine, epipodophyllotoxin and camptothecin (CPT). PTX-CPT conjugates demonstrated higher anti-cancer activity against PC-3 and LN-CAP prostate cancer cells, than PTX itself. Also, the PTX-CPT conjugates exhibited anti-angiogenic properties, as well as reduced inhibitory activity against normal human lung fibroblasts [341].

Another approach which has been exploited is the development of hybrids that link two tubulin targeting agents. For instance, an admantane-based taxane-colchicine conjugate, exhibited superior anti-cancer activity against A549 adenocarcinoma human alveolar basal epithelial cells [354]. An additional colchicine-based hybrid was synthesised by its conjugation with caulerpenyne, a toxin isolated from the marine algae *C. taxifolia* [355], which exhibited inhibition of tubulin polymerisation and proliferation of SK-N-

SH neuroblastoma cells [356]. The activity of the colchicine-caulerpenyne hybrid was disappointing against tubulin polymerisation with IC_{50} value > 100 μM. High concentration (10 μM) of the hybrid was required to inhibit more than 50% of the formation of a capillary network [357]. The fact that the hybrid demonstrated poor tubulin polymerisation activity but still inhibited the capillary tube formation at 10 μM, may indicate that this was as a result of possible hydrolyses into different components.

A re-evaluation on the concept of tubulin targeting agents in hybrid drugs is contained in a review by Breen and Walsh [339].

1.8.1.2 Antibody - Drug Hybrids

1.8.1.2.1 PTX - Cetuximab Hybrid

Tumour-directed drug delivery has been attempted by conjugation of a tubulin targeting agent or a cytotoxic agent to a monoclonal antibody. For instance, PTX-cetuximab (a monoclonal antibody targeting EGFR) was synthesised, where its *in vitro* cytotoxicity results indicated enhancement of PTX's cytocidal effect, compared to that of the free drug, the intact antibody, and a physical mixture of the two. The *in vivo* anti-tumour activity of the conjugate was similar to that of cetuximab alone, which may be due to either a relatively low dose of the antibody-delivered drug (346 μg/kg) or an extensive release of the conjugate in circulation [358].

1.8.1.2.2 Trastuzumab - DM1 Hybrid

Moreover, the monoclonal antibody trastuzumab has been conjugated with the cytotoxic molecule maytansinoid (DM1), a microtubule depolymerising agent. The resulting conjugate, trastuzumab-DM1 (T-DM1), was designed to deliver DM1 into the HER-2-expressing cells *via* receptor mediated endocytosis. T-DM1 conjugate has shown activity both *in vitro* and *in vivo* models of trastuzumab-resistant breast cancer [342]. It has also shown remarkable activity in Phase I and II clinical trials in patients with trastuzumab-resistant HER-2-expressing breast cancer [343-344].

1.8.1.2.3 Cytokine Fusion Chimeras

Immunotherapeutics not only include conjugation to cytotoxic drugs but also fused to cytokines (cytokine fusion chimeras). A monoclonal antibody L19 was developed,

which targets a tumour specific splice form of fibronectin, which is selectively expressed on the tumour vasculature within a variety of tumours [359]. In addition, several derivatives of L19 antibody were generated and showed preclinical and clinical efficacy by specifically targeting the tumour vasculature [360-363]. Furthermore, two high affinity human antibodies, G11 and F16, were shown to bind to the large isoform of tenascin-C, a type of extracellular matrix glycoprotein expressed in different types of connective tissues, with a prominent perivascular pattern [364]. The activity of G11 and F16 antibodies was evaluated in a U87 glioblastoma xenograft model and showed great anti-tumour effect, by demonstrating accumulation at the tumour site, but not in other organs [365].

1.8.1.2.4 Anti-PSMA Conjugates

Further studies with antibody conjugates were carried out using an antibody against PSMA. PSMA is a membrane glycoprotein that is predominantly expressed in the prostate, in the neovasculature of different solid tumours and it's also present in the serum of prostate cancer patients [366-367]. The anti-PSMA antibody was conjugated to the anti-mitotic agent monomethyl auristatin E (MMAE), a microtubule assembly inhibitor, which is a synthetic analogue of dolastatin 10 [368]. The anti-PSMA-MMAE hybrid demonstrated selectivity towards PSMA-expressing cell lines and showed high *in vivo* activity in prostate tumour xenografts following an initial course of docetaxel therapy [369].

An additional example includes the anti-PSMA antibody huJ591, which was conjugated to various toxins and radio-nucleotides. The anti-PSMA conjugate showed promising potential for prostate cancer therapy and other solid tumours [370].

Gerber *et al.* have summarised the recent developments of antibody-drug conjugates which target the tumour vasculature and outlined future directions in that field by indicating some potential targets [371].

1.8.1.3 Toxin - Drug Hybrids

1.8.1.3.1 VEGF - Toxin Hybrids

A different strategy to directly target the tumour vasculature was introduced by Ramakrishnan *et al.* which reported that a toxin polypeptide linked to the $VEGF_{165}$ isoform can be used to target VEGF receptors and to inhibit the proliferation of endothelial cells [372]. In addition, $VEGF_{165}$-toxin conjugate has demonstrated inhibition of angiogenesis in the CAM assay and reduced the tumour growth of ovarian tumour xenogrfats [373].

Once identified that $VEGF_{165}$, binds to the neuropilin-1 receptor (NP-1) which is expressed on endothelial and tumour cells, as well as in adult heart and placenta [374-375], a different VEGF isofrom, $VEGF_{121}$, was used for conjugation with toxins, which binds to VEGFR-2, but not NP-1 [376]. A truncated form of diphtheria toxin (DT385) which contains the catalytic and the translocation domain of diphtheria toxin but lacks the innate receptor-binding domain was employed as the effector molecule. In order to facilitate chemical conjugation with $VEGF_{121}$, DT385 was genetically modified to incorporate a cysteine residue at the carboxyl terminus. The $VEGF_{121}$-DT385 conjugate, demonstrated selective inhibition of endothelial cell proliferation, angiogenesis and tumour growth *in vivo*, without apparent toxicity [377].

1.8.1.3.2 Irofulven - Anginex Hybrid

Furthermore, different types of toxins were used for conjugation with anti-angiogenic agents. Irofulven (MGI-114; 6-hydroxymethylacylfulvene) is a leading member of the acylfulvenes which are a semi-synthetic class of compounds derived from illudin S, a toxin produced by the *Omphalotus illudens* mushroom, which demonstrated *in vitro* and *in vivo* anti-tumour activities. Irofulven alone or in combination with other chemotherapeutic agents, has shown clinical activity against a variety of cancers [378]. However, DLTs were observed, including myelosuppresion, neutropenia, thrombocytopenia, nausea, vomiting and fatigue [379-380]. In order to reduce the systemic toxicity and maintain, or even improve the clinical efficacy, irofulven was conjugated to anginex [381-382], an anti-angiogenic agent which targets galectin-1 [383] (a cell surface glycan binding protein which is highly up-regulated in tumour-

activated endothelial cells) [384-385]. The irofulven-anginex conjugate demonstrated superior activity than the equivalent doses of either compound alone, in an ovarian tumour xenogrfat model, and selectively targeted the tumour vasculature by inhibition of tumour angiogenesis. Interestingly, the conjugate has not shown apparent signs of systemic toxicity, unlike irofulven [345].

1.8.2 RGD/NGR - Related Conjugates

Targeted delivery of cytotoxic agents to the tumour vasculature may be achieved by the identification of molecular markers that differentiate newly formed capillaries from mature vessels. Integrins are heterodimeric transmembrane proteins that represent a family of over 15 α and 8 β subunits which can heterodimerise to form over 20 combinations. A single ECM ligand could be recognised by different integrin combinations, while others may recognise several different ECM proteins. Integrin-mediated adhesion induces intracellular signalling pathways that modulate cell survival, proliferation and migration [26]. These signals involve phosphorylation of non-receptor tyrosine kinases (such as focal adhesion kinase and Src kinases), inositol lipid synthesis and elevation in intracellular calcium and pH. Consequently, a number of downstream signals are triggered, including activation of the Ras/MAPK pathway [26]. Activated endothelial cells express several types of integrins on their surface during angiogenesis, which regulate critical adhesive interactions with several ECM proteins, such as fibronectin, vitronectin, laminin, fibrinogen, von Willebrand factor, collagen types I, IV and denatured collagen. Cell migration, proliferation and differentiation are distinct biological events which are regulated by these adhesive interactions and which are involved in the process of angiogenesis [386]. An interesting expression pattern has been identified by integrin $\alpha_v\beta_3$ with an exposed RGD sequence on endothelial cells undergoing angiogenesis in tumours, wound healing, or inflammatory tissues, and this might be a useful diagnostic or prognostic indicator of tumours [387-390].

One of the best known and specific markers is the $\alpha_v\beta_3$ integrin which mediates the attachment of endothelial cells to sub-matrix proteins such as vitronectin, which forms the capillaries' basement membrane [391]. The $\alpha_v\beta_3$ integrin is found on the luminal surface of the endothelial cells only during angiogenesis and vascular remodelling [388, 392]; although all endothelial cells use the integrin to attach to the extraluminar sub-

matrix. Phage display studies have distinguished a selective ligand sequence RGD which has high affinity for the $\alpha_v\beta_3$ integrin [393]. The tissue distribution of $\alpha_v\beta_3$ integrin is limited in adults but it is expressed on a small percentage of activated macrophages, leukocytes and osteoclasts, where it appears to be involved in bone resorption and immune function. The $\alpha_v\beta_3$ integrin is also expressed in some invasive tumours, such as late-stage glioblastomas and metastatic melanomas, leading to the malignant phenotype of the tumour [394]. Previous studies suggested that $\alpha_v\beta_3$ integrin may serve as an effective diagnostic or prognostic indicator of malignancies.

1.8.2.1 PTX-RGD Conjugate

In order to increase selectivity to tumour blood vessels, different studies have used several chemotherapeutic agents linked to the RGD peptide. Chen *et al.* designed a dimeric RGD peptide E[c(RGDyK)]$_2$, a potent α_v-integrin antagonist, as a carrier for PTX in order to target specifically tumour vasculature and breast cancer cells. RGD peptide inhibited cell cycle proliferation by G_0/G_1-phase arrest, whereas the PTX-RGD conjugate **18**, showed inhibition of cell proliferation mediated by a G_2/M-phase cell cycle arrest followed by apoptosis, and its activity was comparable to that observed for PTX. The integrin binding affinity of **18** was slightly reduced compared to the un-conjugated peptide; however there was specific accumulation of the conjugate in integrin-expressing sites *in vivo*. The highest tumour uptake of 125-I-labeled PTX-RGD was observed after 2h post-injection and the best tumour/background contrast after 4h post-injection. These results demonstrated the potential of the conjugate to be delivered specifically to integrin-rich sites of the tumour and the vasculature, therefore reducing toxicity and improving selectivity [395]. In another study, PTX was conjugated with a divalent cyclic peptide E-[c(RGDfK)2], which is a novel ligand-based vascular targeting agent that binds to $\alpha_v\beta_3$ integrin, and showed high uptake in OVCAR-3 xenograft tumours [396]. Promising results were observed *in vitro*, although the PTX conjugate was inactive *in vivo* following intravenous (i.v.) administration in ovarian cancer xenograft model. A possible reason suggested by the authors which could explain the lack of efficacy of the PTX conjugate *in vivo*, was premature release of PTX into the circulation and thus reduced accumulation of the active drug to the tumour site [397]. Nevertheless, as PTX is a well known anti-cancer agent one might

still have expected a small degree of anti-tumour activity. Perhaps a more likely outcome is extensive metabolism of the conjugate to inactive metabolites *in vivo*.

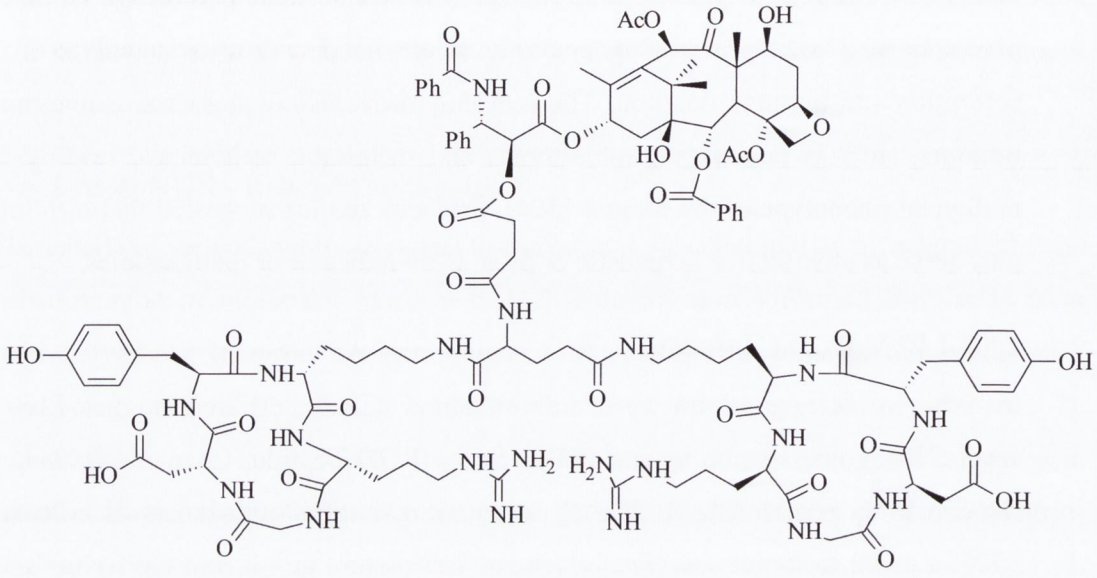

18

Figure 1.20: PTX-RGD conjugate **18** [395].

1.8.2.2. MMAE-HSA - RGD Hybrid

Moreover, the tubulin targeting agent MMAE was bound *via* the valine-citrulline linker to human serum albumin (HSA), which is a biocompatible and biodegradable carrier. Conjugation of cRGD peptides to MMAE-HSA was established either by polyethylene glycol (PEG) linker or a short alkyl linker, in order to promote selectivity to angiogenic endothelial cells. Both conjugates inhibited HUVEC proliferation at nanomolar concentrations and displayed excellent tumour homing properties upon i.v. administration in C26 tumour models [398]. It is worth noting that no control compounds were examined such as MMAE in order to better define the conjugates' activity. Furthermore, MMAE prodrug, which recruits tumour-associated protease (TAP) legumain for its activation, was designed to target cell surface $\alpha_v\beta_3$ integrin. MMAE conjugate strongly induced cell death of MDA-MB-435 breast cancer cells which are positive for $\alpha_v\beta_3$ integrin expression. Treatment of tumour bearing mice with 3 mg/kg every three days for 17 days resulted in decreased tumour growth and

metastasis in 4T1 murine breast cancer, D121 Lewis lung carcinoma and MDA-MB-435 models. These findings suggest that MMAE's activity was enhanced by selective targeting of integrin-rich sites and legumain protease on tumour cells, which otherwise would be too toxic to use for therapeutic applications at the dose evaluated [399].

1.8.2.3 sFlt-1 gene - PEI-g-PEG-RGD Conjugate

A different strategy aiming to selectively target tumour vasculature by inhibiting angiogenesis is gene therapy. Several studies have described RGD-mediated gene delivery systems for transferring siRNA [400] or luciferase reporter gene [401]. A study conducted by Kim *et al.* reported a therapeutic gene encoding Flt-1 (fms-like tyrosine kinase-1) and evaluated its anti-angiogenic activity when conjugated to PEI-g-PEG-RGD (polyethylenimine with a hydrophilic PEG spacer) gene carrier. Flt-1 is a VEGF receptor which upon activation leads to endothelial cell stimulation, proliferation, migration and capillary tube formation [402]. Soluble Flt-1 (sFlt-1) is a potent and selective inhibitor of VEGF. Although the transmembrane and intracellular tyrosine kinase domains are absent, sFlt-1 binds to VEGF with the same affinity and specificity as that of the full-length receptor [403]. The PEI part of the conjugate could increase the transfection efficiency by avoiding degradation of DNA complexes from endosome or lysosome compartments [404], and the PEG could decrease the cytotoxicity and increase the solubility of the conjugate. The results of this study showed that the complex of sFlt-1 gene with PEI-g-PEG-RGD conjugate effectively and selectively inhibited endothelial cell proliferation, by blocking the binding of VEGF to the actual Flt-1 receptor [405].

Further studies evaluated the effect of repeated treatment with the conjugate *in vivo* which resulted in an anti-tumour activity and an increased survival rate; however the effect was not identified in PEI-g-PEG/pCMVsFlt-1 or PEI-g-PEG-RGD/pCMV-GFP control groups. These findings suggest the use of a non-viral gene carrier to deliver an anti-angiogenic gene at a low continuous dosage, where it is not possible to use other vectors [406].

1.8.2.4 TNF-α Associated RGD/NGR Conjugates

Corti and Ponzoni have described two strategies which use TNF-α to increase the local concentration of chemotherapeutic agents at the tumour site. TNF-α is an inflammatory cytokine which increases vascular permeability [407] and is cytotoxic to several tumour cell lines. It induces haemorrhagic necrosis in certain solid tumours and has also showed significant anti-tumour activity in animal models [408-409]. Despite its success *in vivo*, the use of TNF-α therapy in the clinic was limited due to systemic toxicity.

To address this concern, two different approaches were introduced, the first one using TNF-α before the administration of chemotherapy in order to increase vascular permeability and enhance the diffusion of the anti-cancer agent into the tumour. The second strategy was based on direct vascular shutdown targeting APN expression present on blood vessels undergoing angiogenesis but not quiescence vessels [199]. Doxorubicin (DOX)-encapsulated liposomes were coupled with the NGR motif. Improved drug uptake by neuroblastoma tumours and enhanced therapeutic index were observed using DOX-encapsulated liposomes homing to tumour vessels [410]. This strategy could be proven effective in poorly vascularised tumours where therapeutic agents are harder to reach.

The biological effect of NGR-TNF-α (TNF-α coupled to the peptide CNGRC) was also investigated which demonstrated increased leakage of the vasculature in NGR-TNF-α treated murine lymphomas compared with controls. Immunohistochemical analysis showed decreased tumour hypoxia as well as elevated tumour blood flow 2h after treatment. Interestingly, reduction in tumour hypoxia did not lead to additional tumour growth; however tumour volume was decreased within 24h of administration [346]. A Phase I clinical study was designed using the conjugate to determine its DLTs, MTD and its anti-tumour activity in patients, as well as to examine the vascular response determined by dynamic contrast enhanced magnetic resonance imaging (DCE-MRI). NGR-TNF-α was well-tolerated and the results from DCE-MRI confirmed the anti-vascular effect of the agent. Approximately one third of the patients experienced stable disease; however no objective responses were observed [347-348]. A further trial was conducted using NGR-TNF-α as a single agent in HCC patients and was well tolerated, with only mild to moderate chills reported as side effects. The overall response rate was 7%, while 22% of the patients had stabilised disease [349]. There are several completed

and ongoing Phase II clinical trials with NGR-TNF-α as a single agent or in combination therapy for the treatment of mesothelioma, colorectal, liver and ovarian cancer [350-351, 411]. Phase III studies have commenced evaluating its effect in patients with malignant pleural mesothelioma.

Tandle *et al.* have reported a hybrid adeno-associated virus phage vector (AAVP) that was used to target tumour endothelium in order to express TNF-α. The AAVP vector targets gene products to tumour vasculature by using the RGD4C peptide. Human melanoma cells were infected with AAVP-TNF-α and resulted in high expression levels of TNF-α, whereas systemic administration of the RGD-AAVP-TNF-α conjugate to melanoma xenografts, produced targeted delivery of the virus to the tumour vasculature; notably, the non-targeted vector was not delivered specifically to tumour vessels. The RGD-AAVP-TNF-α vector enhanced delivery of TNF-α to the tumour vasculature resulting in induction of apoptosis in tumour vasculature and significantly reduced tumour growth, without observable organ toxicity. Therefore, this approach could be useful to target tumour vasculature by delivering anti-cancer agents directly to integrin-expressing sites [412].

1.8.2.5 5-Fluoro-2-deoxyuridine - CNGRC Conjugate

Furthermore, Zhang *et al.* reported the design and synthesis of two prototypes of tumour targeting 5-fluoro-2-deoxyuridine (5-FdUrd) prodrugs conjugated with a CNGRC by known linkers based on succinate and glutarate esters. 5-FdUrd is a cytotoxic anti-cancer drug which mediates its action by blocking thymidylate synthase to inhibit DNA synthesis and incorporation of its metabolites into DNA or RNA [413-414]. However, treatment with this agents is associated with various side effects including non-specific toxicity toward normal tissues [415]. Both conjugates exhibited lower cytotoxicity compared to 5-FdUrd, showing selectivity towards APN-positive cells over APN-negative cells [416].

1.8.2.6 Platinum - Based RGD/NGR Conjugates

In a further extension of this work, platinum (Pt)-based drugs, such as cisplatin, have been conjugated to peptide motifs containing RGD, NGR, CRGDC and (RGDdK)c. Mukhopadhyay *et al.* reported that the Pt(IV)-RGD conjugates **19 a** and **b** were highly and specifically cytotoxic to $\alpha_v\beta_3$ and $\alpha_v\beta_5$ expressing cell lines, approaching the

activity of cisplatin. The Pt(IV)-NGR complexes **20 a** and **b** were less active than **19 a** and **b**, but nevertheless showed higher activity compared to the control complexes [338]. The difference in activity of those conjugates could be due to the expression patterns of APN and integrins in the cell lines used.

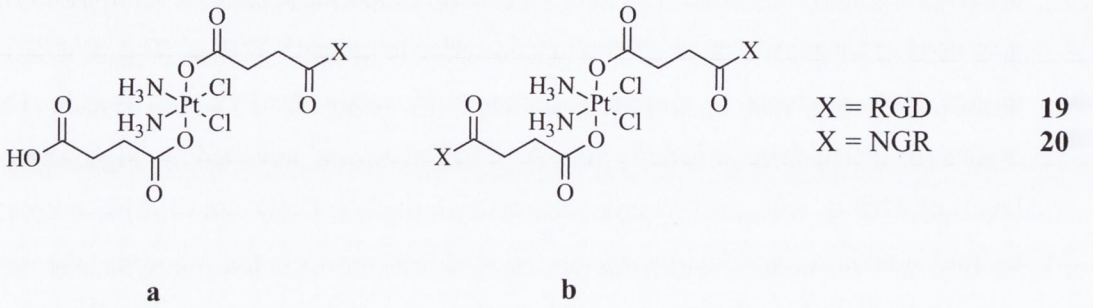

a **b**

Figure 1.21: RGD and NGR platinum-based conjugates **19 a, b** and **20 a, b** [338].

In addition, Ndinguri *et al.* have further synthesised a Pt-based conjugate, cyclic mPEG-CNGRC-Pt and a dichloro(ethylenediamine)platinum(II) (PtenCl2) based conjugate, cyclic mPEG-CNGRC-Pten. Selective delivery of these conjugates was observed in APN-positive PC-3 cells and these agents exhibited significantly higher activity over untargeted carboplatin. Further analysis on the effects of these conjugates on PC-3 cells was determined using caspase-3 and -7 activation, fluorescence microscopy and DNA fragmentation, which confirmed the induction of apoptosis [417]. This targeting approach has been proven effective against integrin-positive and APN-positive cell lines; nevertheless these conjugates have to be examined *in vivo* to establish whether their activity is maintained.

Hybrid based strategies that incorporate RGD/NGR homing ligand have been an active area of recent research in this field. A more comprehensive review of the RGD-conjugates has been presented by Temming *et al.* which concentrate on the structural requirements for RGD-peptides and RGD-mimetics as ligands for $\alpha_v\beta_3$ [418]. Additionally, a review by Corti *et al.* has focused on structural and functional properties of the NGR motif and its applications in anti-angiogenic therapeutics [419].

1.8.3 Heparin - Related Conjugates

Heparin is a highly sulphated natural polysaccharide, which is mainly composed of alternating units of sulphated glucuronic acid and glucosamine units. Heparin is well known for its anticoagulant activity, as well as for its interaction with growth factors, including VEGF and bFGF [420-421]. Heparin treatment was formerly performed in a large number of clinical trials with cancer patients in order to treat venous thrombosis, leading to the suggestion that heparin also prolongs cancer patients' survival [422]. Thus, heparin was found to inhibit angiogenesis and tumour progression and also to diminish metastasis by blocking selectin-mediated intercellular interactions [423-425], and by regulating various proteolytic enzymes essential for invasion of cancer cells and angiogenesis, through the ECM [422, 426].

However, due to its high anticoagulant effect which could induce haemorrhage as a side effect [427], heparin could only be administered at low concentration. Therefore, a number of heparin derivatives have been developed with non anticoagulant activity, while still maintaining their anti-angiogenic effects. A recent clinical trial has demonstrated that low molecular weight heparins (LMWH) may provide an additional advantage in combination with chemotherapeutics, providing an increased tumour uptake and chemo-responsiveness in cancer patients [428].

In contrast, Folkman *et al.* has previously established that heparin alone could enhance tumour angiogenesis and to further investigate that in the CAM assay, cortisone was added in combination with heparin to suppress background inflammation. Unexpectedly, the combination of the heparin and cortisone inhibited angiogenesis, although cortisone alone had little or no effect [429].

1.8.3.1 HAH - Cortisol Hybrid

A non anti-coagulating derivative of heparin, heparin adipic hydrazide (HAH), was designed and linked by an acid-labile bond to cortisol (hydrocortisone). Although heparin receptors are present on other cell types, the majority of systemically administered heparin is taken up by vascular endothelial cells, which bind to sulphated polyanion receptors [430-432], and by cells of the reticuloendothelial system [433-434] (possibly due to the vast surface area of these cells which are in contact with the blood). Dividing endothelial cells are more susceptible to heparin's effect as they bind and

endocytose 10-fold more heparin than non-dividing endothelial cells [435]. In this study, HAH and HAH-cortisol conjugate **21** inhibited DNA synthesis by MPCE cells. The conjugate was more effective than either the individual compounds alone or in combination. HAH-cortisol slowed down the healing of wounded MPCE monolayer, inhibited cell proliferation and migration, whereas combination of free HAH and cortisol showed complete migration of the cells 72h after treatment. Neither the conjugate nor free HAH caused signs of toxicity when administered i.v. to mice at doses of 10 mg/day for 14 days, unlike heparin and cortisol which were lethal at this dose. The anti-tumour effect of the conjugate and free drugs was examined *in vivo* by daily i.v. administration into animals bearing established subcutaneous (s.c.) Lewis lung carcinomas. Treatment with **21** showed highly significant retardation of tumour growth compared with cortisol alone or in combination with HAH, whereas no reduction in tumour growth was observed with HAH alone [436].

1.8.3.2 Heparin - Carrying Polystyrene Conjugate

Heparin-carrying polystyrene (HCPS) has been previously described as a synthetic glycoconjugate that has an amphiphilic structural unit consisting of hydrophilic polysaccharides and hydrophobic polystyrene moieties [437]. This conjugate showed a significantly reduced anticoagulant activity and is able to interact substantially with various heparin-binding growth factors known to stimulate angiogenesis, including FGF-2, $VEGF_{165}$ and hepatocyte growth factor (HGF) [438]. The effect of HCPS on cell growth was examined in growth factor-induced human dermal microvascular endothelial cells (HMVEC), and was found to inhibit growth in a dose-dependent manner, even at low concentrations (2 μg/mL). Strong inhibition of tubular formation was noted following 2 μg/mL HCPS treatment of HMVEC seeded on matrigel and anti-invasive activity and inhibition of cell adhesion was observed in Lewis lung carcinoma (3LL) and B16 mouse melanoma cells at 4 μg/mL. Treatment with HCPS showed a 40% reduction of 3LL tumours and 10% reduction of B16 tumours. Moreover, HCPS treatment reduced the number of CD34 positive vessels in Lewis lung carcinoma tumours and demonstrated anti-metastatic activity on both cancer cell lines, suggesting that this conjugate may be beneficial in a clinical setting [438]. The *in vivo* data obtained suggests a preference for the use of this conjugate in the treatment of Lewis lung carcinoma.

1.8.3.4 Heparin - DOCA Conjugate

In a separate study, a chemically modified heparin derivative, heparin-deoxycholic acid (HD) was designed by covalently coupling N-deoxycholylethylenediamine (DOCA-NH_2) to heparin to serve as a hydrophobic segment [439]. This formulation produce a macromolecule aggregate, which could localised to tumour sites by the enhanced permeability and retention effect (EPR) [440]. The amide conjugate **22** was found to exhibit low anticoagulant activity and to form self-assembled nanoparticles in aqueous condition. During bromodeoxyuridine incorporation assays, **22** inhibited SCC and HUVECs proliferation. The anti-angiogenic activity of **22** and heparin was examined using HUVECs layered onto matrigel-coated plates. The inhibitory effect of 100 μg/mL of **22** was more evident than heparin, as HUVECs gradually lost their intercellular contact. In order to test the ability of HD to inhibit bFGF-induced angiogenesis the matrigel plug assay was performed, where mice were injected s.c. with matrigel containing either bFGF, heparin or **22**. After 10 days, animals were sacrificed and matrigel plugs were excised, fixed and stained with either hematoxylin and eosin (H&E) or CD31 antibody (microvessels staining). Matrigel plugs haemoglobin contents were reduced up to 82% by **22**, indicating that HD effectively inhibited angiogenesis; however, heparin or bFGF alone did not demonstrate any activity. The effect of **22** on the signal pathways (namely phosphorylation of FGFR, ERK and p38 MAPK) induced by bFGF was investigated. HUVECs were incubated with or without **22** in the presence or absence of bFGF and the phosphorylation of FGFR, ERK and p38 MAPK was analysed. The results suggested that **22** interacts with bFGF receptors and interferes with signalling pathways involving FGFR, ERK and p38 MAPK phosphorylation; thus suggesting a possible mechanisms by which **22** inhibits cell proliferation and angiogenesis. The results from the *in vivo* experiments showed that **22** inhibited tumour growth in tumour bearing mice in a dose-dependent manner [441]. The process of angiogenesis is complex and difficult to regulate; however these findings are encouraging because **22** demonstrated interaction with not only one but several signalling pathways, thus making it easier to modulate angiogenesis.

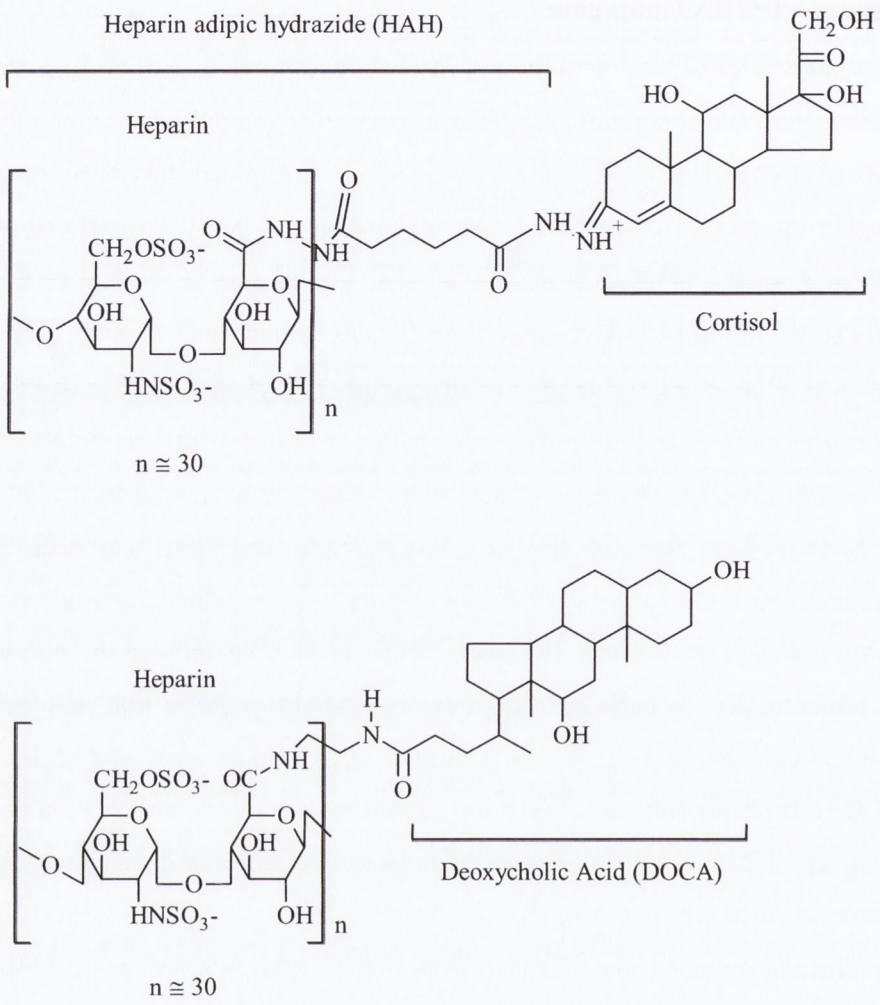

Figure 1.22: HAH-cortisol conjugate **21** [436] and heparin-DOCA or HD conjugate **22** [439, 441]. Heparin is a sulphated polysaccharide with repeating uronic acid and glucosamine residues that vary in number.

An extension of this study involved loading DOX onto the amphiphilic HD conjugate in order to evaluate the use of this formulation in sustained drug release studies. DOX-loaded heparin nanoparticles (DHN) were safer than free DOX. HD conjugate, DOX and DHN activity was evaluated in tumour bearing mice and the reduction in tumour volume was 43%, 56% and 74% respectively, confirming that DHN is more effective than the free agents and might provide a novel therapy for SCC [442]. The fact that DHN treatment had shown a safer toxicological profile than free DOX reveals an additional advantage for this type of therapy.

1.8.3.5 LMWH - DOCA Conjugate

Another conjugate, LHD was synthesised, by conjugating the carboxylic groups of LMWH to the carboxylic group of DOCA. Similar results were obtained when the anti-angiogenic effect of LHD and LMWH was examined in the capillary tube assay. The CAM assay was used to investigate the interaction between LMWH, LHD and bFGF. Although the effect of LMWH was smaller than LHD, the results were not significant enough. The matrigel plug assay was performed and the haemoglobin contents of plugs from animals treated with LHD and LMWH *vs* untreated controls were 34.0 ± 4.8 % and 102.3 ± 7.2 %, respectively, suggesting that angiogenesis was unaffected by LMWH treatment. Microvessel density was also reduced by LHD treatment, but not by LMWH. The size of the tumours in SCC7 murine xenograft models was diminished after LHD treatment and the number of tumour microvessels was decreased at a dose-dependent manner. Combination therapy of LHD and DOX enhanced the anti-tumour effect *in vivo* compared to individual components, which suggests that this treatment may be a useful therapy for SCC [443-444]. Additional studies revealed that LHD oral administration attenuated metastasis in B16F10 murine melanoma or A549 human lung carcinoma cells [445]. Further, LHD conjugates with further reduced anticoagulant activity were synthesised, by controlling the DOCA coupling ratio, and showed inhibition of angiogenesis and tumour growth in SCC7 and A549 xenografts [446].
Additionally, a LMWH-taurocholate conjugate (LHT7) was synthesised and shown to have low anticoagulant activity, bind to VEGF strongly and inhibit VEGF-dependent KDR phosphorylation. When LHT7 was evaluated in the matrigel plug assay it showed a strong anti-angiogenic effect. *In vivo* efficacy studies resulted in a significant reduction in SCC7 tumour growth and increased survival rate [447].

1.8.3.6 Folate - HL Conjugate

Yu *et al.* have designed low anti-coagulant heparin amphiphiles, heparin-lithocholic acid conjugate (HL) and folate-conjugated HL (FHL, **23**). Folate receptors (FR) are over-expressed in various cancer types, including ovarian, endometrial, breast and colorectal cancers [448-451]. They have also been identified as markers of specific tumours for diagnostic and therapeutic purposes. In this study, 100 μg/mL of unfractionated heparin (UFH), HL and **23** were examined in the *in vivo* matrigel plug

assay and the results showed that HL and **23** significantly inhibited plugs' vascularisation, whereas the haemoglobin content was reduced to 29% and 43%, respectively. The effect of UFH was less than that of HL and **23**, although still significant compared to the positive control. Cytotoxicity of the conjugates was evaluated in KB cervical adenocarcinoma cells using the MTT assay and showed that **23** reduced the viability of cells to 25% following 24h incubation; HL had no effect on cell viability. FHL-treated cells induced sub-G_1 phase accumulation, an indication of apoptosis, and induced a high amount of apoptotic cells after Annexin V/propidium iodide (PI) staining; whereas UFH and HL had no effect. Cellular internalisation of HL and **23** in KB cells was investigated and **23** showed higher cellular uptake than HL indicating that folate conjugation provided the ability for cellular endocytosis. *In vivo* results revealed that both administered HL and **23** had similar anti-angiogenic activity and inhibitory effect on tumour growth; however FHL induced higher levels of apoptosis on tumour tissues [352]. The anti-angiogenic activity along with the apoptotic effects on cancer cells may provide an additional advantage for the evaluation of **23** in preclinical and clinical settings.

1.8.3.7 cRGD - HL Conjugate

In a similar study, the investigators designed a cRGD-HL conjugate **24**. Adhesion studies were performed using HUVECs. The addition of heparin, cRGDyK, HL and **24** decreased cell adhesion by 39.1%, 45%, 54.2% and 65.6%, respectively. Additionally, the effect on cell migration was tested and was effectively reduced by 27% (heparin), 47.8% (cRGDyK), 72.1% (HL), and 82.8% (**24**). The anti-adhesion and anti-migration activity of **24** was obvious compared to the other compounds. The inhibition of capillary tube formation was most profound in **24**-treated cells, whereby receptor binding studies have shown that **24** exhibited higher binding affinity for purified $\alpha_v\beta_3$ integrin, over cRGDyK. In the matrigel plug assay, **24** significantly inhibited bFGF-induced angiogenesis and tumour growth activity with superior anti-tumour effect for **24**, compared to heparin and cRGDyK. The enhanced activity of the conjugate was suggested to be due to the anti-angiogenic characteristics of the heparin derivative (mediated through bFGF inhibition) and the additional effect from the integrin-mediated interaction of the functionalised heparin derivative [452].

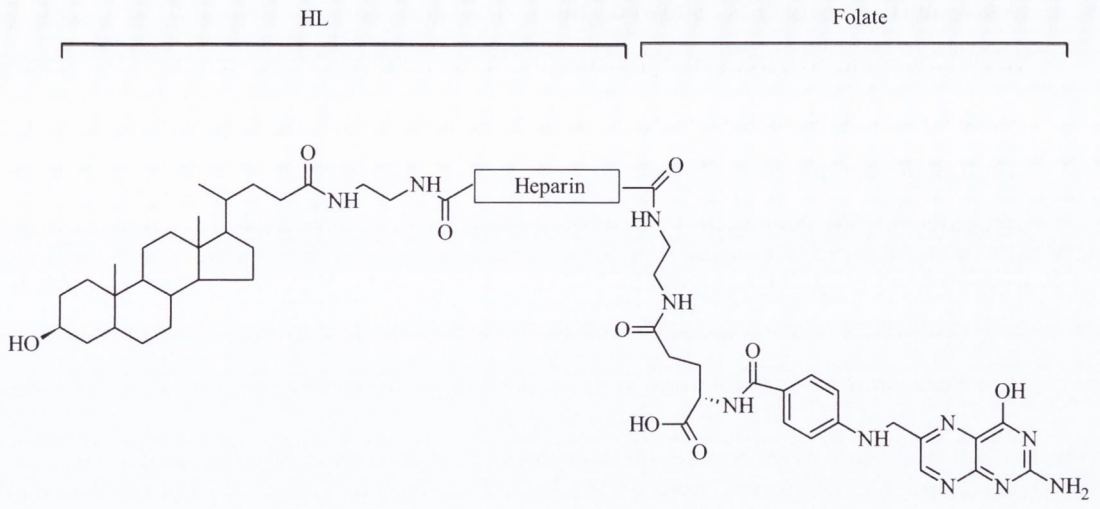

23

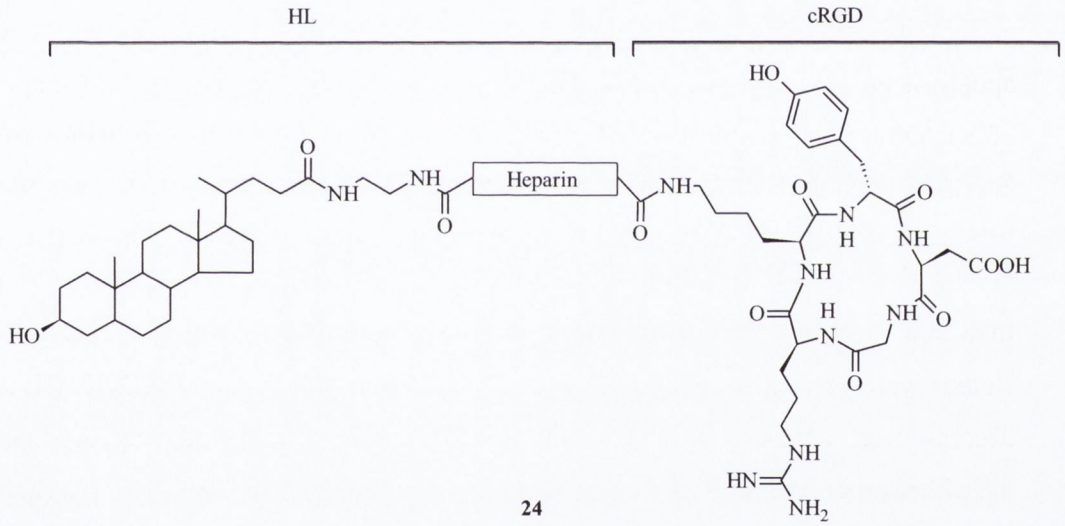

24

Figure 1.23: Folate-heparin-lithocholate conjugate (FHL) **23** [352] and cRGD-heparin-lithocholic acid congugate, (cRGD-HL) **24** [452].

In summary, most of the heparin-related conjugates demonstrated significant differences in activity from their single components and individual 1:1 combination of the two. However, it is important that heparin analogues are properly examined for anticoagulant activity at an early stage, as well as at a more advanced *in vivo* setting, due to the fact that heparin conjugates could be metabolised into toxic analogues which may induce internal haemorrhage.

1.8.4 Multi - Targeted Compounds

Especially in the design of novel anti-angiogenic inhibitors, the idea of synthesising compounds that target multiple molecular events has proven to be an effective strategy, as evidenced by the clinically approved multiple TKIs, sunitinib, sorafenib and pazopanib [139, 143, 150]. However, these inhibitors have demonstrated anti-tumour activity associated with a variety of "off-VEGF target" effects. Their low potency is leading to the administration of higher doses, which in turn, results in increased blockage of non-VEGF kinases due to low selectivity, leading to dose reduction or treatment interruption. A new generation of VEGFR TKIs has emerged which aims for higher selectivity and potency, providing improved anti-tumour efficacy and less treatment-related toxicity.

1.8.4.1 Cediranib

Cediranib **25** (Recentin®) is an oral VEGFR TKI with affinity for VEGFRs, c-Kit, PDGFR-$\beta\beta$, FGFR-1, and several other kinases [453]. In a phase II trial, cediranib monotherapy has shown significantly greater anti-tumour efficacy in patients with advanced or metastatic RCC [454]. In addition, further studies were conducted with cediranib treatment, including patients with head and neck cancer, NSCLC [455], recurrent glioblastoma [456], epithelial ovarian, fallopian tube and peritoneal cancer [457], whereby a variation in response to treatment was observed. Combination studies of cediranib with chemotherapy in patients with advanced lung cancer did not demonstrate significant improvement with the addition of cediranib; instead dose reductions or treatment discontinuation occurred which was associated with cediranib toxicities [458]. The most frequent toxicities observed with cediranib therapy included haematological abnormalities, fatigue, hypertension, anorexia, dysphonia, gastrointestinal events, and hepatobiliary abnormalities [454-455, 457]. Ongoing trials are currently investigating the anti-tumour efficacy of cediranib in patients with advanced biliary tract cancers, leukaemia, melanoma, and soft tissue sarcomas [323].

1.8.4.2 Motesanib

Another TKI is motesanib **26** (AMG 706), which inhibits VEGFR, PDGFR, and c-Kit receptor [459]. A phase I combination study of motesanib with gemcitabine demonstrated good tolerability profile in the treatment of solid tumours [460].

Motesanib has been evaluated in phase II trials in combination with PTX and carboplatin, where the treatment outcome was similar to that observed with bevacizumab plus chemotherapy, in patients with advanced NSCLC [461]. Several ongoing trials are examining the activity of motesanib alone or in combination with other chemotherapeutic agents for the treatment of NSCLC, metastatic colorectal, breast cancer and other solid tumours [323].

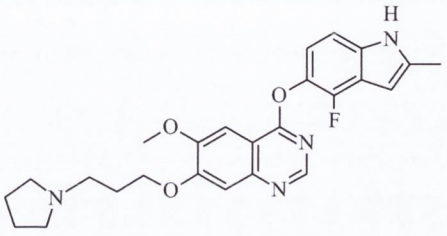

25

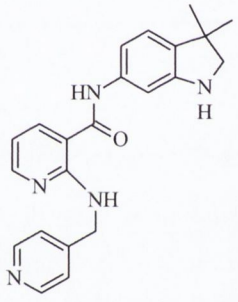

26

Figure 1.24: Multi-TKIs of angiogenesis cediranib **25** [453] and motesanib **26** [459].

1.8.4.3 Canertinib

An additional TKI is canertinib **27** (CI-1033), which inhibits in a non-selective manner all the members of the EGFR-family kinases [462]. This may result in a broader spectrum of anti-tumour efficacy. Reported adverse effects in a Phase I trial included diarrhoea, rash and/or anorexia [463], while in a Phase II study with Pt-refractory or recurrent ovarian cancer patients treated with canertinib, failed to demonstrate activity and appeared to be no association between baseline EGFR expression and disease stability [464]. Further Phase II studies with canertinib in pre-treated advanced NSCLC and metastatic breast cancer patients demonstrated similar unsatisfying results [465-466]. Currently, studies in NSCLC and breast cancer with canertinib are ongoing [323].

1.8.4.4 Vatalanib

Furthermore, vatalanib **28** (PTK787) is a multi-TKI which targets VEGFR1, VEGFR2 and PDGFR [467], and which clearly demonstrated an anti-angiogenic, anti-tumour and anti-metastatic effect in several solid tumours [468-469]. Side effects after treatment with vatalanib include light-headedness, fatigue, transaminase elevation, hypertension, nausea, and vomiting [470]. No beneficial effects were observed in a Phase III trial when vatalanib was added to standard chemotherapy (FOLFOX4) in metastatic colorectal cancer patients [471]. Nevertheless, an additional Phase III study with vatalanib in combination with chemotherapy (FOLFOX4) in metastatic colorectal cancer patients showed an improvement in progression free survival but not in overall survival. Interestingly, the effect of vatalanib was more pronounced in patients with high lactate dehydrogenase (LDH) at baseline [472]. Monotherapy and combination studies were conducted in other advanced malignancies such as mesothelioma but no beneficial effect was proven [473-474].

1.8.4.5 Leflunomide

Leflunomide **29** (Arava®) is an immunomodulatory agent [475] used in rheumatoid arthritis and found to inhibit PDGFR tyrosine kinase, and also partially EGFR and FGFR [476]. It has demonstrated anti-tumour activity both *in vitro* and *in vivo* [477] and showed partial response, great decline in the PSA expression and improvement in pain in some of the hormone-refractory prostate cancer patients [478]. Phase III trials of leflunomide, in combination with other agents, are still in progress in patients with hormone-refractory prostate cancer and glioblastoma multiforme patients [323].

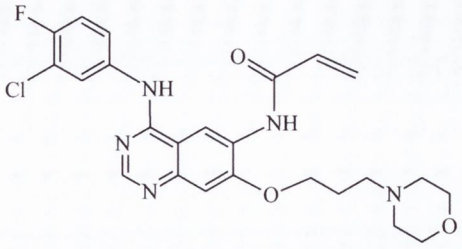

27

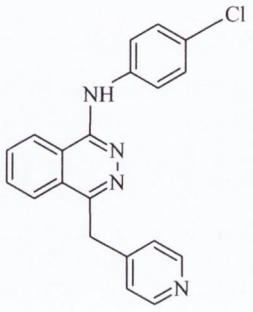

28

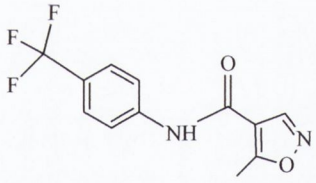

29

Figure 1.25: Multi-targeted TKIs canertinib **27** [462], vatalanib **28** [467] and leflunomide **29** [476].

1.8.4.6 VEGFR2 - Tie-2 Inhibitors

Other recent examples have included studies performed by Miyazaki *et al.* on dual inhibitors of VEGFR2 and angiopoietin-1 receptor (Tie-2), such as compound **30**. VEGFR2 is involved in vessel sprouting through induction of proliferation, migration and survival of endothelial cells [479], whereas Tie-2 plays an important role in stabilising the immature endothelial cell network at a later stage of blood vessel formation [480-481]. The discovery of 4-NH_2-furo[2,3-d]pyrimidines bearing a diarylurea substituent at 5-position led to the identification of potent inhibitors of angiogenesis-receptor tyrosine kinases, including **30**. This compound exhibits both enzymatic and cellular inhibitory activity [482], as well as *in vivo* anti-tumour and anti-

angiogenic activity, when evaluated in a HT-29 colon adenocarcinoma xenograft model [483]. Interestingly, **30** was examined in a kinase screening panel and demonstrated inhibitory activity against multiple kinases, including VEGFR1, VEGFR3 and PDGFR, indicating a similar inhibitory profile as vatalanib, which its evaluation may result in more advanced-stage clinical evaluation.

Furthermore, a novel series of C-3 urea, amide and carbamate fused dihydroindazolocarbazole (DHI) analogues such as compound **31,** were reported by Becknell *et al.* to be highly potent dual inhibitors of VEGFR2 and Tie-2 receptor tyrosine kinases [484]. These compounds showed promising results in tumour models without any observable toxicity [485]. In addition, NVP-AAL881, a small molecule dual inhibitor of VEGFR2 and Raf, was synthesised and shown to block proliferation of bovine aortic endothelial cells (BAECs), inhibit invasion of glioma cells and reduce orthotopic tumour growth in a preclinical glioma model [486]. It also disrupted activation of ERK and transcription factor STAT3, in HCC and decreased cancer cell motility and migration of endothelial cells and vascular smooth muscle cells. *In vivo* studies have demonstrated significant inhibition of cell proliferation, reduction of tumour growth and reduced CD31 tumour vessel area [487]. Moreover, NVP-AAL881 caused reduction of VEGF expression, blocking of VEGF-induced ERK and stress-activated protein kinase (SAPK) phosphorylation, in endothelial cells, whereas STAT3 phosphorylation was diminished by the Raf inhibitor. Promising results were also observed in orthotopic L3.6p1 pancreatic tumours, where oral delivery of NVP-AAL881 at 100 mg/kg/day showed a significant reduction in tumour growth, vascularisation and metastasis [488].

1.8.4.7 VEGFR2 - c-Met Inhibitor

Raeppel *et al.* have synthesised a series of carboximide compounds which exhibit inhibitory effects on both hepatocyte growth factor receptor (c-Met) and VEGFR2 tyrosine kinases. The most promising inhibitor **32** was evaluated in cell-based assays and dramatically impaired HGF-induced epithelial cell migration, proving its ability to inhibit c-Met-dependent cell motility events. VEGF-induced phosphorylation of ERK, VEGF-induced proliferation of HUVECs and tubule formation were potentially inhibited by the most active compounds within the series. Compound **32** was evaluated

against a variety of human cancer cell lines and displayed nanomolar IC_{50} values in cell lines which are particularly sensitive to c-Met inhibition, including MKN-45 gastric cancer cells. *In vivo* results showed that oral administration of **32** once daily for 12 days caused significant reduction of MKN-45 tumours [489].

1.8.4.8 $\alpha_v\beta_3/\alpha_5\beta_1$ Integrin Inhibitor

Considering the role of integrins in cell migration and angiogenesis, integrin inhibitors are promising candidates for the development of cancer therapeutic agents. Interestingly, the $\alpha_5\beta_1$ integrin has shown to regulate the function of $\alpha_v\beta_3$ integrin and to affect the $\alpha_v\beta_3$-mediated endothelial cell migration and angiogenesis [490]. Gentilucci *et al.* have synthesised a series of cyclotetrapeptide mimetics, including compound **33** which contained a Arg-Gly-Asp sequence, and which displayed good inhibitory activity against $\alpha_v\beta_3$ integrin-mediated cell adhesion of vitronectin or fibronectin. Capillary tube formation induced by bFGF was inhibited at sub-micromolar concentrations and these compounds did not exhibit any cytotoxicity to HUVECs [491]. Further evaluation of these compounds in *ex-vivo* and *in vivo* assays may provide a better understanding of their mechanism of action and identify their true potential.

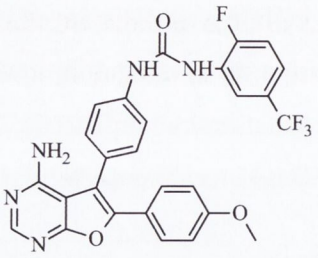

30

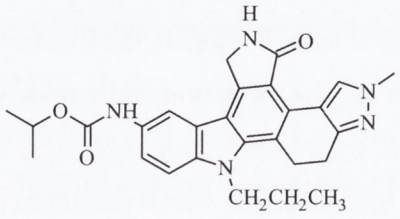

31

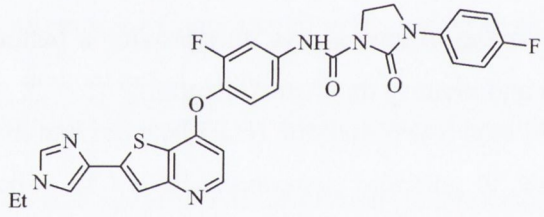

32

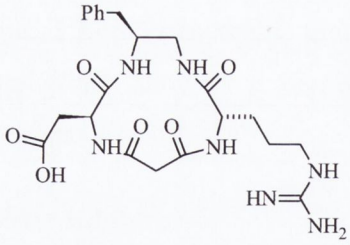

33

Figure 1.26: Multi-target inhibitors of VEGFR2 and Tie-2 tyrosine kinases **30** [483] and **31** [484], VEGFR2/c-Met **32** [489] and $\alpha_v\beta_3/\alpha_5\beta_1$ **33** [491].

The evaluation of multiple-target inhibitors differs from that of hybrids/conjugates. During the evaluation of a true hybrid it is crucial to investigate the effect of a 1:1 combination of both components; however the absence of the two moieties in a dual/multi-targeted inhibitor leads only to the assessment of the actual compound. It is

important to examine thoroughly all the targets of the inhibitor and confirm the mechanism of action by which the inhibition is exerted.

1.9 Project Aims

This project involves the *in vitro*, *ex vivo* and *in vivo* evaluation of novel tubulin polymerisation inhibitors, dual-acting hybrids and a designed multiple ligand (DML), which target tubulin polymerisation and APN.

The tubulin targeting compounds were chosen for evaluation for a number of reasons, including their: a) anti-proliferative effect on both endothelial and tumour cells, b) ability to induce morphological changes to endothelial cells, alter their motility and invasiveness properties, c) anti-vascular activity caused by either morphological changes or by interaction with adhesion molecules, such as E-cadherin and d) anti-angiogenic effect resulted by interfering with either cell proliferation or morphology.

The hybrids were indented to target tubulin polymerisation and APN. APN was chosen as a target due to its over-expression on proliferating vasculature undergoing angiogenesis but not on the normal vasculature, as well as its over-expression on specific type of tumour cell types, including PC-3 cells. The inclusion of an APN targeting moiety, such as bestatin, was due to its well known anti-angiogenic activity and its ability to inhibit invasion and metastasis. In the DML's case, a selected tubulin inhibitor was conjugated to a hydroxamic acid, which exhibit APN inhibitory properties.

The incorporation of bestatin into the design of these hybrids also serves to improve their solubility, by generating more polarised compounds. In addition, this hybrid design enables the formation of prodrugs and salts for *in vivo* purposes.

The novel compounds synthesised in this lab are divided into different groups, according to their target and mechanism of action and which are summarised in Figure 1.29.

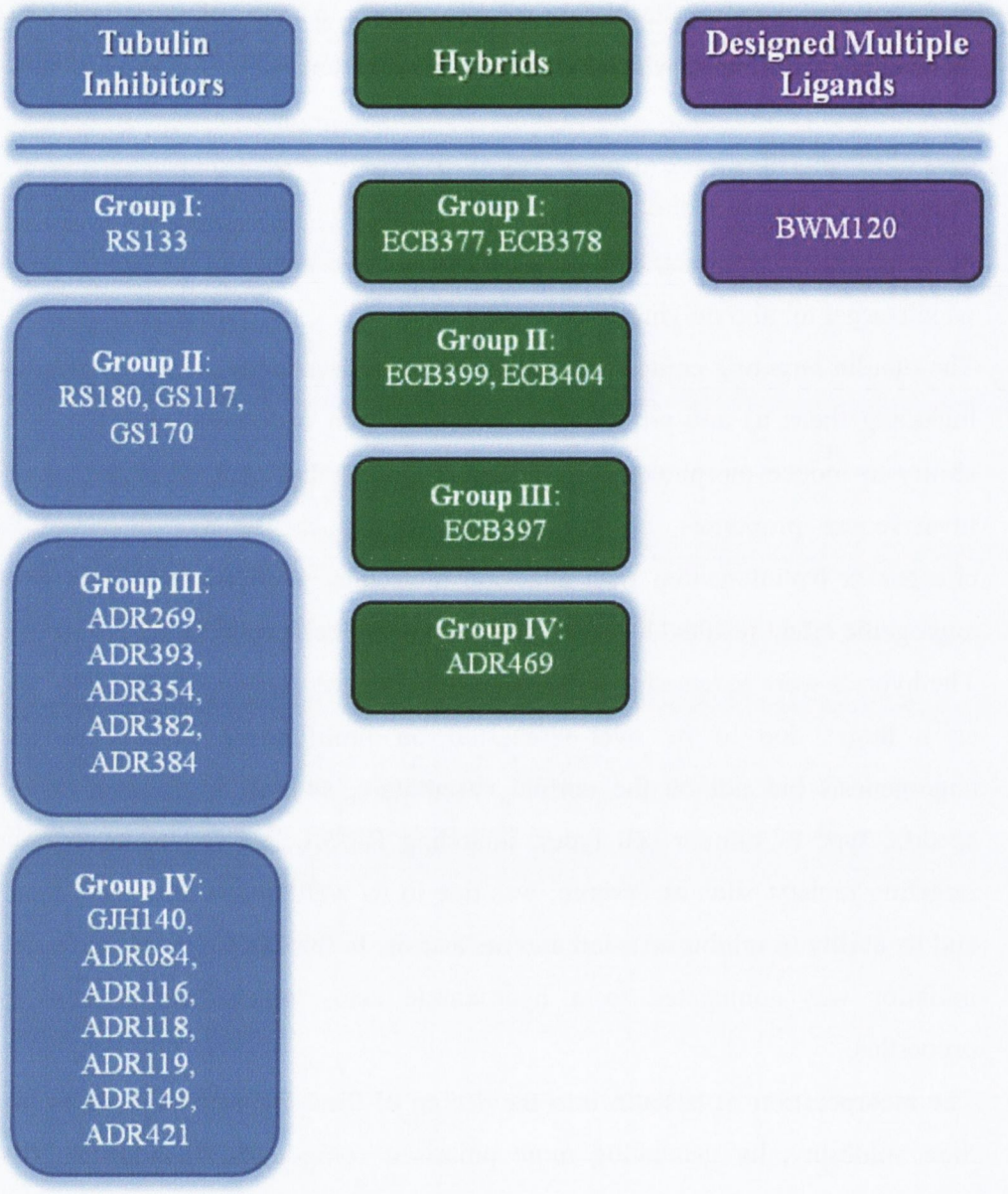

Figure 1.27: The group of compounds evaluated include tubulin polymerisation inhibitors, dual-targeting hybrids and DML.

1.9.1 Overall Aims

Following the design and synthesis of the novel tubulin polymerisation inhibitors, hybrids and DML, it was necessary to evaluate their anti-vascular, anti-angiogenic and anti-tumour activities *in vitro*, *ex vivo* and *in vivo*. Therefore the overall aims of this study were to:

- Determine the anti-proliferation effect of test compounds in proliferating HUVECs and PC-3 human prostate adenocarcinoma cells.
- Investigate the effect of test compounds on the tubulin cytoskeleton of endothelial cells.
- Examine the cell cycle stage of HUVECs and/or PC-3 cells, for evidence of an anti-mitotic effect, following treatment with test compounds.
- Evaluate the *in vitro* anti-vascular effect of test compounds by examining the endothelial cells' morphology and determine the effect's reversibility.
- Assess the anti-vascular and the anti-angiogenic effects of test compounds in the *ex-vivo* aortic ring assay.
- Determine the APN inhibitory activity of hybrids and DML in an enzymatic assay and in two cell-based assays, using HUVECs and PC-3 cells.
- Explore the cell cycle stage of HUVECs and PC-3 cells, for evidence of cell death (apoptosis), following treatment with the hybrids and DML.
- Investigate the *in vivo* anti-tumour activity of selected compounds in a s.c. PC-3 tumour xenograft model and observe any apparent systemic toxicity.
- Examine PC-3 tumour samples following completion of each efficacy study, evaluating the overall tumour necrosis and the anti-vascular effect of test compounds.

-- Chapter 2 --

In Vitro Evaluation of Novel Tubulin Polymerisation Inhibitors

2. Introduction

Novel compounds with potent tubulin polymerisation inhibition were previously developed in our lab. Four different groups of compounds were synthesised with a view to improve the tubulin binding activity, overcome solubility issues, and generate prodrugs or salts for *in vivo* evaluation. The four groups of compounds are as follows:

- Group I: RS133, synthesised by Shah.
- Group II: RS180, GS117 and GS170, synthesised by Stack.
- Group III: ADR269, ADR354, ADR382, ADR384 and ADR393, synthesised by Coogan.
- Group IV: GJH140, ADR084, ADR116, ADR118, ADR119, ADR149 and ADR421, synthesised by Coogan.

2.1 Compound Series

2.1.1 Group I Compound

The most active tubulin polymerisation inhibitor in group I was previously determined by McCormack (2002) to be RS133, which shares structural similarities with phenstatin *i.e.* both structures display a benzyl ring with three methoxy groups (A-ring), and a benzyl ring with a hydroxyl and a methoxy group (C-ring) (Figure 2.1). In addition, RS133 and colchicine both display the A-ring and a seven membered ring (B-ring). Structure-activity relationship (SAR) studies on colchicine have shown that the hydrophobic, electron rich A-ring is essential for binding to tubulin, therefore no modifications were made there. RS133 was previously evaluated in the tubulin polymerisation assay and the IC_{50} was determined to be 6.70 μM. CA-4 was used as a positive control and evaluated in the tubulin polymerisation assay, where its IC_{50} value was 1.45 μM. Further biological evaluation of RS133 was therefore undertaken.

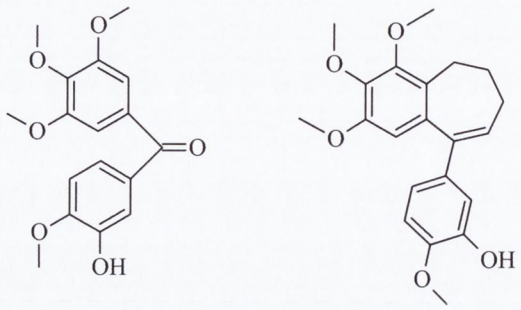

Phenstatin RS133

Figure 2.1: Phenstatin and group I compound RS133.

2.1.2 Group II Compounds

RS180 was the lead compound in this series synthesised first by Shah and later by Stack. A carbonyl group at position-7 on the B-ring was added in order to alter the shape and affect the electronic properties of the A- and C-rings. The low IC_{50} value (1.05 μM) of RS180 previously determined in the tubulin polymerisation assay indicated that RS180 is not only more potent than RS133, but also than CA-4. In order to improve the solubility of RS180 and facilitate the development of prodrugs or salts, the phenol of the C-ring was replaced with aniline, giving GS117. RS180 was also conjugated to a succinate linker unit at position-7 producing GS170, to provide the possibility of generating hybrids or prodrugs (Figure 2.2).

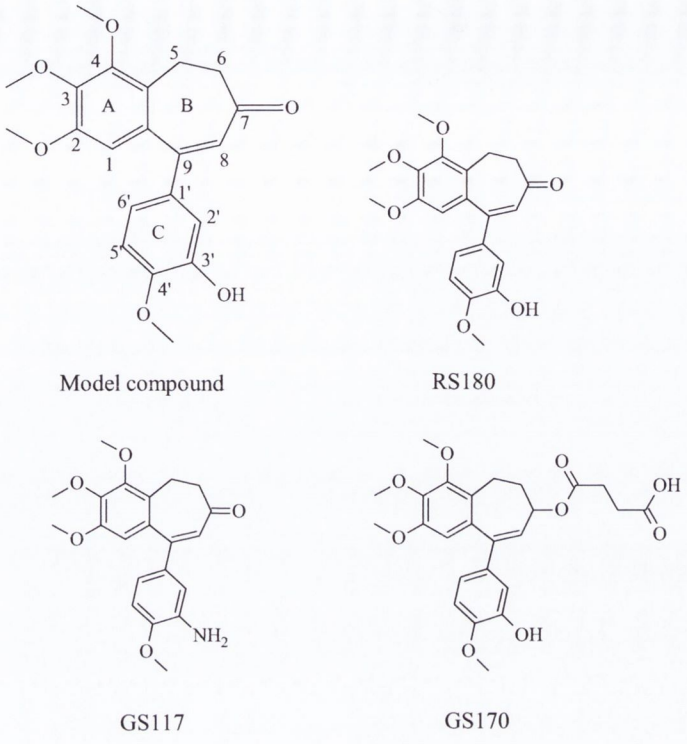

Figure 2.2: Group II compounds: RS180, GS117 and GS170.

2.1.3 Group III Compounds

Group III compounds aimed to improve the tubulin binding affinity by increasing the electronic density in the A-ring and by altering the shape of the B-ring. For that reason, the benzylic methylene group at position-5 of the B-ring was replaced with an oxygen atom to generate ADR269 (first synthesised by Shah and later by Coogan.) The IC_{50} value of ADR269 in the tubulin polymerisation assay was previously determined to be 3.12 μM. Further analogues of ADR269 were developed by Coogan including ADR354, ADR382, ADR384 and ADR393 (Figure 2.3). ADR354 contains a carbonyl group at position-6 and a methoxy group at position-7. ADR382 has a hydroxyl group at position-7 of the B-ring and contains a C-ring without a phenolic group at position-3'. ADR384 is an analogue of ADR269 without a phenolic group at position-3', while ADR393 contains an aniline moiety at position-3', allowing the formation of alanine salts or prodrugs that could be cleaved by APN.

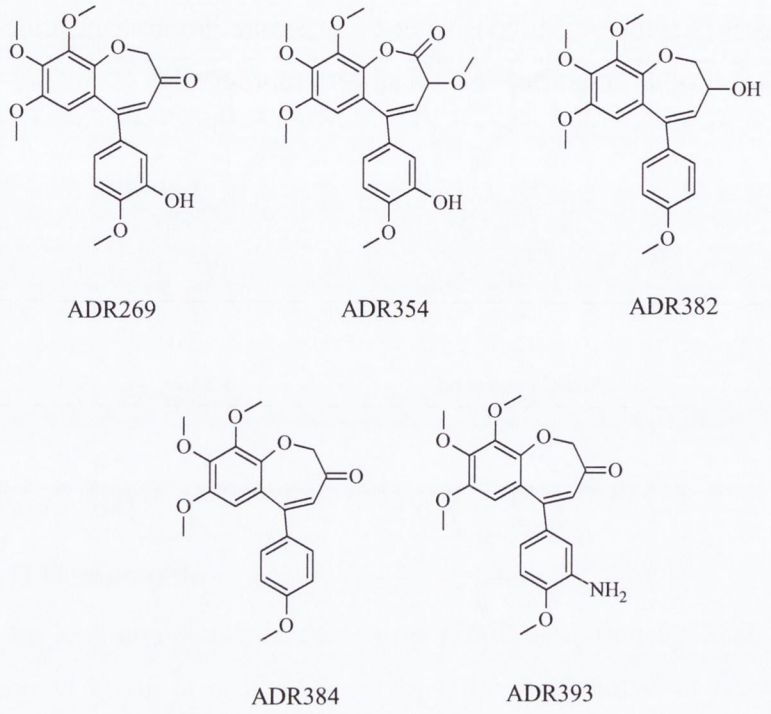

Figure 2.3: Group III compounds, ADR269, ADR354, ADR382, ADR384 and ADR393.

2.1.4 Group IV Compounds

The structure of group IV compounds is based on 4-phenyl-chromanones (1-benzopyran-2-one) which are naturally occurring compounds. Chromanone-based compounds are used in the pharmaceutical industry as precursors in the synthesis of anticoagulants such as warfarin. GJH140 was the first compound designed in this series, initially synthesised by Hudson and then by Coogan, which has a carbonyl group at position-5 of the B-ring, a hydroxyl group at position-8 and a methoxy group at position-9. The IC_{50} value of GJH140 in the tubulin polymerisation assay was previously determined to be 0.6 μM, suggesting that GJH140 is a more potent tubulin binding agent than CA-4 by more than 2-fold. Subsequently, analogues of GJH140 were synthesised by Coogan in order to investigate the best structural design based on their *in vitro* activity (Figure 2.4). ADR084 has an extra hydroxyl group at position-10, whereas ADR116 possess no hydroxyl groups on the C-ring. ADR118 has the hydroxyl group at position-8 replaced by a methyl group. ADR119 displays a similar structure to that of ADR116 with the only difference being the replacement of the methoxy group with a thioether group at position-9. In order to improve the solubility of GJH140,

ADR149 was synthesised, consisting of an amine group at position-8, thus providing the opportunity for the formation of salts or prodrugs.

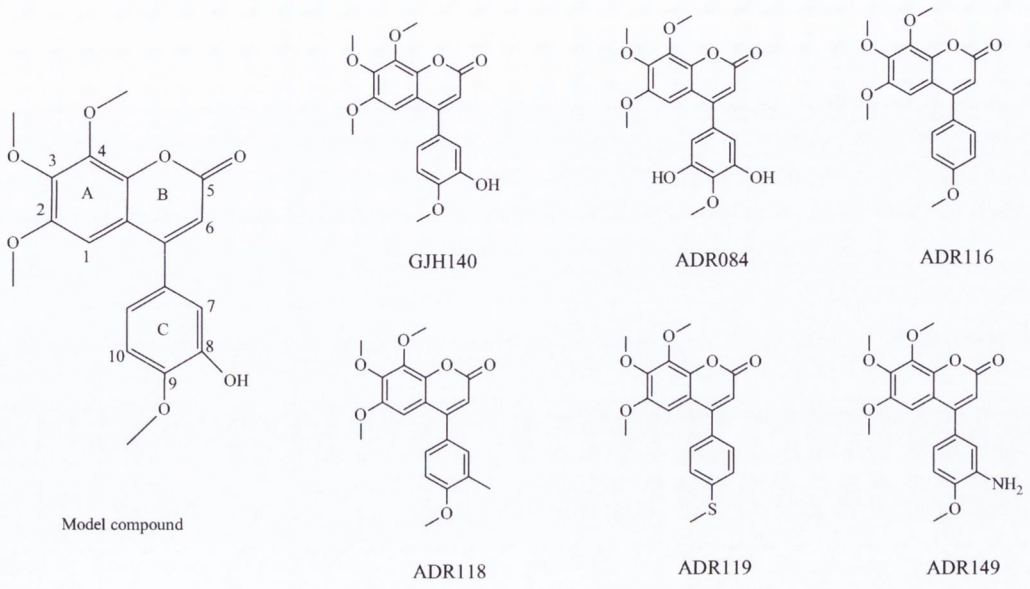

Figure 2.4: Group IV compounds, GJH140, ADR084, ADR116, ADR118, ADR119 and ADR149.

ADR241 is a DML which incorporates within its design part of GJH140 and part of CA-4's structure. In theory, this compound could potentially bind to tubulin from the south-west or the east-south facing side of the molecule, suggesting a possibly stronger tubulin binding affinity (Figure 2.5).

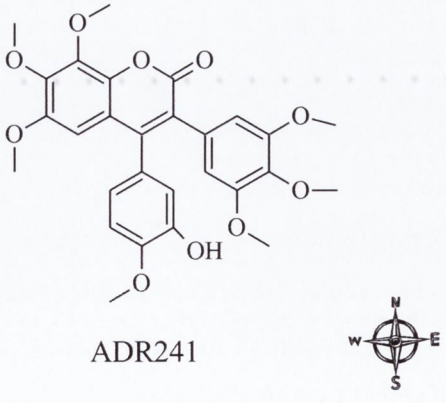

Figure 2.5: The DML ADR241.

2.1.5 Tubulin Polymerisation Inhibitors as VDAs

Tubulin binding agents are well known for their anti-proliferative and anti-mitotic effects, which are mediated by the disruption of the tubulin cytoskeleton, leading to mitotic cell death. Several tubulin binding agents such as PTX and vincristine are used as cytotoxic chemotherapeutic agents. Moreover, the discovery and evaluation of the tubulin targeting agent CA-4, led to its development as a VDA due to the extensive tumour vascular damage observed *in vivo* at relatively non-toxic doses [308]. In addition to the anti-vascular effect, CA-4 also demonstrated anti-angiogenic activity at lower non-toxic concentrations [492].

Once it was established that the test compounds exhibited potent inhibition of tubulin polymerisation, the following step was to select, develop and validate cell-based assays, in order to evaluate their activity *in vitro*. It was hypothesised that due to structural similarities with CA-4, our test compounds would possess similar inhibitory effects on cell proliferation and division and exhibit anti-vascular and anti-angiogenic properties. Therefore, test compounds were mainly evaluated as VDAs, anti-tumour agents and to a lesser extent as anti-angiogenic agents. Firstly, it was essential to examine the effect of test compounds on cell proliferation of human endothelial and prostate cancer cells. In order to establish whether the anti-proliferative effect was as a result of a mitotic arrest, cell cycle analysis was performed. To confirm that inhibition of cell growth and induction of cell cycle arrest was due to a disruption of microtubule dynamics, the tubulin cytoskeleton was visualised, following exposure to test compounds. The next step was to determine the *in vitro* anti-vascular effect of test compounds by examining endothelial cells' morphology. The final *in vitro* study aimed to investigate any evidence of angiogenesis inhibition following continuous treatment with a selected compound, RS180.

The preliminary *in vitro* screening of the test compounds aimed to provide a better understanding of the compounds' mechanism of action and classify which functional groups provide an improved pharmacological profile. Furthermore, the preliminary *in vitro* data obtained served to identify the compounds with the most potential and encourage further *ex vivo* and *in vivo* evaluation.

2.1.6 Aims

The novel tubulin polymerisation inhibitors designed and synthesised in our lab were evaluated *in vitro* as VDAs, therefore the primary aims of this project were to:

- Determine the anti-proliferative effect of test compounds on HUVECs and PC-3 human prostate adenocarcinoma cells, using the MTT assay.
- Establish the anti-mitotic activity of test compounds by analysing the cell cycle stages, using PI staining followed by a flow cytometric technique.
- Visualise the disruption of the tubulin cytoskeleton of endothelial cells following treatment with test compounds, using immunofluorescence staining and confocal microscopy.
- Examine the morphological changes of endothelial cells caused by test compounds and further evaluate the effect's reversibility.
- Assess the anti-angiogenic properties of a selected compound, RS180, using an *in vitro* human angiogenesis assay (AngioKit assay).

2.1.7 Background to the Protocols Used

2.1.7.1 MTT Assay

The MTT assay was used to assess the anti-proliferative activity of test compounds. The assay was first described by Mosmann *et al.* but further modifications were made in order to adjust the assay to the purpose of our experiments [493]. This is a quantitative colorimetric assay which detects viable, but not dead cells, by generating a signal dependent on the degree of cell activation. MTT (3-(4, 5-Dimethylthiazol-2-yl)-2, 5-diphenyltetrazolium bromide) a yellow tetrazole, is reduced by active reductase enzyme present only in viable cells, to purple formazan insoluble crystals which are then solubilised by either dimethyl sulfoxide (DMSO) or an acidified ethanol solution to give a coloured solution. The absorbance of this can be quantified by measuring at a wavelength between 500 and 600 nm using a spectrophotometer. The MTT assay is widely used and is considered a precise and rapid assay that can be used for the screening of multiple compounds [493].

2.1.7.2 Cell Cycle Analysis

Proliferating cells are constantly dividing to produce daughter cells. The most obvious cellular structure that requires duplication and division is the cell nucleus, where DNA is present. During the cell cycle there are changes in the DNA content and thus there are different cycle stages, including G_0, G_1, S, G_2 and M (mitosis). The G_0 stage of the cycle is a subset of G_1 where the cells are quiescent and have limited cellular functions. Cells remain in the G_1 portion of the cycle when not in a process of cell division and thus G_1 phase is the most predominant phase of the cycle appearing as the largest peak. In addition, during the G_1 phase synthesis of many RNA and protein molecules is taking place which are necessary for DNA synthesis. G_2 phase is a period for repair of any damaged DNA and for reorganisation of the DNA structure before entering into the M phase. Cell cycle abnormalities could be a sign of cell damage, for example DNA damage causes interruption of the cell cycle at certain checkpoints such as the spindle assembly checkpoint (SAC), to prevent carcinogenesis [494].

The mitotic spindle is composed of microtubules which together with regulatory proteins assist in the activity of properly segregating replicated chromosomes. It is well established that treatment of cells with tubulin polymerisation inhibitors causes a G_2/M phase arrest of the cell cycle and thus an observable increased DNA content at that stage [495-497].

For this reason, cell cycle analysis was carried out by PI staining followed by flow cytometric analysis. The initial protocol was presented by Krishan *et al.* in 1975 [498]. The first step involves permeabilisation of the cells' plasma membrane by fixating the cells in ethanol, in order to facilitate intracellular uptake of the fluorescent DNA dye. Ribonuclease A (RNase A) serves to eliminate any RNA present within the cells in order to avoid creating artefacts that could affect the results. PI was used for the staining of the cells' DNA content; however other fluorescent dyes can be used instead, including 4', 6-diamidino-2-phenylindole (DAPI) and Hoechst 33342.

Flow cytometry was used to quantify the cells' DNA content. This is a technique which was first introduced by Fulwyler *et al.*, which examines and counts cells or other microscopic particles by suspending them in a stream of fluid and passing them by an electronic detection apparatus [499]. Cells pass through the flow cytometer's laser

where a fluorescence pulse is generated, which correlates with the amount of DNA dye present intracellularly. Cell aggregates are excluded from analysis through double discrimination.

2.1.7.3 Immunofluorescence Staining of the Microtubules

In order to confirm that test compounds are able to interfere with the tubulin cytoskeleton, immunofluorescence staining was performed followed by examination using confocal microscopy. The effect of test compounds on tubulin reorganisation was visualised by staining of the microtubules using an α-tubulin antibody and the cell nuclei using DAPI [497].

2.1.7.4 Analysis of Endothelial Cells' Morphology

Tubulin inhibitors are not only known for their anti-mitotic effects but also for their anti-vascular activity. Treatment with such agents was previously shown to cause vascular shutdown, independently of a direct cytotoxic effect on tumour cells [302]. Hence, the endothelial cells' morphology was examined after treatment with test compounds at 1h and 3h after drug washout. The 1h incubation period aimed to identify any observable morphological changes of endothelial cells, while the 3h incubation period served to indicate any signs of the effect's reversibility [500].

2.1.7.5 *In vitro* Angiogenesis Assay

In addition to their anti-mitotic and anti-vascular activity, tubulin targeting agents such as CA-4 exhibit anti-angiogenic effects at lower doses that do not inhibit the proliferation of endothelial cells [492]. Therefore, the anti-angiogenic effect of RS180 was evaluated using the AngioKit assay which was supplied from TCS Cellworks. This assay is a co-culture of HUVECs and matrix-producing cells which represent a better *in vitro* angiogenesis model than a culture of HUVECs alone [501].

2.2 Materials and Methods

2.2.1 Materials

Dimethyl sulfoxide (DMSO), (3-(4, 5-Dimethylthiazol-2-yl)-2, 5-diphenyltetrazolium bromide (MTT), foetal bovine serum (FBS), streptomycin/penicillin solution, 0.25% trypsin/EDTA solution, CA-4, ribonuclease A from bovine pancreas (RNase), PI, monoclonal mouse anti-α-tubulin antibody and crystal violet were all purchased from Sigma, Ireland. Phosphate buffered saline (PBS) tablets, Alexa Fluor® 488 goat anti-mouse IgG, ProLong® gold antifade reagent with DAPI were purchased from Invitrogen, Ireland. AngioKit assay, endothelial growth medium (EGM), blocking buffer, mouse anti-human CD31 antibody, goat anti-mouse IgG alkaline phosphatise conjugate and insoluble substrate were purchased from TCS Cellworks, UK. Greiner CELLSTAR® 75 cm^2 cell culture flasks, Greiner 96-well PS cell culture microplates, with solid U-bottom, Greiner 6-well plates and Greiner 12-well plates were purchased from Cruinn, Ireland. Frosted end microscopy slides and cover slips were purchased from VWR, Ireland.

2.2.2 Test Compounds

For *in vitro* evaluation, stock solutions of test compounds were prepared in DMSO and then diluted in the appropriate medium or buffer to provide the required concentrations. The maximum final DMSO concentration was $\leq 0.1\%$. Control solutions consisted of 0.1% DMSO in the appropriate medium or buffer. In each experiment a positive control was used. Fresh solutions were prepared prior to each experiment.

2.2.3 Cell Lines

HUVECs were obtained from TCS Cellworks, UK and cultured in endothelial cell basal medium (EBM), supplemented with growth factors and antibiotics (TCS Cellworks, UK). The PC-3 human prostate adenocarcinoma cell line was purchased from LGC Standards, UK and cultured in F12K medium supplemented with 0.02 mg/mL sodium pyruvate, 10% FBS and 10 mL/L penicillin/streptomycin solution. Cell and tissue cultures were kept at 37 °C in a humidified atmosphere, containing 5% CO_2 at all times.

2.2.4 Cell Maintenance and Sub-culture

Cell culture experiments were performed under a NuAire class II biological safety cabinet and aseptic techniques were followed at all times to prevent contamination. HUVECs/PC-3 cells were culture in 75 cm^2 cell culture flasks using 15 mL of the appropriate complete medium. Cells were monitored daily using an Olympus CKX41 inverted microscope (Mason Technology, Ireland). Once the cells reached 70-80 % confluence they were sub-cultured as follows: the old medium was removed from the flasks, the cell monolayer was gently rinsed with 10 mL of PBS, 3 mL of trypsin/EDTA solution was added in each flask and incubated at 37 °C until 90% of the cells rounded up (no longer than 5-10 minutes). The flasks were tapped to detach the cells and 5 mL of complete medium was added into the flasks and then transferred into a centrifuge tube. The flasks were rinsed with a further 5 mL of complete medium to collect residual cells and added to the rest of the cells in the tube. Centrifugation took place for 5 minutes at 1000 rpm at 25 °C. Following that, the supernatant was removed and 3mL of fresh medium was added to gently mix the cells.

In order to reseed the cells, 15 mL of complete medium was added to each flask and pre-equilibrated in the CO_2 incubator for at least 30 minutes. The cell suspension was then sub-cultured in the new flasks at 1:4 or 1:6 seeding densities and returned to the incubator. The following day, cells were examined microscopically to ensure the reseeding was successful and the medium was replaced with pre-equilibrated fresh medium. Every 2-3 days the medium was changed.

2.2.5 Cell Count

The estimation of cell densities was determined using a haemocytometer. Once the cells reached 70-80% confluence the same procedure was followed as previously described (*i.e.* cell trypsinisation and collection). After the centrifugation step, the cell pellet was re-suspended in 10 mL of complete medium and mixed gently. The haemocytometer was cleaned with 70% ethanol and the cover slip was affixed using gentle pressure and circular motions. If the phenomenon of Newton's rings was observed the coverslip was correctly placed on the haemocytometer. The haemocytometer was filled with cell suspension by resting the end of the pipette tip at the edge of the chambers, without overfilling them. The samples were allowed to be drawn out of the pipette by capillary

action. Using the x4 objective of the inverted microscope to focus on the grid lines of the haemocytometer, the cells were counted in each of the 16 corner squares using a hand tally counter. Cells were included in the count only if they were within the square or positioned on the left hand or bottom boundary line. Counting was carried until all 5 sets of 16 corner squares (including the one in the middle) were counted and an average count was obtained using the following formula:

$(C_1+C_2+C_3+C_4+C_5)/5$ where C = count per 16 corner squares.

The haemocytometer is designed so that the number of cells in the 16 corner squares is equivalent to the number of cells x 10^4/mL. Therefore, to calculate the number of cells/mL, the average count of cells was multiplied by 10 (or depending on the total volume of cell suspension) and then by 10^4. In order to determine the required cell density in each experiment, the following formula was used:

$C_1V_1 = C_2V_2$ where C = concentration and V = volume.

2.2.6 Cell Proliferation Assay

Cell growth inhibition was assessed using the MTT assay. $5x10^4$ cells/well HUVECs or PC-3 cells (180 µL) were inoculated into a 96-well plate and incubated overnight at 37 °C. Compounds or control solutions (20 µL) were added into each well and the plates were incubated for 72h at 37 °C. CA-4 was used as a positive control. After the incubation period, the culture medium was removed and replaced by 200 µL of 0.5 mg/mL MTT solution in complete medium. Following further 4h incubation, the solution was removed from each well and replaced by 180 µL of DMSO to solubilise the formazan crystals resulting from the MTT conversion. Absorbance values (Abs) for the resulting solutions were read at 584 nm using a FLUOstar OPTIMA microplate reader (BMG Labtech) and cell survival was calculated as the absorbance of treated cells divided by the control. Each compound concentration was tested in quadruplicate and each experiment was performed three independent times. The percentage growth inhibition was determined using the formula below and the results were expressed in terms of IC_{50} values ± standard error of mean (SEM).

*% growth inhibition = 100-[(mean Abs of test compound)/(mean Abs of control)]*100*

2.2.7 Cell Cycle Analysis – G_2/M Phase

Cell cycle arrest at the G_2/M phase was examined by PI staining. $1x10^6$ cells/well (1 mL) HUVECs and/or PC-3 cells were seeded in 6-well plates and incubated overnight at 37 °C. Stock solutions of test compounds were diluted with complete medium. CA-4 was used as a positive control. Cells were treated with 1 mL of test compounds for 24h at 37 °C. Next, the cells were harvested by trypsinisation, washed with 3 mL of PBS and centrifuged at 1000 rpm at 25 °C for 5 minutes. The cell pellet was first re-suspended in 300 µL of PBS and then in 3mL of 70% ethanol (in PBS). Cell suspensions were kept at 4 °C until ready for analysis. Prior to analysis, cell suspensions were centrifuged at 2000 rpm at 4 °C for 5 minutes and all the ethanol was removed from each tube. The RNAse (10 mg/mL) and PI (1 mg/mL) stock solutions were prepared in PBS. The cell pellet was re-suspended in 300 µL of PBS, and 25 µL of RNAse solution and 75 µL of PI solution were added to each sample and incubated at 37 °C for 30-40 minutes. Samples were analysed using a Beckman Coulter (Dako) 2-laser CyAn ADP analyser, provided by the School of Biochemistry and Immunology, Trinity College Dublin (TCD). Cell cycle analysis was obtained by examining the PI-positive DNA content, particularly focusing on the G_2/M phase. Each compound concentration was tested in duplicate and each experiment was performed three independent times. The results were expressed in terms of mean percentage of cells present in the G_2/M phase ± SEM and statistical significance between the control and treated groups was determined using the Student's *t*-test.

2.2.8 Immunofluorescence Staining of the Microtubules

The effect of the compounds on microtubules disruption was examined by staining the cells for α-tubulin. Sterile cover slips were placed in each well of a 6-well plate and $1x10^6$ cells/well (1 mL) HUVECs were seeded and allowed to attach onto the cover slips overnight at 37 °C. The following day the medium was removed from the wells, replaced with 1 mL of test compounds diluted in medium (final concentration 1 µM), and incubated for 30 minutes at 37 °C. Next, the medium was removed and the cells were fixed in 1 mL of pre-cooled methanol at -20 °C for 30 minutes. Then, the cells were washed twice with 1 mL of PBS (for 5 minutes each time). The primary monoclonal antibody for α-tubulin was diluted in PBS (1:200) and 1 mL of that was

added in each well for 1h at room temperature (RT). After that, the cells were washed three times with 1 mL of PBS and incubated with 1 mL of secondary Alexa Fluor® 488 antibody diluted in PBS (1:1000) for 30 minutes at RT in the dark. The cells were washed a further three times with 1 mL of PBS and allowed to air-dry for 10 minutes. The cover slips containing the attached cells were mounted on microscopy slides using ProLong® gold antifade reagent with DAPI (for nuclear staining) and stored at 4 °C until required for analysis. Images were taken using an Olympus FV1000 point scanning confocal microscope provided by the School of Biochemistry and Immunology, TCD. Experiments were performed in duplicate at two independent times. The results were presented as images of the microtubule disruption of endothelial cells.

2.2.9 Analysis of Endothelial Cells' Morphology

The effect of test compounds on endothelial cells' morphology was examined. $1x10^6$ cells/well HUVECs (1 mL) were seeded into 6-well plates and incubated overnight at 37 °C. The following day, the medium was removed and replaced by test compounds diluted in fresh medium. The cells were incubated for 40 minutes at 37 °C. Following that, each well was washed with medium to remove detached cells and incubated with fresh medium for a further 1h or 3h at 37 °C. Next, the medium was removed, 0.5% crystal violet solution was prepared in 20% ethanol and 1 mL was added in each well for 15 minutes at RT. The wells were then washed 3 times with distilled water (d.w), for 5 minutes each time. Wells were allowed to air dry and cell morphology was examined under an Olympus CKX41 inverted microscope using a x4 objective. Images were captured with an E-330 SLR camera system 1h and 3h after washout. Digital images were processed using Cell^A software (Mason Technology, Ireland). The experiments were performed in triplicate and the results were presented as images of the morphological changes of endothelial cells after 1h and 3h of drug washout.

2.2.10 *In Vitro* Angiogenesis Assay

In order to analyse the effect of test compounds in a co-culture of human endothelial cells and matrix-producing cells (fibroblasts), the AngioKit assay supplied from TCS Cellworks, UK, was performed. The assay consists of a co-culture of HUVECs and fibroblasts at the earliest stages of tubule formation, growing in a 24-well plate format.

The cultures were maintained in EGM at 37 °C within a 5% CO_2 humidified atmosphere. Controls and test compounds diluted in medium were added on day 1. Culture medium was changed every 2-3 days until day 12. A CD31 staining kit was used in order to visualise the tubule formation. Mouse anti-human CD31 antibody was diluted in blocking buffer, added into each well and incubated for 1h at 37 °C. Then the wells were washed with the blocking buffer 3 times (for 5 minutes each time). The secondary antibody (goat anti-mouse IgG alkaline phosphatise conjugate) was also diluted in blocking buffer, added into each well and the plate was incubated for a further 1h at 37 °C. After that, the wells were washed three times with d.w (for 5 minutes each time). The insoluble substrate was dissolved in d.w and added in each well. The plate was incubated at 37 °C for 10-15 minutes until the tubules developed a dark purple colour. Finally, the wells were washed three times with d.w (for 5 minutes each time) and left to air dry. Images were taken using an Olympus CKX41 inverted microscope and images were captured with an E-330 SLR camera system and processed using Cell^A software (Mason Technology, Ireland). The experiments were performed in triplicate. The mean tubule pixel density in each image was estimated using Adobe Photoshop CS4 and results were presented as the mean pixel density area ± SEM, along with images of the tubule formation. Statistical comparison between the treated and control groups was performed, using Student's *t*-test

2.2.14 Statistical Analysis

Statistical analysis of the data was carried out using GraphPad Prism, version 5. Values of each compound at each concentration were expressed as mean ± SEM. Values were tested for Gaussian distribution and where appropriate IC_{50} values were generated. In order to determine whether there was a significant difference between control and each treatment group, Student's *t*-test was applied, using GraphPad Prism, version 5. One-way ANOVA test was also applied for comparison purposes between all groups, using GraphPad Prism.

2.3 Results

2.3.1 Cell Proliferation Assay

All compounds were tested in the MTT assay using HUVECs and PC-3 cells and their IC_{50} values ± SEM were determined.

2.3.1.1 Group I Compound

Group I compound RS133 demonstrated reasonable anti-proliferating activity against HUVECs and PC-3 cells, with IC_{50} values of 20.26 ± 1.43 nM and 150.00 ± 40.01 nM, respectively. Control compound CA-4 was evaluated for its anti-proliferative activity and IC_{50} values were determined to be 4.03 ± 1.73 nM against HUVECs, and 14.01 ± 0.58 nM against PC-3 cells. Table 2.1 summarises the calculated IC_{50} values.

Table 2.1: Best fit IC_{50} values ± SEM of group I compound, following the MTT assay (n=3).

	HUVECs (nM)	PC-3 (nM)
CA-4	4.03 ± 1.73	14.01 ± 0.58
RS133	20.26 ± 1.43	150.00 ± 40.01

2.3.1.2 Group II Compounds

RS180, GS117 and GS170 were assessed for their anti-proliferative activity on both HUVECs (65.05 ± 1.10 nM, 8.58 ± 1.06 nM and 34.02 ± 5.70 nM, respectively) and PC-3 cells (50.65 ± 1.19 nM, 9.70 ± 0.88 nM and 90.00 ± 3.10 nM, respectively) and found to be relatively active anti-proliferative agents with IC_{50} values in the low nanomolar range. GS117 activity was comparable to that of CA-4. Table 2.2 summarises the IC_{50} values of group II compounds.

Table 2.2: Best fit IC_{50} values ± SEM of group II compounds, following the MTT assay (n=3).

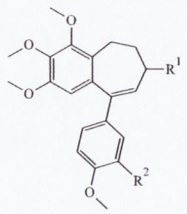

	R^1	R^2	HUVECs (nM)	PC-3 cells (nM)
CA-4	-	-	4.03 ± 1.73	14.01 ± 0.58
RS180	C=O	OH	65.05 ± 1.10	50.65 ± 1.19
GS117	C=O	NH_2	8.58 ± 1.06	9.70 ± 0.88
GS170	Linker	OH	34.02 ± 5.70	90.00 ± 3.10

2.3.1.3 Group III Compounds

The anti-proliferative activity of group III compounds on HUVECs and PC-3 cells was examined. The lead compound ADR269 demonstrated similar potency on HUVECs (4.91 ± 1.01 nM) to that of CA-4, however the inhibitory activity on PC-3 cells (4.67 ± 1.45 nM) was superior to that of CA-4. Although the rest of the analogues in this series displayed inhibition of cell growth, were not as potent as ADR269, with their IC_{50} values varying in the low micromolar range. Table 2.3 summarises the IC_{50} values of group III compounds.

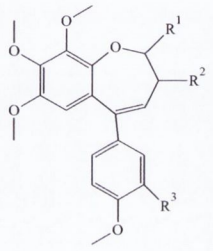

Table 2.3: Best fit IC_{50} values ± SEM of group III compounds, following the MTT assay (n=3).

	R^1	R^2	R^3	HUVECs (μM)	PC-3 cells (μM)
CA-4	-	-	-	4.03 ± 1.73 (nM)	14.01 ± 0.58 (nM)
ADR269	-	C=O	OH	4.91 ± 1.01 (nM)	4.67 ± 1.45 (nM)
ADR354	C=O	OCH_3	OH	1.94 ± 1.73	N/D
ADR382	-	OH	-	4.02 ± 2.80	0.14 ± 0.04
ADR384	-	C=O	-	1.09 ± 0.41	10.00 ± 4.03 (nM)
ADR393	-	C=O	NH_2	0.23 ± 0.15	0.36 ± 0.21

2.3.1.4 Group IV Compounds

The effect of group IV compounds on cell proliferation of HUVECs and PC-3 cells was determined. GJH140's anti-proliferative activity was similar to that of CA-4 against HUVECs (5.56 ± 1.36 nM) and PC-3 cells (4.70 ± 1.19 nM), along with the rest of the compounds in this series which displayed IC_{50} values in the low nanomolar range, the only exception being ADR084 (3.51 ± 2.05 μM against HUVECs and 6.10 ± 3.50 μM against PC-3 cells). The most potent compound in this series was ADR149 with IC_{50} values as low as 1.45 ± 1.15 nM against HUVECs and 3.82 ± 1.15 nM against PC-3 cells. Table 2.4 summarises the IC_{50} values of group IV compounds.

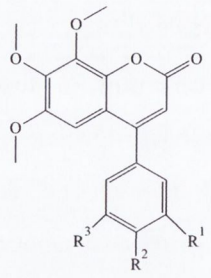

Table 2.4: Best fit IC_{50} values ± SEM of group IV compounds, following the MTT assay (n=3).

	R^1	R^2	R^3	HUVECs (nM)	PC-3 cells (nM)
CA-4	-	-	-	4.03 ± 1.73	14.01 ± 0.58
GJH140	OH	OCH_3	-	5.56 ± 1.36	4.70 ± 1.19
ADR084	OH	OCH_3	OH	3.51 ± 2.05 (μM)	6.10 ± 3.50 (μM)
ADR116	-	OCH_3	-	12.03 ± 0.58	8.50 ± 0.40
ADR118	CH_3	OCH_3	-	7.04 ± 12.12	11.03 ± 1.15
ADR119	-	SCH_3	-	3.01 ± 1.15	8.50 ± 3.46
ADR149	NH_2	OCH_3	-	1.45 ± 1.15	3.82 ± 1.15

The DML ADR241 showed moderate activity in the low micromolar range with IC_{50} values of 14.56 ± 1.54 μM against HUVECs and 4.75 ± 1.13 μM against PC-3 cells. Table 2.5 summarises the IC_{50} for ADR241.

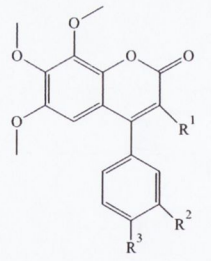

Table 2.5: Best fit IC_{50} values ± SEM of ADR241, following the MTT assay (n=3).

	R^1	R^2	R^3	HUVECs	PC-3 cells
CA-4	-	-	-	4.03 ± 1.73 nM	14.01 ± 0.58 nM
ADR241	Trimethoxybenzene	OH	OCH_3	14.56 ± 1.54 μM	4.75 ± 1.13 μM

2.3.2 Cell Cycle Analysis – G_2/M Phase

Following the preliminary screening of test compounds, the most active tubulin inhibitors were further evaluated. The effect of each compound on the cell cycle of HUVECs was examined for evidence of a G_2/M phase arrest. Statistical comparison between the treated and control groups was performed, using Student's *t*-test.

2.3.2.1 Group I Compound

The cell cycle stage of RS133-treated cells was analysed. The control group showed an ordinary cell cycle profile with the largest peak at the G_1 phase (57.22 ± 0.31 %), followed by a smaller peak at the S phase (15.10 ± 0.93 %) and a final peak at the G_2/M phase (25.21 ± 1.20 %). CA-4 treatment induced a G_2/M phase arrest showing a significant ($p < 0.01$) difference between the treated and control groups at 0.5 μM (80.50 ± 5.82 %) and 1 μM (69.52 ± 8.30 %). RS133-treated cells demonstrated a significant ($p < 0.01$) increase of cells in the G_2/M at 0.5 μM (78.91 ± 2.14 %) and 1 μM (75.95 ± 2.50 %), as shown in Figures 2.6 and 2.7.

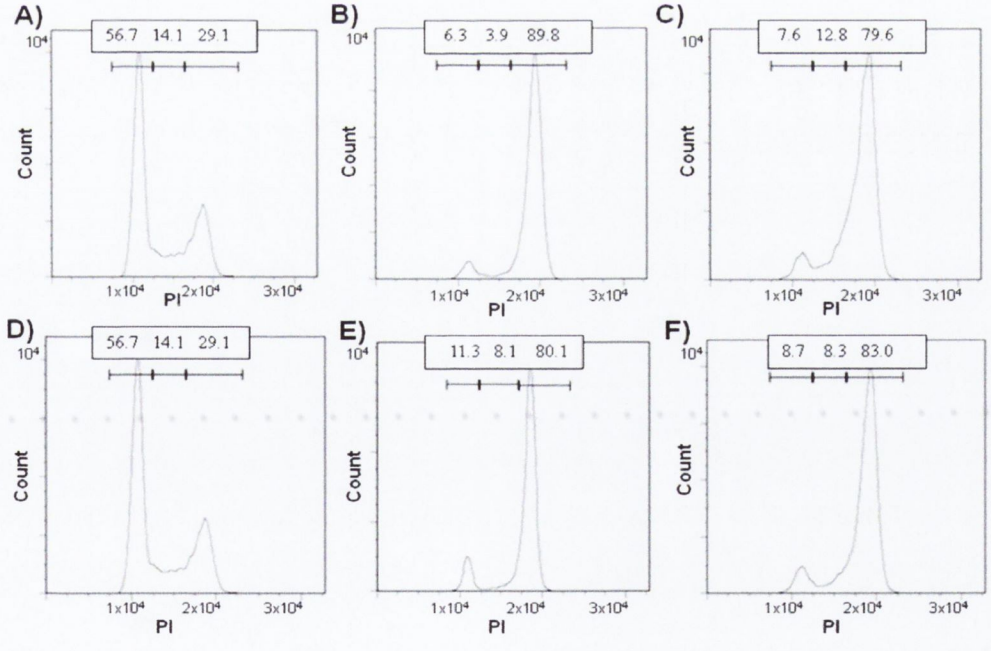

Figure 2.6: Cell cycle histograms of the gated G_1/S/G_2/M cells treated with CA-4 and RS133. HUVECs were treated for 24h, stained with PI and analysed using flow cytometry. **A)** and **D)** Control (0.1% DMSO), **B)** 0.5 μM CA-4, **C)** 1 μM CA-4, **E)** 0.5 μM RS133 and **F)** 1 μM RS133.

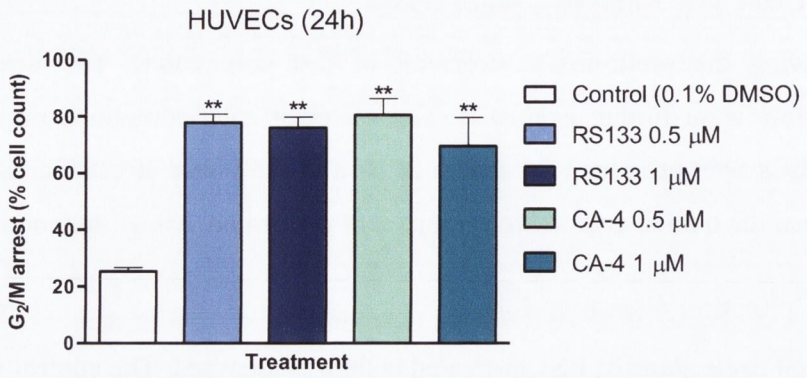

** $p < 0.01$, significantly higher mean % cell count in the G_2/M phase compared with the untreated controls as determined by Student's *t*-test.

Figure 2.7: Percentage of cells in the G_2/M phase treated with RS133 and CA-4. Data represents mean ± SEM (n=3).

2.3.2.2 Group II Compounds

Cell cycle analysis was performed on HUVECs with selected group II compounds, including RS180 and GS117. RS180 exhibited a significant ($p < 0.01$) effect on the cell cycle inducing an arrest at the G_2/M phase (86.30 ± 2.31 % at 0.5 μM and 79.35 ± 1.72 % at 1 μM). Similarly, GS117 at concentrations of 0.5 μM and 1 μM, demonstrated a significant ($p < 0.01$) increase in the percentage of G_2/M phase cells (81.25 ± 0.63 % and 76.07 ± 4.82 %, respectively), as shown in Figures 2.8 and 2.9.

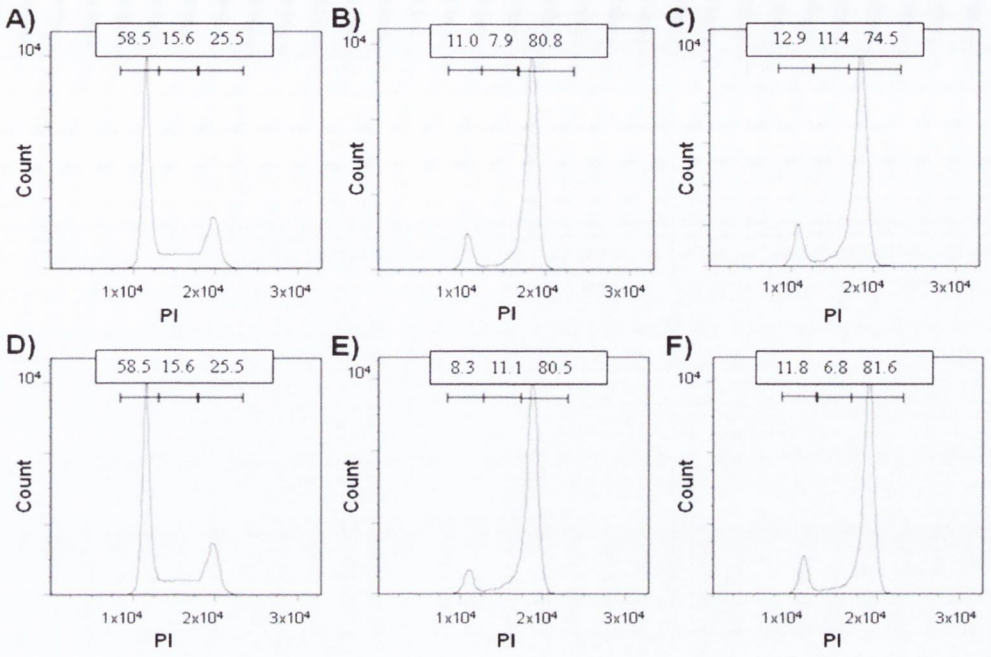

Figure 2.8: Cell cycle histograms of the gated $G_1/S/G_2/M$ cells treated with RS180 and GS117. HUVECs were treated for 24h, stained with PI and analysed using flow cytometry. **A)** and **D)** Control (0.1% DMSO), **B)** 0.5 μM RS180, **C)** 1 μM RS180, **E)** 0.5 μM GS117 and **F)** 1 μM GS117.

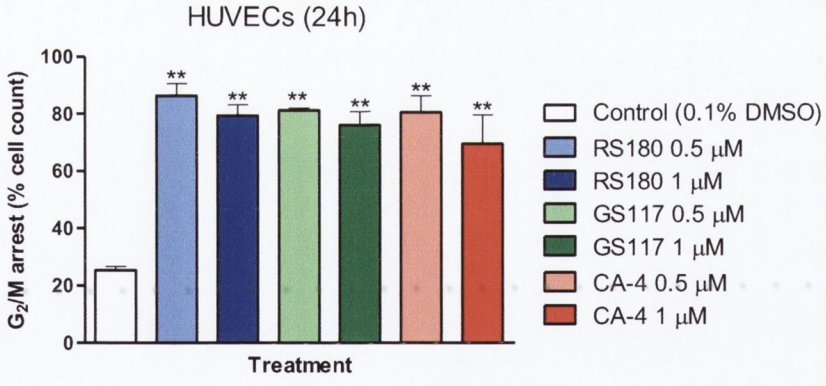

** $p < 0.01$, significantly higher mean % cell count in the G_2/M phase compared with the untreated controls as determined by Student's *t*-test.

Figure 2.9: Percentage of cells in the G_2/M phase treated with RS180, GS117 and CA4. Data represents mean ± SEM (n=3).

2.3.2.3 Group III Compound

Group III compound ADR269 was selected for further evaluation to examine its ability to induce G_2/M phase arrest of endothelial cells. The percentage of ADR269-treated cells (71.20 ± 7.12 %) at 1 μM detected in the G_2/M phase was significantly ($p < 0.01$) higher than that of control treated cells (31.44 ± 0.82 %), as shown in Figures 2.10 and 2.11.

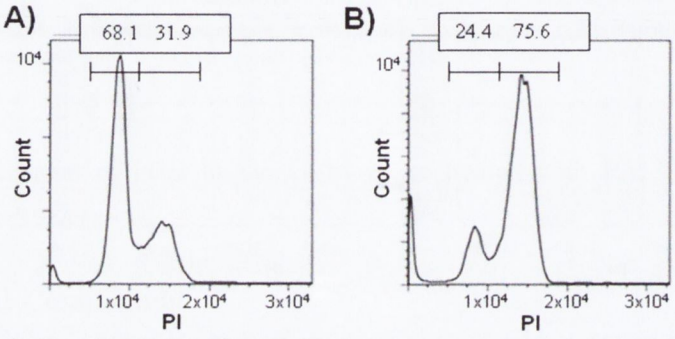

Figure 2.10: Cell cycle histograms of the gated G_2/M cells treated with ADR269. HUVECs were treated for 24h, stained with PI and analysed using flow cytometry. **A)** Control (0.1% DMSO) and **B)** 1 μM ADR269.

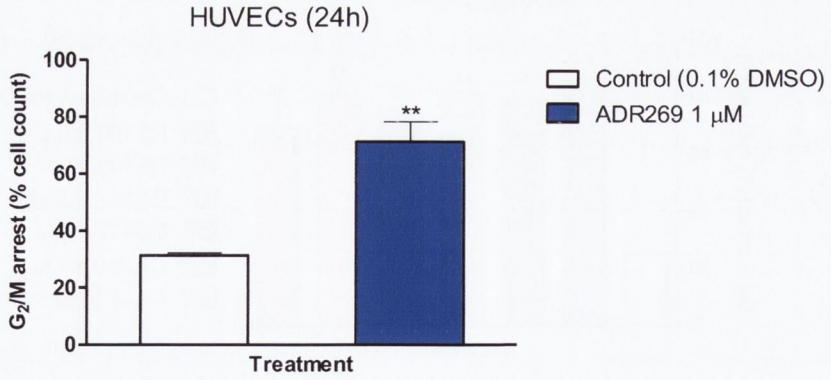

** $p < 0.01$, significantly higher mean % cell count in the G_2/M phase compared with the untreated controls as determined by Student's *t*-test.

Figure 2.11: Percentage of cells in the G_2/M phase treated ADR269. Data represents mean ± SEM (n=3).

2.3.2.4 Group IV Compounds

Group IV compounds, GJH140 and ADR149, were examined in the cell cycle analysis. A significant ($p < 0.01$) G_2/M phase arrest was observed in GJH140-treated cells at 0.5 μM (81.22 ± 1.43 %) and 1 μM (81.42 ± 4.20 %) and in ADR149-treated cells at 0.5 μM (77.91 ± 3.72 %) and 1 μM (69.63 ± 3.11 %), as shown in Figures 2.12 and 2.13.

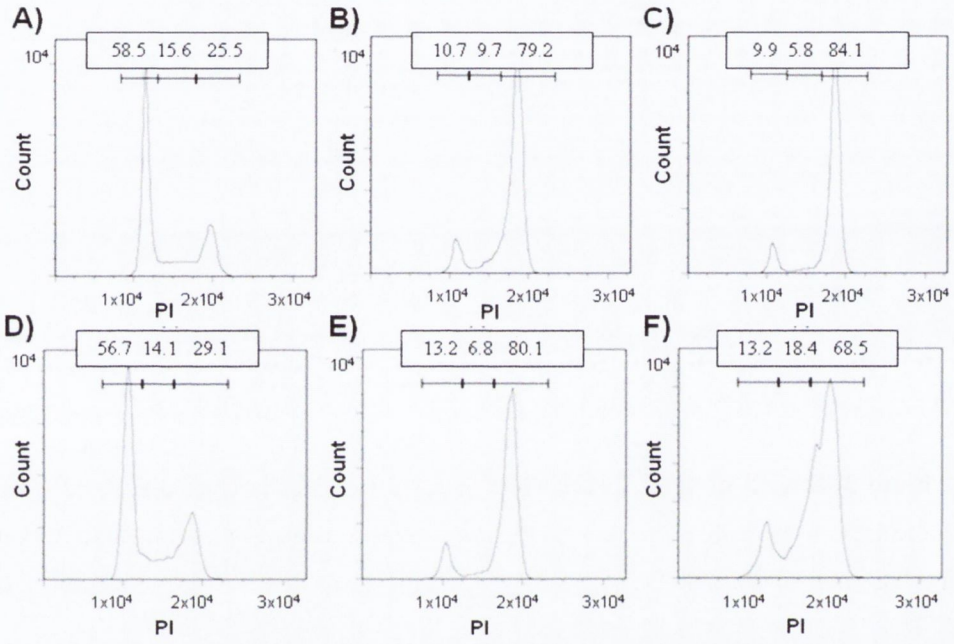

Figure 2.12: Cell cycle histograms of the gated G_1/S/G_2/M cells treated with GJH140 and ADR149. HUVECs were treated for 24h, stained with PI and analysed using flow cytometry. **A)** and **D)** Control (0.1% DMSO), **B)** 0.5 μM GJH140, **C)** 1 μM GJH140, **E)** 0.5 μM ADR149 and **F)** 1 μM ADR149.

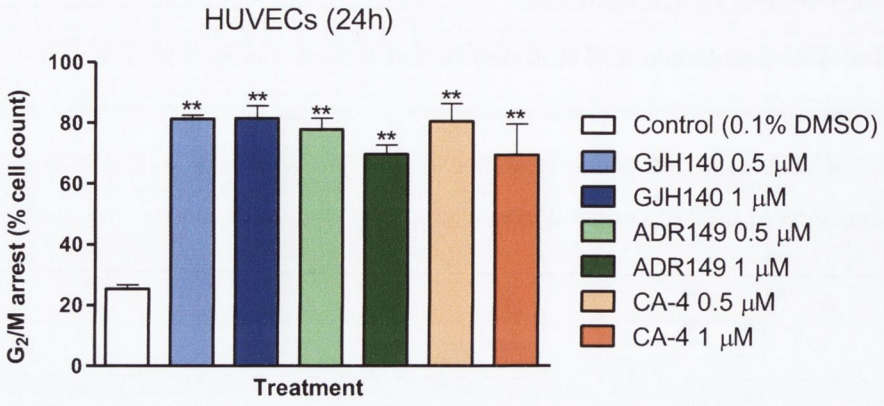

** $p < 0.01$, significantly higher mean % cell count in the G_2/M phase compared with the untreated controls as determined by Student's *t*-test.

Figure 2.13: Percentage of cells in the G_2/M phase treated with GJH140, ADR149 and CA-4. Data represents mean ± SEM (n=3).

2.3.3 Immunofluorescence Staining of the Microtubules

To confirm the ability of test compounds to disrupt the tubulin cytoskeleton, the microtubule organisation of treated endothelial cells was examined using confocal microscopy. Control treated cells showed complex, well organised microtubule networks, with long fibre-like structures present.

2.3.3.1 Group I Compound

HUVECs were incubated with 1 μM of CA-4 or RS133. CA-4 and RS133-treated cells showed an apparent reduction in the microtubules formation, without any long fibres present (Figure 2.14 and 2.15). Fragmentation of the nucleus was also observed in some cases.

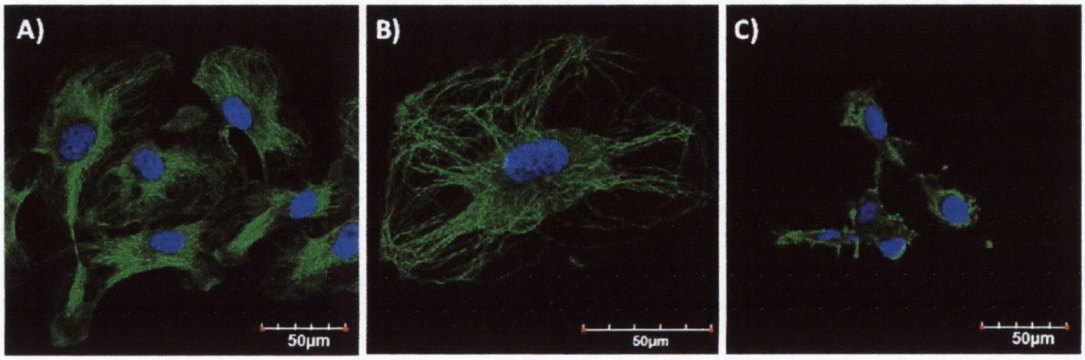

Figure 2.14: Microtubule disruption of endothelial cells by CA-4. HUVECs were treated for 30 minutes and stained for α-tubulin (green) and nucleus (blue). Images were taken using an Olympus FV1000 point scanning confocal microscope (x60). **A-B)** Control (0.1% DMSO) and **C)** 1 µM CA-4.

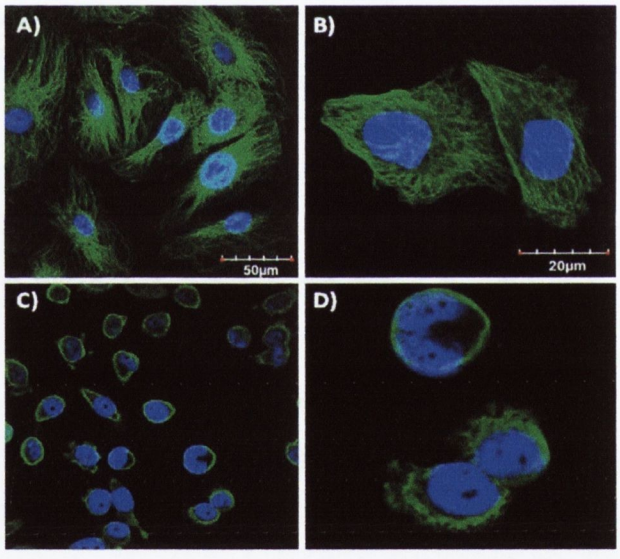

Figure 2.15: Microtubule disruption of endothelial cells by RS133. HUVECs were treated for 30 minutes and stained for α-tubulin (green) and nucleus (blue). Images were taken using an Olympus FV1000 point scanning confocal microscope (x60). **A-B)** Control (0.1% DMSO) and **C-D)** 1 µM RS133.

2.3.3.2 Group II Compounds

The effect of 1 µM of RS180 and GS117 on HUVECs' microtubule organisation was determined. Severe microtubule disruption was observed following treatment with RS180 and GS117, in a similar manner (Figure 2.16). Microtubule fibres were absent in the treated cells. Contraction of the nucleus was also observed.

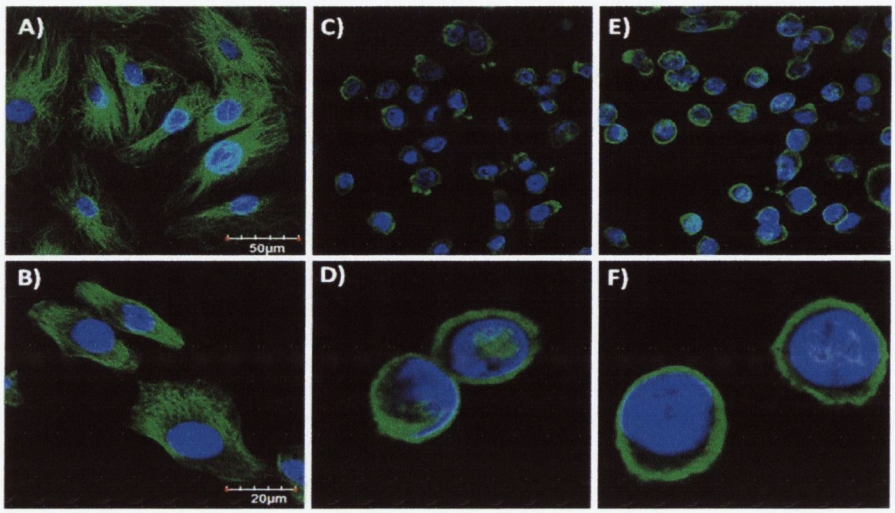

Figure 2.16: Microtubule disruption of endothelial cells by RS180 and GS117. HUVECs were treated for 30 minutes and stained for α-tubulin (green) and nucleus (blue). Images were taken using an Olympus FV1000 point scanning confocal microscope (x60). **A-B)** Control (0.1% DMSO), **C-D)** 1 µM RS180 and **E-F)** 1 µM GS117.

2.3.3.3 Group III Compound

The effect of ADR269 on the tubulin cytoskeleton of endothelial cells was examined. Treatment with 1 µM ADR269 demonstrated an apparent effect on the tubulin organisation and a disruption of the cell monolayer with a reduced cell number (Figure 2.17).

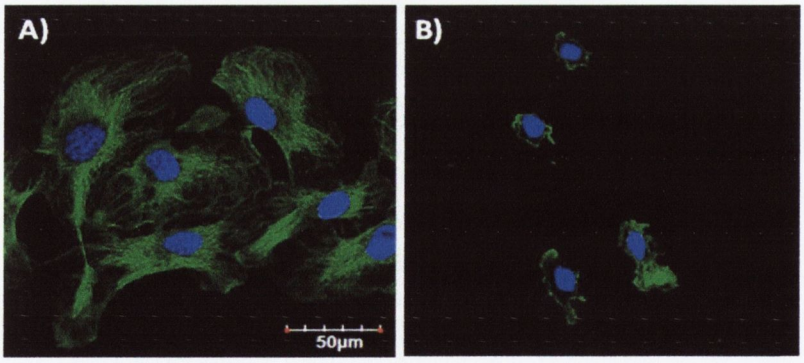

Figure 2.17: Microtubule disruption of endothelial cells by ADR269. HUVECs were treated for 30 minutes and stained for α-tubulin (green) and nucleus (blue). Images were taken using an Olympus FV1000 point scanning confocal microscope (x60). **A)** Control (0.1% DMSO) and **B)** 1 µM ADR269.

2.3.3.4 Group IV Compounds

Microtubules organisation was examined after treatment of endothelial cells with 1 μM of GJH140 and ADR149. The effect of GJH140 and ADR149 on the tubulin cytoskeleton was evident, showing a substantial reduction of the microtubule assembly and an absence of microtubule fibres (Figure 2.18).

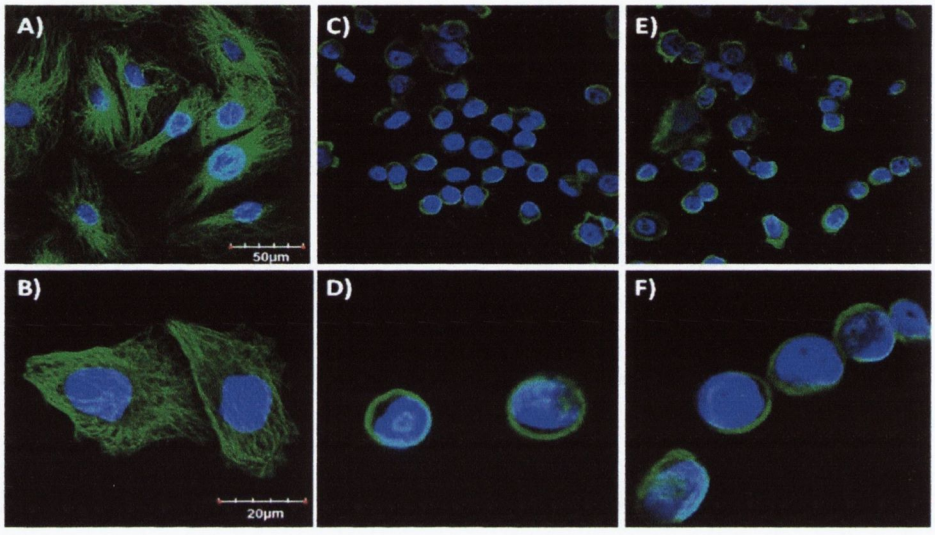

Figure 2.18: Microtubule disruption of endothelial cells by GJH140 and ADR149. HUVECs were treated for 30 minutes and stained for α-tubulin (green) and nucleus (blue). Images were taken using an Olympus FV1000 point scanning confocal microscope (x60). **A-B)** Control (0.1% DMSO), **C-D)** 1 μM GJH140 and **E-F)** 1 μM ADR149.

2.3.4 Analysis of Endothelial Cells' Morphology

The *in vitro* anti-vascular effect of test compounds was assessed by their ability to induce morphological changes to endothelial cells. Control treated cells retained a confluent monolayer and appeared well-structured without apparent abnormalities. Test compounds clearly induced rapid morphological changes to endothelial cells as observed 1h after drug washout, including endothelial cell contraction, membrane blebbing, intercellular gaps and darkening of the cell contents, as well as reduced cell area. However, in most cases treated cells regained their morphology as observed 3h after drug washout and there was no apparent decrease in cell area.

2.3.4.1 Group I Compound

RS133 was evaluated for its ability to induce morphological changes to endothelial cells, as an indication of its *in vitro* anti-vascular effect. Incubation of HUVECs with RS133 caused rapid alterations in the cells' structure and disrupted the cell monolayer at concentrations as low as 0.1 μM. The extent of this effect was reduced, as observed 3h after washout (Figure 2.19).

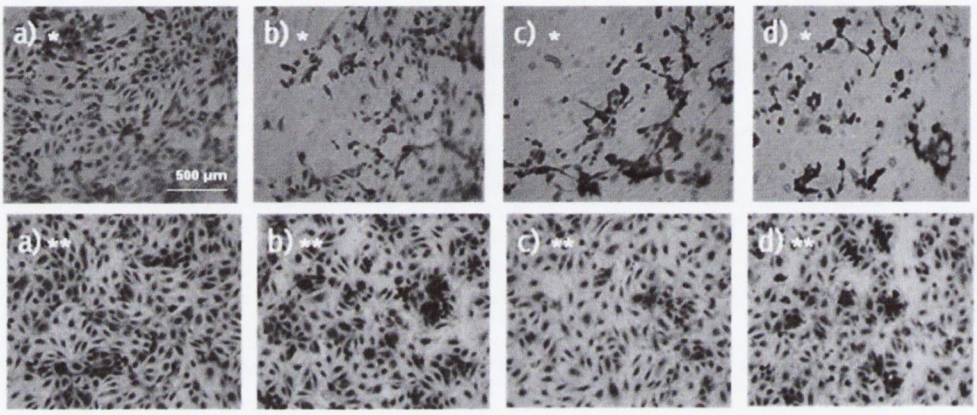

Figure 2.19: The effect of RS133 on endothelial cells' morphology. HUVECs were exposed to the compounds for 40 minutes and photomicrographs (x10) were taken 1h (*) and 3h (**) after drug washout. **A)** Control (0.1% DMSO), **B)** RS133 0.1 μM, **C)** RS133 0.5 μM and **D)** RS133 1 μM.

2.3.4.2 Group II Compounds

The *in vitro* anti-vascular effect of group II compounds, RS180 and GS117, on the endothelial cells' morphology was evaluated. Both compounds exerted their effects at concentrations as low as 0.1 μM by altering the cells' structure and monolayer, and displayed a similar activity profile to that of CA-4 (Figure 2.20). After 3h of drug washout, endothelial cells appeared to regain their structure to some extent (Figure 2.21).

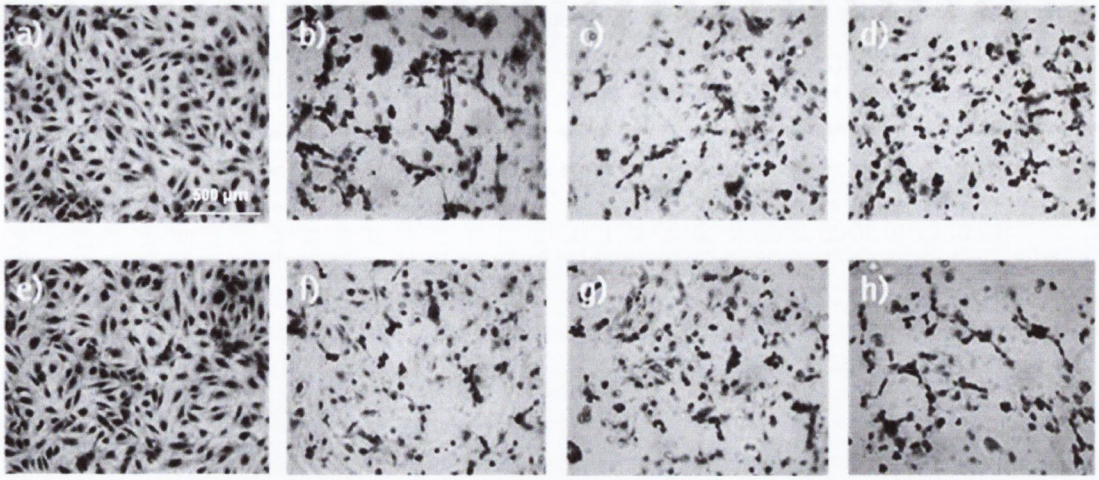

Figure 2.20: The effect of RS180 and CA-4 on endothelial cells' morphology. HUVECs were exposed to the compounds for 40 minutes and photomicrographs (x10) were taken 1h after drug washout. **A/E)** Control (0.1% DMSO), **B)** RS180 0.1 μM, **C)** RS180 0.5 μM, **D)** RS180 1 μM, **F)** CA-4 0.1 μM, **G)** CA-4 0.5 μM and **H)** CA-4 1 μM.

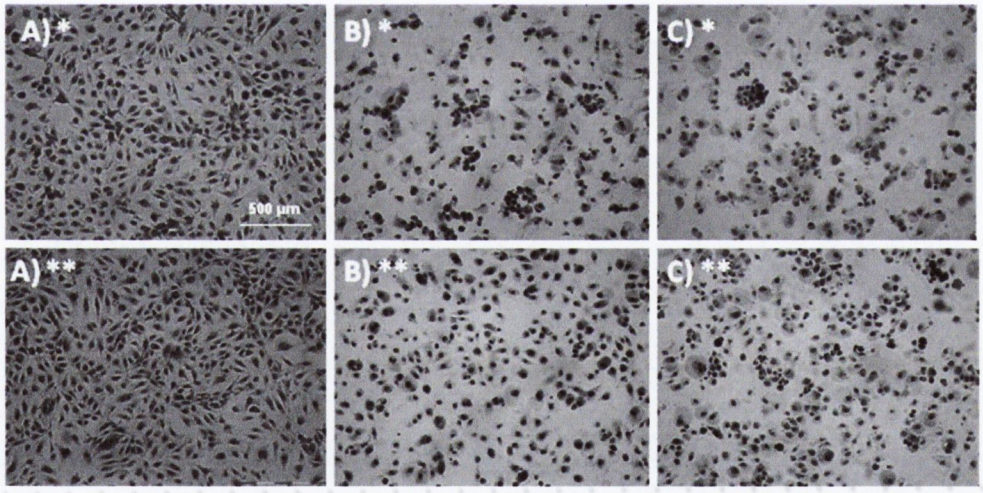

Figure 2.21: The effect of GS117 on endothelial cells' morphology. HUVECs were exposed to the compounds for 40 minutes and photomicrographs (x10) were taken 1h (*) and 3h (**) after drug washout. **A)** Control (0.1% DMSO) **B)** GS117 0.1 μM and **C)** GS117 0.5 μM.

2.3.4.3 Group III Compound

The *in vitro* anti-vascular effect of ADR269 was evaluated by its ability to interfere with the endothelial cells' morphology. HUVECs incubated with 0.1 μM and 1 μM ADR269 showed apparent differences in their morphology, as well as a disturbed monolayer. After 3h of drug washout, a minor recovery of endothelial cells appeared, although morphological changes were still evident (Figure 2.22).

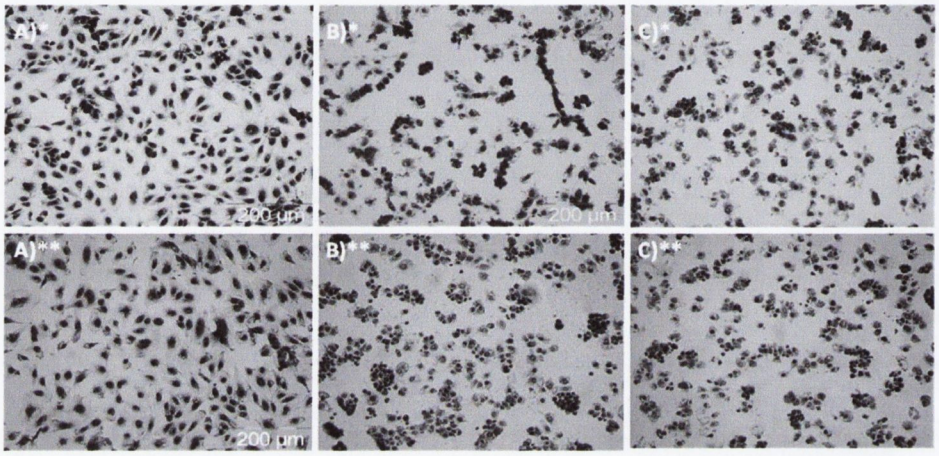

Figure 2.22: The effect of ADR269 on endothelial cells' morphology. HUVECs were exposed to the compounds for 40 minutes and photomicrographs (x10) were taken 1h (*) and 3h (**) after drug washout. **A)** Control (0.1% DMSO) **B)** ADR269 0.1 μM and **C)** ADR269 1 μM.

2.3.4.4 Group IV Compounds

Endothelial cells' morphology was evaluated following treatment with GJH140 and ADR149, in order to determine their *in vitro* anti-vascular effect. Treated cells appeared to have altered structure at 0.1 μM, but started to regain their shape 3h after washout (Figure 2.23 and 2.24).

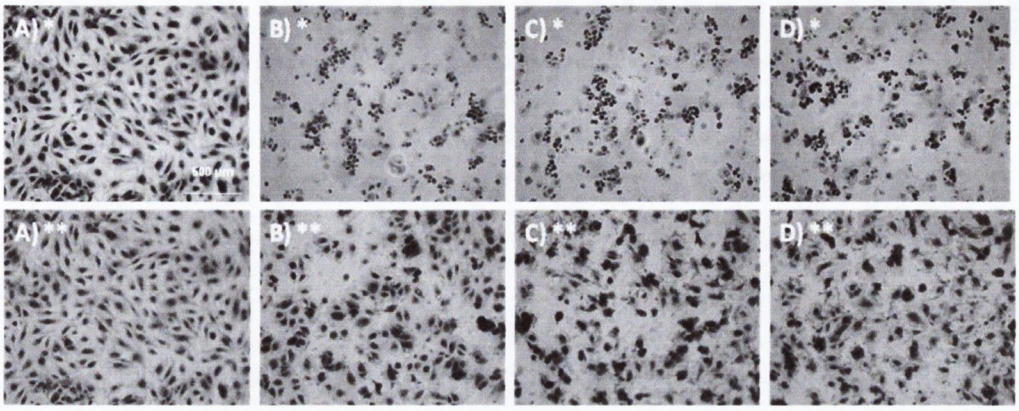

Figure 2.23: The effect of GJH140 on endothelial cells' morphology. HUVECs were exposed to the compounds for 40 minutes and photomicrographs (x10) were taken 1h (*) and 3h (**) after drug washout. **A)** Control (0.1% DMSO) **B)** GJH140 0.1 μM, **C)** GJH140 0.5 μM and **D)** GJH140 1 μM.

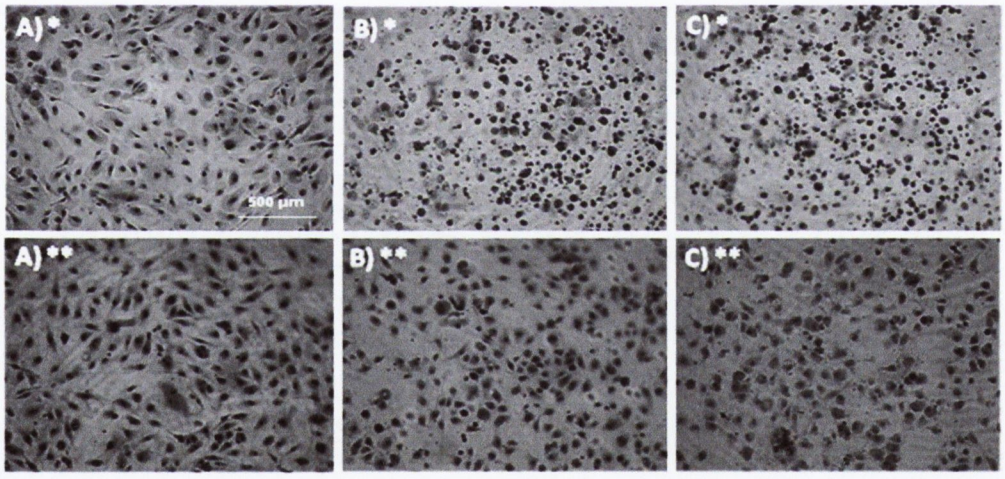

Figure 2.24: The effect of ADR149 on endothelial cells' morphology. HUVECs were exposed to the compounds for 40 minutes and photomicrographs (x10) were taken 1h (*) and 3h (**) after drug washout. **A)** Control (0.1% DMSO), **B)** ADR149 0.1 μM and **C)** ADR149 0.5 μM.

2.3.5 *In Vitro* Angiogenesis Assay

In addition to the anti-proliferative, anti-mitotic and anti-vascular effects, tubulin inhibitors are also known for their anti-angiogenic properties. Inhibition of *in vitro* angiogenesis was investigated using the AngioKit assay provided by TCS Cellworks. RS180 was the only compound evaluated in this assay and suramin served as a positive control, whereas 2 ng/mL VEGF served as a negative control. Treatment of the co-culture with suramin decreased the number of microvessels to some extent. Figure 2.25

illustrates the effect of RS180, clearly showing the reduction of microvessels at concentrations as low as 10 nM. The microvessel density of each treated group was analysed and statistical comparisons between control and treated cells were determined using Student's *t*-test (Figure 2.26). The reduction of microvessels in the suramin-treated group was not of statistical significance. Although RS180 treatment demonstrated a visible decrease in vessel formation at low concentrations (10 nM and 25 nM) this was not statistically significant. Treatment of the co-culture with 50 nM RS180 significantly ($p < 0.01$) reduced the number of tubule structures and shortened their length.

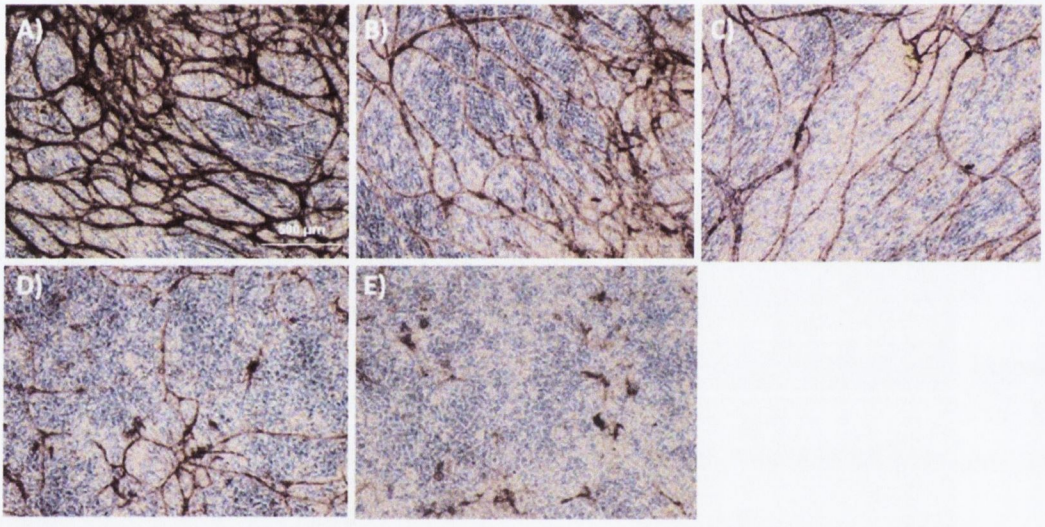

Figure 2.25: The anti-angiogenic effect of RS180 as determined by the AngioKit assay. The co-culture assay was supplied from TCS Cellworks as a growing culture of HUVECs and fibroblasts in 24-well plate format. Cells were cultured for 12 days resulting in a confluent co-culture. **A)** 2 ng/mL VEGF, **B)** Control (0.1% DMSO), **C)** 20 μM suramin, **D)** 25 nM RS180 and **E)** 50 nM RS180.

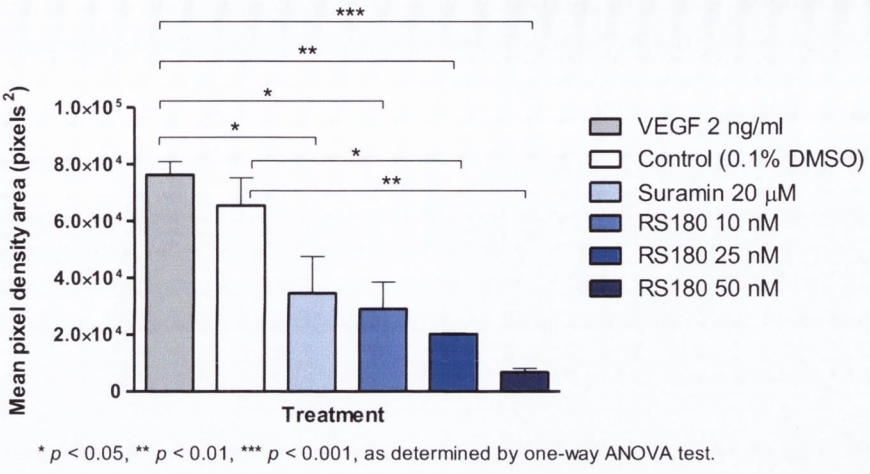

Figure 2.26: The effect of RS180 on microvessels formation. An estimation of the mean pixel density area of the vessels was calculated by Adobe Photoshop CS4. Data represents mean ± SEM (n=3).

2.4 Discussion

2.4.1 Cell Proliferation Assay

2.4.1.1 Group I Compound

In order to validate the assay and compare the obtained IC_{50} values from each test compound, a positive control was required. In this case CA-4 was used, where its anti-proliferative effect was determined using both HUVECs (IC_{50}: 4.03 ± 1.73 nM) and PC-3 cells (IC_{50}: 14.01 ± 0.58 nM). The IC_{50} value of CA-4 against HUVECs was comparable to previously reported data (IC_{50}: 2.2 nM) [502]. RS133 did not possess remarkable anti-proliferative activity against PC-3 cells (IC_{50}: 150.00 ± 40.01 nM); however it showed some selectivity towards HUVECs (IC_{50}: 20.26 ± 1.43 nM), demonstrating a 7-fold increase in activity against these cells (Table 2.1, p.85). This finding suggests that RS133's design may confer selectivity for endothelial cells over cancer cells and may be referred to as a "true" VDA. Similarly, Beale *et al.* reported selectivity for endothelial cells of triazole analogues of CA-1 over SK-OV-3 ovarian cancer cells (IC_{50}: 4.3 nM *vs* 30 nM, respectively) which share the same trimethoxy benzene A-ring with RS133 [502].

Flynn *et al.* examined the effect of benzo[b]furans as tubulin polymerisation inhibitors; in particular the 7-hydroxy-6-methoxy-2-methyl-3-(3, 4, 5-trimethoxybenzoyl)benzo-[b]furan demonstrated higher selectivity against activated endothelial cells (IC_{50} = 1.7 nM) over quiescent endothelial cells (IC_{50} = 3.4 nM) [503]. This property provides an improved pharmacological profile for any VDA or anti-angiogenic agent. The drug-related toxicities could be minimised by selective interaction of the agent with tumour-associated proliferating endothelial cells and to a lesser extent with quiescent endothelial cells.

2.4.1.2 Group II Compounds

Group II compounds, RS180 and GS117, exhibited an improved anti-proliferative activity compared to that of RS133, in both HUVECs and PC-3 cells (IC_{50} range: 65.05 ± 1.10 nM – 8.58 ± 1.06 nM, Table 2.2, p.85). The addition of a carbonyl group at position-3 of the B-ring appeared to alter its shape and facilitate stronger tubulin binding affinity, which confirmed the initial hypothesis. The presence of an amine

group in GS117 conferred even greater activity at the low nanomolar range and improved solubility. There was no observable selectivity towards HUVECs over PC-3 cells.

2.4.1.3 Group III Compounds

Group III compounds displayed a variation in the level of their anti-proliferative activity in both cell lines. In order to further improve the binding affinity of test compounds to tubulin, additional structural modification were attempted on the B-ring, by replacing the benzylic methylene group with an oxygen atom at position-5. This alteration dramatically improved the inhibitory profile of ADR269 against HUVECs and PC-3 cells which showed higher potency than CA-4 (IC_{50}: 4.91 ± 1.01 nM and 4.67 ± 1.45 nM, respectively). The promising preliminary results obtained from group III compounds led to the synthesis of additional analogues of ADR269; however none of them demonstrated superior anti-proliferative activity to that of ADR269 or CA-4 (IC_{50} range: 10.00 ± 4.03 nM – 4.02 ± 2.80 μM, Table 2.3, p.86).

2.4.1.4 Group IV Compounds

The majority of group IV coumarin-based compounds exhibited potent anti-proliferative activity. Lead compound GJH140 demonstrated a similar inhibitory profile to that of CA-4, against HUVECs and PC-3 cells (IC_{50}: 5.56 ± 1.36 nM and 4.70 ± 1.19 nM, respectively). The addition of a hydroxyl group at position-10 on the C-ring of ADR084 resulted in a 1000-fold reduction of its inhibitory activity on both cell lines (IC_{50}: 3.51 ± 2.05 μM and 6.10 ± 3.50 μM, respectively), indicating that position-10 modifications are not favourable. The rest of the compounds in this series displayed potent activity against both cell lines without any notable pattern of selectivity (IC_{50} range: 1.45 ± 1.15 nM – 12.03 ± 0.58 nM, Table 2.4, p.87). The most active compound was ADR149 which showed improved inhibition compared to that of CA-4, in both HUVECs and PC-3 cells (IC_{50}: 1.45 ± 1.15 nM and 3.82 ± 1.15 nM, respectively). The DML ADR241 demonstrated moderate anti-proliferative activity in the micromolar range, against both cell lines (Table 2.5, p.87). The reduced activity may be due the increased bulk of the molecule.

Following the preclinical and clinical success of CA-4, numerous attempts were made to design and synthesise analogues that could mimic or improve its effects. Sun *et al.* evaluated a series of novel 1, 4-diaryl-2-azetidinones, conformationally restricted analogues of CA-4, for cytotoxicity against a number of human tumour and normal cell lines. The best compounds exhibited strong potencies (IC_{50} range: 25 - 74 nM) against IMR32 human neuroblastoma cells and a variety of other cell lines [504]. Furthermore, a different series of CA-4 analogues containing the 1, 4-diaryl-2-azetidinone (β-lactam) ring system in place of the usual ethylene bridge present in the natural CA-4, was synthesised by Carr *et al.* Two of the most potent compounds of this series (3-unsubstituted compound and 3-methyl substituted compound) demonstrated anti-proliferative activity at nanomolar concentrations in MCF-7 (IC_{50}: 17 nM and 10 nM, respectively) and MDA-MB-231 (IC_{50}: 54 nM and 47 nM, respectively) human breast carcinoma cell lines [505]. In addition, O'Boyle *et al.* reported a new series of rigid analogues of CA-4 which contain the 1, 4-diaryl-2-azetidinone (β-lactam) ring system in place of the usual ethylene bridge present in the natural CA-4, where the most active compound showed sub-nanomolar activity in MCF-7 cells (IC_{50}: 0.8 nM), along with significant inhibition of tubulin polymerisation [506]. A new class of compounds in which the 2-amino-5-chlorophenyl ring of a phenstatin analogue was replaced by a 2-amino-5-aryl thiophene was reported by Romagnoli *et al.*, where their anti-proliferative activities ranged between IC_{50}: 2.5 - 6.5 nM against the L1210 mouse lymphocytic leukaemia and K562 human erythromyeloblastoid leukaemia cell lines [507].

Taking into consideration the reported IC_{50} data from different CA-4 analogues, the majority of our test compounds, including GJH140, ADR149 and ADR269 demonstrated high potency against HUVECs and PC-3 cells and showed superiority over several of the discussed CA-4 analogues. An overall increased activity was observed in group IV compounds, where manipulation of the B-ring by the addition of a carbonyl group at position-5 resulted in an improved inhibitory effect.

2.4.2 Cell Cycle Analysis

The anti-mitotic effect of selected test compounds was determined by examination of the cell cycle stages. All compounds demonstrated cell cycle arrest at the G_2/M phase following a 24h incubation treatment, without any particular pattern observed within

each group. This finding suggests that test compounds have a direct effect on the chromosomes' structure, causing them to fail segregation after replication, thus inducing cell cycle arrest at the metaphase checkpoint, resulting in a mitotic arrest.

Tubulin binding agents are well known for their ability to induce a G_2/M phase arrest. In fact, Ding *et al.* reported that treatment of HUVECs with CA-4 resulted in an accumulation of G_2/M phase cells accompanied with DNA fragmentation [508]. Furthermore, incubation with 2 μM CA-4 for 24h showed a significant disturbance on the cell cycle of AGS metastatic gastric cancer cells [495]. Similarly, Zhu *et. al* demonstrated a G_2/M arrest of A549 alveolar adenocarcinoma cells following incubation with XN0502, a CA-4 analogue, where the effect was time- ($\leq$ 48h) and concentration- ($\leq$ 0.1 μM) dependent [509]. In addition, a triazole-based tubulin polymerisation inhibitor T115 was reported to arrest HeLa cells at 40 nM following 24h treatment, and the effect was dose-dependent [497]. Carr *et al.* showed that the CA-4 analogues containing the 1, 4-diaryl-2-azetidinone (*β*-lactam) ring system, exerted anti-mitotic effects through inhibition of tubulin polymerisation and a subsequent G_2/M arrest of MDA-MB231 human breast cancer cells, with similar activity to that of CA-4 [505]. A novel series of 2-(3', 4', 5'-trimethoxybenzoyl)-3-amino-5-aryl/heteroaryl thiophene derivatives not only induced accumulation of HL-60 human promyelocytic leukaemia cells in the G_2/M phase, but also significantly increased the number of apoptotic cells [510]. Furthermore, the effect of 5 and 10 μM of embellistatin, a microtubule polymerisation inhibitor, on BAECs cycle was investigated following 24h exposure. An apparent G_2/M arrest was observed and the effect was dose-dependent. Interestingly, cytotoxicity data of BAECs up to 15 μM of embellistatin following 72h treatment, revealed more than 90% cell viability. This indicated that the G_2/M arrest was not a cytotoxic-induced effect, but was associated with microtubule disruption [496].

The results generated from the cell cycle study are in agreement with the evidence reported in the literature, implying that test compounds indirectly cause cell death by altering the microtubule organisation and by preventing the successful completion of cell division.

2.4.3 Immunofluorescence Staining of the Microtubules

In order to confirm that test compounds interfere with the tubulin cytoskeleton, microtubule organisation was visualised, following exposure to test compounds. Control-treated cells showed a complex microtubule network consisting of long filaments and displayed compact rounded nucleus. All compounds were able to disturb the cells' microtubule arrangement, as evidenced by an apparent reduction of the fluorescence intensity and by the loss of the microtubule network. In some cases, nucleus contraction was noted, indicating inhibition of chromosome separation.

Kanthou *et al.* demonstrated that 1 μM CA-4P caused microtubule disruption of endothelial cells within 30 minutes of treatment [315]. One hypothesis which could explain how CA-4 blocks tubulin polymerisation was related to the association of CA-4 with tubulin dimers, which renders them incompetent for assembly [311]. Kanthou *et al.* further investigated the mechanisms and signalling pathways involved in the effects of CA-4P on the cytoskeleton of endothelial cells. It was reported that microtubule disruption induced by CA-4P caused Rho/Rho-kinase-mediated reorganisation of actin, which led to actinomyosin contractility, assembly of stress fibres and local adhesions, and early membrane blebbing. The cytoskeletal features observed in the early membrane blebbing were similar to those of the apoptotic blebbing; however this was associated with necrosis rather than the onset of an apoptotic pathway [315]. In an attempt to further investigate the signalling pathway involved in the CA-4-induced regression of tumour neovessels, Vincent *et al.* demonstrated that CA-4P mediates its effect by rapidly disrupting the molecular engagement of the endothelial cell-specific junctional molecule, vascular endothelial-cadherin (VE-cadherin), *in vitro* and *in vivo* [511].

The discovery of the 7-hydroxy-6-methoxy-2-methyl-3-(3',4',5'-trimethoxybenzoyl)benzo[b]furan (BNC105) by Flynn *et al.* as a novel tubulin polymerisation inhibitor, led to its evaluation as a tumour vasculature targeting agent. To address whether inhibition of tubulin polymerisation by BNC105 operated *via* the same mechanism as CA-4, endothelial cells were exposed to 10 nM BNC105 and CA-4 for 20 minutes, whereby both agents demonstrated cell blebbing [512].

Furthermore, 24h treatment of HeLa and MCF-7 cells with either CA-4 (25, 100 nM) or a triazole-based anti-mitotic agent T115 (50, 100 nM) resulted in disorder and fragmentation of the microtubule network and disruption of the mitotic spindle formation. At the lower concentration, T115 caused inhibition of chromosome separation during mitosis which resulted in the formation of multinucleated cells. At higher concentration, there was a significant loss of the fluorescence intensity which reflected severe destruction of the microtubule network [497]. Bonezzi *et al.* reported the evaluation of the effect of novel 1, 5-diaryl-1H-imidazole CA-4 analogues on the tubulin cytoskeleton. Alteration of endothelial cells' morphology such as disorganisation of microtubules was induced at 0.1 and 1 μM following 1h exposure to test compounds; however CA-4 exhibited a more pronounced effect [513].

Taken together, these results confirmed that treatment with test compounds causes disruption of the microtubule assembly which is essential for the formation of the mitotic spindle and segregation of condensed chromosomes. Bearing in mind the reported data from the literature, our compounds exert their effects and maintain potency in a similar manner as CA-4 and its related analogues.

2.4.4 Analysis of Endothelial Cells' Morphology

The anti-vascular effect of the tubulin inhibitors is exhibited through direct disruption of the endothelial cells present in the blood vessels' lining. Hence, the *in vitro* anti-vascular activity of test compounds was assessed by their ability to alter endothelial cells' morphology. The control group showed an undisturbed cell monolayer, with ordinary morphological features. In contrast, cells treated with test compounds showed morphological changes, including endothelial cell contraction, membrane blebbing, intercellular gaps and darkening of the cell contents. In fact, endothelial cell retraction is usually associated with alterations in the organisation of both tubulin and actin cytoskeletons. In addition, there was an observable reduction in cell area which might be an indication of cell adhesion disturbances.

Similarly to our compounds, 1 μM CA-4P was previously reported to cause blebbing morphology of endothelial cells, in which F-actin accumulated around the blebs surface, stress fibres misassembled into a spherical network surrounding the cytoplasm and focal adhesions appeared malformed. Time course studies revealed that blebbing

was complete within 1h of treatment when it was evident in 16.0 ± 64.5 % of cells [315]. As a consequence, this could lead into an increased endothelial permeability to macromolecules [514]. Indeed, CA-4P-mediated contractility and blebbing were associated with a Rho-dependent increase in monolayer permeability to dextrans, implying that such functional changes may be important in the rapid response of the tumour endothelium to CA-4P *in vivo* [315].

In addition, Romagnoli *et al.* demonstrated that 0.5 μM of triazole-based CA-4 analogues induced rapid changes to the endothelial cells such as formation of membrane blebs, following 30 minutes incubation [515]. A different series of CA-4 analogues, 1, 5-diaryl-1H-imidazoles-based tubulin inhibitors, were examined for their *in vitro* anti-vascular activity. Following 1h treatment, all compounds caused profound changes in the morphology of endothelial cells at 0.1 and 1 μM, which retracted by assuming a rounded shape and tended to detach from the substrate. However, test compounds did not demonstrate superiority over CA-4 [513].

The activity of CA-4 and its related analogues is comparable to the compounds synthesised in our lab. The abnormal morphological features visualised following exposure to test compounds could be due to their interaction with the cell cytoskeleton, but could also be an indication of cells undergoing apoptosis. However, the fact that 3h after drug washout cells were able to recover in most cases, suggests that treatment with test compounds disturbs cell morphology but it's not cytotoxic; in other words, this effect is reversible. A similar reversibility effect was demonstrated by Joncour *et al.* using a new series of dibenzoxepines-based tubulin targeting compounds which caused morphological alterations to endothelial cells and returned to normality 3h after drug washout [500].

The reversibility of this effect could be beneficial *in vivo*, considering short treatment with these agents is expected to produce rapid damage to the tumour vasculature, while avoiding or minimising possible side effects through prolonged disruption of microtubules in normal tissues.

2.4.5 *In Vitro* Angiogenesis Assay

The *in vitro* human angiogenesis assay was performed in order to demonstrate the anti-angiogenic effect of the tubulin targeting compound RS180. Most *in vitro* assays do not address the entire process of blood vessels development, but only focus on distinct steps, including tubule formation in matrigel or migration of endothelial cells in monocultures. Therefore, the human co-culture of endothelial cells and fibroblasts was used in order to provide a better representation of human angiogenesis *in vivo*. RS180 treatment showed a moderate effect at 10 and 25 nM, and a more pronounced effect at 50 nM (Figure 2.25 and 2.26, p.101-102). A less evident inhibitory activity was seen with the positive control, suramin at 20 μM.

The inhibition of microvessel formation and the reduction in tubule area is an indication of angiogenesis disruption. However, the choice of compound concentration is crucial for the outcome of the study, due to the fact that higher concentrations may interfere with cell proliferation and thus result in a reduction or a complete inhibition of microvessel outgrowth. Ahmed *et al.* reported that 30 ng/mL CA-4 (concentration that had no effect on cell proliferation) significantly decreased tube formation in a collagen gel assay using brain capillary endothelial cells (BCECs), following 24h incubation [492]. In addition, it was reported that following 18h incubation of FGF-2-stimulated HUVECs seeded on matrigel with 10 nM CA-4P, resulted in a disturbed capillary tube formation, with decreased tubule length and reduced branching points. A further investigation revealed that the effect of CA-4P was mediated though disruption of the VE-cadherin/β-cadherin/Akt signalling pathway [511].

Embellistatin was reported by Jung *et al.* to dose-dependently inhibit bFGF-induced tube formation of BAECs, at concentrations of up to 10 μM [496]. In comparison to embellistatin, RS180 demonstrated an approximate 1000-fold greater anti-angiogenic activity, highlighting its potential.

Remarkably, HUVECs co-cultured with smooth muscle cells (SMCs) in the presence or absence of 10 nM CA-4P were able to assemble into capillary tubes only when endothelial cells were stabilised with SMCs [511]. This finding implied that mural protection of endothelial cells may provide a shield for vascular tubes against CA-4P-induced vessel destabilisation. However, this was not the case with RS180 treatment,

where it resulted in inhibition of tubule formation even in the presence of mural cells such as fibroblasts.

Tubulin inhibitors are able to modulate the process of angiogenesis since tubulin is an essential component of the cell cytoskeleton and is involved in many dynamic processes such as cell proliferation, migration and invasion. Therefore, treatment with RS180 was proven to interfere with the rate of angiogenesis and alter the tubules' arrangement.

2.5 Conclusions

The studies undertaken in this Chapter aimed to investigate the effect of novel tubulin polymerisation inhibitors as tumour VDAs. Initially, the effect of test compounds on cell proliferation of HUVECs and PC-3 cells was established. The majority of compounds demonstrated substantial anti-proliferative activity with the most potent compounds being ADR149, GJH140 and ADR269. Next, cell cycle analysis was performed following treatment with test compounds, which showed an accumulation of cells in the G_2/M phase, indicative of an anti-mitotic effect. Furthermore, the effect of test compounds on the tubulin cytoskeleton was determined, where a direct disruption of microtubule network was observed. The *in vitro* anti-vascular activity of test compounds was illustrated by evident morphological changes of endothelial cells. In addition, the reversibility of this effect was established once the endothelial cells recovered from treatment with the compounds following 3h after washout. Moreover, RS180 was examined in the human angiogenesis assay, where it exhibited anti-angiogenic activity at relatively low concentrations.

Although additional mechanisms of action may be investigated, the main aim of this project was to assist in the development of novel tubulin binding agents targeting the tumour vasculature. For that reason it was important to establish whether these compounds maintain their activities in *ex vivo* and *in vivo* models. Therefore, compounds which demonstrated a promising pharmacological profile were further assessed using the *ex vivo* aortic ring assay and an *in vivo* tumour xenograft model for anti-vascular, anti-angiogenic and anti-tumour activities. These studies are outlined further in Chapter 3.

-- Chapter 3 --

Ex Vivo and *In Vivo* Evaluation of Novel Tubulin Polymerisation Inhibitors

3. Introduction

The *in vitro* results documented in Chapter 2 indicated that the majority of novel compounds previously synthesised in our group, possessed anti-proliferative, anti-mitotic, anti-vascular and anti-angiogenic properties, comparable to or superior in some examples, to that of CA-4. Following the preliminary *in vitro* screening of test compounds, the next stage involved the selection of the most promising compounds from each series and further examination of their anti-vascular/anti-angiogenic activities in *ex vivo* and *in vivo* models. The *ex vivo* aortic ring assay was chosen as the most appropriate assay, prior to the development of an *in vivo* model for two reasons. Firstly, to assess the breakdown of existing microvessel networks which represents an anti-vascular property, and secondly to determine the effect of test compounds on the formation of new microvessels, which would identify any anti-angiogenic activity. The final evaluation involved the establishment of a tumour xenograft model as a mean to determining their anti-tumour and anti-vascular/anti-angiogenic properties.

Arising from the *ex vivo* and *in vitro* studies, two compounds, namely ADR149 and RS180 were selected for *in vivo* evaluation. ECB206, a leucine prodrug salt of ADR149 was synthesised by Breen and GS291, a disodium phosphate prodrug form of RS180, was synthesised by Stack, in order to resolve solubility issues (Figure 3.1). ECB206 was designed for site-specific delivery of the active compound (ADR149), by an APN enzymatic cleavage of leucine to APN-rich sites, including proliferating endothelial cells and PC-3 cells, expressed in tumour vasculature and tissue.

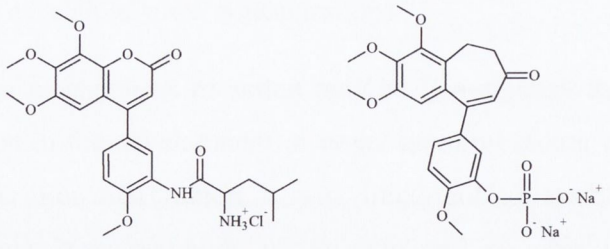

ECB206 GS291

Figure 3.1: ECB206 is the leucine prodrug of ADR149 and GS291 is the disodium phosphate prodrug of RS180.

3.1. Aims

Following their *in vitro* evaluation, the most promising compounds from each series were selected for further investigation as tumour vasculature targeting, anti-angiogenic and anti-tumour agents. Thus, the overall aims of the work described in this Chapter were to:

- Verify the anti-vascular effects of test compounds in the *ex vivo* aortic ring assay.
- Investigate and quantify angiogenesis inhibition of test compounds in the *ex vivo* aortic ring assay.
- Determine a maximum, or close to the maximum, tolerated dose of selected compounds *in vivo*.
- Establish the anti-tumour effect of selected compounds in a PC-3 tumour xenograft model and observe any evident toxicity.
- Histologically examine the tumour samples following completion of the *in vivo* efficacy study and identify any evidence of tumour necrosis.
- Evaluate the anti-vascular activity of selected compounds in a PC-3 tumour xenograft model by visualising the functional tumour vasculature.

3.2 Background to the Protocols Used

3.2.1 Aortic Ring Assay

The aortic ring assay is an ideal assay for testing the activity of anti-vascular, anti-angiogenic or pro-angiongenic agents. This method was originally developed and modified by Nicosia and Ottinetti [516]. The aorta can be excised from either mice or rats, cut into ~ 1 mm rings and cultured in either basement membrane matrix (matrigel) or collagen gel. Following incubation for several days the rings start to generate outgrowths of branching microvessels, which are lined by endothelial cells and supported by pericytes and fibroblasts. The angiogenic response of the aorta is a self-limited process regulated by endogenous growth factors, including bFGF [517], VEGF [518], PDGF [519] and angiopoietins [520].

The rat aorta model is an *ex vivo* assay which combines advantages of both *in vitro* and *in vivo* models. The process of angiogenesis takes place in a defined culture environment which can be easily adapted to different experimental conditions according to the requirements of the study. The cells of the aortic outgrowth are not modified by repeated passages in culture, thus newly formed microvessels reproduce the characteristics of the vasculature formed during *in vivo* angiogenesis [521-522]. There is no influx of leukocytes from circulating blood, therefore inflammatory complications which may affect the interpretation of *in vivo* assays are minimised. For the purpose of this study, rat aortic ring cultures were used to investigate both the anti-vascular and the anti-angiogenic activity of test compounds.

The successful growth of the aortic rings into a mircovessel networks was dependent on several factors including: (i) the amount of periaortic fibroadipose tissue remaining on the ring, (ii) the orientation of the ring (*i.e.* the way the ring was embedded into the matrigel) and (iii) the volume of the matrigel used. Initial attempts involved positioning the ring so as to ensure that the luminal axis was parallel to the bottom of the culture dish, but this did not result in significant microvessel growth. Thus, the rings were placed with their luminal axis perpendicular to the bottom of the dish which promoted the successful development of a microvessel network. Several further attempts were carried out to optimise the assay by changing the way the rings were embedded into the matrigel. For instance, a matrigel layer was added on the bottom of the dish and allowed to solidify; the rings were then placed on top and covered with an extra layer of matrigel. However, this method did not prove to be consistent. The finalised protocol for optimal microvessel growth involved adding an 80 μL-drop of matrigel onto the bottom of the dish. The aortic rings were then placed into the matrigel drop and allowed to solidify for 30 minutes, followed by incubation with the appropriate medium.

3.2.2 Tumour Xenograft Models

One of the most critical parts of this study was to determine the anti-tumour and anti-vascular activity of promising lead compounds in an *in vivo* model, as it is a closer representation of the final desired outcome in a clinical setting. In some cases, compounds exhibiting potent activity *in vitro* often disappoint *in vivo* for a variety of

reasons. For example, they can be readily metabolised to inactive derivatives or have poor bioavailability.

Xenograft refers to a transplantation of living cells or tissues from one species to another. The human tumour xenograft model is the most widely used and effective way of examining the anti-tumour activity of chemotherapeutic agents [308, 523-525]. In this model, human tumour cells/tissues are transplanted, either s.c. (*i.e.* under the skin) or orthotopically (*i.e.* into the organ type in which the tumour originated) into immunocompromised (*i.e.* athymic nude) mice. The rate of tumour growth depends on the number of cells injected, or the size of tumour fragments transplanted. Although some components of the immune system are missing in athymic nude mice, the B cells, dendritic cells and granulocytes are all relatively intact, and there is an increase in both natural killer cells and tumouricidal macrophages [526].

There are several advantages of using human tumour xenografts to examine therapeutic responses to drugs: (i) the actual human tumour tissue can be used, which features the genetic and epigenetic abnormalities that are present in the human tumour population, (ii) the development of individualised molecular therapeutic approaches can be facilitated, (iii) results can be obtained in a matter of a few weeks and (iv) orthotopic xenografts can be developed to reproduce the organ environment in which the tumour originates [526]. However, one disadvantage of xenografts using human cells lines is the poor correlation with clinical activities in patients, due to the fact that tumours usually grow s.c. in an immunodeficient host which does not mimic a pragmatic environment. For this reason, a shift has occurred towards the development of spontaneous mouse tumours arising in transgenic and/or knockout mice engineered to recapitulate various genetic alterations responsible for specific types of human cancers. Alternatively, tumour xenograft models could be improved by the use of either orthotopic implantation which promotes metastasis, or by s.c. "primary" tumour transplants which can remarkably predict the activity of chemotherapeutic agents in humans [527].

Subsequently, for the purpose of this study, the s.c. human PC-3 tumour xenograft model was established following several attempts. In our initial validation of this assay, a single injection of (1×10^6 cells/mL) PC-3 cells was injected s.c. onto the flank region of the animal; however the outcome of this approach was inconsistent and time-

consuming (*i.e.* there was a large variation in tumour growth between the animals and the duration of the primary tumour development was approximately 2-3 months). For these reasons, a different method of tumour growth was established whereby primary tumours were developed in several donor animals using a single PC-3 cells injection, followed by a s.c. implantation of small tumour fragments into the test animals [528-529]. At first, the tumours excised from donor animals were cryo-preserved and used when required. However, this approach resulted in inconsistent tumour growth between the animals. Therefore, tumours were rapidly excised from donor animals and immediately implanted s.c. into the test animals. This method was less time-consuming and more reliable than the cell-based xenograft model, thus this procedure was used throughout this project.

3.2.3 Assessment of Tumour Necrosis

Targeting the tumour vasculature with VDAs leads to blockage of tumour blood supply which can result in an increased level of hypoxia within the tissue and induce high levels of tumour necrosis. The degree of tumour development and progression is directly correlated to the degree of necrosis within the tumour. In situations where necrosis is only present in the centre of the tumour, it is unlikely to have a significant effect on the tumour growth since peripheral tumour tissue can obtain nutrients from unaffected blood vessels in normal surrounding host tissues.

Herein, the degree of tumour necrosis in each group was determined after completion of each treatment. Paraffin-embedded tumour samples were stained with H&E in order to visualise any morphological differences in control *vs* treated groups. This staining protocol is widely used in histology and histopathology especially for the diagnosis of malignant and non-malignant lesions [530].

3.2.4 Assessment of the Tumour Vasculature

Following the *in vivo* anti-tumour evaluation of test compounds it was essential to examine any effects on the tumour vasculature. Initially, studies were carried out by i.v. injection of Hoechst 33342, a DNA-binding fluorescent dye. One minute after injection, mice were sacrificed and tumours were dissected, frozen in liquid nitrogen and cryo-sectioned. Tissue slices were then examined microscopically. The theory

behind this technique is that cells lining the blood vessels are the first to incorporate this agent. Although Hoechst 33342 is not a specific stain for endothelial cells, its rapid uptake into cells and limited diffusion across cell layers makes it a useful substance for identifying functional vascular networks [531]. While in principle the method was quite feasible and had been previously performed by Prokopiou *et al.* [529]; it failed to provide us with reproducible results. This may be due to diverse morphological features between PC-3 tumour vasculature and other solid tumour types which could prevent cellular diffusion of the dye.

A different approach was developed using immuonofluorescence staining of endothelial cells using a primary CD31 antibody, followed by a secondary antibody treatment with Alexa Fluor® 488 [532-533]. Initially, there was uncertainty as to whether the vasculature formed in the human PC-3 tumour xenograft originated from the host or from the tumour. Thus, a trial attempt was carried out using a CD31 antibody recognising human vasculature, but functional endothelial cells were not clearly visible. This issue was clarified once an anti-mouse CD31 antibody was used. Nevertheless, the protocol used required considerable modifications before optimum conditions were attained. In particular the staining protocol was modified, including the samples' fixation, the antigen retrieval and the blocking of nonspecific binding. For the samples' fixation, both paraformaldehyde and ice-cold acetone were tested, whereby acetone was found to be the most effective. When freshly frozen sections were utilised, antigen retrieval was not necessary because the samples were not fixed in paraformaldehyde. In order to block nonspecific binding of the antibody and to avoid background staining, 5% or 10% normal goat serum (from the same species as the secondary antibody) was initially used. This failed to improve the immunofluorescence staining. Therefore, 2% bovine serum albumin (BSA) in PBS was selected as a different blocking buffer and proved to be effective.

3.3 Materials and Methods

3.3.1 Materials

DMSO, FBS, streptomycin/penicillin solution, polypropylene tuberculin syringes (27 x ½ in.), Triton-X 100, BSA were all purchased from Sigma, Ireland. EBM-2 medium was purchased from Lonza, Ireland and basement membrane matrix (matrigel) from BD Biosciences, Ireland. Vetalar® and Rompun® were provided by BioResources Unit (BRU), TCD. Tissue-Tek* optimum cutting temperature (O.C.T.) compound was purchased from Syntec Scientific, Ireland. Superfrost plus microscopy slides and cover slips were purchased from VWR, Ireland. Purified anti-mouse CD31 (PECAM-1) antibody was purchased from BD Biosciences, Ireland. PBS tablets, Alexa Fluor® 488 goat anti-rat IgG and ProLong® gold antifade reagent with DAPI were purchased from Invitrogen, Ireland.

Liquid nitrogen was provided by the School of Chemistry, TCD. All materials used for the paraffin-embedding of tumour samples and their staining with H&E were kindly provided by Peter Stafford, Department of Zoology, TCD.

3.3.2 Cell Line

PC-3 human prostate adenocarcinoma cell line was purchased from LGC Standards, UK and cultured in F12K medium supplemented with 0.02 mg/mL sodium pyruvate, 10% FBS and 10 mL/L penicillin/streptomycin solution. PC-3 cell line was selected for two reasons; firstly for its high expression pattern of APN and secondly due the cells' invasive potential when growing in tumour xenograft models. Cell and tissue cultures were kept at 37 °C in a humidified atmosphere containing 5% CO_2 at all times and maintained as previously described in Chapter 2, section 2.2.4, p.80.

3.3.3 Test Compounds

For the *ex vivo* assays, stock solution of test compounds were dissolved in DMSO and then diluted in the appropriate medium at the required concentrations (final DMSO concentration $\leq 0.1\%$). Control solutions contained 0.1% DMSO in medium. For the *in vivo* studies, control compound CA-4P and test compounds, ECB206 and GS291, were dissolved in DMSO and then diluted at the appropriate concentration in PBS, pH = 7.4

(final DMSO concentration was 5%). The control solution contained 5% DMSO in PBS. Fresh solutions were prepared prior to each treatment.

3.3.4 Animals

Male Wistar rats (200-300 g) were sourced from the BioResources Unit (BRU), TCD. Animals were housed under controlled conditions at 22 °C with 12h light and 12h dark cycles. All animals had access to food and water *ad libitum*.

Male *balb-c* immunodeficient *nu/nu* mice, aged 6-8 weeks were supplied by Harlan, UK and housed in Scrubs, BRU. Immunodeficient mice were maintained in a specific pathogen free (SPF) environment within individual ventilated cages (IVCs) in groups of 10 or less, under controlled conditions at 22 °C with 12h light and 12h dark cycles. Animals received Harlan 2018 diet and had access to food and water *ad libitum*. Animal handling and experimentation were performed using aseptic techniques and under a laminar hood at all times. At the end of each experiment, animals were sacrificed by either CO_2 asphyxiation or cervical dislocation. All animal procedures were carried out under a project licence issued by the Department of Health and Children.

3.3.5 Aortic Ring Assay (anti-vascular model)

The aortic ring assay is an *ex vivo* assay which allows the analyst to examine the inhibition/stimulation of angiogenesis as well as the breakdown of existing vasculature. Matrigel was stored at -20 °C and prior to use, was thawed by placing it on ice and keeping it at 4 °C overnight. The matrigel was kept on ice at all times for the duration of the experiments. Aortic rings were obtained by excising the thoracic aorta of 5-10 week old Wistar male rats and removing the fibroadipose tissue from the aortic wall. The rings were obtained by cross-sectioning the aorta at ~ 1 mm intervals and any blood clots were removed by washing them several times with EBM-2. Matrigel (80 μL) was placed uniformly in each well of a 12-well plate and the aortic rings were then individually placed within the matrigel layer with the lumen perpendicular to the surface of the plate. The matrigel solution was allowed to solidify for 30-40 minutes at 37 °C and 1 mL of EBM-2 medium (supplemented with 2% FBS and 1 mM streptomycin/penicillin solution) was added to each culture. The aortic rings were kept

in a humidified CO_2 incubator at 37 °C and the medium was replaced every other day, starting from day 3. Once an established microvessel network was developed (day 7-9), test compounds diluted in 1 mL of EBM-2 medium were added to each well and incubated at 37 °C for 24h. The cultures were monitored for microvessel breakdown over time and images were taken 4h and 24h after treatment using an Olympus CKX41 inverted microscope. Images were captured with an E-330 SLR camera system and processed using Cell^A software. Each compound concentration was tested in duplicate. Results were presented as images showing the microvessel breakdown at each time point.

3.3.6 Aortic Ring Assay (anti-angiogenic model)

In order to examine the anti-angiogenic effect of test compounds, the aortic ring assay was performed as previously described with a slight modification. The assay was conducted over 8 days with test compounds added on day 1. Relative to the anti-vascular assay the concentration of test compounds used was reduced by a factor of 10. On day 1, once the aortic ring cultures were obtained and embedded in matrigel, the stock solutions of test compounds were diluted in medium at the appropriate concentrations and added to the assigned wells. The cultures were kept in a humidified CO_2 incubator at 37 °C and the medium was replaced with fresh medium containing test compounds every other day, starting from day 3. On day 8, images of the aortic rings were captured as previously described. Each compound concentration was tested in duplicate and each experiment was performed three independent times. Microvessel density was then analysed using Image J software (NIH) and results were presented as the mean pixel density area ± SEM, along with images of the aortic rings. Statistical comparison between the treated and control groups was determined using Student's *t*-test.

3.3.7 Maximum Tolerated Dose

Prior to the anti-tumour evaluation of test compounds it was necessary to determine a suitable well-tolerated dose. Following the method by Burtles *et al.*, individual test compounds were injected i.p. into an individual animal at a starting dose, based on the efficacy of existing marketed compounds. Signs of toxicity or abnormal behaviour were monitored and recorded over 48h. Where no side effects were observed, the dose was

increased in other animals. If signs of toxicity were noted, the dose of the compound was slightly reduced until a dose producing no toxic signs was established (*i.e.* the MTD) [534].

3.3.8 Tumour System

PC-3 human prostate adenocarcinoma cell line was used in this study. The procedure involved re-suspending $1x10^6$/100 µL of PC-3 cells in complete medium, followed by subsequent s.c. injection into the right flank of donor animals. The tumours were allowed to grow for a period of 2-3 months until they reached the appropriate size (~ 350-450 mm^3). Tumours were then excised from the donor animals, placed in culture plates with sterile PBS containing antibiotics and cut into small fragments of ~1 mm^3. Single fragments were implanted s.c. using a trocar into the right flank of each mouse, while under brief general anaesthesia (0.5 mL Vetalar® + 0.25 mL Rompun® + 4.25 mL water for injection (wfi), at 0.1 mL/10 g body weight, i.p. injection). As soon as the tumours could be accurately measured by callipers the mice were allocated randomly into different treatment groups, each group consisting of 7-8 mice. Mean group tumour size variation was kept to a minimum.

3.3.9 Chemotherapy Studies

Test compounds were prepared at the appropriate concentration and administered by an i.p. injection, once a week for three weeks at doses below their previously established MTDs. CA-4P was used as a positive control. Each group had a total of 8 mice and day 0 was designated as the first day of treatment. Where necrotic tumour implants were observed, animals were excluded from the study; therefore the number of animals in each group varied between 7-8 mice. Two-dimensional calliper measurements of the tumours were used to assess tumour growth. Tumour and body weight (BW) measurements were obtained every other day. The experiment was terminated on day 25 and the animals were sacrificed by cervical dislocation. Using the formula $(a^2 \times b) / 2$, tumour volumes were calculated (where a is the smaller and b the larger diameter of the tumour) [535]. Next, the relative tumour volume (RTV) was determined using the following formula: $RTV = (\text{tumour volume on day}_n / \text{tumour volume on day}_0)$

where $n = 0$ - *day of completion*

The mean RTV was calculated for each day and semi-log plots of mean RTV *vs* duration (days) were drawn. The Mann-Whitney *U*-test was used to determine any significant difference between the growth rate of treated tumours and the control group. Where appropriate, statistical significance on individual days of treatment was also determined using the Mann-Whitney *U*-test.

The percentage of BW was calculated using the following formula:

$$\% BW = 100\text{-}(BW \text{ on } day_n / BW \text{ on } day_0) * 100$$

where $n = 0$ - *day of completion*

The mean percentage BW was calculated for each day and plots of mean percentage BW *vs* duration (days) were constructed. A percentage BW above 85%, relative to control, is considered to be within the normal range. Any value below that was considered under the limit and a sign of significant systemic toxicity caused by test compounds.

3.3.10 Assessment of Tumour Necrosis

Following completion of the *in vivo* efficacy studies of test compounds, histological examination of the treated and control tumours was carried out. Tumours were rapidly excised from each animal and immersed in 10% neutral-buffered formalin for 24h. Several steps of tissue dehydration were followed before embedding the tumour samples in paraffin. Each consecutive step required incubation of the tumour samples in each solution for approximately 1-2h (depending on the size of the tumour). The solutions for each incubation step were as follows: 70% ethanol, 90% ethanol, 100% ethanol (twice), histoclear, histoclear/paraffin (1:1, at 65 °C), paraffin (at 65 °C, twice). The tumour samples were then embedded into paraffin blocks and allowed to set for 24h. Tumour-paraffin blocks were kept at RT until required for sectioning.

Leica RM2255 automated rotary microtome was used for the sectioning of the tumours and was kindly provided by the Department of Zoology, TCD. Paraffin sections, 5-μm thick, were taken at 200-μm intervals and placed in a 45 °C waterbath using a small forceps. The paraffin slices were allowed to float and expand on the surface of the waterbath and then placed onto the surface of super frost plus microscopy slides and allowed to air-dry overnight.

In order to examine the tumours for the presence of any extensive necrosis, the slides were stained with H&E. The slides were placed on a slide holder, immersed and consecutively incubated in the following solutions: histoclear, 100% ethanol (twice), 90% ethanol, 70% ethanol (for 2-5 minutes each stage). Then, the slides were treated with 2.5% sodium thiosulphate for 30 seconds to remove picric acid and washed with d.w. Following this step, the slides were placed in Harris' haematoxylin solution for 10 minutes and then washed thoroughly with d.w. Acid alcohol (0.5% aqueous HCl in 70% ethanol) was used to treat the samples for 10 seconds to remove any excess haematoxylin from the cells. The slides were washed with d.w and then placed in alkaline Scott's tap water for 15-30 seconds, followed by 1% aqueous eosin for 15 seconds and washed again with d.w. Next, the slides were placed in 100% ethanol twice, firstly for 30 seconds and then for 2 minutes. They were then placed in histoclear twice, for 3 minutes each time. Finally, the sections were mounted with cover slips using D.P.X medium and allowed to dry. Tumour sections were visualised using an Olympus CKX41 inverted microscope. Images were captured with an E-330 SLR camera system and processed using Cell^A software. Three tumours per group were analysed and the results were presented as images showing the extent of tumour necrosis within control and treated groups.

3.3.11 Assessment of the Tumour Vasculature

The effect of treatment with test compounds on the functional vasculature of PC-3 tumours was evaluated in 3 tumour bearing mice. Tumours were implanted in mice as previously described and were treated as soon as an established tumour vasculature developed (minimum diameter of 7 mm). The animals were injected with test compound or vehicle using a single i.p. injection. After 6h of treatment, animals were sacrificed by cervical dislocation. The tumours were rapidly excised, wrapped in aluminium foil, immersed in liquid nitrogen and stored at -80 °C until ready for ultracryotomy.

Prior to use, tumours were embedded in liquid O.C.T and kept at -20 °C until the O.C.T solidified. Leica CM1850 cryostat was used for the sectioning of the samples and was kindly provided by the Institute of Neuroscience, TCD. Frozen 8-μm sections of each

tumour were taken at 200-μm intervals, placed on super frost plus microscopy slides and kept at -20 °C until required for staining.

For the staining procedure, slides were kept at RT for 30 minutes and then fixed in ice-cold acetone for 10 minutes. The slides were then washed three times in PBS (for 10 minutes each time) and treated with 0.1% Triton-X 100 in PBS for 8 minutes at 4 °C. Next, the slides were washed twice in PBS (for 5 minutes each time) and incubated with 2% BSA in PBS for 1h at RT. Following these steps, 200 µL of anti-mouse CD31 antibody (1:50, diluted in 2% BSA in PBS) was added on top of each tumour sample for 1h at RT. The slides were washed a further three times in PBS (for 5 minutes each time) and then incubated with 200 µL of secondary goat anti-mouse Alexa Fluor® 488 antibody (1:1000, diluted in 2% BSA in PBS) for 30 minutes at RT. After that, the slides were washed twice with PBS (for 5 minutes each time) and allowed to air-dry for 10 minutes. Cover slips were carefully mounted on the slides using ProLong® gold antifade reagent with DAPI (for nuclear staining) and stored at 4 °C until required for analysis. Images were taken using an Olympus FV1000 point scanning confocal microscope provided by the School of Biochemistry and Immunology, TCD. The amount of CD31 staining was analysed using Image J and the results were presented as mean pixel density area ± SEM, together with images of the functional vasculature. Experiments were performed in triplicate.

3.3.12 Statistical Analysis

Statistical analysis of the data was carried out using GraphPad Prism, version 5. Pixel density area of mircovessel networks, tumour measurements, percentage of BW and pixel density area of functional vasculature were expressed as mean ± SEM. The statistical significance between control and treated groups in the *ex vivo* aortic ring assay of angiogenesis and in the *in vivo* anti-vascular study was determined using Student's *t*-test. In order to determine whether there was a significant difference between the control and treated groups in the *in vivo* efficacy study, the Mann-Whitney *U*-test was applied using GraphPad Prism, version 5. Statistical significance was also determined on individual days of treatment in the *in vivo* study, using the Mann-Whitney *U*-test.

3.4 Results

3.4.1 Aortic Ring Assay (anti-vascular model)

The anti-vascular activity of selected compounds from each group was evaluated in the *ex vivo* aortic ring assay. The cultures were monitored microscopically from 1h to 24h after treatment and the degree of vasculature disruption was captured at different time points.

3.4.1.1 Group I Compound

The effect of control compound CA-4 and group I compound RS133 was examined in the aortic ring assay for evidence of microvessel breakdown. Treatment of the aortic rings with 10 nM CA-4 showed a potent anti-vascular effect on the microvessels structure, as soon as 4h after treatment (Figure 3.2). Incubation of the aortic rings with 100 nM RS133 demonstrated disruption of the microvessel network as soon as 4h after treatment, and the effect was time-dependent *i.e.* the breakdown was more apparent 24h after treatment (Figure 3.3).

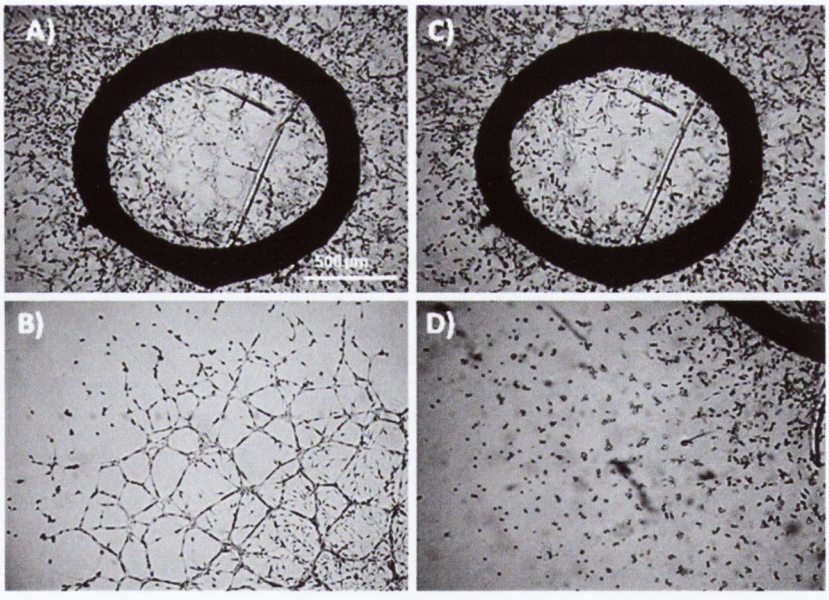

Figure 3.2: The anti-vascular effect of CA-4. The aortic rings were kept in a humidified CO_2 incubator at 37 °C and the medium was changed every other day, starting from day 3. Test compounds were added on day 8. Photomicrographs of the aortic cultures were taken under bright field microscopy using a digital camera (x4). **A-B)** Before the addition of test compound and **C-D)** 10 nM CA-4 (4h).

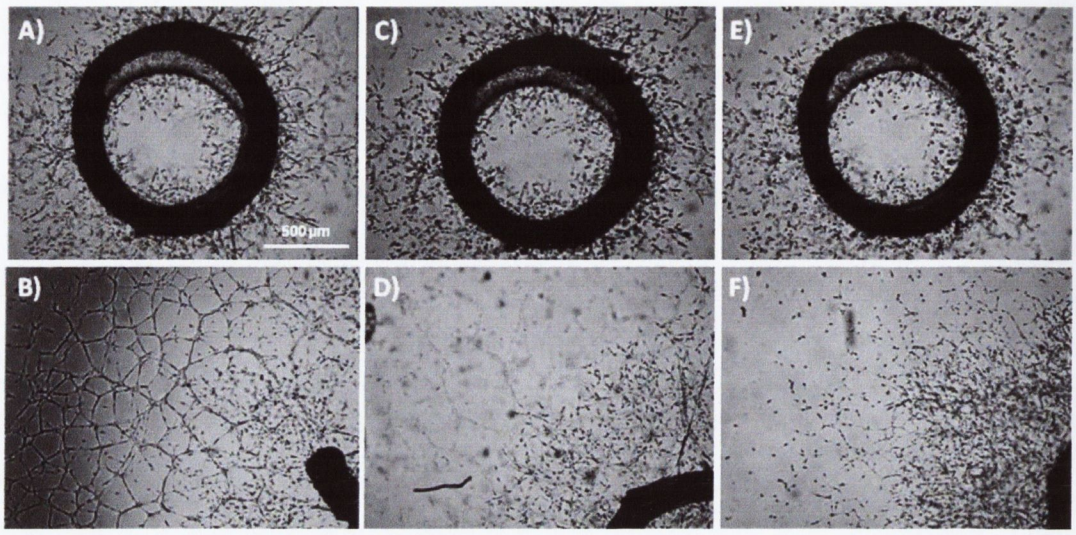

Figure 3.3: The anti-vascular effect of RS133. The aortic rings were kept in a humidified CO_2 incubator at 37 °C and the medium was changed every other day, starting from day 3. Test compounds were added on day 8. Photomicrographs of the aortic cultures were taken under bright field microscopy using a digital camera (x4). **A-B)** Before the addition of test compound, **C-D)** 100 nM RS133 (4h) and **E-F)** 100 nM RS133 (24h).

3.4.1.2 Group II Compounds

Group II compounds, RS180 and GS117, were examined for their anti-vascular effect on existing microvessel networks. Aortic rings treated with 100 nM of either RS180 or GS117, resulted in evident changes in the microvessels' structure after 4h of treatment (Figure 3.4 and 3.5). This effect was time-dependent with the greater disruption following 24h of treatment. Although these compounds showed greater anti-vascular activity than RS133, they were not superior to that of CA-4.

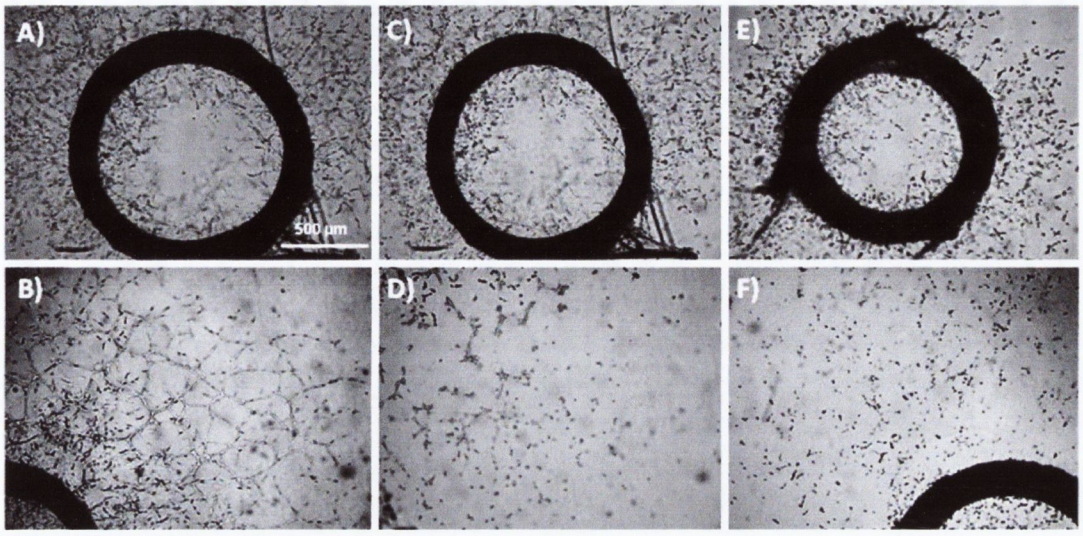

Figure 3.4: The anti-vascular effect of RS180. The aortic rings were kept in a humidified CO_2 incubator at 37 °C and the medium was changed every other day, starting from day 3. Test compounds were added on day 8. Photomicrographs of the aortic cultures were taken under bright field microscopy using a digital camera (x4). **A-B)** Before the addition of test compound, **C-D)** 100 nM RS180 (4h) and **E-F)** 100 nM RS180 (24h).

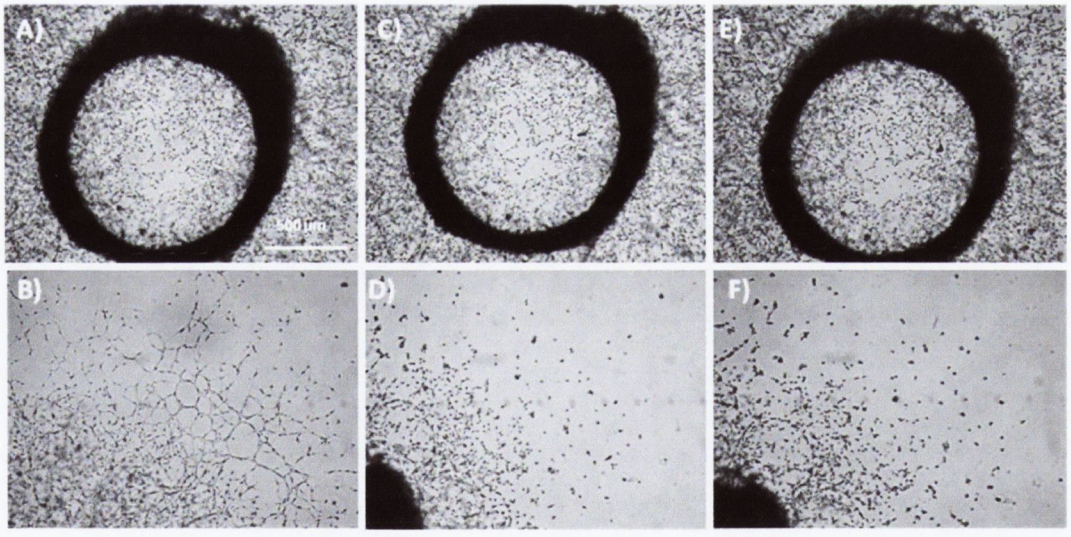

Figure 3.5: The anti-vascular effect of GS117. The aortic rings were kept in a humidified CO_2 incubator at 37 °C and the medium was changed every other day, starting from day 3. Test compounds were added on day 8. Photomicrographs of the aortic cultures were taken under bright field microscopy using a digital camera (x4). **A-B)** Before the addition of test compound, **C-D)** 100 nM GS117 (4h) and **E-F)** 100 nM GS117 (24h).

3.4.1.3 Group III Compound

The anti-vascular effect of group III compound ADR269 was examined in the aortic ring assay. Although ADR269 showed similar *in vitro* activity profile to that of CA-4, did not demonstrate pronounced microvessel breakdown at 10 nM, as observed with CA-4. Instead its anti-vascular activity was more evident at 50 nM, following 4h of treatment and the effect was time-dependent (Figure 3.6).

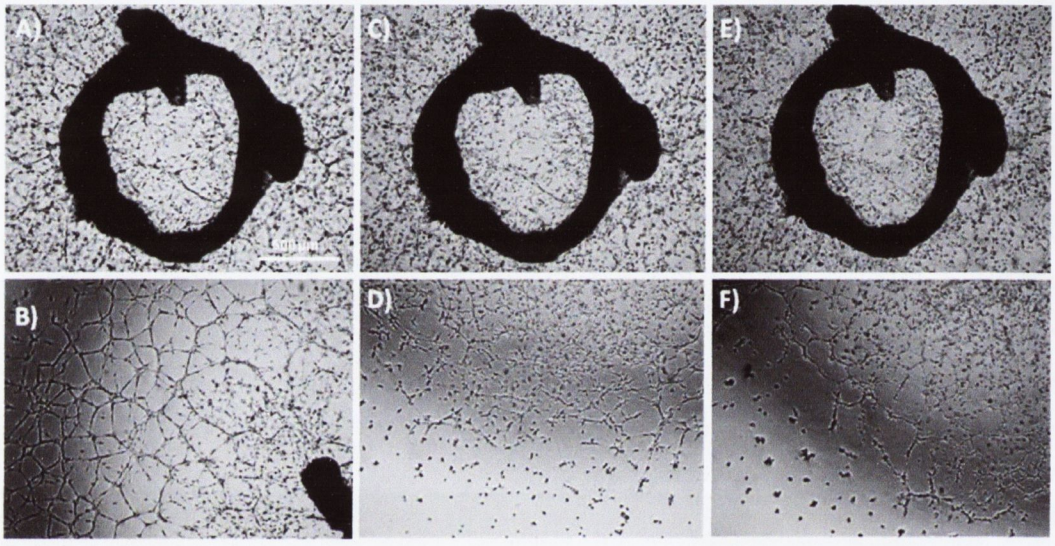

Figure 3.6: The anti-vascular effect of ADR269. The aortic rings were kept in a humidified CO_2 incubator at 37 °C and the medium was changed every other day, starting from day 3. Test compounds were added on day 8. Photomicrographs of the aortic cultures were taken under bright field microscopy using a digital camera (x4). **A-B)** Before the addition of test compound, **C-D)** 50 nM ADR269 (4h) and **E-F)** 50 nM ADR269 (24h).

3.4.1.4 Group IV Compounds

Group IV compounds, GJH140 and ADR149, were assessed in the anti-vascular model of the aortic ring assay. Both compounds demonstrated potent activity at 10 nM with clear microvessel breakdown following 4h of treatment and the effect was time-dependent (Figure 3.7 and 3.8). In fact, their anti-vascular properties were similar to that of CA-4.

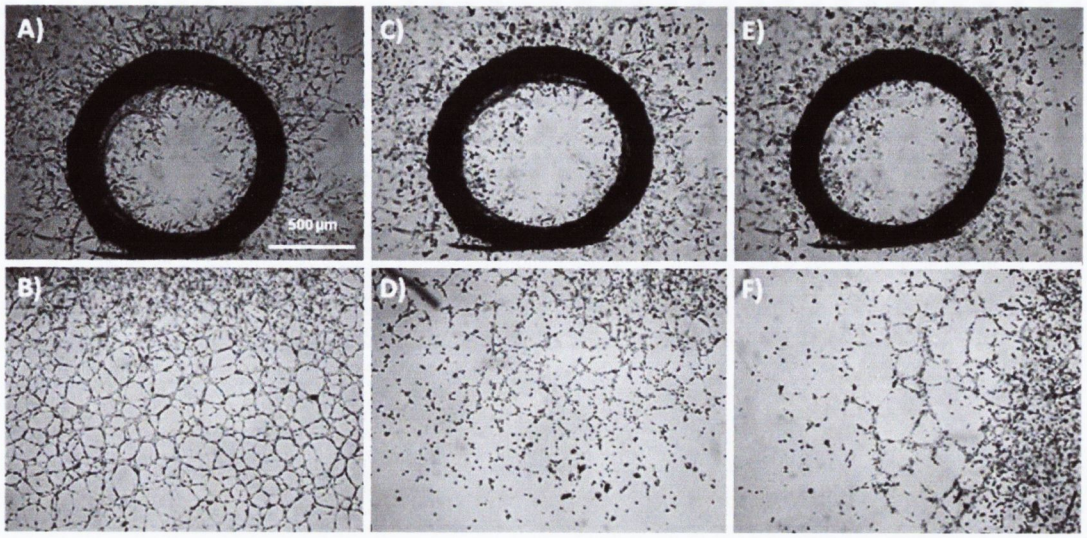

Figure 3.7: The anti-vascular effect of GJH140. The aortic rings were kept in a humidified CO_2 incubator at 37 °C and the medium was changed every other day, starting from day 3. Test compounds were added on day 8. Photomicrographs of the aortic cultures were taken under bright field microscopy using a digital camera (x4). **A-B)** Before the addition of test compound, **C-D)** 10 nM GJH140 (4h) and **E-F)** 10 nM GJH140 (24h).

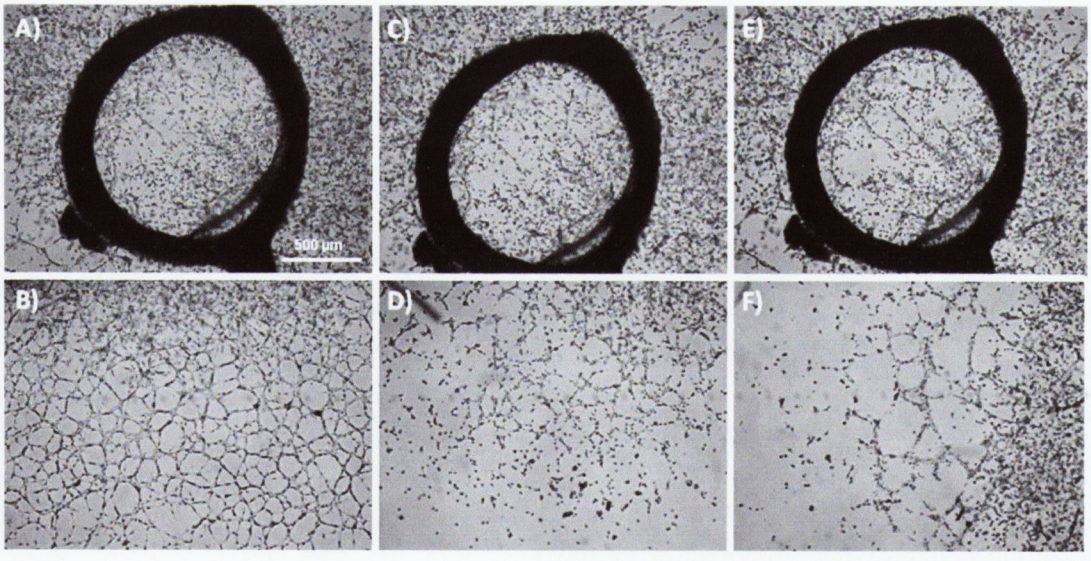

Figure 3.8: The anti-vascular effect of ADR149. The aortic rings were kept in a humidified CO_2 incubator at 37 °C and the medium was changed every other day, starting from day 3. Test compounds were added on day 8. Photomicrographs of the aortic cultures were taken under bright field microscopy using a digital camera (x4). **A-B)** Before the addition of test compound, **C-D)** 10 nM ADR149 (4h) and **E-F)** 10 nM ADR149 (24h).

3.4.2 Aortic Ring Assay (anti-angiogenic model)

In addition to the anti-vascular activity, tubulin inhibitors are known to exhibit anti-angiogenic properties. For this reason, test compounds were examined in the aortic ring assay for inhibition of angiogenesis. The results were presented as the mean pixel density area ± SEM. Statistical analysis of the microvessel density of control and treated cultures was determined using Student's *t*-test

3.4.2.1 Group I Compound

CA-4 and RS133 were examined for their anti-angiogenic activity in the aortic ring assay. CA-4 demonstrated a moderate anti-angiogenic effect at 1 nM but showed a significant ($p < 0.01$) inhibition of microvessels formation at 10 and 50 nM (Figure 3.9 and 3.10). However, RS133 treatment did not inhibit the vessel formation at 10 nM, but significantly reduced the growth of vessels at 100 nM ($p < 0.05$) and at 1 μM ($p < 0.01$) (Figure 3.11 and 3.12).

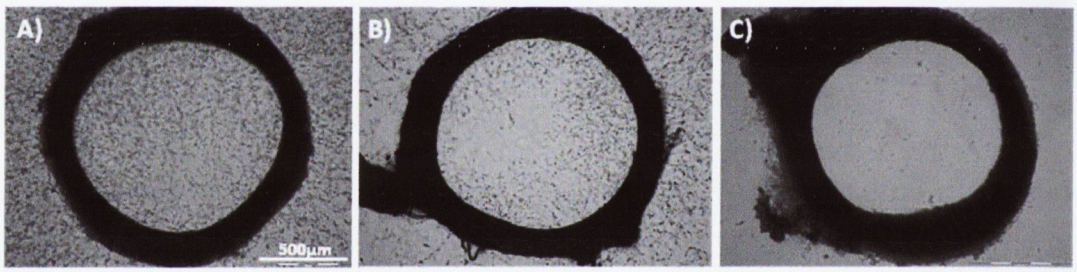

Figure 3.9: The anti-angiogenic effect of CA-4. The aortic rings were kept in a humidified CO_2 incubator at 37 °C and the medium was changed every other day, starting from day 3. Test compounds were added on day 1. Photomicrographs of the aortic cultures were taken under bright field microscopy using a digital camera (x4). **A)** Control (0.1% DMSO), **B)** 1 nM CA-4 and **C)** 10 nM CA-4.

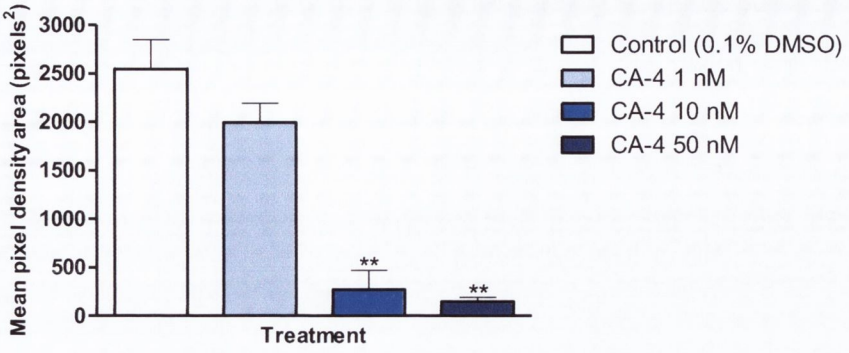

** $p < 0.01$, significantly lower mean pixel density area compared with the untreated controls as determined by Student's *t*-test.

Figure 3.10: The microvessel density of CA-4-treated cultures was obtained using Image J. Data represents mean pixel density area ± SEM (n=3).

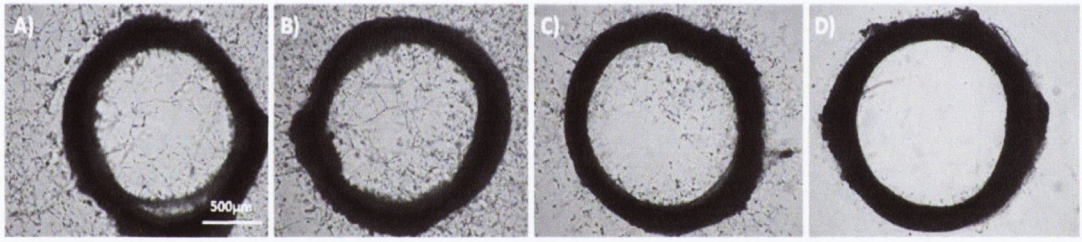

Figure 3.11: The anti-angiogenic effect of RS133. The aortic rings were kept in a humidified CO_2 incubator at 37 °C and the medium was changed every other day, starting from day 3. Test compounds were added on day 1. Photomicrographs of the aortic cultures were taken under bright field microscopy using a digital camera (x4). **A)** Control (0.1% DMSO), **B)** 10 nM RS133, **C)** 100 nM RS133 and **D)** 1 µM RS133.

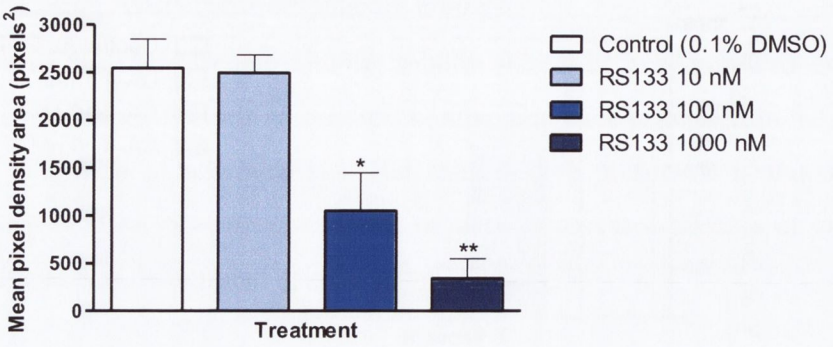

Figure 3.12: The microvessel density of RS133-treated cultures was obtained using Image J. Data represents mean pixel density area ± SEM (n=3).

3.4.2.3 Group II Compounds

The anti-angiogenic effect of RS180 and GS117 was determined using the aortic ring assay. There was no inhibitory effect observed after treatment with 1 nM RS180, however 10 nM and 100 nM significantly ($p < 0.01$) inhibited the formation of microvessels and the response was dose-dependent (Figure 3.13 and 3.14). RS180 activity was proved to be closer to that of CA-4. The aortic rings treated with 10 nM GS117 did not demonstrate a decrease in microvessels formation, but 50 nM were sufficient to cause complete growth inhibition (Figure 3.15 and 3.16).

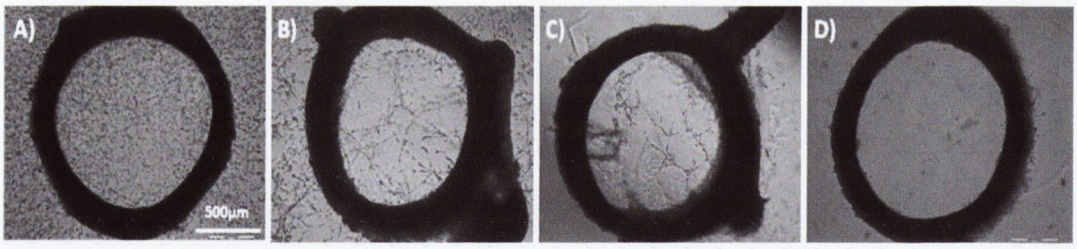

Figure 3.13: The anti-angiogenic effect of RS180. The aortic rings were kept in a humidified CO_2 incubator at 37 °C and the medium was changed every other day, starting from day 3. Test compounds were added on day 1. Photomicrographs of the aortic cultures were taken under bright field microscopy using a digital camera (x4). **A)** Control (0.1% DMSO), **B)** 1 nM RS180, **C)** 10 nM RS180 and **D)** 100 nM RS180.

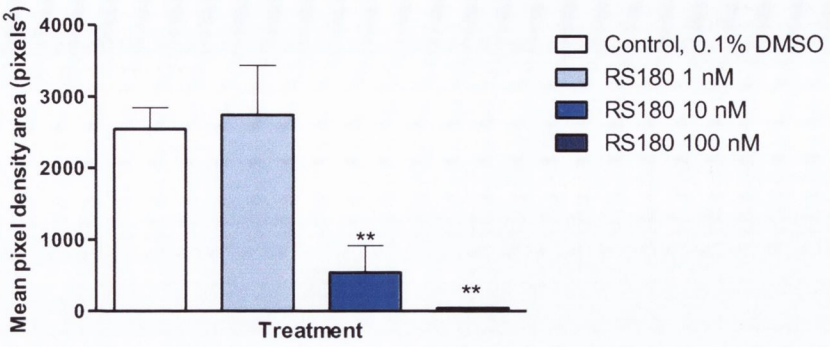

** $p < 0.01$, significantly lower mean pixel density area compared with the untreated controls as determined by Student's *t*-test.

Figure 3.14: The microvessel density of RS180-treated cultures was obtained using Image J. Data represents mean pixel density area ± SEM (n=3).

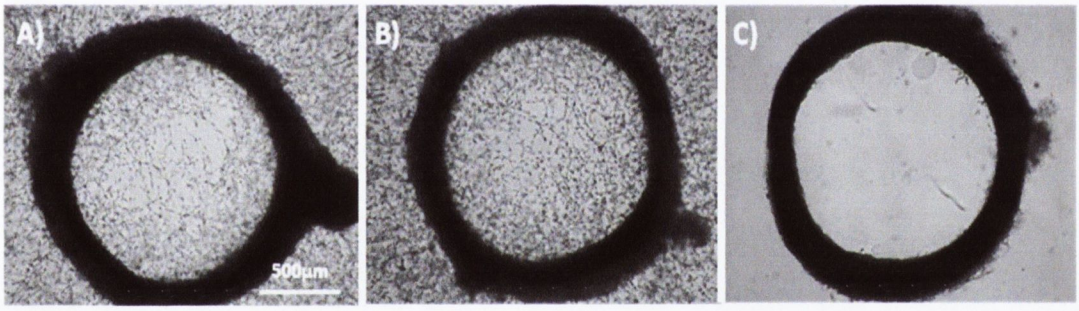

Figure 3.15: The anti-angiogenic effect of GS117. The aortic rings were kept in a humidified CO_2 incubator at 37 °C and the medium was changed every other day, starting from day 3. Test compounds were added on day 1. Photomicrographs of the aortic cultures were taken under bright field microscopy using a digital camera (x4). **A)** Control (0.1% DMSO), **B)** 10 nM GS117 and **C)** 50 nM GS117.

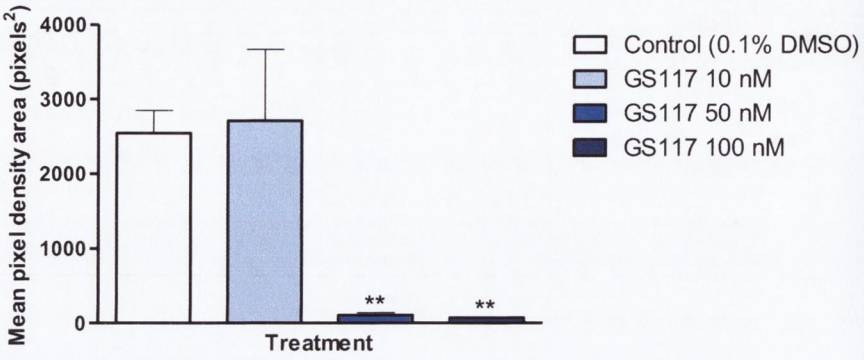

** $p < 0.01$, significantly lower mean pixel density area compared with the untreated controls as determined by Student's *t*-test.

Figure 3.16: The microvessel density of GS117-treated cultures was obtained using Image J. Data represents mean pixel density area ± SEM (n=3).

3.4.2.3 Group III Compound

The anti-vascular effect of ADR269 was investigated using the aortic ring assay. An insignificant reduction in vessel growth after treatment with 10 nM ADR269 was observed. Incubation of the cultured rings with 50 nM and 100 nM ADR269 significantly ($p < 0.01$) inhibited the development of microvessels, as shown in Figure 3.17 and 3.18.

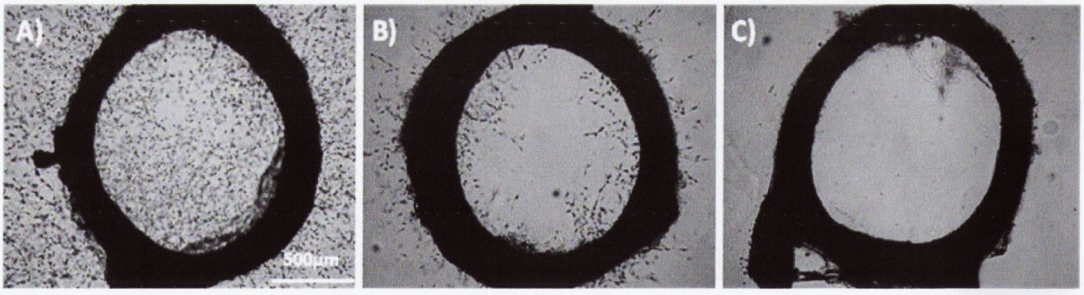

Figure 3.17: The anti-angiogenic effect of ADR269. The aortic rings were kept in a humidified CO_2 incubator at 37 °C and the medium was changed every other day, starting from day 3. Test compounds were added on day 1. Photomicrographs of the aortic cultures were taken under bright field microscopy using a digital camera (x4). **A)** Control (0.1% DMSO), **B)** 10 nM ADR269 and **C)** 50 nM ADR269.

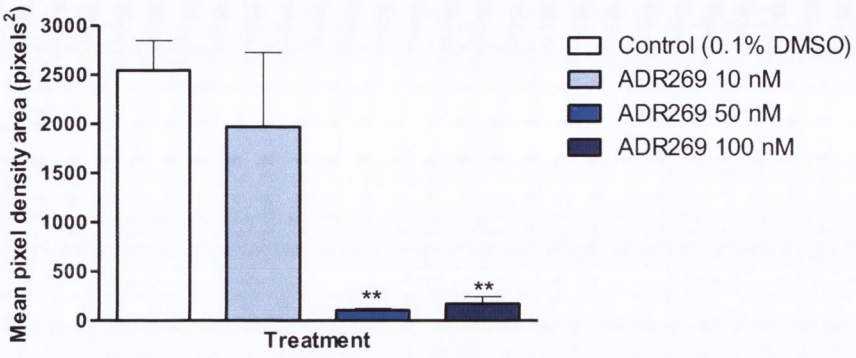

** $p < 0.01$, significantly lower mean pixel density area compared with the untreated controls as determined by Student's *t*-test.

Figure 3.18: The microvessel density of ADR269-treated cultures was obtained using Image J. Data represents mean pixel density area ± SEM (n=3).

3.4.2.4 Group IV Compounds

Group IV compounds, GJH140 and ADR149, were evaluated in the anti-vascular model of the aortic ring assay. GJH140 treatment reduced the microvessel density at concentrations as low as 5 nM, although this was not statistically significant. Incubation of the rings with 10 nM and 50 nM GJH140 significantly ($p < 0.01$) inhibited the microvessel growth, sharing similar inhibitory profile to CA-4 (Figure 3.19 and 3.20). Likewise, ADR149-treated rings showed no effect at 1 nM, decreased microvessel formation at 5 nM and significantly ($p < 0.01$) caused almost complete inhibition at 10 nM, indicating superior activity to that of CA-4 (Figure 3.21 and 3.22).

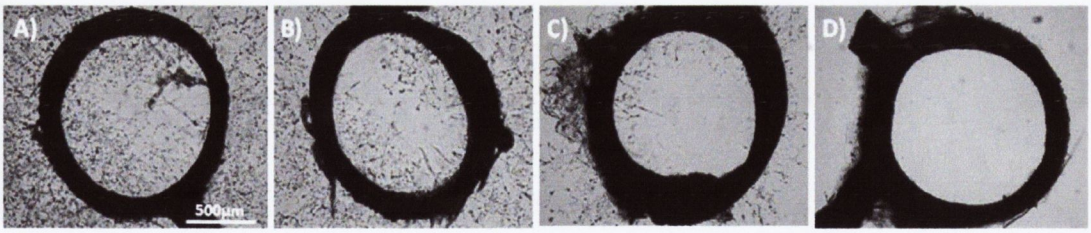

Figure 3.19: The anti-angiogenic effect of GJH140. The aortic rings were kept in a humidified CO_2 incubator at 37 °C and the medium was changed every other day, starting from day 3. Test compounds were added on day 1. Photomicrographs of the aortic cultures were taken under bright field microscopy using a digital camera (x4). **A)** Control (0.1% DMSO), **B)** 5 nM GJH140, **C)** 10 nM GJH140 and **D)** 50 nM GJH140.

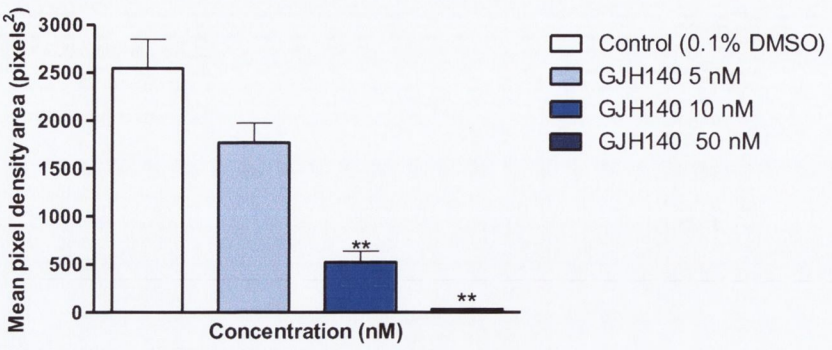

** $p < 0.01$, significantly lower mean pixel density area compared with the untreated controls as determined by Student's *t*-test.

Figure 3.20: The microvessel density of GJH140-treated cultures was obtained using Image J. Data represents mean pixel density area ± SEM (n=3).

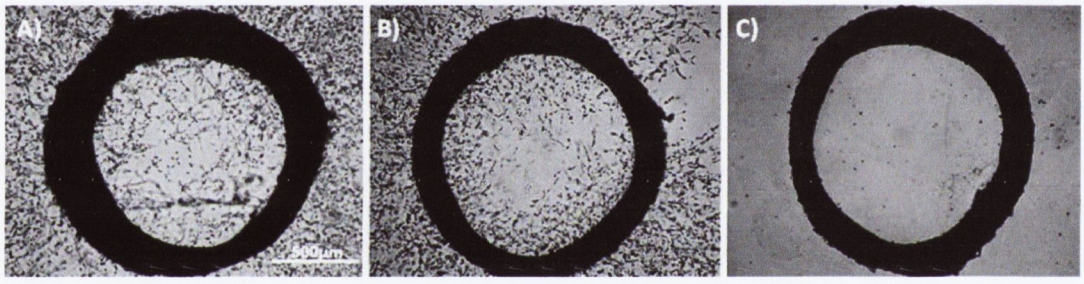

Figure 3.21: The anti-angiogenic effect of ADR149. The aortic rings were kept in a humidified CO_2 incubator at 37 °C and the medium was changed three times a week starting from day 3. Test compounds were added on day 1. Photomicrographs of the aortic cultures were taken under bright field microscopy using a digital camera (x4). A) Control (0.1% DMSO), B) 5 nM ADR149 and C) 10 nM ADR149.

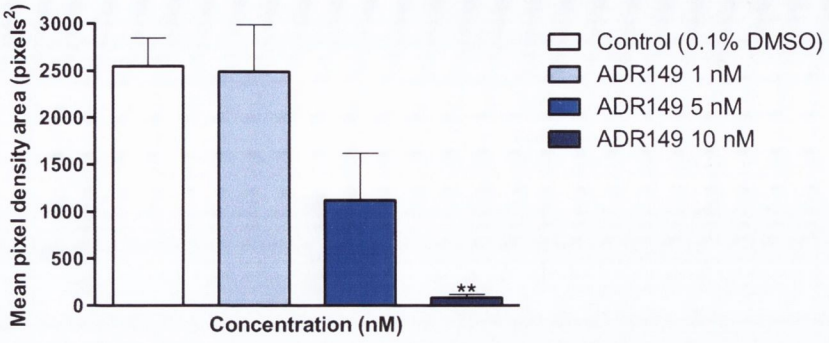

** $p < 0.01$, significantly lower mean pixel density area compared with the untreated controls as determined by Student's *t*-test.

Figure 3.22: The microvessel density of ADR149-treated cultures was obtained using Image J. Data represents mean pixel density area ± SEM (n=3).

3.4.3 *In Vivo* Evaluation of ECB206

The findings from the *in vitro* an *ex vivo* evaluation of test compounds revealed that ADR149 was one of the compounds with the most potential, due to its potency at low nanomolar concentrations. For this reason, a leucine prodrug form of ADR149 was synthesised by Breen, namely ECB206. This was the first *in vivo* study conducted and thus it was considered as a preliminary result and guidance for subsequent studies.

3.4.3.1 Maximum Tolerated Dose

It was essential to establish a maximum tolerated dose before commencing the *in vivo* efficacy study. Due to the fact that ADR149 had similar inhibitory activity to CA-4, a thorough search of the literature indicated that the most commonly used *in vivo* doses for CA-4 was between 100-150 mg/kg [312, 536-537]. Thus, 100 or 150 mg/kg ECB206 was injected as a single i.p. dose in two individual animals and any signs of toxicity were observed. Unexpectedly, the animals did not respond well to the treatment and showed signs of severe pain, hypothermia and dehydration. Therefore, a lower dose was administered at 75 mg/kg ECB206, which similarly showed to exert the same side effects, but to a lesser extent. A lower dose of 50 mg/kg ECB206 was then administered where no observable toxicity was noticed, hence it was chosen as the dose for the *in vivo* efficacy study.

3.4.3.2 *In Vivo* Anti-tumour Efficacy

The PC-3 tumour xenograft model was established and the anti-tumour efficacy of 50 mg/kg ECB206 once a week for three weeks was determined. Semi-log plots of mean RTVs *vs* time were generated as shown in Figure 3.23. According to the data (n=7), treatment with 50 mg/kg ECB206 failed to demonstrate anti-tumour activity compared to the control group (Figure 3.23 A). The mean tumour doubling time (when RTV = 2) of treated and control groups was calculated and the difference in growth delay was determined to be -5.22 days. Outlier tumour measurements were observed in two individual animals where their tumour growth rate was higher than the rest of the animals; for this reason those particular values were excluded from the data. A separate plot of RTVs *vs* time was generated (n=5), as shown in Figure 3.23 B. Statistical analysis using the Mann Whitney *U*-test was performed on individual days in order to examine any significant difference between ECB206 and control group but none was detected. According to the revised data (n=5), a slight decrease in tumour volume was observed after 16 days of treatment. The RTV2 of ECB206-treated and control groups were calculated and the difference in growth delay was 3.59 days. However, this was not statistically significant.

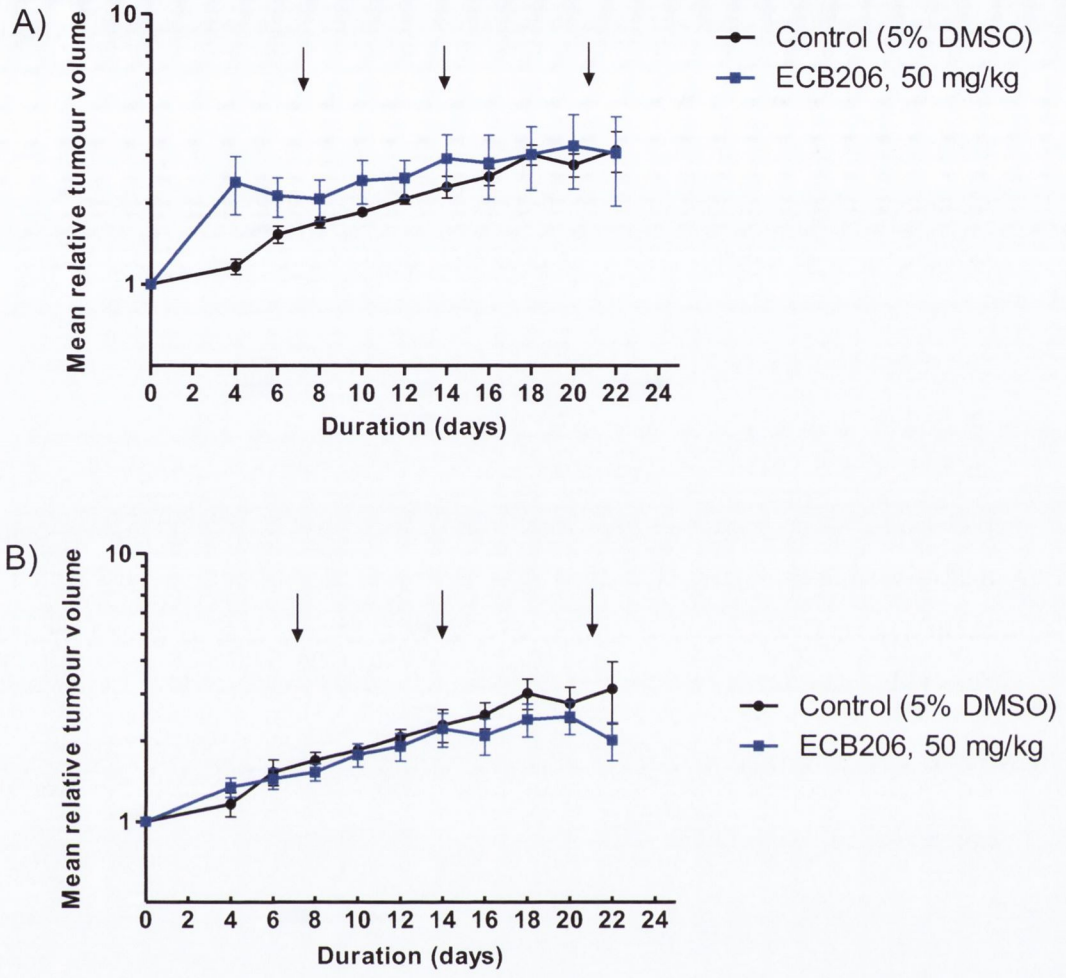

Figure 3.23: Evaluation of the efficacy of 50 mg/kg ECB206 administered once a week for three weeks in a PC-3 tumour xenograft model. Data represents the mean relative tumour volume ± SEM. **A)** n=7 and **B)** n=5. Arrows indicate days of treatment.

BW measurements were recorded every other day in order to determine any systemic toxicity caused during the treatment. The percentage BW was then calculated as shown in Figure 3.24. An observable decline of BW was noted following each treatment with maximum weight loss on day 16; nevertheless this was maintained above the 85% limit and thus was not considered significant.

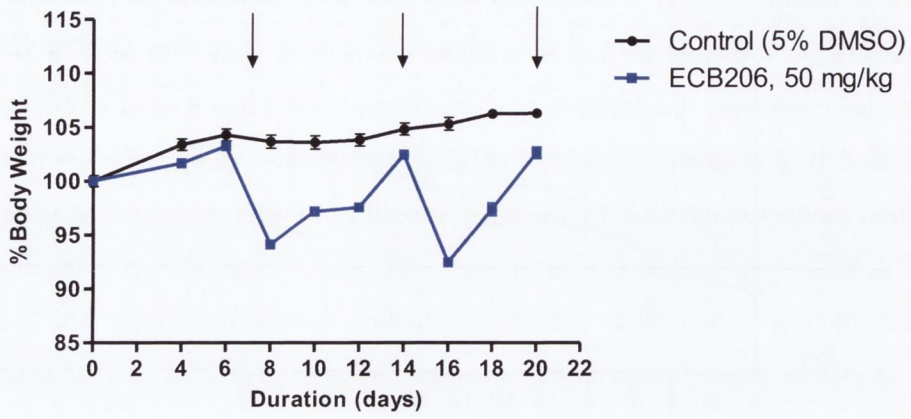

Figure 3.24: Body weight measurements were recorded to monitor any systemic toxicity following treatment with ECB206. Data represents the mean percentage body weight ± SEM (n=7). Arrows indicate days of treatment.

The data from the *in vivo* efficacy study with 50 mg/kg ECB206, including the mean RTV2, the growth delay and the maximum percentage of weight loss is summarised in Table 3.1.

Table 3.1: Summary of ECB206 *in vivo* data.

Treatment	Dose (mg/kg)	Mean RTV2* (days)	Growth delay (days)	Significance**	Max % weight loss (day)
Vehicle (n=7)	5% DMSO	10.94	-	-	None
ECB206 (n=7)	50	5.72	-5.22	NS	7.53 (16)
Vehicle (n=5)	5% DMSO	10.94	-	-	None
ECB206 (n=5)	50	14.53	3.59	NS	7.42 (16)

* Mean tumour volume doubling time, ** Mann-Whitney *U*-test was performed to determine the statistical significance of any differences in growth rate between control and treated groups. NS, not significant.

3.4.3.3 Assessment of Tumour Necrosis

In order to assess tumour necrosis, histological examination of three tumours treated for 24h with a single i.p. injection of 50 mg/kg ECB206 or vehicle (5% DMSO) was carried out. Tumour samples were processed for H&E staining and examined microscopically, whereby images from each treatment group were captured.

Control treated tumours demonstrated negligible amount of tumour necrosis in the centre, whereas all the ECB206-treated tumours displayed large areas of haemorrhagic necrosis with a remaining viable rim on the periphery (Figure 3.25).

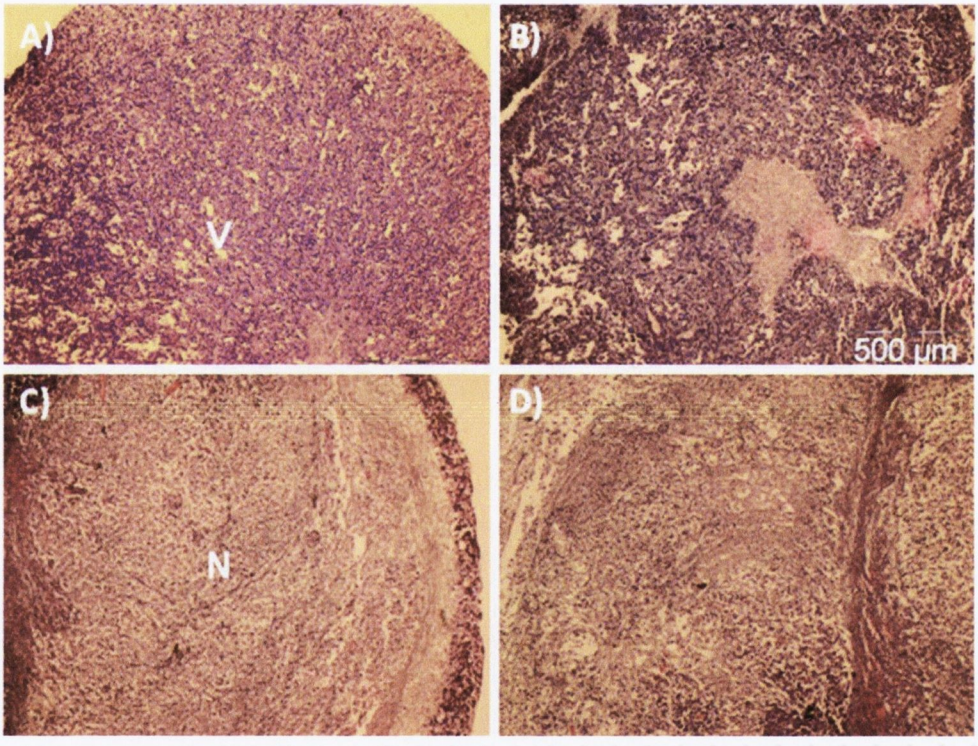

Figure 3.25: H&E stained tumour samples obtained from **A-B)** the control treated group and **C-D)** the ECB206-treated group, following 24h of a single i.p. injection (V=Viable, N=Necrotic, n=3).

3.4.4 *In Vivo* Evaluation of GS291

Following the preliminary results from the first *in vivo* study with ECB206, the next compound selected for evaluation was GS291.

3.4.4.1 Maximum Tolerated Dose

GS291 was firstly administered to animals at 100 or 150 mg/kg, whereby no observable toxicity was noted. Therefore, the dose was increased up to 200 mg/kg, where treated animals did not show any signs of toxicity. Following administration of a higher dose of 250 mg/kg GS291, animals appeared unwell and showed signs of pain and hypothermia. For this reason, the GS291 treatment dose was designated to be 200 mg/kg.

3.4.4.2 *In Vivo* Anti-tumour Efficacy

Tumour bearing mice were administered an i.p. injection of 200 mg/kg GS291 once a week for three weeks and 150 mg/kg CA-4P was used as a positive control (at a similar molar concentration to GS291). A semi-log plot of RTVs *vs* time was generated, as shown in Figure 3.26. Statistical analysis of the RTV of CA-4P- and GS291-treated groups compared to the control group was carried out on individual days using the Mann Whitney *U*-test. CA-4P treatment demonstrated significant ($*p < 0.05$) difference in the RTVs compared to the control, from day 5 until day 21. GS291-treated group showed a significant ($*p < 0.05$) reduction in tumour volume over the control group on days 7, 9, 12, 19 and 21. In comparison with the control group, treatment with 150 mg/kg CA-4P demonstrated significant tumour growth delay ($p < 0.01$, 6.28 days). Treatment with 200 mg/kg GS291 also resulted in a significant growth delay ($p < 0.05$, 4.55 days).

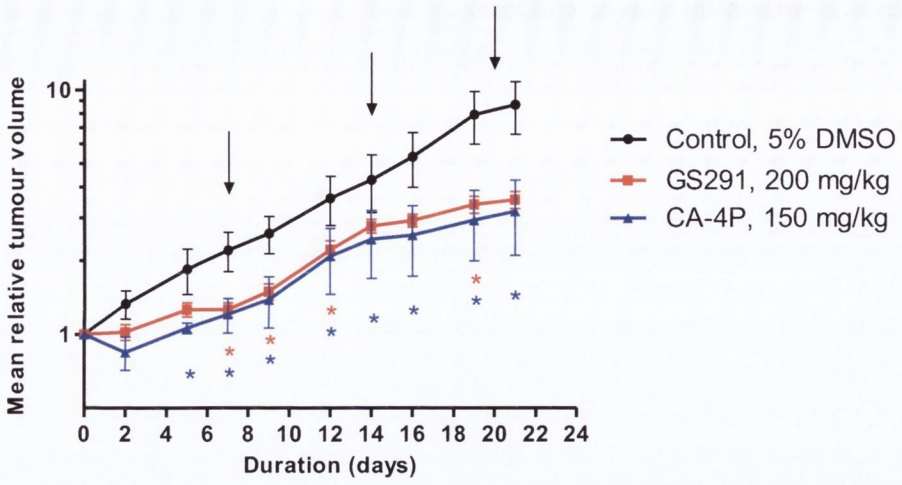

* $p < 0.05$, significantly higher mean relative tumour volume compared with the control group as determined by the Mann-Whitney *U*-test.

Figure 3.26: Evaluation of the efficacy of 200 mg/kg GS291 and 150 mg/kg CA-4P administered once a week for three weeks in a PC-3 tumour xenograft model. Data represents the mean relative tumour volume ± SEM (n=8). Arrows indicate days of treatment.

BW measurements were recorded every other day in order to determine any systemic toxicity caused following treatment. The percentage of mean BW was then calculated as shown in Figure 3.27. There was no reduction of BW following treatment with either CA-4P or GS291.

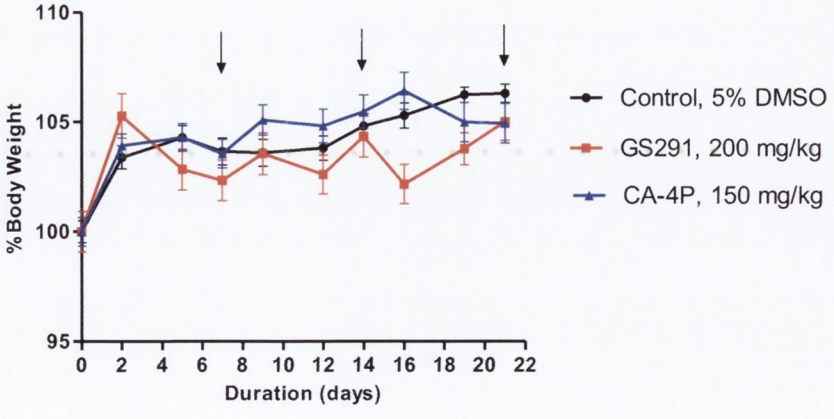

Figure 3.27: Body weight measurements were recorded to monitor any systemic toxicity following treatment with GS291 and CA-4. Data represents the mean percentage body weight ± SEM (n=8). Arrows indicate days of treatment.

The data from the *in vivo* efficacy study with 200 mg/kg GS291 and 150 mg/kg CA-4P, including the mean RTV2, the growth delay and the maximum percentage of weight loss is summarised in Table 3.2.

Table 3.2: Summary of GS291 and CA-4P *in vivo* data.

Treatment	Dose (mg/kg)	Mean RTV2* (days)	Growth delay (days)	Significance**	Max % weight loss (day)
Vehicle	5% DMSO	5.31	-	-	None
GS291	200	9.86	4.55	$p < 0.05$	None
CA-4P	150	11.59	6.28	$p < 0.01$	None

* Mean tumour volume doubling time, ** Mann-Whitney *U*-test was performed to determine the statistical significance of any differences in growth rate between control and treated groups.

3.4.4.3 Assessment of Tumour Necrosis

At the end of the *in vivo* efficacy study, histological examination of the treated tumours was carried out. Upon completion of the efficacy study, tumours were processed for H&E staining. Tumour sections were visualised using an inverted microscope and images from each group were captured.

A variation of tumour size in the control treated group was noted which could affect the extent of tumour necrosis. Once all of the control tumours were analysed it was observed that the larger the tumour size, the higher the degree of necrosis. Therefore, three medium-sized tumours were selected for inclusion in the analysis. Control tumours displayed a small amount of necrosis, whereas all three CA-4- and GS291-treated tumours showed a greater degree of necrotic area in the centre with a residual viable tissue found mainly in the periphery (Figure 3.28).

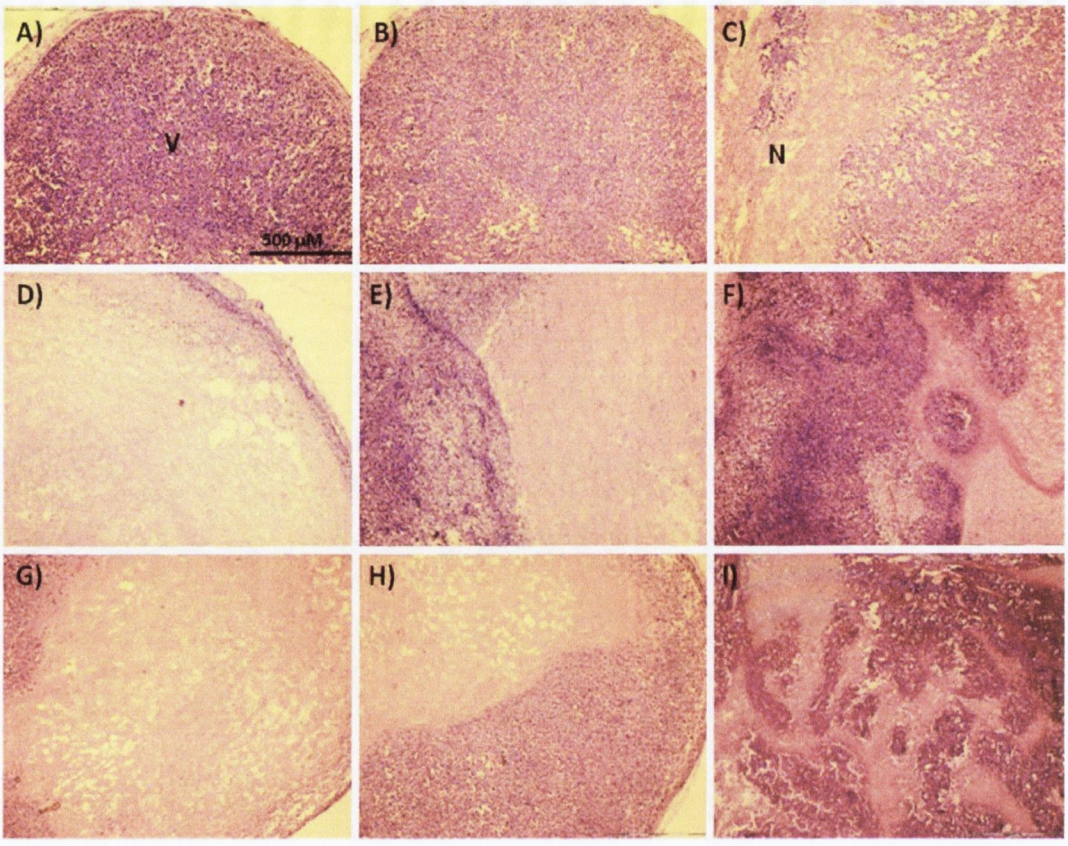

Figure 3.28: H&E stained tumour samples obtained from **A-C)** the control treated group, **D-F)** the CA-4P-treated group and **G-I)** the GS291-treated group (V=Viable, N=Necrotic, n=3).

3.4.4.4 Assessment of the Tumour Vasculature

In order to investigate whether part of the anti-tumour effect of GS291 was caused by tumour vasculature shutdown, 200 mg/kg GS291 was administered by a single i.p. injection. Following a 6h period, tumours were rapidly excised and processed for endothelial cells staining. The tumour slides were visualised using a confocal microscope and the images were analysed for stained endothelial cells using Image J (Figure 3.29).

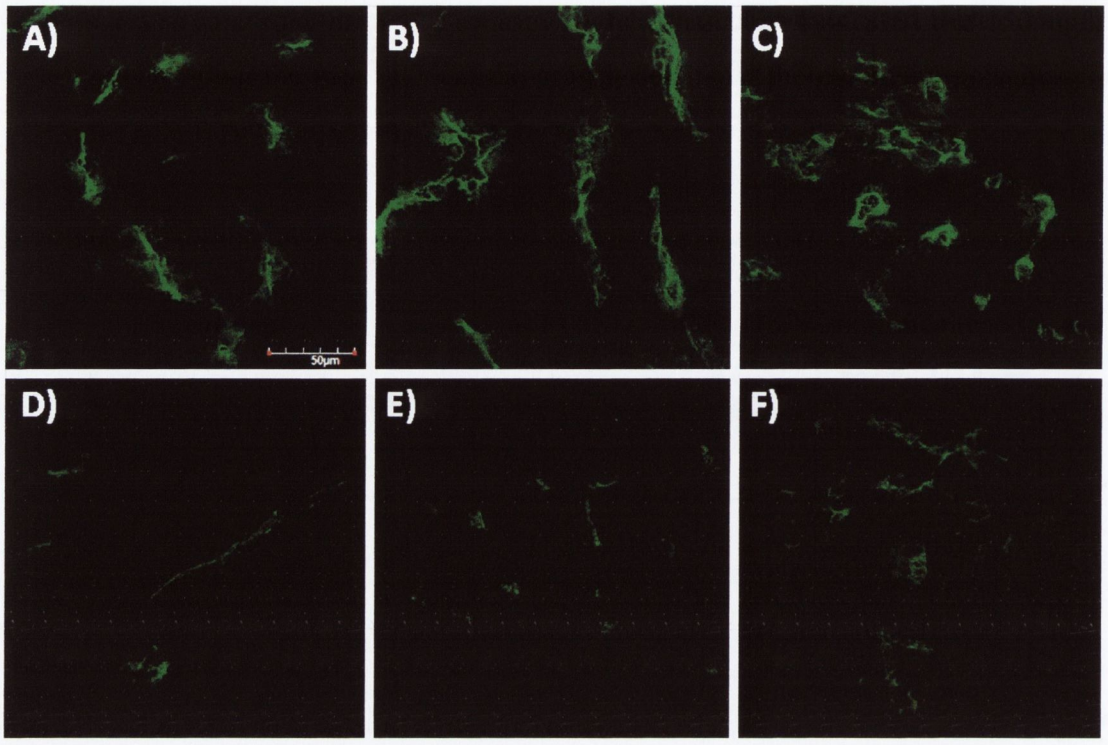

Figure 3.29: The effect of GS291 treatment on the tumour vasculature. Images of CD31-stained endothelial cells in cryo-sections of PC-3 tumours treated with **A-C)** vehicle (5% DMSO) and **D-F)** 200 mg/kg GS291, for 6h (n=3).

The functional vasculature area for control and GS291-treated tumours was estimated (Figure 3.30). A clear reduction in the functional vasculature area was noted in the GS291-treated group compared to the control group; however this was not highly significant ($p < 0.1$). An overall observation between GS291-treated and control tumours was the structural differences in the functional vasculature, *i.e.* the blood vessels' diameter of GS291-treated tumours appeared reduced, compared to those in the control group.

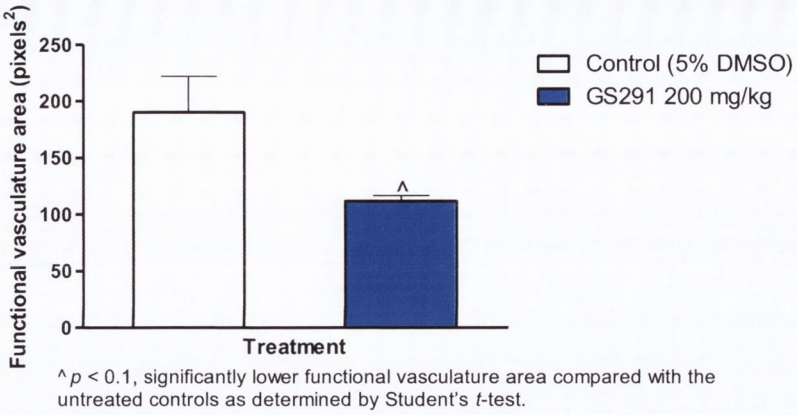

^ $p < 0.1$, significantly lower functional vasculature area compared with the untreated controls as determined by Student's *t*-test.

Figure 3.30: Quantification of functional vasculature area of tumours following 6h after a single i.p. administration of 200 mg/kg GS291. Data represents mean functional vasculature area ± SEM (n=3).

3.5 Discussion

3.5.1 Aortic Ring Assay (anti-vascular model)

The anti-vascular activity of test compounds was demonstrated using the aortic ring assay. All compounds evaluated in this assay displayed an anti-vascular effect on a pre-established microvessel network of the cultured aortic rings. The two most active compounds were GJH140 (Figure 3.7, p.130) and ADR149 (Figure 3.8, p.130). Both compounds exhibited potent microvessel breakdown at 10 nM, even after 4h of treatment, signifying similar activity to that of CA-4 (Figure 3.2, p.126). The anti-vascular effect was dose- and time-dependent. These findings together with the *in vitro* data suggest that test compounds are able to induce structural alterations to endothelial cells and disrupt an established complex microvessel network.

Several studies were conducted using different methods of assessing the anti-vascular properties of tubulin binding agents. For instance, Romagnoli *et al.* reported the synthesis and evaluation of novel 1, 5-diaryl-substituted 1, 2, 4-triazole derivatives designed as *cis*-restricted CA-4 analogues. The chick aortic ring assay was performed in order to examine the anti-vascular activity of test compounds, by implanting the aortic arches in matrigel and allowing 24-48h for them to sprout. Following a 30 minutes exposure to 10 μM of test compounds, a disruption of vascular sprouts was evident [515].

Furthermore, van Wijngaarden *et al.* examined the anti-vascular effect of a tubulin targeting agent, Ang-510, by using foetal mouse bone explants that were cultured for 10 days, in the presence of 50 ng/mL VEGF. Following this, cultures were incubated with 1 μM Ang-510 for 24h, stained for PECAM-1 and quantified for the number of positively stained microvessels. Ang-510 showed a significant suppression of newly established vasculature with an IC_{50} of 0.01 μM, which is comparable to the activity of our compounds [538].

The anti-vascular properties of a novel class of indazole-based tubulin inhibitors, including TH-482, were explored by Meng *et al.* in a cell-based assay. HUVECs were seeded and incubated over matrigel for 6h to allow capillary tube formation. TH-482 (11, 33 and 100 nM) was then added and incubated for an additional 2h, and breakdown

of the existing vasculature was monitored using fluorescent microscopy. TH-482 disrupted the pre-established capillary-like structures in a dose-dependent manner. Furthermore, changes in endothelial cell monolayer permeability were also examined, which provides an additional *in vitro* model of tumour vascular disruption. A significant increase in endothelial cell permeability was observed, when a confluent monolayer was treated with 10 and 100 nM TH-482, whereas CA-4 displayed a similar profile but exhibited lower potency [539].

The aortic ring assay is a closer representation of the vasculature formed *in vivo* compared to the *in vitro* cell-based studies. The microvessels developed in the aortic rings share similar characteristics to the vasculature formed *in vivo*. However, tumour vasculature has unique features due to an increased rate of angiogenesis, thus the aortic ring assay does not precisely mimic tumour vascular growth. For this reason, it was important to assess the effect of test compounds on tumour vasculature in the *in vivo* xenograft model, the discussion on which is outlined in section 3.5.6.

3.5.2 Aortic Ring Assay (anti-angiogenic model)

In addition to their anti-vascular properties, tubulin binding agents exert anti-angiogenic effects at non-toxic concentrations. All compounds either completely inhibited angiogenesis or reduced microvessel formation at different concentrations. Once again, the most potent inhibitors were GJH140 (Figure 3.19, p.136) and ADR149 (Figure 3.21, p.137), which restrained the vessels growth at concentrations as low as 5 nM. This indicated superior activity to that of CA-4 (Figure 3.9, p.131), suggesting a clear correlation between inhibition of tubulin polymerisation and anti-angiogenic activity.

In order to assess the extent of the anti-angiogenic profile within the anti-tumour efficacy of CA-4, Ahmed *et al.* specifically evaluated the capacity of CA-4 to influence endothelial cell migration and tube formation. A significant inhibition of cell migration (40%) in the wound assay was observed at concentrations as low as 10 ng/mL. Sprouting and tube formation were studied using cytodex-3 beads which were overgrown with BCECs on collagen, whereby CA-4 suppressed tube formation in a dose-dependent manner, following 24h incubation. Maximal inhibition of tube formation (90%) was observed at concentrations over 3 ng/mL [492].

Kong *et al.* reported the synthesis and evaluation of a boronic acid chalcone analogue of CA-4, which demonstrated cell growth inhibition towards 16 human cancer cell lines in the 10-200 nM range. Inhibition of *in vitro* angiogenesis was determined in the capillary tube formation assay, where HUVECs were cultured on matrigel and exposed to test compound for 16h. The boronic acid analogue significantly inhibited the capillary tube formation at 1 μM. The aortic ring assay was performed, whereby the boronic acid analogue dramatically inhibited functional angiogenesis at 5 μM, following incubation of cultures for 6 days [540].

Moreover, CC-5079, a small molecule inhibitor of tubulin polymerisation and phosphodiesterase-4 activity, was evaluated by Vu *et al.* for evidence of angiogenesis inhibition. Initially, the effect of CC-5079 on cell proliferation, migration and invasion was examined, where 0.1 μM CC-5079 significantly inhibited the proliferation and migration of HUVECs, fibroblasts and MC38 murine colon cancer cells. Invasion of HUVECs was also inhibited. In the aortic ring assay and the *ex vivo* CAM assay, inhibition of microvessel sprout formation was observed, following exposure to 0.1 and 1 μM CC-5079 [541].

Additionally, the anti-angiogenic effect of LP-261, N-(3-(1H-indol-4-yl)-5-(2 methoxyisonicotinoyl) phenyl)methanesulfonamide, a novel tubulin targeting agent, was determined using the aortic ring assay. LP-261 significantly inhibited microvessel outgrowth of the aortic ring cultures in a dose-dependent manner, with greater than 50% inhibition at 50 nM [542].

The angiogenic response of the aorta is a self-limited process regulated by endogenous growth factors. In contrast, regulation of angiogenesis in the tumour microenvironment involves a more complex signalling pathway. Numerous factors are implicated in the initiation of this process, including high levels of hypoxia. The evaluation of test compounds in the aortic ring assay represents a more controlled environment and the obtained results can be justified when observed in tumour xenograft models.

3.5.3 *In Vivo* Anti-tumour Efficacy of ECB206

Taking into consideration the *in vitro* and *ex vivo* data, group IV compounds and particularly ADR149 demonstrated the most potent activity. Hence, ECB206 prodrug

was synthesised, and its *in vivo* anti-tumour efficacy was determined using a PC-3 tumour xenograft model. According to the tumour volume measurements, treatment with 50 mg/kg ECB206 was not sufficient to significantly reduce the size of PC-3 tumours; although a slight decrease in the rate of tumour growth was observed from day 16 of treatment (when n=5, Table 3.1, p.141).

This finding may suggests that higher ECB206 doses could have resulted in a more evident anti-tumour effect. However, the fact that ECB206 was not tolerable at higher doses may indicate that the systemic toxicity observed could be as a consequence of a different mechanism of action other than tubulin inhibition. In addition, BW loss was observed following each ECB206 administration, indicating a sign of drug-induced systemic toxicity.

ECB206 is a coumarin-based compound which may possess similar properties to that of coumarin. Coumarin is a toxic compound found in many plants including tonka beans (*Dipteryx odorata*) and sweet clover (*Melilotus*) [543]. Bishydroxycoumarin, the active ingredient responsible for haemorrhagic disorders, was discovered by Campbell and Link and is formed when fungi in mouldy sweet clover oxidize coumarin to 4-hydroxycoumarin, an anticoagulant. Bishydroxycoumarin was synthesised and used clinically as an oral anticoagulant named dicoumarol [544]. It has previously been shown that rodents largely metabolise coumarin to 3, 4-coumarin epoxide which is a toxic compound that can cause internal haemorrhage and death [545].

ECB206 treatment at doses higher than 50 mg/kg caused severe toxicity which could possibly be explained by the effect of its coumarin-based properties (possible internal haemorrhage). For this reason, further evaluation of ECB206's efficacy was not pursued.

3.5.4 *In Vivo* Anti-tumour Effect of GS291

Following the unsuccessful outcome from the preliminary *in vivo* study with ECB206, the next potential compound had to be chosen for further evaluation from a different series of compounds, other than the coumarin-based. *In vitro* and *ex vivo* data indicated that group II compound, namely RS180, could be an ideal candidate for the purpose of our studies because of both its non coumarin-like structure as well as its reasonable, but

not overly potent, *in vitro* and *ex vivo* activity. Subsequently, its phosphate derivative namely GS291, was synthesised for the *in vivo* evaluation in the PC-3 tumour xenograft model and CA-4P was used as a positive control.

A significant decline in the tumour growth rate was observed following both treatments; however the CA-4P treated group displayed a slightly better anti-tumour effect according to the RTV2 growth delay (6.28 days) compared to that of GS291 (4.55 days, Table 3.2, p.144). There was no apparent reduction in BW following treatment with either CA-4P or GS291, suggesting that both treatments were well-tolerated.

According to reported data, a single i.p. injection of 100 mg/kg CA-4P was sufficient to cause tumour growth delay in the s.c. MAC 15A murine colon adenocarcinoma model [536]. This result, along with our CA-4P *in vivo* data, indicates the variation in treatment response when dealing with different type of tumours. Numerous studies have reported the anti-tumour effect of CA-4 in several *in vivo* models. For instance, 100 mg/kg CA-4 was administered i.p. in DBA/2 mice bearing P-388 leukaemia on either days 1, 5 and 9 or consecutively on days 1-9, and was only marginally active (25% increased lifespan). A higher i.p. dose of 150 mg/kg CA-4 on days 1, 5 and 9 did not delay s.c. B-16 melanoma tumour growth in C57/B1 mice [537]. There was no consistent anti-tumour activity observed, following treatment with CA-4 in those particular murine tumour models. Furthermore, s.c. WSU-DLCL2-SCID lymphoma tumour bearing mice treated with CA-4P's MTD (up to 800 mg/kg) in different doses/schedules, revealed that best results were obtained when CA-4P was administered in two and four divided doses (400 and 200 mg/kg, respectively) [546].

In addition, the anti-tumour effect of 50 mg/kg CA-4P in two s.c. murine NSCLC tumour xenograft models was determined by daily i.p. administration for 3 weeks, whereby it significantly delayed tumour growth. An additional orthotopic xenotransplantation model was developed which estimated prolongation of survival after intrapulmonary tumour induction with secondary metastatic disease, following daily i.p. administration of 50 mg/kg CA-4P for 3 weeks [547].

Several CA-4 analogues were designed as tumour vasculature targeting agents and evaluated in tumour xenograft models. In particular, Kuo *et al.* synthesised a series of 3-aroylindole compounds as novel heterocyclic CA-4 analogues. The lead compound BPR0L075 was assessed for its anti-tumour efficacy in MKN-45 gastric carcinoma, KB human cervical carcinoma, and KB-derived P-gp170/MDR-over-expressing KB-VIN10 xenografts, by different doses/treatment schedules. The greatest decrease in tumour volume was noted in animals treated daily with i.v. administration of 50 mg/kg BPR0L075 for two weeks [548].

Furthermore, Cai *et al.* reported a different series of VDAs, including the (Z)-3, 4′, 5-trimethoxylstilbene-3′-O-phosphate disodium, M410, whereby its anti-tumour efficacy was explored in a s.c. LoVo colon carcinoma xenograft model. Treatment with 25 mg/kg M410 or CA-4P administrated i.p. every three days for 12 days resulted in a significant inhibitory rate of 44.3% and 42.1%, respectively [549].

Taking into account the variation observed in the reported data, several factors are implicated in tumour xenograft studies which have to be considered: (i) the type of cancer cells used to generate the tumours (*i.e.* some tumours could be more effective/resistant to chemotherapy than others; could be either highly or poorly vascularised; invasive or metastatic), (ii) the tumour volume prior to initiating the treatment is important since tumours at a more advanced-stage (300-400 mm^3) could be less responsive to treatment than early-stage tumours (100-150 mm^3), (iii) the site of tumour growth (*i.e.* s.c. or orthotopic implantation could result in a diverse treatment outcome due to the differences of the tumour microenvironment at the site of growth), (iv) the species of the animals used in such studies could affect the end results, (*e.g.* immunodeficient mice lack the proper immune response that normal mice exhibit).

3.5.5 Assessment of Tumour Necrosis

Tumour samples were histologically examined for evidence of tumour necrosis, following treatment with test compounds. For the assessment of 50 mg/kg ECB206, animals were treated for 24h by a single i.p. injection and the tumours were excised for histological examination (Figure 3.25, p.142). Tumour samples from the CA-4P and GS291 treatments were obtained following completion of the *in vivo* anti-tumour efficacy study and processed for histological examination (Figure 3.28, p.145). Control

treated tumours showed limited necrosis in the centre, whereas ECB206-, CA-4P- and GS291-treated tumours demonstrated large areas of haemorrhagic necrosis. This is an indication of the indirect impact of these compounds on the functional vasculature and a subsequent effect on the tumour tissue.

Disrupting the tubulin cytoskeleton of tumour endothelial cells could lead to congestive thrombi in the tumour microvasculature and result in vessel leakage. This in turn could cause necrosis of the surrounding tumour, due to oxygen and nutrient depletion. In addition, a higher localised concentration of test compounds could increase their exposure and subsequent cytotoxicity within the tumour tissue.

The preclinical evaluation of tubulin targeting agents, such as CA-4, showed that these compounds are able to disrupt tumour blood flow, causing tumour hypoxia and necrosis [550]. For instance, Horsman *et al.* reported that i.p. administration of 100 mg/kg CA-4 in C3H mouse mammary carcinoma xenografts, resulted in an insignificant increase in tumour necrosis within 3h of treatment; however by 24h significantly higher levels of tumour necrosis were observed. Measurements of tumour partial oxygen pressure (pO_2) demonstrated increased tumour hypoxia, following i.p. administration of 100 mg/kg CA-4 and this effect was maintained for at least 6h. At longer time intervals (12-24h), tumours were severely hypoxic, although to a lesser degree. This finding suggested that the apparent reduction in oxygenation was reflected as tumour haemorrhage and oedema from the damage produced [551].

Moreover, a single i.p. dose of 100 mg/kg CA-4P induced marked haemorrhagic necrosis consistent with widespread vascular shutdown 24h post-injection, in both NT murine adenocarcinoma and MDA-MB-231 human breast adenocarcinoma xenografts. A small viable rim on the periphery of the tumour remained, equivalent to less than 5% of the tumour mass [308]. Similar observations in tumour morphology were reported by Grosios *et al.*, whereby 24h treatment of s.c. MAC 15A tumours with i.p. administration of 100 mg/kg CA-4P demonstrated extensive areas of haemorrhagic necrosis with a small rim of viable tumour in the periphery. Necrosis was not seen in avascular tumour nodules, suggesting a vascular mechanism of action [536].

In our situation, a viable rim of tumour tissue was observed on the periphery of each treated tumour, where cells could obtain nutrients from unaffected blood vessels in normal surrounding host tissues. This explanation could justify the fact that tumour growth was not completely restricted following treatment with CA-4P and GS291; although there was a significant difference between the control and treated tumours.

Combination treatment of these compounds with standard chemotherapy or radiation therapy may overcome this issue and prevent tumour growth. For instance, Chaplin *et al.* reported that although administration of 100 mg/kg CA-4P resulted in extensive cell loss following 24h of treatment, this did not translate into any significant effect on tumour growth [329]. The actively proliferating cell population at the periphery of the tumour, depending on the normal tissue vasculature, was responsible for the continued growth of the tumours. For this reason, CA-4P was combined with cytotoxic approaches, including combination treatment with cisplatin or radiation therapy, whereby superior anti-tumour efficacy was achieved [329]. Furthermore, CA-4P treatment potentiated the anti-tumour effect of radiation therapy in a KHT rodent sarcoma model [330], and improved the activity of 5-FU in an experimental murine colon adenocarcinoma model [552]. Both strategies significantly enhanced the tumour response to CA-4 treatment indicating its potential therapeutic usefulness as an adjuvant to conventional cytotoxic approaches.

3.5.6 Assessment of the Tumour Vasculature

To determine whether the delay in tumour growth observed in PC-3 tumour xenografts was due to an anti-vascular effect of GS291, tumour samples were examined for evidence of vascular shutdown. Tumour bearing mice were administered with a single i.p. injection of 200 mg/kg GS291. Following 6h of treatment, tumours were excised and processed for functional endothelial cell staining.

According to the quantified data generated from the CD31-stained tumour samples, an approximate 50% reduction in tumour vasculature was observed following 6h treatment with 200 mg/kg GS291. This finding indicated a direct anti-vascular effect of GS291 within the tumour tissue (Figure 3.29 and 3.30, p.146-147). This is in agreement with previously reported data, whereby a single i.p. administration of 100 mg/kg CA-4P caused a very large decrease in P22 carcinosarcoma blood flow, which was reduced by

almost a 100-fold, within 6h of treatment [312]. CA-4P treatment also showed a 93% reduction in functional vascular volume in NT murine breast carcinomas [308]. Additional studies showed that a single i.p. injection of 100 mg/kg CA-4P was sufficient to induce complete vascular shutdown after 4h of treatment in MAC 15A tumours [536]. Furthermore, 50 mg/kg CA-4P induced approximately 40% vascular shutdown in CaNT murine breast adenocarcinoma tumours [553].

In an attempt to explore the mechanism of action in which CA-4 exerts its effects from initial tubulin binding to vascular shutdown, Tozer *et al.* described the tumour vascular response from a systemic treatment with CA-4P. This mechanism is reminiscent of a classical acute inflammatory reaction, involving a very rapid increase in vascular permeability to plasma proteins. Another common feature included the stacking of red cells to form rouleaux which coincided with the slowing of blood flow, leading to an increase in viscous resistance to blood flow [314].

Moreover, following screening of a chemical library consisting of more than 100 compounds based on diversification of the CA-4 pharmacophore, Kremmidiotis *et al.* attempted to identify compounds with acquired selectivity to activated tumour endothelial cells. A novel tubulin targeting agent, BNC105, was discovered which exhibited a wider therapeutic window than CA-4P. Treatment of animals bearing solid tumours derived from human MDA-MB-231 breast, Calu-6 lung, Colo 205 colon and DU145 prostate cancer cells, with BNC105 disodium phosphate (BNC105-P) at dose levels $\geq$ 10 mg/kg for 24h, resulted in complete tumour vascular disruption. The maximum effect was seen in MDA-MB-231 tumours, with efficacy evident at doses as low as 1 mg/kg; whereas treatment with 20 mg/kg BNC105-P gave rise to > 75% tumour necrosis. A similar level of necrosis was achieved with CA-4P, although at a considerably higher dose (300 mg/kg). Interestingly, in the Colo 205 xenograft model, BNC105-P treatment demonstrated significant disruption of tumour vasculature with a corresponding level of necrosis; however CA-4P treatment was ineffective in this model [512].

These findings highlight the importance of the tumour type used in xenograft models due to the variation in activity observed with CA-4 treatment. In our situation, the anti-vascular activity of GS291 observed in the PC-3 tumour xenograft verified the results

obtained from the *in vitro* and *ex vivo* assays, whereby it demonstrated tubulin targeting properties in cell-based assays and microvessel breakdown in the aortic ring assay.

3.6 Conclusions

Following the successful *in vitro* evaluation of test compounds, the next stage was to examine their anti-vascular activity in the *ex vivo* aortic ring assay. Selected compounds from each group were tested for evidence of microvessel breakdown in the cultured aortic rings. All compounds examined demonstrated anti-vascular activity at different levels of potency and their effect proved to be both dose- and time-dependent. The most active compounds appeared to be GJH140 and ADR149; these findings are in agreement with the preliminary *in vitro* data obtained in Chapter 2.

In addition to the anti-vascular effect, test compounds were assessed for their anti-angiogenic properties in the aortic ring assay. The majority of compounds showed moderate to complete inhibition of microvessel formation at nanomolar concentrations (10-100 nM), suggesting that the rate of angiogenesis was affected. Once again, GJH140 and ADR149 demonstrated the highest potency in the anti-angiogenic model of the aortic ring assay.

According to the *in vitro* and *ex vivo* data, ADR149 proved to be the most promising compound; for this reason ECB206, a leucine prodrug of ADR149, was synthesised and selected for preliminary *in vivo* evaluation in a PC-3 tumour xenograft model. Treatment of tumour bearing mice with i.p. administration of 50 mg/kg ECB206, once a week for three weeks, did not demonstrate any significant difference compared to the vehicle treated group. The percentage BW was reduced over the duration of the treatment, indicating a sign of toxicity; however it was maintained within the limits at all times. Doses of ECB206 greater than 50 mg/kg were not tolerable. This finding may suggest that the systemic toxicity of ECB206 treatment observed at higher doses could possibly be due to the coumarin-based component of the compound, which has previously been established to be a rodenticide. For that reason, further studies were not pursued.

Consequently, GS291, a disodium phosphate salt of RS180, was synthesised to resolve solubility issues. Along with GS291, CA-4P was also examined in the PC-3 tumour

xenograft model. Both compounds exhibited significant anti-tumour activity by reducing the tumour growth rate. No observable systemic toxicity was observed according to the BW measurements.

Following completion of the studies, the level of tumour necrosis was examined in the control and treated groups. Control treated tumours showed limited necrosis whereas ECB206-, GS291- and CA-4P-treated tumours displayed large areas of haemorrhagic necrosis with a viable rim on the periphery. The morphological changes in the tumour tissues may be an indirect effect from the anti-vascular activity of test compounds. This was confirmed by 6h treatment of tumour bearing mice with 200 mg/kg GS291, whereby an approximate 50% reduction in functional vasculature was demonstrated. This implied that part of the anti-tumour effect of GS291 was mediated by direct disruption of functional vasculature.

3.7 Overall Conclusions

To summarise the data obtained from Chapter 2 and 3, four different classes of novel tubulin polymerisation inhibitors demonstrated potent anti-proliferative effects in the low nanomolar range, and their activity was dependent on their design. These compounds induced a G_2/M phase arrest, an indication of their anti-mitotic properties. They disrupted the organisation of the tubulin cytoskeleton and exerted reversible morphological changes to endothelial cells, signifying their anti-vascular potential. The most promising compounds were subsequently selected for further examination in the *ex vivo* aortic ring assay. Test compounds exhibited their effects by disrupting the pre-established microvessel network and inhibited the formation of capillary tubes. ADR149 was chosen as the compound with the most potential, therefore its anti-tumour efficacy was determined in a s.c. PC-3 tumour xenograft model, using a leucine prodrug form, ECB206. The preliminary *in vivo* anti-tumour study with ECB206 failed to provide evidence of efficacy, thus GS291, a disodium phosphate form of RS180, was selected for *in vivo* evaluation. A significant reduction in tumour volume was observed following i.p. administration of 200 mg/kg GS291, once a week for three weeks, whereas treated tumours exhibited large areas of haemorrhagic necrosis compared to the vehicle treated tumours. Finally, a decrease in the functional tumour vasculature was noted following a single i.p. administration of 200 mg/kg GS291, following 6h of treatment.

An additional approach for an improved pharmacological profile is to conjugate two individually active components to form a single agent with dual-targeting properties (*i.e.* a hybrid). The design and evaluation of hybrids and a DML which target tubulin polymerisation and APN will be discussed in Chapter 4.

-- Chapter 4 --

In Vitro Evaluation of Novel Dual-Acting Compounds Targeting Tubulin Polymerisation and APN

4. Introduction

In addition to the evaluation of novel tubulin polymerisation inhibitors as VDAs in cellular, *ex vivo* and *in vivo* models, the aim of the work described in this Chapter was to evaluate the activity of dual-acting tubulin polymerisation and APN inhibitors, in several vascular/angiogenesis assays. Initial studies focussed on developing new assays to add to the repertoire discussed in the previous Chapters for the evaluation of the tubulin targeting agents. Particular emphasis was placed on implementing cellular-based assays for evaluation of the APN inhibitory component of the design, and subsequent evaluation of test compounds in these assay systems. In addition, comparison studies between hybrids, their individual components and their 1:1 combinations were conducted in order to examine evidence of synergy.

4.1 Background to the Dual-Acting Compounds Designed in our Group

The compounds under evaluation were designed to inhibit tubulin polymerisation and APN. Inclusion of the APN targeting moiety in these compounds was based primarily on the fact that it plays a critical role in angiogenesis and tumour cells' invasion and it is expressed on vasculature undergoing angiogenesis, but not on quiescent vasculature. Initial model studies conducted by McCormack (2002) involved using the prototypical tubulin inhibitor colchicine and attaching bestatin-related compounds onto to its derivative, N-deacetylcolchicine. The selection of bestatin was based on its excellent APN inhibition in conjunction with its ability to maintain the activity of the tubulin inhibitor to which it was attached, as demonstrated in previous studies by McCormack. The colchicine-bestatin analogues exhibited equipotent tubulin inhibitory activity to the model compound colchicine and excellent APN inhibition, significantly better than the parent drug, bestatin. Encouraged by these results, further work by Hudson (2007) involved coupling a similar series of bestatin-like molecules onto a new series of tubulin inhibitors, based primarily around the tubulin inhibitor RS180. However, the hybrids synthesised by Hudson were presented as mixtures of diastereoisomers, which necessitated building single stereoisomers of these compounds before extensive studies could be conducted in biological models. Thus the work concluded by Breen (2012) involved the synthesis of single stereoisomers of these hybrids, as well as others, using a yeast mediated biotransformation, to secure the compounds with the appropriate

stereochemical purity [554]. An additional series of pH-sensitive ester-linked hybrids was also synthesised by Breen and Coogan (2012) to allow for the optimal uptake of the hydrophilic bestatin moiety of the hybrid into the cells. Ester derivatives of bestatin have been shown to exhibit superior activity over bestatin, in both *in vitro* and *in vivo* settings. Work conducted by Moran (2012) involved the creation of DMLs with the facility to inhibit tubulin polymerisation and APN. Compounds within this series differ quite significantly from the hybrids of Breen and Coogan, as they rely solely on the inclusion of a hydroxamic acid moiety into the design, for zinc chelating purposes and thus APN inhibition. Therefore, this Chapter concerns the evaluation of these different classes of hybrids and DML.

4.1.1 Compound Series

Overall there are four series of dual-acting hybrids and one DML which are the subject of the work described in this Chapter. The first two series are presented as active dual-target hybrids; group I includes ECB377 and ECB378 (amide series) and group II includes ECB399 and ECB404 (ester series). In group III (ECB397) and group IV (ADR469), hybrids are designed for presentation of the tubulin binding component of the design in a prodrug form, with the APN component in an active form. The tubulin binding component within these designs is expected to be activated following the pH-sensitive release of the APN binding component, as phenolic esters are labile bonds which are prone to hydrolysis under physiological conditions. An additional expected advantage with this hybrid series was that with the hydrophilic bestatin moiety attached, the solubility of the tubulin binding component would be greatly enhanced. Thus the objective within these designs was to both optimise the delivery of the bestatin-like component to the intracellular environment and to enhance the solubility of the tubulin binding component for *in vivo* administration. Within the last group which includes a DML, BWM120, the objective was to create a series of compounds with a similar pharmacological profile to that of the hybrids, but nevertheless substantially smaller in size, to ultimately give compounds with more favourable Lipinski-like drug characteristics.

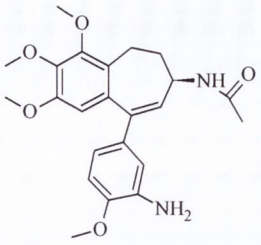

ECB394

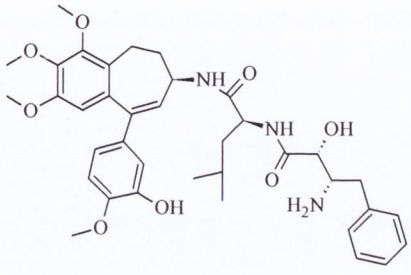

ECB377

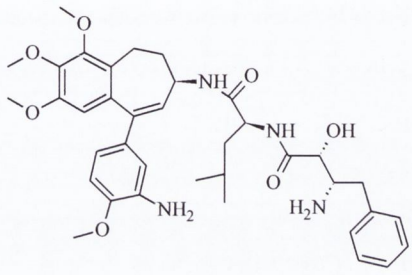

ECB378

Figure 4.1: Group I hybrids ECB377 and ECB378 which incorporate ECB394 and bestatin.

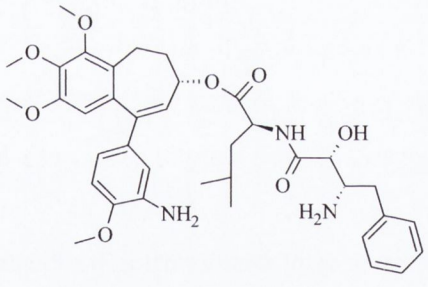

ECB399

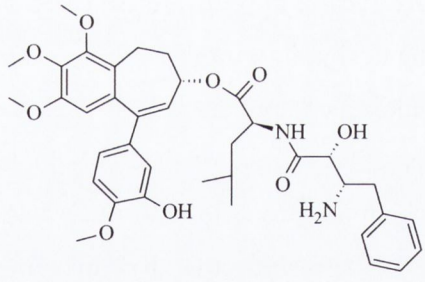

ECB404

Figure 4.2: Group II hybrids ECB399 and ECB404 which incorporate GS117 or RS176 and bestatin, respectively.

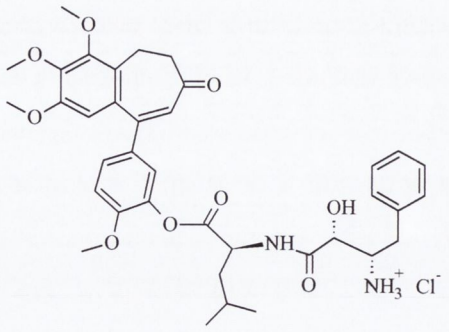

ECB397

Figure 4.3: Group III hybrid ECB397 which incorporates RS180 and bestatin.

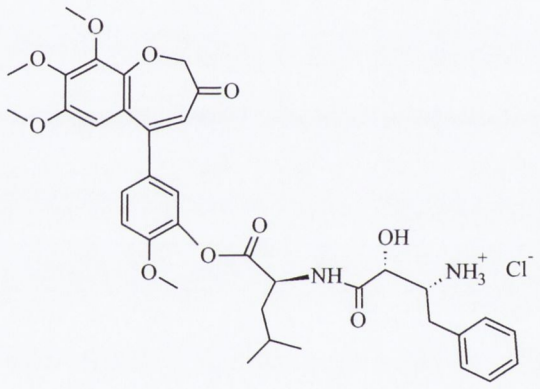

ADR469

Figure 4.4: Group IV hybrid ADR469 which incorporates ADR269 and bestatin.

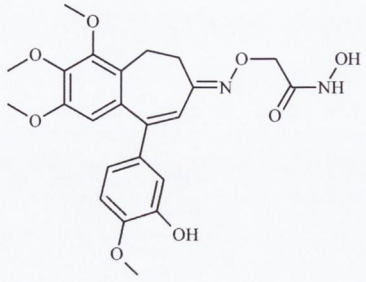

BWM120

Figure 4.5: BWM120, a DML which incorporates RS180 and a hydroxamic acid.

Data from the literature regarding the effectiveness and superiority of hybrid compounds over single agents or 1:1 combinations is encouraging, especially in respect to overcoming issues associated with toxicity, solubility, drug resistance and pharmacokinetic properties [335, 555]. In the work described in this Chapter, initial studies focussed on the implementation and validation of several APN-associated assays. Once established, evaluation of the APN component of the hybrids commenced with a study of their properties against the isolated protein, in an enzyme based assay, and in cell lines expressing APN (HUVECs and PC-3 cells). In addition to that, APN expression was also investigated by flow cytometric techniques using a selected compound, BWM120. The developed assays served not only to verify the APN inhibition of these hybrids but also to determine any enhancement of the APN component with the dual-targeting design. Evaluation of the tubulin component of the hybrid essentially followed the same sequence as that discussed in Chapter 2 for the evaluation of the single-targeting tubulin binding agents. A key objective of the work described in this Chapter was to investigate evidence of additive or synergistic effects of the hybrids over the single agents or their 1:1 combinations in anti-proliferative and apoptosis assays.

4.1.2 Aims

The specific aims of the work described in this Chapter were to:

- Investigate the APN inhibitory profile of test compounds in an APN enzyme-based assay, using a colorimetric technique.
- Select two APN-positive cell lines and confirm their APN expression pattern using immunofluorescence staining and flow cytometric analysis.
- Determine the non-cytotoxic concentration of test compounds and then evaluate their aminopeptidase inhibition in a cell-based assay, using both HUVECs and PC-3 cells.
- Explore the inhibition of APN expression in HUVECs and PC-3 cells after treatment with BWM120 by immunofluorescence staining and flow cytometric analysis.

- Determine whether test compounds inhibit proliferation of HUVECs and PC-3 cells using the MTT assay, and address whether an additive or synergistic effect exists over single agents or their respective 1:1 combinations.

- Confirm and visualise the tubulin inhibition activity of test compounds by immunofluorescence staining of the microtubules of treated endothelial cells.

- Establish the anti-mitotic effect of test compounds on cell cycle (G_2/M arrest), using PI staining followed by flow cytometric analysis.

- Assess the effect of test compounds on cell death (sub-G_0/G_1 arrest) using PI staining followed by flow cytometric analysis, and investigate any additive or synergistic effect compared to single agents or their 1:1 combinations.

- Examine any morphological changes to endothelial cells following treatment with test compounds, an indication of their *in vitro* anti-vascular activity, and further evaluate their reversibility.

4.1.3 Background to the Protocols Used

4.1.3.1 APN Enzyme-based Assay

In order to determine the APN inhibitory activity of the compounds synthesised, the colorimetric APN enzyme assay developed by Melzig *et al.* was performed [556]. In this assay, L-leucine-*p*-nitroanilide is used as a substrate which, following hydrolysis by APN, produces the highly coloured product *p*-nitroaniline. The degree of colour intensity and thus APN activity can be measured spectrophotometrically at 405 nm. This assay has been used widely to investigate the APN inhibitory properties of a variety of test compounds [275-277, 279].

4.1.3.2 APN Expression of HUVECs and PC-3 cells

For the *in vitro* evaluation of hybrids and DML, HUVECs and PC-3 cell lines were selected based on their high expression levels of APN, and for their respective roles in angiogenesis/vascularisation and tumour growth/metastasis [227, 278, 557-558]. In order to confirm this, the APN expression levels of both cell lines were examined by immunofluorescence staining of CD13 and by flow cytometric analysis.

4.1.3.3 APN Cell-based Assay

To further investigate the aminopeptidase inhibitory effect of the hybrids, the APN cell-based assay was carried out as previously described [281, 559-560], using both HUVECs and PC-3 cells. In order to exclude any possible cytotoxic effects (or possible disruption of cell adhesion) induced by the tubulin binding component of the hybrids, it was necessary to perform cytotoxicity assays. For this purpose, the MTT assay was used as previously described; however the duration of compounds' incubation was modified to 2h in order to correlate with the incubation period of the APN cell-based assay. The release of the resulting product *p*-nitroaniline was measured spectrophotometrically at 405 nm and the level of cellular aminopeptidases was directly related to the intensity of the colour absorbance.

4.1.3.4 APN Expression

To further investigate the effect of BWM120 on the inhibition of APN expression in both cell lines, an immunofluorescence staining protocol was performed followed by flow cytometric analysis. This method is widely used for the identification and quantification of the level of cell surface expression markers including APN [281, 559, 561]. APN is anchored to the plasma membrane but is also present in the cytosol. In this study the level of cytosolic APN was not included in the quantification since the APN antigen was detected using non-permeabilised cells [562].

4.1.3.5 Cell Cycle Analysis – Cell Death

The ability of bestatin to induce apoptosis has been established in a variety of cancer cells [242-243], as well as leukaemic cell lines [244, 246]. Tubulin targeting agents, such as CA-4P, demonstrated induction of mitotic cell death after arrest of endothelial cells in mitosis [563-564]. In addition, PTX-induced mitotic block triggered rapid onset of a p53-independent apoptotic pathway [565-566]. As both components of these hybrids are able to induce cells to undergo apoptosis, it was hypothesised that their apoptotic effect may prove to be additive or even synergistic. To investigate the activity of test compounds it was necessary to examine single agents and 1:1 combination treatments in order to determine whether hybrids' activity was superior or similar to the other treatments.

Initial attempts were carried out using the Annexin V/PI staining technique (which is based on changes in the cell membrane's integrity) in order to detect non-apoptotic living cells, early apoptotic and late apoptotic or necrotic cells, following exposure to test compounds [567]. Although this method was able to distinguish the different stages of apoptosis, the results obtained were inconclusive and inconsistent. Therefore, a different method of apoptosis detection was established by examining the cells' DNA contents using flow cytometric analysis. Cell cycle analysis was performed as previously described to detect apoptotic DNA fragmentation. During apoptosis DNA is degraded by cellular endonucleases and therefore the apoptotic cells contain less DNA than healthy cells. This results in a sub-G_0/G_1 peak in the fluorescence histogram that can be quantified as the amount of apoptotic cells in a sample. This method was first described by Nicoletti *et al.* [568] and then optimised by Riccardi *et al.* [569], and is widely used as a way of examining apoptosis after treatment with anti-cancer compounds [570-572].

This approach is the most rapid and cost-effective discrimination of apoptotic cells and is routinely used in laboratories for screening drug effects *in vitro*, especially when large number of samples have to be examined. However, one of the main limitations of this method is the non-specific detection of apoptotic cells, *i.e.* cellular debris, single chromosomes from broken mitotic cells, chromosome clumps *etc.* all having a very low DNA content may be incorrectly classified as apoptotic cells. In order to provide a better assurance that objects with minimal DNA content are excluded from the analysis, a linear rather than logarithmic scale was applied [573]. This was only a preliminary screening study which was going to identify the effect of test compounds on cell death, thus a more sensitive technique would clarify the situation.

4.2 Materials and Methods

4.2.1 Materials

DMSO, MTT, FBS, streptomycin/penicillin solution, 0.25% trypsin/EDTA solution, CA-4, bestatin hydrochloride, L-leucine-*p*-nitroanilide, HEPES, NaCl, microsomal leucine aminopeptidase from porcine kidney (EC 3.4.11.2), RNase, PI, monoclonal mouse anti-α-tubulin antibody and crystal violet were all purchased from Sigma, Ireland. Anti-human CD13 PE was purchased from eBioscience, UK. PBS tablets, Alexa Fluor® 488 goat anti-mouse IgG and ProLong® gold antifade reagent with DAPI were purchased from Invitrogen, Ireland. EBM-2 medium was purchased from Lonza, Ireland and basement membrane matrix (matrigel) from BD Biosciences, Ireland. Greiner CELLSTAR® 75 cm^2 cell culture flasks, Greiner 96-well PS cell culture microplates, with solid U-bottom, Greiner 6-well plates and Greiner 12-well plates were purchased from Cruinn, Ireland. Frosted end microscopy slides and cover slips were purchased from VWR, Ireland.

4.2.2 Test Compounds

For the *in vitro* evaluation, stock solutions of test compounds were prepared in DMSO and then diluted in the appropriate medium or buffer to provide the required concentrations. The maximum final DMSO concentration was $\leq$ 0.1%. Control solutions consisted of 0.1% DMSO in the appropriate medium or buffer. In each experiment a positive control was used. Fresh solutions were prepared prior to use.

4.2.3 APN Assay Buffer

For the APN enzyme and APN cell-based assay, HEPES buffer (50 mM HEPES, 154 mM NaCl) was prepared weekly and kept at 4 °C. The pH was adjusted to 7.3-7.4 prior to use.

4.2.4 Cell Lines

HUVECs were obtained from TCS Cellworks, UK and cultured in EBM supplemented with growth factors and antibiotics (TCS Cellworks, UK). PC-3 human prostate adenocarcinoma cell line was purchased from LGC Standards, UK and cultured in F12K medium supplemented with 0.02 mg/mL sodium pyruvate, 10% FBS and 10

mL/L penicillin/streptomycin solution. Cell and tissue cultures were kept at 37 °C in a humidified atmosphere containing 5% CO_2 at all times. Cell culture experiments were performed under a NuAire class II biological safety cabinet and it was ensured that aseptic techniques were followed at all times. Cell maintenance, subculture and cell count procedures were followed as previously described in Chapter 2, sections 2.2.4 and 2.2.5, p.80.

4.2.5 APN Expression of HUVECs and PC-3 cells

In order to quantify the APN expression level on the surface of HUVECs and PC-3 cells, an immunofluorescence/flow cytometric protocol was followed. Cells were harvested by trypsinisation and washed with 3 mL of ice-cold PBS by centrifugation at 1000 rpm at 25 °C for 5 minutes. The cell pellet was re-suspended in 100 µL of PBS, a PE CD13 conjugated antibody (1:10 in PBS) was added to $1x10^6$ cells/mL and kept on ice for 15 minutes in the dark. The cells were then washed with 3 mL of PBS by centrifugation at 1000 rpm at 25 °C for 5 minutes and immediately analysed by a Beckman Coulter (Dako) 2-laser CyAn ADP analyser, provided by the School of Biochemistry and Immunology, TCD. APN levels were estimated as median fluorescence intensity. The experiments were performed in triplicate at three independent times.

4.2.6 APN Enzyme-based Assay

APN enzyme activity was examined spectrophotometrically using L-leucine-*p*-nitroanilide as an APN substrate. Briefly, 50 µL of L-leucine-*p*-nitroanilide was added to each well of a 96-well plate to give a final concentration of 2 mM. Test compound stock solutions were diluted in HEPES buffer to give a range of concentrations and 100 µL of each was added into each well. Bestatin was used as a positive control, whereas ECB394 and RS180 served as negative controls. A further 40 µL of HEPES buffer was added to bring the final volume in each well to 190 µL. The reaction was initiated by adding 10 µL of microsomal leucine aminopeptidase to give a final concentration of 5 mUnits and the plate was incubated for 1h at 37 °C. The absorbance was measured at 405 nm using a FLUOstar OPTIMA microplate reader (BMG Labtech). Each compound concentration was tested in quadruplicate and each experiment was performed three independent times. The percentage APN inhibition was determined

using the following formula, whereby dose response curves were generated, and where appropriate, IC_{50} values ± SEM were obtained:

*% APN inhibition = 100-[(mean Abs of test compound)/(mean Abs of control)]*100*

4.2.7 Cytotoxicity Assay

It was necessary to establish a non-toxic concentration range of test compounds prior to the APN cell-based assay. For this purpose, the MTT assay was performed as previously described (Chapter 2, section 2.1.7.1, p.76) but the incubation period of test compounds was changed to 2h in order to correlate with the incubation period used in the APN assay. Each compound concentration was tested in quadruplicate and each experiment was performed three independent times. Results were expressed in terms of percentage of inhibition of cell viability using the following formula:

*% Inhibition of cell viability = 100-[(mean Abs of test compound)/(mean Abs of control)]*100*

4.2.8 APN Cell-based Assay

HUVECs/PC-3 cells' surface APN activity was estimated spectrophotometrically using L-leucine-*p*-nitroanilide as an APN substrate. $1x10^6$ cells (150 µL) were seeded in 96-well plates and incubated overnight at 37 °C. The following day cell medium was replaced by 100 µL of various concentrations of compounds diluted in HEPES buffer. Bestatin was dissolved in HEPES buffer and used as a positive control. L-leucine-*p*-nitroanilide (50 µL) was added to each well to give a final concentration of 2 mM. A further 50 µL of HEPES buffer was added to bring the final volume in each well to 200 µL. Following 2h incubation at 37 °C, absorbance was measured at 405 nm using a FLUOstar OPTIMA microplate reader (BMG Labtech). Each compound concentration was tested in quadruplicate and each experiment was performed at three independent times. The percentage APN inhibition was determined using the formula below and where appropriate, IC_{50} values ± SEM were obtained.

*% APN inhibition = 100-[(mean Abs of test compound)/(mean Abs of control)]*100*

4.2.9 Inhibition of APN Expression

APN expression of HUVECs and PC-3 cells was evaluated followed treatment with BWM120. $1x10^6$ cells (1 mL) were seeded in 6-well plates and incubated overnight at 37 °C. The following day, cells were treated for 2h or 24h with test compounds

prepared by diluting stock solutions in complete medium. Bestatin was used as a positive control. Cells were harvested by trypsinisation and washed with 3 mL of ice-cold PBS, centrifuged at 1000 rpm at 25 °C for 5 minutes. The cell pellet was re-suspended in 100 μL of PBS, a PE CD13 conjugated antibody was added to the cells (1:10 in PBS) and kept on ice for 15 minutes. The cells were then washed with 3 mL of PBS by centrifugation at 1000 rpm at 25 °C for 5 minutes and immediately analysed by a Beckman Coulter (Dako) 2-laser CyAn ADP analyser provided by the School of Biochemistry and Immunology, TCD. APN levels were estimated as median fluorescence intensity. Each compound concentration was tested in duplicate and each experiment was performed three independent times. The results were expressed as a percentage of the mean PE CD13 median fluorescence intensity ± SEM.

4.2.10 Cell Proliferation Assay

Cell growth inhibition was assessed using the MTT assay as previously described in Chapter 2, section 2.1.7.1, p.76. Bestatin was used as a single agent and in 1:1 combination with the associated tubulin inhibitor from each hybrid. Each compound concentration was tested in quadruplicate and each experiment was performed three independent times. The percentage growth inhibition was determined using the formula below and the results were expressed in terms of IC_{50} values ± SEM.

*% growth inhibition = 100-[(mean Abs of test compound)/(mean Abs of control)]*100*

4.2.11 Immunofluorescence Staining of the Microtubules

To confirm that the hybrids and DML exhibit an effect on the tubulin cytoskeleton, treated endothelial cells were examined using the α-tubulin staining procedure described in Chapter 2, section 2.1.7.3, p.78. Experiments were performed in duplicate at two independent times. The results were presented as images of the microtubule disruption of endothelial cells.

4.2.12 Cell Cycle Analysis – G_2/M Phase

Cell cycle arrest at the G_2/M phase was examined by PI staining as previously described in Chapter 2, section 2.1.7.2, p.77. Each compound concentration was tested in duplicate and each experiment was performed three independent times. The results

were expressed in terms of the mean percentage of cells found to be present in the G_2/M phase ± SEM.

4.2.13 Cell Cycle Analysis – Sub-G_0/G_1 Phase

In order to examine the apoptotic effect of these compounds, the cell cycle analysis protocol was followed as previously described in Chapter 2, section 2.1.7.2, p.77. Bestatin was used as a single agent or in 1:1 combination with the associated tubulin inhibitor of each hybrid. In addition, CA-4 was used as a positive control. HUVECs were treated for 24h and PC-3 cells were treated for 72h instead. Samples were analysed using a Beckman Coulter (Dako) 2-laser CyAn ADP analyser provided by the School of Biochemistry and Immunology, TCD. Cell cycle analysis was obtained by examining the PI-stained DNA content, in particular focusing on the sub-G_0/G_1 phase. Each compound concentration was tested in duplicate and each experiment was performed three independent times. The results were expressed in terms of the mean percentage of cells found in the sub-G_0/G_1 phase ± SEM.

4.2.14 Analysis of Endothelial Cells' Morphology

The effect of test compounds on endothelial cells' morphology was examined as previously examined in Chapter 2, section 2.1.7.4, p.78. The experiments were performed in triplicate and the results were presented as images of the morphological changes of endothelial cells after 1h and 3h of drug washout.

4.2.15 Statistical Analysis

Statistical analysis of the data was carried out using GraphPad Prism, version 5. Percentage inhibition values of each compound at each concentration were expressed as mean ± SEM. Values were tested for Gaussian distribution and where appropriate, IC_{50} values were generated. In order to determine whether there was a significant difference between control and treated groups, Student's *t*-test was applied using GraphPad Prism, version 5.

4.3 Results

The novel hybrids were synthesised as dual-acting inhibitors of both tubulin and APN activity, hence it was important to investigate their effects in APN- and tubulin-based assays.

4.3.1 APN Enzyme-based Assay

Firstly, it was necessary to evaluate the hybrids' ability to inhibit the APN enzyme using a colorimetric assay, based on the conversion of L-leucine-*p*-nitroanilide to the coloured hydrolysis product *p*-nitroaniline by APN. Dose response curves were generated and IC_{50} values ± SEM were determined.

4.3.1.1 Group I Hybrids

ECB377 and ECB378 hybrids were examined in the APN enzyme-based assay. Bestatin was used as a positive control and ECB394 (the active tubulin inhibitor incorporated into the hybrids' design) served as a negative control. ECB377 and ECB378 demonstrated similar APN inhibitory profiles with IC_{50} values determined to be 29.42 ± 1.24 μM and 28.06 ± 1.20 μM, respectively. In fact, these hybrids exhibited superior APN inhibition to that of bestatin (59.81 ± 1.08 μM) with a 2-fold increase in their activity. ECB394 did not demonstrate any APN inhibitory activity. Table 4.1 summarises the activity of hybrids and bestatin on the APN enzyme-based assay.

Table 4.1: APN enzyme-based assay data of group I hybrids, IC_{50} ± SEM (n=3).

Compounds	5 mUnits APN (μM)
Bestatin	59.81 ± 1.08
ECB377	29.42 ± 1.24
ECB378	28.06 ± 1.20

4.3.1.2 Group II Hybrids

The APN inhibitory activity of ECB399 and ECB404 hybrids was assessed using the APN enzyme-based assay. Both ECB399 and ECB404 demonstrated superior activity to that of bestatin with IC_{50} values of 27.76 ± 1.12 μM and 23.49 ± 1.12 μM,

respectively. Table 4.2 summarises the inhibitory activity of group II hybrids in the APN enzyme-based assay.

Table 4.2: APN enzyme-based assay data of group II hybrids, IC_{50} ± SEM (n=3).

Compounds	5 mUnits APN (μM)
Bestatin	59.81 ± 1.08
ECB399	27.76 ± 1.12
ECB404	23.49 ± 1.12

4.3.1.3 Group III Hybrid

ECB397 was assessed for its APN inhibitory properties in the enzyme-based assay. RS180, the active tubulin inhibitor released following hydrolysis of ECB397, was used as negative control. Group I hybrid, ECB397 demonstrated superior APN inhibitory activity to that of bestatin, exhibiting an IC_{50} value of 32.04 ± 1.19 μM. RS180 did not demonstrate any APN inhibition. Table 4.3 summarises the activity of ECB397 and bestatin on the APN enzyme-based assay.

Table 4.3: APN enzyme-based assay data of group III hybrid, IC_{50} ± SEM (n=3).

Compounds	5 mUnits APN (μM)
Bestatin	59.81 ± 1.08
ECB397	32.04 ± 1.19

4.3.1.4 Group IV Hybrid

The inhibitory effect of ADR469 in the APN enzyme assay was determined. An IC_{50} value was not calculated due to the formation of coloured solution at higher concentrations; thus percentage inhibition was estimated at different concentrations. ADR469 showed APN inhibitory activity at concentrations as low as 5 μM and the effect was dose-dependent. At 100 μM, the APN inhibition of ADR469 was 38.99 ±

3.01 %, whereas 100 μM of bestatin proved to be significantly ($p < 0.01$) more effective with 64.19 ± 1.90 % inhibition. Figure 4.6 represents the percentage APN inhibition of ADR469 at a range of concentration as determined by the APN enzyme assay.

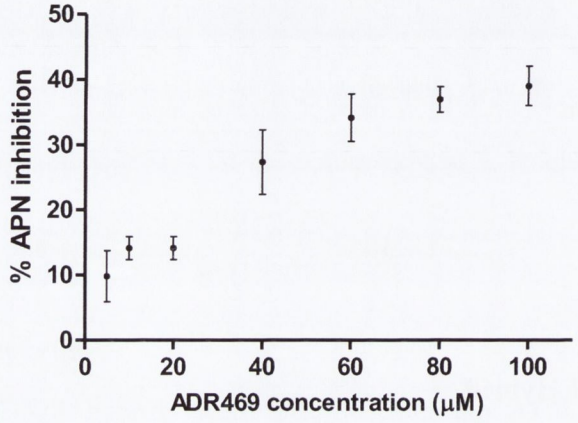

Figure 4.6: The effect of ADR469 on APN inhibition using the enzyme-based assay. Data represents mean ± SEM (n=3).

4.3.1.5 Designed Multiple Ligand

The inhibitory activity of BWM120 was examined in the APN enzyme-based assay. BWM120 exhibited potent APN inhibitory properties with an IC_{50} value of 9.32 ± 1.06 μM. The result obtained from the BWM120 data demonstrated approximately a 6-fold increase in activity compared to that of bestatin. Table 4.4 presents the inhibitory data of BWM120 and bestatin obtained from the APN enzyme-based assay.

Table 4.4: APN enzyme-based assay data of BWM120, IC_{50} ± SEM (n=3).

Compounds	5 mUnits APN (μM)
Bestatin	59.81 ± 1.08
BWM120	9.32 ± 1.06

4.3.2 APN Expression of HUVECs and PC-3 Cells

Following the examination of hybrids and DML in the APN enzyme-based assay, the next stage involved the evaluation of test compounds against APN expressing cell lines.

For the purpose of this study, HUVECs and PC-3 cells were selected and assessed for APN expression using immunofluorescence staining followed by flow cytometric analysis. Membrane-bound APN was detected in both cell lines (Figure 4.7).

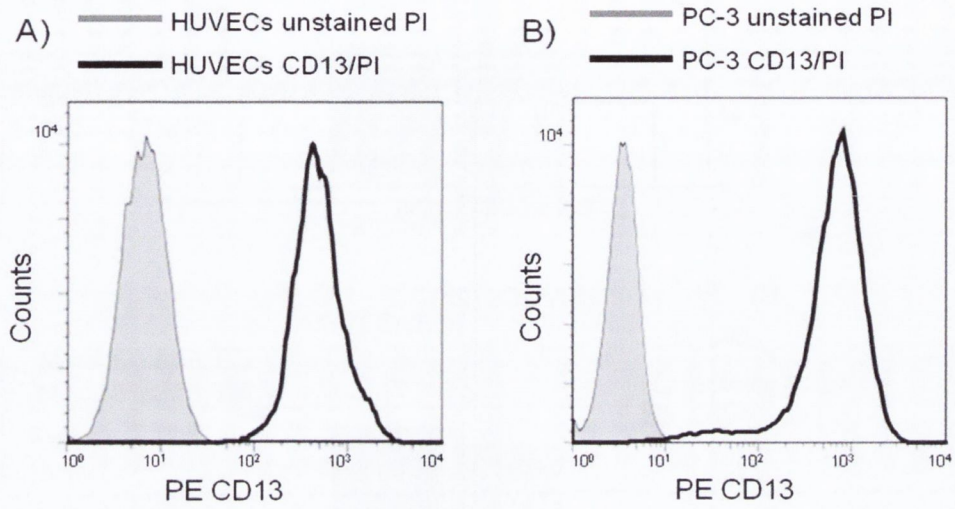

Figure 4.7: APN expression of HUVECs and PC-3 cells. Immunofluorescence staining of **A)** HUVECs and **B)** PC-3 cells with PE CD13, followed by flow cytometric analysis.

4.3.3 Cytotoxicity Assay

Once the APN expression of both cell lines was determined, it was necessary to establish a non-toxic concentration range of test compounds prior to the APN cell-based assay. For the purpose of this study, the MTT assay was performed and cell viability was determined as previously described and expressed in terms of percentage inhibition of cell viability ± SEM.

4.3.3.1 Group I Hybrids

The cell viability of HUVECs and PC-3 cells was determined following incubation with ECB377 and ECB378. Both hybrids exerted their cytotoxic effects on HUVECs at concentrations of 10 and 20 μM, as shown in Figure 4.8. ECB377 at 10 and 20 μM demonstrated a percentage inhibition of cell viability of 23.71 ± 0.72 % and 39.90 ± 11.12 %, whereas ECB378 showed a percentage inhibition of cell viability of 22.13 ± 15.41 % and 54.81 ±13.52 %, respectively. The hybrids did not demonstrate any cytotoxic effect on PC-3 cells up to 20 μM.

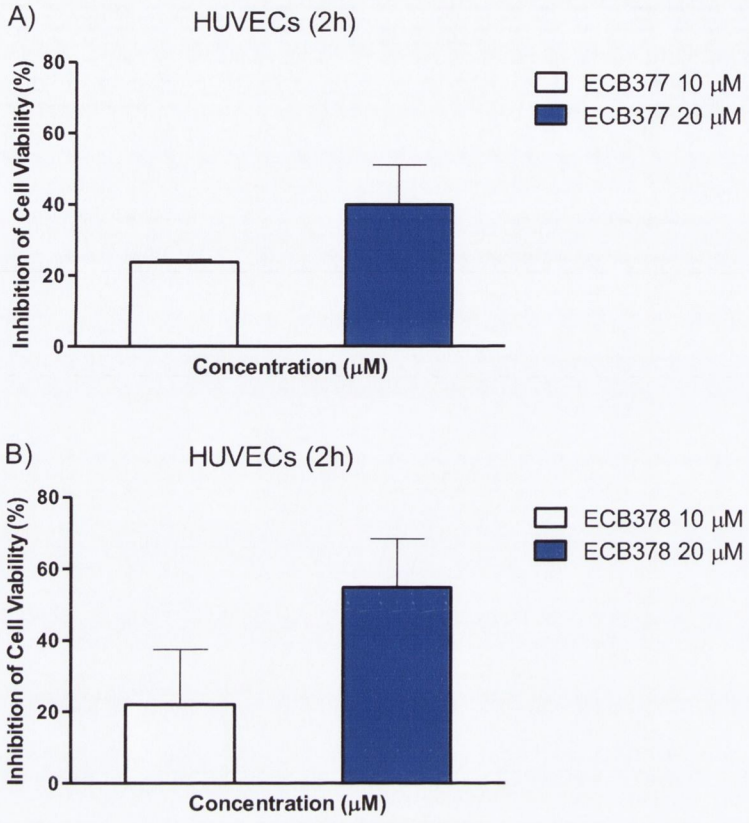

Figure 4.8: The cytotoxic effect of **A)** ECB377 and **B)** ECB378 on HUVECs after 2h incubation, as determined by the MTT assay. Data represents mean ± SEM (n=3).

4.3.3.2 Group II Hybrids

ECB399 and ECB404 were examined for their ability to cause cytotoxicity to HUVECs and PC-3 cells after 2h of treatment. ECB399 demonstrated a reduction in HUVECs' percentage viability at 10 μM (30.32 ± 5.09 %) and at 20 μM (44.90 ± 4.31 %), whereas ECB404 showed greater cell growth inhibition at 10 μM (35.42 ± 9.30 %) and at 20 μM (56.33 ± 7.50 %), as shown in Figure 4.9. There was no cytotoxic effect observed in PC-3 cells when treated with either hybrid at concentrations up to 20 μM.

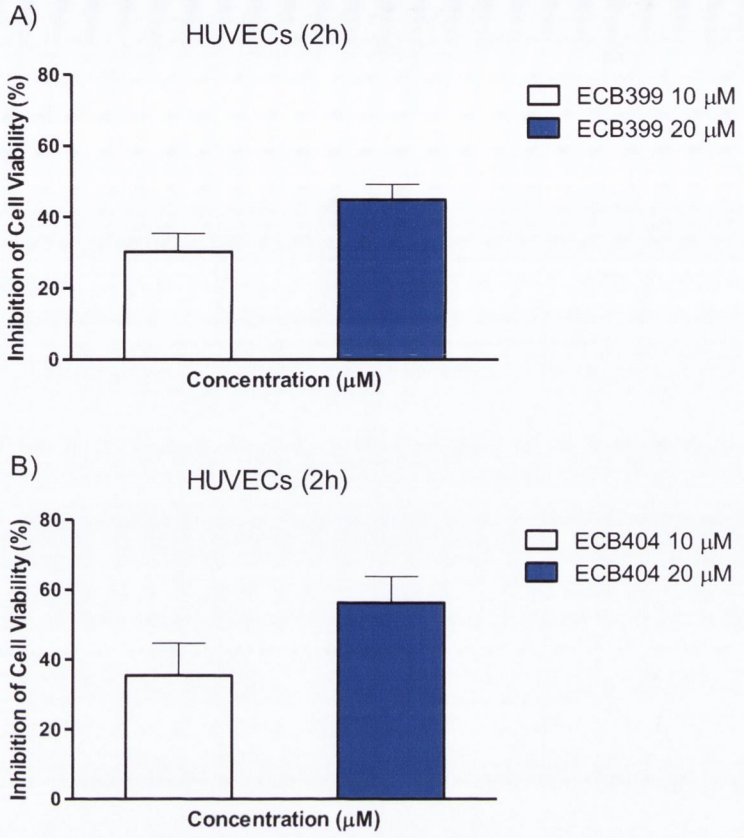

Figure 4.9: The cytotoxic effect of **A)** ECB399 and **B)** ECB404 on HUVECs after 2h incubation, as determined by the MTT assay. Data represents mean ± SEM (n=3).

4.3.3.3 Group III Hybrid

The cytotoxic effect of ECB397 on HUVECs and PC-3 cells was assessed after a 2h incubation period. ECB397 did not exhibit any effect on cell viability on either cell lines at concentrations up to 20 μM.

4.3.3.4 Group IV Hybrid

Due to the fact that ADR269, the active tubulin component of the ADR469 hybrid showed high potency when evaluated *in vitro*, ADR469 was expected to possess similar activity. Thus, ADR469 was evaluated for evidence of cytotoxic activity after 2h incubation at concentrations as low as 1 and 5 μM, using both HUVECs and PC-3 cells. Inhibition of HUVECs' viability following treatment with 1 and 5 μM ADR469 was found to be 28.91 ± 5.32 % and 30.53 ± 7.40 %, respectively (Figure 4.10). The viability of PC-3 cells was not affected by treatment with up to 20 μM ADR469.

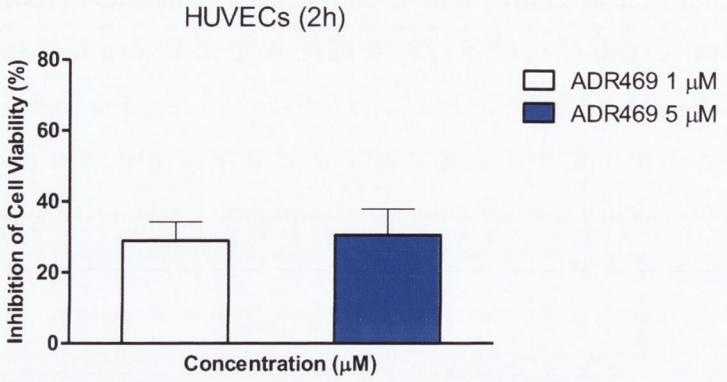

Figure 4.10: The cytotoxic effect of ADR469 on HUVECs after 2h incubation, as determined by the MTT assay. Data represents mean ± SEM (n=3).

4.3.3.5 Designed Multiple Ligand

The cytotoxic effect of BWM120 on HUVECs and PC-3 cells was determined following 2h incubation. Inhibition of HUVECs' viability was observed after treatment with BWM120 at 10 μM (44.00 ± 10.31 %) and at 20 μM (44.46 ± 3.43 %), as shown in Figure 4.11. BWM120 did not alter the viability of PC-3 cells at concentrations up to 20 μM.

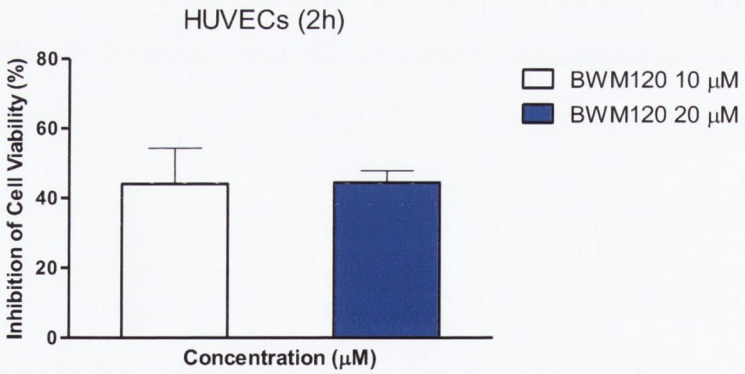

Figure 4.11: The cytotoxic effect of BWM120 on HUVECs after 2h incubation, as determined by the MTT assay. Data represents mean ± SEM (n=3).

4.3.4 APN Cell-based Assay

Once the cytotoxic concentrations of test compounds were determined, it was necessary to examine their inhibitory properties at non-toxic doses in an APN cell-based assay, using either HUVECs or PC-3 cells, instead of the active APN enzyme. Bestatin was used as a positive control and although it was not found to be cytotoxic at higher

concentrations, it was only examined up to 5 μM in the HUVECs-based assay (with the exception of ADR469) and up to 20 μM in the PC-3 cell based assay, in order to be comparative to the test compounds. The results were expressed in terms of percentage APN inhibition relative to untreated cells ± SEM. Statistical significance was determined between the percentage APN inhibition calculated for test compounds and bestatin, using Student's *t*-test.

4.3.4.1 Group I Hybrids

The ability of ECB377 and ECB378 to inhibit the activity of cellular APN present in HUVECs and PC-3 cells was assessed. Firstly, the activity of test compounds and bestatin was examined using HUVECs. Bestatin's APN inhibitory effect was determined at 1 μM and 5 μM to be 11.88 ± 3.27 % and 17.86 ± 0.75 %, respectively (Figure 4.12 A). Both hybrids demonstrated satisfactory APN inhibition against HUVECs at concentrations below 10 μM. ECB377 exhibited 12.15 ± 7.00 % at 1 μM and 46.00 ± 2.31 % at 5 μM, whereas ECB378 showed 23.42 ± 5.80 % at 1 μM and 51.50 ± 2.12 % at 5 μM (Figure 4.12 B and C). ECB377 and ECB378 demonstrated significantly ($p < 0.001$) superior APN inhibition to that of bestatin at 5 μM in HUVECs by an almost 3-fold increase in activity.

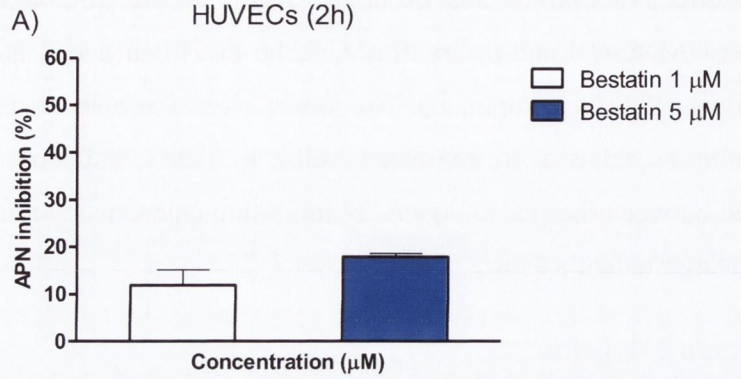

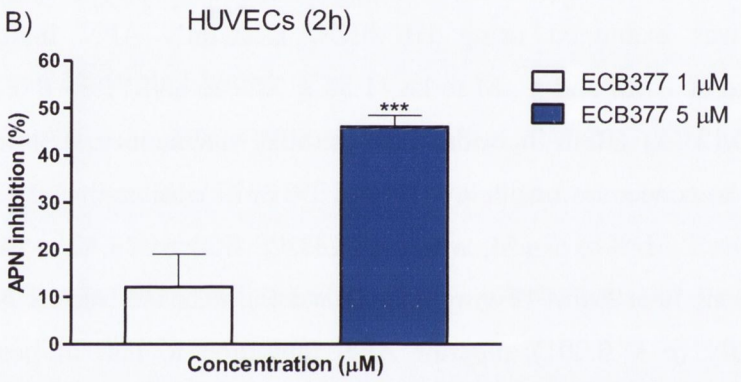

*** $p < 0.001$, significantly higher % APN inhibition compared to that of bestatin at the corresponding concentration, as determined by Student's *t*-test.

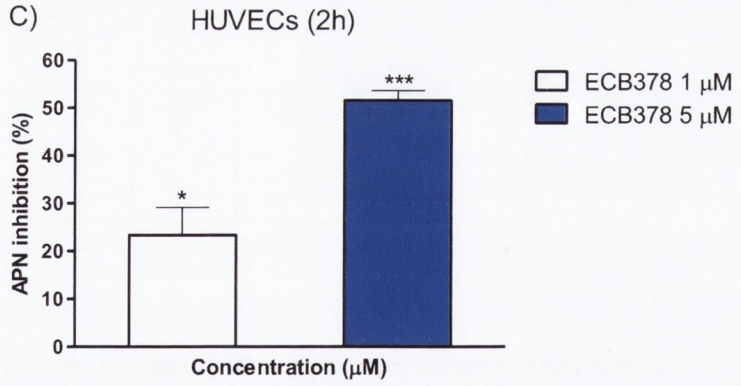

* $p < 0.05$, *** $p < 0.001$, significantly higher % APN inhibition compared to that of bestatin at the corresponding concentration, as determined by Student's *t*-test.

Figure 4.12: APN inhibition of HUVECs after 2h incubation with **A)** bestatin, **B)** ECB377 and **C)** ECB378. Data represents mean ± SEM (n=3).

Next, the effect of hybrids and bestatin on the APN inhibition of PC-3 cells was determined. Bestatin was examined at 1, 5, 10 and 20 μM and the percentage APN inhibition was established to be 10.84 ± 3.24 %, 15.10 ± 0.97 %, 17.31 ± 5.72 % and 36.11 ± 0.90 %, respectively (Figure 4.13 A). Similarly, the activity of ECB377 and ECB378 was evaluated at 1, 5, 10 and 20 μM and the percentage inhibition of ECB377 was determined to be 27.76 ± 2.10 %, 44.61 ± 7.32 %, 63.70 ± 7.68 % and 68.43 ± 8.57 % and for ECB378 31.37 ± 5.48 %, 47.25 ± 2.05 %, 50.72 ± 6.02 % and 61.90 ± 0.99 %, respectively (Figure 4.13 B and C). The inhibitory properties of both hybrids against the APN enzyme present on PC-3 cells were approximately 2-fold better than bestatin.

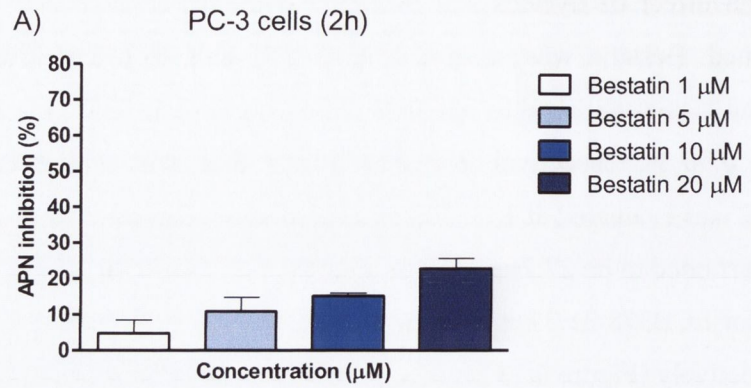

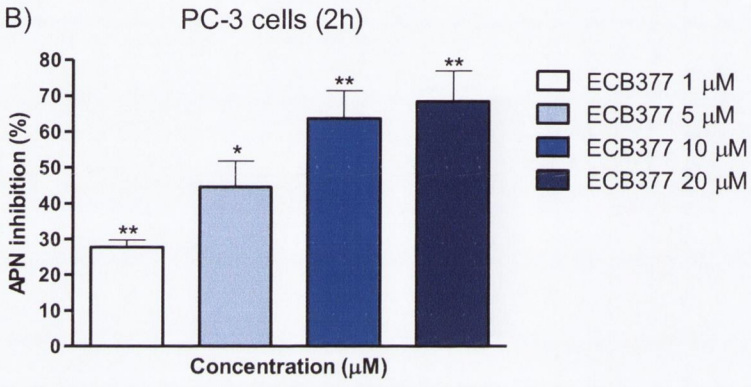

* $p < 0.05$, ** $p < 0.01$, significantly higher % APN inhibition compared to that of bestatin at the corresponding concentration, as determined by Student's *t*-test.

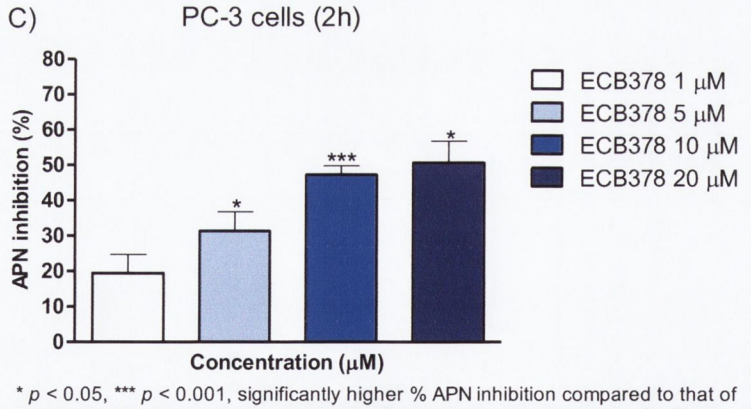

* $p < 0.05$, *** $p < 0.001$, significantly higher % APN inhibition compared to that of bestatin at the corresponding concentration, as determined by Student's *t*-test.

Figure 4.13: APN inhibition of PC-3 cells after 2h incubation with **A)** bestatin, **B)** ECB377 and **C)** ECB378. Data represents mean ± SEM (n=3).

4.3.4.2 Group II Hybrids

ECB399 and ECB404 were examined for their APN inhibitory effects against HUVECs and PC-3 cells. In the HUVECs-based assay, both hybrids demonstrated good inhibitory activity at 1 and 5 μM and the percentage APN inhibition for ECB399 was calculated to be 22.40 ± 0.91 % and 39.00 ± 2.92 % and for ECB404 32.70 ± 4.73 % and 48.61 ± 0.82 %, respectively (Figure 4.14 A and B). Both hybrids demonstrated a significantly greater inhibitory profile against APN in HUVECs compared to that of bestatin by a 3-fold increase in activity.

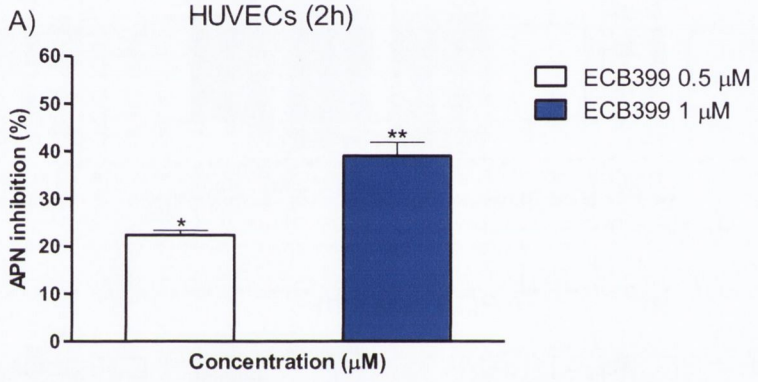

* $p < 0.05$, ** $p < 0.01$, significantly higher % APN inhibition compared to that of bestatin at the corresponding concentration, as determined by Student's *t*-test.

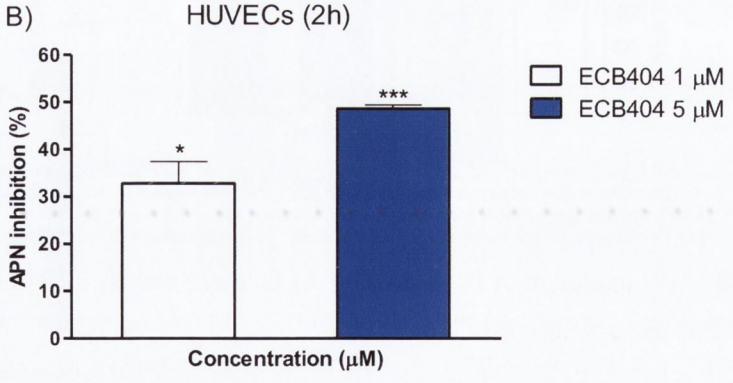

* $p < 0.05$, *** $p < 0.001$, significantly higher % APN inhibition compared to that of bestatin at the corresponding concentration, as determined by Student's *t*-test.

Figure 4.14: APN inhibition of HUVECs by **A)** ECB399 and **B)** ECB404 after 2h incubation. Data represents mean ± SEM (n=3).

The APN inhibition of PC-3 cells by 1, 5, 10 and 20 μM ECB399 and ECB404 was also determined and the extent of inhibition was as follows: 27.30 ± 10.91 %, 48.51 ± 11.62 %, 56.93 ± 8.41 %, 60.35 ± 12.10 % for ECB399 and 40.37 ± 8.23 %, 62.21 ± 3.90 %, 72.90 ± 7.41 % and 77.43 ± 4.91 % for ECB404, respectively (Figure 4.15 A and B). The APN inhibitory effect of both hybrids was 4-fold better than bestatin.

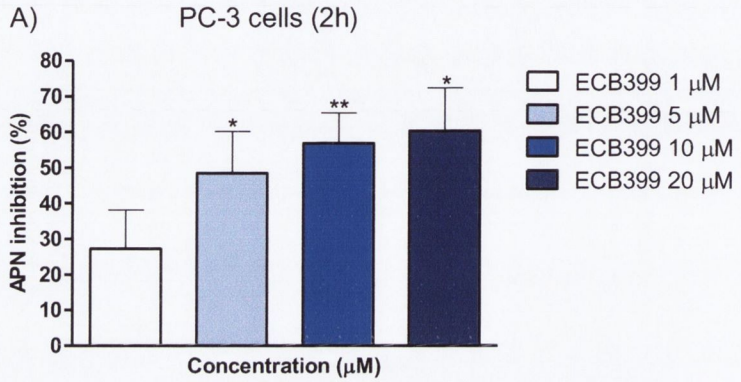

* $p < 0.05$, ** $p < 0.01$, significantly higher % APN inhibition compared to that of bestatin at the corresponding concentration, as determined by Student's *t*-test.

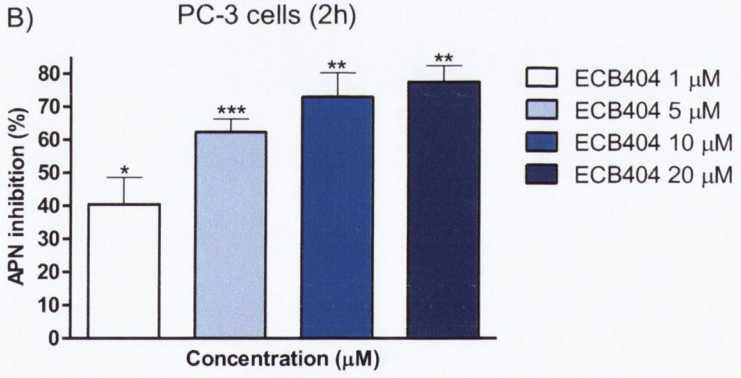

* $p < 0.05$, ** $p < 0.01$, *** $p < 0.001$, significantly higher % APN inhibition compared to that of bestatin at the corresponding concentration, as determined by Student's *t*-test.

Figure 4.15: APN inhibition of PC-3 cells by **A)** ECB399 and **B)** ECB404 after 2h incubation. Data represents mean ± SEM (n=3).

4.3.4.3 Group III Hybrid

ECB397 was evaluated for its APN inhibitory properties against HUVECs and PC-3 cells at non-cytotoxic concentrations. The effect of ECB397 on HUVECs was analysed at 0.1, 1 and 5 μM and the percentage APN inhibition was determined to be 31.90 ± 9.00 %, 52.61 ± 14.70 % and 64.00 ± 16.11 %, respectively (Figure 4.16 A). ECB397

showed improved activity against APN compared to that of bestatin with approximately a 5-fold increase in activity. The APN inhibition of ECB397 was also established using PC-3 cells at 1, 5, 10 and 20 μM and determined to be 31.30 ± 8.90 %, 51.71 ± 8.52 %, 55.71 ± 9.80 % and 71.43 ± 7.52 %, respectively (Figure 4.16 B). Its activity in this cell line was approximately 2-fold better than bestatin.

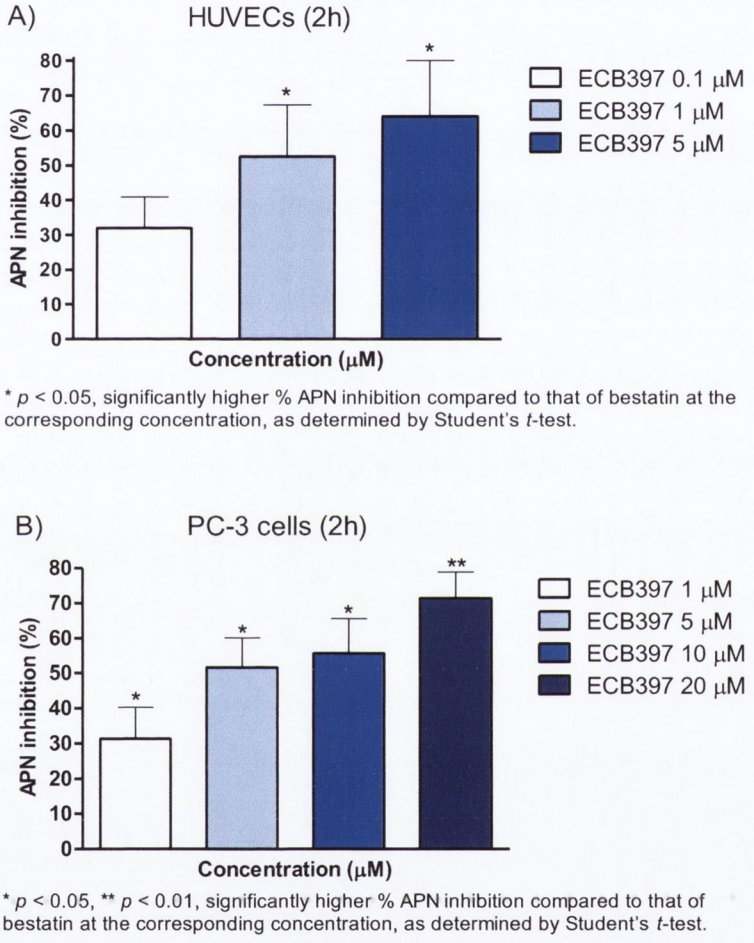

Figure 4.16: APN inhibition by ECB397 of **A)** HUVECs and **B)** PC-3 cells after 2h incubation. Data represents mean ± SEM (n=3).

4.3.4.4 Group IV Hybrid

ADR469 was assessed for its APN inhibitory properties in the APN cell-based assay. Due to its potent cytotoxic effect on HUVECs, ADR469 was only tested at 0.1 and 0.5 μM in the APN assay and the percentages of APN inhibition were 18.11 ± 2.90 % and 21.64 ± 2.22 %, respectively (Figure 4.17 A). This result suggests that ADR469 has a

superior activity to that of bestatin in the HUVECs-based APN assay. The percentages of APN inhibition caused by 1, 5, 10 and 20 μM of ADR469 were determined using PC-3 cells and found to be 47.91 ± 1.23 %, 51.71 ± 1.38 %, 51.87 ± 3.89 % and 56.55 ± 3.13 %, respectively (Figure 4.17 B). At these concentrations, ADR469 was significantly better than bestatin by approximately 3-fold in the PC-3 based assay.

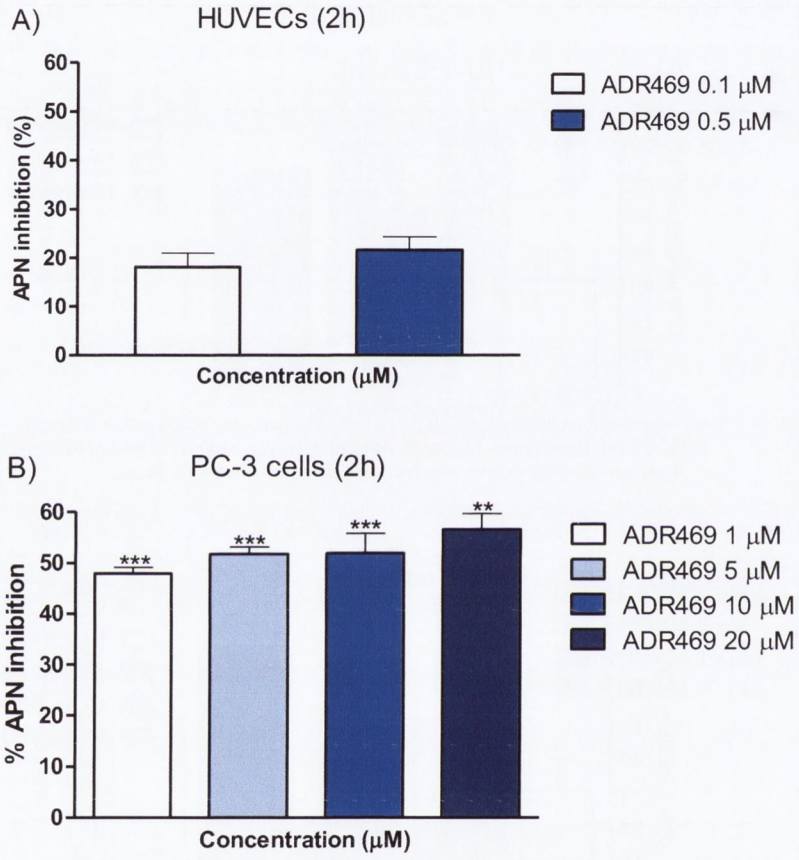

** $p < 0.01$, *** $p < 0.001$ significantly higher % APN inhibition compared to that of bestatin at the corresponding concentration, as determined by Student's *t*-test.

Figure 4.17: APN inhibition by ADR469 of **A)** HUVECs and **B)** PC-3 cells after 2h incubation. Data represents mean ± SEM (n=3).

4.3.4.5 Designed Multiple Ligand

The effect of BWM120 on the APN inhibition of HUVECs and PC-3 cells was investigated. Firstly, BWM120 activity was examined at 1 and 5 μM in the HUVECs-based assay, where the percentages of APN inhibition were 11.25 ± 0.45 % and 20.77 ± 3.81 %, respectively (Figure 4.18 A). Based on this data, the inhibitory effect of BWM120 was similar to that of bestatin. Next, the effect of 1, 5, 10 and 20 μM

BWM120 was determined using PC-3 cells and the percentages of APN inhibition were 21.09 ± 4.04 %, 41.26 ± 6.48 %, 39.18 ± 3.30 % and 55.25 ± 6.62 %, respectively (Figure 4.18 B). Although BWM120 demonstrated a similar inhibitory profile to bestatin with HUVECs, it was proven to be better in PC-3 cells with an approximately a 2-fold increase in activity.

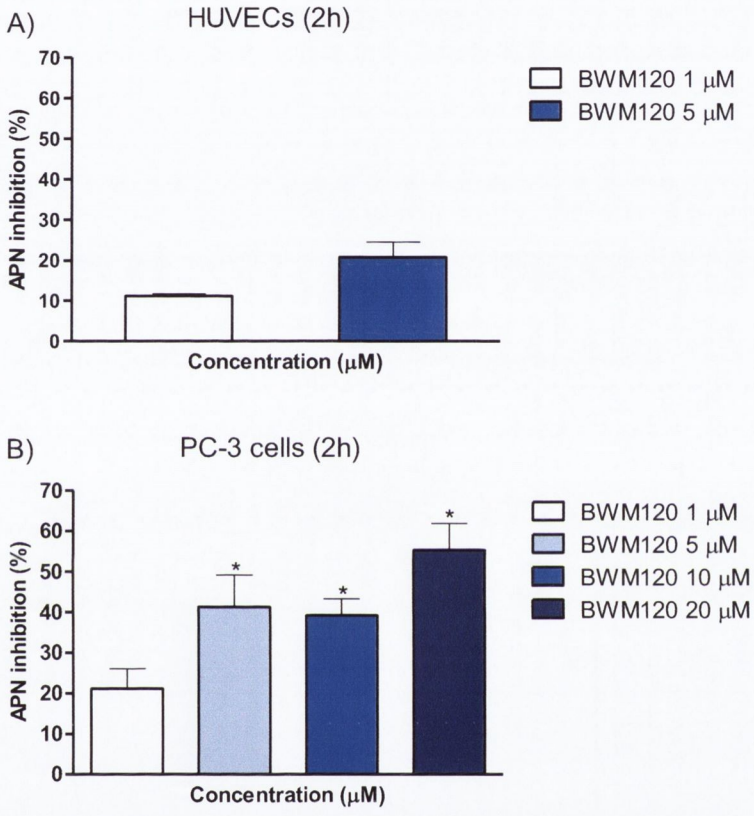

* $p < 0.05$, significantly higher % APN inhibition compared to that of bestatin at the corresponding concentration, as determined by Student's *t*-test.

Figure 4.18: APN inhibition by BWM120 of **A)** HUVECs and **B)** PC-3 cells after 2h incubation. Data represents mean ± SEM (n=3).

4.3.5 Inhibition of APN Expression

The ability of BWM120 to bind to extracellular APN and inhibit its expression was examined in HUVECs and PC-3 cells. Bestatin was used as a positive control. The level of PE CD13 fluorescence intensity was detected on the viable cells' membrane and was expressed in terms of fluorescence median ± SEM. Control treated HUVECs exhibited a percentage PE fluorescence median of 108 ± 16.5 %, whereas 0.1 mM and 0.5 mM bestatin demonstrated 100.51 ± 10.53 % and 93.70 ± 11.62 %, respectively

(Figure 4.19 and 4.20 A). The percentage PE fluorescence median of BWM120-treated HUVECs was determined to be 83.41 ± 5.83 % at 0.1 mM and 53.80 ± 2.41 % at 0.5 mM (Figure 4.19 and 4.20 B). There was no significant effect on the APN expression after treatment of HUVECs with bestatin at either concentration. BWM120 reduced the level of APN at 0.1 mM, but this was not sufficient for statistical significance. However, the APN expression of HUVECs was significantly ($p < 0.05$) reduced after treatment with 0.5 mM BWM120.

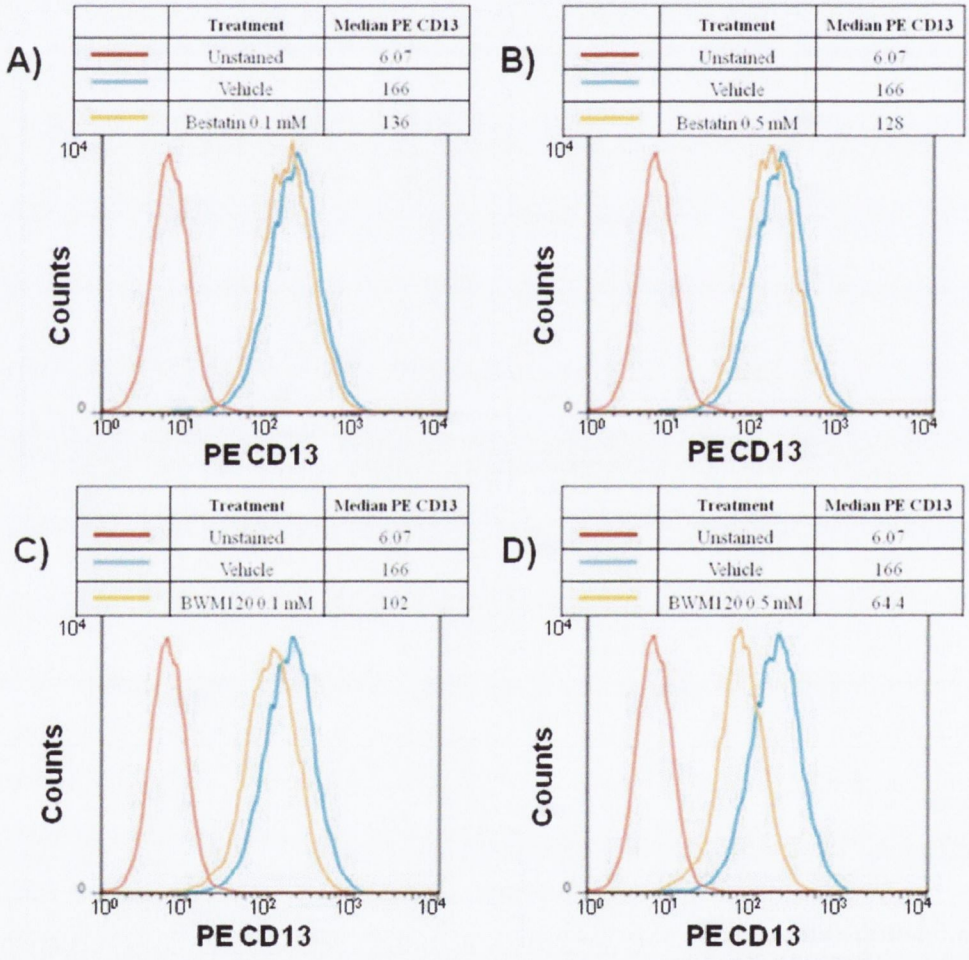

Figure 4.19: Detection of APN expression level (PE CD13) in HUVECs after 2h incubation with **A)** 0.1 mM bestatin, **B)** 0.5 mM bestatin, **C)** 0.1 mM BWM120 and **D)** 0.5 mM BWM120.

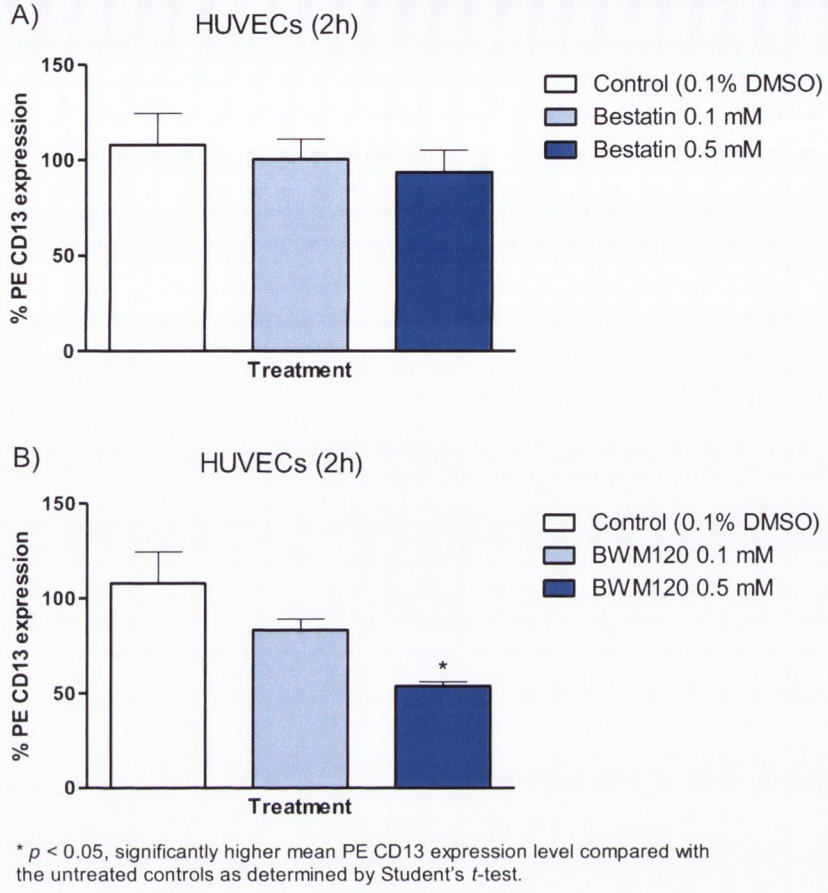

Figure 4.20: Percentage PE CD13 fluorescence median of HUVECs after 2h incubation with **A)** bestatin and **B)** BWM120. Data represents mean ± SEM (n=3).

APN expression of PC-3 cells was also examined after 2h incubation with 0.1 mM and 0.5 mM bestatin or BWM120 (Figure 4.21). The percentage fluorescence median of control treated cells was 206.61 ± 13.16 %, whereas percentage of bestatin treated cells was 193.30 ± 10.78 % at 0.1 mM and 123.16 ± 5.96 % at 0.5 mM (Figure 4.22 A). There was no apparent difference in the percentage fluorescence median of cells treated with 0.1 mM bestatin; however there was a significant ($p < 0.01$) reduction in the percentage PE CD13 fluorescence intensity of cells treated with 0.5 mM bestatin. BWM120-treated PC-3 cells demonstrated a slight decrease in the mean fluorescence median at 0.1 mM (177.00 ± 13.11 %), but showed a significant ($p < 0.01$) reduction at 0.5 mM (124.83 ± 5.90 %, Figure 4.22 B).

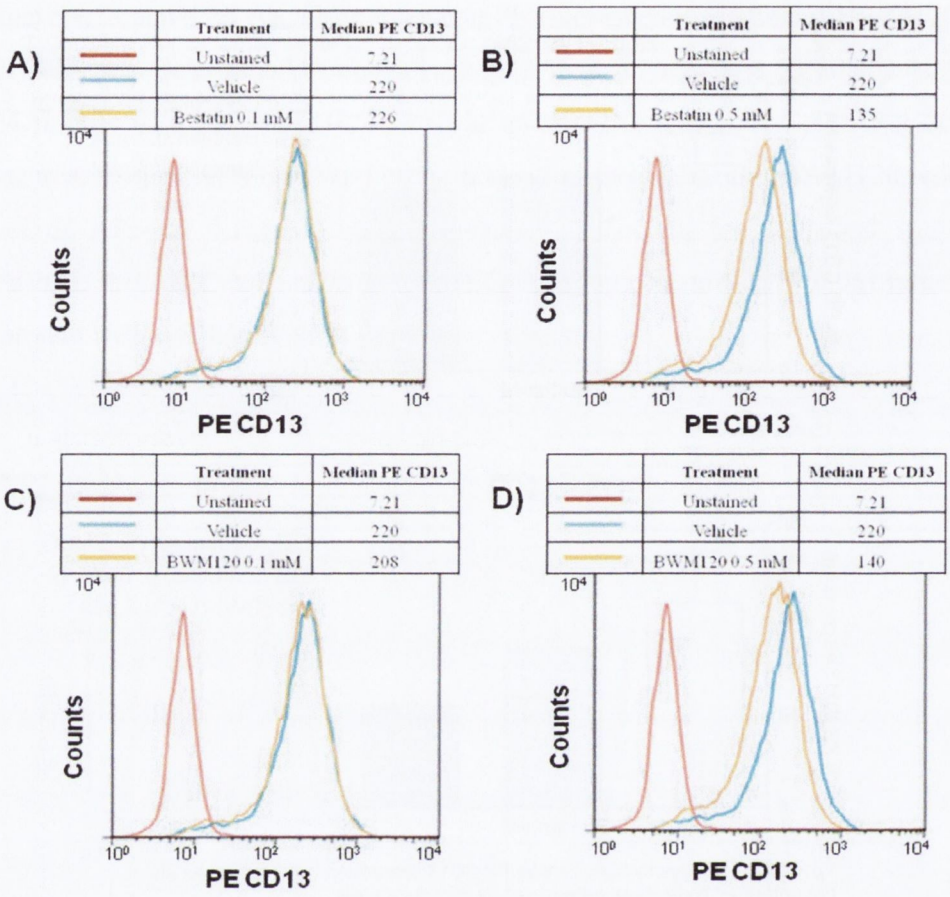

Figure 4.21: Detection of APN expression level (PE CD13) in PC-3 cells after 2h incubation with **A)** 0.1 mM bestatin, **B)** 0.5 mM bestatin, **C)** 0.1 mM BWM120 and **D)** 0.5 mM BWM120.

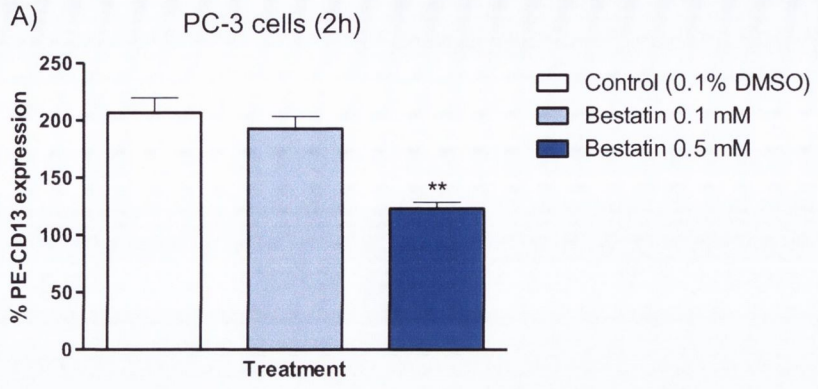

** $p < 0.01$, significantly higher mean PE-CD13 expression level compared with the untreated controls as determined by Student's *t*-test.

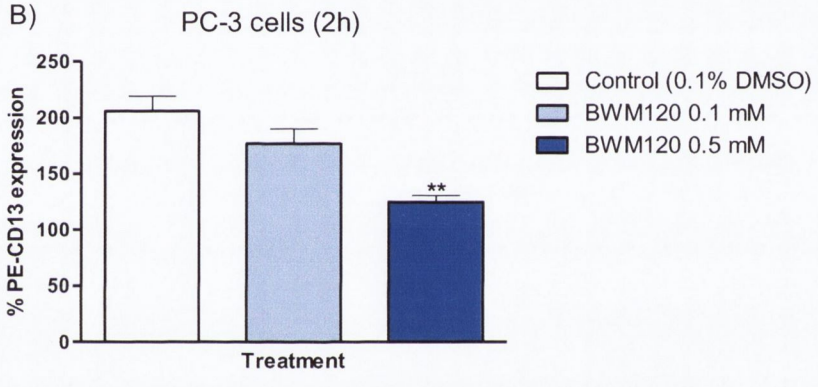

** $p < 0.01$, significantly higher mean PE-CD13 expression level compared with the untreated controls as determined by Student's t-test.

Figure 4.22: Percentage PE CD13 fluorescence median of PC-3 cells after 2h incubation with **A)** bestatin and **B)** BWM120. Data represents mean ± SEM (n=3).

4.3.6 Cell Proliferation Assay

The anti-proliferative activity of test compounds was determined using HUVECs and PC-3 cells in the MTT assay. Dose response curves were generated and IC_{50} values ± SEM were determined.

4.3.6.1 Group I Hybrids

Group I hybrids were examined for their effects on cell proliferation. Using ECB394 as the model tubulin inhibitor (as it closely resembles the tubulin binding component of the hybrids), the effects of bestatin, 1:1 combination of ECB394/bestatin, ECB377 and ECB378 were investigated on HUVECs and PC-3 cell proliferation. Their respective

IC_{50} values for HUVECs and PC-3 cells are displayed in Table 4.5. ECB394 demonstrated satisfactory anti-proliferative activity against HUVECs, with bestatin approximately 10-fold less active when compared to ECB394. Interestingly, the 1:1 combination of ECB394 and bestatin displayed a better anti-proliferative effect over ECB394 alone. Although ECB377 showed similar activity to ECB394, ECB378 exhibited almost a 2-fold reduction in the anti-proliferative effect against HUVECs. ECB394's effect on PC-3 cell proliferation was close to that with HUVECs, whereas bestatin was essentially inactive. The 1:1 combination of ECB394 and bestatin exhibited a slightly reduced effect on PC-3 cells when compared to ECB394 alone. While ECB378 exhibited similar activity to the ECB394/bestatin combination, the activity of ECB377 was 2-fold less.

Table 4.5: Best fit IC_{50} values ± SEM of group I hybrids, following the MTT assay (n=3).

Compounds	HUVECs (μM)	PC-3 cells (μM)
ECB394	4.09 ± 1.41	4.90 ± 1.12
Bestatin	43.03 ± 1.27	> 100
ECB394 + Bestatin (1:1)	2.08 ± 1.44	6.77 ± 1.24
ECB377	4.71 ± 0.52	12.05 ± 3.31
ECB378	7.80 ± 1.13	6.25 ± 1.09

4.3.6.2 Group II Hybrids

The ester-linked hybrids, ECB399 and ECB404, were evaluated for their anti-proliferative activity against HUVECs and PC-3 cells. Again the data generated here was compared to ECB394. ECB399 and ECB404 were firstly examined in the HUVECs-based assay, where their IC_{50} values were determined to be 0.25 ± 0.09 μM and 2.52 ± 1.44 μM, respectively (Table 4.6). These hybrids successfully demonstrated an enhanced inhibition of cell growth compared to that of ECB394, with a wide variation in the increased activity by a 16-fold and 1.6-fold enhancement, respectively. The effect of both hybrids on PC-3 cell proliferation was also determined and their IC_{50}

values were determined to be 0.63 ± 0.02 μM for ECB399 and 0.17 ± 0.06 μM for ECB404 (Table 4.6). Once more, the activity of both hybrids was considerably improved compared to that of ECB394 by 7-fold for ECB399 and a remarkable 29-fold for ECB404. The cell growth inhibition observed with 1:1 combination of ECB394/bestatin was not proven greater than that caused by hybrids in both cell lines.

Table 4.6: Best fit IC_{50} values ± SEM of group II hybrids, following the MTT assay (n=3).

Compounds	HUVECs (μM)	PC-3 cells (μM)
ECB394	4.09 ± 1.41	4.90 ± 1.12
Bestatin	43.03 ± 1.27	> 100
ECB394 + Bestatin (1:1)	2.08 ± 1.44	6.77 ± 1.24
ECB399	0.25 ± 0.09	0.63 ± 0.02
ECB404	2.52 ± 1.44	0.17 ± 0.06

4.3.6.3 Group III Hybrid

The anti-proliferative activity of ECB397 was evaluated in HUVECs and PC-3 cells. The effect of RS180 (the active tubulin component released upon hydrolysis of ECB397) in 1:1 combination with bestatin was also examined on both cell lines. In the HUVECs-based assay, RS180 displayed strong anti-proliferative activity with an IC_{50} value of 65.05 ± 1.10 nM, whereas RS180/bestatin combination revealed more than a 9-fold increase in activity with an IC_{50} value of 7.03 ± 3.41 nM. The ECB397 hybrid demonstrated a potent anti-proliferative effect against HUVECs and the IC_{50} value was 30.00 ± 17.01 nM, which was proven to be superior to that of RS180 alone, but not to that of the 1:1 combination (Table 4.7).

The inhibition of PC-3 cell growth by ECB397 and RS180/bestatin combination was also examined. RS180 exhibited a potent anti-proliferative effect against PC-3 cells (IC_{50}: 50.65 ± 1.19 nM), and when combined with bestatin, the combination demonstrated enhanced activity (IC_{50}: 10.52 ± 1.4 nM). The activity of ECB397 was slightly better than RS180 (42.44 ± 1.55 nM), but was not as effective as the combination (Table 4.7).

Table 4.7: Best fit IC_{50} values ± SEM of group III hybrid, following the MTT assay (n=3).

Compounds	HUVECs (nM)	PC-3 cells (nM)
RS180	65.05 ± 1.10	50.65 ± 1.19
Bestatin	43.03 ± 1.27 (μM)	> 100 (μM)
RS180 + Bestatin (1:1)	7.03 ± 3.41	10.52 ± 1.14
ECB397	30.00 ± 17.01	42.44 ± 1.55

4.3.6.4 Group IV Hybrid

The effect of group IV hybrid ADR469 on the proliferation of HUVECs and PC-3 cells was investigated. Comparison studies of ADR269 (the active tubulin inhibitor of the hybrid), a 1:1 combination of ADR269/bestatin and ADR469 hybrid was carried out in both cell lines. Their respective best fit IC_{50} values are displayed in Table 4.8. Within this group, a remarkably similar level of activity in PC-3 cells was observed between all forms regardless of the presentation of the tubulin binding component.

Table 4.8: Best fit IC_{50} values ± SEM of group IV hybrid, following the MTT assay (n=3).

Compounds	HUVECs (nM)	PC-3 cells (nM)
ADR269	4.91 ± 1.01	4.67 ± 1.45
Bestatin	43.03 ± 1.27 (μM)	> 100 (μM)
ADR269 + Bestatin (1:1)	14.80 ± 1.13	5.43 ± 1.07
ADR469	10.31 ± 1.22	5.41 ± 1.37

4.3.6.5 Designed Multiple Ligand

The anti-proliferative activity of BWM120 against both HUVECs and PC-3 cells was examined. BWM120 demonstrated modest inhibition, in comparison to RS180, against HUVECs' growth with an IC_{50} value of 1.10 ± 0.09 μM, but exhibited a more pronounced effect on PC-3 cells with an IC_{50} value of 0.49 ± 0.03 μM (Table 4.9).

Table 4.9: Best fit IC_{50} values ± SEM of BWM120, following the MTT assay (n=3).

Compounds	HUVECs	PC-3 cells
RS180	65.05 ± 1.10 nM	50.65 ± 1.19 nM
BWM120	1.10 ± 0.09 μM	0.49 ± 0.03 μM

4.3.7 Immunofluorescence Staining of the Microtubules

The next stage of the *in vitro* evaluation of the novel hybrids and DML was to explore their effects on the tubulin cytoskeleton of intact cells. Selected compounds were chosen for further evaluation including ECB378, ECB397, ADR469 and BWM120, in order to examine the disruption of tubulin organisation of endothelial cells. Samples were visualised using a confocal microscope and images were captured.

4.3.7.1 Group I Hybrid

ECB378 was selected for further evaluation in order to examine its effect on the microtubule organisation of HUVECs. The effect of ECB378 on the tubulin cytoskeleton was not apparent at 1 μM, unlike the rest of the tubulin inhibitors examined previously, and for this reason higher concentrations were used. An observable difference in the tubulin structure was more evident at 40 μM ECB378, where there was a disruption of the cell monolayer and absence of tubulin microfilaments (Figure 4.23).

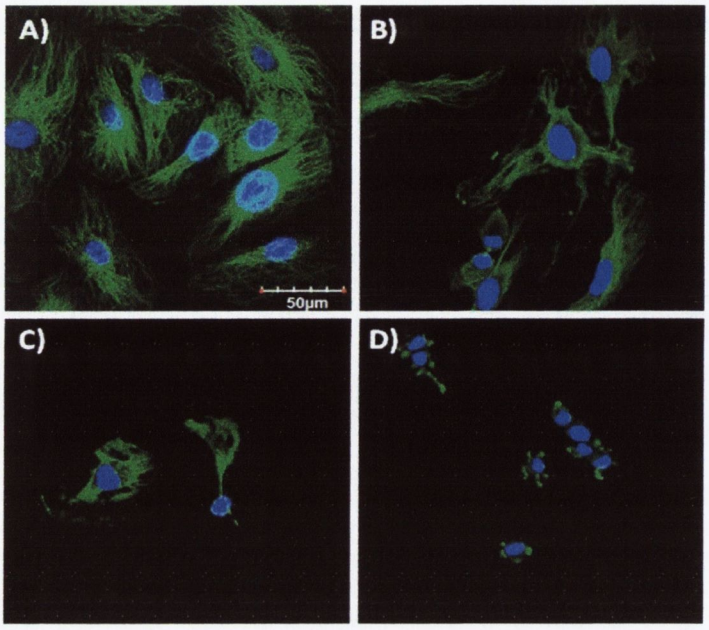

Figure 4.23: Microtubule disruption of endothelial cells by ECB378. HUVECs were treated for 30 minutes and stained for α-tubulin (green) and nucleus (blue). Images were taken using an Olympus FV1000 point scanning confocal microscope (x60). **A)** Control (0.1% DMSO), **B)** 10 µM ECB378, **C)** 20 µM ECB378 and **D)** 40 µM ECB378.

4.3.7.2 Group III Hybrid

ECB397 was examined for its ability to affect microtubule assembly in HUVECs. Treatment with 1 µM of ECB397 induced microtubule disruption as evidenced by the reduced degree of microtubule staining (Figure 4.24). Long microtubule fibres were present in the control treated cells, whereas in the ECB397-treated cells a microtubule network was absent.

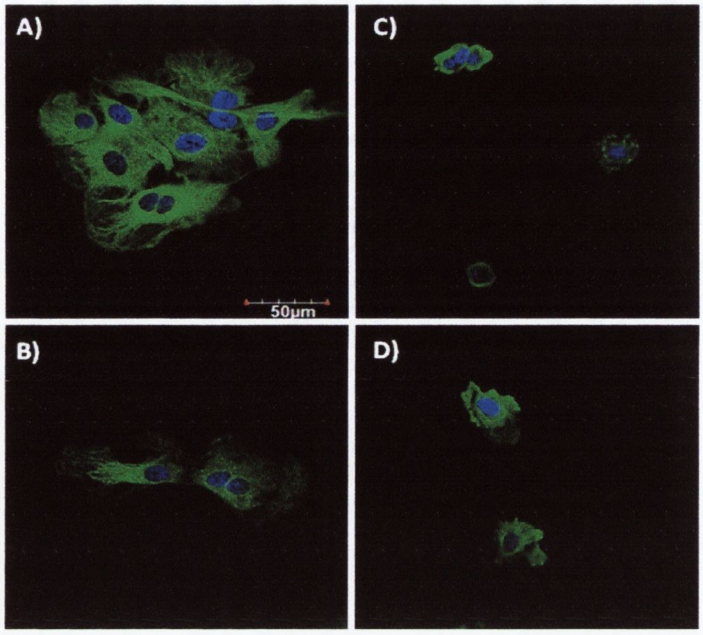

Figure 4.24: Microtubule disruption of endothelial cells by ECB397. HUVECs were treated for 30 minutes and stained for α-tubulin (green) and nucleus (blue). Images were taken using an Olympus FV1000 point scanning confocal microscope (x60). **A-B)** Control (0.1% DMSO), **C-D)** 1 µM ECB397.

4.3.7.3 Group IV Hybrid

The tubulin cytoskeleton of HUVECs was examined after treatment with 1 µM ADR469. The disruption of microtubule organisation by ADR469 was clear, as the amount of stained tubulin was dramatically reduced and no long microtubule filaments were present (Figure 4.25).

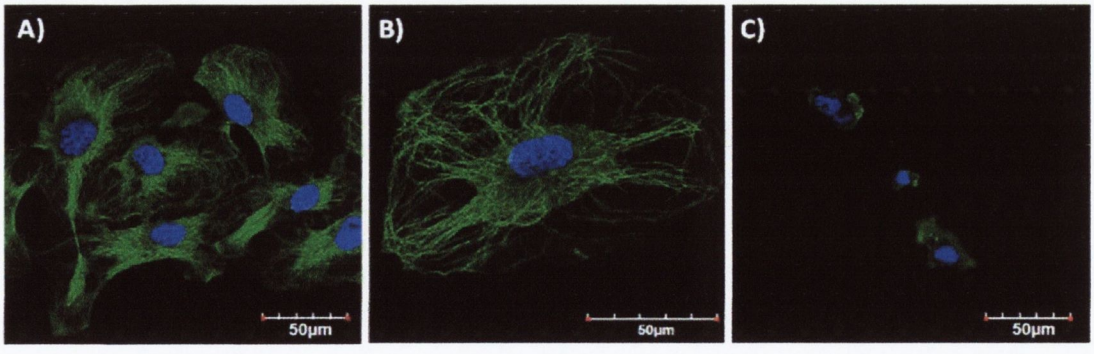

Figure 4.25: Microtubule disruption of endothelial cells by ADR469. HUVECs were treated for 30 minutes and stained for α-tubulin (green) and nucleus (blue). Images were taken using an Olympus FV1000 point scanning confocal microscope (x60). **A-B)** Control (0.1% DMSO) and **C)** 1 µM ADR469.

4.3.7.4 Designed Multiple Ligand

The ability of BWM120 to disrupt the tubulin cytoskeleton of HUVECs was investigated. Endothelial cells were incubated with 1 μM of BWM120. A minor effect was observed on the tubulin cytoskeleton when cells were treated with 1 μM BWM120, thus a higher concentration was used. A more evident disruption of the cytoskeleton was observed after treatment of cells with 5 μM BWM120, where there was a clear decrease in the amount of stained tubulin and loss of the complex microtubule network (Figure 4.26).

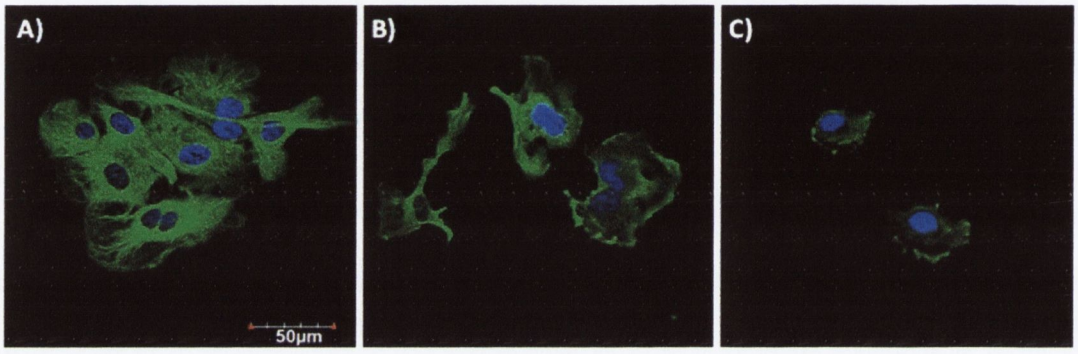

Figure 4.26: Microtubule disruption of endothelial cells by BWM120. HUVECs were treated for 30 minutes and stained for α-tubulin (green) and nucleus (blue). Images were taken using an Olympus FV1000 point scanning confocal microscope (x60). **A)** Control (0.1% DMSO), **B)** 1 μM BWM120 and **C)** 5 μM BWM120.

4.3.8 Cell Cycle Analysis – G_2/M Phase

Furthermore, the effect of each compound on the cell cycle of HUVECs and PC-3 cells was examined in order to establish their ability to interfere with cell mitosis. In all the control treated cells, the highest peak for DNA-stained cells appeared to be in the G_1 phase. The results were expressed in terms of percentage of cells in the G_2/M phase ± SEM.

4.3.8.1 Group I Hybrid

HUVECs and PC-3 cells were incubated with 1 and 10 μM of ECB378 and examined for their cell cycle stage (Figure 4.27). Control treated HUVECs appeared to accumulate in the G_1 phase and the percentage in the G_2/M phase was 25.71 ± 1.66 %. Interestingly, ECB378-treated HUVECs did not show a higher percentage of cells in the G_2/M phase at 1 or 10 μM with percentages of 24.33 ± 0.61 % and 24.42 ± 2.90 %,

respectively (Figure 4.28 A). Instead, the highest peaks appeared to be in the G_1 phase without any noticeable difference to that of control treated cells. Treatment of HUVECs with higher concentrations of ECB378, 20 and 40 μM, did not result in a significant accumulation of cells in the G_2/M phase, with respective percentages of 31.95 ± 2.16 % and 22.25 ± 0.40 %. Higher concentrations of ECB378 were not used due to the increased percentage of apoptotic cells detected in the sub-G_0/G_1 phase.

In addition, PC-3 cells were incubated with 1, 10, 20 and 40 μM of ECB378 and then analysed for the percentage of cells in the G_2/M phase. Control treated cells demonstrated an accumulation in the G_1 phase and the percentage of cells in the G_2/M phase was 25.51 ± 2.79 %. ECB378-treated PC-3 cells did not demonstrate any significant increase of DNA content in the G_2/M phase at 1, 10, 20 or 40 μM with percentages of 27.00 ± 4.21 %, 24.53 ± 4.42 %, 27.91 ± 0.38 % and 22.40 ± 0.22 %, respectively (Figure 4.28 B).

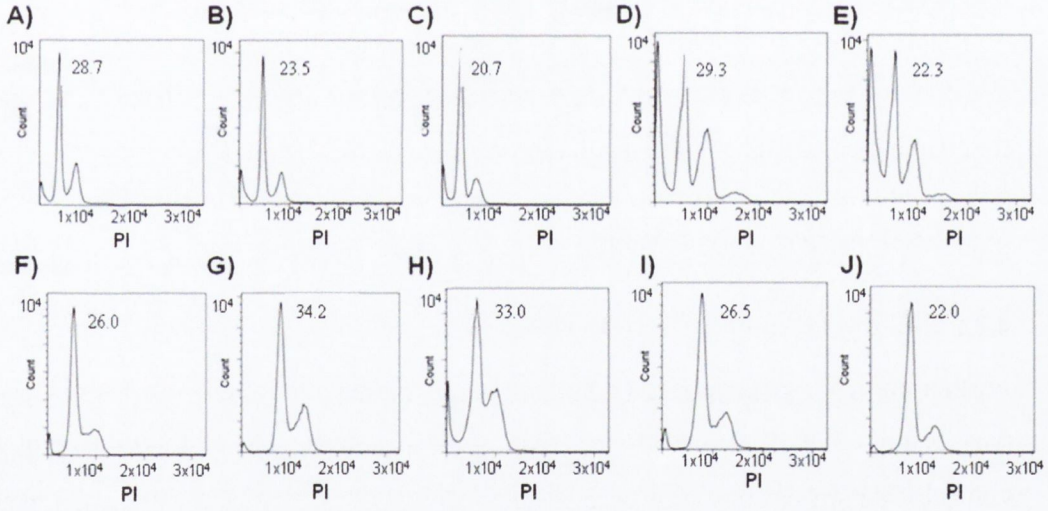

Figure 4.27: Cell cycle histograms of the gated G_2/M cells treated with ECB378. HUVECs (H) and PC-3 cells (P) were treated for 24h, stained with PI and analysed using flow cytometry. **A)** Control (0.1% DMSO) (H), **B)** 1 μM ECB378 (H), **C)** 10 μM ECB378 (H), **D)** 20 μM ECB378 (H) **E)** 40 μM ECB378 (H), **F)** Control (0.1% DMSO) (P), **G)** 1 μM ECB378 (P), **H)** 10 μM ECB378 (P), **I)** 20 μM ECB378 (P) and **J)** 40 μM ECB378 (P).

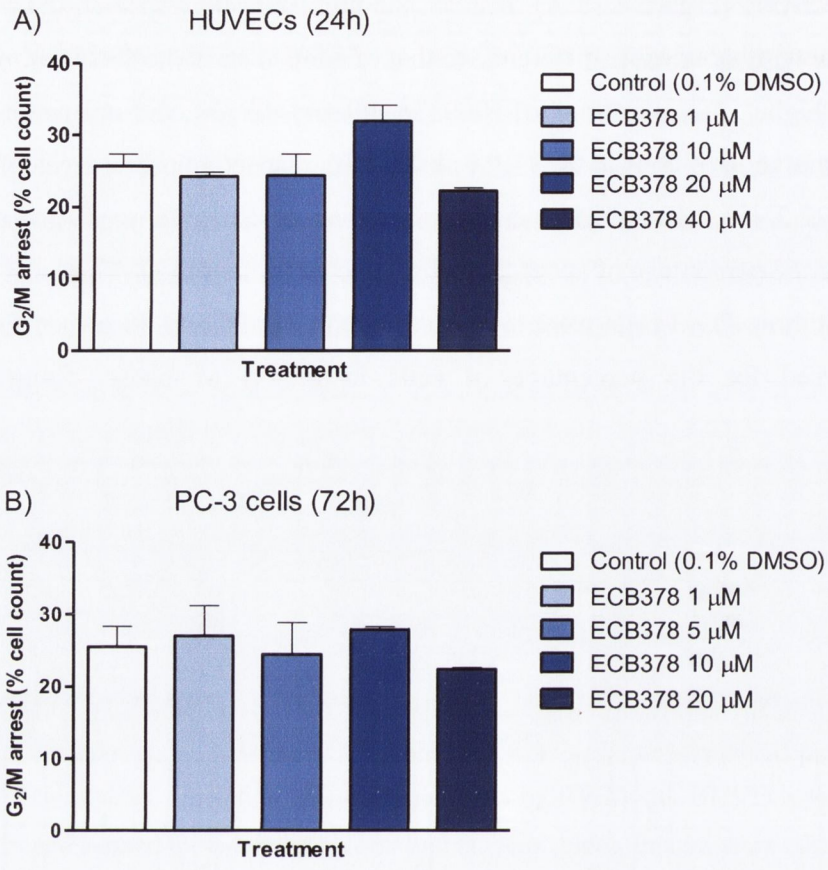

Figure 4.28: Percentage of cells in the G_2/M phase **A)** HUVECs and **B)** PC-3 cells incubated with ECB378. Data represents mean ± SEM (n=3).

4.3.8.2 Group III Hybrid

ECB397 was evaluated for its ability to induce cell cycle arrest of HUVECs and PC-3 cells at the G_2/M phase (Figure 4.29). The percentage of control treated HUVECs present in the G_2/M phase was 25.71 ± 1.66 %. ECB397-treated HUVECs showed a significant ($p < 0.05$) difference in the percentage of G_2/M cells compared to that of control cells at 1 μM (33.30 ± 1.19 %) and 10 μM (32.52 ± 1.31 %), as shown in Figure 4.30 A. Although the difference in the G_2/M of HUVECs between ECB397 and the control treated group was statistically significant, there was no obvious G_2/M mitotic arrest. Control treated PC-3 cells showed 25.50 ± 2.81 % of cells in the G_2/M phase, whereas ECB397-treated cells demonstrated a significant ($p < 0.01$) accumulation of cells in the G_2/M phase at 1 μM (83.33 ±1.49 %), as shown in Figure 4.30 B.

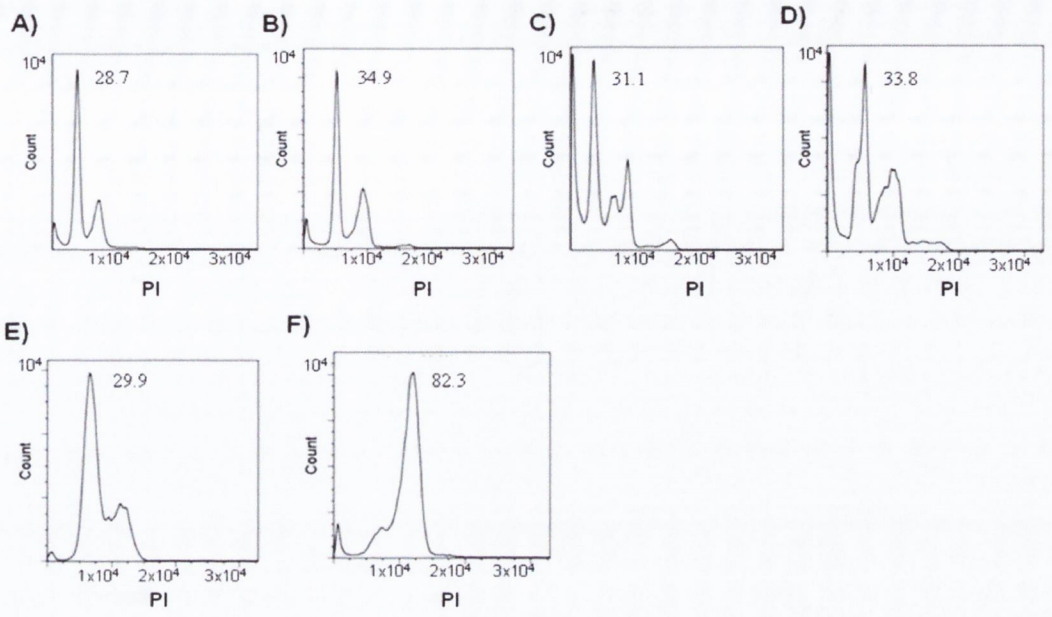

Figure 4.29: Cell cycle histograms of the gated G_2/M cells treated with ECB397. HUVECs (H) or PC-3 cells (P) were treated for 24h, stained with PI and analysed using flow cytometry **A)** Control (0.1% DMSO) (H), **B)** 1 μM ECB397 (H), **C)** 5 μM ECB397 (H), **D)** 10 μM ECB397 (H), **E)** Control (0.1% DMSO) (P) and **F)** 1 μM ECB397 (P).

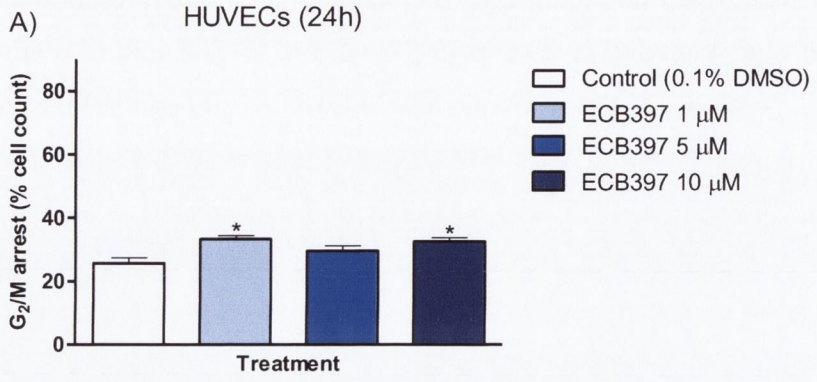

* $p < 0.05$, significantly higher mean % cell count in the G_2/M phase compared with the untreated controls as determined by Student's *t*-test.

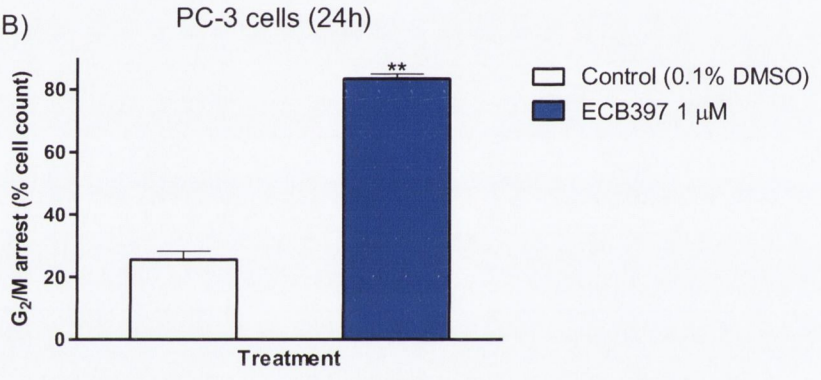

** $p < 0.01$, significantly higher mean % cell count in the G_2/M phase compared with the untreated controls as determined by Student's *t*-test.

Figure 4.30: Percentage of cells in the G_2/M phase **A)** HUVECs and **B)** PC-3 cells incubated with ECB397. Data represents mean ± SEM (n=3).

4.3.8.3 Group IV Hybrid

The anti-mitotic effect of group IV hybrid ADR469 was investigated by examining the cell cycle of HUVECs and PC-3 cells (Figure 4.31). The percentage of control treated HUVECs at the G_2/M phase was 28.00 ± 0.30 %, whereas the percentages for the ADR469-treated cells at 1 and 5 μM were 35.72 ± 1.61 % and 36.50 ± 1.13 %, respectively (Figure 4.32 A). Although the percentage of G_2/M HUVECs was significantly ($p < 0.05$) higher in the ADR469 treated group compared to the control, there was no apparent accumulation of cells in the G_2/M phase.

As expected, control treated PC-3 cells demonstrated an accumulation of cells in the G_1 phase and the percentage of cells in the G_2/M phase was 29.54 ± 1.59 %. Treatment of

PC-3 cells with 1 and 5 μM ADR469 induced cell cycle arrest at the G_2/M phase with percentage counts of 79.02 ± 0.72 % and 79.12 ± 0.56 % respectively, which were significantly ($p < 0.001$) higher compared to the control group (Figure 4.32 B).

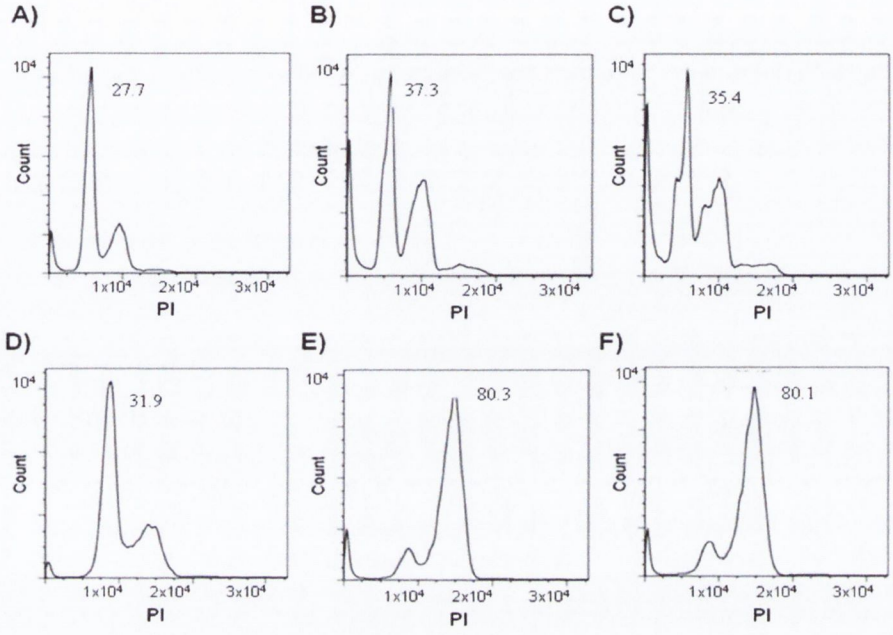

Figure 4.31: Cell cycle histograms of the gated G_2/M cells treated with ADR469. HUVECs (H) or PC-3 cells (P) were treated for 24h, stained with PI and analysed using flow cytometry **A)** Control (0.1% DMSO) (H), **B)** 1 μM ADR469 (H), **C)** 5 μM ADR469 (H), **D)** Control (0.1% DMSO) (P), **E)** 1 μM ADR469 (P) and **F)** 5 μM ADR469 (P).

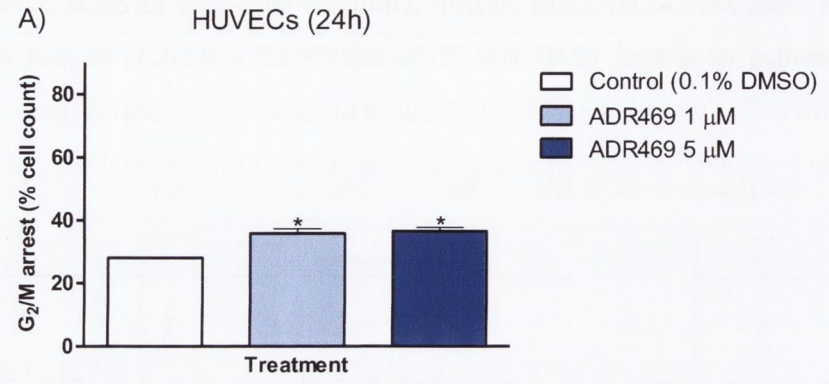

* $p < 0.05$, significantly higher mean % cell count in the G_2/M phase compared with the untreated controls as determined by Student's *t*-test.

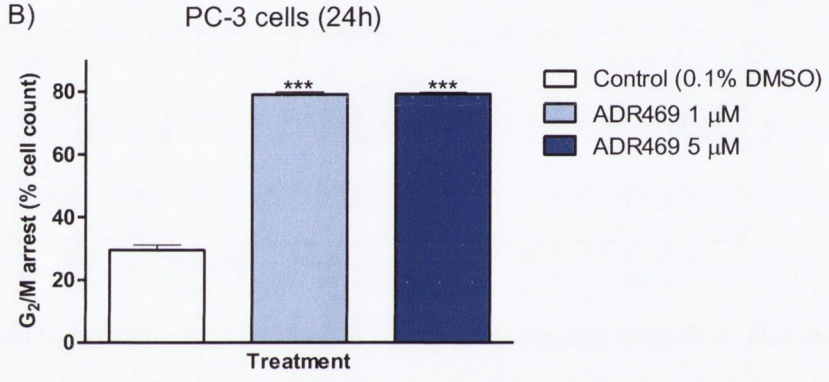

*** $p < 0.001$, significantly higher mean % cell count in the G_2/M phase compared with the untreated controls as determined by Student's *t*-test.

Figure 4.32: Percentage of cells in the G_2/M phase **A)** HUVECs and **B)** PC-3 cells incubated with ADR469. Data represents mean ± SEM (n=3).

4.3.8.4 Designed Multiple Ligand

The cell cycle stage of HUVECs and PC-3 cells was analysed after treatment with BWM120 as shown in Figure 4.33. An insignificant increase in the percentage of HUVECs present in the G_2/M phase was observed after treatment with 1 μM of BWM120 (33.38 ± 1.38 %) compared to that of the control group (25.71 ± 1.66 %), as shown in Figure 4.34 A. A higher concentration (5 μM) of BWM120 did not result in a G_2/M phase arrest; instead cells appeared to undergone cell death as indicated by the accumulation of cells in the sub-G_0/G_1 phase. BWM120-treated PC-3 cells demonstrated an evident amplification in the percentage of G_2/M phase cells at 1 μM

(83.01 ± 3.00 %) compared to the control treated cells (25.51 ± 2.79 %), and the difference was significant ($p < 0.01$), as shown in Figure 4.34 B.

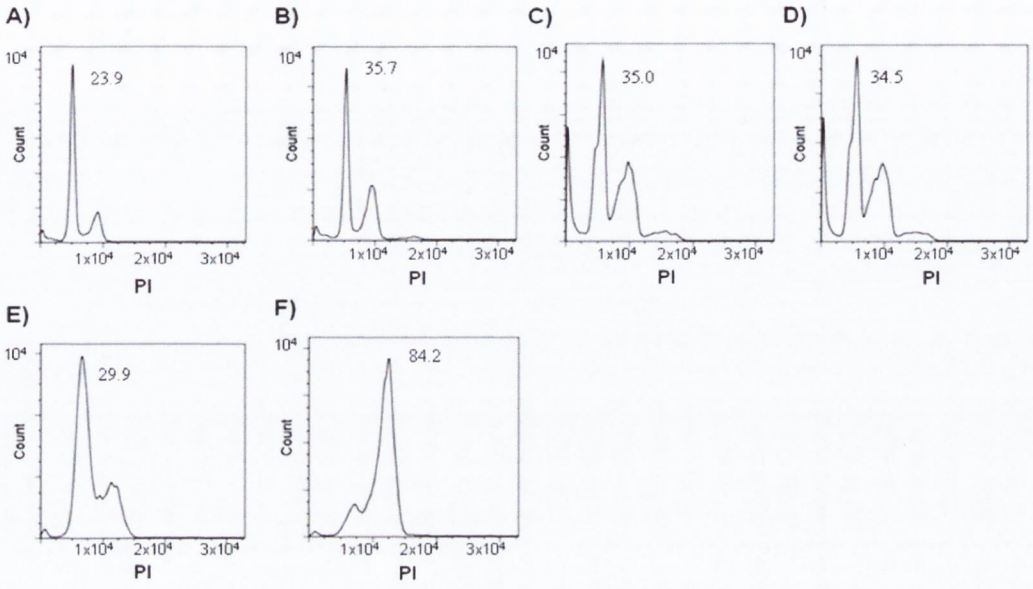

Figure 4.33: Cell cycle histograms of the gated G_2/M cells treated with BWM120. HUVECs (H) or PC-3 cells (P) were treated for 24h, stained with PI and analysed using flow cytometry **A)** Control (0.1% DMSO) (H), **B)** 1 μM BWM120 (H), **C)** 5 μM BWM120 (H), **D)** 10 μM BWM120 (H), **E)** Control (0.1% DMSO) (P) and **F)** 1 μM BWM120 (P).

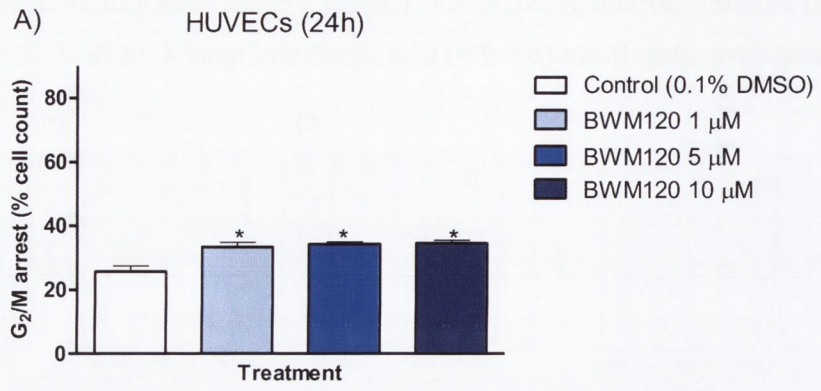

* $p < 0.05$, significantly higher mean % cell count in the G_2/M phase compared with the untreated controls as determined by Student's *t*-test.

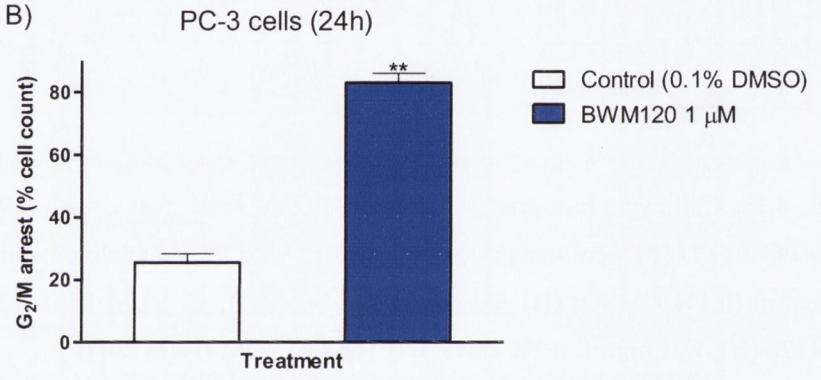

** $p < 0.01$, significantly higher mean % cell count in the G_2/M phase compared with the untreated controls as determined by Student's *t*-test.

Figure 4.34: Percentage of cells in the G_2/M phase **A)** HUVECs and **B)** PC-3 cells incubated with BWM120. Data represents mean ± SEM (n=3).

4.3.9 Cell Cycle Analysis – Sub-G_0/G_1 Phase

It was hypothesised that hybrids and DML could possibly induce higher levels of cell death compared to either their associated tubulin inhibitor or bestatin alone, due to the fact that both components of the dual targeting compounds were previously shown to induce apoptosis [242, 564]. It was essential to examine not only the effect of the hybrid but also the effect of the hybrid's corresponding tubulin inhibitor and bestatin alone and in 1:1 combination.

Hence, cell cycle analysis was performed on treated HUVECs (24h) and PC-3 cells (72h) as previously described. The proportion of sub-G_0/G_1 stained cells correlates to the level of apoptotic DNA fragmentation and thus represents an indication of cell

death. The results were expressed in terms of percentage of cells detected in the sub-G_0/G_1 phase ± SEM.

CA-4 served as a positive control at 10, 50 and 100 μM using both HUVECs and PC-3 cells (Figure 4.35). The percentages of sub-G_0/G_1 HUVECs at 10, 50 and 100 μM CA-4 were 36.62 ± 8.07 % ($p < 0.05$), 37.18 ± 6.05 % ($p < 0.05$) and 34.80 ± 2.55 % ($p < 0.01$) respectively, which were significantly higher than the control treated cells (Figure 4.36 A). Following treatment of PC-3 cells with 10, 50 and 100 μM CA-4, the percentages of sub-G_0/G_1 cells were determined to be 27.80 ± 5.18 % ($p < 0.05$), 27.35 ± 7.10 % ($p < 0.05$) and 36.80 ± 6.32 % ($p < 0.01$) respectively, which were significantly higher than the control treated cells (Figure 4.36 B).

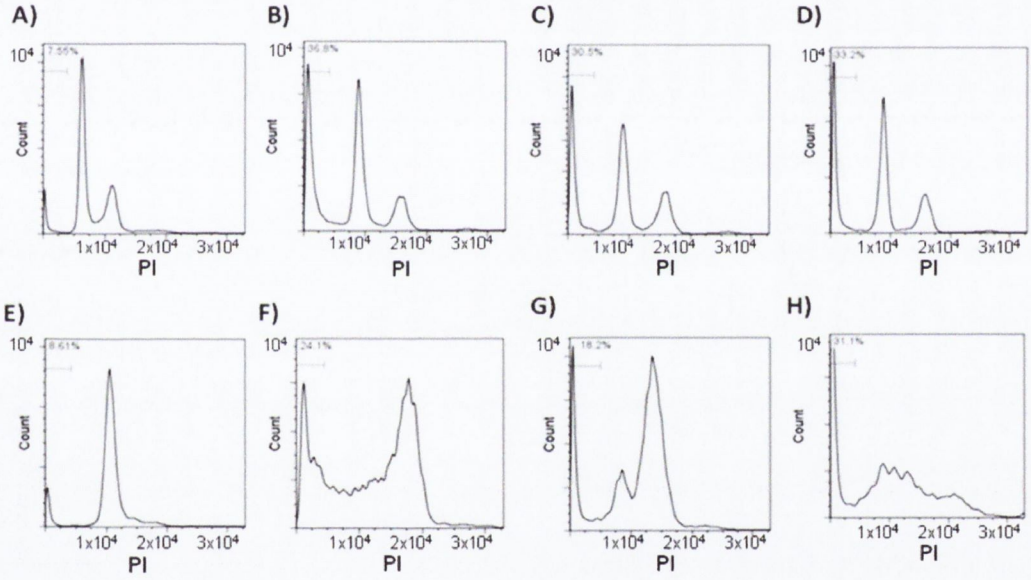

Figure 4.35: Cell cycle histograms of the gated sub-G_0/G_1 cells treated with CA-4. HUVECs (H) were treated for 24h and PC-3 cells (P) for 72h, stained with PI and analysed using flow cytometry. **A)** Control (0.1% DMSO) (H), **B)** 10 μM CA-4 (H), **C)** 50 μM CA-4 (H), **D)** 100 μM CA-4 (H), **E)** Control (0.1% DMSO) (P), **F)** 10 μM CA-4 (P), **G)** 50 μM CA-4 (P) and **H)** 100 μM CA-4 (P).

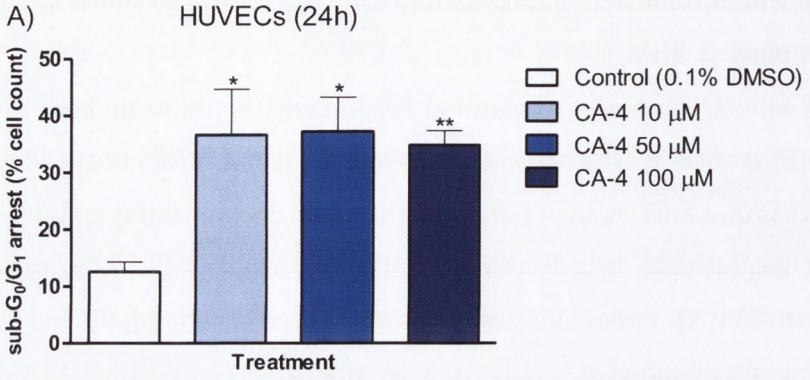

* $p < 0.05$, ** $p < 0.01$, significantly higher mean % cell count in the sub-G_0/G_1 phase compared with the untreated controls as determined by the Student's *t*-test.

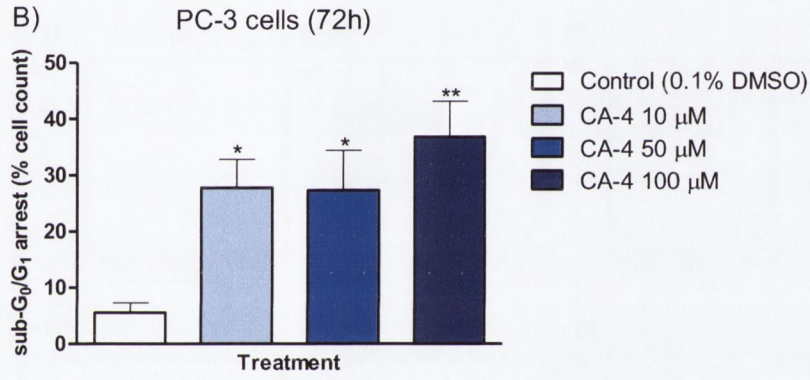

* $p < 0.05$, ** $p < 0.01$, significantly higher mean % cell count in the sub-G_0/G_1 phase compared with the untreated controls as determined by the Student's *t*-test.

Figure 4.36: Percentage of cells in the sub-G_0/G_1 phase **A)** HUVECs and **B)** PC-3 cells incubated with CA-4. Data represents mean ± SEM (n=3).

4.3.9.1 Group I Hybrid

In order to examine any additive or synergistic effect of group I hybrid, ECB378, the effects of ECB394 (Figure 4.37), bestatin (Figure 4.39), a 1:1 combination of ECB394/bestatin (Figure 4.41) and ECB378 (Figure 4.43) were assessed in the cell cycle analysis using both HUVECs and PC-3 cells.

The percentages of sub-G_0/G_1 HUVECs after treatment with 10, 50 and 100 μM of ECB394 were 12.60 ± 0.65 %, 21.95 ± 0.94 % and 26.01 ± 0.16 % (Figure 4.38 A); for bestatin 8.18 ± 1.80 %, 7.58 ± 1.36 % and 8.27 ± 1.32 % (Figure 4.40 A); for ECB394/bestatin combinations 10.13 ± 0.13 %, 31.16 ± 1.81 % and 28.40 ± 0.57 %

(Figure 4.42 A) and for ECB378 13.01 ± 2.93 %, 42.44 ± 4.01 % and 51.38 ± 4.82 % (Figure 4.44 A), respectively.

Furthermore, ECB394, bestatin, ECB394/bestatin combination and ECB378 were examined in the cell cycle analysis for any evidence of cell death using PC-3 cells. The percentages of sub-G_0/G_1 PC-3 cells following treatment with 10, 50 and 100 μM of ECB394 were 25.65 ± 5.30 %, 22.03 ± 4.66 % and 21.36 ± 0.86 % (Figure 4.38 B); for bestatin 8.13 ± 0.75 %, 7.70 ± 2.45 % and 7.28 ± 1.87 % (Figure 4.40 B); for ECB394/bestatin 23.37 ± 2.05 %, 25.96 ± 1.73 % and 23.76 ± 0.86 % (Figure 4.42 B) and for ECB378 26.33 ± 14.43 %, 60.62 ± 5.71 % and 69.00 ± 3.82 % (Figure 4.44 B), respectively. These results are summarised in Table 4.10.

Table 4.10: Percentage of cells in the sub-G_0/G_1 ± SEM (n=3), for group I hybrid.

Treatment	HUVECs (%)			PC-3 cells (%)		
	10 μM	50 μM	100 μM	10 μM	50 μM	100 μM
CA-4	36.62 ± 8.07	37.18 ± 6.05	34.80 ± 2.55	22.33 ± 1.54	12.33 ± 2.84	24.95 ± 5.00
ECB394	12.60 ± 0.65	21.95 ± 0.94	26.01 ± 0.16	25.65 ± 5.30	22.03 ± 4.66	21.36 ± 0.86
Bestatin	8.18 ± 1.80	7.58 ± 1.36	8.27 ± 1.32	8.13 ± 0.75	7.70 ± 2.45	7.28 ± 1.87
E394/Bes	10.13 ± 0.13	31.16 ± 1.81	28.40 ± 0.57	23.37 ± 2.05	25.96 ± 1.73	23.76 ± 0.86
ECB378	13.01 ± 2.93	42.44 ± 4.01	51.38 ± 4.82	26.33 ± 14.43	60.62 ± 5.71	69.00 ± 3.82

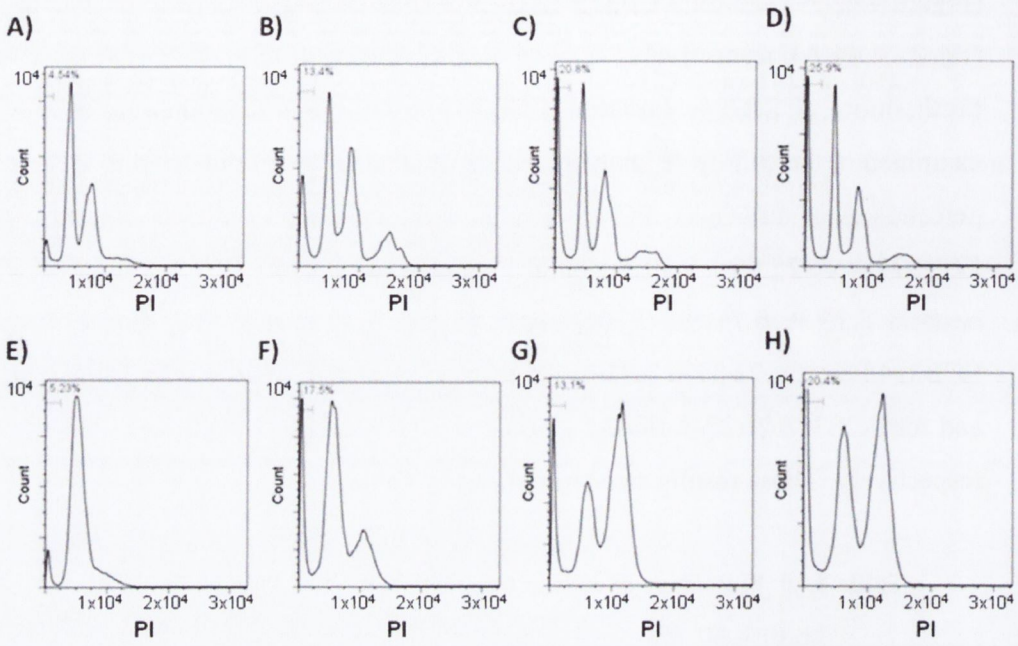

Figure 4.37: Cell cycle histograms of the gated sub-G_0/G_1 cells treated with ECB394. HUVECs (H) were treated for 24h and PC-3 cells (P) for 72h, stained with PI and analysed using flow cytometry. **A)** Control (0.1% DMSO) (H), **B)** 10 μM ECB394 (H), **C)** 50 μM ECB394 (H), **D)** 100 μM ECB394 (H), **E)** Control (0.1% DMSO) (P), **F)** 10 μM ECB394 (P), **G)** 50 μM ECB394 (P) and **H)** 100 μM ECB394 (P).

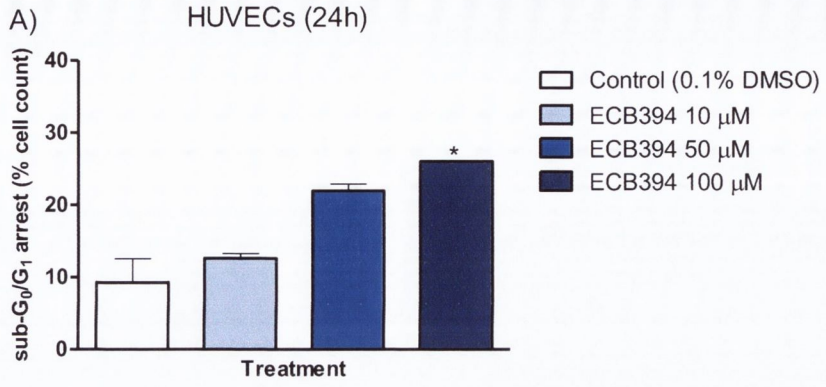

* $p < 0.05$, significantly higher mean % cell count in the sub-G_0/G_1 phase compared with the untreated controls as determined by Student's *t*-test.

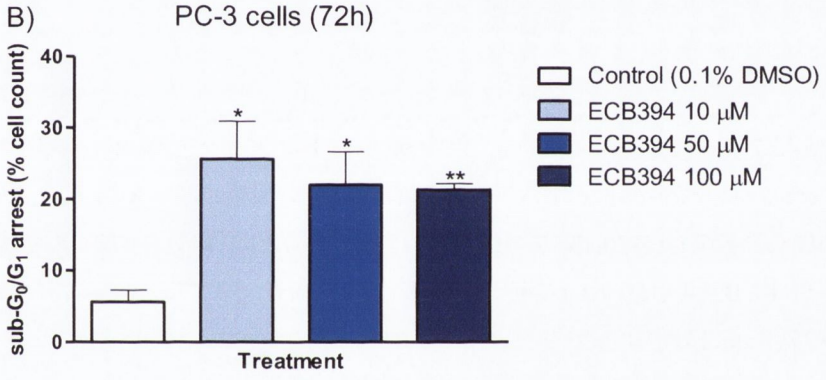

* $p < 0.05$, ** $p < 0.01$, significantly higher mean % cell count in the sub-G_0/G_1 phase compared with the untreated controls as determined by Student's *t*-test.

Figure 4.38: Percentage of cells in the sub-G_0/G_1 phase **A)** HUVECs and **B)** PC-3 cells incubated with ECB394. Data represents mean ± SEM (n=3).

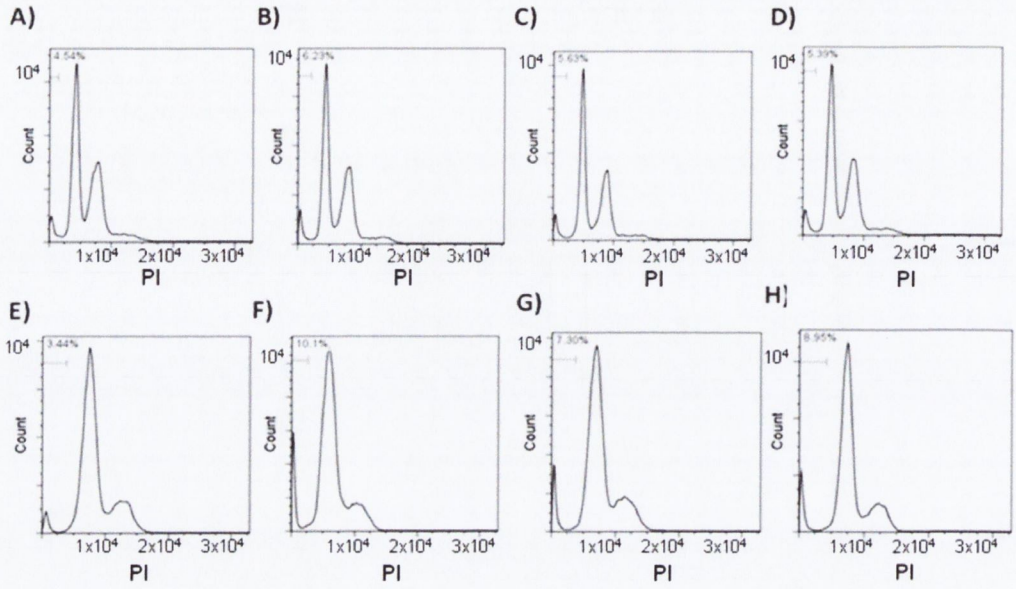

Figure 4.39: Cell cycle histograms of the gated sub-G_0/G_1 cells treated with bestatin. HUVECs (H) were treated for 24h and PC-3 cells (P) for 72h, stained with PI and analysed using flow cytometry. **A)** Control (0.1% DMSO) (H), **B)** 10 μM bestatin (H), **C)** 50 μM bestatin (H), **D)** 100 μM bestatin (H), **E)** Control (0.1% DMSO) (P), **F)** 10 μM bestatin (P), **G)** 50 μM bestatin (P) and **H)** 100 μM bestatin (P).

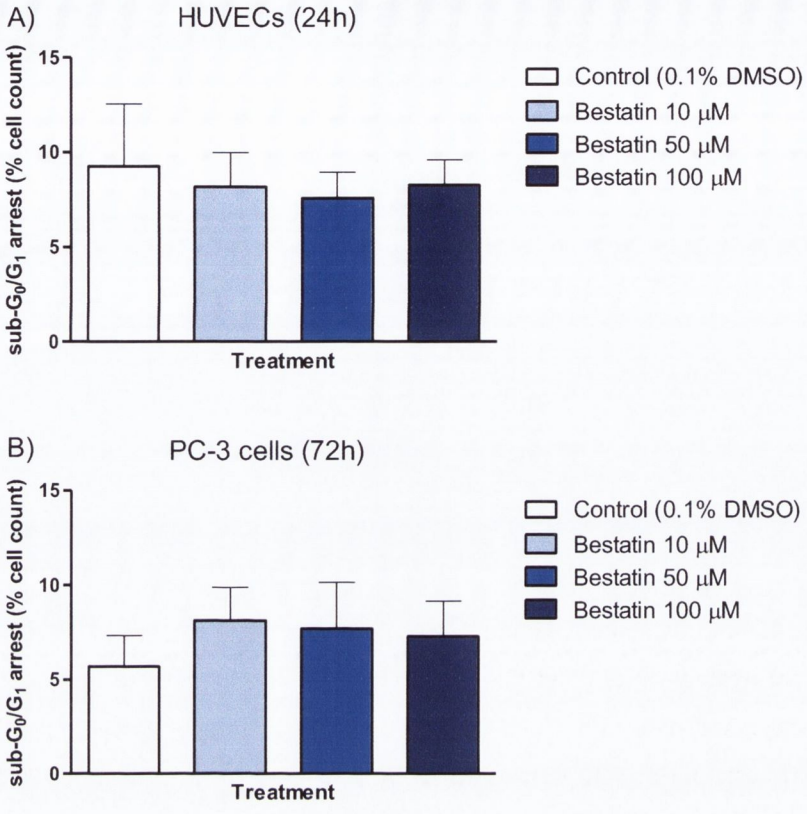

Figure 4.40: Percentage of cells in the sub-G_0/G_1 phase **A)** HUVECs and **B)** PC-3 cells incubated with bestatin. Data represents mean ± SEM (n=3).

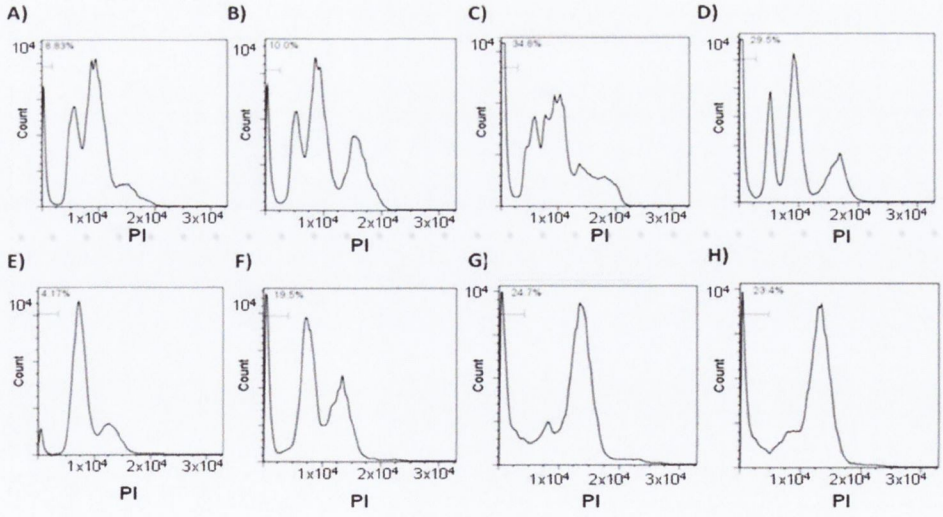

Figure 4.41: Cell cycle histograms of the gated sub-G_0/G_1 cells treated with ECB394 and bestatin. HUVECs (H) were treated for 24h and PC-3 cells (P) for 72h, stained with PI and analysed using flow cytometry. **A)** Control (0.1% DMSO) (H), **B)** 10 μM E394 + 10 μM bes (H), **C)** 50 μM E394 + 50 μM bes (H), **D)** 100 μM E394 + 100 μM bes (H), **E)** Control (0.1%

DMSO) (P), **F)** 10 μM E394 + 10 μM bes (P), **G)** 50 μM E394 + 50 μM best (P) and **H)** 100 μM E394 + 100 μM bes (P).

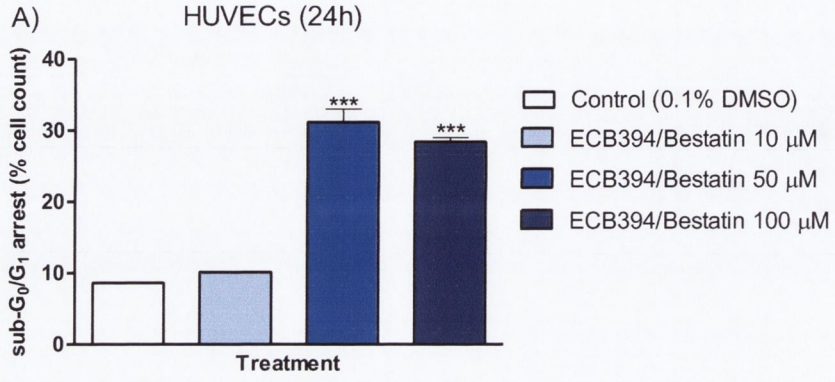

*** $p < 0.001$, significantly higher mean % cell count in the sub-G_0/G_1 phase compared with the untreated controls as determined by Student's *t*-test.

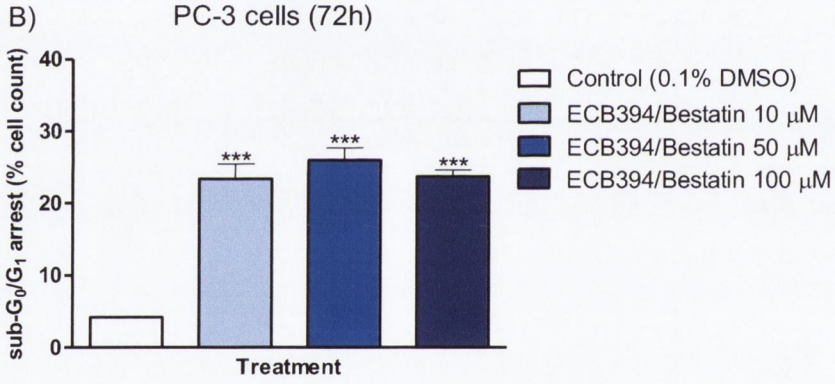

*** $p < 0.001$, significantly higher mean % cell count in the sub-G_0/G_1 phase compared with the untreated controls as determined by Student's *t*-test.

Figure 4.42: Percentage of cells in the sub-G_0/G_1 phase **A)** HUVECs and **B)** PC-3 cells incubated with 1:1 ECB394/bestatin combinations. Data represents mean ± SEM (n=3).

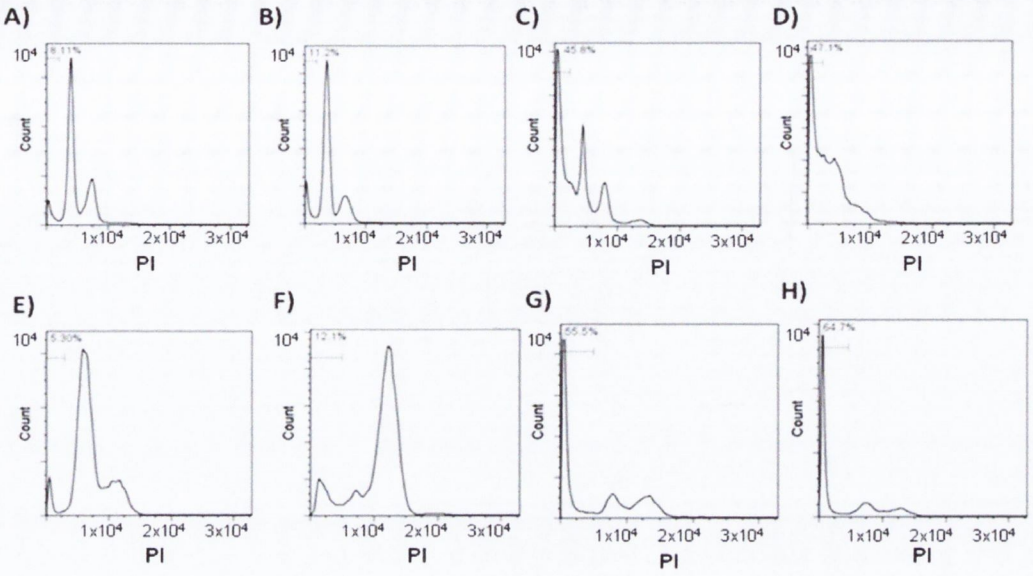

Figure 4.43: Cell cycle histograms of the gated sub-G_0/G_1 cells treated with ECB378. HUVECs (H) were treated for 24h and PC-3 cells (P) for 72h, stained with PI and analysed using flow cytometry. **A)** Control (0.1% DMSO) (H), **B)** 10 μM ECB378 (H), **C)** 50 μM ECB378 (H), **D)** 100 μM ECB378 (H), **E)** Control (0.1% DMSO) (P), **F)** 10 μM ECB378 (P), **G)** 50 μM ECB378 (P) and **H)** 100 μM ECB378 (P).

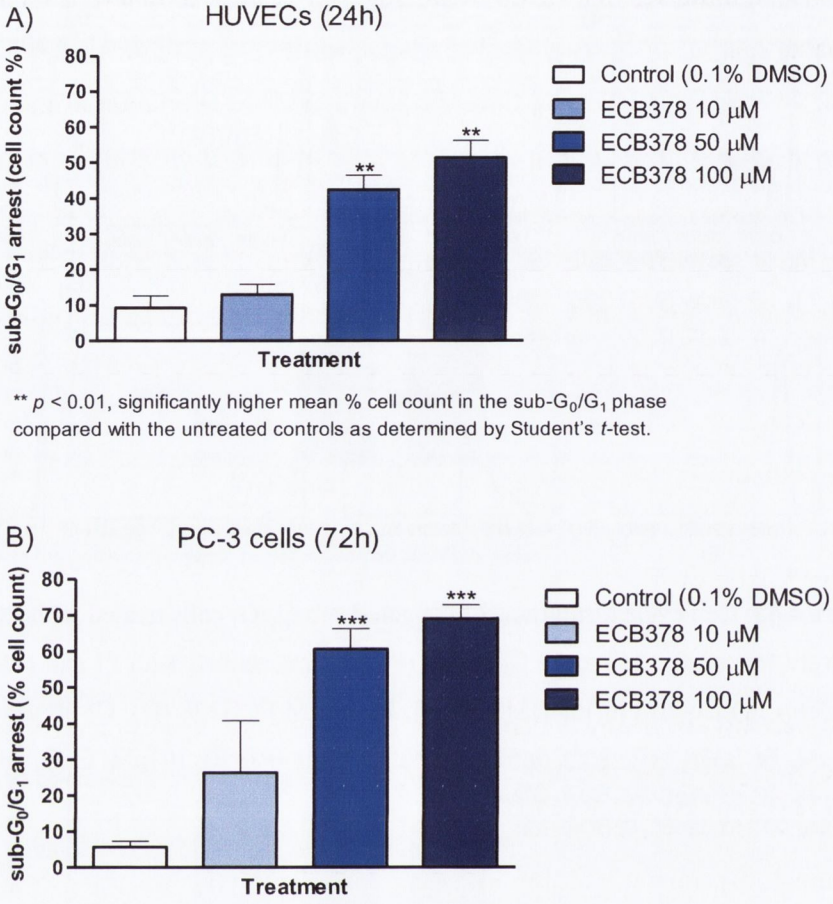

Figure 4.44: Percentage of cells in the sub-G_0/G_1 phase **A)** HUVECs and **B)** PC-3 cells incubated with ECB378. Data represents mean ± SEM (n=3).

ECB394 treatment at 100 μM resulted in a significantly ($p < 0.05$) higher percentage of sub-G_0/G_1 HUVECs compared to the control cells, whereas bestatin did not demonstrate any observable increase in the sub-G_0/G_1 cells even at 100 μM. Combination treatment of HUVECs with 50 and 100 μM ECB394/bestatin revealed a significant ($p < 0.001$) accumulation of cells at the sub-G_0/G_1 phase. Similarly, treatment with 50 and 100 μM ECB378 significantly ($p < 0.01$) induced a sub-G_0/G_1 arrest. Statistical comparison of ECB378 with ECB394 at each concentration showed significant ($p < 0.05$) differences at 50 and 100 μM, indicating that ECB378 caused higher percentage of cell death than ECB394. In addition, significant ($p < 0.01$) difference was detected between ECB378 and ECB394/bestatin combination at 100

μM, which indicates that ECB378 has superior activity to that of a 1:1 ECB394/bestatin combination.

ECB394-treated PC-3 cells showed a significant accumulation at the sub-G_0/G_1 phase at 10 μM ($p < 0.05$), 50 μM ($p < 0.05$) and 100 μM ($p < 0.01$) compared to the control cells, whereas bestatin treatment failed to elicit any significant difference in the percentage of sub-G_0/G_1 cells. Treatment with 1:1 ECB394/bestatin combinations resulted in a significantly ($p < 0.001$) higher amount of sub-G_0/G_1 PC-3 cells at each concentration compared to the control group, while ECB378 also demonstrated significance at 50 and 100 μM. ECB378, ECB394 and ECB394/bestatin combinations were statistically analysed for any difference in activity and it was found that ECB378 induced a significantly ($p < 0.01$) higher proportion of cell death than ECB394 alone or in combination with bestatin at 50 and 100 μM.

4.3.9.2 Group III Hybrid

Group III hybrid ECB397 was evaluated in the cell cycle analysis assay in order to assess its effect on HUVECs and PC-3 cells. It was necessary to examine RS180 (Figure 4.45), a 1:1 combination of RS180/bestatin (Figure 4.47) and ECB397 hybrid (Figure 4.49), for their ability to induce HUVEC or PC-3 cell death at 10, 50 and 100 μM.

The percentages of HUVECs detected in the sub-G_0/G_1 phase, treated with 10, 50 and 100 μM RS180 were 25.71 ± 1.04 %, 31.55 ± 1.20 % and 26.72 ± 0.97 % (Figure 4.46 A); for RS180/bestatin combination they were 25.10 ± 0.32 %, 33.72 ± 6.51 % and 28.43 ± 1.41 % (Figure 4.48 A), and for ECB397 they were 29.80 ± 3.32 %, 39.91 ± 2.24 % and 39.10 ± 3.49 % (Figure 4.50 A), respectively.

Additionally, the percentages of sub-G_0/G_1 PC-3 cells treated with 10, 50 and 100 μM RS180 were 12.97 ± 2.03 %, 27.90 ± 3.71 % and 21.93 ± 2.60 % (Figure 4.46 B); for RS180/bestatin combination they were 25.82 ± 1.91 %, 39.10 ± 6.70 % and 13.35 ± 4.80 % (Figure 4.48 B), and for ECB397 they were 10.82 ± 4.22 %, 6.41 ± 3.24 % and 5.20 ± 1.53 % (Figure 4.50 B), respectively. These results are summarised in Table 4.11.

Table 4.11: Percentage of cells in the sub-G_0/G_1 ± SEM (n=3), for group III hybrid.

Treatment	HUVECs (%)			PC-3 cells (%)		
	10 μM	50 μM	100 μM	10 μM	50 μM	100 μM
CA-4	36.62 ± 8.07	37.18 ± 6.05	34.80 ± 2.55	22.33 ± 1.54	12.33 ± 2.84	24.95 ± 5.00
RS180	25.71 ± 1.04	31.55 ± 1.20	26.72 ± 0.97	12.97 ± 2.03	27.90 ± 3.71	21.93 ± 2.60
Bestatin	8.18 ± 1.80	7.58 ± 1.36	8.27 ± 1.32	8.13 ± 0.75	7.70 ± 2.45	7.28 ± 1.87
R180/Bes	25.10 ± 0.32	33.72 ± 6.51	28.43 ± 1.41	25.82 ± 1.91	39.10 ± 6.70	13.35 ± 4.80
ECB397	29.80 ± 3.32	39.91 ± 2.24	39.10 ± 3.49	10.82 ± 4.22	6.41 ± 3.24	5.20 ± 1.53

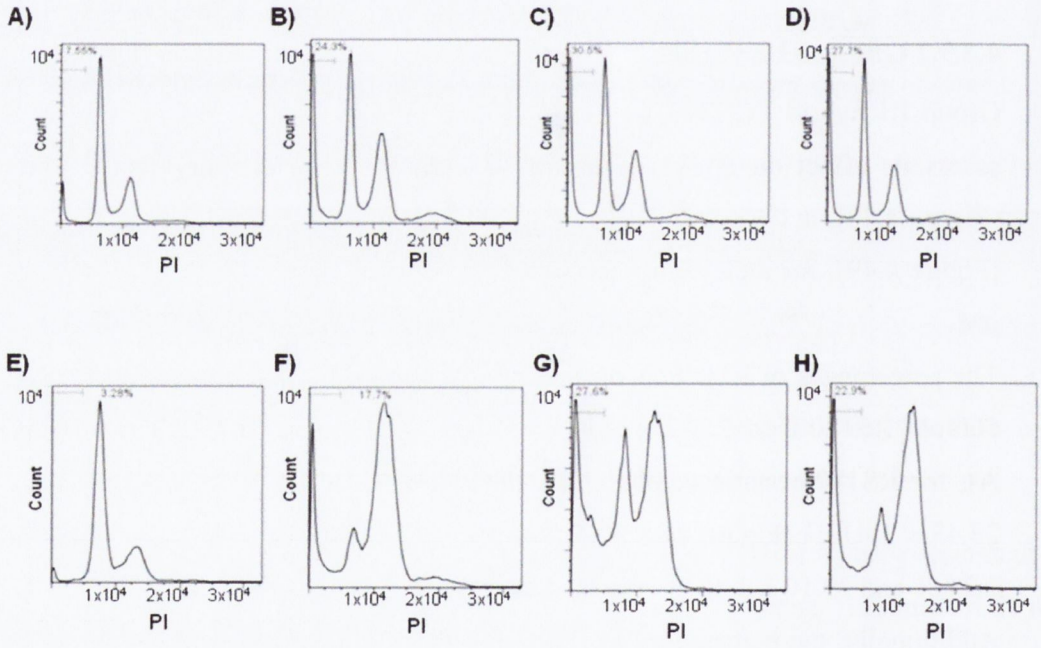

Figure 4.45: Cell cycle histograms of the gated sub-G_0/G_1 cells treated with RS180. HUVECs (H) were treated for 24h and PC-3 cells (P) for 72h, stained with PI and analysed using flow cytometry. **A)** Control (0.1% DMSO) (H), **B)** 10 μM RS180 (H), **C)** 50 μM RS180 (H), **D)** 100 μM RS180 (H), **E)** Control (0.1% DMSO) (P), **F)** 10 μM RS180 (P), **G)** 50 μM RS180 (P) and **H)** 100 μM RS180 (P).

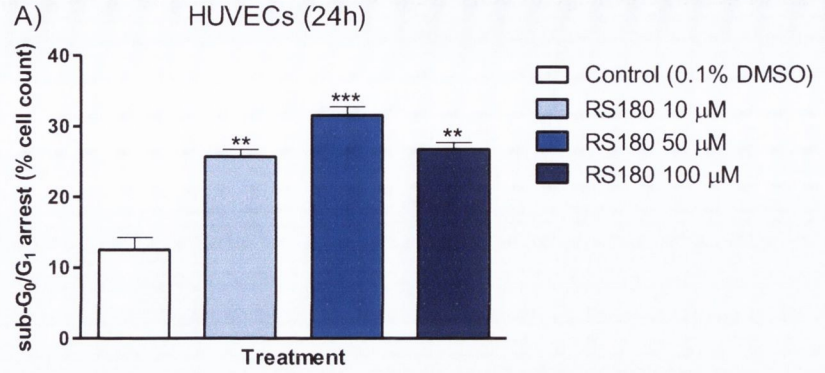

** $p < 0.01$, *** $p < 0.001$, significantly higher mean % cell count in the sub-G_0/G_1 phase compared with the untreated controls as determined by Student's *t*-test.

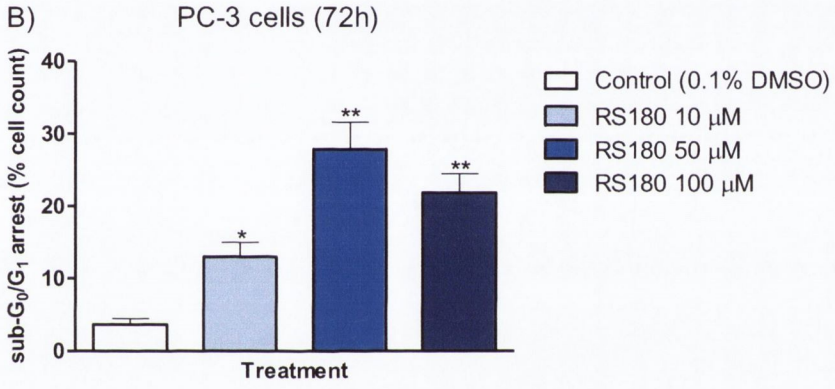

* $p < 0.05$, ** $p < 0.01$, significantly higher mean % cell count in the sub-G_0/G_1 phase compared with the untreated controls as determined by Student's *t*-test.

Figure 4.46: Percentage of cells in the sub-G_0/G_1 phase **A)** HUVECs and **B)** PC-3 cells incubated with RS180. Data represents mean ± SEM (n=3).

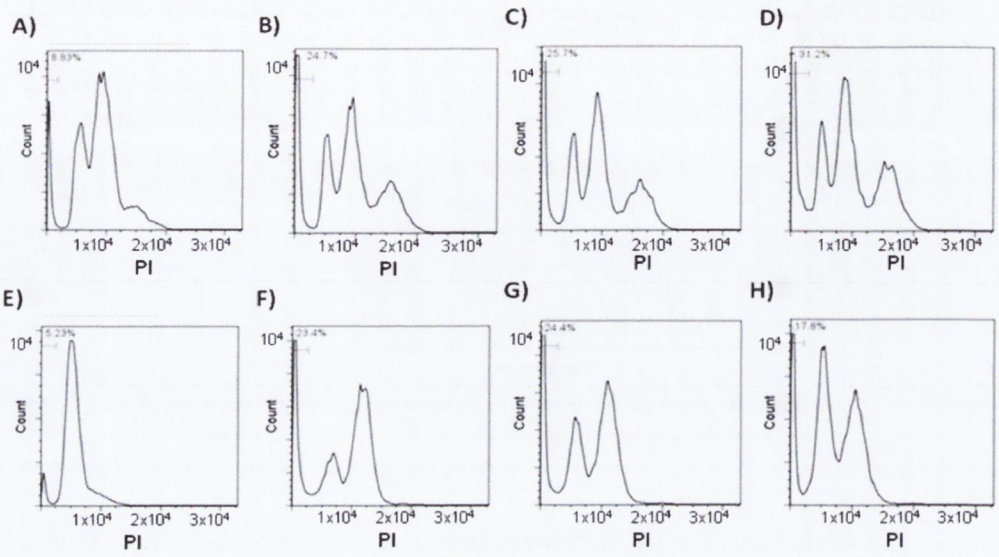

Figure 4.47: Cell cycle histograms of the gated sub-G_0/G_1 cells treated with RS180 and bestatin. HUVECs (H) were treated for 24h and PC-3 cells (P) for 72h, stained with PI and analysed using flow cytometry. **A)** Control (0.1% DMSO) (H), **B)** 10 μM RS180 + 10 μM best (H), **C)** 50 μM RS180 + 50 μM bes (H), **D)** 100 μM RS180 + 100 μM bes (H), **E)** Control (0.1% DMSO) (P), **F)** 10 μM RS180 + 10 μM bes (P), **G)** 50 μM RS180 + 50 μM bes (P) and **H)** 100 μM RS180 + 100 μM bes (P).

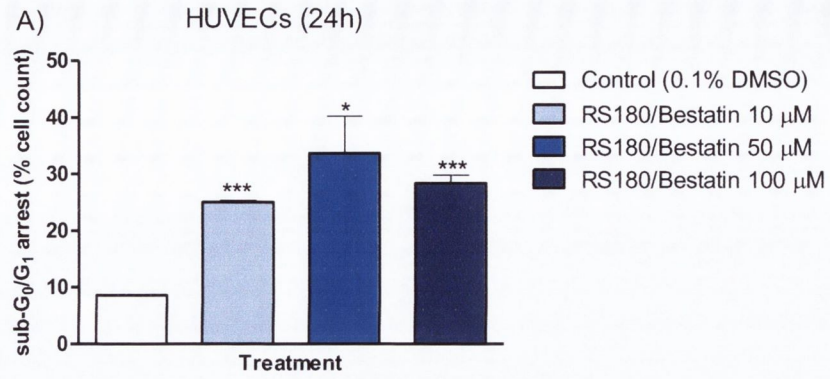

* $p < 0.05$, *** $p < 0.001$, significantly higher mean % cell count in the sub-G_0/G_1 phase compared with the untreated controls as determined by Student's *t*-test.

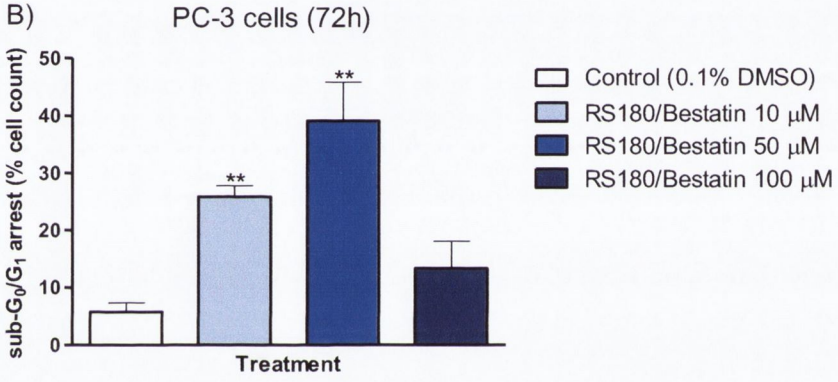

** $p < 0.01$, significantly higher mean % cell count in the sub-G_0/G_1 phase compared with the untreated controls as determined by Student's *t*-test.

Figure 4.48: Percentage of cells in the sub-G_0/G_1 phase **A)** HUVECs and **B)** PC-3 cells incubated with 1:1 RS180/bestatin combinations. Data represents mean ± SEM (n=3).

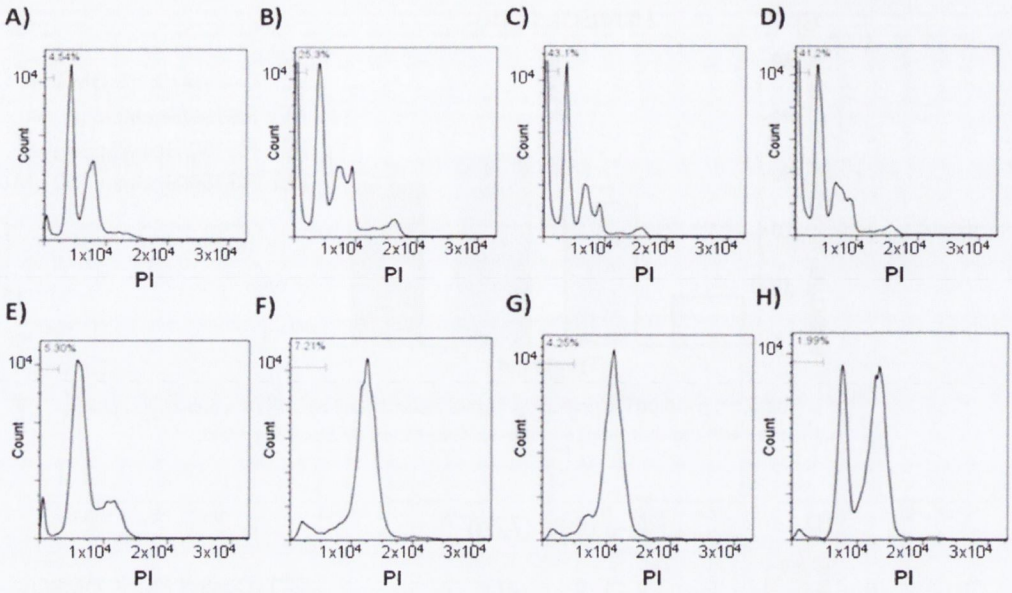

Figure 4.49: Cell cycle histograms of the gated sub-G_0/G_1 cells treated with ECB397. HUVECs (H) were treated for 24h and PC-3 cells (P) for 72h, stained with PI and analysed using flow cytometry. **A)** Control (0.1% DMSO) (H), **B)** 10 μM ECB397 (H), **C)** 50 μM ECB397 (H), **D)** 100 μM ECB397 (H), **E)** Control (0.1% DMSO) (P), **F)** 10 μM ECB397 (P), **G)** 50 μM ECB397 (P) and **H)** 100 μM ECB397 (P).

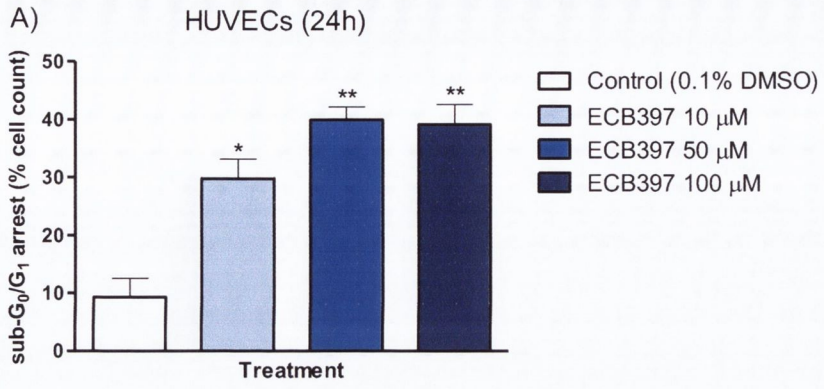

* $p < 0.05$, ** $p < 0.01$, significantly higher mean % cell count in the sub-G_0/G_1 phase compared with the untreated controls as determined by Student's *t*-test.

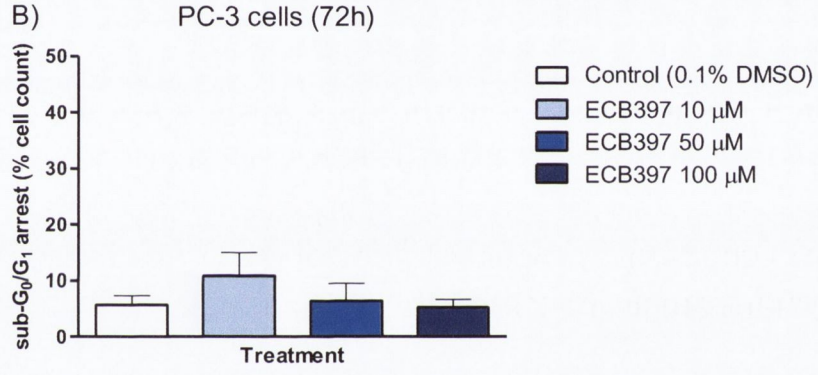

Figure 4.50: Percentage of cells in the sub-G_0/G_1 phase **A)** HUVECs and **B)** PC-3 cells incubated with ECB397. Data represents mean ± SEM (n=3).

Incubation of HUVECs for 24h with 10, 50 and 100 μM RS180, 1:1 RS180/bestatin combinations and ECB397 resulted in significantly higher proportion of sub-G_0/G_1 cells compared to the control group at all concentrations. Statistical comparisons of ECB397 with either RS180 or a 1:1 RS180/bestatin combination revealed significant ($p < 0.05$) difference at 100 μM, indicating that ECB397 induced a higher level of HUVECs in the sub-G_0/G_1 phase.

The data obtained from PC-3 cells treated with 10, 50 and 100 μM RS180 showed a significantly increased sub-G_0/G_1 cell population compared to the control group, whereas RS180/bestatin combination attained significance ($p < 0.01$) at 10 and 50 μM. ECB397 treatment failed to demonstrate an accumulation of PC-3 cells in the sub-G_0/G_1 phase, whereas statistical comparison indicated that RS180 alone or in

combination with bestatin induced a significantly larger population of PC-3 cells in the sub-G_0/G_1 phase.

4.3.9.3 Designed Multiple Ligand

The ability of BWM120 to induce cell death of HUVECs or PC-3 cells was determined (Figure 4.51). HUVECs were incubated with 10, 50 and 100 μM BWM120 and analysed for their DNA-content. The percentages of sub-G_0/G_1 HUVECs treated with 10, 50 and 100 μM BWM120 were 12.27 ± 6.87 %, 20.30 ± 6.53 % and 39.39 ± 11.81 %, respectively (Figure 4.52 A).

In addition, the effect of BWM120 on PC-3 cell death was examined following a 72h incubation period. The percentages of sub-G_0/G_1 PC-3 cells treated with 10, 50 and 100 μM BWM120 were as follows: 12.02 ± 1.44 %, 34.61 ± 9.60 % and 81.83 ± 2.11 %, respectively (Figure 4.52 B). These results are summarised in Table 4.12.

Table 4.12: Percentage of cells in the sub-G_0/G_1 ± SEM (n=3), for BWM120.

Treatment	HUVECs (%)			PC-3 cells (%)		
	10 μM	50 μM	100 μM	10 μM	50 μM	100 μM
CA-4	36.62 ± 8.07	37.18 ± 6.05	34.80 ± 2.55	22.33 ± 1.54	12.33 ± 2.84	24.95 ± 5.00
RS180	25.71 ± 1.04	31.55 ± 1.20	26.72 ± 0.97	12.97 ± 2.03	27.90 ± 3.71	21.93 ± 2.60
BWM120	12.27 ± 6.87	20.30 ± 6.53	39.39 ± 11.81	12.02 ± 1.44	34.61 ± 9.60	81.83 ± 2.11

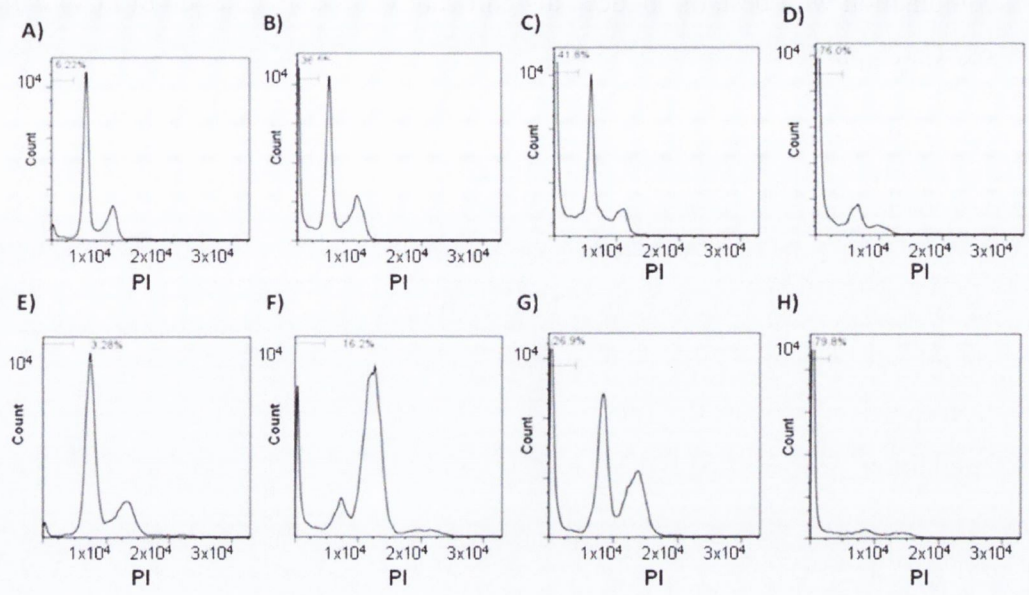

Figure 4.51: Cell cycle histograms of the gated sub-G_0/G_1 cells treated with BWM120. HUVECs (H) were treated for 24h and PC-3 cells (P) for 72h, stained with PI and analysed using flow cytometry. **A)** Control (0.1% DMSO) (H), **B)** 10 μM BWM120 (H), **C)** 50 μM BWM120 (H), **D)** 100 μM BWM120 (H), **E)** Control (0.1% DMSO) (P), **F)** 10 μM BWM120 (P), **G)** 50 μM BWM120 (P) and **H)** 100 μM BWM120 (P).

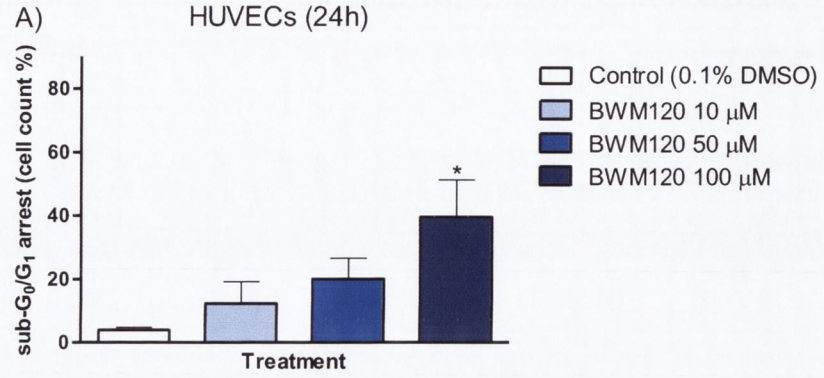

* $p < 0.05$, significantly higher mean % cell count in the sub-G_0/G_1 phase compared with the untreated controls as determined by Student's *t*-test.

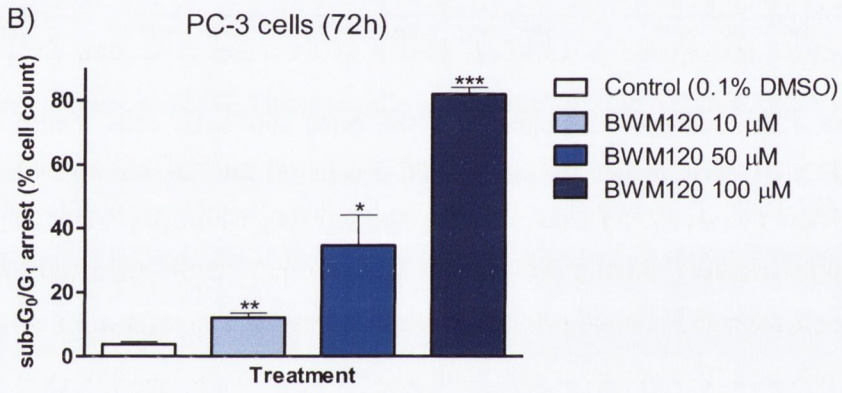

* $p < 0.05$, ** $p < 0.01$, *** $p < 0.001$, significantly higher mean % cell count in the sub-G_0/G_1 phase compared with the untreated controls as determined by Student's *t*-test.

Figure 4.52: Percentage of cells in the sub-G_0/G_1 phase **A)** HUVECs and **B)** PC-3 cells incubated with BWM120. Data represents mean ± SEM (n=3).

Statistical analysis was performed and found a significant ($p < 0.05$) difference in the percentage cell count of sub-G_0/G_1 cells between the 100 μM BWM120-treated cells and the control group. Due to the structural relationship of BWM120 to RS180, statistical comparison was carried out between the two at the corresponding concentrations but no significant different in the percentage of apoptotic cells was detected.

A significant difference between the BWM120 group and the control group was detected at all three concentrations. Statistical comparison of BWM120 and RS180 group at each concentration revealed a significantly ($p < 0.001$) higher percentage of PC-3 cell death at 100 μM BWM120.

4.3.10 Analysis of Endothelial Cells' Morphology

As previously discussed in Chapter 2, the ability of test compounds to alter the morphology of endothelial cells is an indication of an anti-vascular effect. Control treated HUVECs retained a confluent monolayer and appeared to be well-structured with no observable abnormalities. Hybrids and DML clearly induced rapid changes in the morphology of cells, 1h after drug washout, including shrinkage, darkness and round-up of the cells as well as reduced cell area. However, in most cases, cells treated with test compounds were shown to regain their shape and structure after 3h of drug washout.

4.3.10.1 Group I Hybrid

The effect of ECB378 on the endothelial cell morphology was investigated at 1, 5 and 10 μM, where there was no observable difference between the treated and the control cells (Figure 4.53). Therefore, higher concentrations of ECB378 were used at 20 and 40 μM (Figure 4.54). Endothelial cells treated with 20 μM ECB378 did not show any signs of morphological disruption, however at 40 μM cells appeared morphologically different from the control group but the changes were not severe, neither the cell area was reduced. Following a 3h incubation period, cells treated at 40 μM ECB378 regained their appearance and were similar to the control treated cells.

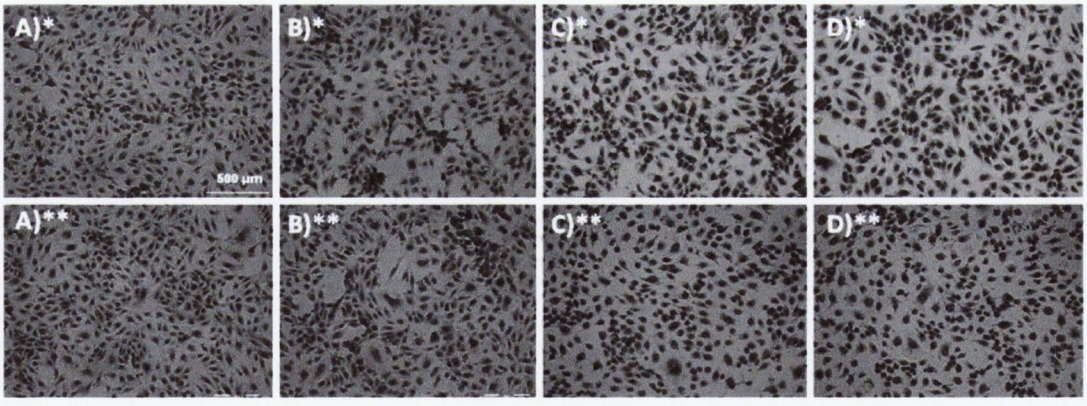

Figure 4.53: The effect of ECB378 on endothelial cells' morphology. HUVECs were exposed to the compounds for 40 minutes and photomicrographs (x10) were taken 1h (*) and 3h (**) after drug washout. **A)** Control (0.1% DMSO) **B)** 1 μM ECB378, **C)** 5 μM ECB378 and **D)** 10 μM ECB378.

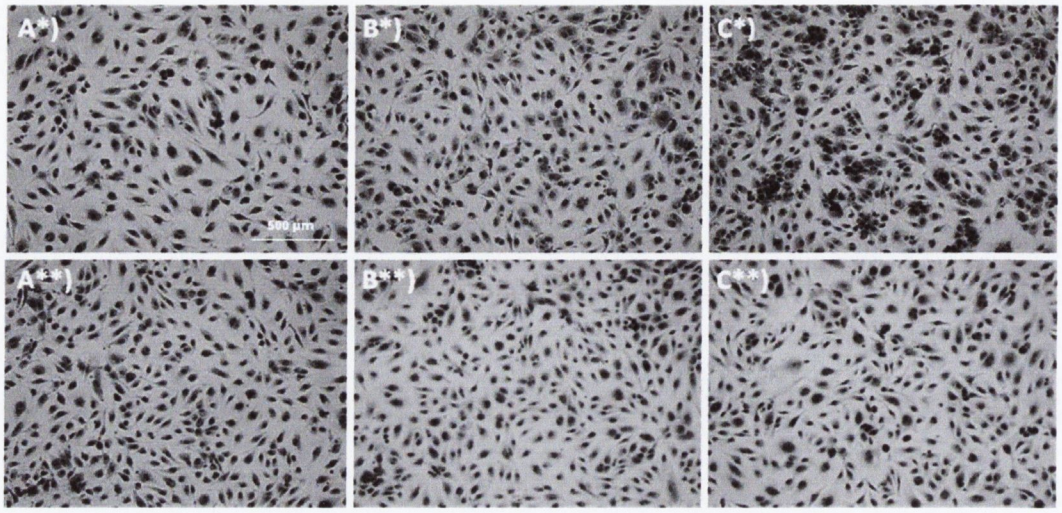

Figure 4.54: The effect of ECB378 on endothelial cells' morphology. HUVECs were exposed to the compounds for 40 minutes and photomicrographs (x10) were taken 1h (*) and 3h (**) after drug washout. **A)** Control (0.1% DMSO), **B)** 20 µM ECB378 and **C)** 40 µM ECB378.

4.3.10.2 Group III Hybrid

ECB397 was assessed for its ability to disrupt endothelial cell morphology. HUVECs were treated with 0.1 and 1 μM ECB397 and examined microscopically (Figure 4.55). Minor changes to endothelial cell morphology were noted when 0.1 μM ECB397 was used with a more significant effect at 1 μM ECB397, where the cell monolayer was disturbed and the morphology of the endothelial was altered. Despite the drastic morphological changes, endothelial cells regained normality after 3h of drug washout.

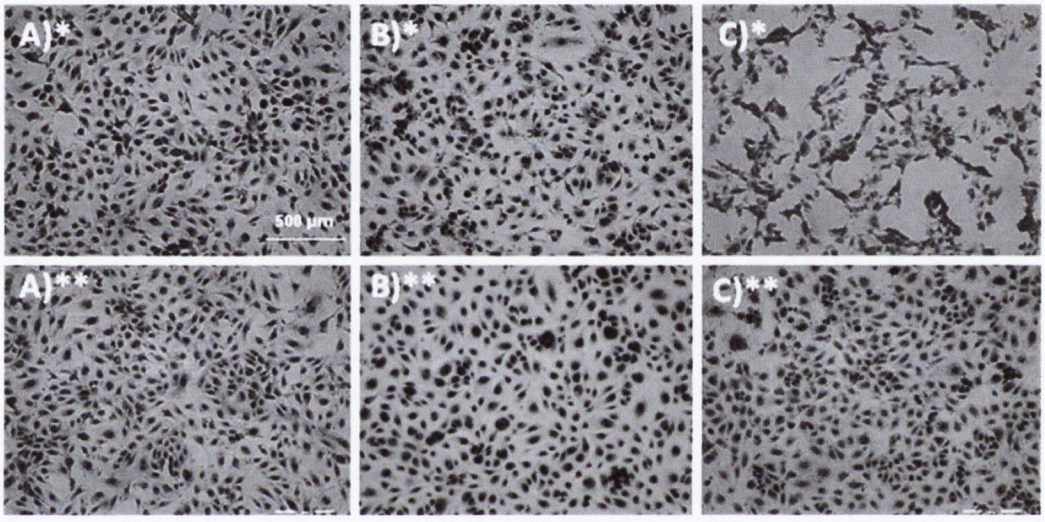

Figure 4.55: The effect of ECB397 on endothelial cells' morphology. HUVECs were exposed to the compounds for 40 minutes and photomicrographs (x10) were taken 1h (*) and 3h (**) after drug washout. **A)** Control (0.1% DMSO), **B)** 0.1 μM ECB397 and **C)** 1 μM ECB397.

4.3.10.3 Group IV Hybrid

The indirect anti-vascular effect of ADR469 on endothelial cell morphology was determined. HUVECs were incubated with 0.1 and 1 μM ADR469 and their appearance was examined (Figure 4.56). A severe effect on cell morphology was noted after treatment with ADR469 at both concentrations, where the cell monolayer seemed disrupted and cells appeared to shrink and round up. As observed 3h after drug washout, cells did not seem to regain their original shape, signifying ADR469 potency.

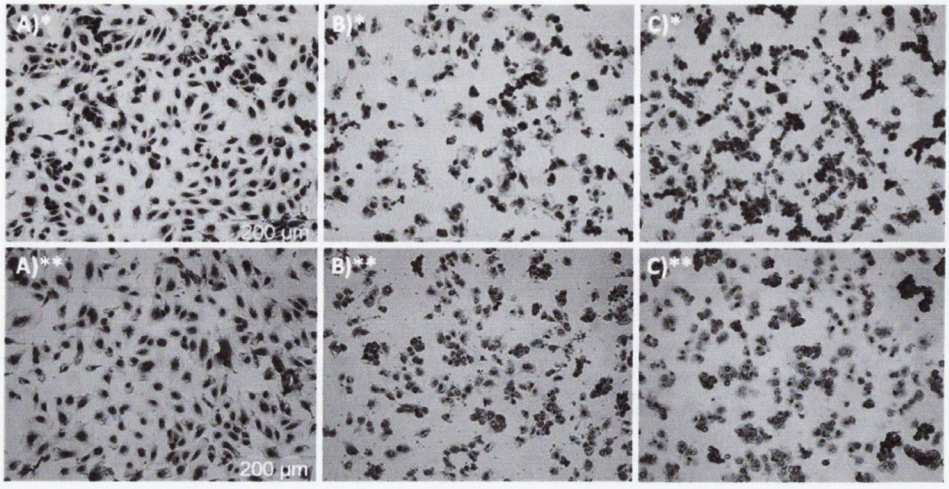

Figure 4.56: The effect of ADR469 on endothelial cells' morphology. HUVECs were exposed to the compounds for 40 minutes and photomicrographs (x10) were taken 1h (*) and 3h (**) after drug washout. **A)** Control (0.1% DMSO), **B)** 0.1 µM ADR469 and **C)** 1 µM ADR469.

4.3.10.4 Designed Multiple Ligand

The effect of BWM120 on endothelial cell morphology was evaluated at 1 and 5 µM (Figure 4.57). BWM120-treated HUVECs resulted in structural alterations and disruption of the cell monolayer. This effect was more evident at 5 µM, where cell morphology appeared even more disturbed. Treated cells fully regained normality after treatment with 1 µM BWM120 and to a lesser extent with 5 µM, as observed 3h after drug washout.

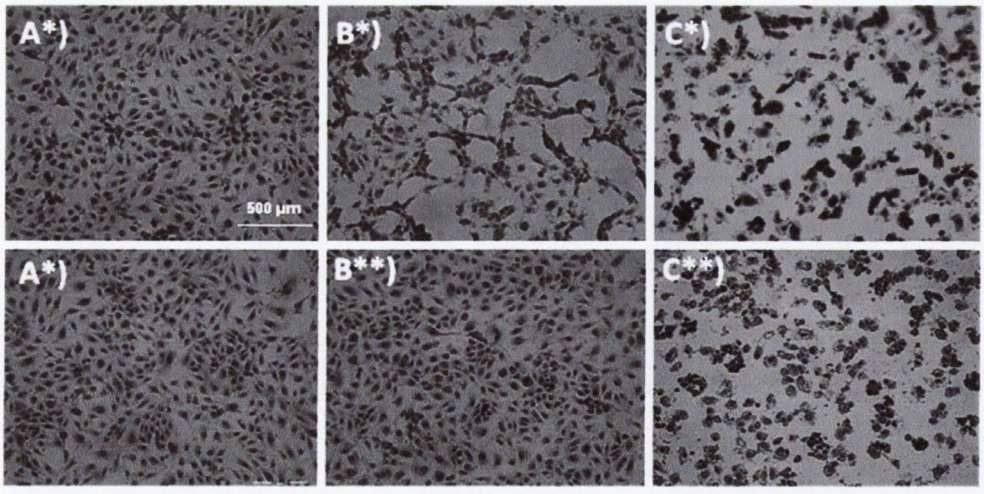

Figure 4.57: The effect of BWM120 on endothelial cells' morphology. HUVECs were exposed to the compounds for 40 minutes and photomicrographs (x10) were taken 1h (*) and 3h (**) after drug washout. **A)** Control (0.1% DMSO), **B)** 1 µM BWM120 and **C)** 5 µM BWM120.

4.4 Discussion

Presented here is the evaluation of several dual-acting inhibitors of tubulin polymerisation and APN. While bestatin is used clinically as an adjuvant in the treatment of AML, its use in this project was primarily to elucidate the evidence in support of its use in hybrid forms for the targeting of drugs to the tumour vasculature and inhibition of APN. This enzyme is considered essential for tumour vasculature growth and metastasis. The tubulin binding component of the design was largely incorporated to inhibit endothelial and tumour cell proliferation, cause tumour vasculature shutdown and exert a direct anti-tumour effect *in vivo*. Initial studies focused on the evaluation of test compounds in APN-based assays, followed by examination of cell proliferation, disruption of the tubulin cytoskeleton, cell cycle stages and endothelial cells' morphology.

4.4.1 APN Enzyme-based Assay

The APN enzyme-based assay was performed in order to determine the APN enzyme inhibitory activity of hybrids and DML. Bestatin was used as a positive control in order to compare its activity with test compounds. All hybrids, whether presented as dual active agents or in a prodrug form (IC_{50} range: 32.04 ± 1.19 to 23.49 ± 1.12 μM, p.174-176), demonstrated superior inhibition of APN compared to that of bestatin (IC_{50}: 59.81 ± 1.08 μM). The only exception was ADR469, where it was not possible to generate an IC_{50} value, owing to the colour intensity of the solution at the higher concentration of test compound used. There was no particular pattern in the hybrids' activity between the various groups, which implies that the hybrids' design was not associated with potency at the enzymatic level. The most potent hybrid was ECB404 (IC_{50}: 23.49 ± 1.12 μM, Table 4.2, p.175) which showed more than a 2-fold increase in activity compared to bestatin and caused significantly ($p < 0.05$) greater APN inhibition than the rest of the hybrids (ECB377, ECB378 and ECB397). This result suggests that structural modifications generated from conjugation of bestatin with a tubulin binding agent may enhance the binding affinity to the APN enzyme, and thus greater inhibition is observed with the hybrids compared to that of bestatin. Interestingly, these results are in agreement with previous work performed by McCormack during his PhD studies (2002), where colchicine-bestatin hybrids exhibited equipotent tubulin inhibitory

activity to the model compound colchicines, and excellent APN inhibition, significantly better than the parent drug, bestatin.

In addition, (2S,3R)-3-amino-2-hydroxy-4-phenylbutanoyl-L-valyl-L-prolyl-L-proline), namely probestin, which is a non-specific aminopeptidase inhibitor, demonstrated greater APN inhibition (IC_{50}: 0.03 μg/mL) compared to that of bestatin (IC_{50}: 6.2 μg/mL) [274]. This could be due to the more hydrophobic proline moiety of the molecule which binds better to the hydrophobic pockets of the enzyme.

Evaluation of BWM120 resulted in a 6-fold increase in activity (IC_{50}: 9.32 ± 1.06 μM, Table 4.4, p.176) compared to bestatin, implying that BWM120 was the most active compound evaluated in the APN enzyme-based assay. The conjugation of a hydroxamic acid to the tubulin targeting compound RS180 resulted in a potent APN inhibitor. This finding complies with several findings from the literature which suggest that hydroxamic acid-related compounds demonstrated strong APN inhibition, including a series of phosphinates (IC_{50} range: 0.24-155 μM) and a N-hydroxy-2-(naphthalene-2-ylsulfanyl)-acetamide (IC_{50}: 3.4 μM) [574-575]. In addition, CHR-2797, a hydroxamate-containing ester, demonstrated greater APN inhibition (IC_{50}: 0.22 μM) compared to that of bestatin (IC_{50}: 0.30 μM) [576].

4.4.2 APN Cell-based Assay

The APN inhibitory properties of test compounds were assessed in two cell-based assays, involving APN-positive HUVECs and PC-3 cells. Non-toxic concentrations of test compounds were determined prior to the APN cell-based assays, in order to avoid any misinterpretation of the results. The theory behind this procedure was similar to the APN enzyme assay; except the active enzyme is replaced by cellular APN. All hybrids demonstrated superior APN inhibitory activity compared to that of bestatin, when using both HUVECs and PC-3 cells (p.182-188). There was a slight variation in activity between HUVECs and PC-3 cells which could be associated with the level of cellular APN present in each cell population. The hybrids within each group displayed an inhibitory effect in a similar manner; however ECB404, ECB397 and ADR469 (the ester-link hybrids) showed high levels of activity against both cell lines. It is worthwhile to note that ADR469 showed APN inhibitory activity at concentrations as

low as 0.1 μM with HUVECs, which highlights its potency in a cellular environment, in contrast with its observable decreased activity at the enzymatic level.

The results may suggest that these hybrids are more active in a cell-based than an enzyme-based assay for two hypothetical reasons. The design of these compounds (which are more hydrophobic than bestatin) may facilitate their intracellular uptake, which could inhibit the cytosolic APN, as well as the membrane-bound APN. The final outcome from this effect could be an overall higher percentage of APN inhibition. These results are comparable to data reported by Sekine *et al.* which demonstrated that bestatin methyl ester, which is more hydrophobic and thus more cell permeable than bestatin, showed a higher APN inhibition in HeLa cells (IC_{50}: 10.2 ng/mL) compared to that of bestatin (IC_{50}: 14.2 ng/mL) [243]. In addition, a bestatin dimethylaminoethyl ester, LYP, suppressed the APN activity of ES-2 and SKOV-3 ovarian carcinoma cells, to a greater extent than bestatin. It was suggested that the ester moiety in the LYP molecule may contribute to the effect of LYP on cancer cells [281].

A different theory that could possibly explain this result is the non-specific inhibition of APN by bestatin, *i.e.* bestatin is a known inhibitor of aminopeptidase B [577], leucine and arginine aminopeptidases [578]. In the presence of other aminopeptidases in the particular cell population used, there is a possibility that the bestatin component of the hybrids interfered with them leading to greater overall inhibition.

The APN inhibitory data obtained from BWM120 treatment did not reveal higher potency than bestatin in the HUVECs-based assay, and was only significantly more active than bestatin at the highest concentration in the PC-3 cell-based assay (p.189). In contrast to the results generated from the enzyme-based assay, BWM120 showed only moderate activity in the cell-based assay which highlights the importance of the compounds' design in the outcome of the study based in a cellular environment. It is interesting to note that 24F, a hydroxamic acid derivative ((S)-2-amino-N-((S)-1-(2-(hydroxyamino)-2-oxoethyl)-2,6-dioxopiperidin-3-yl)-3 phenylpropanamide) was reported to react strongly with APN *in vitro* by inhibiting its enzyme activity but demonstrated moderate inhibition of APN activity using HL-60 cells (IC_{50}: 1.88 mM) [579]. In both cases (BWM120 and 24F), this might be as a result of the "less hydrophobic nature" of these types of compounds, leading to decreased intracellular

uptake. Another possible explanation may involve the fact that higher binding affinity of such compounds for APN could result in a stronger binding to the membrane-bound APN, which in turn results in less intracellular uptake and thus less APN inhibition.

4.4.3 Inhibition of APN Expression

The ability of BWM120 to bind to the extracellular APN and inhibit its expression was investigated. A significantly lower level of PE CD13 was detected in the BWM120-treated HUVECs (83.41 ± 5.83 % at 0.1 mM and 53.80 ± 2.41 % at 0.5 mM) and PC-3 cells at the highest concentration (124.83 ± 5.90 % at 0.5 mM) compared to that of the control (p.190-193). A possible explanation could be that BWM120 binds strongly to the APN and prevents its recognition by the CD13 antibody, thus lower APN expression was detected.

A similar APN expression pattern was reported by Cui *et al.*, where a cyclic-imide peptidomimetics compound, CIP-13F, designed to fit to the active pockets S1 and S′1 of APN, demonstrated significant suppression of APN activity and expression in ES-2 cells, when analysed using flow cytometric and Western blot techniques [560]. Gao *et al.* also reported that the APN expression of ES-2 cells was significantly decreased following 24h exposure to LYP, when compared to the untreated control cells, and showed greater inhibition than that of the bestatin-treated cells [281].

4.4.4 Cell Proliferation Assay

The effect of test compounds on the proliferation of HUVECs and PC-3 cells was determined using the MTT assay. For comparison purposes individual components of the hybrids and their 1:1 combination were also examined. The potency of the hybrids varied depending upon their design. Bestatin's effect on HUVECs' proliferation was moderate (IC_{50}: 43.03 ± 1.27 μM); this is in agreement with data reported by Mishima *et al.*, where 50 μM bestatin inhibited approximately 80% of HUVECs' proliferation [580]. However in the PC-3 cell based assay, bestatin was evaluated up to 100 μM but no effect was observed. In fact, bestatin is a weak anti-proliferating agent which demonstrated IC_{50} values in the low millimolar range (0.87 ± 0.07 mM and 1.98 ± 0.09 mM against HL-60 and SKOV3 cells, respectively) [581]. In addition, bestatin showed selectivity to SQ-5 and EBC-1 squamous lung cancer cells (IC_{50} values: 72.7 ± 17.0

and 94.7 ± 9.9 μg/mL, respectively), over ABC-1, RERF-LC-OK and RERF-LC-MS adenocarcinoma lung cancer cells, where IC_{50} values were not obtained (> 200 μg/mL) [242].

ECB394, the tubulin-binding agent related to group I hybrids, demonstrated reasonable anti-proliferative effect against HUVECs or PC-3 cells (IC_{50}: 4.09 ± 1.41 μM and 4.90 ± 1.12 μM, respectively); this was similar to ECB377 or ECB378 hybrids which had IC_{50} values varying in the low micromolar range (IC_{50} range: 4.71 ± 0.52 μM to 12.05 ± 3.31 μM, Table 4.5, p.194). Taking into consideration the data generated from the hybrids, there is no evidence to support the hypothesis that group I hybrids demonstrated a greater anti-proliferative effect on HUVECs or PC-3 cells than their individual components, alone or in 1:1 combinations. In theory, group I hybrids were designed to remain intact under physiological conditions, which may suggest that such larger-sized molecules provoke a weaker binding affinity to tubulin, resulting in decreased potency. In fact, hydrolysis studies conducted by Breen confirmed that group I hybrids remained intact under physiological conditions [554].

Group II hybrids, ECB399 and ECB404, showed a substantial increase in their anti-proliferative activity (IC_{50} range: 0.17 ± 0.06 μM to 2.52 ± 1.44 μM, Table 4.6, p.195) compared to their associated tubulin inhibitor ECB394, in both HUVECs and PC-3 cells (IC_{50}: 4.09 ± 1.41 μM and 4.90 ± 1.12 μM, respectively). Although it was not clear whether these hybrids remained intact or were degraded by a slow release of their individual components, they demonstrated relatively strong anti-proliferative activity, implying that their design facilitates their activity. In theory, group II hybrids have an aliphatic ester linkage, which is more stable than the phenol ester, because it could undergo elimination instead of hydrolysis, thus resulting in a stronger conjugation. Studies conducted by Breen suggested that group II compounds hydrolysed under physiological conditions to generate both bestatin and the thermodynamically more stable alkene derivative [554].

Group III hybrid ECB397 showed superior anti-proliferative activity against HUVECs and PC-3 cells (IC_{50}: 30.00 ± 17.01 nM and 42.44 ± 1.55 nM, respectively, Table 4.7, p.196) to that of RS180 (IC_{50}: 65.05 ± 1.10 nM and 50.65 ± 1.19 nM, respectively); however the 1:1 combination of bestatin and RS180 was proven to be more effective

(IC_{50}: 7.03 ± 3.41 nM and 10.52 ± 1.14 nM, respectively). ECB397's prodrug design demonstrated an advantage over RS180 which either indicates a higher cell accumulation of the active agent due to hydrolysis or perhaps provides an additive effect by the involvement of two different mechanism of action. Preliminary hydrolysis studies confirmed that ECB397 was hydrolysed to release its individual components under physiological conditions [554].

Group IV hybrid ADR469 demonstrated the highest potency compared to the rest of the hybrids in the MTT assay, in both HUVECs and PC-3 cells (IC_{50}: 10.31 ± 1.22 nM and 5.41 ± 1.37 nM, respectively, Table 4.8, p.196), but did not show greater activity than ADR269 (IC_{50}: 4.91 ± 1.01 nM and 4.67 ± 1.45 nM, respectively). Interestingly, 1:1 combination of ADR269/bestatin resulted in a similar anti-proliferative effect (IC_{50}: 14.80 ± 1.13 nM and 5.43 ± 1.07 nM) to that of ADR469, suggesting possible release of ADR269 and bestatin under physiological conditions.

The preliminary *in vitro* studies proposed that the prodrug-form hybrid approach was more effective than the active hybrid approach. Several dual-targeting hybrids have previously been developed that incorporate a tubulin binding agent with a view to improve their overall pharmacological properties, with varying degrees of success. In particular, Ohtsu *et al.* reported a series of PTX–CPT hybrids which were more active against HCT-8 cell proliferation than either PTX or CPT, and their potency differed from the 1:1 combination of single agents [582]. Perhaps a different mechanism of action is involved following conjugation of the two individual moieties. In addition, an ester-link tubulin targeting hybrid, CA-4–chlorambucil (DNA alkylating agent), demonstrated higher potency than CA-4 in a SH-SY5Y human neuroblastoma cell line, but was comparable to the 1:1 combination of CA-4 and chlorambucil. However, this hybrid did not exhibit superior activity to CA-4 in RBL mastocyte and REN mesothelioma cell lines, but still remained relatively potent (IC_{50} < 3 nM). A possible reason for the varied activity might be due to the relative esterase activity present in different cell lines [583].

In contrast, Kar *et al.* designed and synthesised bifunctional heterodimers targeting both microtubule stabilisation (using PTX) and DNA replication (using daunorubicin, a DNA-intercalating anthracycline). The PTX-daunorubicin conjugates which contained

ester and amide linkages, failed to demonstrate greater growth inhibition than PTX or daunorubicin. This might be due to the increased bulk of the hybrid and perhaps inadequate release of the individual compounds (upon *in vitro* cleavage) [584].

Although in our case the anti-proliferative activity of hybrids is believed to be mainly due to their tubulin binding component which is more active than bestatin, a synergistic effect may be observed with the ester-link hybrids (ECB397, ECB399, ECB404 and ADR469). According to Gao *et al.*, LYP had a dose-dependent anti-proliferative effect on ES-2 cells in the concentration range 50-800 μM following 72h of exposure, and demonstrated a significantly stronger inhibitory effect than bestatin [281].

BWM120's design incorporates a hydroxamic acid unit onto the carbonyl of RS180, and as such we refer to this compound as a DML. The anti-proliferative effect of BWM120 against HUVECs and PC-3 cells was slightly reduced (IC_{50}: 1.10 ± 0.92 μM and 0.49 ± 0.25 μM, respectively, Table 4.9, p.197) compared to RS180 (IC_{50}: 65.05 ± 1.10 nM and 50.65 ± 1.19 nM, respectively); however this compound was still considered relatively potent. Although it is uncertain whether BWM120 is hydrolysed under physiological conditions, the data from the cell proliferation assay may suggest that this compound either remains intact or slowly hydrolyses due to the decreased activity observed, compared to that of RS180.

Krige *et al.* reported that the hydroxamate-containing ester CHR-2797, which is converted to the active acid product CHR-79888, exerted anti-proliferative effects against a range of human leukaemic and lymphoma cell lines. Against these cell lines its activity was 300 times greater than bestatin (IC_{50} range: 10-10000 nM). However when CHR-79888 itself was evaluated it demonstrated much weaker anti-proliferative properties (IC_{50} > 10 μM), suggesting that the prodrug ester form, as in CHR-2797, is essential for optimal intracellular uptake. To confirm this hypothesis, the fate of CHR-2797 was investigated upon incubation with U-937 cells, where CHR-79888 accumulated intracellularly in a time-dependent manner [576]. The presented evidence supports our hypothesis and indicates that the ester link-prodrug design is preferable to the active acid form for optimal cellular uptake.

4.4.5 Immunofluorescence Staining of the Microtubules

Once it was established that test compounds exhibited APN inhibitory properties, the next stage of their *in vitro* evaluation was to verify the properties of the tubulin targeting component of the design. Endothelial cells treated with group I hybrid ECB378 did not demonstrate sufficient evidence of microtubule disruption at 1 or 10 μM, whereas at 20 and 40 μM a more apparent reduction of the fluorescence intensity was noticed, and the effect was dose-dependent (Figure 4.23, p.198). This observation may imply that ECB378 is a weak tubulin binding agent. A possible explanation for the reduced activity could be due to steric hindrance of ECB378 to the tubulin binding site.

Examination of ECB397 (Figure 4.24, p.199) and ADR469-treated cells (Figure 4.25, p.199) revealed a considerable reduction in the tubulin cytoskeleton at 1 μM, whereas this effect was comparable to that observed with their associated tubulin targeting components, RS180 (Chapter 2, Figure 2.16, p.95) and ADR269 (Chapter 2, Figure 2.17, p.95), respectively. As these hybrids were designed to specifically present the tubulin binding component in a prodrug form it is further evidence that once uptaken, cellular hydrolysis occurred to liberate the tubulin binding component.

As might have been anticipated, based on the anti-proliferative data, the effect of 1 μM BWM120 on microtubule organisation was apparent but not comparable to RS180; however it was more evident at 5 μM (Figure 4.26, p.200).

Interestingly, several reported hybrids associated with a tubulin binding agent revealed variation in their activity with regard to tubulin inhibition. In particular, a PTX-daunorubicin conjugate showed a > 10-fold decrease in tubulin binding affinity compared to PTX alone, in an *in vitro* tubulin-binding competition assay [584]. Taking into consideration the increased bulk of the dimers, a possible explanation for the reduced activity may be steric hindrance.

In contrast, Huang *et al.* synthesised and evaluated a PTX-octreotide conjugate which retained the ability of PTX to bind to tubulin and cause bundle formation in MCF-7 cells [353]. Additionally, a hybrid with two tubulin targeting components, vindoline and thiocolchicine, demonstrated inhibition of tubulin polymerisation and showed comparable shortening of microtubule assembly in A549 human lung carcinoma cells

to that of thiocolchicine [585]. The potentiation of the hybrid's activity may be due to the choice of linker (non-cleavable alkyne) used to conjugate the two moieties; it was proposed that this was of sufficient length between the two components and thus allowed adequate binding to the two target sites. Moreover, Sharifi *et al.* designed a colchicine-cyanonilutamide (an androgen receptor antagonist) hybrid, which demonstrated binding to tubulin with a similar affinity to thiocolchicine, and inhibited tubulin assembly more effectively than colchicine or CA-4 [586]. In addition, one of the hybrids designed by Kamal *et al.* composed of two tubulin targeting moieties using 3, 5-diaryl isoxazoline/isoxazoles and linked to quinazolinones through different alkane spacers, disrupted microtubule organisation at 5 μM, following a 48h incubation period in MCF-7 cells, and the effect was comparable to that of CA-4 [587].

4.4.6 Cell Cycle Analysis – G_2/M Phase

In order to determine whether test compounds were able to induce mitotic arrest of HUVECs and PC-3 cells and to establish whether their anti-proliferative effect is due to their anti-mitotic effect, cell cycle analysis was performed on treated and control cells. In the control treated cells, the highest peak for DNA-stained cells appeared to be in the G_1 phase, an indication of normal cell behaviour. Group I hybrid ECB378 did not demonstrate an apparent G_2/M phase arrest at 1-40 μM with HUVECs or up to 20 μM with PC-3 cells when incubated for 24h (Figure 4.28, p.202). At the higher concentrations (20 and 40 μM), ECB378 caused HUVECs' death and thus was not further examined. Data obtained from the apoptosis study using the cell cycle method showed that PC-3 cells showed an accumulation in the G_2/M phase when treated with 10 μM ECB378 for 72h, an indication of an anti-mitotic effect (Figure 4.43, p.217). This result may suggest that ECB378 is a weak tubulin binding agent and thus its effect required a longer period of time to be observed. In fact, this finding is in agreement with the tubulin visualisation study, where ECB378 demonstrated moderate microtubule disruption.

Incubation of HUVECs with ECB397, ADR469 or BWM120 showed a moderate increase of G_2/M phase cells compared to the vehicle, whereas PC-3 treated cells demonstrated an apparent G_2/M phase arrest (Figures 4.30, p.204; 4.32, p.206 and 4.34, p.208, respectively). This finding verifies that ECB397, ADR469 and BWM120

acquire anti-mitotic properties. Tubulin binding agents are well known for their ability to induce a G_2/M phase arrest and this is a confirmation that test compounds are indeed targeting tubulin.

Passarella *et al.* reported that following 24h incubation of A549 cells with 10 μM of the vindoline-thiocolchicine hybrid, a substantial increase in the G_2/M phase was observed compared to the vehicle control [585]. Additional hybrids of 3, 5-diaryl isoxazoline/isoxazoles and quinazolinones demonstrated a variation in the cell cycle analysis; a particular hybrid (at 5 μM) caused a moderate increase of MCF-7 cells in the G_2/M phase (43.9%) following 24h incubation, whereas the rest of the compounds failed to provide evidence of an anti-mitotic effect. However, treatment of cells with positive control CA-4 resulted in a higher accumulation in the G_2/M phase (65.5%) than the hybrids [587].

4.4.7 Cell Cycle Analysis – Sub-G_0/G_1 Phase

According to the results obtained previously, test compounds may indirectly cause cell death by altering the microtubule organisation and by preventing the successful completion of cell division. It was hypothesised that hybrids and DML could possibly induce higher levels of cell death compared to either a tubulin inhibitor or bestatin, due to the fact that both components of the dual-acting design were previously shown to induce apoptosis [242, 564].

Initially, several attempts were made in order to establish the appropriate concentration or time points that would result in an accumulation of cells in the sub-G_0/G_1 phase. No significant effect was observed following treatment with test compounds at < 10 μM including both cell lines and thus the selected concentrations were ≥ 10 μM. A substantial effect was noted following 24h incubation of HUVECs with test compounds; however PC-3 cells appeared to be more resistant to cell death and did not provide any evidence of apoptosis following 24h or 48h incubation. Hence, the treatment duration for PC-3 cells was chosen to be 72h.

The effect on cell death of group I hybrid ECB378, its individual components ECB394 and bestatin, and their 1:1 combination were examined in the cell cycle analysis, by determining the percentage of DNA degradation represented by a sub-G_0/G_1 peak.

Bestatin did not demonstrate any evidence of cell death with either cell line at any concentration. ECB394 and ECB394/bestatin combination showed a similar pattern; however ECB378 resulted in a significantly higher percentage of sub-G_0/G_1 cells in both cell lines compared to single and combination treatment (summarised in Table 4.10, p.211). This finding may suggest that a synergistic effect is taking place or that the apoptotic effect of ECB378 is partly mediated by a different mechanism of action, other than mitotic arrest.

Group III hybrid ECB397, RS180 and RS180/bestatin combination were investigated for evidence of cell death, following treatment of HUVECs and PC-3 cells. The degree of apoptosis was similar between RS180 and RS180/bestatin combination in both cell lines. ECB397 demonstrated a higher percentage of sub-G_0/G_1 HUVECs than both of the treatments, which may indicate synergy or perhaps a different mechanism of action other than mitotic arrest. In contrast, ECB397 treatment failed to demonstrate a similar effect with PC-3 cells (summarised in Table 4.11, p.220). The fact that DNA degradation was not detectable at a sub-G_0/G_1 peak does not constitute proof of no apoptosis [588]. The method of apoptosis detection using a flow cytometric technique relies on the fact that small fragments of DNA are eluted after washing off alcohol-fixed apoptotic cells with buffer. Following DNA staining, cells which have lost DNA will take up less stain and will only appear on the left of the G_1 peak. However, if cells enter apoptosis from the S or G_2/M phases, they are less likely to appear in the sub-G_0/G_1 area. For instance, Kanthou *et al.* reported that 24h treatment of endothelial cells with 100 nM CA-4P resulted in a G_2/M phase arrest, without any observable accumulation in the sub-G_0/G_1 phase. On the other hand, an enzyme-linked immunosorbent assay (ELISA)-based cell death assay which detects cytoplasmic DNA-histone complexes generated during apoptotic DNA fragmentation into nucleosomes, showed that 100 nM CA-4P induced apoptosis following a continuous 8h exposure of the cells to the agent [563]. Therefore, absence of a sub-G_0/G1 peak in PC-3 cells treated with ECB397 is consistent with apoptotic cells derived from other phases of the cell cycle except G_1.

The effect of BWM120 on apoptosis was assessed using both HUVECs and PC-3 cells. Considerable high levels of cell death were noted in HUVECs but were similar to that

of RS180; however BWM120 treatment of PC-3 cells resulted in a substantial increase of apoptosis which was significantly higher than that observed with RS180 (summarised in Table 4.12, p.226). The results generated from this study may imply that BWM120 design is beneficial over RS180 and the addition of the hydroxamic acid along with RS180 may promote a synergistic effect in terms of apoptosis or perhaps a different mechanism of action may be involved.

Overall, the fact that hybrids and BWM120's design was proven advantageous over single agents, alone or combination treatments, may indicate a synergistic apoptotic effect which supports the initial hypothesis. Nevertheless, the fact that bestatin alone did not show any evidence of cell death at the particular concentrations used, implies that the increased apoptotic effect observed after treatment with hybrids or DML may be due to their design *i.e.* a different mechanism of action may be involved or perhaps their activity was enhanced by a higher intracellular uptake of bestatin. Perhaps the enhanced APN inhibition observed by test compounds may be involved in the synergistic apoptotic effect. It is still inconclusive as to how these compounds exert their effect on apoptosis and further studies could clarify this.

There is evidence to support that bestatin methyl ester induced leukaemic cell apoptosis more potently than bestatin, probably because bestatin methyl ester is more hydrophobic than bestatin and thus intracellular uptake is enhanced. Additional studies revealed that bestatin methyl ester induced activation of caspase-3 more rapidly, at lower concentrations than bestatin [244]. Furthermore, Ezawa *et al.* reported that higher concentration (100 mg/mL) of bestatin induced apoptosis in some human NSCLC cell lines, whereas lower concentration (10 mg/mL) did not demonstrate any growth inhibition or apoptosis in most cell lines [242]. In a further attempt to investigate the apoptotic effect of bestatin in solid tumour cell lines (PC-1, EBC-1, HeLa S-3 and HT-1080), neither direct growth inhibition nor induction of apoptosis was observed. Instead, bestatin significantly augmented death lignad-induced (by agonistic anti-Fas antibody, CH11) growth inhibitory effect and induction of apoptosis. It is worthwhile to note that bestatin did not show any effects even in an APN-expressing cell line (HT-1080), which may indicate that cell surface expression of APN and augmentation of apoptosis by bestatin were not correlated. It is believed, that the apoptotic pathways in

leukaemic cells but not in solid tumour cells, might be partially stimulated and thus leukaemia cell lines are more sensitive to apoptotic stimuli than solid tumour cell lines [243]. With regard to our case, this could be a possible explanation for bestatin's inability to induce apoptosis in HUVECs or PC-3 cells at relatively low concentrations (10-100 μM).

In addition to the bestatin component, the tubulin binding agent of the hybrids was most likely the greatest contributor to apoptotic induction as observed with our hybrids. Data from the literature indicated that the selective cytotoxic effect of CA-4 was mediated by the induction of apoptosis and not necrosis. For instance, incubation of endothelial cells with 0.1 mM CA-4 resulted in the conversion of the CPP32 proenzyme to active caspase-3 and also increased the activity of caspase-3. Moreover, there was an increase in Annexin V binding (50%) of the cells 8h after CA-4 incubation, internucleosomal DNA fragmentation was detected in cells treated with 0.1 mM CA-4 for 24h and 75% of cells exhibited nuclear morphological features, characteristic of apoptosis [564].

Several dual-acting conjugates have been examined for their apoptotic effect. Lee *et al.* reported the evaluation of an immunoconjugate MEDI-547, composed of fully humanised monoclonal antibody (1C1) against human and murine ephrin receptor EphA2 (which is frequently over-expressed in endometrial cancer) and the tubulin polymerisation inhibitor monomethyl auristatin F (MMAF) *via* stable maleimidocaproyl (mc) linker. The apoptotic effects of MEDI-547, 1C1 and IgG-mcMMAF (non-specific binding IgG monoclonal antibody conjugated to MMAF *via* the mc linker), on Hec-1A endometrial cancer cells were determined using the Annexin V/PI staining. Significantly higher percentages of apoptotic cells were observed following 48h, 72h and 96h incubation with MEDI-547 compared to the effect of 1C1 and IgG-mcMMAF. However, the fact that comparison combination studies of 1C1 and IgG-mcMMAF were not conducted means it is not possible to distinguish whether there is a synergistic effect or an unknown mechanism of action [589].

Furthermore, an additional immunoconjugate composed of cAC10, a chimeric monoclonal antibody directed against CD30 (a TNF receptor over-expressed in anaplastic large cell lymphoma (ALCL) and a subset of non-Hodgkin lymphomas) and MMAE was synthesised and evaluated. In order to assess the cell cycle and apoptotic

effects of cAC10-vcMMAE conjugate, Hodgkin-derived L450 cells were exposed to 1 μg/mL of cAC10, cAC10-vcMMAE, or an isotype-matched, irrelevant cIgG-vcMMAE for 12h, 24h and 48h. Following this, cells were labelled with bromodeoxyuridine to detect nascent DNA synthesis and with PI to detect total DNA content, followed by flow cytometric analysis. By 48 hours, 53% of the cells showed a sub-G_1 DNA content, consistent with apoptotic DNA fragmentation and this effect was not observed after exposure to equivalently high concentrations of control cAC10 or IgG-vcMMAE [590]. Once more, 1:1 combination studies of individual components were not performed for comparison purposes and thus the results are inconclusive as to whether the conjugate exhibits a synergistic effect or is similar to the combination treatment.

Huang *et al.* reported that exposure of MCF-7 cells to 1 nM PTX or PTX-octreotide conjugate for 24h resulted in chromatin condensation in a similar manner, which was assessed by fluorescent microscopic analysis of nuclei stained with Hoechst 33258, and by electron microscopy. Treatment of cells with octreotide alone failed to induce apoptosis, although comparison combination studies were not performed. This finding verified that the conjugate retained PTX's activity; however it has not yet proven to be advantageous over combination therapy [353].

Moreover, Zhang *et al.* synthesised a series of α-methylene-γ-lactone and 2-phenyl indole hybrids including S9, which target the PI3K/Akt/mammalian target of rapamycin (mTOR) pathway, which plays a central role in tumour formation and progression [591]. In particular, S9 not only functioned as a PI3K and mTOR inhibitor but also as a microtubule destabiliser. The apoptotic effect of S9 was examined in a variety of human cancer cell lines, which were subjected to Annexin V/PI staining following incubation with 10 μM S9 for 8h. S9 successfully induced rapid apoptosis, whereas PI3K inhibitors are usually associated with G_1 phase arrest, rather than apoptosis. This indicated that the S9-induced effect may represent its combinatorial activity on the PI3K-Akt-mTOR pathway and the microtubule cytoskeleton [592].

In summary, published data provides evidence to support the idea that dual-targeting conjugates induced apoptosis in a similar manner to their associated tubulin inhibitor; however most cases are inconclusive due to the lack of combination studies. In our case, the hybrids' design proved advantageous over single or combination treatment,

independent of whether the hybrid remained intact (*e.g.* ECB378) or released its individual components (*e.g.* ECB397 and ADR469).

4.4.8 Analysis of Endothelial Cells' Morphology

The final study conducted, involved the *in vitro* evaluation of test compounds as potential modulators of endothelial cells' morphology, which is a direct indication of an *in vitro* anti-vascular effect. The control treated group appeared to have an undisturbed monolayer of cells, with normal structural features. In contrast, cells treated with test compounds showed morphological changes including endothelial cell contraction, membrane blebbing, intercellular gaps and darkening of the cell contents.

Although group I hybrid ECB378 failed to show evidence of morphological disruption up to 20 μM, it demonstrated a moderate effect on endothelial cells' structure at 40 μM, and the effect was reversible as observed 3h after drug washout (Figure 4.53 and 4.54, p.229-230). This result is in agreement with the microtubule disruption study, where 40 μM ECB378 showed a substantial decrease in the level of microtubule staining. Again, the results from this assay confirmed that ECB378 is a weak anti-vascular agent due to its poor tubulin binding properties.

Treatment of endothelial cells with group III hybrid ECB397 at 1 μM resulted in an evident disruption of cell morphology, but this effect was reversible as observed 3h after drug washout (Figure 4.55, p.231). The activity of ECB397 was comparable to that of RS180, verifying that ECB397 was hydrolysed to release its individual components (Chapter 2, Figure 2.20, p.98). Taking into consideration the findings from the microtubule disruption studies, along with the changes in endothelial cell morphology, we can conclude that ECB397 is a relatively potent anti-vascular agent *in vitro*.

The effect of ADR469 on endothelial cells was apparent even at 0.1 μM, highlighting its potency and confirming its anti-vascular effect *in vitro* (Figure 4.56, p.232). However, endothelial cells did not fully regain their normal appearance after 3h of drug washout. The activity of ADR469 on cell morphology was similar to that of ADR269 (Chapter 2, Figure 2.22, p.99), where in both cases a potent effect was observed at 0.1 μM. However, cells did not fully recover from exposure to these agents. This finding

may suggest that this effect was either irreversible at those particular concentrations (0.1 and 1 μM), or a longer incubation period was required to observe reversibility. Once more, ADR469 retained its anti-vascular activity *in vitro* and demonstrated a comparable effect to that of its tubulin binding components, suggesting the release of its individual moieties.

Furthermore, moderate morphological changes of endothelial cells were observed after treatment with 1 μM BWM120 and were more evident at 5 μM (Figure 4.57, p.233). Although this effect was reversible at 1 μM BWM120, at higher concentration cells did not appear to fully regain normality. In comparison to RS180, BWM120 appeared to have slightly reduced activity; however it can still be considered a relatively active anti-vascular agent. This finding confirmed that BWM120 maintained, to some extent, the tubulin binding properties of RS180 and verified its *in vitro* anti-vascular activity.

In a similar manner, 1 μM CA-4P was previously reported to cause blebbing morphology in endothelial cells, in which F-actin accumulated around surface blebs, stress fibres misassembled into a spherical network surrounding the cytoplasm and focal adhesions appeared malformed [315]. As a result of these effects, there is an increase in endothelial permeability which facilitates the uptake of macromolecules and provides an advantage for combination chemotherapy *in vivo* [514].

In theory, treatment with the ester-link hybrids designed to release individual components upon hydrolysis, including ECB397 and ADR469, will lead to a highly permeable tumour endothelium, disrupted by the tubulin targeting component, and an increased exposure of bestatin at the tumour site. To justify this hypothesis *in vivo* anti-tumour studies were required which will be discussed in Chapter 5.

4.5 Conclusions

Novel hybrids and DML were designed to target tubulin polymerisation and APN activity. It was essential to design and develop assays in order to examine separately both targets of the hybrids and verify the effects of their design. Initially, test compounds were evaluated in an APN enzyme-based assay and found to possess APN inhibitory properties superior to that of control compound bestatin, with BWM120 being the most potent. Next, the APN inhibition of test compounds was determined in a

cell-based assay using HUVECs and PC-3 cells, where the majority of the compounds demonstrated greater inhibition than bestatin, where ECB397 and ADR469 were the most active. BWM120 was further examined for its ability to interfere with APN expression of HUVECs and PC-3 cells using a flow cytometric method, and showed a significantly decreased level of APN expression compared to the control treated cells.

Following this, the effect of test compounds on cell proliferation was investigated, along with their individual components alone or in 1:1 combination. Group I hybrids showed reasonable anti-proliferative activity against both cell lines, similar to their individual components alone or in combination, whereas the anti-proliferative activity of group II hybrids was improved. Group III and IV hybrids inhibited cell growth in a similar manner as their tubulin binding components alone or in combination with bestatin. The DML demonstrated slightly decreased anti-proliferative activity compared to its parent compound RS180, but was still relatively potent. Furthermore, all hybrids and DML showed a substantial disruption of the microtubule of endothelial cells with variation in potency, implying their ability to interfere with the tubulin cytoskeleton. In addition, the anti-mitotic effects of test compounds were assessed by examining the cell cycle of treated endothelial and PC-3 cells, where a G_2/M phase arrest was observed, signifying their effect on cell division. In order to determine evidence of a synergistic effect with test compounds in the degree of drug-induced apoptosis, DNA fragmentation was analysed at the sub-G_0/G_1. It was found that in most cases hybrids and DML induced higher levels of apoptotic cells than their individual components (alone or in combination). These results proved that the design of the hybrids and DML is advantageous over single agents and may suggest a different mechanism of action (other than the mitotic arrest) in which the compounds induced their apoptotic effects. Finally, test compounds demonstrated their anti-vascular properties in proliferating endothelial cells by reversibly altering their morphological features.

Taking into consideration the results obtained from the *in vitro* evaluation of hybrids, their degree of potency depends upon their design *i.e.* whether the hybrids are hydrolysed or remained intact. According to the obtained data, in addition with studies conducted by Breen [554], group I hybrids remained intact as dual-acting compounds due to their reduced activity as tubulin binding agents, whereas group II hybrids were

hydrolysed by a slow-release hydrolysis, due to the observed moderate activity. Group III and IV hybrids were hydrolysed to release their individual components under physiological conditions, due their potent activity observed as tubulin binding agents.

Bearing in mind the evidence obtained from the literature regarding a wide variation in results, it is believed that the hybrid's design plays a crucial role in the outcome of the study, including its presentation (active or prodrug form), the type and length of the linker unit which conjugates the two components of the hybrid, the type of the enzymatic cleavage requires to release the active agents, the choice of cell line (*i.e.* enzyme presence) and the conditions in which the hybrid is hydrolysed (*i.e.* pH, temperature *etc.*).

In conclusion, these compounds inhibited both enzymatic and cellular APN, cell proliferation of endothelial and prostate cancer cells, showed evidence of microtubule disruption, induced anti-mitotic and apoptotic effects and caused reversible morphological changes to endothelial cells indicating their anti-vascular potential. Although additional mechanisms of action may be involved, the main aim of this study was to assist in the development of novel hybrids and DML of tubulin and APN, which aim to target tumour vasculature and angiogenesis. For this reason it was important to establish whether these compounds maintain their activity in *ex vivo* and *in vivo* models. Therefore, selected compounds were assessed using the *ex vivo* aortic ring assay and a PC-3 tumour xenograft model for anti-vascular, anti-angiogenic and anti-tumour activities. This is further discussed in Chapter 5.

-- Chapter 5 --

Ex Vivo and *In Vivo* Evaluation of Novel Dual-Acting Compounds Targeting Tubulin Polymerisation and APN

5. Introduction

The *in vitro* results obtained from Chapter 4 revealed that the hybrids and the DML previously synthesised in our group, target tubulin polymerisation and APN. These compounds possess APN inhibitory activities, both at the enzymatic and the cellular level, and consecutively have anti-proliferative, anti-mitotic, apoptotic and anti-vascular properties *in vitro*. Given that the preliminary evaluation of these compounds supported the theory based on their design, it was necessary to evaluate them in a more complex *ex vivo* model in order to further establish their anti-vascular and anti-angiogenic activities. Next, once their solubility issues were addressed, selected compounds were chosen for their final evaluation in a tumour xenograft model to determine their *in vivo* anti-tumour efficacy, and examine the tumour samples for any evidence of tumour necrosis or vasculature disruption. The compounds selected for *in vivo* evaluation included ECB378, ECB397, ADR469 and BWM10 (Figure 5.1). For comparison purposes, a 1:1 combination of RS180-leucine(leu)/bestatin was also examined.

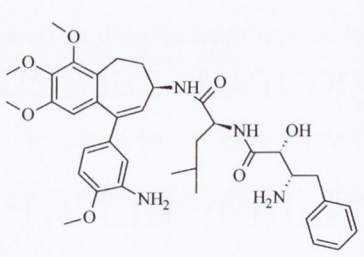

ECB378

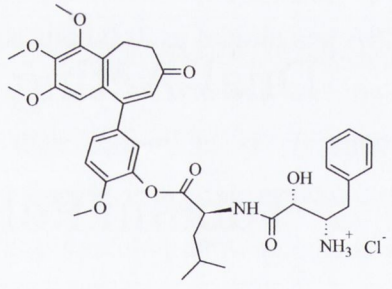

ECB397

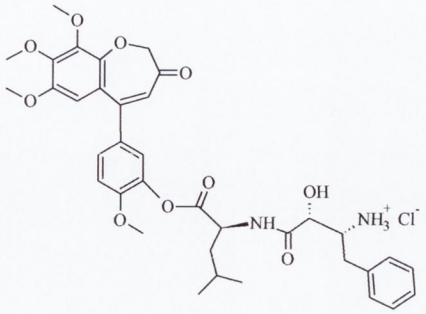

ADR469

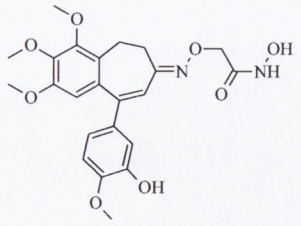

BWM120

Figure 5.1: Hybrids ECB397, ECB378, ADR469 and DML BWM120.

5.1 Aims

The specific aims of the work described in this Chapter were to:

- Verify the anti-vascular effect of test compounds in the *ex vivo* aortic ring assay.
- Determine and quantify the anti-angiogenic activity of test compounds in the *ex vivo* aortic ring assay.
- Develop suitable medium to solubilise test compounds, prior to their *in vivo* administration.
- Establish the anti-tumour efficacy activity of selected compounds in a s.c. PC-3 tumour xenograft model and observe any obvious toxicity following their administration.
- Histologically examine the tumour samples following completion of the *in vivo* efficacy studies for evidence of tumour necrosis.
- Evaluate the functional vasculature of tumour samples following completion of the *in vivo* efficacy studies.

5.2 Materials and Methods

5.2.1 Materials

DMSO, FBS, streptomycin/penicillin solution, polypropylene tuberculin syringes (27 x ½ in.), Triton-X 100, BSA and Tween® 80 were all purchased from Sigma, Ireland. EBM-2 medium was purchased from Lonza, Ireland and basement membrane matrix (matrigel) from BD Biosciences, Ireland. Vetalar® and Rompun® were provided by BRU, TCD. Tissue-Tek* O.C.T. compound was purchased from Syntec Scientific, Ireland. Superfrost plus microscopy slides and cover slips were purchased from VWR, Ireland. Purified anti-mouse CD31 (PECAM-1) antibody was purchased from BD Biosciences, Ireland. PBS tablets, Alexa Fluor® 488 goat anti-rat IgG and ProLong® gold antifade reagent with DAPI were purchased from Invitrogen, Ireland.

Liquid nitrogen was provided by the School of Chemistry, TCD. All the materials used for the paraffin-embedding of tumour samples and their staining with H&E were kindly provided by Peter Stafford, Department of Zoology, TCD.

5.2.2 Cell Line

PC-3 human prostate adenocarcinoma cell line was purchased from LGC Standards, UK and cultured in F12K medium supplemented with 0.02 mg/mL sodium pyruvate, 10% FBS and 10 mL/L penicillin/streptomycin solution. PC-3 cell line was selected for its APN expression and its invasive potential when growing in tumour xenograft models. Cell and tissue cultures were kept at 37 °C in a humidified atmosphere containing 5% CO_2 at all times and maintained as previously described in Chapter 2, section 2.2.4, p.80.

5.2.3 Test Compounds

For the *ex vivo* assays, stock solutions of test compounds were prepared in DMSO and then diluted in the appropriate medium at the required concentrations (final DMSO concentration $\leq$ 0.1%). Control solutions contained 0.1% DMSO in medium. With regard to the *in vivo* studies, poor solubility issues were associated with ECB378 and BWM120. The maximum DMSO concentration used for *in vivo* administration varies between 5-10%. Initial attempts were carried out by dissolving test compounds in DMSO, followed by adjustment to the required concentration with PBS, pH=7.4 (final

DMSO concentration was either 5% or 10%). This did not improve the solubility and thus further attempts were made by replacing PBS with wfi. Although some improvement was noted, test compounds were still not fully in solution. Next, in addition to DMSO, Tween® 80 was also used, followed by adjustment of the required concentration with wfi (final DMSO and Tween® 80 concentration was 5% each). This dramatically improved the solubility and hence it was used to solubilise ECB378, ECB397, RS180-leu/bestatin and BWM120. The control solutions contained 5% DMSO and 5% Tween® 80 in wfi. ADR469 was dissolved in 10% DMSO and then diluted in wfi; the corresponding control solutions contained 10% DMSO in wfi. Fresh solutions were prepared prior to each treatment.

5.2.4 Animals

Male Wistar rats (200-300 g) were sourced from the BRU, TCD. Animals were housed under controlled conditions at 22 °C with 12h light and 12h dark cycles. All animals had access to food and water *ad libitum*.

Male *balb-c* immunodeficient *nu/nu* mice, aged 6-8 weeks, were supplied by Harlan, UK and housed in Scrubs, BRU. Immunodeficient mice were maintained in a SPF environment, within IVCs in groups of 10 or less, under controlled conditions at 22 °C with 12h light and 12h dark cycles. Animals received Harlan 2018 diet and had access to food and water *ad libitum*. Animal handling and experimentation were performed using aseptic techniques and under a laminar hood at all times. At the end of each experiment, animals were sacrificed by either CO_2 asphyxiation or cervical dislocation. All animal procedures were carried out under a project licence issued by the Department of Health and Children.

5.2.5 Aortic Ring Assay (anti-vascular and anti-angiogenic model)

The aortic ring assay was performed in order to evaluate the anti-vascular and anti-angiogenic properties of test compounds. The same procedures were followed as previously described in Chapter 3, section 3.3.5 and 3.3.6, p.120-121. For the anti-vascular study, each compound concentration was tested in duplicate and results were presented as images showing the microvessels breakdown at each time point. For the anti-angiogenic study, each compound concentration was tested in duplicate and each

experiment was performed three independent times. Microvessel density was then analysed using Image J software (NIH) and results were presented as the mean pixel density area ± SEM, along with images of the aortic rings.

5.2.6 Dose Establishment

The anti-tumour effect of bestatin and its related analogues has been previously examined in several tumour xenograft models using continuous treatment at low doses. It was indicated that bestatin's anti-tumour efficacy was in part due to its cytostatic as well as its anti-angiogenic properties, when administered consecutively [281-282, 593]. Therefore, it was hypothesised that our bestatin-related hybrids should demonstrate comparable anti-tumour effect when evaluated at a similar dosing regimen as bestatin. In addition, it was proposed that an additive or synergistic effect could be observed, due to the vascular disrupting properties of the tubulin targeting component of the hybrids. Herein, a MTD was not established and the selected dose for ECB378, ECB397 and BWM120 was 40 mg/kg. RS180-leu/bestatin combination was used at an equimolar dose as per ECB397. ADR469 was administered at 50 mg/kg.

5.2.7 Tumour System

PC-3 human prostate adenocarcinoma cell line was used and the s.c. tumour xenografts were established as previously described in Chapter 3, section 3.3.8, p.122. As soon as the tumours were accurately measurable by callipers the mice were allocated randomly into different treatment groups, each group consisting of 8 mice. Where necrotic tumour implants were observed, animals were excluded from the study; therefore the number of animals in each group varied between 6-8 mice. Mean group tumour size variation was kept to a minimum.

5.2.8 Chemotherapy Studies

Test compounds were prepared at the appropriate concentration and administered by an i.p. injection on alternate days. The duration of treatment with ECB378, ECB397, BWM120 and RS180-leu/bestatin was 12 days, whereas with ADR469 was 24 days. Day 0 was designated as the first day of treatment. Two-dimensional calliper measurements of the tumours were used to assess tumour growth. Tumour and BW measurements were obtained every other day. At the end of each experiment animals

were sacrificed using cervical dislocation. The RTV and percentage BW were estimated as previously described in Chapter 3, section 3.3.9, p.122.

5.2.9 Assessment of Tumour Necrosis

Following the *in vivo* anti-tumour efficacy study of test compounds, histological examination of tumour samples was carried out. Three tumours per group were rapidly excised and processed for paraffin embedding, sectioning and H&E staining as previously described in Chapter 3, section 3.3.10, p.123. Tumours from each group were analysed and the results were presented as images showing the extent of tumour necrosis within control and treated groups.

5.2.10 Assessment of the Tumour Vasculature

The effect on functional vasculature of PC-3 tumours following treatment with test compounds was evaluated after completion of each efficacy study. Three tumours per group were rapidly excised and cryo-preserved at -80 °C until ready for ultracryotomy. Tumour samples were processed for cryo-sectioning and then stained for functional endothelial cells using a CD31 antibody as described in Chapter 3, section 3.3.11, p.124. The level of CD31 staining was analysed using Image J (NIH) and the results were presented as mean pixel density area ± SEM, together with images of the functional vasculature.

5.2.11 Statistical Analysis

Statistical analysis of the generated data was carried out using GraphPad Prism, version 5. Pixel density area of mircovessel network, tumour measurements, percentage of BW and pixel density area of functional vasculature were expressed as mean ± SEM. The statistical significance between control and treated groups in the *ex vivo* aortic ring assay of angiogenesis and in the *in vivo* anti-vascular study was determined using Student's *t*-test. In order to determine any significant difference between the tumour growth of the control and treated groups in each *in vivo* efficacy study, Mann-Whitney *U*-test was applied using GraphPad Prism, version 5. Statistical significance along individual days of treatment in the *in vivo* studies was also determined using the Mann-Whitney *U*-test.

5.3 Results

5.3.1 Aortic Ring Assay (anti-vascular model)

The anti-vascular activity of test compounds was evaluated in the *ex vivo* aortic ring assay. The cultures were monitored microscopically from 1h to 24h after treatment and images were captured to show the degree of vasculature disruption at different time points.

5.3.1.1 Group I Hybrid

The effect of ECB378 was determined in the aortic ring assay for any evidence of microvessel breakdown. Initially, ECB378 was examined at 1 and 10 μM, where no activity was observed; for this reason higher concentrations were used at 25 and 50 μM. Minor microvessel breakdown was noted at 25 μM following 24h incubation; however the anti-vascular effect was more evident at 50 μM and the effect was time-dependent (Figure 5.2).

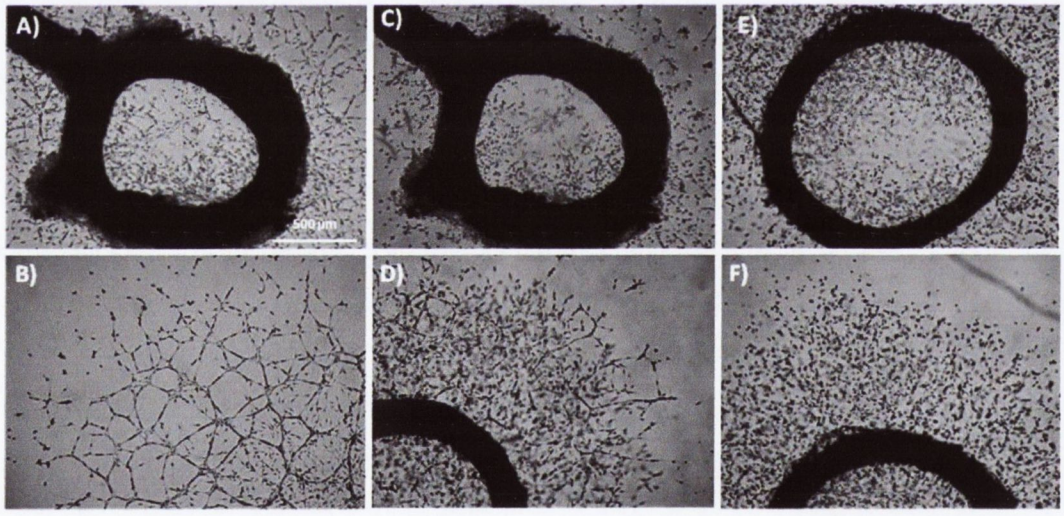

Figure 5.2: The anti-vascular effect of ECB378. The aortic rings were kept in a humidified CO_2 incubator at 37 °C and the medium was changed every other day, starting from day 3. Test compounds were added on day 8. Photomicrographs of the aortic cultures were taken under bright field microscopy using a digital camera (x4). **A-B)** Before the addition of test compound, **C-D)** 25 μM ECB378 (24h) and **E-F)** 50 μM ECB378 (24h).

5.3.1.2 Group II Hybrid

ECB397 was evaluated for its ability to interfere with established microvessel network. Incubation of the aortic rings with 0.1 μM did not result in an evident anti-vascular effect, and thus 1 μM was used. An apparent microvessel breakdown was observed at 1 μM ECB397 following a 24h incubation period (Figure 5.3).

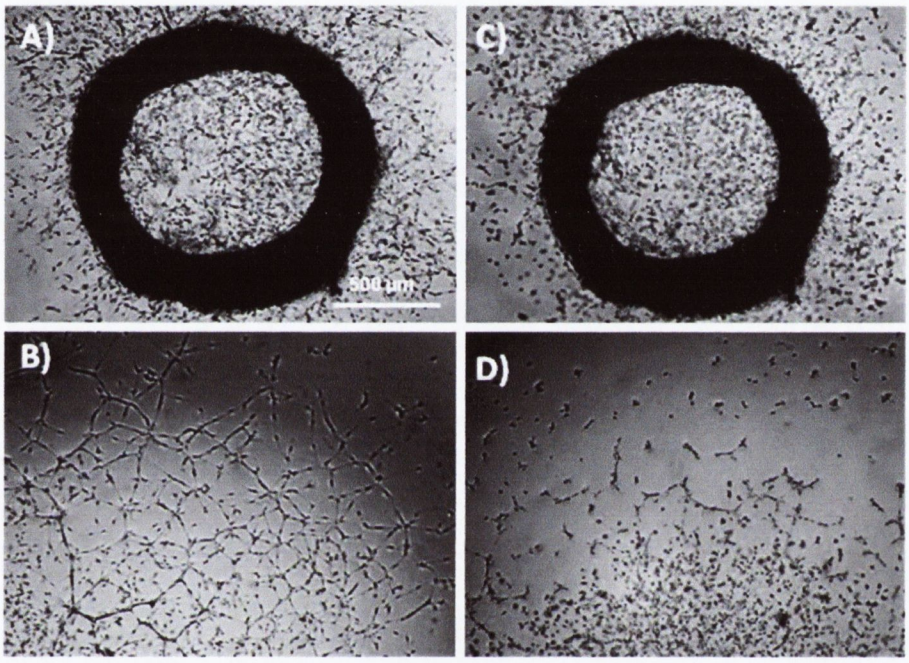

Figure 5.3: The anti-vascular effect of ECB397. The aortic rings were kept in a humidified CO_2 incubator at 37 °C and the medium was changed every other day, starting from day 3. Test compounds were added on day 8. Photomicrographs of the aortic cultures were taken under bright field microscopy using a digital camera (x4). **A-B)** Before the addition of test compound and **C-D)** 1 μM ECB397 (24h).

5.3.1.3 Group IV Hybrid

The anti-vascular effect of ADR469 was investigated in the aortic ring assay. Treatment of the ring cultures with 1 and 10 nM ADR469 did not demonstrate any obvious anti-vascular activity, whereas 50 nM was sufficient to disrupt the microvessel network, even after 4h treatment. The effect was more evident after 24h (Figure 5.4).

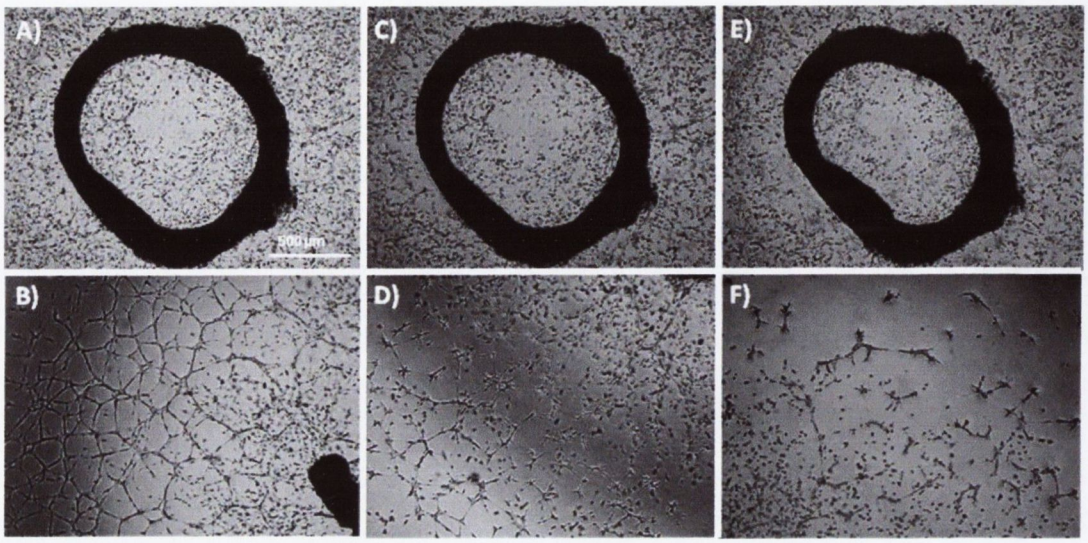

Figure 5.4: The anti-vascular effect of ADR469. The aortic rings were kept in a humidified CO_2 incubator at 37 °C and the medium was changed every other day, starting from day 3. Test compounds were added on day 8. Photomicrographs of the aortic cultures were taken under bright field microscopy using a digital camera (x4). **A-B)** Before the addition of test compound, **C-D)** 50 nM ADR469 (4h) and **E-F)** 50 nM ADR469 (24h).

5.3.1.4 Designed Multiple Ligand

BWM120 was examined for evidence of anti-vascular activity in the aortic ring assay. At 1 μM, BWM120 demonstrated satisfactory activity following 4h incubation and the effect was more evident following 24h treatment, whereby a clear microvessel disruption was observed (Figure 5.5).

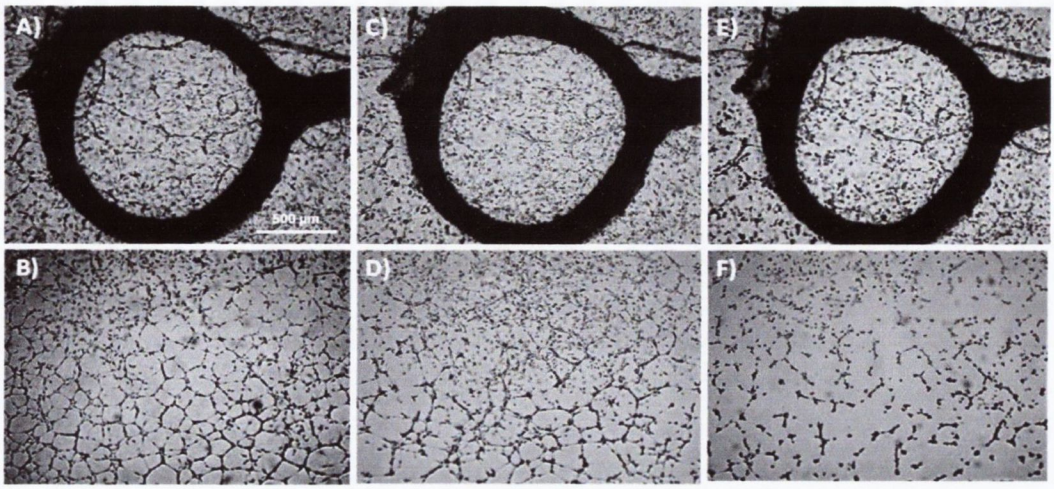

Figure 5.5: The anti-vascular effect of BWM120. The aortic rings were kept in a humidified CO_2 incubator at 37 °C and the medium was changed every other day, starting from day 3. Test compounds were added on day 8. Photomicrographs of the aortic cultures were taken under bright field microscopy using a digital camera (x4). **A-B)** Before the addition of test compound, **C-D)** 1 μM BWM120 (4h) and **E-F)** 1 μM BWM120 (24h).

5.3.2 Aortic Ring Assay (anti-angiogenic model)

In addition to the anti-vascular activity, the anti-angiogenic properties of test compounds were assessed in the aortic ring assay. These compounds were designed to target tubulin polymerisation and APN. The anti-angiogenic activity of both tubulin and APN inhibitors has been well-established in the literature. It was hypothesised that an additive or synergistic effect should be observed following treatment with test compounds. The microvessel density was determined by analysing the images using Image J and the results were expressed in terms of mean pixel density area ± SEM.

5.3.2.1 Group I Hybrid

ECB378 was assessed for its ability to inhibit the formation of a microvessel network in the aortic ring assay. Cultures incubated with 1 μM ECB378 resulted in an insignificant lower microvessel density compared to that of the control treated cultures; however 10 μM ECB378 significantly ($p < 0.01$) inhibited the vessel growth (Figure 5.6 and 5.7).

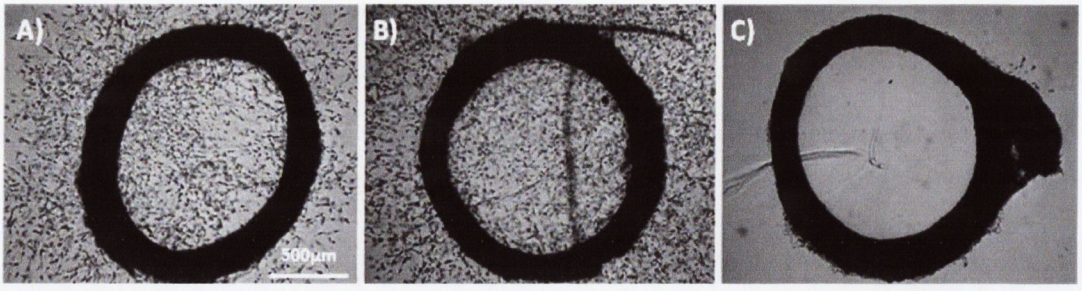

Figure 5.6: The anti-angiogenic effect of ECB378. The aortic rings were kept in a humidified CO_2 incubator at 37 °C and the medium was changed every other day, starting from day 3. Test compounds were added on day 1. Photomicrographs of the aortic cultures were taken under bright field microscopy using a digital camera (x4). **A)** Control (0.1% DMSO), **B)** 1 µM ECB378 and **C)** 10 µM ECB378.

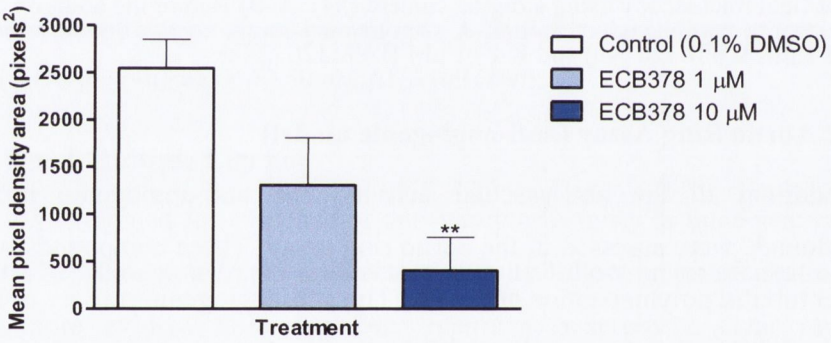

** $p < 0.01$, significantly lower mean pixel density area compared with the untreated controls as determined by Student's *t*-test.

Figure 5.7: The microvessel density of ECB378-treated cultures was obtained using Image J. Data represents mean pixel density area ± SEM (n=3).

5.3.2.2 Group II Hybrid

The anti-angiogenic properties of ECB397 were examined in the aortic ring assay. At 10 nM ECB397 an insignificant decrease in the microvessel density of the aortic rings was observed. Moreover, treatment with 100 nM ECB397 demonstrated a significant ($p < 0.05$) reduction in the number of microvessel growth (Figure 5.8 and 5.9).

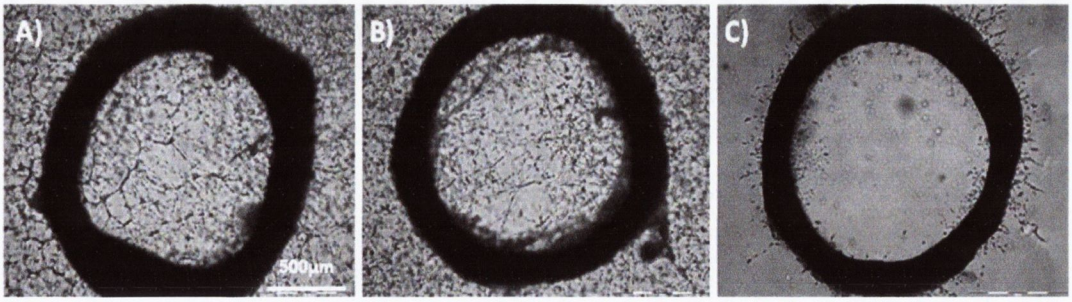

Figure 5.8: The anti-angiogenic effect of ECB397. The aortic rings were kept in a humidified CO_2 incubator at 37 °C and the medium was changed every other day, starting from day 3. Test compounds were added on day 1. Photomicrographs of the aortic cultures were taken under bright field microscopy using a digital camera (x4). **A)** Control (0.1% DMSO), **B)** 10 nM ECB397 and **C)** 100 nM ECB397.

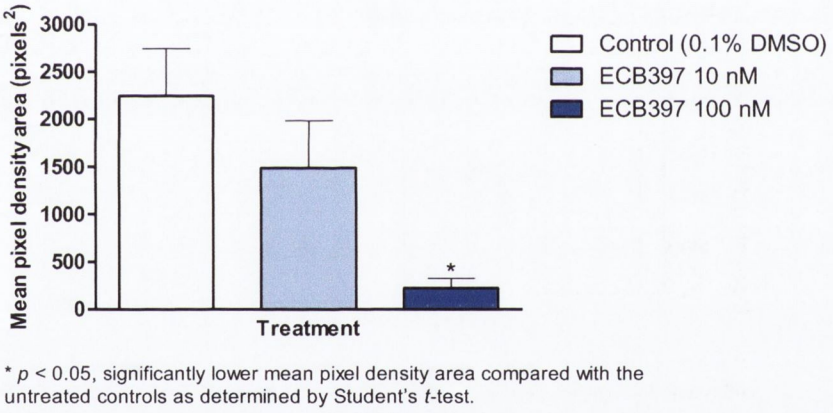

Figure 5.9: The microvessel density of ECB397-treated cultures was obtained using Image J. Data represents mean pixel density area ± SEM (n=3).

5.3.2.3 Group IV Hybrid

The ability of ADR469 to inhibit angiogenesis was evaluated in the aortic ring assay. Microvessel density was insignificantly decreased at 10 nM ADR469, whereas 50 nM caused almost complete inhibition ($p < 0.01$) of the microvessel growth (Figure 5.10 and 5.11).

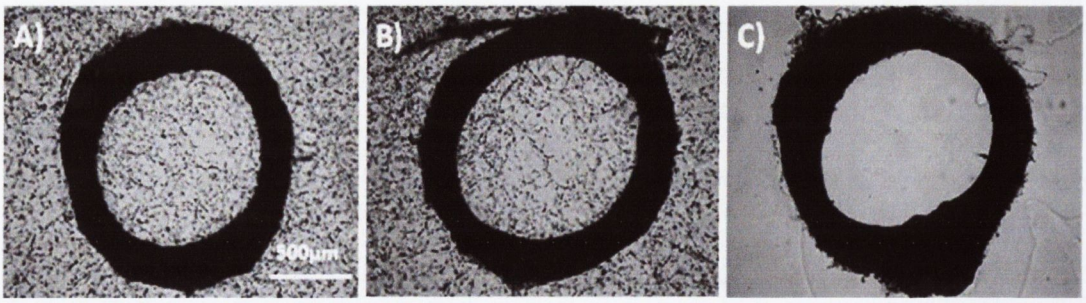

Figure 5.10: The anti-angiogenic effect of ADR469. The aortic rings were kept in a humidified CO_2 incubator at 37 °C and the medium was changed every other day, starting from day 3. Test compounds were added on day 1. Photomicrographs of the aortic cultures were taken under bright field microscopy using a digital camera (x4). **A)** Control (0.1% DMSO), **B)** 10 nM ADR469 and **C)** 50 nM ADR469.

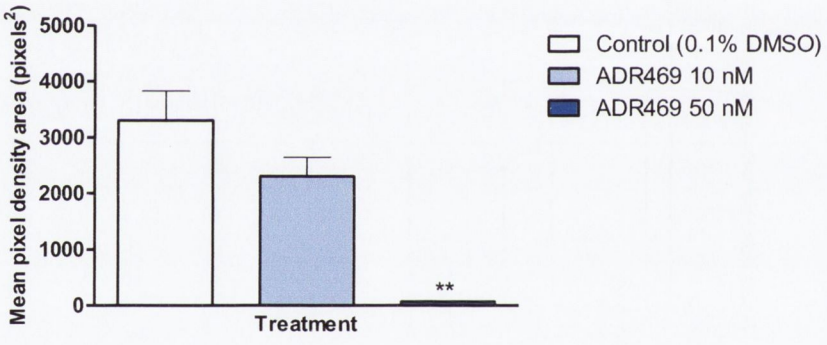

Figure 5.11: The microvessel density of ADR469-treated cultures was obtained using Image J. Data represents mean pixel density area ± SEM (n=3).

5.3.2.4 Designed Multiple Ligand

The anti-angiogenic effect of BWM120 was determined in the aortic ring assay. Cultured rings treated with 0.1 µM BWM120 showed a negligible reduction in the microvessel area, whereas treatment with 1 µM BWM120 resulted in a significantly ($p < 0.01$) lower microvessel density compared to the control cultures (Figure 5.12 and 5.13).

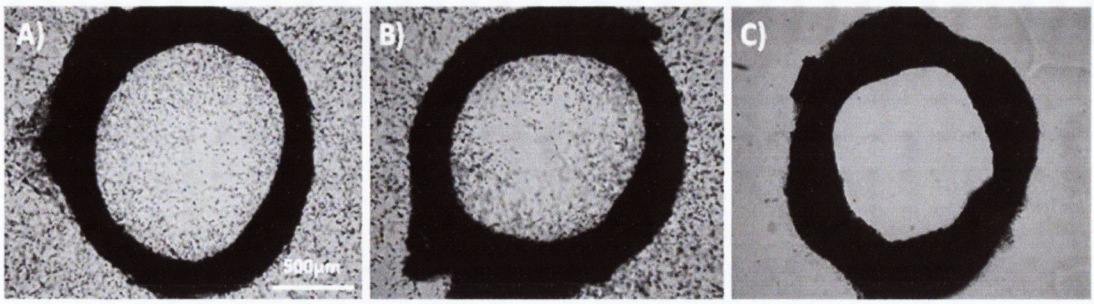

Figure 5.12: The anti-angiogenic effect of BWM120. The aortic rings were kept in a humidified CO_2 incubator at 37 °C and the medium was changed every other day, starting from day 3. Test compounds were added on day 1. Photomicrographs of the aortic cultures were taken under bright field microscopy using a digital camera (x4). **A)** Control (0.1% DMSO), **B)** 0.1 µM BWM120 and **C)** 1 µM BWM120.

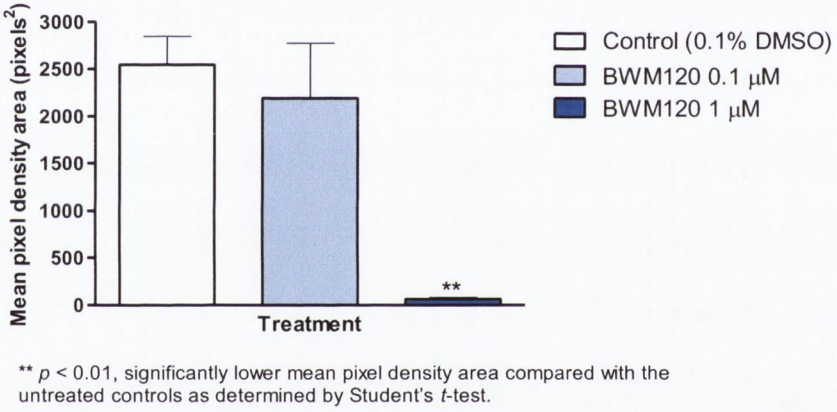

Figure 5.13: The microvessel density of BWM120-treated cultures was obtained using Image J. The data represents mean pixel density area ± SEM (n=3).

5.3.3 *In Vivo* Anti-tumour Evaluation

Following the promising results obtained from the *in vitro* and *ex vivo* assays, selected compounds were evaluated in a s.c. PC-3 tumour xenograft model. Two-dimensional tumour measurements were recorded every other day and tumour volumes were calculated as previously described. Semi-log plots of mean RTVs *vs* duration (days) were generated for each treatment.

5.3.3.1 Group I Hybrid

The anti-tumour effect of 40 mg/kg ECB378 was investigated in a PC-3 tumour xenograft by i.p. administration on alternate days for 12 days. The control group was administered with the vehicle (5% DMSO, 5% Tween® 80 in wfi) at the same dose regimen. According to the estimated RTVs, treatment with 40 mg/kg ECB378 did not demonstrate any apparent reduction in the rate of tumour growth. However, on the final day of the study a noticeable difference between the tumour volume of the ECB378-treated and control tumours was observed (Figure 5.14). The RTV2 of treated and control groups was calculated with the difference in growth delay determined to be 2.2 days. However, the minor reduction in tumour growth delay was not statistically significant.

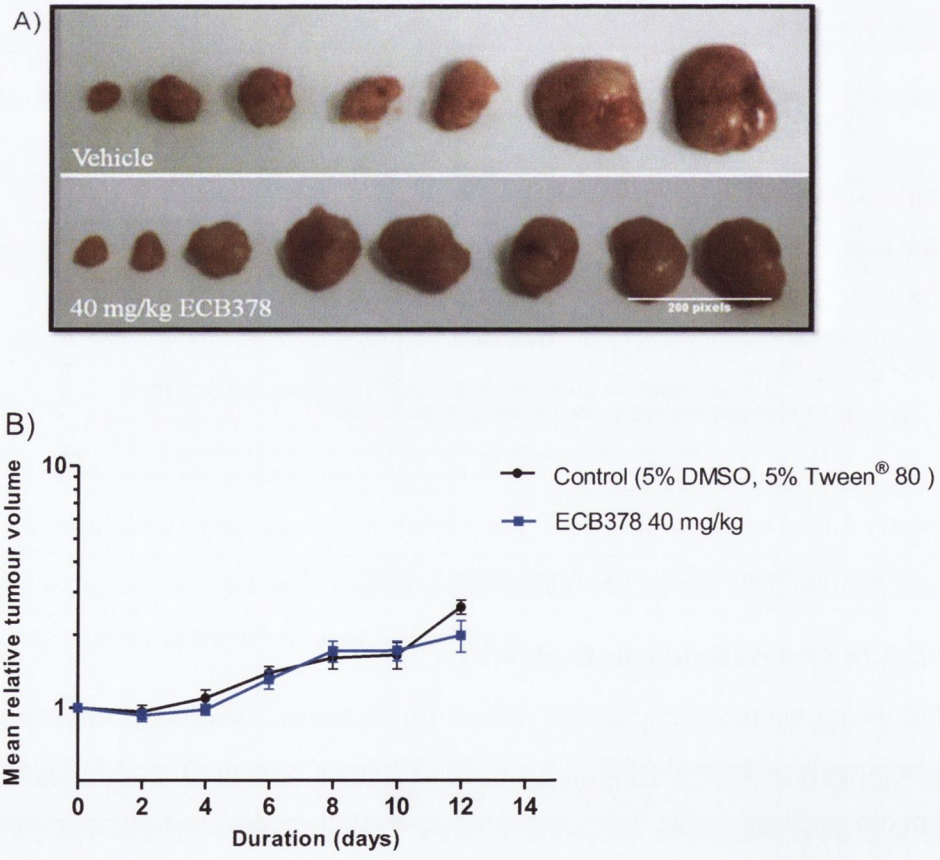

Figure 5.14: Evaluation of the efficacy of 40 mg/kg ECB378 administered i.p. on alternate days for 12 days in a PC-3 tumour xenograft model. **A)** Control and treated tumours obtained after completion of the study, **B)** data represents the mean relative tumour volume ± SEM (n=7-8).

BW measurements were recorded every other day in order to determine any systemic toxicity caused by the duration of the treatment. The percentage of BW was then calculated as shown in Figure 5.15. A noticeable but insignificant decline of BW was observed following treatment with ECB378, which was maintained above the 85% limit; however the BW showed some recovery from day 8 of treatment.

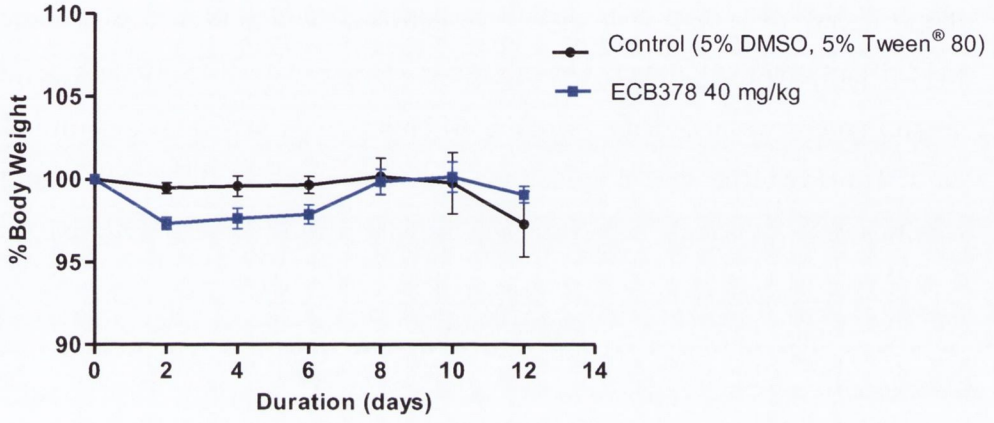

Figure 5.15: Body weight measurements were recorded to monitor any systemic toxicity following treatment with ECB378. Data represents the mean percentage body weight ± SEM (n=7-8).

The data obtained from the *in vivo* efficacy study with 40 mg/kg ECB378, including the mean RTV2, the growth delay and the maximum percentage of weight loss is summarised in Table 5.1.

Table 5.1: Summary of ECB378 *in vivo* data.

Treatment	Dose (mg/kg)	Mean RTV2 (days)	Growth delay (days)	Max % weight loss (day)
Vehicle	5% DMSO 5% Tween® 80	10.45	-	2.71 (12)
ECB378	40	12.65	2.2	2.67 (2)

5.3.3.2 Group II Hybrid

The *in vivo* efficacy of 40 mg/kg ECB397 was evaluated in a s.c. PC-3 tumour xenograft model by i.p. administration on alternate days for 12 days. For comparison

purposes, a 1:1 combination of RS180-leu/bestatin was administered i.p. at an equimolar concentration as per ECB397. The control group was treated with i.p. administration of vehicle (5% DMSO, 5% Tween® 80 in wfi) at the same dose regimen. Treatment with 40 mg/kg ECB397 demonstrated a noticeable reduction in the tumour volume compared to that of the vehicle treatment, whereas RS180-leu/bestatin combination did not show any evidence of anti-tumour activity (Figure 5.16). Statistical analysis using the Mann-Whitney *U*-test was performed individually on each day in order to examine any significant difference between the ECB397 and control group, where significance ($p < 0.05$) was detected on days 2, 6 and 12. The estimated RTV2 of ECB397-treated and control groups was calculated and the difference in growth delay was 10.8 days, whereas for RS180-leu/bestatin treatment the growth delay was -4.08 days.

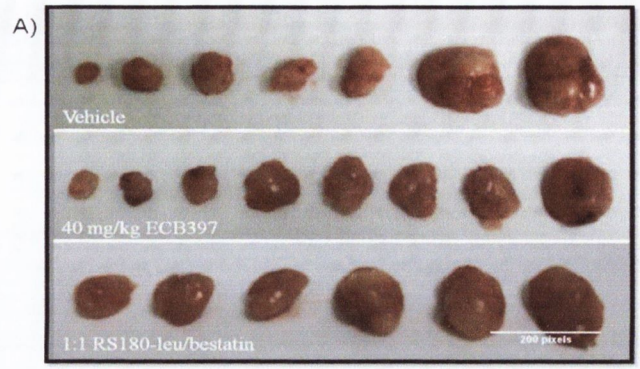

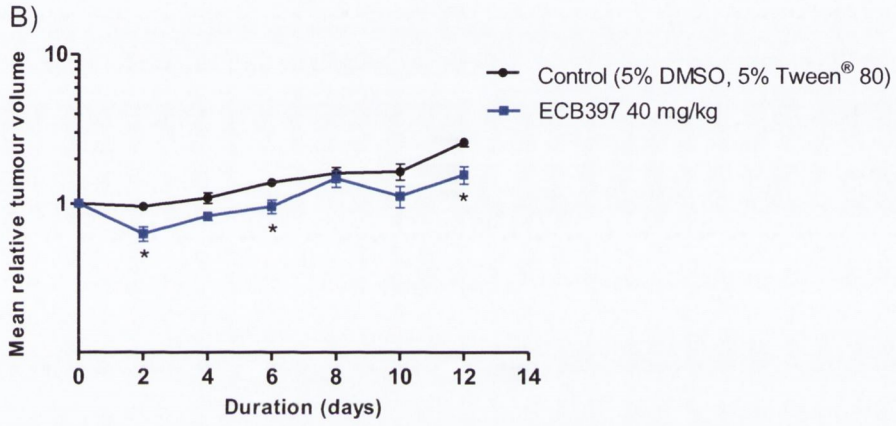

* $p < 0.05$, significantly lower mean relative tumour volume compared with the control group as determined by the Mann-Whitney *U*-test.

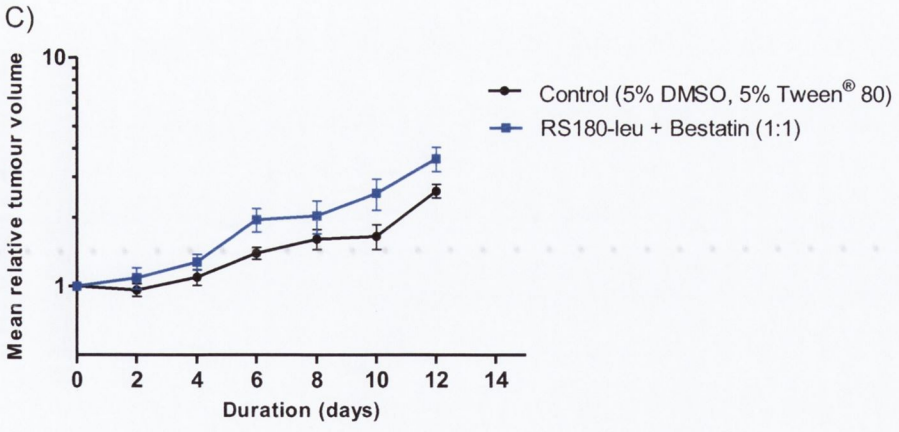

Figure 5.16: **A)** Control and treated tumours obtained after completion of the study. Evaluation of the efficacy of **B)** 40 mg/kg ECB397 and **C)** 1:1 RS180-leu/bestatin combination at equimolar concentration as per ECB397 administered i.p. on alternate days for 12 days in a PC-3 tumour xenograft model. Data represents the mean relative tumour volume ± SEM (n=6-8).

To monitor any potential systemic toxicity caused throughout the duration of the treatments, BW measurements were recorded every other day. The percentage of BW was then calculated for each group (Figure 5.17). There was no observable reduction in BW in either treated group.

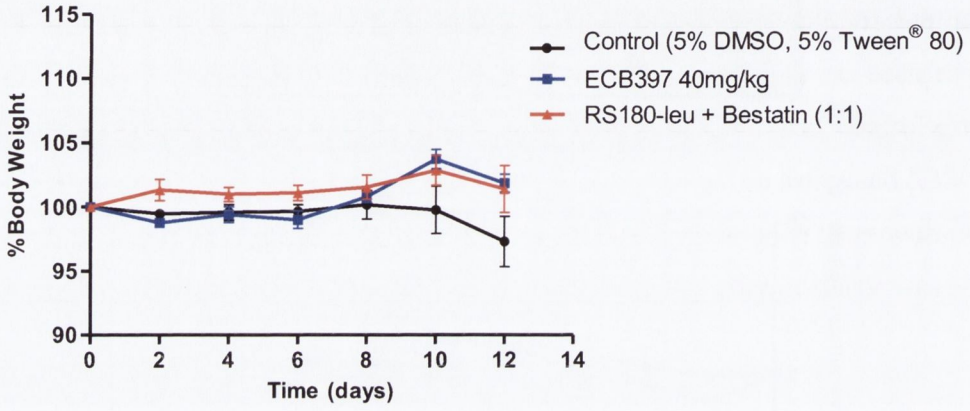

Figure 5.17: Body weight measurements were recorded to monitor any systemic toxicity following treatment with ECB397 and RS180-leu/bestatin. Data represents the mean percentage body weight ± SEM (n=6-8).

The data generated from the *in vivo* efficacy study with 40 mg/kg ECB397 and a 1:1 combination of RS180-leu/bestatin, including the mean RTV2, the growth delay and the maximum percentage of weight loss is summarised in Table 5.2.

Table 5.2: Summary of ECB397 and RS180-leu/bestatin *in vivo* data.

Treatment	Dose (mg/kg)	Mean RTV2 (days)	Growth delay (days)	Max % weight loss (day)
Vehicle	5% DMSO 5% Tween® 80	10.45	-	2.71 (12)
ECB397	40	21.25	10.8	1.23 (2)
RS180-leu + Bestatin	Equimolar dose	6.37	-4.08	None

5.3.3.3 Group IV Hybrid

The anti-tumour activity of 50 mg/kg ADR469 was examined in a PC-3 tumour xenograft model by i.p. administration on alternate days for 24 days. Control treated group was administered with vehicle (10% DMSO in wfi) at the same dose regimen. An evident difference of tumour growth was observed between the ADR469 and control treated groups (Figure 5.18). Statistical analysis using the Mann-Whitney *U*-test was performed individually on each day in order to examine any significant difference between ADR469 and control group, where significance ($p < 0.05$) was detected on days 4, 6, 10, 12 and 16. According to the estimated RTV2s, the difference in tumour growth delay between the ADR469 and control treated groups was 4.42 days.

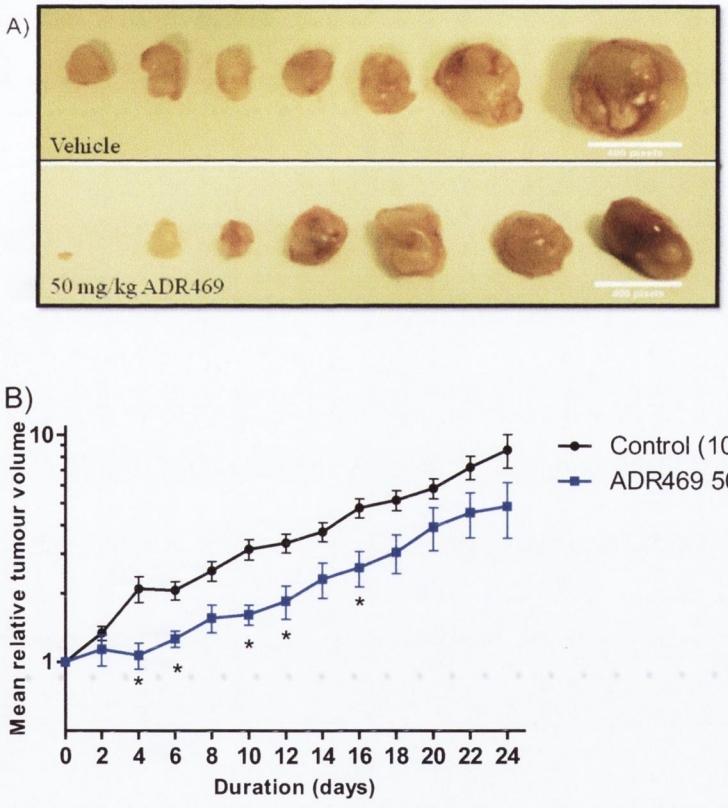

* $p < 0.05$, significantly lower mean relative tumour volume compared with the control group as determined by the Mann-Whitney *U*-test.

Figure 5.18: **A)** Control and treated tumours obtained after completion of the study. **B)** Evaluation of the efficacy of 50 mg/kg ADR469 administered i.p. on alternate days for 24 days in a PC-3 tumour xenograft model. Data represents the mean relative tumour volume ± SEM (n=7).

BW measurements were recorded every other day in order to observe any systemic toxicity caused throughout the duration of the treatment. The percentage of BW was then calculated for each group (Figure 5.19). A slight decrease of BW was noted in the ADR469-treated group, with maximum loss on day 14; however this was within the limits and the animals showed evidence of recovery from day 16.

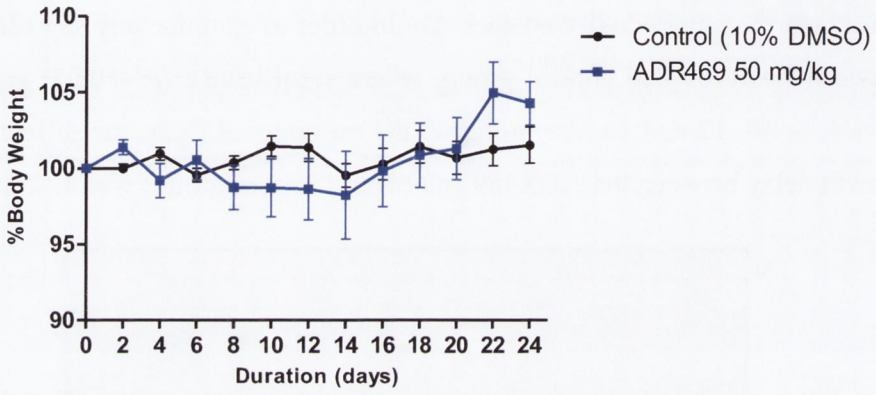

Figure 5.19: Body weight measurements were recorded to monitor any systemic toxicity following treatment with ADR469. Data represents the mean percentage body weight ± SEM (n=7).

The data obtained from the *in vivo* efficacy study with 50 mg/kg ADR469 including the mean RTV2, the growth delay and the maximum percentage of weight loss is summarised in Table 5.3.

Table 5.3: Summary of ADR469 *in vivo* data.

Treatment	Dose (mg/kg)	Mean RTV2 (days)	Growth delay (days)	Max % weight loss (day)
Vehicle	10% DMSO	5.33	-	0.46 (14)
ADR469	50	9.75	4.42	1.77 (14)

5.3.3.4 Designed Multiple Ligand

The effect of 40 mg/kg BWM120 on tumour growth was investigated in a s.c. PC-3 tumour xenograft by i.p. administration on alternate days for 12 days. The control treated group was administered with vehicle (5% DMSO, 5% Tween® 80 in wfi) at the

same dose regimen. Initially, a minor reduction in the volume of BWM120-treated tumours was noted up to day 4; however following this, BWM120 treatment did not provide any evidence of an anti-tumour effect (Figure 5.20). According to the estimated RTV2s, the difference in tumour growth between the BWM120 and control treated groups was -1.51 days.

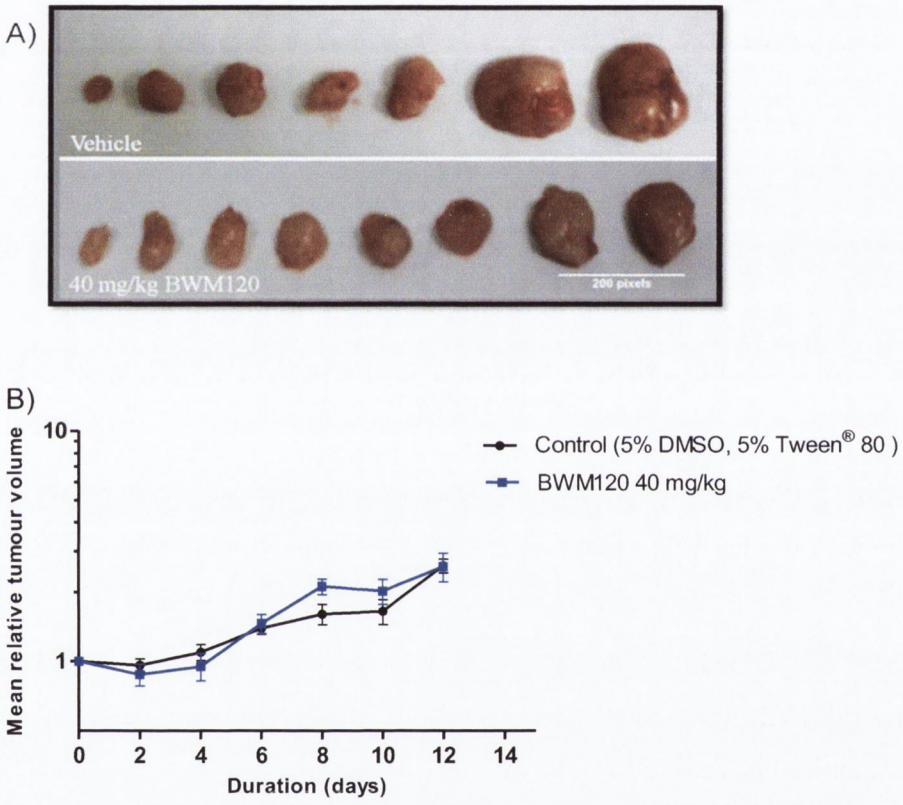

Figure 5.20: **A)** Control and treated tumours obtained after completion of the study. **B)** Evaluation of the efficacy of 40 mg/kg BWM120 administered i.p. on alternate days for 12 days in a PC-3 tumour xenograft model. Data represents the mean relative tumour volume ± SEM (n=7-8).

BW was monitored and recorded on alternate days in order to observe any signs of systemic toxicity induced by the treatment. The percentage of BW was then calculated for each group (Figure 5.21). A negligible weight loss was noted in the BWM120-treated group up to day 6, with maximum loss on day 2. Following that, animals' BW returned to normal.

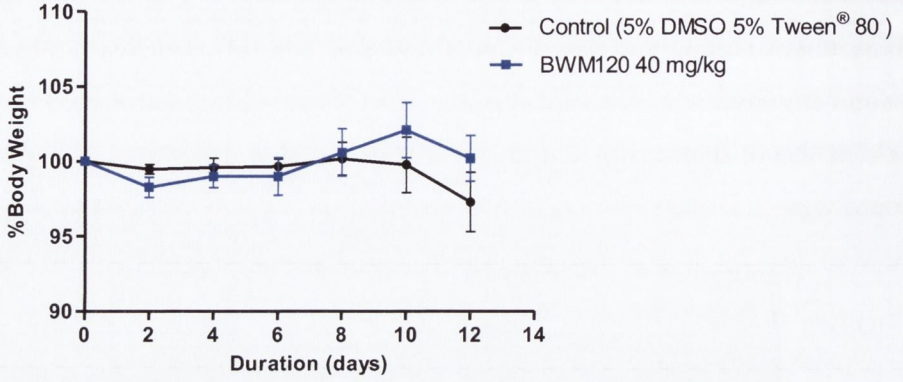

Figure 5.21: Body weight measurements were recorded to monitor any systemic toxicity following treatment with BWM120. Data represents the mean percentage body weight ± SEM (n=7-8).

The data generated from the *in vivo* efficacy study with 40 mg/kg BWM120 including the mean RTV2, the growth delay and the maximum percentage of weight loss is summarised in Table 5.4.

Table 5.4: Summary of BWM120 *in vivo* data.

Treatment	Dose (mg/kg)	Mean RTV2 (days)	Growth delay (days)	Max % weight loss (day)
Vehicle	5% DMSO 5% Tween® 80	10.45	-	2.71 (12)
BWM120	40	8.94	-1.51	1.73 (2)

5.3.4 Assessment of Tumour Necrosis

Following the completion of the *in vivo* efficacy study with test compounds, histological examination of tumours from each group was carried out. Treated and control tumours were processed for H&E staining. Tumour sections were examined microscopically and images from each group were captured. Due to technical error in the paraffin-embedding procedure, processing of tumour samples from the ECB378, ECB397, RS180-leu/bestatin and BWM120 groups was not possible.

5.3.4.1 Group IV Hybrid

Three tumour samples from the ADR469 and control group were obtained and the extent of tumour necrosis was examined. It was noted that tumour size was correlated with the level of necrosis, *i.e.* the larger the tumour size, the higher the degree of necrosis observed. In this study, the variation of tumour size led to complications in data interpretation. Two of the control treated tumours exhibited a relatively smaller area of necrosis, whereas one larger-sized tumour displayed increased level of necrosis. In the ADR469-treated group, a small-sized tumour did not show any evidence of necrosis; however the remaining two medium-sized tumours showed large areas of haemorrhagic necrosis in the centre with a residual viable tissue found mainly in the periphery (Figure 5.22).

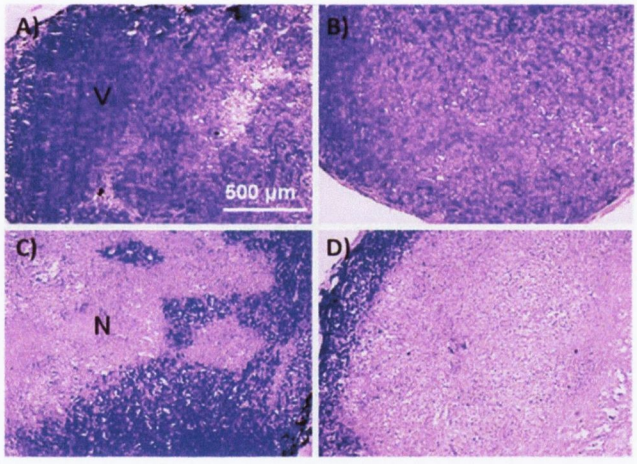

Figure 5.22: H&E stained tumour samples obtained from the **A-B)** control treated group and **C-D)** the ADR469-treated group. Images were capture using an inverted microscope (V=Viable, N=Necrotic, n=3).

5.3.5 Assessment of the Tumour Vasculature

To determine whether treatment with test compounds exerted an effect on the tumour vasculature, three tumours per group were excised at the end of the efficacy study and processed for endothelial cell staining. The tumour slides were examined using a confocal microscope and the images were analysed for functional endothelial cells. The results were expressed in terms of mean pixel density area ± SEM, as well as images of the tumour vasculature.

5.3.5.1 Group I Hybrid

The effect of 40 mg/kg ECB378 on tumour vasculature was examined following completion of the *in vivo* efficacy study. Three tumours from the ECB378 and control treated groups were analysed for the level of CD31 staining (Figure 5.23).

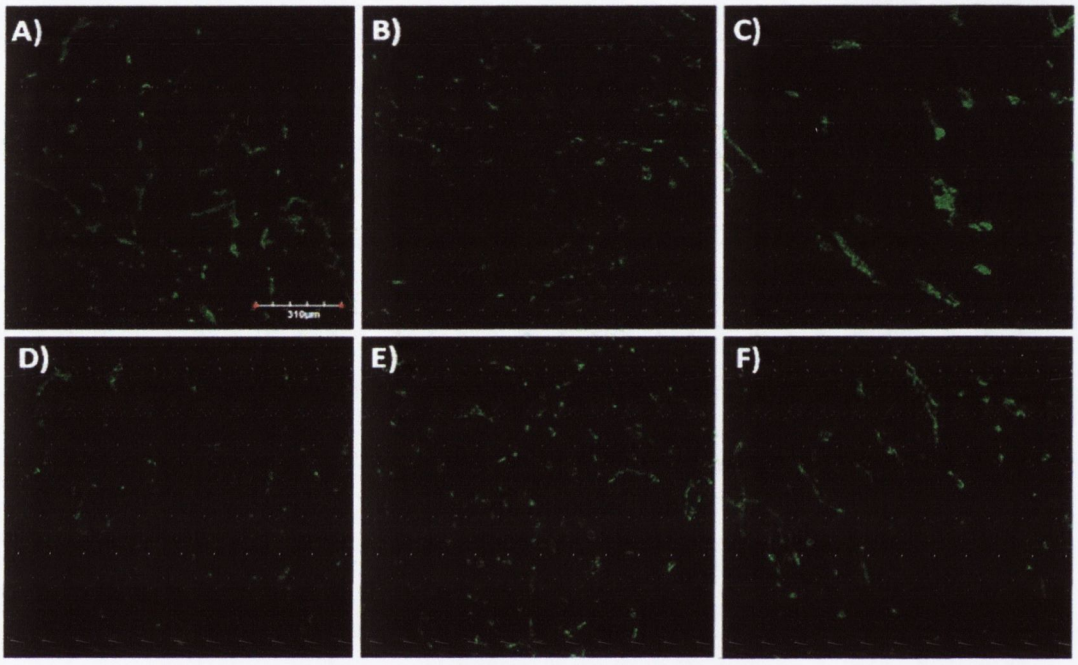

Figure 5.23: The effect of ECB378 treatment on the tumour vasculature. Images were captured using a confocal microscope (x10) of CD31-stained endothelial cells in cryo-sections of PC-3 tumours treated with **A-C)** control (5% DMSO, 5% Tween® 80) and **D-F)** 40 mg/kg ECB378 by i.p. administration on alternate days for 12 days (n=3).

ECB378-treated tumours did not show any evidence of anti-vascular or anti-angiogenic effect; instead the level of tumour vasculature area appeared slightly higher than that of the control treated tumours (Figure 5.24).

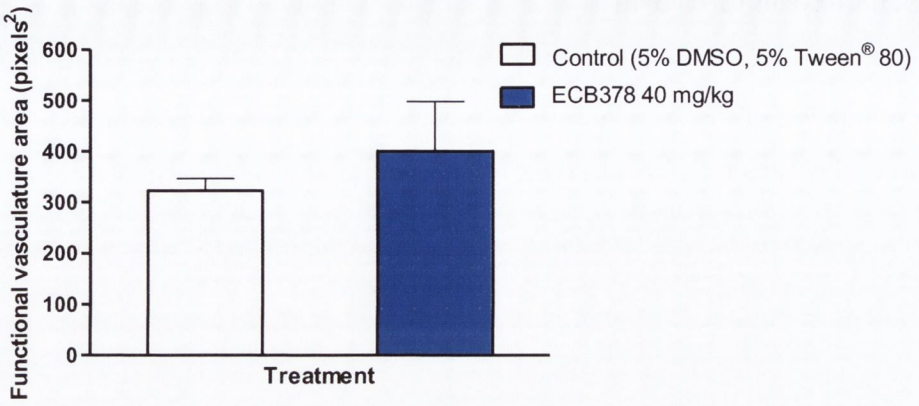

Figure 5.24: Quantification of functional vasculature area of tumours following i.p. administration of 40 mg/kg ECB378 on alternate days for 12 days, using Image J. Data represents mean functional vasculature area ± SEM (n=3).

5.3.5.2 Group II Hybrid

The effect of 40 mg/kg ECB397 and 1:1 combination of equimolar dose of RS180-leu/bestatin treatment on the tumour vasculature was determined following completion of the *in vivo* efficacy study. Treated and control tumours were analysed for the level of CD31-positive cells (Figure 5.25).

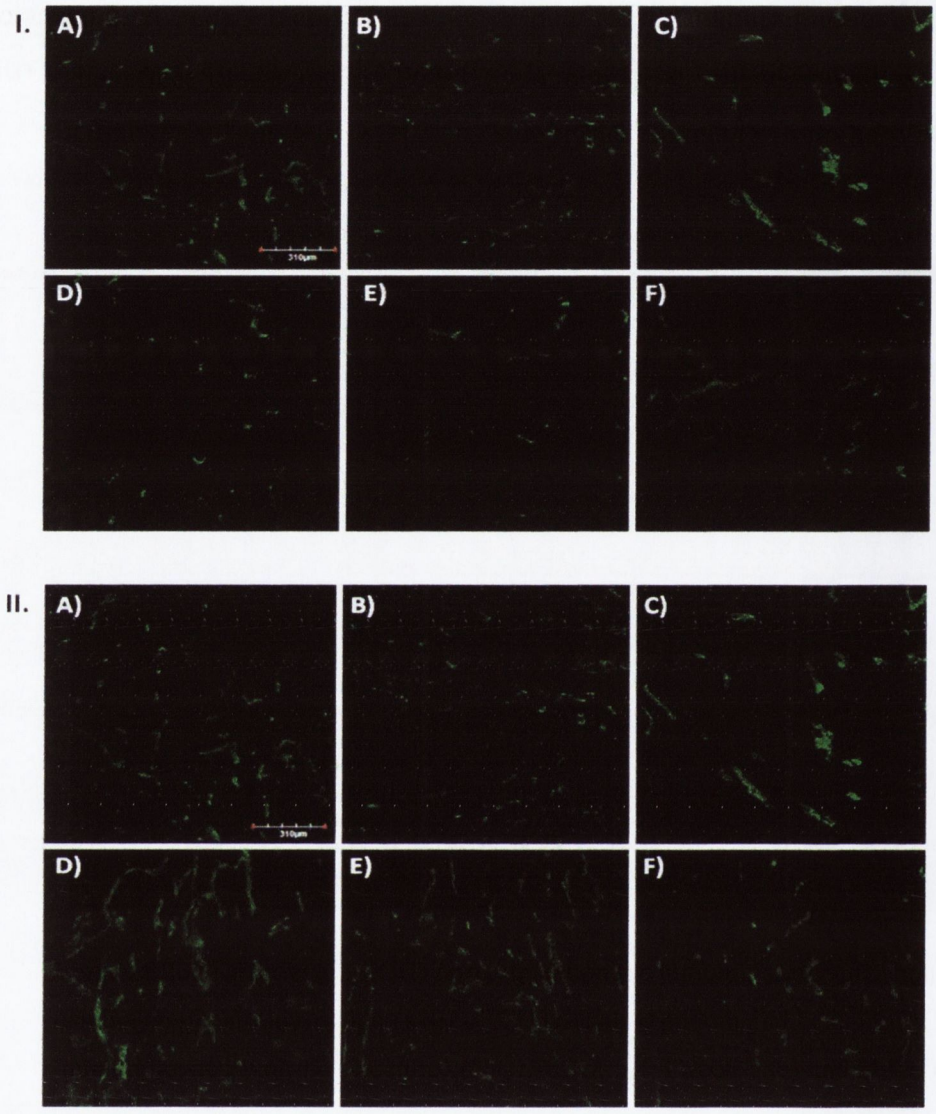

Figure 5.25: The effect of **I.** 40 mg/kg ECB397 and **II.** equimolar dose of RS180-leu/bestatin (1:1) treatment on tumour vasculature. Images were captured using a confocal microscope (x10) of CD31-stained endothelial cells in cryo-sections of PC-3 tumours treated with **A-C)** control (5% DMSO, 5% Tween® 80) and **D-F)** test compound by i.p. administration on alternate days for 12 days (n=3).

Following imaging processing of individual samples, a variation in the functional vasculature area between the ECB397 and control treated tumours was observed (Figure 5.26). Although the overall effect was not statistically significant (Figure 5.26 B), an evident reduction in the amount of CD31 staining was clearly noted in two out of three ECB397-treated tumour samples (Figure 5.26 A). In contrast, the 1:1 RS180-

leu/bestatin combination demonstrated a minor increase in the amount of functional tumour vasculature compared to that of the control tumours (Figure 5.25 B).

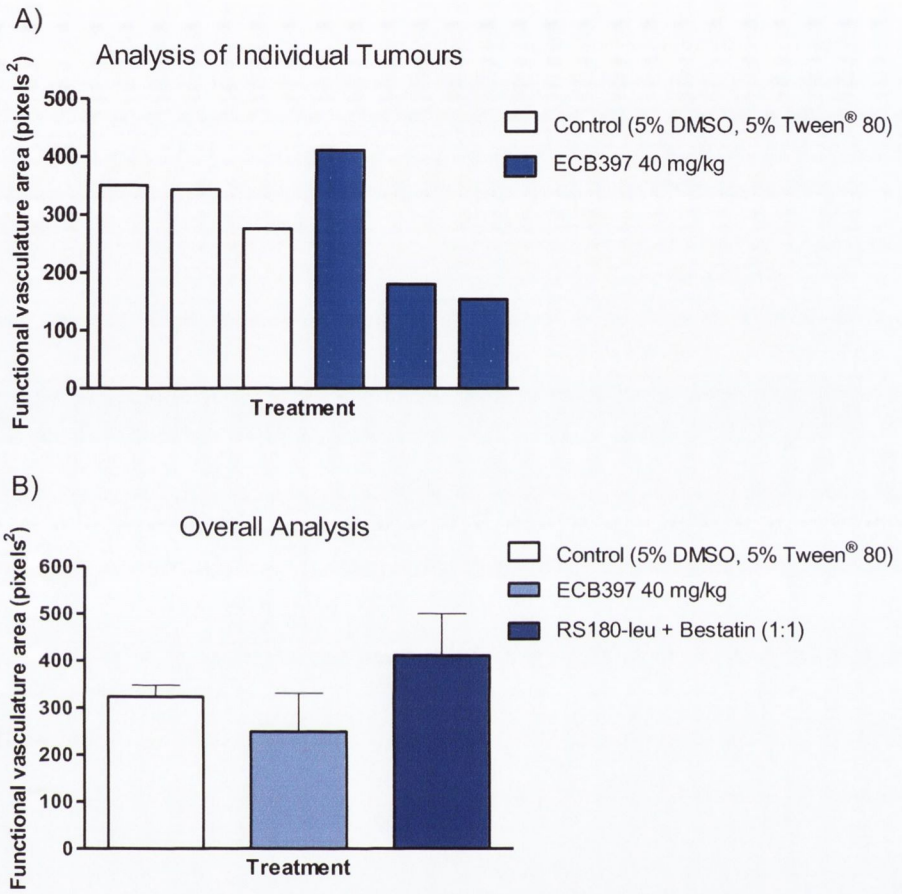

Figure 5.26: Quantification of functional vasculature area of tumours following i.p. administration of 40 mg/kg ECB397 or equimolar dose of RS180-leu/bestatin combination on alternate days for 12 days, using Image J. **A)** Analysis of individual control and ECB397-treated tumours and **B)** overall analysis. Data represents mean functional vasculature area ± SEM (n=3).

5.3.5.3 Group IV Hybrid

Once the *in vivo* efficacy study was completed, the anti-vascular/anti-angiogenic activity of 50 mg/kg ADR469 was assessed by examining the functional tumour vasculature. Three tumours from the ADR469 and control group were processed for endothelial cell staining (Figure 5.27).

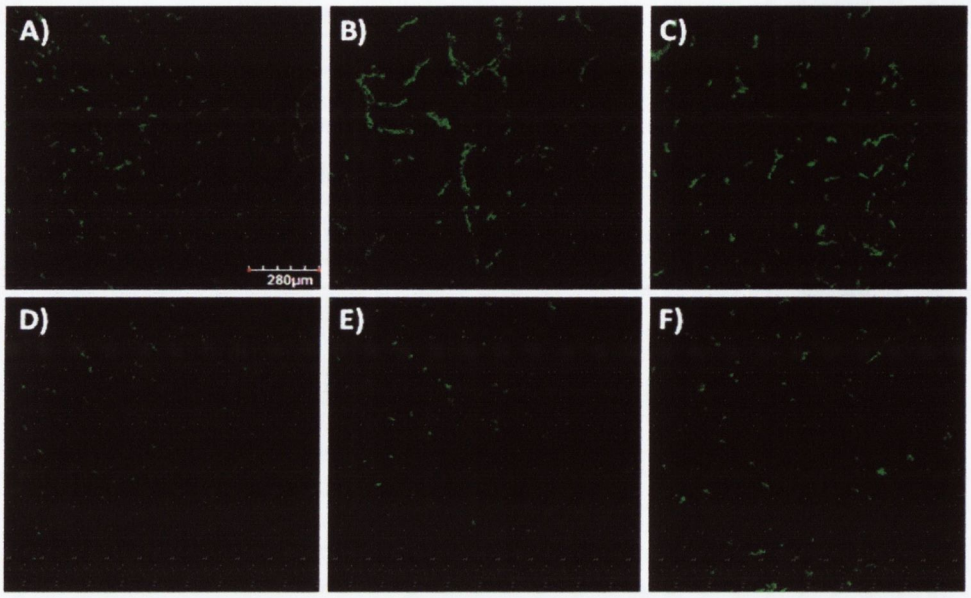

Figure 5.27: The effect of ADR469 treatment on tumour vasculature. Images were captured using a confocal microscope (x10) of CD31-stained endothelial cells in cryo-sections of PC-3 tumours treated with **A-C)** control (10% DMSO) and **D-F)** 50 mg/kg ADR469 by i.p. administration on alternate days for 24 days (n=3).

According to the analysed data of individual samples, all three of the ADR469-treated tumours showed considerable reduction in their tumour vasculature area compared to the two control tumours, which displayed larger areas of functional vasculature. However, the remaining control treated tumour exhibited lower amount of CD31-positive cells compared to the other two (Figure 5.28 A). Therefore, analysis of the overall vasculature area from each group showed a noticeable yet insignificant reduction in the ADR469-treated tumours compared to that of the control tumours (Figure 5.28 B). In addition, stained blood vessels in the ADR469-treated tumours appeared to have a thinner diameter compared to those in the control group.

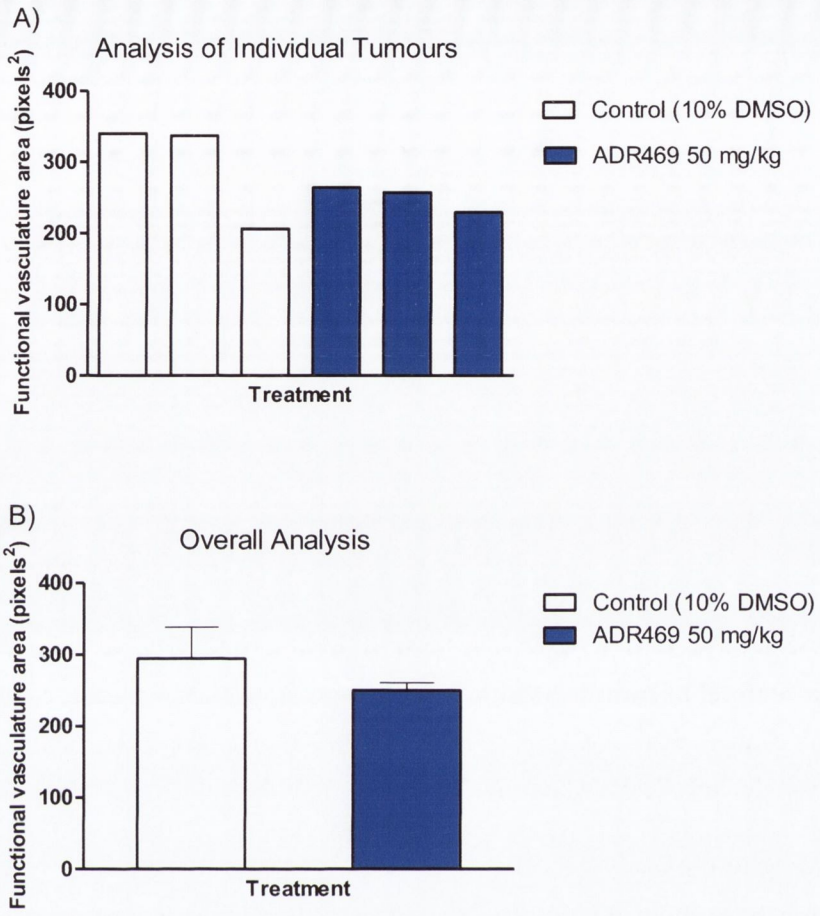

Figure 5.28: Quantification of functional vasculature area of tumours following i.p. administration of 50 mg/kg ADR469 on alternate days for 24 days, using Image J. **A)** Analysis of individual control and ADR469-treated tumours and **B)** overall analysis. Data represents mean functional vasculature area ± SEM (n=3).

5.3.5.4 Designed Multiple Ligand

Following the *in vivo* efficacy study with 40 mg/kg BWM120, the effect of treatment on the tumour vasculature was determined. Tumour samples obtained from the BWM120 and control treated group were processed for endothelial cells staining (Figure 5.29).

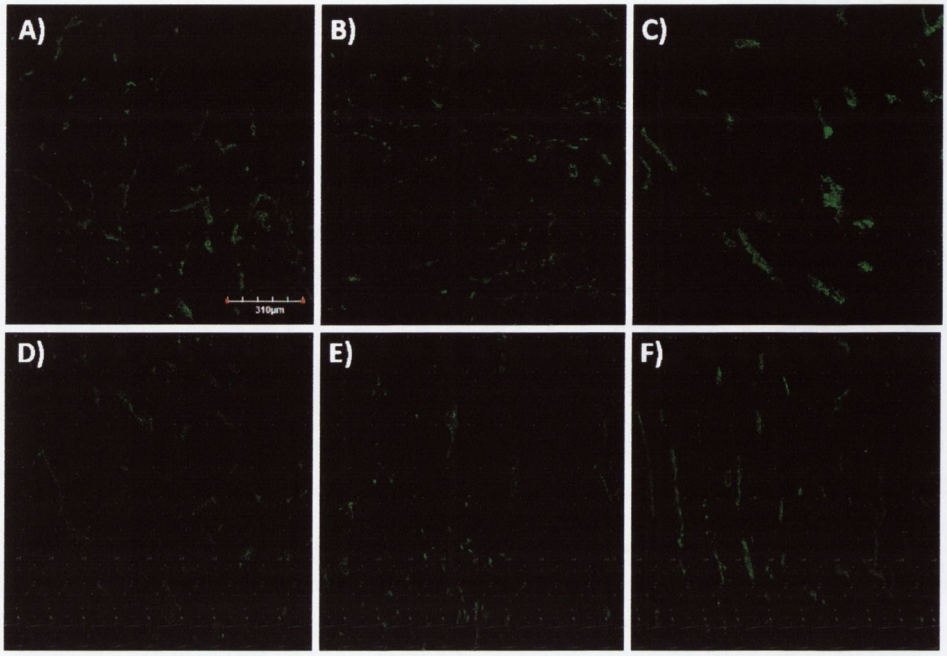

Figure 5.29: The effect of BWM120 treatment on tumour vasculature. Images were captured using a confocal microscope (x10) of CD31-stained endothelial cells in cryo-sections of PC-3 tumours treated with **A-C)** control (5% DMSO, 5% Tween® 80) and **D-F)** 40 mg/kg BWM120 by i.p. administration on alternate days for 12 days (n=3).

Imaging analysis of BWM120 and control treated tumours demonstrated similar levels in their functional vasculature without any noticeable decrease in the BWM120 tumours (Figure 5.30).

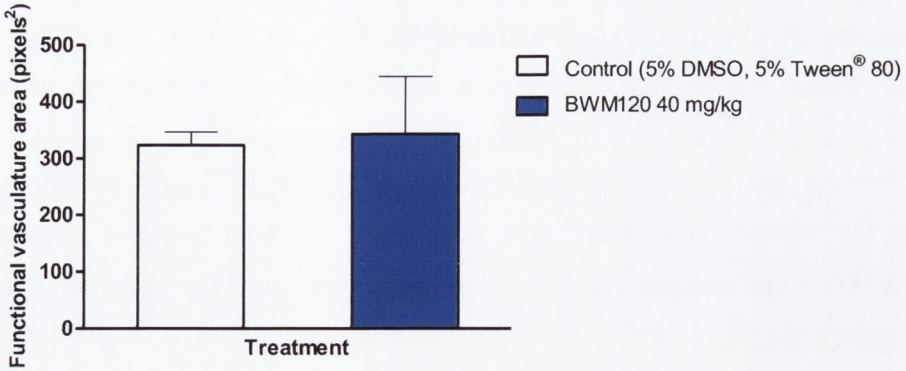

Figure 5.30: Quantification of functional vasculature area of tumours following i.p. administration of 40 mg/kg BWM120 on alternate days for 12 days, using Image J. Data represents mean functional vasculature area ± SEM (n=3).

5.4 Discussion

5.4.1 Aortic Ring Assay (anti-vascular model)

In addition to their *in vitro* anti-vascular effects, test compounds were further examined in the *ex vivo* aortic ring assay. All test compounds demonstrated an evident anti-vascular effect by disrupting the pre-established microvessel network of the aortic rings. However, depending upon the hybrid's design, the degree of potency varied. For instance, treatment with the active dual-targeting hybrid ECB378 resulted in a moderate anti-vascular activity at 25 μM (Figure 5.2, p.258). In contrast, ECB397 and ADR469 which were presented in a prodrug form demonstrated an anti-vascular effect at 1 μM (Figure 5.3, p.259) and 50 nM (Figure 5.4, p.260), respectively, verifying the release of their individual components. Similar observations were noted with RS180, the active tubulin targeting component of ECB397, which exhibited anti-vascular activity at 0.1 μM (Chapter 3, Figure 3.4, p.128). ADR269, the active tubulin targeting component of ADR469, displayed its effect at 50 nM (Chapter 3, Figure 3.6, p.129). The presentation of the tubulin binding component of the prodrug-from hybrids is not active, unless hydrolysis takes place. Although the bestatin component of these hybrids remains active in this presentation, the true anti-vascular effect was only going to be observed once the tubulin targeting component was released.

BWM120, whose design was largely inspired by RS180, exerted reasonable anti-vascular activity at 1 μM (Figure 5.5, p.261), suggesting incorporating the APN hydroxamic acid binding motif does not adversely affect its anti-vascular activity.

These findings concur with the *in vitro* preliminary data, confirming that test compounds do indeed disrupt the complex microvessel networks by inducing morphological changes to endothelial cells. The anti-vascular properties of the tubulin binding compounds were previously discussed in Chapter 3, section 3.5.1, p.148.

5.4.2 Aortic Ring Assay (anti-angiogenic model)

To determine the anti-angiogenic activity of test compounds, the aortic ring assay was performed. All compounds demonstrated reduction in the microvessel growth, an indication of angiogenesis inhibition. Once more, the level of potency was very much dependent on the hybrid's design. ECB378 was the least active hybrid which displayed

inhibition of angiogenesis at 10 μM (Figure 5.7, p.262). Although ECB397 demonstrated significant anti-angiogenic activity at 100 nM (Figure 5.9, p.263), it was slightly less potent than RS180 which inhibited the formation of microvessels at 10 nM (Chapter 3, Figure 3.14, p.134). ADR469 was the most potent hybrid which showed a significant anti-angiogenic effect at 50 nM (Figure 5.11, p.264), similar to that of ADR269 (Chapter 3, Figure 3.18, p.136). Treatment of the rings with 1 μM BWM120 resulted in a significant inhibitory effect at 1 μM (Figure 5.13, p.265), displaying a reduction in potency relative to RS180.

It was hypothesised that the angiogenic inhibitory profile of hybrids should demonstrate evidence of synergy, due to the anti-angiogenic properties exerted by both their tubulin targeting and bestatin component. However, bestatin's anti-angiogenic activity was previously established to be only evident at higher concentrations than those used in the aortic ring assay. For instance, 10 and 100 μg/mL (~ 30 and 300 μM) bestatin significantly inhibited the capillary tube formation of HUVECs seeded on matrigel [241]. In addition, 80 μM of bestatin and LYP demonstrated suppression of vascular endothelial cell tube formation *in vitro* [282]. Taking into account the lower potency of bestatin compared to the individual tubulin inhibitors of the hybrids, it is believed that the anti-angiogenic activity observed in the aortic ring assay was mostly contributed by the tubulin targeting component of the hybrids. The anti-angiogenic properties of tubulin binding agents were previously discussed in Chapter 3, section 3.5.2, p.149.

Although the evaluation of test compounds in this assay represented a more controlled environment, the results obtained can be justified when observed in tumour xenograft models.

5.4.3 *In Vivo* Anti-tumour Efficacy

Following the successful *in vitro* and *ex vivo* evaluation of test compounds, the next stage was to determine their anti-tumour efficacy in a s.c. PC-3 tumour xenograft model. It was previously established that continuous treatment with bestatin (or its related analogues) at doses as low as 2 and 20 mg/kg was sufficient to demonstrate an effective reduction in tumour growth [281-282, 593]. Hence, it was decided that treatment of tumour bearing mice with test compounds at relatively low doses should not only exhibit an anti-tumour effect but should also demonstrate evidence of synergy.

Interestingly, i.p. administration of 40 mg/kg ECB378 on alternate days for 12 days did not cause reduction in tumour growth (Figure 5.14, p.266) and was associated with moderate systemic toxicity according to the BW measurements.

The anti-tumour effect of 40 mg/kg ECB397 following i.p. administration on alternate days for 12 days was not explicit (Figure 5.16, p.269). Although a decreased tumour growth was observed, the difference between it and control groups was significant only on days 2, 6 and 12. The 1:1 combination of RS180-leu/bestatin did not prove effective, suggesting that the design of ECB397 may provide an improved therapeutic outcome when administered *in vivo*, over the 1:1 combination treatment. The prodrug presentation of ECB397 was designed to selectively target APN-rich sites (such as proliferating endothelial cells mostly expressed in the tumour vasculature and also PC-3 cells), hence once residing in these regions was expected to undergo hydrolysis and release its individual component. BW measurements did not show any signs of drug-related toxicity, suggesting that treatment with ECB397 at the particular dose regimen was well-tolerated.

Taking into consideration the results acquired from the previous *in vivo* studies, some adjustments were made in an attempt to potentiate the activity of ADR469. Subsequently, the treatment dose was increased to 50 mg/kg and the duration of the study was prolonged up to 24 days. The anti-tumour effect of i.p. administration of 50 mg/kg ADR469 on alternate days was noticeable throughout the duration of the study (Figure 5.18, p.271). A decreased rate of tumour growth was observed in the ADR469-treated group compared to that of the control group, with significant differences on days 4, 6, 10, 12 and 16. An observable decrease in BW was noted following treatment with ADR469, which indicated an insignificant drug-induced toxicity.

To date, ADR469 has proven to be the hybrid with the most potential *in vivo* and this was in agreement with the *in vitro* and *ex vivo* data. However, 1:1 combination studies of ADR269 and bestatin are essential in order to investigate whether its design provides an improved pharmacological profile over combination treatment.

It is worthwhile to note that the anti-tumour effect of bestatin was examined using the NaUCC-4 choriocarcinoma xenograft model and demonstrated a significant effect by

daily i.p. administration for 4 weeks at doses of 2 and 20 mg/kg [593]. Furthermore, Gao *et al.* reported that 100 μmol/kg of bestatin or LYP significantly reduced the tumour growth of ES-2 xenografts in athymic mice, following daily i.v. administration for 2 weeks [281]. Pasqualini *et al.* showed that i.p. administration of 250 μg/mouse bestatin once a week for 3 weeks resulted in an evident decrease of MDA-MB-435 breast carcinoma xenografts [199]. Moreover, i.v. administration of 100 mg/kg bestatin or CIP-13F (a cyclic-imide peptidomimetics compound) performed daily for 3 consecutive weeks using a s.c. Lewis lung carcinoma xenograft model, resulted in a significant tumour growth delay [594].

The evidence from the literature indicated that bestatin's anti-tumour effect was evident in a variety of human tumour xenografts. In addition, bestatin inhibited the growth of syngeneic tumours, including colon adenocarcinoma 26 (colon 26) and myeloid leukaemia C1498 (C1498), but not the growth of colon 26 tumours in *balb-c* athymic mice [247]. Spleen cells taken from mice bearing colon 26 and C1498 did not neutralise the corresponding tumour. In contrast, when bestatin was administered to these mice, spleen cells obtained from the administered mice did neutralise the corresponding tumour. This result suggested that bestatin enhanced natural killer cell activity of the spleen cells of colon 26-bearing mice. It was indicated that bestatin exhibited its anti-tumour effect indirectly by immunomodulation *via* spleen cells and possibly *via* T cells [247]. In addition, bestatin has shown to modulate macrophage-mediated cytotoxicity, by increasing their secretory activity of acid hydrolases and the prostaglandins E2 and F2a [595]. Although athymic mice have been previously used in bestatin-related *in vivo* models, the use of immunocompromised mice in our studies could be a possible explanation for the reduced anti-tumour activity observed with our hybrids, due to the absence of bestatin's immunomodulator effect.

Furthermore, 40 mg/kg BWM120 was evaluated in the PC-3 tumour xenograft model, by i.p. administration on alternate days for 12 days. Treatment with BWM120 failed to verify its anti-tumour effect *in vivo* (Figure 5.20, p.273), where it demonstrated reasonable activity *in vitro* and *ex vivo* and particularly exhibited potent APN inhibitory properties. According to the BW measurements, there was no sign of systemic toxicity observed following treatment with BWM120 at the particular dose regimen. Possible

explanations for BWM120 minimal anti-tumour effect could be due to its administration at a non-effective dose (40 mg/kg).

Krige *et al.* reported that i.p. administration of 100 mg/kg/day CHR-2797 (a hydroxamate-based APN inhibitor) for two weeks resulted in a moderate anti-tumour effect using the MDA-MB-468 human breast adenocarcinoma xenograft, whereas daily oral administration of 3, 10 or 30 mg/kg CHR-2797 demonstrated a more pronounced effect using HOSP-1 and HSN LV10 rodent cancer models [576].

The *in vivo* anti-tumour efficacy mediated directly by a tubulin targeting agent, was previously discussed in Chapter 3, section 3.5.4, p.151. Several *in vivo* studies were conducted using dual-targeting conjugates or immunoconjugates, with one of their components being a tubulin binding agent. For instance, MTC-220 hybrid comprised of PTX and a muramyl dipeptide analogue (an immunomodulator), was synthesised as a novel agent possessing dual anti-tumour and anti-metastatic activities. *In vivo* studies indicated that the hybrid exhibited inhibition of tumour growth, superior to that of PTX alone, and prevented tumour metastasis in Lewis lung carcinoma and 4T1 tumour bearing mice [596]. In addition, SAR3419, a novel anti-CD19 humanised monoclonal antibody (for B-cell selectivity) conjugated to a maytansine derivate (a tubulin targeting agent) through a cleavable linker, was reported for the treatment of B-cell malignancies. Single or multiple dose administration of SAR3419 resulted in a complete treatment response with tumour-free animals at the study termination point, at the highest doses administered. At the lower doses, SAR3419 treatment resulted in a significant tumour growth delay, as observed in different lymphoma models (Burkitt's lymphomas and diffuse large B-cell lymphoma) [597]. Moreover, h1F6-mcMMAF conjugates, targeting CD70 and tubulin, demonstrated potent anti-tumour effect following i.p. administration every 4 days for 28 days, at doses of 1.5 or 4.5 mg/kg, using orthotopic or s.c. RCC tumour xenografts [598].

5.4.4 Assessment of Tumour Necrosis

Following completion of the *in vivo* efficacy study with 50 mg/kg ADR469, tumours were excised and processed for histological examination in order to determine the extent of tumour necrosis induced by the treatment (Figure 5.22, p.275). Variation in tumour size interfered with the interpretation of the results, since larger-sized tumours

displayed higher levels of necrosis than smaller ones. The extent of tumour necrosis observed in the larger control tumours could be associated with higher levels of hypoxia, induced by inadequate tumour vascular supply. This in turn could stimulate angiogenesis in order to improve the oxygen influx [599]. The evidence of haemorrhagic necrosis observed in the ADR469-treated tumours was most probably related to treatment-induced hypoxia following disruption of the vasculature. However, it is imprecise as to whether tumour necrosis was mainly induced by ADR469 treatment, due to the tumour size variation and the limited number of tumour samples.

It is worthwhile to note, that unsuccessful *in vivo* studies with ECB378 and BWM120 at that particular dose, could be as a result of an angiogenic stimulation following depletion of the tumour vasculature. Upon activation of hypoxia-induced signalling pathways, various angiogenic, inflammatory and profibrotic cytokines are secreted, eventually leading to wound resolution and restoring normoxia [600-602]. In high proliferating regions of well-developed tumours, hypoxia can be induced which is not directly related to the degree of vascularity, perfusion, or oxygen supply. For instance, other cell types within the tumour can serve as "oxygen sinks", contributing to the development of hypoxia. Tumour-associated macrophages (TAMs) infiltrate developing tumours which are associated with increased angiogenesis [603-604], by their ability to secrete pro-angiogenic cytokines [605].

5.4.5 Assessment of the Tumour Vasculature

To establish whether test compounds maintained their anti-vascular and anti-angiogenic activity *in vivo*, tumour samples from each group were analysed for functional tumour vasculature, following completion of the efficacy studies. In theory, dual-acting compounds targeting tubulin polymerisation and APN should exhibit potent effects on the tumour vasculature by either direct disruption (induced by the tubulin binging agent) or by angiogenesis depletion (generated from both components of the hybrids).

Tumour bearing mice treated with 40 mg/kg ECB378 or BWM120 failed to show any reduction in tumour vasculature which was correlated with the outcome from their *in vivo* efficacy study (Figure 5.24, p.277 and 5.30 p.282, respectively). Absence of an *in vivo* anti-vascular/anti-angiogenic effect could be a possible explanation as to why ECB378 and BWM120 did not exhibit an anti-tumour effect. In addition, the fact that

animals treated with these compounds showed a slight increased tumour vasculature compared to that of the control tumours, may be explained by an angiogenic stimulation following depletion of the tumour blood vessels. Although treatment with either 40 mg/kg ECB397 or 50 mg/kg ADR469 showed a variation between individual tumour samples, an overall insignificant decrease in the amount of functional tumour vasculature was observed (Figure 5.26, p.279 and 5.28, p.281, respectively). Yet again, these results were related with the anti-tumour efficacy study, where both ECB397 and ADR469 exhibited an anti-tumour activity *in vivo*. These findings may indicate that part of ECB397's and ADR469's anti-tumour activity was mediated through direct anti-vascular and anti-angiogenic effects. Moreover, this finding verified an improved pharmacological profile of ECB397 and ADR469 over ECB378 and BWM120, suggesting along with the *in vitro* data, that the prodrug presentation was favourable compared to the active dual-acting design.

The *in vivo* anti-vascular and anti-angiogenic effects exerted by tubulin targeting agents were discussed in Chapter 3, section 3.5.6, p.155. Several *in vivo* anti-angiogenic studies have also determined the effect of bestatin and its related analogues. Aozuka *et al.* showed that i.p. administration of 50-100 mg/kg/day bestatin for 4 days significantly reduced the number of vessels oriented towards the established primary tumour in orthotopic B15-BL6 melanoma xenografts [241]. In addition, immunohistochemical staining for CD34 expression in an ES-2 xenograft model following by daily i.v. administation with 100 μM bestatin or LYP for 2 weeks resulted in a significant decrease in the vascular density of tumours [282]. This finding was in agreement with the *in vivo* efficacy study of bestatin and LYP, implying that their anti-tumour effect was directly associated with a diminished vasculature.

Taking into consideration the promising *in vitro* data obtained with these hybrids, as outlined in Chapter 4, the *in vivo* findings did not directly correlate with the anti-tumour, anti-vascular and anti-angiogenic effects of test compounds. In an *in vivo* setting, additional complications in the experimental design are always involved and issues such as compound's solubility, selection of a dose regimen, route of administration, tumour type, poor bioavailability, and drug metabolism have to be taken into account. Furthermore, for comparison purposes, it is important to examine

individual components of the hybrids as well as their 1:1 combination. Without providing this data for each compound, it's not precise whether the hybrid's pharmacological profile is improved compared to that of single or combination treatment.

5.5 Conclusions

Novel hybrids and a DML were designed to target tubulin polymerisation and APN. Following the encouraging *in vitro* results obtained in Chapter 4, it was essential to further examine the potential of these compounds in a more complex *ex vivo* assay. The anti-vascular effect of hybrids and DML was assessed in the aortic ring assay, where all compounds demonstrated microvessel breakdown at different levels of potency and the effect was proven to be dose- and time-dependent. The most active hybrids were ADR469 and ECB397.

In addition to the anti-vascular effect, test compounds were assessed for their anti-angiogenic activity in the aortic ring assay. All compounds showed moderate to complete inhibition of microvessels formation at different concentrations, indicating angiogenesis inhibition. Once more, ADR469 and ECB397 demonstrated the highest potency in the anti-angiogenic model of the aortic ring assay, which are in agreement with the *in vitro* data.

Test compounds were examined in a PC-3 tumour xenograft model for evidence of anti-tumour efficacy. ECB378 and BWM120 did not show any evident reduction of tumour growth at 40 mg/kg, whereas 40 mg/kg ECB397 and 50 mg/kg ADR469 demonstrated a significant decrease in the rate of tumour growth at particular days compared to the control group. According to the BW measurements, none of the treatments caused significant systemic toxicity.

The level of tumour necrosis was examined in control and ADR469-treated groups following completion of the efficacy study. The histological examination of tumours did not provide any conclusive results as to whether ADR469 treatment caused extensive areas of tumour necrosis.

To further investigate the effect of treatment on their vasculature, tumour samples were processed for endothelial cell staining following completion of the anti-tumour study.

ECB378 and BWM120 treatment did not demonstrate any effect on the tumour vasculature. ECB397 and ADR469 showed some effect, verifying that part of their anti-tumour effect was mediated through direct vasculature shutdown and angiogenesis inhibition.

5.6 Overall Conclusions

To summarise the findings obtained from Chapter 4 and 5, four groups of hybrids and one DML, BWM120, were designed and synthesised in our group to target tubulin polymerisation and APN. Initial studies involved the evaluation of test compounds in APN-related assays. All groups of hybrids and DML demonstrated superior inhibition of APN compared to that of bestatin, both at the enzymatic and the cellular level. The effect of BWM120 on APN expression of HUVECs and PC-3 cells was examined using a flow cytometric technique and showed a significantly decreased level of APN expression compared to the control treated cells. Following this study, the anti-proliferative activity of test compounds was determined along with their individual components alone or in 1:1 combinations. All compounds exhibited inhibition of cell proliferation at different levels of activity, with ADR469 and ECB397 being the most potent agents, showing similar effects to their tubulin binding components alone or in combination. Furthermore, test compounds caused a substantial disruption to the microtubule network of endothelial cells with considerable variation in potency, confirming their ability to interfere with the tubulin cytoskeleton. Following treatment of cells with test compounds, cell cycle analysis was performed, whereby a G_2/M phase arrest was observed, signifying their anti-mitotic activity. In addition, DNA fragmentation was analysed at the sub-G_0/G_1 and found that in most cases test compounds induced higher levels of apoptotic cells than their individual components (alone or in combination). Perhaps, the design of the hybrids and DML is advantageous over single agents and may suggest a different mechanism of action (other than the mitotic arrest) in which the compounds induced their apoptotic effects. The *in vitro* anti-vascular effect of test compounds was observed by the reversible morphological changes of proliferating endothelial cells.

Following the promising *in vitro* evaluation of test compounds, their anti-vascular and anti-angiogenic effects were assessed in the *ex vivo* aortic ring assay, where all compounds demonstrated microvessel breakdown and depletion of angiogenesis at different levels of potency. In agreement with the *in vitro* data, the two most active compounds were ADR469 and ECB397. The final stage of evaluation involved the assessment of compounds in a s.c. PC-3 tumour xenograft model. Treatment of tumour bearing mice with 40 mg/kg ECB378 or BWM120 was not sufficient to provide

evidence of an anti-tumour effect, whereas 40 mg/kg ECB397 and 50 mg/kg ADR469 demonstrated a tumour growth delay compared to the control group. Histological examination of tumour samples following completion of the ADR469 efficacy study did not provide conclusive evidence as to whether ADR469 treatment caused extensive areas of tumour necrosis. Finally, the effect of each treatment on the tumour vasculature was examined following completion of the anti-tumour study. A minor reduction was observed in the ECB397- and ADR469-treated tumours, verifying that part of their anti-tumour effect was mediated through direct vasculature shutdown and angiogenesis inhibition.

Taking into consideration the results obtained from the *in vitro*, *ex vivo* and *in vivo* evaluation of hybrids, their degree of potency depends upon their design *i.e.* whether the hybrids were presented in an active or a prodrug form. According to these findings and in addition with studies conducted by Breen [554], group I hybrids remain intact as dual-acting compounds and hence their reduced activity as tubulin binding agents, whereas group II hybrids are hydrolysed by a slow-release reaction, thus the observed moderate activity. Group III and IV hybrids are hydrolysed to release their individual components under physiological conditions, and for this reason they maintained their potency of their corresponding tubulin binding agent.

To conclude, novel hybrids and DML designed to target tumour vasculature and angiogenesis, demonstrated promising *in vitro* and *ex vivo* activities; however the results obtained from the *in vivo* data were not directly correlated to their actual potential, possibly due to their administration at non-effective doses. Additional studies are encouraged to be carried out with different experimental settings in order to reveal their true potential as anti-vascular, anti-angiogenic and anti-tumour agents. Future work is discussed in Chapter 6.

-- Chapter 6 --

Future Work

6. Future Work

6.1 Inhibition of Cell Proliferation

The majority of tubulin polymerisation inhibitors, hybrids and the DML synthesised in our lab, demonstrated potent anti-proliferative activity against HUVECs and PC-3 prostate cancer cells, as determined by the MTT assay. Additional assays could also be used to confirm the anti-proliferative effect of test compounds, including an LDH-based assay [606], and an ATP-based bioluminescent assay [607]. It would be interesting to expand the investigation of the inhibitory effect of test compounds using additional primary cells lines (*e.g.* fibroblasts). This could distinguish any type of selectivity over normal cells in general or specifically over HUVECs. In addition, it is worthwhile to determine the anti-proliferative effect of test compounds on quiescent HUVECs and observe any significant selectivity over proliferating HUVECs. This will identify whether these compounds exert "true" vascular disrupting properties, by selectively targeting proliferating endothelial cells, but not quiescent endothelial cells. In theory, this property would be beneficial *in vivo*, which could lead to a minimised drug-associated systemic toxicity. Furthermore, screening of test compounds against a variety of solid tumour cell lines could identify possible selectivity over a particular tumour type.

The anti-proliferative activity of the bestatin-related hybrids could be examined in myeloid cell lines, since bestatin demonstrated selectivity over several myeloid cell lines, by induction of apoptosis [244-245]. In addition, it would be interesting to explore the effect of hybrids on proliferation of APN-negative cell lines and compare their activities to that of APN-positive cells' proliferation. This would be an indication as to whether their effects are directly mediated through an APN-associated pathway.

6.2 Inhibition of Tubulin Polymerisation

Considering the data obtained from the cell cycle analysis (G_2/M arrest) and the visualisation of the microtubule disruption of endothelial cells, following drug exposure, it is reasonable to conclude that test compounds were directly targeting tubulin. It is important to determine the degree of tubulin polymerisation inhibition of each compound and correlate that to the *in vitro* activity demonstrated at the cellular

level [608]. Furthermore, it is only assumed that similar to CA-4, our compounds bind to tubulin at the colchicine-binding site; however additional studies are required to confirm that [609]. The exact molecular mechanism in which our compounds interfere with microtubule organisation it is still unclear and perhaps they share similar properties with CA-4. However, further investigation is encouraged to take place in order to clarify this by examining the involvement of actin, actinomyosin and VE-cadherin [315, 511].

6.3 Inhibition of Cell Migration, Invasion, Adhesion and Angiogenesis

Although the primary aim of this study was to evaluate the novel tubulin polymerisation inhibitors as tumour VDAs, a supplementary assay was performed in order to investigate the effect of RS180 on *in vitro* angiogenesis (AngioKit assay). In addition, the anti-angiogenic inhibition of tubulin binding agents and dual-acting compounds was examined in the *ex vivo* aortic ring assay. Angiogenesis involves multiple cellular processes and it is associated with several different growth factors. It would be worthwhile to determine the effect of selected compounds, particularly the bestatin-related hybrids, on angiogenesis-associated cellular processes including migration, invasion and adhesion [223, 240, 579]. Furthermore, the regulation of particular growth factors, including hypoxia inducible factor 1 (HIF-1) and VEGF [610-611] could be investigated following continuous drug exposure. The effect of hybrids on cell invasion and metastasis could also be assessed by exploring the expression pattern of certain MMPs involved in matrix degradation [240, 612-613].

6.4 Inhibition of APN

The inhibitory effect of hybrids on APN was determined at the enzymatic and the cellular level using a colorimetric technique. Further enzyme kinetic studies could identify how the compounds inhibit APN and could classify them as competitive or non-competitive, reversible or irreversible inhibitors [271]. Additional hydrolysis studies could be carried out using the prodrug-form hybrids in order to quantify their levels both in an extracellular and intracellular environment, using a liquid chromatography–mass spectrometry (LCMS) technique. Moreover, the APN expression profile of BWM120-treated cells was examined using immunofluorescence staining, followed by flow cytometric analysis. Additional methods of detection could establish

the level of APN expression using Western blotting [282], ELISA [580] and real-time polymerase chain reaction techniques [614].

6.5 Induction of Apoptosis

An additional study involved the examination of hybrids and their individual components alone or in 1:1 combination for evidence of synergistic induction of cell death. Cell cycle analysis was performed using PI staining, followed by detection of sub-G_0/G_1 arrest, using a flow cytometric technique. A significant increase of apoptotic cells was observed following treatment with hybrids, compared to the single agents alone or in combination. It is still unknown whether this observation was due to a synergistic effect or due to an undiscovered mechanism of action. Further studies are encouraged to clarify the situation, using different methods of apoptosis detection, including Annexin V/PI staining followed by flow cytometric analysis, DNA fragmentation using electrophoresis, exploring specific caspases activity and examination of any cell morphological abnormalities associated with apoptosis-induced nuclear degradation [244-245, 563-564].

6.6 *In Vivo* Anti-tumour Efficacy

The *in vivo* anti-tumour efficacy of test compounds was evaluated in a s.c. PC-3 tumour xenograft model. From the preliminary *in vivo* data obtained in Chapter 3, a significant decrease in tumour volume was observed following i.p. administration once a week for three weeks with 200 mg/kg of GS291 and 150 mg/kg of CA-4P; however GS291 treatment was not superior to that of CA-4P. Perhaps, an increased frequency of treatment (*e.g.* on alternate days), a different route of administration (*e.g.* i.v.) or combination therapy could enhance the anti-tumour effect of test compounds. In fact, there are numerous evidences to support that the activity of VDAs can be augmented by combination therapy with a standard cytotoxic agent [529, 615-616]. This theory is based on the fact that the anti-vascular agent will cause disruption of the tumour vasculature, resulting in a higher permeability of tumour vessels and thus facilitating the release of the cytotoxic agent within the tumour tissue. Additional *in vivo* studies could explore the anti-tumour activity of test compounds on other xenograft models, including different types of tumours, or by using orthotopic implantation of tumour cells/tissues [527, 617].

The *in vivo* evaluation of hybrids showed a variation in their anti-tumour efficacy. For instance, i.p. administration with 50 mg/kg ADR469 on alternate days for three weeks demonstrated the largest decrease in tumour volume in the PC-3 tumour xenografts. Treatment of tumour bearing mice with 40 mg/kg ECB397 on alternate days for two weeks resulted in a smaller reduction of tumour volume, which may indicate that a prolonged treatment is beneficial for the outcome of the study. Following i.p. administration of 40 mg/kg of ECB378 or BWM120 on alternate days for two weeks was not sufficient to demonstrate any anti-tumour effect. Additional *in vivo* efficacy studies with longer duration of treatment, perhaps i.v. administration and an increase in treatment dose are encouraged in order to reveal the hybrids' and DML's true anti-tumour potential. Moreover, comparison studies with individual components of the hybrids, alone or in 1:1 combinations, will clarify the situation and reveal any advantageous effect of the hybrids. *In vivo* pharmacokinetic studies could also address any issues associated with poor bioavailability and drug metabolism. It is worthwhile to investigate the degree of hydrolysis of the prodrug-form hybrids by determining the level of their individual components in plasma, tumour samples and other APN-rich sites, including the liver and kidneys. Furthermore, it would be interesting to evaluate the anti-tumour effect of hybrids in other solid tumours including APN-positive and APN-negative cancer cell lines and identify any selectivity patterns.

The aim of the *in vivo* study with regard to the hybrids' evaluation was to identify any synergistic effect in terms of anti-tumour efficacy, as a result of a direct tumour vasculature disruption and angiogenesis inhibition. However, immunotherapy with bestatin previously demonstrated activity against haematological cancers [264-265, 267]; thus the adjuvant effect of bestatin-related hybrids could also be examined in haematological malignancies. It is worthwhile to note that the anti-tumour effect of bestatin observed against syngeneic colon tumours was through indirect immunomodulation *via* spleen cells and possibly *via* T cells [247]. In our studies, immunodeficient mice were used, lacking certain components of the immune system, including T cells. This could minimise the immunomodulatory properties of bestatin and as a consequence reduce its anti-tumour activity. Further studies using non-immunodeficient animals are encouraged, in order to observe any enhancement of bestatin's anti-tumour effect, through indirect immunomodulation. As an extension to

the efficacy study, the effect of bestatin-related hybrids on *in vivo* metastasis could also be investigated, by examination of potentially-metastatic organs, including the lungs and liver [594, 618].

6.7 Examination of Tumour Samples

Following completion of the *in vivo* efficacy studies, tumour samples were collected and processed for histological examination. The degree of tumour necrosis and vasculature disruption was determined following H&E and CD31 staining, respectively. Tumour vasculature was examined for evidence of vascular disruption, contributed by the tubulin binding component of the hybrids, and evidence of an anti-angiogenic effect, mediated by their bestatin component. However, there was no distinguishable marker in this method to reveal a separate effect induced from each individual component of the hybrid. It is worthwhile to investigate the effect of the hybrids on the tumours' APN expression pattern, using immunostaining techniques or to quantify the APN levels in tumour homogenate samples, using flow cytometric analysis [594, 618].

6.8 Hybrids' Design

It is reasonable to conclude that the effect of the bestatin-component of the hybrids did not contribute mostly to their potency and effectiveness, both *in vitro* and *in vivo*. Therefore, it is only rational to assume that perhaps a different ratio (*e.g.* 1:2) in the hybrids' design between the tubulin targeting agent and bestatin, could pronounce the activity of bestatin and potentiate an overall greater synergistic effect. In addition, targeted delivery of the compounds to the tumour site could be facilitated by their conjugation to a NGR or RGD moiety, which could recognise APN- or integrin-rich sites within the tumour, and provide a prolonged release of the active drugs.

Bibliography

[1] Raven, R. W., *The Theory and Practice of Oncology - Historical evolution and present principles*, ed. e.T.P.P. Group. 1990, Lancs - England / Park Ridge, New Jersey - USA.

[2] *The National Cancer Registry Ireland.* [cited 2012; Available from: http://www.ncri.ie.

[3] Hanahan, D. and Weinberg, R. A. The hallmarks of cancer. *Cell.* **2000**, *100*(1), 57-70.

[4] Hanahan, D. and Weinberg, R. A. Hallmarks of cancer: the next generation. *Cell.* **2011**, *144*(5), 646-674.

[5] Kinzler, K. W. and Vogelstein, B. Lessons from hereditary colorectal cancer. *Cell.* **1996**, *87*(2), 159-170.

[6] Slamon, D. J.; Clark, G. M.; Wong, S. G.; Levin, W. J.; Ullrich, A.McGuire, W. L. Human breast cancer: correlation of relapse and survival with amplification of the HER-2/neu oncogene. *Science.* **1987**, *235*(4785), 177-182.

[7] Yarden, Y. and Ullrich, A. Growth factor receptor tyrosine kinases. *Annu Rev Biochem.* **1988**, *57*, 443-478.

[8] Medema, R. H. and Bos, J. L. The role of p21ras in receptor tyrosine kinase signaling. *Crit Rev Oncog.* **1993**, *4*(6), 615-661.

[9] Weinberg, R. A. The retinoblastoma protein and cell cycle control. *Cell.* **1995**, *81*(3), 323-330.

[10] Wyllie, A. H.; Kerr, J. F.Currie, A. R. Cell death: the significance of apoptosis. *Int Rev Cytol.* **1980**, *68*, 251-306.

[11] Lotem, J. and Sachs, L. Control of apoptosis in hematopoiesis and leukemia by cytokines, tumor suppressor and oncogenes. *Leukemia.* **1996**, *10*(6), 925-931.

[12] Butt, A. J.; Firth, S. M.Baxter, R. C. The IGF axis and programmed cell death. *Immunol Cell Biol.* **1999**, *77*(3), 256-262.

[13] Ashkenazi, A. and Dixit, V. M. Apoptosis control by death and decoy receptors. *Curr Opin Cell Biol.* **1999**, *11*(2), 255-260.

[14] Green, D. R. and Reed, J. C. Mitochondria and apoptosis. *Science.* **1998**, *281*(5381), 1309-1312.

[15] Thornberry, N. A. and Lazebnik, Y. Caspases: enemies within. *Science.* **1998**, *281*(5381), 1312-1316.

[16] Vaux, D. L.; Cory, S.Adams, J. M. Bcl-2 gene promotes haemopoietic cell survival and cooperates with c-myc to immortalize pre-B cells. *Nature.* **1988**, *335*(6189), 440-442.

[17] Strasser, A.; Harris, A. W.; Bath, M. L.Cory, S. Novel primitive lymphoid tumours induced in transgenic mice by cooperation between myc and bcl-2. *Nature.* **1990**, *348*(6299), 331-333.

[18] Hayflick, L. Mortality and immortality at the cellular level. A review. *Biochemistry (Mosc).* **1997**, *62*(11), 1180-1190.

[19] Wright, W. E.; Pereira-Smith, O. M.Shay, J. W. Reversible cellular senescence: implications for immortalization of normal human diploid fibroblasts. *Mol Cell Biol.* **1989**, *9*(7), 3088-3092.

[20] Counter, C. M.; Avilion, A. A.; LeFeuvre, C. E.; Stewart, N. G.; Greider, C. W.; Harley, C. B.Bacchetti, S. Telomere shortening associated with chromosome instability is arrested in immortal cells which express telomerase activity. *EMBO J.* **1992**, *11*(5), 1921-1929.

[21] Bryan, T. M. and Cech, T. R. Telomerase and the maintenance of chromosome ends. *Curr Opin Cell Biol.* **1999**, *11*(3), 318-324.
[22] Shay, J. W. and Bacchetti, S. A survey of telomerase activity in human cancer. *Eur J Cancer.* **1997**, *33*(5), 787-791.
[23] Bouck, N.; Stellmach, V.Hsu, S. C. How tumors become angiogenic. *Adv Cancer Res.* **1996**, *69*, 135-174.
[24] Hanahan, D. and Folkman, J. Patterns and emerging mechanisms of the angiogenic switch during tumorigenesis. *Cell.* **1996**, *86*(3), 353-364.
[25] Sporn, M. B. The war on cancer. *Lancet.* **1996**, *347*(9012), 1377-1381.
[26] Aplin, A. E.; Howe, A.; Alahari, S. K.Juliano, R. L. Signal transduction and signal modulation by cell adhesion receptors: the role of integrins, cadherins, immunoglobulin-cell adhesion molecules, and selectins. *Pharmacol Rev.* **1998**, *50*(2), 197-263.
[27] Varner, J. A. and Cheresh, D. A. Integrins and cancer. *Curr Opin Cell Biol.* **1996**, *8*(5), 724-730.
[28] Coussens, L. M. and Werb, Z. Matrix metalloproteinases and the development of cancer. *Chem Biol.* **1996**, *3*(11), 895-904.
[29] Warburg, O. On the origin of cancer cells. *Science.* **1956**, *123*(3191), 309-314.
[30] Warburg, O. On respiratory impairment in cancer cells. *Science.* **1956**, *124*(3215), 269-270.
[31] Bindea, G.; Mlecnik, B.; Fridman, W. H.; Pages, F.Galon, J. Natural immunity to cancer in humans. *Curr Opin Immunol.* **2010**, *22*(2), 215-222.
[32] Ferrone, C. and Dranoff, G. Dual roles for immunity in gastrointestinal cancers. *J Clin Oncol.* **2010**, *28*(26), 4045-4051.
[33] Gimbrone, M. A., Jr.; Leapman, S. B.; Cotran, R. S.Folkman, J. Tumor dormancy in vivo by prevention of neovascularization. *J Exp Med.* **1972**, *136*(2), 261-276.
[34] Ferrara, N. Vascular endothelial growth factor. *Arterioscler Thromb Vasc Biol.* **2009**, *29*(6), 789-791.
[35] Mac Gabhann, F. and Popel, A. S. Systems biology of vascular endothelial growth factors. *Microcirculation.* **2008**, *15*(8), 715-738.
[36] Carmeliet, P. VEGF as a key mediator of angiogenesis in cancer. *Oncology.* **2005**, *69 Suppl 3*, 4-10.
[37] Littlepage, L. E.; Sternlicht, M. D.; Rougier, N.; Phillips, J.; Gallo, E.; Yu, Y.; Williams, K.; Brenot, A.; Gordon, J. I.Werb, Z. Matrix metalloproteinases contribute distinct roles in neuroendocrine prostate carcinogenesis, metastasis, and angiogenesis progression. *Cancer Res.* **2010**, *70*(6), 2224-2234.
[38] Pandya, N. M.; Dhalla, N. S.Santani, D. D. Angiogenesis--a new target for future therapy. *Vascul Pharmacol.* **2006**, *44*(5), 265-274.
[39] Kazerounian, S.; Yee, K. O.Lawler, J. Thrombospondins in cancer. *Cell Mol Life Sci.* **2008**, *65*(5), 700-712.
[40] Pasquale, E. B. Eph receptors and ephrins in cancer: bidirectional signalling and beyond. *Nat Rev Cancer.* **2010**, *10*(3), 165-180.
[41] Ahmed, Z. and Bicknell, R. Angiogenic signalling pathways. *Methods Mol Biol.* **2009**, *467*, 3-24.
[42] Dejana, E.; Orsenigo, F.; Molendini, C.; Baluk, P.McDonald, D. M. Organization and signaling of endothelial cell-to-cell junctions in various

regions of the blood and lymphatic vascular trees. *Cell Tissue Res.* **2009**, *335*(1), 17-25.

[43] Carmeliet, P. and Jain, R. K. Angiogenesis in cancer and other diseases. *Nature.* **2000**, *407*(6801), 249-257.

[44] O'Reilly, M. S. Angiostatin: an endogenous inhibitor of angiogenesis and of tumor growth. *EXS.* **1997**, *79*, 273-294.

[45] Galligioni, E. and Ferro, A. Angiogenesis and antiangiogenic agents in non-small cell lung cancer. *Lung Cancer.* **2001**, *34 Suppl 4*, S3-7.

[46] Nyberg, P.; Xie, L.Kalluri, R. Endogenous inhibitors of angiogenesis. *Cancer Res.* **2005**, *65*(10), 3967-3979.

[47] Cao, Y. Tumor angiogenesis and therapy. *Biomed Pharmacother.* **2005**, *59 Suppl 2*, S340-343.

[48] Abdollahi, A.; Hlatky, L.Huber, P. E. Endostatin: the logic of antiangiogenic therapy. *Drug Resist Updat.* **2005**, *8*(1-2), 59-74.

[49] Maeshima, Y.; Manfredi, M.; Reimer, C.; Holthaus, K. A.; Hopfer, H.; Chandamuri, B. R.; Kharbanda, S.Kalluri, R. Identification of the anti-angiogenic site within vascular basement membrane-derived tumstatin. *J Biol Chem.* **2001**, *276*(18), 15240-15248.

[50] Kamphaus, G. D.; Colorado, P. C.; Panka, D. J.; Hopfer, H.; Ramchandran, R.; Torre, A.; Maeshima, Y.; Mier, J. W.; Sukhatme, V. P.Kalluri, R. Canstatin, a novel matrix-derived inhibitor of angiogenesis and tumor growth. *J Biol Chem.* **2000**, *275*(2), 1209-1215.

[51] North, S.; Moenner, M.Bikfalvi, A. Recent developments in the regulation of the angiogenic switch by cellular stress factors in tumors. *Cancer Lett.* **2005**, *218*(1), 1-14.

[52] Arbiser, J. L.; Moses, M. A.; Fernandez, C. A.; Ghiso, N.; Cao, Y.; Klauber, N.; Frank, D.; Brownlee, M.; Flynn, E.; Parangi, S.; Byers, H. R.Folkman, J. Oncogenic H-ras stimulates tumor angiogenesis by two distinct pathways. *Proc Natl Acad Sci U S A.* **1997**, *94*(3), 861-866.

[53] Ravi, R.; Mookerjee, B.; Bhujwalla, Z. M.; Sutter, C. H.; Artemov, D.; Zeng, Q.; Dillehay, L. E.; Madan, A.; Semenza, G. L.Bedi, A. Regulation of tumor angiogenesis by p53-induced degradation of hypoxia-inducible factor 1alpha. *Genes Dev.* **2000**, *14*(1), 34-44.

[54] Bergers, G. and Benjamin, L. E. Tumorigenesis and the angiogenic switch. *Nat Rev Cancer.* **2003**, *3*(6), 401-410.

[55] Ribatti, D. The crucial role of vascular permeability factor/vascular endothelial growth factor in angiogenesis: a historical review. *Br J Haematol.* **2005**, *128*(3), 303-309.

[56] Alon, T.; Hemo, I.; Itin, A.; Pe'er, J.; Stone, J.Keshet, E. Vascular endothelial growth factor acts as a survival factor for newly formed retinal vessels and has implications for retinopathy of prematurity. *Nat Med.* **1995**, *1*(10), 1024-1028.

[57] Benjamin, L. E.; Golijanin, D.; Itin, A.; Pode, D.Keshet, E. Selective ablation of immature blood vessels in established human tumors follows vascular endothelial growth factor withdrawal. *J Clin Invest.* **1999**, *103*(2), 159-165.

[58] Yuan, F.; Chen, Y.; Dellian, M.; Safabakhsh, N.; Ferrara, N.Jain, R. K. Time-dependent vascular regression and permeability changes in established human tumor xenografts induced by an anti-vascular endothelial growth factor/vascular

permeability factor antibody. *Proc Natl Acad Sci U S A*. **1996**, *93*(25), 14765-14770.

[59] Plouet, J.; Schilling, J.Gospodarowicz, D. Isolation and characterization of a newly identified endothelial cell mitogen produced by AtT-20 cells. *EMBO J.* **1989**, *8*(12), 3801-3806.

[60] Leung, D. W.; Cachianes, G.; Kuang, W. J.; Goeddel, D. V.Ferrara, N. Vascular endothelial growth factor is a secreted angiogenic mitogen. *Science*. **1989**, *246*(4935), 1306-1309.

[61] Ferrara, N. Pathways mediating VEGF-independent tumor angiogenesis. *Cytokine Growth Factor Rev.* **2010**, *21*(1), 21-26.

[62] Ferrara, N. and Davis-Smyth, T. The biology of vascular endothelial growth factor. *Endocr Rev.* **1997**, *18*(1), 4-25.

[63] Dvorak, H. F.; Brown, L. F.; Detmar, M.Dvorak, A. M. Vascular permeability factor/vascular endothelial growth factor, microvascular hyperpermeability, and angiogenesis. *Am J Pathol.* **1995**, *146*(5), 1029-1039.

[64] Ferrara, N. and Alitalo, K. Clinical applications of angiogenic growth factors and their inhibitors. *Nat Med.* **1999**, *5*(12), 1359-1364.

[65] Kim, K. J.; Li, B.; Winer, J.; Armanini, M.; Gillett, N.; Phillips, H. S.Ferrara, N. Inhibition of vascular endothelial growth factor-induced angiogenesis suppresses tumour growth in vivo. *Nature*. **1993**, *362*(6423), 841-844.

[66] *Medscape*. 2012; Available from: http://www.medscape.com/.

[67] Ornitz, D. M. and Itoh, N. Fibroblast growth factors. *Genome Biol.* **2001**, *2*(3), REVIEWS3005.

[68] Burgess, W. H. and Maciag, T. The heparin-binding (fibroblast) growth factor family of proteins. *Annu Rev Biochem.* **1989**, *58*, 575-606.

[69] Kwan, C. P.; Venkataraman, G.; Shriver, Z.; Raman, R.; Liu, D.; Qi, Y.; Varticovski, L.Sasisekharan, R. Probing fibroblast growth factor dimerization and role of heparin-like glycosaminoglycans in modulating dimerization and signaling. *J Biol Chem*. **2001**, *276*(26), 23421-23429.

[70] Matsumoto, T.; Turesson, I.; Book, M.; Gerwins, P.Claesson-Welsh, L. p38 MAP kinase negatively regulates endothelial cell survival, proliferation, and differentiation in FGF-2-stimulated angiogenesis. *J Cell Biol.* **2002**, *156*(1), 149-160.

[71] Arbeit, J. M.; Olson, D. C.Hanahan, D. Upregulation of fibroblast growth factors and their receptors during multi-stage epidermal carcinogenesis in K14-HPV16 transgenic mice. *Oncogene*. **1996**, *13*(9), 1847-1857.

[72] Nakamura, T.; Mochizuki, Y.; Kanetake, H.Kanda, S. Signals via FGF receptor 2 regulate migration of endothelial cells. *Biochem Biophys Res Commun*. **2001**, *289*(4), 801-806.

[73] Baeriswyl, V. and Christofori, G. The angiogenic switch in carcinogenesis. *Semin Cancer Biol*. **2009**, *19*(5), 329-337.

[74] Kandel, J.; Bossy-Wetzel, E.; Radvanyi, F.; Klagsbrun, M.; Folkman, J.Hanahan, D. Neovascularization is associated with a switch to the export of bFGF in the multistep development of fibrosarcoma. *Cell*. **1991**, *66*(6), 1095-1104.

[75] Nguyen, M.; Watanabe, H.; Budson, A. E.; Richie, J. P.Folkman, J. Elevated levels of the angiogenic peptide basic fibroblast growth factor in urine of bladder cancer patients. *J Natl Cancer Inst*. **1993**, *85*(3), 241-242.

[76] Nguyen, M.; Watanabe, H.; Budson, A. E.; Richie, J. P.; Hayes, D. F.Folkman, J. Elevated levels of an angiogenic peptide, basic fibroblast growth factor, in the urine of patients with a wide spectrum of cancers. *J Natl Cancer Inst.* **1994**, *86*(5), 356-361.

[77] Bottcher, R. T. and Niehrs, C. Fibroblast growth factor signaling during early vertebrate development. *Endocr Rev.* **2005**, *26*(1), 63-77.

[78] Heldin, C. H.; Ostman, A.Ronnstrand, L. Signal transduction via platelet-derived growth factor receptors. *Biochim Biophys Acta.* **1998**, *1378*(1), F79-113.

[79] Kazlauskas, A. A new member of an old family. *Nat Cell Biol.* **2000**, *2*(5), E78-79.

[80] Lindahl, P.; Hellstrom, M.; Kalen, M.Betsholtz, C. Endothelial-perivascular cell signaling in vascular development: lessons from knockout mice. *Curr Opin Lipidol.* **1998**, *9*(5), 407-411.

[81] Li, X.; Ponten, A.; Aase, K.; Karlsson, L.; Abramsson, A.; Uutela, M.; Backstrom, G.; Hellstrom, M.; Bostrom, H.; Li, H.; Soriano, P.; Betsholtz, C.; Heldin, C. H.; Alitalo, K.; Ostman, A.Eriksson, U. PDGF-C is a new protease-activated ligand for the PDGF alpha-receptor. *Nat Cell Biol.* **2000**, *2*(5), 302-309.

[82] LaRochelle, W. J.; Jeffers, M.; McDonald, W. F.; Chillakuru, R. A.; Giese, N. A.; Lokker, N. A.; Sullivan, C.; Boldog, F. L.; Yang, M.; Vernet, C.; Burgess, C. E.; Fernandes, E.; Deegler, L. L.; Rittman, B.; Shimkets, J.; Shimkets, R. A.; Rothberg, J. M.Lichenstein, H. S. PDGF-D, a new protease-activated growth factor. *Nat Cell Biol.* **2001**, *3*(5), 517-521.

[83] Zwerner, J. P. and May, W. A. PDGF-C is an EWS/FLI induced transforming growth factor in Ewing family tumors. *Oncogene.* **2001**, *20*(5), 626-633.

[84] Uutela, M.; Lauren, J.; Bergsten, E.; Li, X.; Horelli-Kuitunen, N.; Eriksson, U.Alitalo, K. Chromosomal location, exon structure, and vascular expression patterns of the human PDGFC and PDGFD genes. *Circulation.* **2001**, *103*(18), 2242-2247.

[85] Ostman, A. and Heldin, C. H. Involvement of platelet-derived growth factor in disease: development of specific antagonists. *Adv Cancer Res.* **2001**, *80*, 1-38.

[86] Yu, J.; Ustach, C.Kim, H. R. Platelet-derived growth factor signaling and human cancer. *J Biochem Mol Biol.* **2003**, *36*(1), 49-59.

[87] Betsholtz, C. Biology of platelet-derived growth factors in development. *Birth Defects Res C Embryo Today.* **2003**, *69*(4), 272-285.

[88] Heinrich, M. C.; Corless, C. L.; Duensing, A.; McGreevey, L.; Chen, C. J.; Joseph, N.; Singer, S.; Griffith, D. J.; Haley, A.; Town, A.; Demetri, G. D.; Fletcher, C. D.Fletcher, J. A. PDGFRA activating mutations in gastrointestinal stromal tumors. *Science.* **2003**, *299*(5607), 708-710.

[89] Baxter, E. J.; Hochhaus, A.; Bolufer, P.; Reiter, A.; Fernandez, J. M.; Senent, L.; Cervera, J.; Moscardo, F.; Sanz, M. A.Cross, N. C. The t(4;22)(q12;q11) in atypical chronic myeloid leukaemia fuses BCR to PDGFRA. *Hum Mol Genet.* **2002**, *11*(12), 1391-1397.

[90] Xie, J., *PDGF Pathways and Growth of Basal Cell and Squamous Cell Carcinomas*, in *Molecular Mechanisms of Basal Cell and Squamous Cell Carcinomas*, J. Reichrath, Editor. 2006.

[91] Olayioye, M. A.; Neve, R. M.; Lane, H. A.Hynes, N. E. The ErbB signaling network: receptor heterodimerization in development and cancer. *EMBO J.* **2000**, *19*(13), 3159-3167.

[92] Ferguson, K. M.; Berger, M. B.; Mendrola, J. M.; Cho, H. S.; Leahy, D. J.Lemmon, M. A. EGF activates its receptor by removing interactions that autoinhibit ectodomain dimerization. *Mol Cell.* **2003**, *11*(2), 507-517.

[93] Ogiso, H.; Ishitani, R.; Nureki, O.; Fukai, S.; Yamanaka, M.; Kim, J. H.; Saito, K.; Sakamoto, A.; Inoue, M.; Shirouzu, M.Yokoyama, S. Crystal structure of the complex of human epidermal growth factor and receptor extracellular domains. *Cell.* **2002**, *110*(6), 775-787.

[94] Yarden, Y. and Sliwkowski, M. X. Untangling the ErbB signalling network. *Nat Rev Mol Cell Biol.* **2001**, *2*(2), 127-137.

[95] Citri, A. and Yarden, Y. EGF-ERBB signalling: towards the systems level. *Nat Rev Mol Cell Biol.* **2006**, *7*(7), 505-516.

[96] Baselga, J. and Albanell, J. Epithelial growth factor receptor interacting agents. *Hematol Oncol Clin North Am.* **2002**, *16*(5), 1041-1063.

[97] De Luca, A.; Carotenuto, A.; Rachiglio, A.; Gallo, M.; Maiello, M. R.; Aldinucci, D.; Pinto, A.Normanno, N. The role of the EGFR signaling in tumor microenvironment. *J Cell Physiol.* **2008**, *214*(3), 559-567.

[98] Ferrara, N. and Kerbel, R. S. Angiogenesis as a therapeutic target. *Nature.* **2005**, *438*(7070), 967-974.

[99] Goldman, C. K.; Kim, J.; Wong, W. L.; King, V.; Brock, T.Gillespie, G. Y. Epidermal growth factor stimulates vascular endothelial growth factor production by human malignant glioma cells: a model of glioblastoma multiforme pathophysiology. *Mol Biol Cell.* **1993**, *4*(1), 121-133.

[100] Pore, N.; Liu, S.; Haas-Kogan, D. A.; O'Rourke, D. M.Maity, A. PTEN mutation and epidermal growth factor receptor activation regulate vascular endothelial growth factor (VEGF) mRNA expression in human glioblastoma cells by transactivating the proximal VEGF promoter. *Cancer Res.* **2003**, *63*(1), 236-241.

[101] Ladanyi, M. and Pao, W. Lung adenocarcinoma: guiding EGFR-targeted therapy and beyond. *Mod Pathol.* **2008**, *21 Suppl 2*, S16-22.

[102] Page-McCaw, A.; Ewald, A. J.Werb, Z. Matrix metalloproteinases and the regulation of tissue remodelling. *Nat Rev Mol Cell Biol.* **2007**, *8*(3), 221-233.

[103] Parks, W. C.; Wilson, C. L.Lopez-Boado, Y. S. Matrix metalloproteinases as modulators of inflammation and innate immunity. *Nat Rev Immunol.* **2004**, *4*(8), 617-629.

[104] Egeblad, M. and Werb, Z. New functions for the matrix metalloproteinases in cancer progression. *Nat Rev Cancer.* **2002**, *2*(3), 161-174.

[105] Sternlicht, M. D. and Werb, Z. How matrix metalloproteinases regulate cell behavior. *Annu Rev Cell Dev Biol.* **2001**, *17*, 463-516.

[106] Deryugina, E. I. and Quigley, J. P. Matrix metalloproteinases and tumor metastasis. *Cancer Metastasis Rev.* **2006**, *25*(1), 9-34.

[107] Bergers, G.; Brekken, R.; McMahon, G.; Vu, T. H.; Itoh, T.; Tamaki, K.; Tanzawa, K.; Thorpe, P.; Itohara, S.; Werb, Z.Hanahan, D. Matrix metalloproteinase-9 triggers the angiogenic switch during carcinogenesis. *Nat Cell Biol.* **2000**, *2*(10), 737-744.

[108] Ahn, G. O. and Brown, J. M. Matrix metalloproteinase-9 is required for tumor vasculogenesis but not for angiogenesis: role of bone marrow-derived myelomonocytic cells. *Cancer Cell.* **2008**, *13*(3), 193-205.

[109] Sounni, N. E.; Dehne, K.; van Kempen, L.; Egeblad, M.; Affara, N. I.; Cuevas, I.; Wiesen, J.; Junankar, S.; Korets, L.; Lee, J.; Shen, J.; Morrison, C. J.; Overall, C. M.; Krane, S. M.; Werb, Z.; Boudreau, N.Coussens, L. M. Stromal regulation of vessel stability by MMP14 and TGFbeta. *Dis Model Mech.* **2010**, *3*(5-6), 317-332.

[110] Boire, A.; Covic, L.; Agarwal, A.; Jacques, S.; Sherifi, S.Kuliopulos, A. PAR1 is a matrix metalloprotease-1 receptor that promotes invasion and tumorigenesis of breast cancer cells. *Cell.* **2005**, *120*(3), 303-313.

[111] Seals, D. F. and Courtneidge, S. A. The ADAMs family of metalloproteases: multidomain proteins with multiple functions. *Genes Dev.* **2003**, *17*(1), 7-30.

[112] Wu, E.; Croucher, P. I.McKie, N. Expression of members of the novel membrane linked metalloproteinase family ADAM in cells derived from a range of haematological malignancies. *Biochem Biophys Res Commun.* **1997**, *235*(2), 437-442.

[113] Iba, K.; Albrechtsen, R.; Gilpin, B.; Frohlich, C.; Loechel, F.; Zolkiewska, A.; Ishiguro, K.; Kojima, T.; Liu, W.; Langford, J. K.; Sanderson, R. D.; Brakebusch, C.; Fassler, R.Wewer, U. M. The cysteine-rich domain of human ADAM 12 supports cell adhesion through syndecans and triggers signaling events that lead to beta1 integrin-dependent cell spreading. *J Cell Biol.* **2000**, *149*(5), 1143-1156.

[114] Yavari, R.; Adida, C.; Bray-Ward, P.; Brines, M.Xu, T. Human metalloprotease-disintegrin Kuzbanian regulates sympathoadrenal cell fate in development and neoplasia. *Hum Mol Genet.* **1998**, *7*(7), 1161-1167.

[115] Kessenbrock, K.; Plaks, V.Werb, Z. Matrix metalloproteinases: regulators of the tumor microenvironment. *Cell.* **2010**, *141*(1), 52-67.

[116] Dvorak, H. F.; Nagy, J. A.; Dvorak, J. T.Dvorak, A. M. Identification and characterization of the blood vessels of solid tumors that are leaky to circulating macromolecules. *Am J Pathol.* **1988**, *133*(1), 95-109.

[117] Eberhard, A.; Kahlert, S.; Goede, V.; Hemmerlein, B.; Plate, K. H.Augustin, H. G. Heterogeneity of angiogenesis and blood vessel maturation in human tumors: implications for antiangiogenic tumor therapies. *Cancer Res.* **2000**, *60*(5), 1388-1393.

[118] Kobayashi, H.; Tsuruchi, N.; Sugihara, K.; Kaku, T.; Saito, T.; Kamura, T.; Tsukamoto, N.; Nakano, H.Taniguchi, S. Expression of alpha-smooth muscle actin in benign or malignant ovarian tumors. *Gynecol Oncol.* **1993**, *48*(3), 308-313.

[119] Hashizume, H.; Baluk, P.; Morikawa, S.; McLean, J. W.; Thurston, G.; Roberge, S.; Jain, R. K.McDonald, D. M. Openings between defective endothelial cells explain tumor vessel leakiness. *Am J Pathol.* **2000**, *156*(4), 1363-1380.

[120] Paku, S. and Paweletz, N. First steps of tumor-related angiogenesis. *Lab Invest.* **1991**, *65*(3), 334-346.

[121] Baluk, P.; Morikawa, S.; Haskell, A.; Mancuso, M.McDonald, D. M. Abnormalities of basement membrane on blood vessels and endothelial sprouts in tumors. *Am J Pathol.* **2003**, *163*(5), 1801-1815.

[122] Less, J. R.; Skalak, T. C.; Sevick, E. M.Jain, R. K. Microvascular architecture in a mammary carcinoma: branching patterns and vessel dimensions. *Cancer Res.* **1991**, *51*(1), 265-273.

[123] Gillies, R. J.; Schornack, P. A.; Secomb, T. W.Raghunand, N. Causes and effects of heterogeneous perfusion in tumors. *Neoplasia.* **1999**, *1*(3), 197-207.

[124] Konerding, M. A.; Malkusch, W.; Klapthor, B.; van Ackern, C.; Fait, E.; Hill, S. A.; Parkins, C.; Chaplin, D. J.; Presta, M.Denekamp, J. Evidence for characteristic vascular patterns in solid tumours: quantitative studies using corrosion casts. *Br J Cancer.* **1999**, *80*(5-6), 724-732.

[125] Pasqualini, R.; Arap, W.McDonald, D. M. Probing the structural and molecular diversity of tumor vasculature. *Trends Mol Med.* **2002**, *8*(12), 563-571.

[126] Kelland, L. R. Targeting Established Tumor Vasculature: A Novel Approach to Cancer Treatment. *Current Cancer Therapy Reviews.* **2005**, *1*, 1-9.

[127] Folkman, J. Tumor angiogenesis: therapeutic implications. *N Engl J Med.* **1971**, *285*(21), 1182-1186.

[128] Hurwitz, H.; Fehrenbacher, L.; Novotny, W.; Cartwright, T.; Hainsworth, J.; Heim, W.; Berlin, J.; Baron, A.; Griffing, S.; Holmgren, E.; Ferrara, N.; Fyfe, G.; Rogers, B.; Ross, R.Kabbinavar, F. Bevacizumab plus irinotecan, fluorouracil, and leucovorin for metastatic colorectal cancer. *N Engl J Med.* **2004**, *350*(23), 2335-2342.

[129] Semenza, G. L. A new weapon for attacking tumor blood vessels. *N Engl J Med.* **2008**, *358*(19), 2066-2067.

[130] Slamon, D. J.; Leyland-Jones, B.; Shak, S.; Fuchs, H.; Paton, V.; Bajamonde, A.; Fleming, T.; Eiermann, W.; Wolter, J.; Pegram, M.; Baselga, J.Norton, L. Use of chemotherapy plus a monoclonal antibody against HER2 for metastatic breast cancer that overexpresses HER2. *N Engl J Med.* **2001**, *344*(11), 783-792.

[131] Baselga, J. Clinical trials of Herceptin(trastuzumab). *Eur J Cancer.* **2001**, *37 Suppl 1*, S18-24.

[132] Cuello, M.; Ettenberg, S. A.; Clark, A. S.; Keane, M. M.; Posner, R. H.; Nau, M. M.; Dennis, P. A.Lipkowitz, S. Down-regulation of the erbB-2 receptor by trastuzumab (herceptin) enhances tumor necrosis factor-related apoptosis-inducing ligand-mediated apoptosis in breast and ovarian cancer cell lines that overexpress erbB-2. *Cancer Res.* **2001**, *61*(12), 4892-4900.

[133] Nagata, Y.; Lan, K. H.; Zhou, X.; Tan, M.; Esteva, F. J.; Sahin, A. A.; Klos, K. S.; Li, P.; Monia, B. P.; Nguyen, N. T.; Hortobagyi, G. N.; Hung, M. C.Yu, D. PTEN activation contributes to tumor inhibition by trastuzumab, and loss of PTEN predicts trastuzumab resistance in patients. *Cancer Cell.* **2004**, *6*(2), 117-127.

[134] Lane, H. A.; Motoyama, A. B.; Beuvink, I.Hynes, N. E. Modulation of p27/Cdk2 complex formation through 4D5-mediated inhibition of HER2 receptor signaling. *Ann Oncol.* **2001**, *12 Suppl 1*, S21-22.

[135] Izumi, Y.; Xu, L.; di Tomaso, E.; Fukumura, D.Jain, R. K. Tumour biology: herceptin acts as an anti-angiogenic cocktail. *Nature.* **2002**, *416*(6878), 279-280.

[136] Seidman, A.; Hudis, C.; Pierri, M. K.; Shak, S.; Paton, V.; Ashby, M.; Murphy, M.; Stewart, S. J.Keefe, D. Cardiac dysfunction in the trastuzumab clinical trials experience. *J Clin Oncol.* **2002**, *20*(5), 1215-1221.

[137] Schoffski, P.; Dumez, H.; Clement, P.; Hoeben, A.; Prenen, H.; Wolter, P.; Joniau, S.; Roskams, T.Van Poppel, H. Emerging role of tyrosine kinase inhibitors in the treatment of advanced renal cell cancer: a review. *Ann Oncol.* **2006**, *17*(8), 1185-1196.

[138] Hirota, S.; Isozaki, K.; Moriyama, Y.; Hashimoto, K.; Nishida, T.; Ishiguro, S.; Kawano, K.; Hanada, M.; Kurata, A.; Takeda, M.; Muhammad Tunio, G.; Matsuzawa, Y.; Kanakura, Y.; Shinomura, Y.Kitamura, Y. Gain-of-function mutations of c-kit in human gastrointestinal stromal tumors. *Science.* **1998**, *279*(5350), 577-580.

[139] Adams, V. R. and Leggas, M. Sunitinib malate for the treatment of metastatic renal cell carcinoma and gastrointestinal stromal tumors. *Clin Ther.* **2007**, *29*(7), 1338-1353.

[140] Socinski, M. A.; Novello, S.; Brahmer, J. R.; Rosell, R.; Sanchez, J. M.; Belani, C. P.; Govindan, R.; Atkins, J. N.; Gillenwater, H. H.; Pallares, C.; Tye, L.; Selaru, P.; Chao, R. C.Scagliotti, G. V. Multicenter, phase II trial of sunitinib in previously treated, advanced non-small-cell lung cancer. *J Clin Oncol.* **2008**, *26*(4), 650-656.

[141] Kulke, K. L., H. J.; Meropol, N. J.; Posey, J.; Ryan, D. P.; Picus, J.; Bergsland, E.; Stuart, K.; Baum, C. M.; Fuchs, C. S. A phase 2 study to evaluate the efficacy and safety of SU11248 in patients (pts) with unresectable neuroendocrine tumors (NETs). *Journal of Clinical Oncology.* **2005**, (23).

[142] Wilhelm, S. M.; Adnane, L.; Newell, P.; Villanueva, A.; Llovet, J. M.Lynch, M. Preclinical overview of sorafenib, a multikinase inhibitor that targets both Raf and VEGF and PDGF receptor tyrosine kinase signaling. *Mol Cancer Ther.* **2008**, *7*(10), 3129-3140.

[143] Keating, G. M. and Santoro, A. Sorafenib: a review of its use in advanced hepatocellular carcinoma. *Drugs.* **2009**, *69*(2), 223-240.

[144] Sridhar, S. S.; Hedley, D.Siu, L. L. Raf kinase as a target for anticancer therapeutics. *Mol Cancer Ther.* **2005**, *4*(4), 677-685.

[145] Perez-Soler, R. Can rash associated with HER1/EGFR inhibition be used as a marker of treatment outcome? *Oncology (Williston Park).* **2003**, *17*(11 Suppl 12), 23-28.

[146] Strumberg, D.; Awada, A.; Hirte, H.; Clark, J. W.; Seeber, S.; Piccart, P.; Hofstra, E.; Voliotis, D.; Christensen, O.; Brueckner, A.Schwartz, B. Pooled safety analysis of BAY 43-9006 (sorafenib) monotherapy in patients with advanced solid tumours: Is rash associated with treatment outcome? *Eur J Cancer.* **2006**, *42*(4), 548-556.

[147] Maitland, M. L. M., K.; Imperial, J.; Kasza, K. E.; Karrison, T.; Elliott, W.; Undevia, S. D.; Stadler, W. A.; Desai, A.; J. Ratain, M. Blood pressure (BP) as a biomarker for sorafenib (S), an inhibitor of the vascular endothelial growth factor (VEGF) signaling pathway. *Journal of Clinical Oncology.* **2006**, *24*.

[148] Sonpavde, G. and Hutson, T. E. Pazopanib: a novel multitargeted tyrosine kinase inhibitor. *Curr Oncol Rep.* **2007**, *9*(2), 115-119.

[149] Sternberg, C. N.; Davis, I. D.; Mardiak, J.; Szczylik, C.; Lee, E.; Wagstaff, J.; Barrios, C. H.; Salman, P.; Gladkov, O. A.; Kavina, A.; Zarba, J. J.; Chen, M.; McCann, L.; Pandite, L.; Roychowdhury, D. F.Hawkins, R. E. Pazopanib in locally advanced or metastatic renal cell carcinoma: results of a randomized phase III trial. *J Clin Oncol.* **2010**, *28*(6), 1061-1068.

[150] Pick, A. M. and Nystrom, K. K. Pazopanib for the treatment of metastatic renal cell carcinoma. *Clin Ther.* **2012**, *34*(3), 511-520.

[151] Rugo, H. S.; Herbst, R. S.; Liu, G.; Park, J. W.; Kies, M. S.; Steinfeldt, H. M.; Pithavala, Y. K.; Reich, S. D.; Freddo, J. L.Wilding, G. Phase I trial of the oral antiangiogenesis agent AG-013736 in patients with advanced solid tumors: pharmacokinetic and clinical results. *J Clin Oncol.* **2005**, *23*(24), 5474-5483.

[152] Kenney, P. A. and Wood, C. G. Re: Comparative Effectiveness of Axitinib Versus Sorafenib in Advanced Renal Cell Carcinoma (AXIS): A Randomised Phase 3 Trial. *Eur Urol.* **2012**, *62*(1), 182-183.

[153] Cohen, E. E.; Rosen, L. S.; Vokes, E. E.; Kies, M. S.; Forastiere, A. A.; Worden, F. P.; Kane, M. A.; Sherman, E.; Kim, S.; Bycott, P.; Tortorici, M.; Shalinsky, D. R.; Liau, K. F.Cohen, R. B. Axitinib is an active treatment for all histologic subtypes of advanced thyroid cancer: results from a phase II study. *J Clin Oncol.* **2008**, *26*(29), 4708-4713.

[154] Fruehauf, J.; Lutzky, J.; McDermott, D.; Brown, C. K.; Meric, J. B.; Rosbrook, B.; Shalinsky, D. R.; Liau, K. F.; Niethammer, A. G.; Kim, S.Rixe, O. Multicenter, phase II study of axitinib, a selective second-generation inhibitor of vascular endothelial growth factor receptors 1, 2, and 3, in patients with metastatic melanoma. *Clin Cancer Res.* **2011**, *17*(23), 7462-7469.

[155] Schiller, J. H.; Larson, T.; Ou, S. H.; Limentani, S.; Sandler, A.; Vokes, E.; Kim, S.; Liau, K.; Bycott, P.; Olszanski, A. J.von Pawel, J. Efficacy and safety of axitinib in patients with advanced non-small-cell lung cancer: results from a phase II study. *J Clin Oncol.* **2009**, *27*(23), 3836-3841.

[156] Rugo, H. S.; Stopeck, A. T.; Joy, A. A.; Chan, S.; Verma, S.; Lluch, A.; Liau, K. F.; Kim, S.; Bycott, P.; Rosbrook, B.; Bair, A. H.Soulieres, D. Randomized, placebo-controlled, double-blind, phase II study of axitinib plus docetaxel versus docetaxel plus placebo in patients with metastatic breast cancer. *J Clin Oncol.* **2011**, *29*(18), 2459-2465.

[157] Sharma, S.; Abhyankar, V.; Burgess, R. E.; Infante, J.; Trowbridge, R. C.; Tarazi, J.; Kim, S.; Tortorici, M.; Chen, Y.Robles, R. L. A phase I study of axitinib (AG-013736) in combination with bevacizumab plus chemotherapy or chemotherapy alone in patients with metastatic colorectal cancer and other solid tumors. *Ann Oncol.* **2010**, *21*(2), 297-304.

[158] Fukuoka, M.; Yano, S.; Giaccone, G.; Tamura, T.; Nakagawa, K.; Douillard, J. Y.; Nishiwaki, Y.; Vansteenkiste, J.; Kudoh, S.; Rischin, D.; Eek, R.; Horai, T.; Noda, K.; Takata, I.; Smit, E.; Averbuch, S.; Macleod, A.; Feyereislova, A.; Dong, R. P.Baselga, J. Multi-institutional randomized phase II trial of gefitinib for previously treated patients with advanced non-small-cell lung cancer (The IDEAL 1 Trial) [corrected]. *J Clin Oncol.* **2003**, *21*(12), 2237-2246.

[159] Ranson, M.; Hammond, L. A.; Ferry, D.; Kris, M.; Tullo, A.; Murray, P. I.; Miller, V.; Averbuch, S.; Ochs, J.; Morris, C.; Feyereislova, A.; Swaisland, H.Rowinsky, E. K. ZD1839, a selective oral epidermal growth factor receptor-tyrosine kinase inhibitor, is well tolerated and active in patients with solid, malignant tumors: results of a phase I trial. *J Clin Oncol.* **2002**, *20*(9), 2240-2250.

[160] Giaccone, G.; Herbst, R. S.; Manegold, C.; Scagliotti, G.; Rosell, R.; Miller, V.; Natale, R. B.; Schiller, J. H.; Von Pawel, J.; Pluzanska, A.; Gatzemeier, U.; Grous, J.; Ochs, J. S.; Averbuch, S. D.; Wolf, M. K.; Rennie, P.; Fandi,

A.Johnson, D. H. Gefitinib in combination with gemcitabine and cisplatin in advanced non-small-cell lung cancer: a phase III trial--INTACT 1. *J Clin Oncol.* **2004**, *22*(5), 777-784.

[161] Herbst, R. S.; Giaccone, G.; Schiller, J. H.; Natale, R. B.; Miller, V.; Manegold, C.; Scagliotti, G.; Rosell, R.; Oliff, I.; Reeves, J. A.; Wolf, M. K.; Krebs, A. D.; Averbuch, S. D.; Ochs, J. S.; Grous, J.; Fandi, A.Johnson, D. H. Gefitinib in combination with paclitaxel and carboplatin in advanced non-small-cell lung cancer: a phase III trial--INTACT 2. *J Clin Oncol.* **2004**, *22*(5), 785-794.

[162] Kim, Y. H.; Ishii, G.; Goto, K.; Nagai, K.; Tsuta, K.; Shiono, S.; Nitadori, J.; Kodama, T.; Nishiwaki, Y.Ochiai, A. Dominant papillary subtype is a significant predictor of the response to gefitinib in adenocarcinoma of the lung. *Clin Cancer Res.* **2004**, *10*(21), 7311-7317.

[163] Perez-Soler, R.; Chachoua, A.; Hammond, L. A.; Rowinsky, E. K.; Huberman, M.; Karp, D.; Rigas, J.; Clark, G. M.; Santabarbara, P.Bonomi, P. Determinants of tumor response and survival with erlotinib in patients with non--small-cell lung cancer. *J Clin Oncol.* **2004**, *22*(16), 3238-3247.

[164] Nakamura, H.; Kawasaki, N.; Taguchi, M.Kabasawa, K. Survival impact of epidermal growth factor receptor overexpression in patients with non-small cell lung cancer: a meta-analysis. *Thorax.* **2006**, *61*(2), 140-145.

[165] Lynch, T. J.; Bell, D. W.; Sordella, R.; Gurubhagavatula, S.; Okimoto, R. A.; Brannigan, B. W.; Harris, P. L.; Haserlat, S. M.; Supko, J. G.; Haluska, F. G.; Louis, D. N.; Christiani, D. C.; Settleman, J.Haber, D. A. Activating mutations in the epidermal growth factor receptor underlying responsiveness of non-small-cell lung cancer to gefitinib. *N Engl J Med.* **2004**, *350*(21), 2129-2139.

[166] Paez, J. G.; Janne, P. A.; Lee, J. C.; Tracy, S.; Greulich, H.; Gabriel, S.; Herman, P.; Kaye, F. J.; Lindeman, N.; Boggon, T. J.; Naoki, K.; Sasaki, H.; Fujii, Y.; Eck, M. J.; Sellers, W. R.; Johnson, B. E.Meyerson, M. EGFR mutations in lung cancer: correlation with clinical response to gefitinib therapy. *Science.* **2004**, *304*(5676), 1497-1500.

[167] Tokumo, M.; Toyooka, S.; Kiura, K.; Shigematsu, H.; Tomii, K.; Aoe, M.; Ichimura, K.; Tsuda, T.; Yano, M.; Tsukuda, K.; Tabata, M.; Ueoka, H.; Tanimoto, M.; Date, H.; Gazdar, A. F.Shimizu, N. The relationship between epidermal growth factor receptor mutations and clinicopathologic features in non-small cell lung cancers. *Clin Cancer Res.* **2005**, *11*(3), 1167-1173.

[168] Meyerhardt, J. A.; Zhu, A. X.; Enzinger, P. C.; Ryan, D. P.; Clark, J. W.; Kulke, M. H.; Earle, C. C.; Vincitore, M.; Michelini, A.; Sheehan, S.Fuchs, C. S. Phase II study of capecitabine, oxaliplatin, and erlotinib in previously treated patients with metastatic colorectal cancer. *J Clin Oncol.* **2006**, *24*(12), 1892-1897.

[169] Townsley, C. A.; Major, P.; Siu, L. L.; Dancey, J.; Chen, E.; Pond, G. R.; Nicklee, T.; Ho, J.; Hedley, D.; Tsao, M.; Moore, M. J.Oza, A. M. Phase II study of erlotinib (OSI-774) in patients with metastatic colorectal cancer. *Br J Cancer.* **2006**, *94*(8), 1136-1143.

[170] Philip, P. A.; Mahoney, M. R.; Allmer, C.; Thomas, J.; Pitot, H. C.; Kim, G.; Donehower, R. C.; Fitch, T.; Picus, J.Erlichman, C. Phase II study of erlotinib in patients with advanced biliary cancer. *J Clin Oncol.* **2006**, *24*(19), 3069-3074.

[171] Philip, P. A.; Mahoney, M. R.; Allmer, C.; Thomas, J.; Pitot, H. C.; Kim, G.; Donehower, R. C.; Fitch, T.; Picus, J.Erlichman, C. Phase II study of Erlotinib

(OSI-774) in patients with advanced hepatocellular cancer. *J Clin Oncol.* **2005**, *23*(27), 6657-6663.

[172] Hainsworth, J. D.; Sosman, J. A.; Spigel, D. R.; Edwards, D. L.; Baughman, C.Greco, A. Treatment of metastatic renal cell carcinoma with a combination of bevacizumab and erlotinib. *J Clin Oncol.* **2005**, *23*(31), 7889-7896.

[173] Kobayashi, T.; Koizumi, T.; Agatsuma, T.; Yasuo, M.; Tsushima, K.; Kubo, K.; Eda, S.; Kuraishi, H.; Koyama, S.; Hachiya, T.Ohura, N. A phase II trial of erlotinib in patients with EGFR wild-type advanced non-small-cell lung cancer. *Cancer Chemother Pharmacol.* **2012**, *69*(5), 1241-1246.

[174] Nelson, M. H. and Dolder, C. R. Lapatinib: a novel dual tyrosine kinase inhibitor with activity in solid tumors. *Ann Pharmacother.* **2006**, *40*(2), 261-269.

[175] Burris, H. A., 3rd; Hurwitz, H. I.; Dees, E. C.; Dowlati, A.; Blackwell, K. L.; O'Neil, B.; Marcom, P. K.; Ellis, M. J.; Overmoyer, B.; Jones, S. F.; Harris, J. L.; Smith, D. A.; Koch, K. M.; Stead, A.; Mangum, S.Spector, N. L. Phase I safety, pharmacokinetics, and clinical activity study of lapatinib (GW572016), a reversible dual inhibitor of epidermal growth factor receptor tyrosine kinases, in heavily pretreated patients with metastatic carcinomas. *J Clin Oncol.* **2005**, *23*(23), 5305-5313.

[176] Fields, A. L. R., D. A.; Henderson, C. A.; Germond, C. J.; Chu, L.; Brill, K. J.; Leopold, L. H.; Berger M. S. An Open-Label Multicenter Phase II Study of Oral Lapatinib (GW572016) as Single Agent, Second-Line Therapy in Patients with Metastatic Colorectal Cancer

Journal of Clinical Oncology. **2005**, *23*(16S), 3583.

[177] Geyer, C. E.; Forster, J.; Lindquist, D.; Chan, S.; Romieu, C. G.; Pienkowski, T.; Jagiello-Gruszfeld, A.; Crown, J.; Chan, A.; Kaufman, B.; Skarlos, D.; Campone, M.; Davidson, N.; Berger, M.; Oliva, C.; Rubin, S. D.; Stein, S.Cameron, D. Lapatinib plus capecitabine for HER2-positive advanced breast cancer. *N Engl J Med.* **2006**, *355*(26), 2733-2743.

[178] Ravaud, A.; Hawkins, R.; Gardner, J. P.; von der Maase, H.; Zantl, N.; Harper, P.; Rolland, F.; Audhuy, B.; Machiels, J. P.; Petavy, F.; Gore, M.; Schoffski, P.El-Hariry, I. Lapatinib versus hormone therapy in patients with advanced renal cell carcinoma: a randomized phase III clinical trial. *J Clin Oncol.* **2008**, *26*(14), 2285-2291.

[179] Crivellari, D.; Spazzapan, S.; Lombardi, D.; Militello, L.; Torrisi, E.; Russo, A. E.; Sorio, R.; Talamini, R.; Miolo, G.; Carli, P.Veronesi, A. Lapatinib-based therapy in heavily pretreated HER2-positive metastatic breast cancer: a single institution experience. *Tumori.* **2012**, *98*(1), 33-38.

[180] Baselga, J.; Bradbury, I.; Eidtmann, H.; Di Cosimo, S.; de Azambuja, E.; Aura, C.; Gomez, H.; Dinh, P.; Fauria, K.; Van Dooren, V.; Aktan, G.; Goldhirsch, A.; Chang, T. W.; Horvath, Z.; Coccia-Portugal, M.; Domont, J.; Tseng, L. M.; Kunz, G.; Sohn, J. H.; Semiglazov, V.; Lerzo, G.; Palacova, M.; Probachai, V.; Pusztai, L.; Untch, M.; Gelber, R. D.Piccart-Gebhart, M. Lapatinib with trastuzumab for HER2-positive early breast cancer (NeoALTTO): a randomised, open-label, multicentre, phase 3 trial. *Lancet.* **2012**, *379*(9816), 633-640.

[181] Breast cancer drug approved for new indication. *Womens Health (Lond Engl).* **2010**, *6*(2), 173.

[182] Wedge, S. R.; Ogilvie, D. J.; Dukes, M.; Kendrew, J.; Chester, R.; Jackson, J. A.; Boffey, S. J.; Valentine, P. J.; Curwen, J. O.; Musgrove, H. L.; Graham, G. A.; Hughes, G. D.; Thomas, A. P.; Stokes, E. S.; Curry, B.; Richmond, G. H.; Wadsworth, P. F.; Bigley, A. L.Hennequin, L. F. ZD6474 inhibits vascular endothelial growth factor signaling, angiogenesis, and tumor growth following oral administration. *Cancer Res.* **2002**, *62*(16), 4645-4655.

[183] Ciardiello, F.; Caputo, R.; Damiano, V.; Troiani, T.; Vitagliano, D.; Carlomagno, F.; Veneziani, B. M.; Fontanini, G.; Bianco, A. R.Tortora, G. Antitumor effects of ZD6474, a small molecule vascular endothelial growth factor receptor tyrosine kinase inhibitor, with additional activity against epidermal growth factor receptor tyrosine kinase. *Clin Cancer Res.* **2003**, *9*(4), 1546-1556.

[184] Ryan, A. J. and Wedge, S. R. ZD6474--a novel inhibitor of VEGFR and EGFR tyrosine kinase activity. *Br J Cancer.* **2005**, *92 Suppl 1*, S6-13.

[185] Heymach, J. V. ZD6474--clinical experience to date. *Br J Cancer.* **2005**, *92 Suppl 1*, S14-20.

[186] Heymach, J. V.; Johnson, B. E.; Prager, D.; Csada, E.; Roubec, J.; Pesek, M.; Spasova, I.; Belani, C. P.; Bodrogi, I.; Gadgeel, S.; Kennedy, S. J.; Hou, J.Herbst, R. S. Randomized, placebo-controlled phase II study of vandetanib plus docetaxel in previously treated non small-cell lung cancer. *J Clin Oncol.* **2007**, *25*(27), 4270-4277.

[187] Miller, K. D.; Trigo, J. M.; Wheeler, C.; Barge, A.; Rowbottom, J.; Sledge, G.Baselga, J. A multicenter phase II trial of ZD6474, a vascular endothelial growth factor receptor-2 and epidermal growth factor receptor tyrosine kinase inhibitor, in patients with previously treated metastatic breast cancer. *Clin Cancer Res.* **2005**, *11*(9), 3369-3376.

[188] Kovacs, M. J.; Reece, D. E.; Marcellus, D.; Meyer, R. M.; Mathews, S.; Dong, R. P.Eisenhauer, E. A phase II study of ZD6474 (Zactima, a selective inhibitor of VEGFR and EGFR tyrosine kinase in patients with relapsed multiple myeloma--NCIC CTG IND.145. *Invest New Drugs.* **2006**, *24*(6), 529-535.

[189] Wells, S. A., Jr.; Gosnell, J. E.; Gagel, R. F.; Moley, J.; Pfister, D.; Sosa, J. A.; Skinner, M.; Krebs, A.; Vasselli, J.Schlumberger, M. Vandetanib for the treatment of patients with locally advanced or metastatic hereditary medullary thyroid cancer. *J Clin Oncol.* **2010**, *28*(5), 767-772.

[190] Wells, S. A., Jr.; Robinson, B. G.; Gagel, R. F.; Dralle, H.; Fagin, J. A.; Santoro, M.; Baudin, E.; Elisei, R.; Jarzab, B.; Vasselli, J. R.; Read, J.; Langmuir, P.; Ryan, A. J.Schlumberger, M. J. Vandetanib in patients with locally advanced or metastatic medullary thyroid cancer: a randomized, double-blind phase III trial. *J Clin Oncol.* **2012**, *30*(2), 134-141.

[191] Lee, J. S.; Hirsh, V.; Park, K.; Qin, S.; Blajman, C. R.; Perng, R. P.; Chen, Y. M.; Emerson, L.; Langmuir, P.Manegold, C. Vandetanib Versus Placebo in Patients With Advanced Non-Small-Cell Lung Cancer After Prior Therapy With an Epidermal Growth Factor Receptor Tyrosine Kinase Inhibitor: A Randomized, Double-Blind Phase III Trial (ZEPHYR). *J Clin Oncol.* **2012**, *30*(10), 1114-1121.

[192] Natale, R. B.; Thongprasert, S.; Greco, F. A.; Thomas, M.; Tsai, C. M.; Sunpaweravong, P.; Ferry, D.; Mulatero, C.; Whorf, R.; Thompson, J.; Barlesi, F.; Langmuir, P.; Gogov, S.; Rowbottom, J. A.Goss, G. D. Phase III Trial of

Vandetanib Compared With Erlotinib in Patients With Previously Treated Advanced Non-Small-Cell Lung Cancer. *J Clin Oncol.* **2011**, *29*(8), 1059-1066.

[193] Herbst, R. S.; Sun, Y.; Eberhardt, W. E.; Germonpre, P.; Saijo, N.; Zhou, C.; Wang, J.; Li, L.; Kabbinavar, F.; Ichinose, Y.; Qin, S.; Zhang, L.; Biesma, B.; Heymach, J. V.; Langmuir, P.; Kennedy, S. J.; Tada, H.Johnson, B. E.
(ZODIAC): a double-blind, randomised, phase 3 trial. *Lancet Oncol.* **2010**, *11*(7), 619-626.

[194] Heinrich, M. C.; Griffith, D. J.; Druker, B. J.; Wait, C. L.; Ott, K. A.Zigler, A. J. Inhibition of c-kit receptor tyrosine kinase activity by STI 571, a selective tyrosine kinase inhibitor. *Blood.* **2000**, *96*(3), 925-932.

[195] Carroll, M.; Ohno-Jones, S.; Tamura, S.; Buchdunger, E.; Zimmermann, J.; Lydon, N. B.; Gilliland, D. G.Druker, B. J. CGP 57148, a tyrosine kinase inhibitor, inhibits the growth of cells expressing BCR-ABL, TEL-ABL, and TEL-PDGFR fusion proteins. *Blood.* **1997**, *90*(12), 4947-4952.

[196] van Oosterom, A. T.; Judson, I. R.; Verweij, J.; Stroobants, S.; Dumez, H.; Donato di Paola, E.; Sciot, R.; Van Glabbeke, M.; Dimitrijevic, S.Nielsen, O. S. Update of phase I study of imatinib (STI571) in advanced soft tissue sarcomas and gastrointestinal stromal tumors: a report of the EORTC Soft Tissue and Bone Sarcoma Group. *Eur J Cancer.* **2002**, *38 Suppl 5*, S83-87.

[197] Demetri, G. D.; von Mehren, M.; Blanke, C. D.; Van den Abbeele, A. D.; Eisenberg, B.; Roberts, P. J.; Heinrich, M. C.; Tuveson, D. A.; Singer, S.; Janicek, M.; Fletcher, J. A.; Silverman, S. G.; Silberman, S. L.; Capdeville, R.; Kiese, B.; Peng, B.; Dimitrijevic, S.; Druker, B. J.; Corless, C.; Fletcher, C. D.Joensuu, H. Efficacy and safety of imatinib mesylate in advanced gastrointestinal stromal tumors. *N Engl J Med.* **2002**, *347*(7), 472-480.

[198] Rubin, B. P.; Singer, S.; Tsao, C.; Duensing, A.; Lux, M. L.; Ruiz, R.; Hibbard, M. K.; Chen, C. J.; Xiao, S.; Tuveson, D. A.; Demetri, G. D.; Fletcher, C. D.Fletcher, J. A. KIT activation is a ubiquitous feature of gastrointestinal stromal tumors. *Cancer Res.* **2001**, *61*(22), 8118-8121.

[199] Pasqualini, R.; Koivunen, E.; Kain, R.; Lahdenranta, J.; Sakamoto, M.; Stryhn, A.; Ashmun, R. A.; Shapiro, L. H.; Arap, W.Ruoslahti, E. Aminopeptidase N is a receptor for tumor-homing peptides and a target for inhibiting angiogenesis. *Cancer Res.* **2000**, *60*(3), 722-727.

[200] Friedlander, M.; Brooks, P. C.; Shaffer, R. W.; Kincaid, C. M.; Varner, J. A.Cheresh, D. A. Definition of two angiogenic pathways by distinct alpha v integrins. *Science.* **1995**, *270*(5241), 1500-1502.

[201] Hammes, H. P.; Brownlee, M.; Jonczyk, A.; Sutter, A.Preissner, K. T. Subcutaneous injection of a cyclic peptide antagonist of vitronectin receptor-type integrins inhibits retinal neovascularization. *Nat Med.* **1996**, *2*(5), 529-533.

[202] Korpelainen, E. I. and Alitalo, K. Signaling angiogenesis and lymphangiogenesis. *Curr Opin Cell Biol.* **1998**, *10*(2), 159-164.

[203] Lappi, D. A. Tumor targeting through fibroblast growth factor receptors. *Semin Cancer Biol.* **1995**, *6*(5), 279-288.

[204] Haas, T. L.; Davis, S. J.Madri, J. A. Three-dimensional type I collagen lattices induce coordinate expression of matrix metalloproteinases MT1-MMP and MMP-2 in microvascular endothelial cells. *J Biol Chem.* **1998**, *273*(6), 3604-3610.

[205] Vu, T. H.; Shipley, J. M.; Bergers, G.; Berger, J. E.; Helms, J. A.; Hanahan, D.; Shapiro, S. D.; Senior, R. M.Werb, Z. MMP-9/gelatinase B is a key regulator of growth plate angiogenesis and apoptosis of hypertrophic chondrocytes. *Cell.* **1998**, *93*(3), 411-422.

[206] Schlingemann, R. O.; Rietveld, F. J.; de Waal, R. M.; Ferrone, S.Ruiter, D. J. Expression of the high molecular weight melanoma-associated antigen by pericytes during angiogenesis in tumors and in healing wounds. *Am J Pathol.* **1990**, *136*(6), 1393-1405.

[207] Burg, M. A.; Pasqualini, R.; Arap, W.; Ruoslahti, E.Stallcup, W. B. NG2 proteoglycan-binding peptides target tumor neovasculature. *Cancer Res.* **1999**, *59*(12), 2869-2874.

[208] Wex, T.; Buhling, F.; Arndt, M.; Frank, K.; Ansorge, S.Lendeckel, U. The activation-dependent induction of APN-(CD13) in T-cells is controlled at different levels of gene expression. *FEBS Lett.* **1997**, *412*(1), 53-56.

[209] Bhagwat, S. V.; Petrovic, N.; Okamoto, Y.Shapiro, L. H. The angiogenic regulator CD13/APN is a transcriptional target of Ras signaling pathways in endothelial morphogenesis. *Blood.* **2003**, *101*(5), 1818-1826.

[210] Hooper, N. M. Families of zinc metalloproteases. *FEBS Lett.* **1994**, *354*(1), 1-6.

[211] Taylor, A. Aminopeptidases: structure and function. *FASEB J.* **1993**, *7*(2), 290-298.

[212] Look, A. T.; Ashmun, R. A.; Shapiro, L. H.Peiper, S. C. Human myeloid plasma membrane glycoprotein CD13 (gp150) is identical to aminopeptidase N. *J Clin Invest.* **1989**, *83*(4), 1299-1307.

[213] Firla, B.; Arndt, M.; Frank, K.; Thiel, U.; Ansorge, S.; Tager, M.Lendeckel, U. Extracellular cysteines define ectopeptidase (APN, CD13) expression and function. *Free Radic Biol Med.* **2002**, *32*(7), 584-595.

[214] Favaloro, E. J.; Browning, T.Facey, D. CD13 (GP150; aminopeptidase-N): predominant functional activity in blood is localized to plasma and is not cell-surface associated. *Exp Hematol.* **1993**, *21*(13), 1695-1701.

[215] Kawai, M.; Otake, Y.Hara, Y. High-molecular-mass isoform of aminopeptidase N/CD13 in serum from cholestatic patients. *Clin Chim Acta.* **2003**, *330*(1-2), 141-149.

[216] Matsas, R.; Stephenson, S. L.; Hryszko, J.; Kenny, A. J.Turner, A. J. The metabolism of neuropeptides. Phase separation of synaptic membrane preparations with Triton X-114 reveals the presence of aminopeptidase N. *Biochem J.* **1985**, *231*(2), 445-449.

[217] Xu, Y.; Wellner, D.Scheinberg, D. A. Substance P and bradykinin are natural inhibitors of CD13/aminopeptidase N. *Biochem Biophys Res Commun.* **1995**, *208*(2), 664-674.

[218] Laouar, A.; Wietzerbin, J.Bauvois, B. Divergent regulation of cell surface protease expression in HL-60 cells differentiated into macrophages with granulocyte macrophage colony stimulating factor or neutrophils with retinoic acid. *Int Immunol.* **1993**, *5*(8), 965-973.

[219] Delmas, B.; Gelfi, J.; L'Haridon, R.; Vogel, L. K.; Sjostrom, H.; Noren, O.Laude, H. Aminopeptidase N is a major receptor for the entero-pathogenic coronavirus TGEV. *Nature.* **1992**, *357*(6377), 417-420.

[220] Yeager, C. L.; Ashmun, R. A.; Williams, R. K.; Cardellichio, C. B.; Shapiro, L. H.; Look, A. T.Holmes, K. V. Human aminopeptidase N is a receptor for human coronavirus 229E. *Nature*. **1992**, *357*(6377), 420-422.

[221] Riemann, D.; Kehlen, A.Langner, J. CD13--not just a marker in leukemia typing. *Immunol Today*. **1999**, *20*(2), 83-88.

[222] Saiki, I.; Murata, J.; Watanabe, K.; Fujii, H.; Abe, F.Azuma, I. Inhibition of tumor cell invasion by ubenimex (bestatin) in vitro. *Jpn J Cancer Res*. **1989**, *80*(9), 873-878.

[223] Yoneda, J.; Saiki, I.; Fujii, H.; Abe, F.; Kojima, Y.Azuma, I. Inhibition of tumor invasion and extracellular matrix degradation by ubenimex (bestatin). *Clin Exp Metastasis*. **1992**, *10*(1), 49-59.

[224] Saiki, I.; Fujii, H.; Yoneda, J.; Abe, F.; Nakajima, M.; Tsuruo, T.Azuma, I. Role of aminopeptidase N (CD13) in tumor-cell invasion and extracellular matrix degradation. *Int J Cancer*. **1993**, *54*(1), 137-143.

[225] Fujii, H.; Nakajima, M.; Saiki, I.; Yoneda, J.; Azuma, I.Tsuruo, T. Human melanoma invasion and metastasis enhancement by high expression of aminopeptidase N/CD13. *Clin Exp Metastasis*. **1995**, *13*(5), 337-344.

[226] Bhagwat, S. V.; Lahdenranta, J.; Giordano, R.; Arap, W.; Pasqualini, R.Shapiro, L. H. CD13/APN is activated by angiogenic signals and is essential for capillary tube formation. *Blood*. **2001**, *97*(3), 652-659.

[227] Fukasawa, K.; Fujii, H.; Saitoh, Y.; Koizumi, K.; Aozuka, Y.; Sekine, K.; Yamada, M.; Saiki, I.Nishikawa, K. Aminopeptidase N (APN/CD13) is selectively expressed in vascular endothelial cells and plays multiple roles in angiogenesis. *Cancer Lett*. **2006**, *243*(1), 135-143.

[228] Petrovic, N.; Schacke, W.; Gahagan, J. R.; O'Conor, C. A.; Winnicka, B.; Conway, R. E.; Mina-Osorio, P.Shapiro, L. H. CD13/APN regulates endothelial invasion and filopodia formation. *Blood*. **2007**, *110*(1), 142-150.

[229] Rangel, R.; Sun, Y.; Guzman-Rojas, L.; Ozawa, M. G.; Sun, J.; Giordano, R. J.; Van Pelt, C. S.; Tinkey, P. T.; Behringer, R. R.; Sidman, R. L.; Arap, W.Pasqualini, R. Impaired angiogenesis in aminopeptidase N-null mice. *Proc Natl Acad Sci U S A*. **2007**, *104*(11), 4588-4593.

[230] Mechtersheimer, G. and Moller, P. Expression of aminopeptidase N (CD13) in mesenchymal tumors. *Am J Pathol*. **1990**, *137*(5), 1215-1222.

[231] Alliot, F.; Rutin, J.; Leenen, P. J.Pessac, B. Pericytes and periendothelial cells of brain parenchyma vessels co-express aminopeptidase N, aminopeptidase A, and nestin. *J Neurosci Res*. **1999**, *58*(3), 367-378.

[232] Dixon, J.; Kaklamanis, L.; Turley, H.; Hickson, I. D.; Leek, R. D.; Harris, A. L.Gatter, K. C. Expression of aminopeptidase-n (CD 13) in normal tissues and malignant neoplasms of epithelial and lymphoid origin. *J Clin Pathol*. **1994**, *47*(1), 43-47.

[233] Hashida, H.; Takabayashi, A.; Kanai, M.; Adachi, M.; Kondo, K.; Kohno, N.; Yamaoka, Y.Miyake, M. Aminopeptidase N is involved in cell motility and angiogenesis: its clinical significance in human colon cancer. *Gastroenterology*. **2002**, *122*(2), 376-386.

[234] Murakami, H.; Yokoyama, A.; Kondo, K.; Nakanishi, S.; Kohno, N.Miyake, M. Circulating aminopeptidase N/CD13 is an independent prognostic factor in patients with non-small cell lung cancer. *Clin Cancer Res*. **2005**, *11*(24 Pt 1), 8674-8679.

[235] Tokuhara, T.; Hattori, N.; Ishida, H.; Hirai, T.; Higashiyama, M.; Kodama, K.Miyake, M. Clinical significance of aminopeptidase N in non-small cell lung cancer. *Clin Cancer Res*. **2006**, *12*(13), 3971-3978.

[236] Ishii, K.; Usui, S.; Sugimura, Y.; Yoshida, S.; Hioki, T.; Tatematsu, M.; Yamamoto, H.Hirano, K. Aminopeptidase N regulated by zinc in human prostate participates in tumor cell invasion. *Int J Cancer*. **2001**, *92*(1), 49-54.

[237] Umezawa, H.; Aoyagi, T.; Suda, H.; Hamada, M.Takeuchi, T. Bestatin, an inhibitor of aminopeptidase B, produced by actinomycetes. *J Antibiot (Tokyo)*. **1976**, *29*(1), 97-99.

[238] Orning, L.; Krivi, G.Fitzpatrick, F. A. Leukotriene A4 hydrolase. Inhibition by bestatin and intrinsic aminopeptidase activity establish its functional resemblance to metallohydrolase enzymes. *J Biol Chem*. **1991**, *266*(3), 1375-1378.

[239] Braun, R. K.; Foerster, M.; Workalemahu, G.; Haefner, D.; Kroegel, C.Walker, C. Differential regulation of aminopeptidase N (CD13) by transendothelial migration and cytokines on human eosinophils. *Exp Lung Res*. **2003**, *29*(2), 59-77.

[240] Fujii, H.; Nakajima, M.; Aoyagi, T.Tsuruo, T. Inhibition of tumor cell invasion and matrix degradation by aminopeptidase inhibitors. *Biol Pharm Bull*. **1996**, *19*(1), 6-10.

[241] Aozuka, Y.; Koizumi, K.; Saitoh, Y.; Ueda, Y.; Sakurai, H.Saiki, I. Anti-tumor angiogenesis effect of aminopeptidase inhibitor bestatin against B16-BL6 melanoma cells orthotopically implanted into syngeneic mice. *Cancer Lett*. **2004**, *216*(1), 35-42.

[242] Ezawa, K.; Minato, K.Dobashi, K. Induction of apoptosis by ubenimex (Bestatin) in human non-small-cell lung cancer cell lines. *Biomed Pharmacother*. **1996**, *50*(6-7), 283-289.

[243] Sekine, K.; Fujii, H.; Abe, F.Nishikawa, K. Augmentation of death ligand-induced apoptosis by aminopeptidase inhibitors in human solid tumor cell lines. *Int J Cancer*. **2001**, *94*(4), 485-491.

[244] Sekine, K.; Fujii, H.Abe, F. Induction of apoptosis by bestatin (ubenimex) in human leukemic cell lines. *Leukemia*. **1999**, *13*(5), 729-734.

[245] Sawafuji, K.; Miyakawa, Y.; Weisberg, E.; Griffin, J. D.; Ikeda, Y.Kizaki, M. Aminopeptidase inhibitors inhibit proliferation and induce apoptosis of K562 and STI571-resistant K562 cell lines through the MAPK and GSK-3beta pathways. *Leuk Lymphoma*. **2003**, *44*(11), 1987-1996.

[246] Lin, M.; He, J.; Cai, Z.Qian, W. [Aminopeptidase inhibitor Bestatin induces HL-60 cell apoptosis through activating caspase 3]. *Zhonghua Xue Ye Xue Za Zhi*. **2001**, *22*(7), 348-350.

[247] Abe, F.; Shibuya, K.; Uchida, M.; Takahashi, K.; Horinishi, H.; Matsuda, A.; Ishizuka, M.; Takeuchi, T.Umezawa, H. Effect of bestatin on syngeneic tumors in mice. *Gann*. **1984**, *75*(1), 89-94.

[248] Ishizuka, M.; Masuda, T.; Mizutani, S.; Takeuchi, T.Umezawa, H. Antitumor cells found in tumor-bearing mice given ubenimex. *J Antibiot (Tokyo)*. **1987**, *40*(5), 697-701.

[249] Abe, F.; Yamashita, T.; Takahashi, K.; Matsuda, A.; Ichikawa, T.Umezawa, H. [Antitumor effect of bestatin combined with bleomycin against hepatoma AH 66 subcutaneously transplanted in rats]. *Jpn J Antibiot*. **1984**, *37*(4), 589-592.

[250] Tsuruo, T.; Naganuma, K.; Iida, H.; Yamori, T.; Tsukagoshi, S.Sakurai, Y. Inhibition of lymph node metastasis of P388 leukemia by bestatin in mice. *J Antibiot (Tokyo)*. **1981**, *34*(9), 1206-1209.

[251] Pisha, E.; Chai, H.; Lee, I. S.; Chagwedera, T. E.; Farnsworth, N. R.; Cordell, G. A.; Beecher, C. W.; Fong, H. H.; Kinghorn, A. D.; Brown, D. M.et al. Discovery of betulinic acid as a selective inhibitor of human melanoma that functions by induction of apoptosis. *Nat Med.* **1995**, *1*(10), 1046-1051.

[252] Oka, S. A review of clinical studies of bestatin. *Recent Results Cancer Res.* **1980**, *75*, 126-132.

[253] Blomgren, H.; Edsmyr, F.; Esposti, P. L.Naslund, I. Immunological and haematological monitoring in bladder cancer patients receiving adjuvant bestatin treatment following radiation therapy. A prospective randomized trial. *Biomed Pharmacother.* **1984**, *38*(3), 143-149.

[254] Mouritzen, C. Bestatin as adjuvant treatment in operated stage I and stage II non-small cell lung cancer. European Lung Cancer Study Group. *Acta Oncol.* **1990**, *29*(6), 817-820.

[255] Ikeda, S.; Ishihara, K.Taguchi, G. [Phase III study of bestatin in patients with malignant skin tumors. (1) Malignant melanoma]. *Gan To Kagaku Ryoho.* **1985**, *12*(1), 77-85.

[256] Ikeda, S.; Ishihara, K.Taguchi, G. [Phase III controlled studies of bestatin in malignant tumors of the skin--results of treatment of squamous cell carcinoma and genital Paget's disease]. *Gan To Kagaku Ryoho.* **1985**, *12*(6), 1260-1266.

[257] Tanaka, T.; Oka, T.Hashimoto, I. [Randomized controlled trial of postoperative adjuvant chemotherapy with bestatin for gastric cancer]. *Gan To Kagaku Ryoho.* **1985**, *12*(1), 125-133.

[258] Ozono, S.; Iwai, A.; Babaya, K.; Hiramatsu, T.; Yoshida, K.; Yamada, K.; Hirao, Y.; Aoyama, H.; Ohara, S.Okajima, E. Effects of bestatin on the host immunity in patients treated for urogenital cancer. *Acta Oncol.* **1990**, *29*(6), 813-816.

[259] Furuse, K.; Fukuoka, M.; Genka, K.; Kato, H.; Tsubura, E.; Ohta, M.; Nakai, H.; Kinuwaki, E.; Nakano, M.; Ishikawa, S.et al. [Double blind controlled study of ubenimex (Bestatin) against squamous cell lung cancer--a multicenter cooperative study]. *Gan To Kagaku Ryoho.* **1993**, *20*(9), 1187-1194.

[260] Ashmun, R. A. and Look, A. T. Metalloprotease activity of CD13/aminopeptidase N on the surface of human myeloid cells. *Blood.* **1990**, *75*(2), 462-469.

[261] Pinto, A.; Del Vecchio, L.; Carbone, A.; Roncadin, M.; Volpe, R.; Serraino, D.; Monfardini, S.; Colombatti, A.Zagonel, V. Expression of myelomonocytic antigens is associated with unfavourable clinicoprognostic factors in B-cell chronic lymphocytic leukaemia. *Ann Oncol.* **1991**, *2 Suppl 2*, 107-113.

[262] Bassan, R.; Biondi, A.; Benvestito, S.; Tini, M. L.; Abbate, M.; Viero, P.; Barbui, T.Rambaldi, A. Acute undifferentiated leukemia with CD7+ and CD13+ immunophenotype. Lack of molecular lineage commitment and association with poor prognostic features. *Cancer.* **1992**, *69*(2), 396-404.

[263] Favaloro, E. J.; Browning, T.; Nandurkar, H.; Sartor, M.; Bradstock, K. F.Koutts, J. Aminopeptidase-N (CD13; gp 150): contrasting patterns of enzymatic activity in blood from patients with myeloid or lymphoid leukemia. *Leuk Res.* **1995**, *19*(9), 659-666.

[264] Kurita, S.; Ota, K.; Yamada, K.; Massaoka, T.; Uzuka, Y.Ogawa, N. [Immunotherapy with bestatin for acute non-lymphocytic leukemia (ANLL) in adults]. *Gan To Kagaku Ryoho*. **1984**, *11*(12 Pt 2), 2742-2750.

[265] Ota, K.; Kurita, S.; Yamada, K.; Masaoka, T.; Uzuka, Y.Ogawa, N. Immunotherapy with bestatin for acute nonlymphocytic leukemia in adults. *Cancer Immunol Immunother*. **1986**, *23*(1), 5-10.

[266] Ota, K.; Kurita, S.; Yamada, K.; Masaoka, T.; Uzuka, Y.Ogawa, N. [Results of follow-up studies on prognosis after immunotherapy with bestatin in acute nonlymphocytic leukemia]. *Gan To Kagaku Ryoho*. **1986**, *13*(4 Pt 1), 1017-1025.

[267] Ota, K. and Ogawa, N. Randomized controlled study of chemoimmunotherapy with bestatin of acute nonlymphocytic leukemia in adults. *Biomed Pharmacother*. **1990**, *44*(2), 93-101.

[268] Kobayashi, T.; Miyawaki, S.; Tanimoto, M.; Kuriyama, K.; Murakami, H.; Yoshida, M.; Minami, S.; Minato, K.; Tsubaki, K.; Ohmoto, E.; Oh, H.; Jinnai, I.; Sakamaki, H.; Hiraoka, A.; Kanamaru, A.; Takahashi, I.; Saito, K.; Naoe, T.; Yamada, O.; Asou, N.; Kageyama, S.; Emi, N.; Matsuoka, A.; Tomonaga, M.; Ohno, R.et al. Randomized trials between behenoyl cytarabine and cytarabine in combination induction and consolidation therapy, and with or without ubenimex after maintenance/intensification therapy in adult acute myeloid leukemia. The Japan Leukemia Study Group. *J Clin Oncol*. **1996**, *14*(1), 204-213.

[269] Ino, K.; Bierman, P. J.; Varney, M. L.; Heimann, D. G.; Kuszynski, C. A.; Walker, S. A.Talmadge, J. E. Monocyte activation by an oral immunomodulator (bestatin) in lymphoma patients following autologous bone marrow transplantation. *Cancer Immunol Immunother*. **1996**, *43*(4), 206-212.

[270] Aoyagi, T.; Tobe, H.; Kojima, F.; Hamada, M.; Takeuchi, T.Umezawa, H. Amastatin, an inhibitor of aminopeptidase A, produced by actinomycetes. *J Antibiot (Tokyo)*. **1978**, *31*(6), 636-638.

[271] Rich, D. H.; Moon, B. J.Harbeson, S. Inhibition of aminopeptidases by amastatin and bestatin derivatives. Effect of inhibitor structure on slow-binding processes. *J Med Chem*. **1984**, *27*(4), 417-422.

[272] Matsuda, N.; Katsuragi, Y.; Saiga, Y.; Tanaka, T.Nakamura, M. Effects of aminopeptidase inhibitors actinonin and amastatin on chemotactic and phagocytic responses of human neutrophils. *Biochem Int*. **1988**, *16*(2), 383-390.

[273] Nagai, M.; Kojima, F.; Naganawa, H.; Hamada, M.; Aoyagi, T.Takeuchi, T. Phebestin, a new inhibitor of aminopeptidase N, produced by Streptomyces sp. MJ716-m3. *J Antibiot (Tokyo)*. **1997**, *50*(1), 82-84.

[274] Aoyagi, T.; Yoshida, S.; Nakamura, Y.; Shigihara, Y.; Hamada, M.Takeuchi, T. Probestin, a new inhibitor of aminopeptidase M, produced by Streptomyces azureus MH663-2F6. I. Taxonomy, production, isolation, physico-chemical properties and biological activities. *J Antibiot (Tokyo)*. **1990**, *43*(2), 143-148.

[275] Andersson, L.; Isley, T. C.Wolfenden, R. alpha-aminoaldehydes: transition state analogue inhibitors of leucine aminopeptidase. *Biochemistry*. **1982**, *21*(17), 4177-4180.

[276] Lejczak, B.; Kafarski, P.Zygmunt, J. Inhibition of aminopeptidases by aminophosphonates. *Biochemistry*. **1989**, *28*(8), 3549-3555.

[277] Flipo, M.; Florent, I.; Grellier, P.; Sergheraert, C.Deprez-Poulain, R. Design, synthesis and antimalarial activity of novel, quinoline-based, zinc metallo-aminopeptidase inhibitors. *Bioorg Med Chem Lett.* **2003**, *13*(16), 2659-2662.

[278] Iguchi, K.; Nakano, T.; Usui, S.Hirano, K. Incadronate inhibits aminopeptidase N expression in prostatic PC-3 cells. *Cancer Lett.* **2006**, *237*(2), 223-233.

[279] Albrecht, S.; Defoin, A.; Salomon, E.; Tarnus, C.; Wetterholm, A.Haeggstrom, J. Z. Synthesis and structure activity relationships of novel non-peptidic metallo-aminopeptidase inhibitors. *Bioorg Med Chem.* **2006**, *14*(21), 7241-7257.

[280] Luan, Y. P., Wang, X.J., Zhu, H.W., Qu, X.J., Fang, H., Xu, W.F The synthesis and activity evaluation of a bestatin derivative (LYP) as an aminopeptidase N inhibitor. *Lett. Drug Des. Discov.* **2009**, (6), 420–423.

[281] Gao, J. J.; Gao, Z. H.; Zhao, C. R.; Yuan, Y.; Cui, S. X.; Zhang, X. F.; Cheng, Y. N.; Xu, W. F.; Tang, W.Qu, X. J. LYP, a novel bestatin derivative, inhibits cell growth and suppresses APN/CD13 activity in human ovarian carcinoma cells more potently than bestatin. *Invest New Drugs.* **2011**, *29*(4), 574-582.

[282] Gao, J. J.; Xue, X.; Gao, Z. H.; Cui, S. X.; Cheng, Y. N.; Xu, W. F.; Tang, W.Qu, X. J. LYP, a bestatin dimethylaminoethyl ester, inhibited cancer angiogenesis both in vitro and in vivo. *Microvasc Res.* **2011**, *82*(2), 122-130.

[283] Bauvois, B. and Dauzonne, D. Aminopeptidase-N/CD13 (EC 3.4.11.2) inhibitors: chemistry, biological evaluations, and therapeutic prospects. *Med Res Rev.* **2006**, *26*(1), 88-130.

[284] Zhang, X.; Fang, H.; Zhang, J.; Yuan, Y.Xu, W. Recent advance in aminopeptidase N (APN/CD13) inhibitor research. *Curr Med Chem.* **2011**, *18*(32), 5011-5021.

[285] Bottaro, D. P. and Liotta, L. A. Cancer: Out of air is not out of action. *Nature.* **2003**, *423*(6940), 593-595.

[286] Tsuzuki, Y.; Fukumura, D.; Oosthuyse, B.; Koike, C.; Carmeliet, P.Jain, R. K. Vascular endothelial growth factor (VEGF) modulation by targeting hypoxia-inducible factor-1alpha--> hypoxia response element--> VEGF cascade differentially regulates vascular response and growth rate in tumors. *Cancer Res.* **2000**, *60*(22), 6248-6252.

[287] Kadambi, A.; Mouta Carreira, C.; Yun, C. O.; Padera, T. P.; Dolmans, D. E.; Carmeliet, P.; Fukumura, D.Jain, R. K. Vascular endothelial growth factor (VEGF)-C differentially affects tumor vascular function and leukocyte recruitment: role of VEGF-receptor 2 and host VEGF-A. *Cancer Res.* **2001**, *61*(6), 2404-2408.

[288] Lee, C. G.; Heijn, M.; di Tomaso, E.; Griffon-Etienne, G.; Ancukiewicz, M.; Koike, C.; Park, K. R.; Ferrara, N.; Jain, R. K.; Suit, H. D.Boucher, Y. Anti-Vascular endothelial growth factor treatment augments tumor radiation response under normoxic or hypoxic conditions. *Cancer Res.* **2000**, *60*(19), 5565-5570.

[289] Hansen-Algenstaedt, N.; Stoll, B. R.; Padera, T. P.; Dolmans, D. E.; Hicklin, D. J.; Fukumura, D.Jain, R. K. Tumor oxygenation in hormone-dependent tumors during vascular endothelial growth factor receptor-2 blockade, hormone ablation, and chemotherapy. *Cancer Res.* **2000**, *60*(16), 4556-4560.

[290] Carmeliet, P. and Jain, R. K. Molecular mechanisms and clinical applications of angiogenesis. *Nature.* **2011**, *473*(7347), 298-307.

[291] Weis, S. M. and Cheresh, D. A. Tumor angiogenesis: molecular pathways and therapeutic targets. *Nat Med.* **2011**, *17*(11), 1359-1370.
[292] Jain, R. K. Normalization of tumor vasculature: an emerging concept in antiangiogenic therapy. *Science.* **2005**, *307*(5706), 58-62.
[293] Lowe, J.; Li, H.; Downing, K. H.Nogales, E. Refined structure of alpha beta-tubulin at 3.5 A resolution. *J Mol Biol.* **2001**, *313*(5), 1045-1057.
[294] Jordan, A.; Hadfield, J. A.; Lawrence, N. J.McGown, A. T. Tubulin as a target for anticancer drugs: agents which interact with the mitotic spindle. *Med Res Rev.* **1998**, *18*(4), 259-296.
[295] Li, H.; DeRosier, D. J.; Nicholson, W. V.; Nogales, E.Downing, K. H. Microtubule structure at 8 A resolution. *Structure.* **2002**, *10*(10), 1317-1328.
[296] Weingarten, M. D.; Lockwood, A. H.; Hwo, S. Y.Kirschner, M. W. A protein factor essential for microtubule assembly. *Proc Natl Acad Sci U S A.* **1975**, *72*(5), 1858-1862.
[297] Ringel, I. and Horwitz, S. B. Effect of alkaline pH on taxol-microtubule interactions. *J Pharmacol Exp Ther.* **1991**, *259*(2), 855-860.
[298] Usui, T.; Kondoh, M.; Cui, C. B.; Mayumi, T.Osada, H. Tryprostatin A, a specific and novel inhibitor of microtubule assembly. *Biochem J.* **1998**, *333 (Pt 3)*, 543-548.
[299] Moritz, M. and Agard, D. A. Gamma-tubulin complexes and microtubule nucleation. *Curr Opin Struct Biol.* **2001**, *11*(2), 174-181.
[300] Lobert, S.; Ingram, J. W.Correia, J. J. Additivity of dilantin and vinblastine inhibitory effects on microtubule assembly. *Cancer Res.* **1999**, *59*(19), 4816-4822.
[301] Conde, C. and Caceres, A. Microtubule assembly, organization and dynamics in axons and dendrites. *Nat Rev Neurosci.* **2009**, *10*(5), 319-332.
[302] Nihei, Y.; Suzuki, M.; Okano, A.; Tsuji, T.; Akiyama, Y.; Tsuruo, T.; Saito, S.; Hori, K.Sato, Y. Evaluation of antivascular and antimitotic effects of tubulin binding agents in solid tumor therapy. *Jpn J Cancer Res.* **1999**, *90*(12), 1387-1395.
[303] Colchicine in the Chemotherapy of Cancer. *Br Med J.* **1950**, *2*(4681), 718-719.
[304] Hill, S. A.; Lonergan, S. J.; Denekamp, J.Chaplin, D. J. Vinca alkaloids: anti-vascular effects in a murine tumour. *Eur J Cancer.* **1993**, *29A*(9), 1320-1324.
[305] Wani, M. C.; Taylor, H. L.; Wall, M. E.; Coggon, P.McPhail, A. T. Plant antitumor agents. VI. The isolation and structure of taxol, a novel antileukemic and antitumor agent from Taxus brevifolia. *J Am Chem Soc.* **1971**, *93*(9), 2325-2327.
[306] Dutcher, J. P.; Novik, Y.; O'Boyle, K.; Marcoullis, G.; Secco, C.Wiernik, P. H. 20th-century advances in drug therapy in oncology--Part. II. *J Clin Pharmacol.* **2000**, *40*(10), 1079-1092.
[307] Baguley, B. C.; Holdaway, K. M.; Thomsen, L. L.; Zhuang, L.Zwi, L. J. Inhibition of growth of colon 38 adenocarcinoma by vinblastine and colchicine: evidence for a vascular mechanism. *Eur J Cancer.* **1991**, *27*(4), 482-487.
[308] Dark, G. G.; Hill, S. A.; Prise, V. E.; Tozer, G. M.; Pettit, G. R.Chaplin, D. J. Combretastatin A-4, an agent that displays potent and selective toxicity toward tumor vasculature. *Cancer Res.* **1997**, *57*(10), 1829-1834.
[309] Pettit, G. R.; Cragg, G. M.Singh, S. B. Antineoplastic agents, 122. Constituents of Combretum caffrum. *J Nat Prod.* **1987**, *50*(3), 386-391.

[310] Pettit, G. R.; Temple, C., Jr.; Narayanan, V. L.; Varma, R.; Simpson, M. J.; Boyd, M. R.; Rener, G. A.Bansal, N. Antineoplastic agents 322. synthesis of combretastatin A-4 prodrugs. *Anticancer Drug Des.* **1995**, *10*(4), 299-309.

[311] McGown, A. T. and Fox, B. W. Structural and biochemical comparison of the anti-mitotic agents colchicine, combretastatin A4 and amphethinile. *Anticancer Drug Des.* **1989**, *3*(4), 249-254.

[312] Tozer, G. M.; Prise, V. E.; Wilson, J.; Locke, R. J.; Vojnovic, B.; Stratford, M. R.; Dennis, M. F.Chaplin, D. J. Combretastatin A-4 phosphate as a tumor vascular-targeting agent: early effects in tumors and normal tissues. *Cancer Res.* **1999**, *59*(7), 1626-1634.

[313] Murata, R.; Overgaard, J.Horsman, M. R. Comparative effects of combretastatin A-4 disodium phosphate and 5,6-dimethylxanthenone-4-acetic acid on blood perfusion in a murine tumour and normal tissues. *Int J Radiat Biol.* **2001**, *77*(2), 195-204.

[314] Tozer, G. M.; Prise, V. E.; Wilson, J.; Cemazar, M.; Shan, S.; Dewhirst, M. W.; Barber, P. R.; Vojnovic, B.Chaplin, D. J. Mechanisms associated with tumor vascular shut-down induced by combretastatin A-4 phosphate: intravital microscopy and measurement of vascular permeability. *Cancer Res.* **2001**, *61*(17), 6413-6422.

[315] Kanthou, C. and Tozer, G. M. The tumor vascular targeting agent combretastatin A-4-phosphate induces reorganization of the actin cytoskeleton and early membrane blebbing in human endothelial cells. *Blood.* **2002**, *99*(6), 2060-2069.

[316] Stevenson, J. P.; Rosen, M.; Sun, W.; Gallagher, M.; Haller, D. G.; Vaughn, D.; Giantonio, B.; Zimmer, R.; Petros, W. P.; Stratford, M.; Chaplin, D.; Young, S. L.; Schnall, M.O'Dwyer, P. J. Phase I trial of the antivascular agent combretastatin A4 phosphate on a 5-day schedule to patients with cancer: magnetic resonance imaging evidence for altered tumor blood flow. *J Clin Oncol.* **2003**, *21*(23), 4428-4438.

[317] Dowlati, A.; Robertson, K.; Cooney, M.; Petros, W. P.; Stratford, M.; Jesberger, J.; Rafie, N.; Overmoyer, B.; Makkar, V.; Stambler, B.; Taylor, A.; Waas, J.; Lewin, J. S.; McCrae, K. R.Remick, S. C. A phase I pharmacokinetic and translational study of the novel vascular targeting agent combretastatin a-4 phosphate on a single-dose intravenous schedule in patients with advanced cancer. *Cancer Res.* **2002**, *62*(12), 3408-3416.

[318] Rustin, G. J.; Galbraith, S. M.; Anderson, H.; Stratford, M.; Folkes, L. K.; Sena, L.; Gumbrell, L.Price, P. M. Phase I clinical trial of weekly combretastatin A4 phosphate: clinical and pharmacokinetic results. *J Clin Oncol.* **2003**, *21*(15), 2815-2822.

[319] Mooney, C. J.; Nagaiah, G.; Fu, P.; Wasman, J. K.; Cooney, M. M.; Savvides, P. S.; Bokar, J. A.; Dowlati, A.; Wang, D.; Agarwala, S. S.; Flick, S. M.; Hartman, P. H.; Ortiz, J. D.; Lavertu, P. N.Remick, S. C. A phase II trial of fosbretabulin in advanced anaplastic thyroid carcinoma and correlation of baseline serum-soluble intracellular adhesion molecule-1 with outcome. *Thyroid.* **2009**, *19*(3), 233-240.

[320] Philpott, M.; Baguley, B. C.Ching, L. M. Induction of tumour necrosis factor-alpha by single and repeated doses of the antitumour agent 5,6-

dimethylxanthenone-4-acetic acid. *Cancer Chemother Pharmacol.* **1995**, *36*(2), 143-148.

[321] Mahadevan, V.; Malik, S. T.; Meager, A.; Fiers, W.; Lewis, G. P.Hart, I. R. Role of tumor necrosis factor in flavone acetic acid-induced tumor vasculature shutdown. *Cancer Res.* **1990**, *50*(17), 5537-5542.

[322] Baguley, B. C. Antivascular therapy of cancer: DMXAA. *Lancet Oncol.* **2003**, *4*(3), 141-148.

[323] *clinicaltrials.gov*. 2012; Available from: http://www.clinicaltrials.gov.

[324] Huang, X.; Molema, G.; King, S.; Watkins, L.; Edgington, T. S.Thorpe, P. E. Tumor infarction in mice by antibody-directed targeting of tissue factor to tumor vasculature. *Science.* **1997**, *275*(5299), 547-550.

[325] Ran, S.; Gao, B.; Duffy, S.; Watkins, L.; Rote, N.Thorpe, P. E. Infarction of solid Hodgkin's tumors in mice by antibody-directed targeting of tissue factor to tumor vasculature. *Cancer Res.* **1998**, *58*(20), 4646-4653.

[326] Nilsson, F.; Kosmehl, H.; Zardi, L.Neri, D. Targeted delivery of tissue factor to the ED-B domain of fibronectin, a marker of angiogenesis, mediates the infarction of solid tumors in mice. *Cancer Res.* **2001**, *61*(2), 711-716.

[327] Liu, C.; Huang, H.; Donate, F.; Dickinson, C.; Santucci, R.; El-Sheikh, A.; Vessella, R.Edgington, T. S. Prostate-specific membrane antigen directed selective thrombotic infarction of tumors. *Cancer Res.* **2002**, *62*(19), 5470-5475.

[328] Tozer, G. M.; Kanthou, C.; Parkins, C. S.Hill, S. A. The biology of the combretastatins as tumour vascular targeting agents. *Int J Exp Pathol.* **2002**, *83*(1), 21-38.

[329] Chaplin, D. J.; Pettit, G. R.Hill, S. A. Anti-vascular approaches to solid tumour therapy: evaluation of combretastatin A4 phosphate. *Anticancer Res.* **1999**, *19*(1A), 189-195.

[330] Li, L.; Rojiani, A.Siemann, D. W. Targeting the tumor vasculature with combretastatin A-4 disodium phosphate: effects on radiation therapy. *Int J Radiat Oncol Biol Phys.* **1998**, *42*(4), 899-903.

[331] Horsman, M. R.; Murata, R.; Breidahl, T.; Nielsen, F. U.; Maxwell, R. J.; Stodkiled-Jorgensen, H.Overgaard, J. Combretastatins novel vascular targeting drugs for improving anti-cancer therapy. Combretastatins and conventional therapy. *Adv Exp Med Biol.* **2000**, *476*, 311-323.

[332] Murata, R.; Siemann, D. W.; Overgaard, J.Horsman, M. R. Improved tumor response by combining radiation and the vascular-damaging drug 5,6-dimethylxanthenone-4-acetic acid. *Radiat Res.* **2001**, *156*(5 Pt 1), 503-509.

[333] Dohn, L. H.; Jensen, B. V.Larsen, F. O. Short time infusion of bevacizumab in combination with 5FU-based chemotherapy as first-line therapy in a non-selective patient group with metastatic colorectal cancer. *Acta Oncol.* **2010**, *49*(3), 395-396.

[334] Nathan, P.; Zweifel, M.; Padhani, A. R.; Koh, D. M.; Ng, M.; Collins, D. J.; Harris, A.; Carden, C.; Smythe, J.; Fisher, N.; Taylor, N. J.; Stirling, J. J.; Lu, S. P.; Leach, M. O.; Rustin, G. J.Judson, I. Phase I trial of combretastatin A4 phosphate (CA4P) in combination with bevacizumab in patients with advanced cancer. *Clin Cancer Res.* **2012**, *18*(12), 3428-3439.

[335] Walsh, J. J. and Bell, A. Hybrid drugs for malaria. *Curr Pharm Des.* **2009**, *15*(25), 2970-2985.

[336] Chow, L. M. and Chan, T. H. Novel classes of dimer antitumour drug candidates. *Curr Pharm Des.* **2009**, *15*(6), 659-674.

[337] Kim, J. W. and Lee, H. S. Tumor targeting by doxorubicin-RGD-4C peptide conjugate in an orthotopic mouse hepatoma model. *Int J Mol Med.* **2004**, *14*(4), 529-535.

[338] Mukhopadhyay, S.; Barnes, C. M.; Haskel, A.; Short, S. M.; Barnes, K. R.Lippard, S. J. Conjugated platinum(IV)-peptide complexes for targeting angiogenic tumor vasculature. *Bioconjug Chem.* **2008**, *19*(1), 39-49.

[339] Breen E.C., W. J. J. Tubulin-Targeting Agents in Hybrid Drugs. *Current Medicinal Chemistry.* **2010**, *17*(7), 609-639.

[340] Rejniak, K. A. and Anderson, A. R. Hybrid models of tumor growth. *Wiley Interdiscip Rev Syst Biol Med.* **2010**.

[341] Nakagawa-Goto, K.; Nakamura, S.; Bastow, K. F.; Nyarko, A.; Peng, C. Y.; Lee, F. Y.; Lee, F. C.Lee, K. H. Antitumor agents. 256. Conjugation of paclitaxel with other antitumor agents: evaluation of novel conjugates as cytotoxic agents. *Bioorg Med Chem Lett.* **2007**, *17*(10), 2894-2898.

[342] Lewis Phillips, G. D.; Li, G.; Dugger, D. L.; Crocker, L. M.; Parsons, K. L.; Mai, E.; Blattler, W. A.; Lambert, J. M.; Chari, R. V.; Lutz, R. J.; Wong, W. L.; Jacobson, F. S.; Koeppen, H.; Schwall, R. H.; Kenkare-Mitra, S. R.; Spencer, S. D.Sliwkowski, M. X. Targeting HER2-positive breast cancer with trastuzumab-DM1, an antibody-cytotoxic drug conjugate. *Cancer Res.* **2008**, *68*(22), 9280-9290.

[343] Krop, I. E.; Beeram, M.; Modi, S.; Jones, S. F.; Holden, S. N.; Yu, W.; Girish, S.; Tibbitts, J.; Yi, J. H.; Sliwkowski, M. X.; Jacobson, F.; Lutzker, S. G.Burris, H. A. Phase I study of trastuzumab-DM1, an HER2 antibody-drug conjugate, given every 3 weeks to patients with HER2-positive metastatic breast cancer. *J Clin Oncol.* **2010**, *28*(16), 2698-2704.

[344] Burris, H. A., 3rd; Rugo, H. S.; Vukelja, S. J.; Vogel, C. L.; Borson, R. A.; Limentani, S.; Tan-Chiu, E.; Krop, I. E.; Michaelson, R. A.; Girish, S.; Amler, L.; Zheng, M.; Chu, Y. W.; Klencke, B.O'Shaughnessy, J. A. Phase II study of the antibody drug conjugate trastuzumab-DM1 for the treatment of human epidermal growth factor receptor 2 (HER2)-positive breast cancer after prior HER2-directed therapy. *J Clin Oncol.* **2011**, *29*(4), 398-405.

[345] Dings, R. P.; Van Laar, E. S.; Loren, M.; Webber, J.; Zhang, Y.; Waters, S. J.; Macdonald, J. R.Mayo, K. H. Inhibiting tumor growth by targeting tumor vasculature with galectin-1 antagonist anginex conjugated to the cytotoxic acylfulvene, 6-hydroxylpropylacylfulvene. *Bioconjug Chem.* **2010**, *21*(1), 20-27.

[346] van Laarhoven, H. W.; Gambarota, G.; Heerschap, A.; Lok, J.; Verhagen, I.; Corti, A.; Toma, S.; Gallo Stampino, C.; van der Kogel, A.Punt, C. J. Effects of the tumor vasculature targeting agent NGR-TNF on the tumor microenvironment in murine lymphomas. *Invest New Drugs.* **2006**, *24*(1), 27-36.

[347] Bordignon C., C. C. F., Toma S., Manenti L., Rizzardi P., Curnis F., Gallo Stampino C., Corti A. NGRhTNF, a new vascular targeting agent with a dual mechanism of action: preliminary clinical results. *Journal of Clinical Oncology.* **2006**, *24*(18).

[348] van Laarhoven, H. W.; Fiedler, W.; Desar, I. M.; van Asten, J. J.; Marreaud, S.; Lacombe, D.; Govaerts, A. S.; Bogaerts, J.; Lasch, P.; Timmer-Bonte, J. N.; Lambiase, A.; Bordignon, C.; Punt, C. J.; Heerschap, A.van Herpen, C. M. Phase I clinical and magnetic resonance imaging study of the vascular agent NGR-hTNF in patients with advanced cancers (European Organization for Research and Treatment of Cancer Study 16041). *Clin Cancer Res.* **2010**, *16*(4), 1315-1323.

[349] Santoro, A.; Pressiani, T.; Citterio, G.; Rossoni, G.; Donadoni, G.; Pozzi, F.; Rimassa, L.; Personeni, N.; Bozzarelli, S.; Colombi, S.; De Braud, F. G.; Caligaris-Cappio, F.; Lambiase, A.Bordignon, C. Activity and safety of NGR-hTNF, a selective vascular-targeting agent, in previously treated patients with advanced hepatocellular carcinoma. *Br J Cancer.* **2010**, *103*(6), 837-844.

[350] Mammoliti, S.; Andretta, V.; Bennicelli, E.; Caprioni, F.; Comandini, D.; Fornarini, G.; Guglielmi, A.; Pessino, A.; Sciallero, S.; Sobrero, A. F.; Mazzola, G.; Lambiase, A.Bordignon, C. Two doses of NGR-hTNF in combination with capecitabine plus oxaliplatin in colorectal cancer patients failing standard therapies. *Ann Oncol.* **2010**.

[351] Gregorc, V.; Zucali, P. A.; Santoro, A.; Ceresoli, G. L.; Citterio, G.; De Pas, T. M.; Zilembo, N.; De Vincenzo, F.; Simonelli, M.; Rossoni, G.; Spreafico, A.; Grazia Vigano, M.; Fontana, F.; De Braud, F. G.; Bajetta, E.; Caligaris-Cappio, F.; Bruzzi, P.; Lambiase, A.Bordignon, C. Phase II study of asparagine-glycine-arginine-human tumor necrosis factor alpha, a selective vascular targeting agent, in previously treated patients with malignant pleural mesothelioma. *J Clin Oncol.* **2010**, *28*(15), 2604-2611.

[352] Yu, M. K.; Lee, D. Y.; Kim, Y. S.; Park, K.; Park, S. A.; Son, D. H.; Lee, G. Y.; Nam, J. H.; Kim, S. Y.; Kim, I. S.; Park, R. W.Byun, Y. Antiangiogenic and apoptotic properties of a novel amphiphilic folate-heparin-lithocholate derivative having cellular internality for cancer therapy. *Pharm Res.* **2007**, *24*(4), 705-714.

[353] Huang, C. M.; Wu, Y. T.Chen, S. T. Targeting delivery of paclitaxel into tumor cells via somatostatin receptor endocytosis. *Chem Biol.* **2000**, *7*(7), 453-461.

[354] Zefirova, O. N.; Nurieva, E. V.; Lemcke, H.; Ivanov, A. A.; Shishov, D. V.; Weiss, D. G.; Kuznetsov, S. A.Zefirov, N. S. Design, synthesis, and bioactivity of putative tubulin ligands with adamantane core. *Bioorg Med Chem Lett.* **2008**, *18*(18), 5091-5094.

[355] Amico, V. O., G.; Piatelli, M.; Tringali, C.; Fattorusso, E.; Magno, S.; Mayol, L., *Caulerpenyne an unusual sesquiterpenoid from the green alga Caulerpa prolifera* Tetrahedron Lett. Vol. 38. 1978.

[356] Barbier, P.; Guise, S.; Huitorel, P.; Amade, P.; Pesando, D.; Briand, C.Peyrot, V. Caulerpenyne from Caulerpa taxifolia has an antiproliferative activity on tumor cell line SK-N-SH and modifies the microtubule network. *Life Sci.* **2001**, *70*(4), 415-429.

[357] Bourdron, J.; Commeiras, L.; Barbier, P.; Bourgarel-Rey, V.; Pasquier, E.; Vanthuyne, N.; Hubaud, J. C.; Peyrot, V.Parrain, J. L. Caulerpenyne-colchicine hybrid: synthesis and biological evaluation. *Bioorg Med Chem.* **2006**, *14*(16), 5540-5548.

[358] Safavy, A.; Bonner, J. A.; Waksal, H. W.; Buchsbaum, D. J.; Gillespie, G. Y.; Khazaeli, M. B.; Arani, R.; Chen, D. T.; Carpenter, M.Raisch, K. P. Synthesis

and biological evaluation of paclitaxel-C225 conjugate as a model for targeted drug delivery. *Bioconjug Chem.* **2003**, *14*(2), 302-310.

[359] Castellani, P.; Viale, G.; Dorcaratto, A.; Nicolo, G.; Kaczmarek, J.; Querze, G.Zardi, L. The fibronectin isoform containing the ED-B oncofetal domain: a marker of angiogenesis. *Int J Cancer.* **1994**, *59*(5), 612-618.

[360] Viti, F.; Tarli, L.; Giovannoni, L.; Zardi, L.Neri, D. Increased binding affinity and valence of recombinant antibody fragments lead to improved targeting of tumoral angiogenesis. *Cancer Res.* **1999**, *59*(2), 347-352.

[361] Tarli, L.; Balza, E.; Viti, F.; Borsi, L.; Castellani, P.; Berndorff, D.; Dinkelborg, L.; Neri, D.Zardi, L. A high-affinity human antibody that targets tumoral blood vessels. *Blood.* **1999**, *94*(1), 192-198.

[362] Borsi, L.; Balza, E.; Bestagno, M.; Castellani, P.; Carnemolla, B.; Biro, A.; Leprini, A.; Sepulveda, J.; Burrone, O.; Neri, D.Zardi, L. Selective targeting of tumoral vasculature: comparison of different formats of an antibody (L19) to the ED-B domain of fibronectin. *Int J Cancer.* **2002**, *102*(1), 75-85.

[363] Santimaria, M.; Moscatelli, G.; Viale, G. L.; Giovannoni, L.; Neri, G.; Viti, F.; Leprini, A.; Borsi, L.; Castellani, P.; Zardi, L.; Neri, D.Riva, P. Immunoscintigraphic detection of the ED-B domain of fibronectin, a marker of angiogenesis, in patients with cancer. *Clin Cancer Res.* **2003**, *9*(2), 571-579.

[364] Carnemolla, B.; Castellani, P.; Ponassi, M.; Borsi, L.; Urbini, S.; Nicolo, G.; Dorcaratto, A.; Viale, G.; Winter, G.; Neri, D.Zardi, L. Identification of a glioblastoma-associated tenascin-C isoform by a high affinity recombinant antibody. *Am J Pathol.* **1999**, *154*(5), 1345-1352.

[365] Brack, S. S.; Silacci, M.; Birchler, M.Neri, D. Tumor-targeting properties of novel antibodies specific to the large isoform of tenascin-C. *Clin Cancer Res.* **2006**, *12*(10), 3200-3208.

[366] Bostwick, D. G.; Grignon, D. J.; Hammond, M. E.; Amin, M. B.; Cohen, M.; Crawford, D.; Gospadarowicz, M.; Kaplan, R. S.; Miller, D. S.; Montironi, R.; Pajak, T. F.; Pollack, A.; Srigley, J. R.Yarbro, J. W. Prognostic factors in prostate cancer. College of American Pathologists Consensus Statement 1999. *Arch Pathol Lab Med.* **2000**, *124*(7), 995-1000.

[367] Liu, H.; Moy, P.; Kim, S.; Xia, Y.; Rajasekaran, A.; Navarro, V.; Knudsen, B.Bander, N. H. Monoclonal antibodies to the extracellular domain of prostate-specific membrane antigen also react with tumor vascular endothelium. *Cancer Res.* **1997**, *57*(17), 3629-3634.

[368] Pettit, G. R. The dolastatins. *Fortschr Chem Org Naturst.* **1997**, *70*, 1-79.

[369] Wang, X.; Ma, D.; Olson, W. C.Heston, W. D. In vitro and in vivo responses of advanced prostate tumors to PSMA ADC, an auristatin-conjugated antibody to prostate-specific membrane antigen. *Mol Cancer Ther.* **2011**, *10*(9), 1728-1739.

[370] Milowsky, M. I.; Nanus, D. M.; Kostakoglu, L.; Sheehan, C. E.; Vallabhajosula, S.; Goldsmith, S. J.; Ross, J. S.Bander, N. H. Vascular targeted therapy with anti-prostate-specific membrane antigen monoclonal antibody J591 in advanced solid tumors. *J Clin Oncol.* **2007**, *25*(5), 540-547.

[371] Gerber, H. P.; Senter, P. D.Grewal, I. S. Antibody drug-conjugates targeting the tumor vasculature: Current and future developments. *MAbs.* **2009**, *1*(3), 247-253.

[372] Ramakrishnan, S.; Olson, T. A.; Bautch, V. L.Mohanraj, D. Vascular endothelial growth factor-toxin conjugate specifically inhibits KDR/flk-1-

positive endothelial cell proliferation in vitro and angiogenesis in vivo. *Cancer Res.* **1996**, *56*(6), 1324-1330.

[373] Olson, T. A.; Mohanraj, D.; Roy, S.Ramakrishnan, S. Targeting the tumor vasculature: inhibition of tumor growth by a vascular endothelial growth factor-toxin conjugate. *Int J Cancer.* **1997**, *73*(6), 865-870.

[374] Soker, S.; Fidder, H.; Neufeld, G.Klagsbrun, M. Characterization of novel vascular endothelial growth factor (VEGF) receptors on tumor cells that bind VEGF165 via its exon 7-encoded domain. *J Biol Chem.* **1996**, *271*(10), 5761-5767.

[375] Soker, S.; Gollamudi-Payne, S.; Fidder, H.; Charmahelli, H.Klagsbrun, M. Inhibition of vascular endothelial growth factor (VEGF)-induced endothelial cell proliferation by a peptide corresponding to the exon 7-encoded domain of VEGF165. *J Biol Chem.* **1997**, *272*(50), 31582-31588.

[376] Gitay-Goren, H.; Cohen, T.; Tessler, S.; Soker, S.; Gengrinovitch, S.; Rockwell, P.; Klagsbrun, M.; Levi, B. Z.Neufeld, G. Selective binding of VEGF121 to one of the three vascular endothelial growth factor receptors of vascular endothelial cells. *J Biol Chem.* **1996**, *271*(10), 5519-5523.

[377] Wild, R.; Dhanabal, M.; Olson, T. A.Ramakrishnan, S. Inhibition of angiogenesis and tumour growth by VEGF121-toxin conjugate: differential effect on proliferating endothelial cells. *Br J Cancer.* **2000**, *83*(8), 1077-1083.

[378] Baekelandt, M. Irofulven (MGI Pharma). *Curr Opin Investig Drugs.* **2002**, *3*(10), 1517-1526.

[379] Eckhardt, S. G.; Baker, S. D.; Britten, C. D.; Hidalgo, M.; Siu, L.; Hammond, L. A.; Villalona-Calero, M. A.; Felton, S.; Drengler, R.; Kuhn, J. G.; Clark, G. M.; Smith, S. L.; MacDonald, J. R.; Smith, C.; Moczygemba, J.; Weitman, S.; Von Hoff, D. D.Rowinsky, E. K. Phase I and pharmacokinetic study of irofulven, a novel mushroom-derived cytotoxin, administered for five consecutive days every four weeks in patients with advanced solid malignancies. *J Clin Oncol.* **2000**, *18*(24), 4086-4097.

[380] Alexandre, J.; Raymond, E.; Kaci, M. O.; Brain, E. C.; Lokiec, F.; Kahatt, C.; Faivre, S.; Yovine, A.; Goldwasser, F.; Smith, S. L.; MacDonald, J. R.; Misset, J. L.Cvitkovic, E. Phase I and pharmacokinetic study of irofulven administered weekly or biweekly in advanced solid tumor patients. *Clin Cancer Res.* **2004**, *10*(10), 3377-3385.

[381] Griffioen, A. W.; van der Schaft, D. W.; Barendsz-Janson, A. F.; Cox, A.; Struijker Boudier, H. A.; Hillen, H. F.Mayo, K. H. Anginex, a designed peptide that inhibits angiogenesis. *Biochem J.* **2001**, *354*(Pt 2), 233-242.

[382] Dings, R. P. and Mayo, K. H. A journey in structure-based drug discovery: from designed peptides to protein surface topomimetics as antibiotic and antiangiogenic agents. *Acc Chem Res.* **2007**, *40*(10), 1057-1065.

[383] Thijssen, V. L.; Postel, R.; Brandwijk, R. J.; Dings, R. P.; Nesmelova, I.; Satijn, S.; Verhofstad, N.; Nakabeppu, Y.; Baum, L. G.; Bakkers, J.; Mayo, K. H.; Poirier, F.Griffioen, A. W. Galectin-1 is essential in tumor angiogenesis and is a target for antiangiogenesis therapy. *Proc Natl Acad Sci U S A.* **2006**, *103*(43), 15975-15980.

[384] Camby, I.; Le Mercier, M.; Lefranc, F.Kiss, R. Galectin-1: a small protein with major functions. *Glycobiology.* **2006**, *16*(11), 137R-157R.

[385] Rabinovich, G. A. Galectin-1 as a potential cancer target. *Br J Cancer*. **2005**, *92*(7), 1188-1192.

[386] Eliceiri, B. P. and Cheresh, D. A. The role of alphav integrins during angiogenesis: insights into potential mechanisms of action and clinical development. *J Clin Invest*. **1999**, *103*(9), 1227-1230.

[387] Enenstein, J. and Kramer, R. H. Confocal microscopic analysis of integrin expression on the microvasculature and its sprouts in the neonatal foreskin. *J Invest Dermatol*. **1994**, *103*(3), 381-386.

[388] Brooks, P. C.; Clark, R. A.Cheresh, D. A. Requirement of vascular integrin alpha v beta 3 for angiogenesis. *Science*. **1994**, *264*(5158), 569-571.

[389] Brooks, P. C.; Montgomery, A. M.; Rosenfeld, M.; Reisfeld, R. A.; Hu, T.; Klier, G.Cheresh, D. A. Integrin alpha v beta 3 antagonists promote tumor regression by inducing apoptosis of angiogenic blood vessels. *Cell*. **1994**, *79*(7), 1157-1164.

[390] Storgard, C. M.; Stupack, D. G.; Jonczyk, A.; Goodman, S. L.; Fox, R. I.Cheresh, D. A. Decreased angiogenesis and arthritic disease in rabbits treated with an alphavbeta3 antagonist. *J Clin Invest*. **1999**, *103*(1), 47-54.

[391] Ruoslahti, E. RGD and other recognition sequences for integrins. *Annu Rev Cell Dev Biol*. **1996**, *12*, 697-715.

[392] Cleaver, O. and Melton, D. A. Endothelial signaling during development. *Nat Med*. **2003**, *9*(6), 661-668.

[393] Pasqualini, R.; Koivunen, E.Ruoslahti, E. Alpha v integrins as receptors for tumor targeting by circulating ligands. *Nat Biotechnol*. **1997**, *15*(6), 542-546.

[394] Felding-Habermann, B.; Mueller, B. M.; Romerdahl, C. A.Cheresh, D. A. Involvement of integrin alpha V gene expression in human melanoma tumorigenicity. *J Clin Invest*. **1992**, *89*(6), 2018-2022.

[395] Chen, X.; Plasencia, C.; Hou, Y.Neamati, N. Synthesis and biological evaluation of dimeric RGD peptide-paclitaxel conjugate as a model for integrin-targeted drug delivery. *J Med Chem*. **2005**, *48*(4), 1098-1106.

[396] Janssen, M. L.; Oyen, W. J.; Dijkgraaf, I.; Massuger, L. F.; Frielink, C.; Edwards, D. S.; Rajopadhye, M.; Boonstra, H.; Corstens, F. H.Boerman, O. C. Tumor targeting with radiolabeled alpha(v)beta(3) integrin binding peptides in a nude mouse model. *Cancer Res*. **2002**, *62*(21), 6146-6151.

[397] Ryppa, C.; Mann-Steinberg, H.; Biniossek, M. L.; Satchi-Fainaro, R.Kratz, F. In vitro and in vivo evaluation of a paclitaxel conjugate with the divalent peptide E-[c(RGDfK)2] that targets integrin alpha v beta 3. *Int J Pharm*. **2009**, *368*(1-2), 89-97.

[398] Temming, K.; Meyer, D. L.; Zabinski, R.; Dijkers, E. C.; Poelstra, K.; Molema, G.Kok, R. J. Evaluation of RGD-targeted albumin carriers for specific delivery of auristatin E to tumor blood vessels. *Bioconjug Chem*. **2006**, *17*(6), 1385-1394.

[399] Liu, Y.; Bajjuri, K. M.; Liu, C.Sinha, S. C. Targeting cell surface alpha(v)beta(3) integrin increases therapeutic efficacies of a legumain protease-activated auristatin prodrug. *Mol Pharm*. **2012**, *9*(1), 168-175.

[400] Schiffelers, R. M.; Ansari, A.; Xu, J.; Zhou, Q.; Tang, Q.; Storm, G.; Molema, G.; Lu, P. Y.; Scaria, P. V.Woodle, M. C. Cancer siRNA therapy by tumor selective delivery with ligand-targeted sterically stabilized nanoparticle. *Nucleic Acids Res*. **2004**, *32*(19), e149.

[401] Kunath, K.; Merdan, T.; Hegener, O.; Haberlein, H.Kissel, T. Integrin targeting using RGD-PEI conjugates for in vitro gene transfer. *J Gene Med.* **2003**, *5*(7), 588-599.

[402] de Vries, C.; Escobedo, J. A.; Ueno, H.; Houck, K.; Ferrara, N.Williams, L. T. The fms-like tyrosine kinase, a receptor for vascular endothelial growth factor. *Science.* **1992**, *255*(5047), 989-991.

[403] Kendall, R. L.; Wang, G.Thomas, K. A. Identification of a natural soluble form of the vascular endothelial growth factor receptor, FLT-1, and its heterodimerization with KDR. *Biochem Biophys Res Commun.* **1996**, *226*(2), 324-328.

[404] Boussif, O.; Lezoualc'h, F.; Zanta, M. A.; Mergny, M. D.; Scherman, D.; Demeneix, B.Behr, J. P. A versatile vector for gene and oligonucleotide transfer into cells in culture and in vivo: polyethylenimine. *Proc Natl Acad Sci U S A.* **1995**, *92*(16), 7297-7301.

[405] Kim, W. J.; Yockman, J. W.; Lee, M.; Jeong, J. H.; Kim, Y. H.Kim, S. W. Soluble Flt-1 gene delivery using PEI-g-PEG-RGD conjugate for anti-angiogenesis. *J Control Release.* **2005**, *106*(1-2), 224-234.

[406] Kim, W. J.; Yockman, J. W.; Jeong, J. H.; Christensen, L. V.; Lee, M.; Kim, Y. H.Kim, S. W. Anti-angiogenic inhibition of tumor growth by systemic delivery of PEI-g-PEG-RGD/pCMV-sFlt-1 complexes in tumor-bearing mice. *J Control Release.* **2006**, *114*(3), 381-388.

[407] Curnis, F.; Sacchi, A.Corti, A. Improving chemotherapeutic drug penetration in tumors by vascular targeting and barrier alteration. *J Clin Invest.* **2002**, *110*(4), 475-482.

[408] Fiers, W., *Biologic therapy with TNF: preclinical studies. In Biologic Therapy of Cancer: Principles and Practice*, ed. Lippincott. 1995, Philadelphia.

[409] Fraker, D. L., Alexander H.R. & Pass H.I. , *Biologic therapy with TNF: systemic administration and isolation-perfusion. In Biologic Therapy of Cancer: Principles and Practice*, ed. Lippincott. 1995, Philadelphia.

[410] Corti, A. and Ponzoni, M. Tumor vascular targeting with tumor necrosis factor alpha and chemotherapeutic drugs. *Ann N Y Acad Sci.* **2004**, *1028*, 104-112.

[411] Gregorc, V.; Santoro, A.; Bennicelli, E.; Punt, C. J.; Citterio, G.; Timmer-Bonte, J. N.; Caligaris Cappio, F.; Lambiase, A.; Bordignon, C.van Herpen, C. M. Phase Ib study of NGR-hTNF, a selective vascular targeting agent, administered at low doses in combination with doxorubicin to patients with advanced solid tumours. *Br J Cancer.* **2009**, *101*(2), 219-224.

[412] Tandle, A.; Hanna, E.; Lorang, D.; Hajitou, A.; Moya, C. A.; Pasqualini, R.; Arap, W.; Adem, A.; Starker, E.; Hewitt, S.Libutti, S. K. Tumor vasculature-targeted delivery of tumor necrosis factor-alpha. *Cancer.* **2009**, *115*(1), 128-139.

[413] Myers, C. E. The pharmacology of the fluoropyrimidines. *Pharmacol Rev.* **1981**, *33*(1), 1-15.

[414] van Laar, J. A.; Rustum, Y. M.; Ackland, S. P.; van Groeningen, C. J.Peters, G. J. Comparison of 5-fluoro-2'-deoxyuridine with 5-fluorouracil and their role in the treatment of colorectal cancer. *Eur J Cancer.* **1998**, *34*(3), 296-306.

[415] Chu, E. M., A. and Fogarasi, M. C., *Pharmacology of cancer chemotherapy*. 6 ed. Cancer Principles & Practice of Oncology, ed. S.H.a.S.A.R. In V. T. DeVita. Vol. 1. 2001, Philadelphia.

[416] Zhang, Z.; Hatta, H.; Tanabe, K.Nishimoto, S. A new class of 5-fluoro-2'-deoxyuridine prodrugs conjugated with a tumor-homing cyclic peptide CNGRC by ester linkers: synthesis, reactivity, and tumor-cell-selective cytotoxicity. *Pharm Res*. **2005**, *22*(3), 381-389.

[417] Ndinguri, M. W.; Solipuram, R.; Gambrell, R. P.; Aggarwal, S.Hammer, R. P. Peptide targeting of platinum anti-cancer drugs. *Bioconjug Chem*. **2009**, *20*(10), 1869-1878.

[418] Temming, K.; Schiffelers, R. M.; Molema, G.Kok, R. J. RGD-based strategies for selective delivery of therapeutics and imaging agents to the tumour vasculature. *Drug Resist Updat*. **2005**, *8*(6), 381-402.

[419] Corti, A.; Curnis, F.; Arap, W.Pasqualini, R. The neovasculature homing motif NGR: more than meets the eye. *Blood*. **2008**, *112*(7), 2628-2635.

[420] Lindahl, U.; Lidholt, K.; Spillmann, D.Kjellen, L. More to "heparin" than anticoagulation. *Thromb Res*. **1994**, *75*(1), 1-32.

[421] Soker, S.; Goldstaub, D.; Svahn, C. M.; Vlodavsky, I.; Levi, B. Z.Neufeld, G. Variations in the size and sulfation of heparin modulate the effect of heparin on the binding of VEGF165 to its receptors. *Biochem Biophys Res Commun*. **1994**, *203*(2), 1339-1347.

[422] Zacharski, L. R. and Ornstein, D. L. Heparin and cancer. *Thromb Haemost*. **1998**, *80*(1), 10-23.

[423] Mannori, G.; Crottet, P.; Cecconi, O.; Hanasaki, K.; Aruffo, A.; Nelson, R. M.; Varki, A.Bevilacqua, M. P. Differential colon cancer cell adhesion to E-, P-, and L-selectin: role of mucin-type glycoproteins. *Cancer Res*. **1995**, *55*(19), 4425-4431.

[424] Borsig, L.; Wong, R.; Hynes, R. O.; Varki, N. M.Varki, A. Synergistic effects of L- and P-selectin in facilitating tumor metastasis can involve non-mucin ligands and implicate leukocytes as enhancers of metastasis. *Proc Natl Acad Sci U S A*. **2002**, *99*(4), 2193-2198.

[425] Borsig, L. Selectins facilitate carcinoma metastasis and heparin can prevent them. *News Physiol Sci*. **2004**, *19*, 16-21.

[426] Engelberg, H. Actions of heparin that may affect the malignant process. *Cancer*. **1999**, *85*(2), 257-272.

[427] Hirsh, J. Heparin induced bleeding. *Nouv Rev Fr Hematol*. **1984**, *26*(4), 261-266.

[428] Phillips, P. G.; Yalcin, M.; Cui, H.; Abdel-Nabi, H.; Sajjad, M.; Bernacki, R.; Veith, J.Mousa, S. A. Increased Tumor Uptake of Chemotherapeutics and Improved Chemoresponse by Novel Non-anticoagulant Low Molecular Weight Heparin. *Anticancer Res*. **2011**, *31*(2), 411-419.

[429] Folkman, J.; Langer, R.; Linhardt, R. J.; Haudenschild, C.Taylor, S. Angiogenesis inhibition and tumor regression caused by heparin or a heparin fragment in the presence of cortisone. *Science*. **1983**, *221*(4612), 719-725.

[430] Florey, H. W.; Poole, J. C.Meek, G. A. Endothelial cells and cement lines. *J Pathol Bacteriol*. **1959**, *77*(2), 625-636.

[431] Hiebert, L. M. and Jaques, L. B. The observation of heparin on endothelium after injection. *Thromb Res*. **1976**, *8*(2), 195-204.

[432] Mahadoo, J.; Heibert, L.Jaques, L. B. Vascular sequestration of heparin. *Thromb Res*. **1978**, *12*(1), 79-90.

[433] Schaefer, C.; Lo Bue, J.Gollub, S. The biodistribution of exogenous [35S]heparin in the dog. *Proc Soc Exp Biol Med.* **1980**, *164*(1), 69-74.

[434] Fabian, I.; Bleiberg, I.Aronson, M. Increased uptake and desulphation of heparin by mouse macrophages in the presence of polycations. *Biochim Biophys Acta.* **1978**, *544*(1), 69-76.

[435] Sakamoto, N., and Tanaka. N. G. Mechanism of the synergistic effect of heparin and cortisone against angiogenesis and tumor growth. *Cancer J.* **1988**, *2*, 9-16.

[436] Thorpe, P. E.; Derbyshire, E. J.; Andrade, S. P.; Press, N.; Knowles, P. P.; King, S.; Watson, G. J.; Yang, Y. C.Rao-Bette, M. Heparin-steroid conjugates: new angiogenesis inhibitors with antitumor activity in mice. *Cancer Res.* **1993**, *53*(13), 3000-3007.

[437] Ishihara, M.; Saito, Y.; Yura, H.; Ono, K.; Ishikawa, K.; Hattori, H.; Akaike, T.Kurita, A. Heparin-carrying polystyrene to mediate cellular attachment and growth via interaction with growth factors. *J Biomed Mater Res.* **2000**, *50*(2), 144-152.

[438] Ishihara, M.; Ono, K.; Ishikawa, K.; Hattori, H.; Saito, Y.; Yura, H.; Akaike, T.; Ozeki, Y.; Tanaka, S.; Mochizuki, H.Kurita, A. Enhanced ability of heparin-carrying polystyrene (HCPS) to bind to heparin-binding growth factors and to inhibit growth factor-induced endothelial cell growth. *J Biochem.* **2000**, *127*(5), 797-803.

[439] Park, K.; Kim, K.; Kwon, I. C.; Kim, S. K.; Lee, S.; Lee, D. Y.Byun, Y. Preparation and characterization of self-assembled nanoparticles of heparin-deoxycholic acid conjugates. *Langmuir.* **2004**, *20*(26), 11726-11731.

[440] Maeda, H.; Wu, J.; Sawa, T.; Matsumura, Y.Hori, K. Tumor vascular permeability and the EPR effect in macromolecular therapeutics: a review. *J Control Release.* **2000**, *65*(1-2), 271-284.

[441] Park, K.; Kim, Y. S.; Lee, G. Y.; Nam, J. O.; Lee, S. K.; Park, R. W.; Kim, S. Y.; Kim, I. S.Byun, Y. Antiangiogenic effect of bile acid acylated heparin derivative. *Pharm Res.* **2007**, *24*(1), 176-185.

[442] Park, K.; Lee, G. Y.; Kim, Y. S.; Yu, M.; Park, R. W.; Kim, I. S.; Kim, S. Y.Byun, Y. Heparin-deoxycholic acid chemical conjugate as an anticancer drug carrier and its antitumor activity. *J Control Release.* **2006**, *114*(3), 300-306.

[443] Lee, D. Y.; Kim, S. K.; Kim, Y. S.; Son, D. H.; Nam, J. H.; Kim, I. S.; Park, R. W.; Kim, S. Y.Byun, Y. Suppression of angiogenesis and tumor growth by orally active deoxycholic acid-heparin conjugate. *J Control Release.* **2007**, *118*(3), 310-317.

[444] Lee, Y.; Nam, J. H.; Shin, H. C.Byun, Y. Conjugation of low-molecular-weight heparin and deoxycholic acid for the development of a new oral anticoagulant agent. *Circulation.* **2001**, *104*(25), 3116-3120.

[445] Lee, D. Y.; Park, K.; Kim, S. K.; Park, R. W.; Kwon, I. C.; Kim, S. Y.Byun, Y. Antimetastatic effect of an orally active heparin derivative on experimentally induced metastasis. *Clin Cancer Res.* **2008**, *14*(9), 2841-2849.

[446] Park, J. W.; Jeon, O. C.; Kim, S. K.; Al-Hilal, T. A.; Jin, S. J.; Moon, H. T.; Yang, V. C.; Kim, S. Y.Byun, Y. High antiangiogenic and low anticoagulant efficacy of orally active low molecular weight heparin derivatives. *J Control Release.* **2010**, *148*(3), 317-326.

[447] Lee, E.; Kim, Y. S.; Bae, S. M.; Kim, S. K.; Jin, S.; Chung, S. W.; Lee, M.; Moon, H. T.; Jeon, O. C.; Park, R. W.; Kim, I. S.; Byun, Y.Kim, S. Y.

Polyproline-type helical-structured low-molecular weight heparin (LMWH)-taurocholate conjugate as a new angiogenesis inhibitor. *Int J Cancer.* **2009**, *124*(12), 2755-2765.

[448] Miotti, S.; Canevari, S.; Menard, S.; Mezzanzanica, D.; Porro, G.; Pupa, S. M.; Regazzoni, M.; Tagliabue, E.Colnaghi, M. I. Characterization of human ovarian carcinoma-associated antigens defined by novel monoclonal antibodies with tumor-restricted specificity. *Int J Cancer.* **1987**, *39*(3), 297-303.

[449] Coney, L. R.; Tomassetti, A.; Carayannopoulos, L.; Frasca, V.; Kamen, B. A.; Colnaghi, M. I.Zurawski, V. R., Jr. Cloning of a tumor-associated antigen: MOv18 and MOv19 antibodies recognize a folate-binding protein. *Cancer Res.* **1991**, *51*(22), 6125-6132.

[450] Weitman, S. D.; Lark, R. H.; Coney, L. R.; Fort, D. W.; Frasca, V.; Zurawski, V. R., Jr.Kamen, B. A. Distribution of the folate receptor GP38 in normal and malignant cell lines and tissues. *Cancer Res.* **1992**, *52*(12), 3396-3401.

[451] Parker, N.; Turk, M. J.; Westrick, E.; Lewis, J. D.; Low, P. S.Leamon, C. P. Folate receptor expression in carcinomas and normal tissues determined by a quantitative radioligand binding assay. *Anal Biochem.* **2005**, *338*(2), 284-293.

[452] Park, K.; Kim, Y. S.; Lee, G. Y.; Park, R. W.; Kim, I. S.; Kim, S. Y.Byun, Y. Tumor endothelial cell targeted cyclic RGD-modified heparin derivative: inhibition of angiogenesis and tumor growth. *Pharm Res.* **2008**, *25*(12), 2786-2798.

[453] Lindsay, C. R.; MacPherson, I. R.Cassidy, J. Current status of cediranib: the rapid development of a novel anti-angiogenic therapy. *Future Oncol.* **2009**, *5*(4), 421-432.

[454] Mulders, P.; Hawkins, R.; Nathan, P.; de Jong, I.; Osanto, S.; Porfiri, E.; Protheroe, A.; van Herpen, C. M.; Mookerjee, B.; Pike, L.; Jurgensmeier, J. M.Gore, M. E. Cediranib monotherapy in patients with advanced renal cell carcinoma: results of a randomised phase II study. *Eur J Cancer.* **2012**, *48*(4), 527-537.

[455] Saura, C. B., J.; Herbst, R.; del Campo, J.; Marotti, M.; Tessier, J.; Collins, B.; Heymach, J. Antitumor activity of cediranib in patients with metastatic or recurrent head and neck cancer (HNC) or recurrent non-small cell lung cancer (NSCLC): An open-label exploratory study. *J Clin Oncol.* **2009**, *27*(15).

[456] Batchelor, T. T.; Duda, D. G.; di Tomaso, E.; Ancukiewicz, M.; Plotkin, S. R.; Gerstner, E.; Eichler, A. F.; Drappatz, J.; Hochberg, F. H.; Benner, T.; Louis, D. N.; Cohen, K. S.; Chea, H.; Exarhopoulos, A.; Loeffler, J. S.; Moses, M. A.; Ivy, P.; Sorensen, A. G.; Wen, P. Y.Jain, R. K. Phase II study of cediranib, an oral pan-vascular endothelial growth factor receptor tyrosine kinase inhibitor, in patients with recurrent glioblastoma. *J Clin Oncol.* **2010**, *28*(17), 2817-2823.

[457] Matulonis, U. A.; Berlin, S.; Ivy, P.; Tyburski, K.; Krasner, C.; Zarwan, C.; Berkenblit, A.; Campos, S.; Horowitz, N.; Cannistra, S. A.; Lee, H.; Lee, J.; Roche, M.; Hill, M.; Whalen, C.; Sullivan, L.; Tran, C.; Humphreys, B. D.Penson, R. T. Cediranib, an oral inhibitor of vascular endothelial growth factor receptor kinases, is an active drug in recurrent epithelial ovarian, fallopian tube, and peritoneal cancer. *J Clin Oncol.* **2009**, *27*(33), 5601-5606.

[458] Goss, G. D.; Arnold, A.; Shepherd, F. A.; Dediu, M.; Ciuleanu, T. E.; Fenton, D.; Zukin, M.; Walde, D.; Laberge, F.; Vincent, M. D.; Ellis, P. M.; Laurie, S. A.; Ding, K.; Frymire, E.; Gauthier, I.; Leighl, N. B.; Ho, C.; Noble, J.; Lee, C.

W.Seymour, L. Randomized, double-blind trial of carboplatin and paclitaxel with either daily oral cediranib or placebo in advanced non-small-cell lung cancer: NCIC clinical trials group BR24 study. *J Clin Oncol.* **2010**, *28*(1), 49-55.

[459] Polverino, A.; Coxon, A.; Starnes, C.; Diaz, Z.; DeMelfi, T.; Wang, L.; Bready, J.; Estrada, J.; Cattley, R.; Kaufman, S.; Chen, D.; Gan, Y.; Kumar, G.; Meyer, J.; Neervannan, S.; Alva, G.; Talvenheimo, J.; Montestruque, S.; Tasker, A.; Patel, V.; Radinsky, R.Kendall, R. AMG 706, an oral, multikinase inhibitor that selectively targets vascular endothelial growth factor, platelet-derived growth factor, and kit receptors, potently inhibits angiogenesis and induces regression in tumor xenografts. *Cancer Res.* **2006**, *66*(17), 8715-8721.

[460] Price, T. J.; Lipton, L.; McGreivy, J.; McCoy, S.; Sun, Y. N.Rosenthal, M. A. Safety and pharmacokinetics of motesanib in combination with gemcitabine for the treatment of patients with solid tumours. *Br J Cancer.* **2008**, *99*(9), 1387-1394.

[461] Blumenschein, G. R., Jr.; Kabbinavar, F.; Menon, H.; Mok, T. S.; Stephenson, J.; Beck, J. T.; Lakshmaiah, K.; Reckamp, K.; Hei, Y. J.; Kracht, K.; Sun, Y. N.; Sikorski, R.Schwartzberg, L. A phase II, multicenter, open-label randomized study of motesanib or bevacizumab in combination with paclitaxel and carboplatin for advanced nonsquamous non-small-cell lung cancer. *Ann Oncol.* **2011**.

[462] Slichenmyer, W. J.; Elliott, W. L.Fry, D. W. CI-1033, a pan-erbB tyrosine kinase inhibitor. *Semin Oncol.* **2001**, *28*(5 Suppl 16), 80-85.

[463] Nemunaitis, J.; Eiseman, I.; Cunningham, C.; Senzer, N.; Williams, A.; Lenehan, P. F.; Olson, S. C.; Bycott, P.; Schlicht, M.; Zentgraff, R.; Shin, D. M.Zinner, R. G. Phase 1 clinical and pharmacokinetics evaluation of oral CI-1033 in patients with refractory cancer. *Clin Cancer Res.* **2005**, *11*(10), 3846-3853.

[464] Campos, S.; Hamid, O.; Seiden, M. V.; Oza, A.; Plante, M.; Potkul, R. K.; Lenehan, P. F.; Kaldjian, E. P.; Varterasian, M. L.; Jordan, C.; Charbonneau, C.Hirte, H. Multicenter, randomized phase II trial of oral CI-1033 for previously treated advanced ovarian cancer. *J Clin Oncol.* **2005**, *23*(24), 5597-5604.

[465] Janne, P. A.; von Pawel, J.; Cohen, R. B.; Crino, L.; Butts, C. A.; Olson, S. S.; Eiseman, I. A.; Chiappori, A. A.; Yeap, B. Y.; Lenehan, P. F.; Dasse, K.; Sheeran, M.Bonomi, P. D. Multicenter, randomized, phase II trial of CI-1033, an irreversible pan-ERBB inhibitor, for previously treated advanced non small-cell lung cancer. *J Clin Oncol.* **2007**, *25*(25), 3936-3944.

[466] Rixe, O.; Franco, S. X.; Yardley, D. A.; Johnston, S. R.; Martin, M.; Arun, B. K.; Letrent, S. P.Rugo, H. S. A randomized, phase II, dose-finding study of the pan-ErbB receptor tyrosine-kinase inhibitor CI-1033 in patients with pretreated metastatic breast cancer. *Cancer Chemother Pharmacol.* **2009**, *64*(6), 1139-1148.

[467] Wood, J. M.; Bold, G.; Buchdunger, E.; Cozens, R.; Ferrari, S.; Frei, J.; Hofmann, F.; Mestan, J.; Mett, H.; O'Reilly, T.; Persohn, E.; Rosel, J.; Schnell, C.; Stover, D.; Theuer, A.; Towbin, H.; Wenger, F.; Woods-Cook, K.; Menrad, A.; Siemeister, G.; Schirner, M.; Thierauch, K. H.; Schneider, M. R.; Drevs, J.; Martiny-Baron, G.Totzke, F. PTK787/ZK 222584, a novel and potent inhibitor of vascular endothelial growth factor receptor tyrosine kinases, impairs vascular

endothelial growth factor-induced responses and tumor growth after oral administration. *Cancer Res.* **2000**, *60*(8), 2178-2189.

[468] Drevs, J.; Hofmann, I.; Hugenschmidt, H.; Wittig, C.; Madjar, H.; Muller, M.; Wood, J.; Martiny-Baron, G.; Unger, C.Marme, D. Effects of PTK787/ZK 222584, a specific inhibitor of vascular endothelial growth factor receptor tyrosine kinases, on primary tumor, metastasis, vessel density, and blood flow in a murine renal cell carcinoma model. *Cancer Res.* **2000**, *60*(17), 4819-4824.

[469] Solorzano, C. C.; Baker, C. H.; Bruns, C. J.; Killion, J. J.; Ellis, L. M.; Wood, J.Fidler, I. J. Inhibition of growth and metastasis of human pancreatic cancer growing in nude mice by PTK 787/ZK222584, an inhibitor of the vascular endothelial growth factor receptor tyrosine kinases. *Cancer Biother Radiopharm.* **2001**, *16*(5), 359-370.

[470] Thomas, A. L.; Morgan, B.; Horsfield, M. A.; Higginson, A.; Kay, A.; Lee, L.; Masson, E.; Puccio-Pick, M.; Laurent, D.Steward, W. P. Phase I study of the safety, tolerability, pharmacokinetics, and pharmacodynamics of PTK787/ZK 222584 administered twice daily in patients with advanced cancer. *J Clin Oncol.* **2005**, *23*(18), 4162-4171.

[471] Tyagi, P. Vatalanib (PTK787/ZK 222584) in combination with FOLFOX4 versus FOLFOX4 alone as first-line treatment for colorectal cancer: preliminary results from the CONFIRM-1 trial. *Clin Colorectal Cancer.* **2005**, *5*(1), 24-26.

[472] Van Cutsem, E.; Bajetta, E.; Valle, J.; Kohne, C. H.; Hecht, J. R.; Moore, M.; Germond, C.; Berg, W.; Chen, B. L.; Jalava, T.; Lebwohl, D.; Meinhardt, G.; Laurent, D.Lin, E. Randomized, placebo-controlled, phase III study of oxaliplatin, fluorouracil, and leucovorin with or without PTK787/ZK 222584 in patients with previously treated metastatic colorectal adenocarcinoma. *J Clin Oncol.* **2011**, *29*(15), 2004-2010.

[473] Jones, S. F.; Spigel, D. R.; Yardley, D. A.; Thompson, D. F.Burris, H. A., 3rd A phase I trial of vatalanib (PTK/ZK) in combination with bevacizumab in patients with refractory and/or advanced malignancies. *Clin Adv Hematol Oncol.* **2011**, *9*(11), 845-852.

[474] Jahan, T.; Gu, L.; Kratzke, R.; Dudek, A.; Otterson, G. A.; Wang, X.; Green, M.; Vokes, E. E.Kindler, H. L. Vatalanib in malignant mesothelioma: A phase II trial by the Cancer and Leukemia Group B (CALGB 30107). *Lung Cancer.* **2012**, *76*(3), 393-396.

[475] Chong, A. S.; Gebel, H.; Finnegan, A.; Petraitis, E. E.; Jiang, X. L.; Sankary, H. N.; Foster, P.Williams, J. W. Leflunomide, a novel immunomodulatory agent: in vitro analyses of the mechanism of immunosuppression. *Transplant Proc.* **1993**, *25*(1 Pt 1), 747-749.

[476] Mattar, T.; Kochhar, K.; Bartlett, R.; Bremer, E. G.Finnegan, A. Inhibition of the epidermal growth factor receptor tyrosine kinase activity by leflunomide. *FEBS Lett.* **1993**, *334*(2), 161-164.

[477] Xu, X.; Shen, J.; Mall, J. W.; Myers, J. A.; Huang, W.; Blinder, L.; Saclarides, T. J.; Williams, J. W.Chong, A. S. In vitro and in vivo antitumor activity of a novel immunomodulatory drug, leflunomide: mechanisms of action. *Biochem Pharmacol.* **1999**, *58*(9), 1405-1413.

[478] Ko, Y. J.; Small, E. J.; Kabbinavar, F.; Chachoua, A.; Taneja, S.; Reese, D.; DePaoli, A.; Hannah, A.; Balk, S. P.Bubley, G. J. A multi-institutional phase ii

study of SU101, a platelet-derived growth factor receptor inhibitor, for patients with hormone-refractory prostate cancer. *Clin Cancer Res.* **2001**, *7*(4), 800-805.

[479] Boyer, S. J. Small molecule inhibitors of KDR (VEGFR-2) kinase: an overview of structure activity relationships. *Curr Top Med Chem.* **2002**, *2*(9), 973-1000.

[480] Davis, S.; Aldrich, T. H.; Jones, P. F.; Acheson, A.; Compton, D. L.; Jain, V.; Ryan, T. E.; Bruno, J.; Radziejewski, C.; Maisonpierre, P. C.Yancopoulos, G. D. Isolation of angiopoietin-1, a ligand for the TIE2 receptor, by secretion-trap expression cloning. *Cell.* **1996**, *87*(7), 1161-1169.

[481] Suri, C.; Jones, P. F.; Patan, S.; Bartunkova, S.; Maisonpierre, P. C.; Davis, S.; Sato, T. N.Yancopoulos, G. D. Requisite role of angiopoietin-1, a ligand for the TIE2 receptor, during embryonic angiogenesis. *Cell.* **1996**, *87*(7), 1171-1180.

[482] Miyazaki, Y.; Matsunaga, S.; Tang, J.; Maeda, Y.; Nakano, M.; Philippe, R. J.; Shibahara, M.; Liu, W.; Sato, H.; Wang, L.Nolte, R. T. Novel 4-amino-furo[2,3-d]pyrimidines as Tie-2 and VEGFR2 dual inhibitors. *Bioorg Med Chem Lett.* **2005**, *15*(9), 2203-2207.

[483] Miyazaki, Y.; Tang, J.; Maeda, Y.; Nakano, M.; Wang, L.; Nolte, R. T.; Sato, H.; Sugai, M.; Okamoto, Y.; Truesdale, A. T.; Hassler, D. F.; Nartey, E. N.; Patrick, D. R.; Ho, M. L.Ozawa, K. Orally active 4-amino-5-diarylurea-furo[2,3-d]pyrimidine derivatives as anti-angiogenic agent inhibiting VEGFR2 and Tie-2. *Bioorg Med Chem Lett.* **2007**, *17*(6), 1773-1778.

[484] Becknell, N. C.; Zulli, A. L.; Angeles, T. S.; Yang, S.; Albom, M. S.; Aimone, L. D.; Robinson, C.; Chang, H.Hudkins, R. L. Novel C-3 N-urea, amide, and carbamate dihydroindazolo[5,4-a]pyrrolo[3,4-c]carbazole analogs as potent TIE-2 and VEGF-R2 dual inhibitors. *Bioorg Med Chem Lett.* **2006**, *16*(20), 5368-5372.

[485] Dandu, R.; Zulli, A. L.; Bacon, E. R.; Underiner, T.; Robinson, C.; Chang, H.; Miknyoczki, S.; Grobelny, J.; Ruggeri, B. A.; Yang, S.; Albom, M. S.; Angeles, T. S.; Aimone, L. D.Hudkins, R. L. Design and synthesis of dihydroindazolo[5,4-a]pyrrolo[3,4-c]carbazole oximes as potent dual inhibitors of TIE-2 and VEGF-R2 receptor tyrosine kinases. *Bioorg Med Chem Lett.* **2008**, *18*(6), 1916-1921.

[486] Sathornsumetee, S.; Hjelmeland, A. B.; Keir, S. T.; McLendon, R. E.; Batt, D.; Ramsey, T.; Yusuff, N.; Rasheed, B. K.; Kieran, M. W.; Laforme, A.; Bigner, D. D.; Friedman, H. S.Rich, J. N. AAL881, a novel small molecule inhibitor of RAF and vascular endothelial growth factor receptor activities, blocks the growth of malignant glioma. *Cancer Res.* **2006**, *66*(17), 8722-8730.

[487] Lang, S. A.; Brecht, I.; Moser, C.; Obed, A.; Batt, D.; Schlitt, H. J.; Geissler, E. K.Stoeltzing, O. Dual inhibition of Raf and VEGFR2 reduces growth and vascularization of hepatocellular carcinoma in an experimental model. *Langenbecks Arch Surg.* **2008**, *393*(3), 333-341.

[488] Lang, S. A.; Schachtschneider, P.; Moser, C.; Mori, A.; Hackl, C.; Gaumann, A.; Batt, D.; Schlitt, H. J.; Geissler, E. K.Stoeltzing, O. Dual targeting of Raf and VEGF receptor 2 reduces growth and metastasis of pancreatic cancer through direct effects on tumor cells, endothelial cells, and pericytes. *Mol Cancer Ther.* **2008**, *7*(11), 3509-3518.

[489] Raeppel, S.; Claridge, S.; Saavedra, O.; Gaudette, F.; Zhan, L.; Mannion, M.; Zhou, N.; Raeppel, F.; Granger, M. C.; Isakovic, L.; Deziel, R.; Nguyen, H.; Beaulieu, N.; Beaulieu, C.; Dupont, I.; Robert, M. F.; Lefebvre, S.; Dubay, M.;

Rahil, J.; Wang, J.; Ste-Croix, H.; Robert Macleod, A.; Besterman, J.Vaisburg, A. N-(3-fluoro-4-(2-arylthieno[3,2-b]pyridin-7-yloxy)phenyl)-2-oxo-3-phenylim idazolidine-1-carboxamides: a novel series of dual c-Met/VEGFR2 receptor tyrosine kinase inhibitors. *Bioorg Med Chem Lett.* **2009**, *19*(5), 1323-1328.

[490] Okada, N.; Watarai, M.; Ozeri, V.; Hanski, E.; Caparon, M.Sasakawa, C. A matrix form of fibronectin mediates enhanced binding of Streptococcus pyogenes to host tissue. *J Biol Chem.* **1997**, *272*(43), 26978-26984.

[491] Gentilucci, L.; Cardillo, G.; Spampinato, S.; Tolomelli, A.; Squassabia, F.; De Marco, R.; Bedini, A.; Baiula, M.; Belvisi, L.Civera, M. Antiangiogenic effect of dual/selective alpha(5)beta(1)/alpha(v)beta(3) integrin antagonists designed on partially modified retro-inverso cyclotetrapeptide mimetics. *J Med Chem.* **2010**, *53*(1), 106-118.

[492] Ahmed, B.; Van Eijk, L. I.; Bouma-Ter Steege, J. C.; Van Der Schaft, D. W.; Van Esch, A. M.; Joosten-Achjanie, S. R.; Lambin, P.; Landuyt, W.Griffioen, A. W. Vascular targeting effect of combretastatin A-4 phosphate dominates the inherent angiogenesis inhibitory activity. *Int J Cancer.* **2003**, *105*(1), 20-25.

[493] Mosmann, T. Rapid colorimetric assay for cellular growth and survival: application to proliferation and cytotoxicity assays. *J Immunol Methods.* **1983**, *65*(1-2), 55-63.

[494] Rabinovitch, P. *Introduction to Cell Cycle Analysis*. Basics of DNA Cell Cycle Analysis.

[495] Lin, H. L.; Chiou, S. H.; Wu, C. W.; Lin, W. B.; Chen, L. H.; Yang, Y. P.; Tsai, M. L.; Uen, Y. H.; Liou, J. P.Chi, C. W. Combretastatin A4-induced differential cytotoxicity and reduced metastatic ability by inhibition of AKT function in human gastric cancer cells. *J Pharmacol Exp Ther.* **2007**, *323*(1), 365-373.

[496] Jung, H. J.; Shim, J. S.; Lee, H. B.; Kim, C. J.; Kuwano, T.; Ono, M.Kwon, H. J. Embellistatin, a microtubule polymerization inhibitor, inhibits angiogenesis both in vitro and in vivo. *Biochem Biophys Res Commun.* **2007**, *353*(2), 376-380.

[497] Arora, S.; Wang, X. I.; Keenan, S. M.; Andaya, C.; Zhang, Q.; Peng, Y.Welsh, W. J. Novel microtubule polymerization inhibitor with potent antiproliferative and antitumor activity. *Cancer Res.* **2009**, *69*(5), 1910-1915.

[498] Krishan, A. Rapid flow cytofluorometric analysis of mammalian cell cycle by propidium iodide staining. *J Cell Biol.* **1975**, *66*(1), 188-193.

[499] Fulwyler, M. J. Electronic separation of biological cells by volume. *Science.* **1965**, *150*(3698), 910-911.

[500] Joncour, A.; Liu, J. M.; Decor, A.; Thoret, S.; Wdzieczak-Bakala, J.; Bignon, J.Baudoin, O. Synthesis of anti-microtubule biaryls and preliminary evaluation as vascular-disrupting agents. *ChemMedChem.* **2008**, *3*(11), 1731-1739.

[501] Giuliani, N.; Colla, S.; Lazzaretti, M.; Sala, R.; Roti, G.; Mancini, C.; Bonomini, S.; Lunghi, P.; Hojden, M.; Genestreti, G.; Svaldi, M.; Coser, P.; Fattori, P. P.; Sammarelli, G.; Gazzola, G. C.; Bataille, R.; Almici, C.; Caramatti, C.; Mangoni, L.Rizzoli, V. Proangiogenic properties of human myeloma cells: production of angiopoietin-1 and its potential relationship to myeloma-induced angiogenesis. *Blood.* **2003**, *102*(2), 638-645.

[502] Beale, T. M.; Bond, P. J.; Brenton, J. D.; Charnock-Jones, D. S.; Ley, S. V.Myers, R. M. Increased endothelial cell selectivity of triazole-bridged

dihalogenated A-ring analogues of combretastatin A-1. *Bioorg Med Chem.* **2012**, *20*(5), 1749-1759.

[503] Flynn, B. L.; Gill, G. S.; Grobelny, D. W.; Chaplin, J. H.; Paul, D.; Leske, A. F.; Lavranos, T. C.; Chalmers, D. K.; Charman, S. A.; Kostewicz, E.; Shackleford, D. M.; Morizzi, J.; Hamel, E.; Jung, M. K.Kremmidiotis, G. Discovery of 7-hydroxy-6-methoxy-2-methyl-3-(3,4,5-trimethoxybenzoyl)benzo[b]furan (BNC105), a tubulin polymerization inhibitor with potent antiproliferative and tumor vascular disrupting properties. *J Med Chem.* **2011**, *54*(17), 6014-6027.

[504] Sun, L.; Vasilevich, N. I.; Fuselier, J. A.; Hocart, S. J.Coy, D. H. Examination of the 1,4-disubstituted azetidinone ring system as a template for combretastatin A-4 conformationally restricted analogue design. *Bioorg Med Chem Lett.* **2004**, *14*(9), 2041-2046.

[505] Carr, M.; Greene, L. M.; Knox, A. J.; Lloyd, D. G.; Zisterer, D. M.Meegan, M. J. Lead identification of conformationally restricted beta-lactam type combretastatin analogues: synthesis, antiproliferative activity and tubulin targeting effects. *Eur J Med Chem.* **2010**, *45*(12), 5752-5766.

[506] O'Boyle, N. M.; Carr, M.; Greene, L. M.; Bergin, O.; Nathwani, S. M.; McCabe, T.; Lloyd, D. G.; Zisterer, D. M.Meegan, M. J. Synthesis and evaluation of azetidinone analogues of combretastatin A-4 as tubulin targeting agents. *J Med Chem.* **2010**, *53*(24), 8569-8584.

[507] Romagnoli, R.; Baraldi, P. G.; Pavani, M. G.; Tabrizi, M. A.; Preti, D.; Fruttarolo, F.; Piccagli, L.; Jung, M. K.; Hamel, E.; Borgatti, M.Gambari, R. Synthesis and biological evaluation of 2-amino-3-(3',4',5'-trimethoxybenzoyl)-5-aryl thiophenes as a new class of potent antitubulin agents. *J Med Chem.* **2006**, *49*(13), 3906-3915.

[508] Ding, X.; Zhang, Z.; Li, S.Wang, A. Combretastatin A4 phosphate induces programmed cell death in vascular endothelial cells. *Oncol Res.* **2011**, *19*(7), 303-309.

[509] Zhu, H.; Zhang, J.; Xue, N.; Hu, Y.; Yang, B.He, Q. Novel combretastatin A-4 derivative XN0502 induces cell cycle arrest and apoptosis in A549 cells. *Invest New Drugs.* **2010**, *28*(4), 493-501.

[510] Romagnoli, R.; Baraldi, P. G.; Remusat, V.; Carrion, M. D.; Cara, C. L.; Preti, D.; Fruttarolo, F.; Pavani, M. G.; Tabrizi, M. A.; Tolomeo, M.; Grimaudo, S.; Balzarini, J.; Jordan, M. A.Hamel, E. Synthesis and biological evaluation of 2-(3',4',5'-trimethoxybenzoyl)-3-amino 5-aryl thiophenes as a new class of tubulin inhibitors. *J Med Chem.* **2006**, *49*(21), 6425-6428.

[511] Vincent, L.; Kermani, P.; Young, L. M.; Cheng, J.; Zhang, F.; Shido, K.; Lam, G.; Bompais-Vincent, H.; Zhu, Z.; Hicklin, D. J.; Bohlen, P.; Chaplin, D. J.; May, C.Rafii, S. Combretastatin A4 phosphate induces rapid regression of tumor neovessels and growth through interference with vascular endothelial-cadherin signaling. *J Clin Invest.* **2005**, *115*(11), 2992-3006.

[512] Kremmidiotis, G.; Leske, A. F.; Lavranos, T. C.; Beaumont, D.; Gasic, J.; Hall, A.; O'Callaghan, M.; Matthews, C. A.Flynn, B. BNC105: a novel tubulin polymerization inhibitor that selectively disrupts tumor vasculature and displays single-agent antitumor efficacy. *Mol Cancer Ther.* **2010**, *9*(6), 1562-1573.

[513] Bonezzi, K.; Taraboletti, G.; Borsotti, P.; Bellina, F.; Rossi, R.Giavazzi, R. Vascular disrupting activity of tubulin-binding 1,5-diaryl-1H-imidazoles. *J Med Chem.* **2009**, *52*(23), 7906-7910.

[514] van Hinsbergh, V. W. Endothelial permeability for macromolecules. Mechanistic aspects of pathophysiological modulation. *Arterioscler Thromb Vasc Biol.* **1997**, *17*(6), 1018-1023.

[515] Romagnoli, R.; Baraldi, P. G.; Cruz-Lopez, O.; Lopez Cara, C.; Carrion, M. D.; Brancale, A.; Hamel, E.; Chen, L.; Bortolozzi, R.; Basso, G.Viola, G. Synthesis and antitumor activity of 1,5-disubstituted 1,2,4-triazoles as cis-restricted combretastatin analogues. *J Med Chem.* **2010**, *53*(10), 4248-4258.

[516] Nicosia, R. F. and Ottinetti, A. Growth of microvessels in serum-free matrix culture of rat aorta. A quantitative assay of angiogenesis in vitro. *Lab Invest.* **1990**, *63*(1), 115-122.

[517] Villaschi, S. and Nicosia, R. F. Angiogenic role of endogenous basic fibroblast growth factor released by rat aorta after injury. *Am J Pathol.* **1993**, *143*(1), 181-190.

[518] Nicosia, R. F.; Nicosia, S. V.Smith, M. Vascular endothelial growth factor, platelet-derived growth factor, and insulin-like growth factor-1 promote rat aortic angiogenesis in vitro. *Am J Pathol.* **1994**, *145*(5), 1023-1029.

[519] Nicosia, R. F.; Lin, Y. J.; Hazelton, D.Qian, X. Endogenous regulation of angiogenesis in the rat aorta model. Role of vascular endothelial growth factor. *Am J Pathol.* **1997**, *151*(5), 1379-1386.

[520] Zhu, W. H.; MacIntyre, A.Nicosia, R. F. Regulation of angiogenesis by vascular endothelial growth factor and angiopoietin-1 in the rat aorta model: distinct temporal patterns of intracellular signaling correlate with induction of angiogenic sprouting. *Am J Pathol.* **2002**, *161*(3), 823-830.

[521] Nicosia, R. F.; Bonanno, E.Villaschi, S. Large-vessel endothelium switches to a microvascular phenotype during angiogenesis in collagen gel culture of rat aorta. *Atherosclerosis.* **1992**, *95*(2-3), 191-199.

[522] Nicosia, R. F.; Tchao, R.Leighton, J. Angiogenesis-dependent tumor spread in reinforced fibrin clot culture. *Cancer Res.* **1983**, *43*(5), 2159-2166.

[523] Ain, K. B.; Tofiq, S.Taylor, K. D. Antineoplastic activity of taxol against human anaplastic thyroid carcinoma cell lines in vitro and in vivo. *J Clin Endocrinol Metab.* **1996**, *81*(10), 3650-3653.

[524] Chang, Y. S.; Adnane, J.; Trail, P. A.; Levy, J.; Henderson, A.; Xue, D.; Bortolon, E.; Ichetovkin, M.; Chen, C.; McNabola, A.; Wilkie, D.; Carter, C. A.; Taylor, I. C.; Lynch, M.Wilhelm, S. Sorafenib (BAY 43-9006) inhibits tumor growth and vascularization and induces tumor apoptosis and hypoxia in RCC xenograft models. *Cancer Chemother Pharmacol.* **2007**, *59*(5), 561-574.

[525] Bagi, C. M.; Gebhard, D. F.Andresen, C. J. Antitumor effect of vascular endothelial growth factor inhibitor sunitinib in preclinical models of hepatocellular carcinoma. *Eur J Gastroenterol Hepatol.* **2012**, *24*(5), 563-574.

[526] Richmond, A. and Su, Y. Mouse xenograft models vs GEM models for human cancer therapeutics. *Dis Model Mech.* **2008**, *1*(2-3), 78-82.

[527] Kerbel, R. S. Human tumor xenografts as predictive preclinical models for anticancer drug activity in humans: better than commonly perceived-but they can be improved. *Cancer Biol Ther.* **2003**, *2*(4 Suppl 1), S134-139.

[528] Shnyder, S. D.; Cooper, P. A.; Millington, N. J.; Pettit, G. R.Bibby, M. C. Auristatin PYE, a novel synthetic derivative of dolastatin 10, is highly effective in human colon tumour models. *Int J Oncol.* **2007**, *31*(2), 353-360.

[529] Prokopiou, E. M.; Cooper, P. A.; Pettit, G. R.; Bibby, M. C.Shnyder, S. D. Potentiation of the activity of cisplatin in a human colon tumour xenograft model by auristatin PYE, a structural modification of dolastatin 10. *Mol Med Report.* **2010**, *3*(2), 309-313.

[530] Avwioro, G. HISTOCHEMICAL USES OF HAEMATOXYLIN - A REVIEW. *JPCS.* **2011**, *1*.

[531] Smith, K. A.; Hill, S. A.; Begg, A. C.Denekamp, J. Validation of the fluorescent dye Hoechst 33342 as a vascular space marker in tumours. *Br J Cancer.* **1988**, *57*(3), 247-253.

[532] Tozer, G. M.; Akerman, S.; Cross, N. A.; Barber, P. R.; Bjorndahl, M. A.; Greco, O.; Harris, S.; Hill, S. A.; Honess, D. J.; Ireson, C. R.; Pettyjohn, K. L.; Prise, V. E.; Reyes-Aldasoro, C. C.; Ruhrberg, C.; Shima, D. T.Kanthou, C. Blood vessel maturation and response to vascular-disrupting therapy in single vascular endothelial growth factor-A isoform-producing tumors. *Cancer Res.* **2008**, *68*(7), 2301-2311.

[533] Loi, M.; Marchio, S.; Becherini, P.; Di Paolo, D.; Soster, M.; Curnis, F.; Brignole, C.; Pagnan, G.; Perri, P.; Caffa, I.; Longhi, R.; Nico, B.; Bussolino, F.; Gambini, C.; Ribatti, D.; Cilli, M.; Arap, W.; Pasqualini, R.; Allen, T. M.; Corti, A.; Ponzoni, M.Pastorino, F. Combined targeting of perivascular and endothelial tumor cells enhances anti-tumor efficacy of liposomal chemotherapy in neuroblastoma. *J Control Release.* **2010**, *145*(1), 66-73.

[534] Burtles, S. S.; Newell, D. R.; Henrar, R. E.Connors, T. A. Revisions of general guidelines for the preclinical toxicology of new cytotoxic anticancer agents in Europe. The Cancer Research Campaign (CRC) Phase I/II Clinical Trials Committee and the European Organization for Research and Treatment of Cancer (EORTC) New Drug Development Office. *Eur J Cancer.* **1995**, *31A*(3), 408-410.

[535] Geran, R. I. G., N.H. and MacDonald M.M., *Protocols for screening chemical agents and natural products against tumours and other biological systems*. Cancer Chemother Rep. Vol. 3. 1972.

[536] Grosios, K.; Holwell, S. E.; McGown, A. T.; Pettit, G. R.Bibby, M. C. In vivo and in vitro evaluation of combretastatin A-4 and its sodium phosphate prodrug. *Br J Cancer.* **1999**, *81*(8), 1318-1327.

[537] Dorr, R. T.; Dvorakova, K.; Snead, K.; Alberts, D. S.; Salmon, S. E.Pettit, G. R. Antitumor activity of combretastatin-A4 phosphate, a natural product tubulin inhibitor. *Invest New Drugs.* **1996**, *14*(2), 131-137.

[538] van Wijngaarden, J.; Snoeks, T. J.; van Beek, E.; Bloys, H.; Kaijzel, E. L.; van Hinsbergh, V. W.Lowik, C. W. An in vitro model that can distinguish between effects on angiogenesis and on established vasculature: actions of TNP-470, marimastat and the tubulin-binding agent Ang-510. *Biochem Biophys Res Commun.* **2010**, *391*(2), 1161-1165.

[539] Meng, F.; Cai, X.; Duan, J.; Matteucci, M. G.Hart, C. P. A novel class of tubulin inhibitors that exhibit potent antiproliferation and in vitro vessel-disrupting activity. *Cancer Chemother Pharmacol.* **2008**, *61*(6), 953-963.

[540] Kong, Y.; Wang, K.; Edler, M. C.; Hamel, E.; Mooberry, S. L.; Paige, M. A.Brown, M. L. A boronic acid chalcone analog of combretastatin A-4 as a potent anti-proliferation agent. *Bioorg Med Chem.* **2010**, *18*(2), 971-977.

[541] Vu, H. N.; Miller, W. J.; O'Connor, S. A.; He, M.; Schafer, P. H.; Payvandi, F.; Muller, G. W.; Stirling, D. I.Libutti, S. K. CC-5079: a small molecule with MKP1, antiangiogenic, and antitumor activity. *J Surg Res.* **2010**, *164*(1), 116-125.

[542] Gardner, E. R.; Kelly, M.; Springman, E.; Lee, K. J.; Li, H.; Moore, W.Figg, W. D. Antiangiogenic and antitumor activity of LP-261, a novel oral tubulin binding agent, alone and in combination with bevacizumab. *Invest New Drugs.* **2012**, *30*(1), 90-97.

[543] Majerus, P. W. a. D. M. T., *Anticoagulant,Thrombolytic and Antiplatelet Drugs.* 11th ed. Goodman and Gilman's The Pharmacological Basis of Therapeutics, ed. L.L. Brunton, J.S. Lazo and K.L. Parker. 2006, New York.

[544] Nutrition classics from The Journal of Biological Chemistry 138:21-33, 1941. Studies on the hemorrhagic sweet clover disease. IV. The isolation and crystallization of the hemorrhagic agent by Harold A. Campbell and Karl Paul Link. *Nutr Rev.* **1974**, *32*(8), 244-246.

[545] Cain, D.; Hutson, S. M.Wallin, R. Assembly of the warfarin-sensitive vitamin K 2,3-epoxide reductase enzyme complex in the endoplasmic reticulum membrane. *J Biol Chem.* **1997**, *272*(46), 29068-29075.

[546] Nabha, S. M.; Mohammad, R. M.; Wall, N. R.; Dutcher, J. A.; Salkini, B. M.; Pettit, G. R.Al-Katib, A. M. Evaluation of combretastatin A-4 prodrug in a non-Hodgkin's lymphoma xenograft model: preclinical efficacy. *Anticancer Drugs.* **2001**, *12*(1), 57-63.

[547] Boehle, A. S.; Sipos, B.; Kliche, U.; Kalthoff, H.Dohrmann, P. Combretastatin A-4 prodrug inhibits growth of human non-small cell lung cancer in a murine xenotransplant model. *Ann Thorac Surg.* **2001**, *71*(5), 1657-1665.

[548] Kuo, C. C.; Hsieh, H. P.; Pan, W. Y.; Chen, C. P.; Liou, J. P.; Lee, S. J.; Chang, Y. L.; Chen, L. T.; Chen, C. T.Chang, J. Y. BPR0L075, a novel synthetic indole compound with antimitotic activity in human cancer cells, exerts effective antitumoral activity in vivo. *Cancer Res.* **2004**, *64*(13), 4621-4628.

[549] Cai, Y. C.; Zou, Y.; Ye, Y. L.; Sun, H. Y.; Su, Q. G.; Wang, Z. X.; Zeng, Z. L.Xian, L. J. Anti-tumor activity and mechanisms of a novel vascular disrupting agent, (Z)-3,4',5-trimethoxylstilbene-3'-O-phosphate disodium (M410). *Invest New Drugs.* **2011**, *29*(2), 300-311.

[550] Tozer, G. M.; Kanthou, C.Baguley, B. C. Disrupting tumour blood vessels. *Nat Rev Cancer.* **2005**, *5*(6), 423-435.

[551] Horsman, M. R.; Ehrnrooth, E.; Ladekarl, M.Overgaard, J. The effect of combretastatin A-4 disodium phosphate in a C3H mouse mammary carcinoma and a variety of murine spontaneous tumors. *Int J Radiat Oncol Biol Phys.* **1998**, *42*(4), 895-898.

[552] Grosios, K.; Loadman, P. M.; Swaine, D. J.; Pettit, G. R.Bibby, M. C. Combination chemotherapy with combretastatin A-4 phosphate and 5-fluorouracil in an experimental murine colon adenocarcinoma. *Anticancer Res.* **2000**, *20*(1A), 229-233.

[553] Hill, S. A.; Toze, G. M.; Pettit, G. R.Chaplin, D. J. Preclinical evaluation of the antitumour activity of the novel vascular targeting agent Oxi 4503. *Anticancer Res.* **2002**, *22*(3), 1453-1458.

[554] Breen, E. C., *The Design, Synthesis and Preliminary Evaluation of Prodrugs and Hybrid Drugs with Tubulin Polymerisation Inhibitory Activity and Anti-Proliferative Activity*, in *School of Pharmacy and Pharmaceutical Sciences*. 2012, Trinity College Dublin: Dublin.

[555] Breen, E. C. and Walsh, J. J. Tubulin-targeting agents in hybrid drugs. *Curr Med Chem.* **2010**, *17*(7), 609-639.

[556] Melzig, M. F. and Bormann, H. Betulinic acid inhibits aminopeptidase N activity. *Planta Med.* **1998**, *64*(7), 655-657.

[557] Ishii, K.; Usui, S.; Sugimura, Y.; Yamamoto, H.; Yoshikawa, K.Hirano, K. Inhibition of aminopeptidase N (AP-N) and urokinase-type plasminogen activator (uPA) by zinc suppresses the invasion activity in human urological cancer cells. *Biol Pharm Bull.* **2001**, *24*(3), 226-230.

[558] Yang, E.; Shim, J. S.; Woo, H. J.; Kim, K. W.Kwon, H. J. Aminopeptidase N/CD13 induces angiogenesis through interaction with a pro-angiogenic protein, galectin-3. *Biochem Biophys Res Commun.* **2007**, *363*(2), 336-341.

[559] Terauchi, M.; Kajiyama, H.; Shibata, K.; Ino, K.; Nawa, A.; Mizutani, S.Kikkawa, F. Inhibition of APN/CD13 leads to suppressed progressive potential in ovarian carcinoma cells. *BMC Cancer.* **2007**, *7*, 140.

[560] Cui, S. X.; Qu, X. J.; Gao, Z. H.; Zhang, Y. S.; Zhang, X. F.; Zhao, C. R.; Xu, W. F.; Li, Q. B.Han, J. X. Targeting aminopeptidase N (APN/CD13) with cyclic-imide peptidomimetics derivative CIP-13F inhibits the growth of human ovarian carcinoma cells. *Cancer Lett.* **2010**, *292*(2), 153-162.

[561] Bauvois, B.; Van Weyenbergh, J.; Rouillard, D.Wietzerbin, J. TGF-beta 1-stimulated adhesion of human mononuclear phagocytes to fibronectin and laminin is abolished by IFN-gamma: dependence on alpha 5 beta 1 and beta 2 integrins. *Exp Cell Res.* **1996**, *222*(1), 209-217.

[562] Jamur, M. C. and Oliver, C. Permeabilization of cell membranes. *Methods Mol Biol.* **2010**, *588*, 63-66.

[563] Kanthou, C.; Greco, O.; Stratford, A.; Cook, I.; Knight, R.; Benzakour, O.Tozer, G. The tubulin-binding agent combretastatin A-4-phosphate arrests endothelial cells in mitosis and induces mitotic cell death. *Am J Pathol.* **2004**, *165*(4), 1401-1411.

[564] Iyer, S.; Chaplin, D. J.; Rosenthal, D. S.; Boulares, A. H.; Li, L. Y.Smulson, M. E. Induction of apoptosis in proliferating human endothelial cells by the tumor-specific antiangiogenesis agent combretastatin A-4. *Cancer Res.* **1998**, *58*(20), 4510-4514.

[565] Woods, C. M.; Zhu, J.; McQueney, P. A.; Bollag, D.Lazarides, E. Taxol-induced mitotic block triggers rapid onset of a p53-independent apoptotic pathway. *Mol Med.* **1995**, *1*(5), 506-526.

[566] Jordan, M. A.; Wendell, K.; Gardiner, S.; Derry, W. B.; Copp, H.Wilson, L. Mitotic block induced in HeLa cells by low concentrations of paclitaxel (Taxol) results in abnormal mitotic exit and apoptotic cell death. *Cancer Res.* **1996**, *56*(4), 816-825.

[567] Koopman, G.; Reutelingsperger, C. P.; Kuijten, G. A.; Keehnen, R. M.; Pals, S. T.van Oers, M. H. Annexin V for flow cytometric detection of

phosphatidylserine expression on B cells undergoing apoptosis. *Blood.* **1994**, *84*(5), 1415-1420.

[568] Nicoletti, I.; Migliorati, G.; Pagliacci, M. C.; Grignani, F.Riccardi, C. A rapid and simple method for measuring thymocyte apoptosis by propidium iodide staining and flow cytometry. *J Immunol Methods.* **1991**, *139*(2), 271-279.

[569] Riccardi, C. and Nicoletti, I. Analysis of apoptosis by propidium iodide staining and flow cytometry. *Nat Protoc.* **2006**, *1*(3), 1458-1461.

[570] Lin, C. F.; Chen, C. L.; Chiang, C. W.; Jan, M. S.; Huang, W. C.Lin, Y. S. GSK-3beta acts downstream of PP2A and the PI 3-kinase-Akt pathway, and upstream of caspase-2 in ceramide-induced mitochondrial apoptosis. *J Cell Sci.* **2007**, *120*(Pt 16), 2935-2943.

[571] Chiu, W. H.; Luo, S. J.; Chen, C. L.; Cheng, J. H.; Hsieh, C. Y.; Wang, C. Y.; Huang, W. C.; Su, W. C.Lin, C. F. Vinca alkaloids cause aberrant ROS-mediated JNK activation, Mcl-1 downregulation, DNA damage, mitochondrial dysfunction, and apoptosis in lung adenocarcinoma cells. *Biochem Pharmacol.* **2012**, *83*(9), 1159-1171.

[572] Sanchez, A. M.; Sanchez, M. G.; Malagarie-Cazenave, S.; Olea, N.Diaz-Laviada, I. Induction of apoptosis in prostate tumor PC-3 cells and inhibition of xenograft prostate tumor growth by the vanilloid capsaicin. *Apoptosis.* **2006**, *11*(1), 89-99.

[573] Darzynkiewicz, Z.; Juan, G.; Li, X.; Gorczyca, W.; Murakami, T.Traganos, F. Cytometry in cell necrobiology: analysis of apoptosis and accidental cell death (necrosis). *Cytometry.* **1997**, *27*(1), 1-20.

[574] Drag, M.; Grzywa, R.Oleksyszyn, J. Novel hydroxamic acid-related phosphinates: inhibition of neutral aminopeptidase N (APN). *Bioorg Med Chem Lett.* **2007**, *17*(6), 1516-1519.

[575] Lee, J.; Shim, J. S.; Jung, S. A.; Lee, S. T.Kwon, H. J. N-hydroxy-2-(naphthalene-2-ylsulfanyl)-acetamide, a novel hydroxamic acid-based inhibitor of aminopeptidase N and its anti-angiogenic activity. *Bioorg Med Chem Lett.* **2005**, *15*(1), 181-183.

[576] Krige, D.; Needham, L. A.; Bawden, L. J.; Flores, N.; Farmer, H.; Miles, L. E.; Stone, E.; Callaghan, J.; Chandler, S.; Clark, V. L.; Kirwin-Jones, P.; Legris, V.; Owen, J.; Patel, T.; Wood, S.; Box, G.; Laber, D.; Odedra, R.; Wright, A.; Wood, L. M.; Eccles, S. A.; Bone, E. A.; Ayscough, A.Drummond, A. H. CHR-2797: an antiproliferative aminopeptidase inhibitor that leads to amino acid deprivation in human leukemic cells. *Cancer Res.* **2008**, *68*(16), 6669-6679.

[577] Umezawa, H.; Ishizuka, M.; Aoyagi, T.Takeuchi, T. Enhancement of delayed-type hypersensitivity by bestatin, an inhibitor of aminopeptidase B and leucine aminopeptidase. *J Antibiot (Tokyo).* **1976**, *29*(8), 857-859.

[578] Burley, S. K.; David, P. R.Lipscomb, W. N. Leucine aminopeptidase: bestatin inhibition and a model for enzyme-catalyzed peptide hydrolysis. *Proc Natl Acad Sci U S A.* **1991**, *88*(16), 6916-6920.

[579] Inagaki, Y.; Tang, W.; Zhang, L.; Du, G.; Xu, W.Kokudo, N. Novel aminopeptidase N (APN/CD13) inhibitor 24F can suppress invasion of hepatocellular carcinoma cells as well as angiogenesis. *Biosci Trends.* **2010**, *4*(2), 56-60.

[580] Mishima, Y.; Terui, Y.; Sugimura, N.; Matsumoto-Mishima, Y.; Rokudai, A.; Kuniyoshi, R.Hatake, K. Continuous treatment of bestatin induces anti-angiogenic property in endothelial cells. *Cancer Sci.* **2007**, *98*(3), 364-372.

[581] Yang, K.; Fen, J.; Fang, H.; Zhang, L.; Gong, J.Xu, W. Synthesis of a novel series of L-isoserine derivatives as aminopeptidase N inhibitors. *J Enzyme Inhib Med Chem.* **2012**, *27*(2), 302-310.

[582] Ohtsu, H.; Nakanishi, Y.; Bastow, K. F.; Lee, F. Y.Lee, K. H. Antitumor agents 216. Synthesis and evaluation of paclitaxel-camptothecin conjugates as novel cytotoxic agents. *Bioorg Med Chem.* **2003**, *11*(8), 1851-1857.

[583] Coggiola, B.; Pagliai, F.; Allegrone, G.; Genazzani, A. A.Tron, G. C. Synthesis and biological activity of mustard derivatives of combretastatins. *Bioorg Med Chem Lett.* **2005**, *15*(15), 3551-3554.

[584] Kar, A. K.; Braun, P. D.Wandless, T. J. Synthesis and evaluation of daunorubicin-paclitaxel dimers. *Bioorg Med Chem Lett.* **2000**, *10*(3), 261-264.

[585] Passarella, D.; Giardini, A.; Peretto, B.; Fontana, G.; Sacchetti, A.; Silvani, A.; Ronchi, C.; Cappelletti, G.; Cartelli, D.; Borlak, J.Danieli, B. Inhibitors of tubulin polymerization: synthesis and biological evaluation of hybrids of vindoline, anhydrovinblastine and vinorelbine with thiocolchicine, podophyllotoxin and baccatin III. *Bioorg Med Chem.* **2008**, *16*(11), 6269-6285.

[586] Sharifi, N.; Hamel, E.; Lill, M. A.; Risbood, P.; Kane, C. T., Jr.; Hossain, M. T.; Jones, A.; Dalton, J. T.Farrar, W. L. A bifunctional colchicinoid that binds to the androgen receptor. *Mol Cancer Ther.* **2007**, *6*(8), 2328-2336.

[587] Kamal, A.; Bharathi, E. V.; Reddy, J. S.; Ramaiah, M. J.; Dastagiri, D.; Reddy, M. K.; Viswanath, A.; Reddy, T. L.; Shaik, T. B.; Pushpavalli, S. N.Bhadra, M. P. Synthesis and biological evaluation of 3,5-diaryl isoxazoline/isoxazole linked 2,3-dihydroquinazolinone hybrids as anticancer agents. *Eur J Med Chem.* **2011**, *46*(2), 691-703.

[588] Darzynkiewicz, Z.; Bedner, E.Smolewski, P. Flow cytometry in analysis of cell cycle and apoptosis. *Semin Hematol.* **2001**, *38*(2), 179-193.

[589] Lee, J. W.; Stone, R. L.; Lee, S. J.; Nam, E. J.; Roh, J. W.; Nick, A. M.; Han, H. D.; Shahzad, M. M.; Kim, H. S.; Mangala, L. S.; Jennings, N. B.; Mao, S.; Gooya, J.; Jackson, D.; Coleman, R. L.Sood, A. K. EphA2 targeted chemotherapy using an antibody drug conjugate in endometrial carcinoma. *Clin Cancer Res.* **2010**, *16*(9), 2562-2570.

[590] Francisco, J. A.; Cerveny, C. G.; Meyer, D. L.; Mixan, B. J.; Klussman, K.; Chace, D. F.; Rejniak, S. X.; Gordon, K. A.; DeBlanc, R.; Toki, B. E.; Law, C. L.; Doronina, S. O.; Siegall, C. B.; Senter, P. D.Wahl, A. F. cAC10-vcMMAE, an anti-CD30-monomethyl auristatin E conjugate with potent and selective antitumor activity. *Blood.* **2003**, *102*(4), 1458-1465.

[591] Cantley, L. C. The phosphoinositide 3-kinase pathway. *Science.* **2002**, *296*(5573), 1655-1657.

[592] Zhang, C.; Yang, N.; Yang, C. H.; Ding, H. S.; Luo, C.; Zhang, Y.; Wu, M. J.; Zhang, X. W.; Shen, X.; Jiang, H. L.; Meng, L. H.Ding, J. S9, a novel anticancer agent, exerts its anti-proliferative activity by interfering with both PI3K-Akt-mTOR signaling and microtubule cytoskeleton. *PLoS One.* **2009**, *4*(3), e4881.

[593] Inoi, K.; Goto, S.; Nomura, S.; Isobe, K.; Nawa, A.; Okamoto, T.Tomoda, Y. Aminopeptidase inhibitor ubenimex (bestatin) inhibits the growth of human

choriocarcinoma in nude mice through its direct cytostatic activity. *Anticancer Res.* **1995**, *15*(5B), 2081-2087.

[594] Pei, K. L.; Yuan, Y.; Qin, S. H.; Wang, Y.; Zhou, L.; Zhang, H. L.; Qu, X. J.Cui, S. X. CIP-13F, a novel aminopeptidase N (APN/CD13) inhibitor, inhibits Lewis lung carcinoma growth and metastasis in mice. *Cancer Chemother Pharmacol.* **2012**, *69*(4), 1029-1038.

[595] Schorlemmer, H. U.; Bosslet, K.; Dickneite, G.; Luben, G.Sedlacek, H. H. Studies on the mechanisms of action of the immunomodulator Bestatin in various screening test systems. *Behring Inst Mitt.* **1984**, (74), 157-173.

[596] Ma, Y.; Zhao, N.Liu, G. Conjugate (MTC-220) of muramyl dipeptide analogue and paclitaxel prevents both tumor growth and metastasis in mice. *J Med Chem.* **2011**, *54*(8), 2767-2777.

[597] Blanc, V.; Bousseau, A.; Caron, A.; Carrez, C.; Lutz, R. J.Lambert, J. M. SAR3419: an anti-CD19-Maytansinoid Immunoconjugate for the treatment of B-cell malignancies. *Clin Cancer Res.* **2011**, *17*(20), 6448-6458.

[598] Oflazoglu, E.; Stone, I. J.; Gordon, K.; Wood, C. G.; Repasky, E. A.; Grewal, I. S.; Law, C. L.Gerber, H. P. Potent anticarcinoma activity of the humanized anti-CD70 antibody h1F6 conjugated to the tubulin inhibitor auristatin via an uncleavable linker. *Clin Cancer Res.* **2008**, *14*(19), 6171-6180.

[599] Moeller, B. J.; Cao, Y.; Vujaskovic, Z.; Li, C. Y.; Haroon, Z. A.Dewhirst, M. W. The relationship between hypoxia and angiogenesis. *Semin Radiat Oncol.* **2004**, *14*(3), 215-221.

[600] Sakuda, H.; Nakashima, Y.; Kuriyama, S.Sueishi, K. Media conditioned by smooth muscle cells cultured in a variety of hypoxic environments stimulates in vitro angiogenesis. A relationship to transforming growth factor-beta 1. *Am J Pathol.* **1992**, *141*(6), 1507-1516.

[601] Shweiki, D.; Itin, A.; Soffer, D.Keshet, E. Vascular endothelial growth factor induced by hypoxia may mediate hypoxia-initiated angiogenesis. *Nature.* **1992**, *359*(6398), 843-845.

[602] Albina, J. E.; Mastrofrancesco, B.; Vessella, J. A.; Louis, C. A.; Henry, W. L., Jr.Reichner, J. S. HIF-1 expression in healing wounds: HIF-1alpha induction in primary inflammatory cells by TNF-alpha. *Am J Physiol Cell Physiol.* **2001**, *281*(6), C1971-1977.

[603] Leek, R. D.; Lewis, C. E.; Whitehouse, R.; Greenall, M.; Clarke, J.Harris, A. L. Association of macrophage infiltration with angiogenesis and prognosis in invasive breast carcinoma. *Cancer Res.* **1996**, *56*(20), 4625-4629.

[604] Yu, J. L. and Rak, J. W. Host microenvironment in breast cancer development: inflammatory and immune cells in tumour angiogenesis and arteriogenesis. *Breast Cancer Res.* **2003**, *5*(2), 83-88.

[605] Leek, R. D.; Talks, K. L.; Pezzella, F.; Turley, H.; Campo, L.; Brown, N. S.; Bicknell, R.; Taylor, M.; Gatter, K. C.Harris, A. L. Relation of hypoxia-inducible factor-2 alpha (HIF-2 alpha) expression in tumor-infiltrative macrophages to tumor angiogenesis and the oxidative thymidine phosphorylase pathway in Human breast cancer. *Cancer Res.* **2002**, *62*(5), 1326-1329.

[606] Decker, T. and Lohmann-Matthes, M. L. A quick and simple method for the quantitation of lactate dehydrogenase release in measurements of cellular cytotoxicity and tumor necrosis factor (TNF) activity. *J Immunol Methods.* **1988**, *115*(1), 61-69.

the tumor microenvironment. *Proc Natl Acad Sci U S A*. **2012**, *109*(5), 1637-1642.

[607] Fan, F. and Wood, K. V. Bioluminescent assays for high-throughput screening. *Assay Drug Dev Technol.* **2007**, *5*(1), 127-136.

[608] O'Boyle, N. M.; Carr, M.; Greene, L. M.; Keely, N. O.; Knox, A. J.; McCabe, T.; Lloyd, D. G.; Zisterer, D. M.Meegan, M. J. Synthesis, biochemical and molecular modelling studies of antiproliferative azetidinones causing microtubule disruption and mitotic catastrophe. *Eur J Med Chem.* **2011**, *46*(9), 4595-4607.

[609] Pettit, G. R.; Singh, S. B.; Hamel, E.; Lin, C. M.; Alberts, D. S.Garcia-Kendall, D. Isolation and structure of the strong cell growth and tubulin inhibitor combretastatin A-4. *Experientia.* **1989**, *45*(2), 209-211.

[610] Dachs, G. U.; Steele, A. J.; Coralli, C.; Kanthou, C.; Brooks, A. C.; Gunningham, S. P.; Currie, M. J.; Watson, A. I.; Robinson, B. A.Tozer, G. M. Anti-vascular agent Combretastatin A-4-P modulates hypoxia inducible factor-1 and gene expression. *BMC Cancer.* **2006**, *6*, 280.

[611] Sheng, Y.; Hua, J.; Pinney, K. G.; Garner, C. M.; Kane, R. R.; Prezioso, J. A.; Chaplin, D. J.Edvardsen, K. Combretastatin family member OXI4503 induces tumor vascular collapse through the induction of endothelial apoptosis. *Int J Cancer.* **2004**, *111*(4), 604-610.

[612] Zhang, J.; Li, X.; Zhu, H. W.; Wang, Q.; Feng, J. H.; Mou, J. J.; Li, Y. G.; Fang, H.Xu, W. F. Design, synthesis, and primary activity evaluation of pyrrolidine derivatives as matrix metalloproteinase inhibitors. *Drug Discov Ther.* **2010**, *4*(1), 5-12.

[613] Zhang, X.; Zhang, J.; Zhang, L.; Feng, J.; Xu, Y.; Yuan, Y.; Fang, H.Xu, W. Design, synthesis and biological evaluation of novel 1,2,3,4-tetrahydroisoquinoline-3-carboxylic acid derivatives as aminopeptidase N/CD13 inhibitors. *Bioorg Med Chem.* **2011**, *19*(20), 6015-6025.

[614] van Hensbergen, Y.; Broxterman, H. J.; Peters, E.; Rana, S.; Elderkamp, Y. W.; van Hinsbergh, V. W.Koolwijk, P. Aminopeptidase inhibitor bestatin stimulates microvascular endothelial cell invasion in a fibrin matrix. *Thromb Haemost.* **2003**, *90*(5), 921-929.

[615] Yang, T.; Wang, Y.; Li, Z.; Dai, W.; Yin, J.; Liang, L.; Ying, X.; Zhou, S.; Wang, J.; Zhang, X.Zhang, Q. Targeted delivery of a combination therapy consisting of combretastatin A4 and low-dose doxorubicin against tumor neovasculature. *Nanomedicine.* **2012**, *8*(1), 81-92.

[616] Zhang, C.; Wu, R.; Zhu, H.; Hu, Y. Z.; Jiang, H.; Lin, N. M.; He, Q. J.Yang, B. Enhanced anti-tumor activity by the combination of TRAIL/Apo-2L and combretastatin A-4 against human colon cancer cells via induction of apoptosis in vitro and in vivo. *Cancer Lett.* **2011**, *302*(1), 11-19.

[617] Stangelberger, A.; Schally, A. V.; Varga, J. L.; Zarandi, M.; Szepeshazi, K.; Armatis, P.Halmos, G. Inhibitory effect of antagonists of bombesin and growth hormone-releasing hormone on orthotopic and intraosseous growth and invasiveness of PC-3 human prostate cancer in nude mice. *Clin Cancer Res.* **2005**, *11*(1), 49-57.

[618] Guzman-Rojas, L.; Rangel, R.; Salameh, A.; Edwards, J. K.; Dondossola, E.; Kim, Y. G.; Saghatelian, A.; Giordano, R. J.; Kolonin, M. G.; Staquicini, F. I.; Koivunen, E.; Sidman, R. L.; Arap, W.Pasqualini, R. Cooperative effects of aminopeptidase N (CD13) expressed by nonmalignant and cancer cells within